NEW AGE

FACTS CONTROLLERS IN POWER TRANSMISSION AND DISTRIBUTION

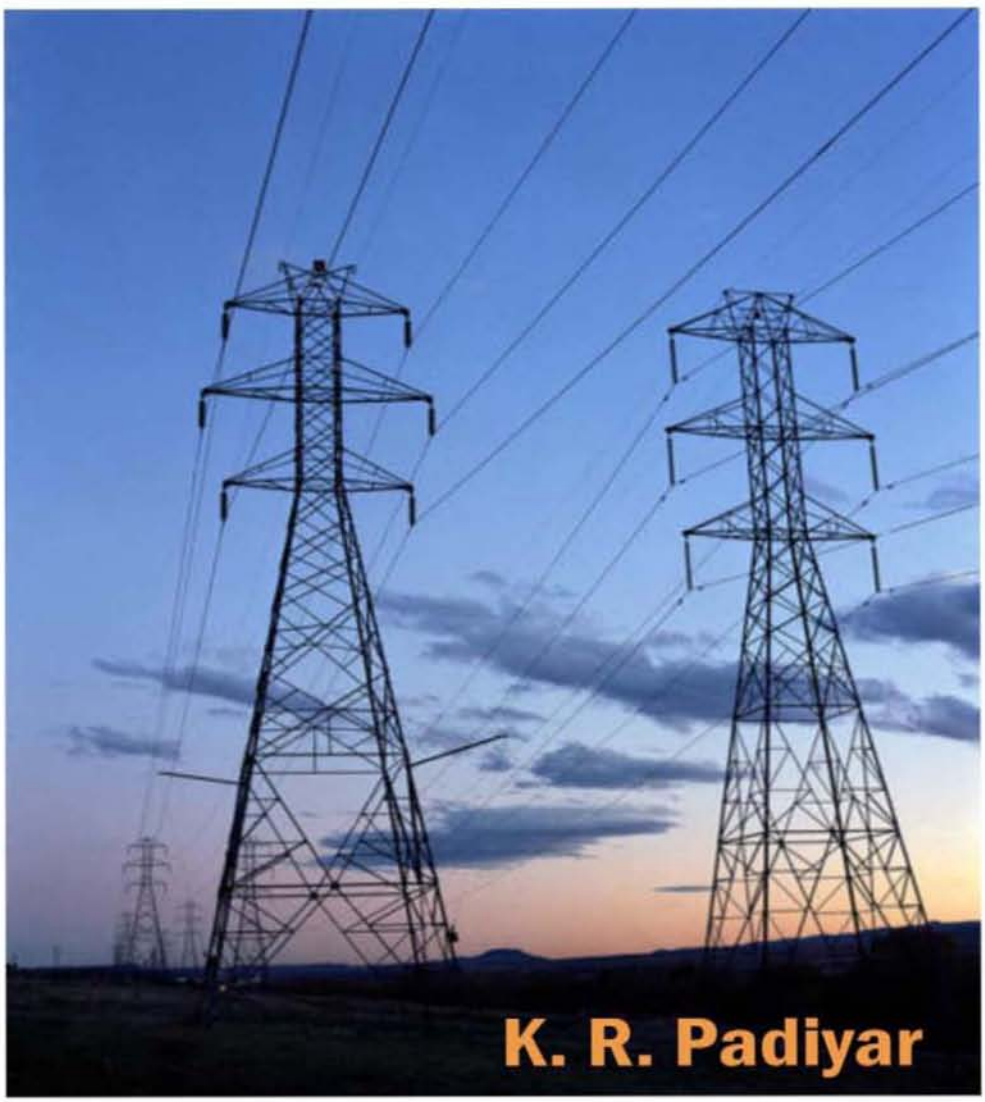

K. R. Padiyar

NEW AGE INTERNATIONAL PUBLISHERS

FACTS CONTROLLERS
IN POWER TRANSMISSION AND DISTRIBUTION

This page intentionally left blank

FACTS CONTROLLERS
IN POWER TRANSMISSION AND DISTRIBUTION

K. R. Padiyar
Department of Electrical Engineering
Indian Institute of Science
Bangalore-560 012
India

PUBLISHING FOR ONE WORLD
NEW AGE INTERNATIONAL (P) LIMITED, PUBLISHERS
New Delhi • Bangalore • Chennai • Cochin • Guwahati • Hyderabad
Jalandhar • Kolkata • Lucknow • Mumbai • Ranchi
Visit us at www.newagepublishers.com

Published by New Age International (P) Ltd., Publishers

ISBN (13) : 978-81-224-2541-3

PUBLISHING FOR ONE WORLD

NEW AGE INTERNATIONAL (P) LIMITED, PUBLISHERS
4835/24, Ansari Road, Daryaganj, New Delhi - 110002
Visit us at **www.newagepublishers.com**

This book is dedicated to

Dr. Narain G. Hingorani

who pioneered the concepts of
Flexible AC Transmission Systems (FACTS) and Custom Pcwer

This page intentionally left blank

Preface

Modern power systems are highly complex and are expected to fulfill the growing demands of power wherever required, with acceptable quality and costs. The economic and environmental factors necessitate the location of generation at places away from load centres. The restructuring of power utilities has increased the uncertainties in system operation. The regulatory constraints on the expansion of the transmission network has resulted in reduction of stability margins and increased the risks of cascading outages and blackouts. This problem can be effectively tackled by the introduction of high power electronic controllers for the regulation of power flows and voltages in AC transmission networks. This allows 'flexible' operation of AC transmission systems whereby the changes can be accommodated easily without stressing the system. Power electronic based systems and other static equipment that provide controllability of power flow and voltage are termed as FACTS Controllers.

It is to be noted that power electronic controllers were first introduced in HVDC transmission for not only regulation of power flow in HVDC links, but also for modulation to improve system stability (both angle and voltage). The technology of thyristor valves and digital controls was initially extended to the development of Static Var Compensator (SVC) for load compensation and voltage regulation in long transmission lines. In 1988,Dr.Narain G. Hingorani introduced the concept of Flexible AC Transmission Systems (FACTS) by incorporating power electronic controllers to enhance power transfer in existing AC transmission lines, improve voltage regulation and system security without adding new lines. The FACTS controllers can also be used to regulate power flow in critical lines and hence, ease congestion in electrical networks. FACTS does not refer to any single device, but a host of controllers such as SVC, Thyristor Controlled Series Capacitor (TCSC), Static Phase Shifting Transformer (SPST), and newer controllers based on Voltage Source Converters (VSC)-Static synchronous Compensator (STATCOM), Static Synchronous Series Compensator (SSSC), Unified Power Flow Controller (UPFC), Interline Power Flow Controller (IPFC) etc. The advent of FACTS controllers has already made a major impact on the planning and operation of power delivery systems. The concept of Custom Power introduced by Dr.Hingorani in 1995 has extended the application of FACTS controllers for distribution systems with the objective of improving power quality. An understanding of the working of individual FACTS controllers and issues that affect their operation under various conditions is essential for both students and engineers (in industry) who are interested in the subject. This book aims to provide detailed information for students, researchers, and development and application engineers in industry. It contains

comprehensive and up-to-date coverage of the FACTS controllers that have been proposed and developed both for transmission and distribution. It is hoped that this book will complement the excellent book on "Understanding FACTS-Concepts and Technology of Flexible AC Transmission Systems" by the pioneers, Dr. Narain G. Hingorani and Dr.Laszlo Gyugyi. The present book covers many analytical issues that affect the design of FACTS Controllers, which are of interest to academics and application engineers. It can be used as a text or reference for a course on FACTS Controllers. The author has been working in the area of HVDC and FACTS Controllers over many years. He has taught a course on FACTS for graduate students at Indian Institute of Science and has guided several Masters and PhD students who have worked on various aspects of different FACTS controllers. He has delivered many lectures in short- term intensive courses attended by teachers from engineering colleges and engineers from industry. He is the author of a book on HVDC Power Transmission Systems (published by Wiley Eastern and John Wiley in 1991), which is widely used. Hence, it was natural to attempt this book based on the expertise and experience gained.

The book is organized into 14 chapters and 4 appendices. The first chapter introduces FACTS controllers and their application in transmission and distribution networks in the context of operational problems of modern power systems involving transmission congestion, loop flows, system security and power quality issues. The second chapter reviews the modeling and steady state characteristics of AC transmission lines. It also covers the analysis of how an individual FACTS controller can modify the power flow and voltage profile in a line.

Chapters 3 to 9 cover the various FACTS controllers -SVC, TCSC and GCSC, Static PST, STATCOM, SSSC, UPFC, IPFC, CSC, IPC and other devices such as Fault Current Limiter (FCL), Thyristor Controlled Braking Resistor (TCBR), NGH Damping and Thyristor Controlled Voltage Limiter (TCVL). In each case, the function of the FACTS device is explained with the description of power circuit, associated controllers and operating modes. The modeling of each FACTS Controller is derived from first principles and simplifications where appropriate are discussed. The applications and control interactions involving Subsynchronous Resonance (SSR), electromagnetic interactions and harmonic interactions are also discussed in some detail wherever required.

A major function of a FACTS Controller is power oscillation damping involving low frequency oscillations that threaten system security under peak power flow conditions. Chapter 10 covers the analysis of this problem with solutions involving control strategies for voltage and power modulation. Illustrative examples are included to explain the techniques.

Another important control function is the improvement of transient stability using bang-bang control technique. This is also termed as discrete control. The analysis and control strategies for this function are discussed in detail in chapter 11 with the help of case studies.

Chapter 12 introduces the power quality issues involving voltage fluctuations, flicker, sags and swells, momentary interruptions, unbalance and harmonics. The measures for power quality are described and introduction to Custom Power Devices (CPD) is presented. Chapter 13 deals with load

compensation and application of distribution STATCOM (DSTATCOM) for fast voltage regulation or reactive power compensation, balancing of source currents and active filtering. Chapter 14 covers series power quality conditioner involving dynamic voltage restoration and harmonic isolation. The Unified Power Quality Conditioner (UPQC), which includes both shunt and series compensators is also described. In all cases considered, the operation of the individual device is described along with modeling, control algorithms and simulation of the system to evaluate the performance. The case studies are presented to illustrate the analysis.

The Appendix A describes the modeling of synchronous machines for both stability and transient analysis. The mechanical system of rotor masses and shafts is also modeled. The major Pulse Width Modulation (PWM) techniques such as Sine PWM and Space Vector modulation are discussed in Appendix B. The per unit system for a STATCOM is discussed in Appendix C. The Appendix D lists the abbreviations used.

It is assumed that the reader has an exposure to elementary power electronics, power systems and basic control theory. Hence, topics on power semiconductor devices and converters have been deliberately left out. Still, the book contains more material than what can be covered in a one-semester course.

Acknowledgements

I would like to acknowledge with gratitude the contributions of several individuals in the preparation of this book. First and foremost, I wish to acknowledge the encouragement and help received from Dr.Narain Hingorani who pioneered the concepts of FACTS and Custom Power. Drs. John Vithayathil (who explained the RANI concept), R.Mohan Mathur, R.S.Thallam, Rambabu Adapa, Rajiv Varma and Subhashish Bhattacharya have helped in getting information and literature on FACTS. I acknowledge the research work carried out by my graduate students on FACTS. Starting with Dr.Rajiv Varma, other PhD students who contributed are: Drs. Vijayan Immanuel, K. Uma Rao, M.K. Geetha, Anil Kulkarni, Sujatha Subhash, Parthasarathy Sensarma, S.Krishna, H.V.Saikumar and Nagesh Prabhu. There are many Masters Students who have worked on FACTS. In particular, I wish to acknowledge the contributions of Lakshmi Devi, Sreekumar, Jayati, Sriram, Sreekantha, Dhiman, Renuka, Sandeep, Anjali, Rajesh Kumar, Manmayjyoti, Mohanraj, Mahesh Sitaram, Swayam Prakash, Venkatesh, Dhananjay and Anand Kumar.

I thank Dr. S. Krishna for assisting in proof reading and the preparation of CRC. Thanks are also due to Dr. Nagesh Prabhu and Mr. Anand Kumar for their help in the preparation of the final manuscript and Mr. Kiran Kumar for the drawings. Dr. Kalyani Gopal made available the Latex style file used. I thank Mr. Saumya Gupta of New Age International Publishers for his keen interest and help in publishing this book on time.

This book was catalyzed and supported by the Department of Science and Technology (DST), Government of India under its Utilization of Scientific Expertise of Retired Scientists (USERS) scheme. The DST has

also supported research schemes during the period from 1994 to 2003. The author also wishes to gratefully acknowledge the financial assistance from All India Council of Technical Education (AICTE) under the Emeritus Fellowship Scheme during the period (August 1,2003-June 30,2006). Finally, I am deeply indebted to Indian Institute of Science for permitting me to pursue academic activities as an Honorary Professor from May 2003.

Last, but not the least, I thank my wife Usha for her patience and quiet support during the long hours of working on this book.

K.R.Padiyar

Contents

This page intentionally left blank

Chapter 1

Introduction

1.1 General

Modern power systems are designed to operate efficiently to supply power on demand to various load centres with high reliability. The generating stations are often located at distant locations for economic, environmental and safety reasons. For example, it may be cheaper to locate a thermal power station at pithead instead of transporting coal to load centres. Hydropower is generally available in remote areas. A nuclear plant may be located at a place away from urban areas. Thus, a grid of transmission lines operating at high or extra high voltages is required to transmit power from the generating stations to the load centres.

In addition to transmission lines that carry power from the sources to loads, modern power systems are also highly interconnected for economic reasons. The interconnected systems benefit by (a) exploiting load diversity (b) sharing of generation reserves and (c) economy gained from the use of large efficient units without sacrificing reliability. However, there is also a downside to ac system interconnection – the security can be adversely affected as the disturbances initiated in a particular area can spread and propagate over the entire system resulting in major blackouts caused by cascading outages.

1.2 Basics of Power Transmission Networks

A large majority of power transmission lines are AC lines operating at different voltages (10 kV to 800 kV). The distribution networks generally operate below 100 kV while the bulk power is transmitted at higher voltages. The lines operating at different voltages are connected through transformers which operate at high efficiency. Traditionally, AC lines have no provision for the control of power flow. The mechanically operated circuit breakers (CB) are meant for protection against faults (caused by flashovers due to overvoltages on the lines or reduced clearances to ground). A CB is rated for a limited number of open and close operations at a time and cannot be used

for power flow control. (unlike a high power electronic switch such as thyristor, GTO, IGBT, IGCT, etc.). Fortunately, ac lines have inherent power flow control as the power flow is determined by the power at the sending end or receiving end. For example, consider a trasmission line connecting a generating station to a load centre in Fig.1.1(a). Assuming the line to be lossless and ignoring the line charging, the power flow (P) is given by

$$P = \frac{V_1 V_2}{X} \sin(\theta_1 - \theta_2) \tag{1.1}$$

where X is the series line reactance. Assuming V_1 and V_2 to be held constants (through voltage regulators at the two ends), the power injected by the power station determines the flow of power in the line. The difference in the bus angles is automatically adjusted to enable $P = P_G$ (Note that usually there could be more than one line transmitting power from a generating station to a load centre). If one or more lines trip, the output of the power station may have to be reduced by tripping generators, so as to avoid overloading the remaining lines in operation.

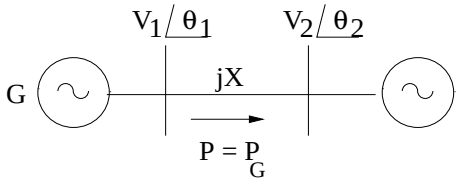

(a) A line transmitting power from a generating station

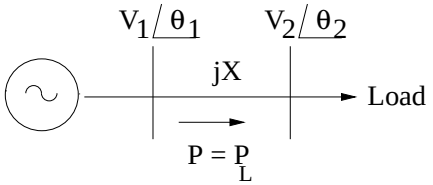

(b) A line supplying power to a load

Figure 1.1: A transmission line carrying power

Fig. 1.1(b) shows another situation where a line supplies power to a load located at bus (2). Here also the eq. (1.1) applies but the power flow in the line is determined by the load supplied. The essential difference between the two situations is that in Fig. 1.1(a), the load centre is modelled as an infinite bus which can absorb (theoretically) any amount of power supplied to it from the generating station. This model of the load centre assumes that the generation available at the load centre is much higher than the power supplied from the remote power station (obviously, the total load supplied at the load centre is equal to the net generation available at that bus).

The reliability of the power supply at a load bus can be improved by arranging two (or more) sources of power as shown in Fig. 1.2. Here, P_1 is the output of $G1$ while P_2 is the output of $G2$ (Note that we are neglecting losses as before). However, the tripping of any one line will reduce the availability of power at the load bus. This problem can be overcome by providing a line (shown dotted in Fig. 1.2) to interconnect the two power stations. Note that this results in the creation of a mesh in the transmission network. This improves the system reliability, as tripping of any one line does not result in curtailment of the load. However, in steady state, P_1 can be higher or lower than P_{G1} (the output of G1). The actual power flows in the 3 lines forming a mesh are determined by Kirchhoff's Voltage Law (KVL). In general, the addition of an (interconnecting) line can result in increase of power flow in a line (while decreasing the power flow in some other line). This is an interesting feature of AC transmission lines and not usually well understood (in the context of restructuring). In general, it can be stated that in an uncontrolled AC transmission network with loops (to improve system reliability), the power flows in individual lines are determined by KVL and do not follow the requirements of the contracts (between energy producers and customers). In other words, it is almost impossible to ensure that the power flow between two nodes follows a predetermined path. This is only feasible in radial networks (with no loops), but the reliability is adversely affected as even a single outage can result in load curtailment. Consider two power systems, each with a single power station meeting its own local load, interconnected by a tie line as shown in Fig. 1.3(a). In this case, the power flow in the tie line (P) in steady state is determined by the mismatch between the generation and load in the individual areas. Under dynamic conditions, this power flow is determined from the equivalent circuit shown in Fig. 1.3(b). If the capacity of the tie is small compared to the size (generation) of the two areas, the angles δ_1 and δ_2 are not affected much by the tie line power flow. Thus, power flow in AC tie is generally uncontrolled and it becomes essential to trip the tie during a disturbance, either to protect the tie line or preserve system security.

In comparison with a AC transmission line, the power flow in a HVDC line in controlled and regulated. However, HVDC converter stations are expensive and HVDC option is used primarily for (a) long distance bulk power transmission (b) interconnection of asynchronous systems and (c) underwater (submarine) transmission. The application of HVDC transmission (using thyristor converters) is also constrained by the problem of commutation failures affecting operation of multiterminal or multi-feed HVDC systems. This implies that HVDC links are primarily used for point-to-point transmission of power and asynchronous interconnection (using Back to Back (BTB) links).

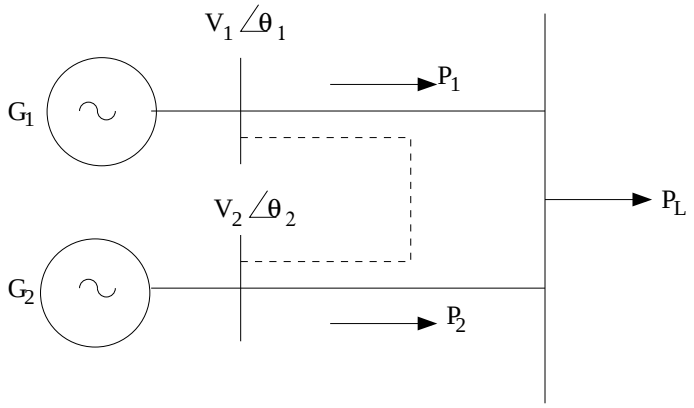

Figure 1.2: Two generating stations supplying a load

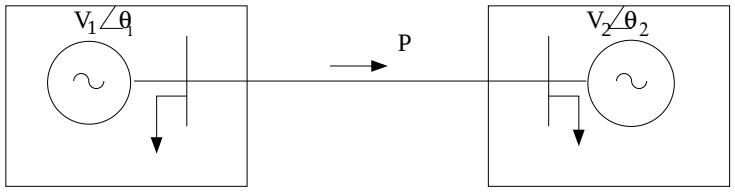

(a)Single line diagram

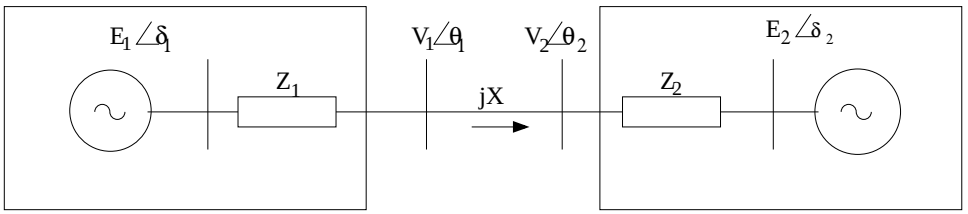

Thevenin equivalent of area 1 Thevenin equivalent of area 2

(b)Equivalent circuit

Figure 1.3: Two areas connected by a tie line

1.3 Control of Power Flow in AC Transmission Line

We may like to control the power flow in a AC transmission line to (a) enhance power transfer capacity and or (b) to change power flow under dynamic conditions (subjected to disturbances such as sudden increase in load, line trip or generator outage) to ensure system stability and security. The stability can be affected by growing low frequency, power oscillations (due to generator rotor swings), loss of synchronism and voltage collapse caused by major disturbances.

From eq. (1.1), we have the maximum power ($P_{\max}$) transmitted over a line as

$$P_{\max} = \frac{V_1 V_2}{X} \sin \delta_{\max} \tag{1.2}$$

where $\delta_{\max}$ (30°–40°) is selected depending on the stability margins and the stiffness of the terminal buses to which the line is connected. For line lengths exceeding a limit, $P_{\max}$ is less than the thermal limit on the power transfer determined by the current carrying capacity of the conductors (Note this is also a function of the ambient temperature). As the line length increases, X increases in a linear fashion and $P_{\max}$ reduces as shown in Fig. 1.4.

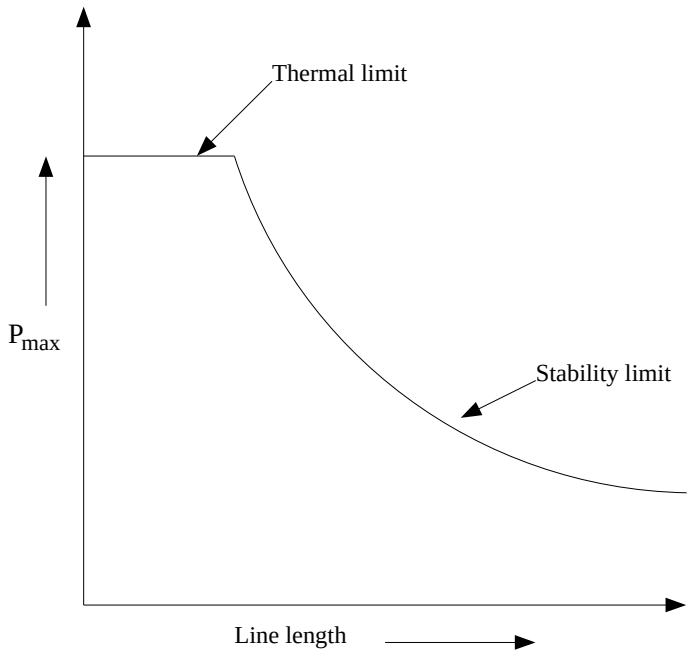

Figure 1.4: Power transfer capacity as a function of line length

The series compensation using series connected capacitors increases $P_{\max}$ as the compensated value of the series reactance (X_c) is given by

$$X_c = X(1 - k_{se}) \tag{1.3}$$

where k_{se} is the degree of series compensation. The maximum value of k_{se} that can be used depends on several factors including the resistance of the conductors. Typically k_{se} does not exceed 0.7.

Fixed series capacitors have been used since a long time for increasing power transfer in long lines. They are also most economical solutions for this purpose. However, the control of series compensation using thyristor

switches has been introduced only 10–15 years ago for fast power flow control. The use of Thyristor Controlled Reactors (TCR) in parallel with fixed capacitors for the control of X_c, also helps in overcoming a major problem of Subsynchronous Resonance (SSR) that causes instability of torsional modes when series compensated lines are used to transmit power from turbogenerators in steam power stations.

In tie lines of short lengths, the power flow can be controlled by introducing Phase Shifting Transformer (PST) which has a complex turns ratio with magnitude of unity. The power flow in a lossless transmission line with an ideal PST (see Fig. 1.5) is given by

$$P = \frac{V_1 V_2}{X} \sin(\theta \pm \phi) \tag{1.4}$$

where $\theta = \theta_1 - \theta_2$.

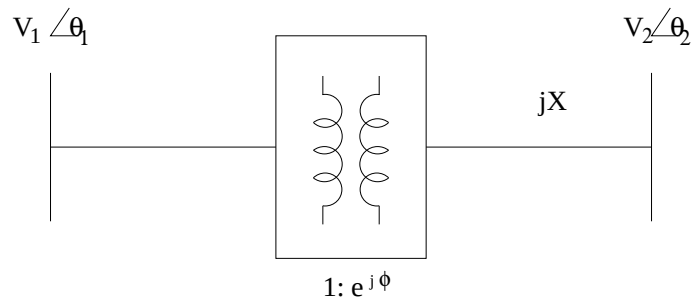

Figure 1.5: A lossless line with an ideal PST

Again, manually controlled PST is not fast enough under dynamic conditions. Thyristor switches can ensure fast control over discrete (or continuous) values of ϕ, depending on the configuration of PST used. $P_{\max}$ can also be increased by controlling (regulating) the receiving end voltage of the AC line. When a generator supplies a unity power factor load (see Fig. 1.1(b)), the maximum power occurs when the load resistance is equal to the line reactance. It is to be noted that V_2 varies with the load and can be expressed as

$$V_2 = V_1 \cos(\theta_1 - \theta_2) \tag{1.5}$$

Substituting (1.5) in (1.1) gives

$$P = \frac{V_1^2 \sin[2(\theta_1 - \theta_2)]}{2X} \tag{1.6}$$

By providing dynamic reactive power support at bus (2) as shown in Fig. (1.6), it is possible to regulate the bus voltage magnitude. The reactive

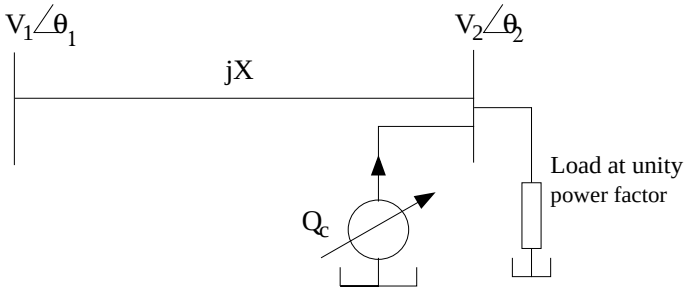

Figure 1.6: Transmission line compensated by controllable reactive power source at receiving end

power (Q_C) that has to be injected is given by

$$Q_C = \frac{V_2^2 - V_1 V_2 \cos(\theta_1 - \theta_2)}{X} \tag{1.7}$$

Comparing eq. (1.6) with (1.1), it can be seen that the maximum power transfer can be doubled just by providing dynamic reactive power support at the receiving end of the transmission line. This is in addition to the voltage support at the sending end. It is to be noted that while steady state voltage support can be provided by mechanically switched capacitors, the dynamic voltage support requires synchronous condenser or a power electronic controller such as Static Var Compensator (SVC) or STATic synchronous COMpensator (STATCOM).

1.4 Flexible AC Transmission System Controllers

1.4.1 General Description

The large interconnected transmission networks (made up of predominantly overhead transmission lines) are susceptible to faults caused by lightning discharges and decrease in insulation clearances by undergrowth. The power flow in a transmission line is determined by Kirchhoff's laws for a specified power injections (both active and reactive) at various nodes. While the loads in a power system vary by the time of the day in general, they are also subject to variations caused by the weather (ambient temperature) and other unpredictable factors. The generation pattern in a deregulated environment also tends to be variable (and hence less predictable). Thus, the power flow in a transmission line can vary even under normal, steady state conditions. The occurrence of a contingency (due to the tripping of a line, generator) can result in a sudden increase/decrease in the power flow. This can result in overloading of some lines and consequent threat to system security.

A major disturbance can also result in the swinging of generator rotors which contribute to power swings in transmission lines. It is possible that the system is subjected to transient instability and cascading outages as individual components (lines and generators) trip due to the action of protective relays. If the system is operating close to the boundary of the small signal stability region, even a small disturbance can lead to large power swings and blackouts.

The increase in the loading of the transmission lines sometimes can lead to voltage collapse due to the shortage of reactive power delivered at the load centres. This is due to the increased consumption of the reactive power in the transmission network and the characteristics of the load (such as induction motors supplying constant torque).

The factors mentioned in the previous paragraphs point to the problems faced in maintaining economic and secure operation of large interconnected systems. The problems are eased if sufficient margins (in power transfer) can be maintained. This is not feasible due to the difficulties in the expansion of the transmission network caused by economic and environmental reasons. The required safe operating margin can be substantially reduced by the introduction of fast dynamic control over reactive and active power by high power electronic controllers. This can make the AC transmission network 'flexible' to adapt to the changing conditions caused by contingencies and load variations. Flexible AC Transmission System (FACTS) is defined as 'Alternating current transmission systems incorporating power electronic-based and other static controllers to enhance controllability and increase power transfer capability' [1,2]. The FACTS controller is defined as 'a power electronic based system and other static equipment that provide control of one or more AC transmission system parameters'.

The FACTS controllers can be classified as

1. Shunt connected controllers
2. Series connected controllers
3. Combined series-series controllers
4. Combined shunt-series controllers

Depending on the power electronic devices used in the control, the FACTS controllers can be classified as

(A) Variable impedance type

(B) Voltage Source Converter (VSC) – based.

The variable impedance type controllers include:

(i) Static Var Compensator (SVC), (shunt connected)

(ii) Thyrister Controlled Series Capacitor or compensator (TCSC), (series connected)

(iii) Thyristor Controlled Phase Shifting Transformer (TCPST) of Static PST (combined shunt and series)

The VSC based FACTS controllers are:

(i) Static synchronous Compensator (STATCOM) (shunt connected)

(ii) Static Synchronous Series Compensator (SSSC) (series connected)

(iii) Interline Power Flow Controller (IPFC) (combined series-series)

(iv) Unified Power Flow Controller (UPFC) (combined shunt-series)

Some of the special purpose FACTS controllers are

(a) Thyristor Controller Braking Resistor (TCBR)

(b) Thyristor Controlled Voltage Limiter (TCVL)

(c) Thyristor Controlled Voltage Regulator (TCVR)

(d) Interphase Power Controller (IPC)

(e) NGH-SSR damping

The FACTS controllers based on VSC have several advantages over the variable impedance type. For example, a STATCOM is much more compact than a SVC for similar rating and is technically superior. It can supply required reactive current even at low values of the bus voltage and can be designed to have in built short term overload capability. Also, a STATCOM can supply active power if it has an energy source or large energy storage at its DC terminals.

The only drawback with VSC based controllers is the requirement of using self commutating power semiconductor devices such as Gate Turn-off (GTO) thyristors, Insulated Gate Bipolar Transistors (IGBT), Integrated Gate Commutated Thyristors (IGCT). Thyristors do not have this capability and cannot be used although they are available in higher voltage ratings and tend to be cheaper with reduced losses. However, the technical advantages with VSC based controllers coupled will emerging power semiconductor devices using silicon carbide technology are expected to lead to the wide spread use of VSC based controllers in future.

It is interesting to note that while SVC was the first FACTS controllers (which utilized the thyristor valves developed in connection with HVDC line commutated convertors) several new FACTS controller based on VSC have been developed. This has led to the introduction of VSC in HVDC transmission for ratings up to 300 MW.

1.4.2 Voltage Source Converter Based Controllers - An Introduction

This section is aimed at giving a brief introduction to the VSC based controller. The individual controllers are discussed in detail in the following chapters (6-8). The schematic diagram of a STATCOM is shown in Fig. 1.7 while that of a SSSC is shown in Fig.1.8. The diagram of a UPFC is shown in Fig. 1.9.

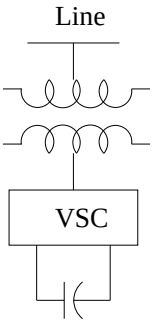

Figure 1.7: Shunt connected STATCOM

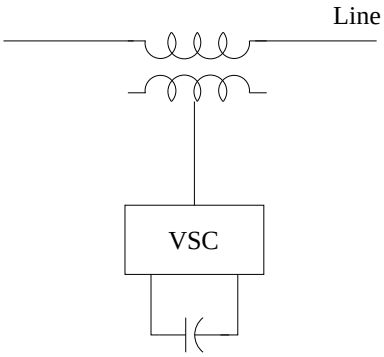

Figure 1.8: Series connected SSSC

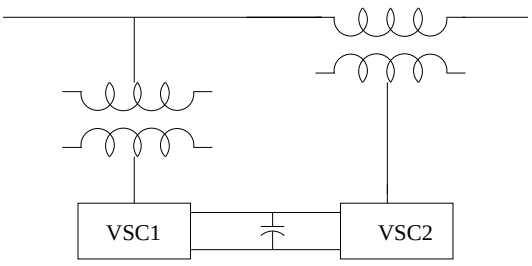

Figure 1.9: Unified power flow controller

A six pulse Voltage Source Converter (VSC) is shown in Fig. 1.10. By suitable control, the phase and the magnitude of the AC voltage injected by the VSC can be controlled. The Phase Lock Loop (PLL) ensures that the sinusoidal component of the injected voltage is synchronized (matching in frequency and required phase angle) with the voltage of the AC bus to which VSC is connected through an inductor. Often, the leakage impedance of the interconnecting transformer serves as the inductive impedance that has to separate the sinusoidal bus voltage and the voltage injected by the VSC (which contains harmonics). The injection of harmonic voltages can be minimized by multipulse (12, 24 or 48), and/or multilevel convertors. At low power levels, it is feasible to provide pulse width modulation (PWM) to control the magnitude of the fundamental component of the injected voltage. The high voltage IGBT devices can be switched up to 2 kHz and high frequency of sinusoidal modulation enables the use of simple L-C (low pass) filters to reduce harmonic components.

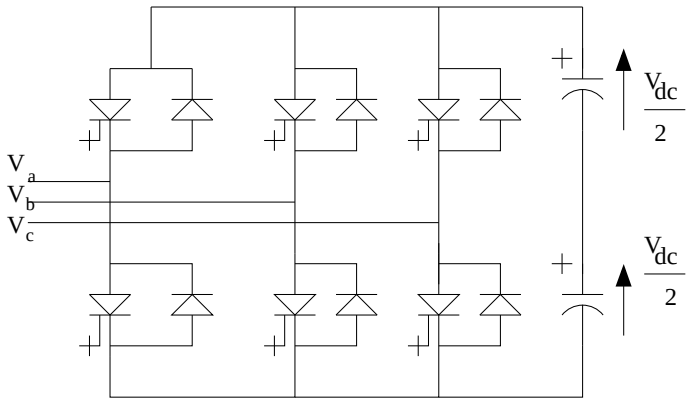

Figure 1.10: A three phase, six pulse VSC

The operation of a VSC can be explained with reference to a single phase (half-wave) convertor shown in Fig. 1.11. This can represent one leg of the 3 phase VSC.

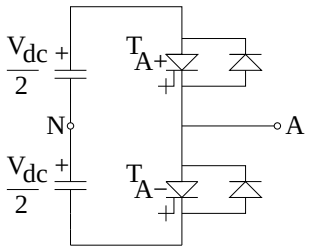

Figure 1.11: A single phase half wave converter

T_{A+} and T_{A-} are controllable switches which can be switched on or off at controllable instants in a cycle. The diodes ensure that the current can flow in both directions in the DC capacitor. The switches T_{A+} and T_{A-} work in complementary fashion – only one of them is on while the other is off. If the switch is turned on only once during a cycle, this is called as the square-wave switching scheme with each switch conducting for 180° in a cycle. The peak value of the fundamental component (V_{AN1}) is given by

$$V_{AN1} = \frac{4}{\pi}\left(\frac{V_{dc}}{2}\right) = 1.273\left(\frac{V_{dc}}{2}\right) \tag{1.8}$$

The waveform contains odd harmonics with the magnitudes

$$V_{ANh} = \frac{V_{AN1}}{h}, \quad h = 3, 5, 7, \ldots \tag{1.9}$$

It is to be noted that in the square wave switching scheme, only the phase angle of the voltage injected by the VSC can be controlled (and not the magnitude). It will be shown in chapter 6 that in a three phase converter with 3 legs the triplen harmonics will disappear such that the non-zero harmonic order (h) is given by

$$h = 6n \pm 1, \quad n = 1, 2, \ldots \tag{1.10}$$

Increasing the pulse number from six to twelve has the effect of eliminating the harmonics corresponding to odd values of n.

The introduction of PWM has the effect of controlling the magnitude of the fundamental component of the injected voltage by the VSC. For this case, the waveform of the voltage v_{AN} is shown in Fig. 1.12. Using sinusoidal modulation (with triangular carrier wave), the peak value of the injected sinusoidal voltage can be expressed as

$$V_{AN1} = m\left(\frac{V_{dc}}{2}\right), \quad 0 < m \leq 1 \tag{1.11}$$

where m is called the modulation index.

The maximum modulation index can be achieved with space vector modulation and is given by [10]

$$m_{\max} = \frac{2}{\sqrt{3}} = 1.1547 \tag{1.12}$$

It is to be noted that the modulation index (m) and the phase angle (α) are controlled to regulate the injected current by the shunt connected VSC. Neglecting losses, a STATCOM can only inject reactive current in

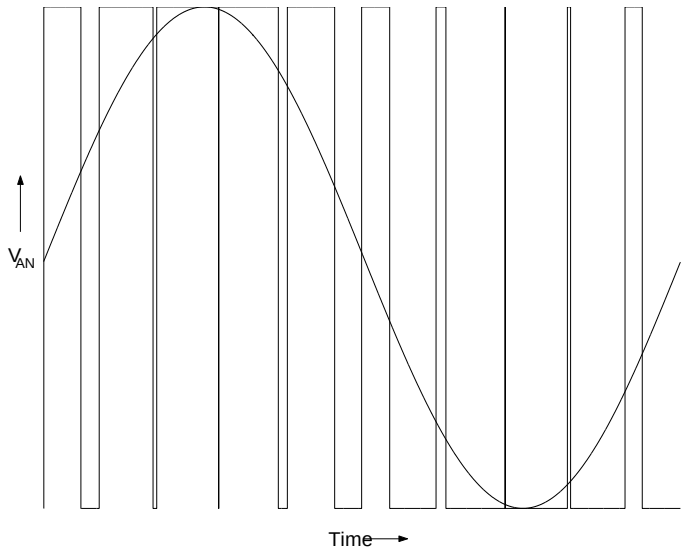

Figure 1.12: Waveform of v_{AN} and the fundamental component

steady state. The reactive current reference can be controlled to regulate the bus voltage. In a similar fashion the reactive voltage injected by a lossless SSSC can be controlled to regulate the power flow in a line within limits. The combination of a STATCOM and a SSSC, in which the STATCOM feeds (or absorbs) power on the DC side to SSSC, can be used to regulate both active and reactive power flow in a line (subject to the constraints imposed by the ratings of the converters in addition to the limits on bus voltages).

1.4.3 A General Equivalent Circuit for FACTS Controllers

The UPFC (shown in Fig. 1.9) is the most versatile FACTS controller with 3 control variables (the magnitude and phase angle of the series injected voltage in addition to the reactive current drawn by the shunt connected VSC). The equivalent circuit of a UPFC on a single phase basis is shown in Fig. 1.13. The current i is drawn by the shunt connected VSC while the voltage e is injected by the series connected VSC. Neglecting harmonics, both the quantities can be represented by phasors I and E.

Neglecting power losses in the UPFC, the following constraint equation applies.

$$Re[V_1 I^*] = Re[E I_2^*] \tag{1.13}$$

Assuming that $\hat{V}_1 = V_1 e^{j\theta_1}$, $\hat{I}_2 = I_2 e^{j\phi_2}$, $\hat{I}$ and $\hat{E}$ can be expressed as

$$\hat{I} \;=\; (I_p - jI_r)e^{j\theta_1} \tag{1.14}$$

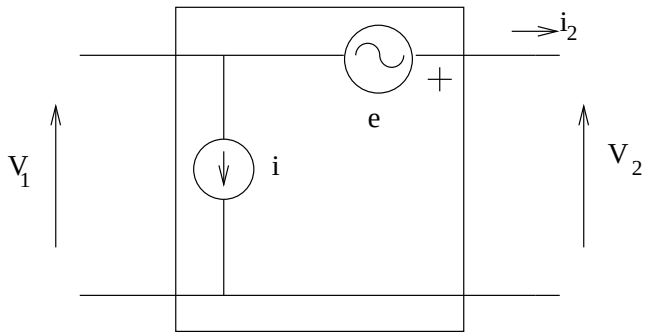

Figure 1.13: An equivalent circuit for UPFC

$$\hat{E} = (V_p + jV_r)e^{j\phi_2} \tag{1.15}$$

where I_p and I_r are 'real' and 'reactive' components of the current drawn by the shunt connected VSC. Similarly V_p and V_r and the 'real' and 'reactive' voltages injected by the series connected VSC. Positive I_p and V_p indicate positive 'real' (active) power flowing into the shunt connected VSC and flowing out of the series connected VSC. The positive values of I_r and V_r indicate reactive power drawn by the shunt convertor and supplied by the series converter. These conventions will be used throughout this book.

Using eqs (1.14) and (1.15), (1.13) can be expressed as

$$V_1 I_p = I_2 V_p \tag{1.16}$$

The remaining shunt and series connected FACTS controllers can be viewed as special cases of a UPFC. For example in a SVC,

$$V_p = 0, V_r = 0, I_p = 0, I_r = -B_{SVC} V_1, \tag{1.17}$$

There are 3 constraint equations and one control variable (B_{SVC}) in a SVC. In a STATCOM, I_r is the control variable. Table 1.1 gives the constraint equations and control variables for all the FACTS controllers. Note that in a STATCOM or SSSC with an energy source at the DC terminals, there are 2 control variables as I_p or V_p is non-zero.

1.4.4 Benefits with the Application of FACTS Controllers

Primarily, the FACTS controllers provide voltage support at critical buses in the system (with shunt connected controllers) and regulate power flow in critical lines (with series connected controllers). Both voltage and power flow are controlled by the combined series and shunt controller (UPFC). The power electronic control is quite fast and this enables regulation both

Table 1.1: Constraint Equations and Control Variables for FACTS Controllers.

Controller	Constraint Equations	Control Variable(s)
SVC	$V_p = 0$, $V_r = 0$, $I_p = 0$ $I_r = -B_{SVC}V_1$	B_{SVC}
TCSC	$I_p = 0$, $I_r = 0$, $V_p = 0$ $V_r = X_{TCSC}I_2$	X_{TCSC}
SPST (TCPAR)	$\hat{E} = V_1(e^{j\phi} - 1) \simeq jV_1\phi$ $V_1I_p = V_pI_2$, $V_1I_r = I_2V_r$	ϕ
STATCOM	$V_p = 0$, $V_r = 0$, $I_p = 0$	I_r
STATCOM with energy source	$V_p = 0$, $V_r = 0$	I_p, I_r
SSSC	$I_p = 0$, $I_r = 0$, $V_p = 0$	V_r
SSSC with energy source	$I_p = 0$, $I_r = 0$	V_p, V_r

under steady state and dynamic conditions (when the system is subjected to disturbances). The benefits due to FACTS controllers are listed below.

1. They contribute to optimal system operation by reducing power losses and improving voltage profile.
2. The power flow in critical lines can be enhanced as the operating margins can be reduced due to fast controllability. In general, the power carrying capacity of lines can be increased to values upto the thermal limits (imposed by current carrying capacity of the conductors).
3. The transient stability limit is increased thereby improving dynamic security of the system and reducing the incidence of blackouts caused by cascading outages.
4. The steady state or small signal stability region can be increased by providing auxiliary stabilizing controllers to damp low frequency oscillations.
5. FACTS controllers such as TCSC can counter the problem of Subsynchronous Resonance (SSR) experienced with fixed series capacitors connected in lines evacuating power from thermal power stations (with turbogenerators).
6. The problem of voltage fluctuations and in particular, dynamic overvoltages can be overcome by FACTS controllers.

The capital investment and the operating costs (essentially the cost of power losses and maintenance) are offset against the benefits provided by the FACTS controllers and the 'payback period' is generally used as an index in the planning. The major issues in the deployment of FACTS controllers are (a) the location (b) ratings (continuous and short term) and (c) control strategies required for the optimal utilization. Here, both steady-state and dynamic operating conditions have to be considered. Several systems studies involving power flow, stability, short circuit analysis are required to prepare the specifications. The design and testing of the control and protection equipment is based on Real Time Digital Simulator (RTDS) or physical simulators.

It is to be noted that a series connected FACTS controller (such as TCSC) can control power flow not only in the line in which it is connected, but also in the parallel paths (depending on the control strategies). This will be explained in chapter 4.

1.5 Application of FACTS Controllers in Distribution Systems

Although the concept of FACTS was developed originally for transmission network; this has been extended since last 10 years for improvement of Power Quality (PQ) in distribution systems operating at low or medium voltages.

In the early days, the power quality referred primarily to the continuity of power supply at acceptable voltage and frequency. However, the prolific increase in the use of computers, microprocessors and power electronic systems has resulted in power quality issues involving transient disturbances in voltage magnitude, waveform and frequency. The nonlinear loads not only cause PQ problems but are also very sensitive to the voltage deviations.

In the modern context, PQ problem is defined as "Any problem manifested in voltage, current or frequency deviations that result in failure or misoperation of customer equipment" [5].

The PQ problems are categorized as follows

1. Transients
   (a) Impulsive
   (b) Oscillatory
2. Short-duration and Long-duration variations
   (a) Interruptions

   (b) Sag (dip)
   (c) Swell

3. Voltage unbalance
4. Waveform distortion

   (a) DC offset
   (b) Harmonics
   (c) Interharmonics
   (d) Notching
   (e) Noise

5. Voltage Flicker
6. Power frequency variations

More details about these problems are discussed in chapter 12.

Hingorani [7] was the first to propose FACTS controllers for improving PQ. He termed them as Custom Power Devices (CPD). These are based on VSC and are of 3 types given below.

1. Shunt connected Distribution STATCOM (DSTATCOM)
2. Series connected Dynamic Voltage Restorer (DVR)
3. Combined shunt and series, Unified Power Quality Conditioner (UPQC).

The DVR is similar to SSSC while UPQC is similar to UPFC. In spite of the similarities, the control strategies are quite different for improving PQ. A major difference involves the injection of harmonic currents and voltages to isolate the source from the load. For example, a DVR can work as a harmonic isolator to prevent the harmonics in the source voltage reaching the load in addition to balancing the voltages and providing voltage regulation. A UPQC can be considered as the combination of DSTATCOM and DVR. A DSTATCOM is utilized to eliminate the harmonics from the source currents and also balance them in addition to providing reactive power compensation (to improve power factor or regulate the load bus voltage).

The terminology is yet to be standardized. The term 'active filters' or 'power conditioners' is also employed to describe the custom power devices. ABB terms DSTATCOM as 'SVC light'. Irrespective of the name, the trend is to increasingly apply VSC based compensators for power quality improvement.

References and Bibliography

1. N.G. Hingorani, "Flexible AC transmission". IEEE Spectrum, v. 30, n. 4, pp. 40-44, 1993.
2. N.G. Hingorani and L Gyugyi, **Understanding FACTS - Concepts and Technology of Flexible AC Transmission Systems**, IEEE Press, New York, 2000.
3. Y.H. Song and A.T. Johns, Eds., **Flexible AC Transmission Systems (FACTS)**, IEE Press, London, 1999.
4. R.M. Mathur and R.K. Varma, **Thyristor-Based FACTS Controller for Electrical Transmission Systems**, IEEE Press and Wiley Interscience, New York, 2002.
5. R.C. Dugan, M.F. McGranaghan and H.W. Beaty, **Electrical Power Systems Quality**, McGraw-Hill, New York, 1996.
6. A. Ghosh and G. Ledwich, **Power Quality Enhancement Using Custom Power Devices** , Kluwer Academic Publishers, Boston, 2002.
7. N.G. Hingorani, "Introducing Custom Power", IEEE Spectrum, v. 32, n. 6, pp. 41–48, 1995.
8. K.R. Padiyar and A.M. Kulkarni, "Flexible AC transmission systems: A status review", Sādhanā, v. 22, Part 6, pp. 781–796, December 1997.
9. H. Akagi, "New trends in active filters for power conditioning", IEEE Trans., Ind. Appl., v. 32, pp. 1312–1322, 1996.
10. H.W. Van Der Broeck, H.C. Skudelny and G.V. Stanke, "Analysis and realization of a pulsewidth modulator based on voltage space vectors", IEEE Trans., Ind. Appl., v. 24, n. 1, pp. 142–150, 1988.

Chapter 2

AC Transmission Line and Reactive Power Compensation

In this chapter, the reactive power control in AC power transmission lines is examined. The requirements are to

(a) transmit as much power as feasible on a line of specified voltage and
(b) to control the voltage along the line within limits.

The steady-state characteristics of a transmission line are first studied based on equations derived from first principles. The benefits of reactive power compensation (both shunt and series) are described with analysis and examples. Several FACTS controllers (such as STATCOM, SSSC) can be viewed as fast acting reactive power controllers. Their influence on power angle characteristics are investigated.

2.1 Analysis of Uncompensated AC Line

2.1.1 General

A transmission line has distributed circuit parameters. We will be assuming the line to be symmetric in three phases and operating with balanced (positive sequence) voltages and currents. Hence it is adequate to consider only a single phase positive sequence equivalent network of the line (see Fig. 2.1).

In Fig. 2.1, it is assumed that the sending end is connected to a generator and the receiving end is connected to a (unity power factor) load. The line has series resistance r and inductance l, shunt conductance g and capacitance c (all parameters expressed per unit length).

2.1.2 Transmission Line Equations

It is assumed that in steady state all the voltages and currents in the line are sinusoidal of frequency (ω rad/sec) and expressed in phasors.

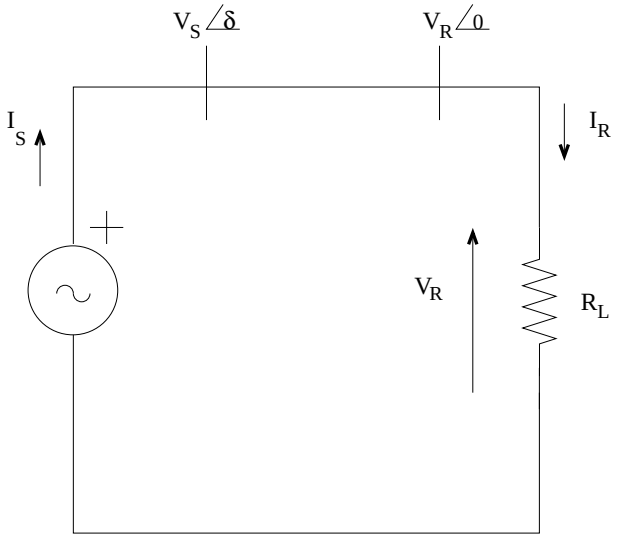

Figure 2.1: A transmission line supplying a unity power factor load

Considering a small element of the line of length (dx) at a distance x from the receiving end, (see Fig. 2.2) the following equations apply,

$$I(x+dx) = I(x) + (ydx)V(x+dx) \tag{2.1}$$

$$V(x+dx) = V(x) + (zdx)I(x) \tag{2.2}$$

where $y = g + jb, z = r + jx, b = \omega c, x = \omega l$.

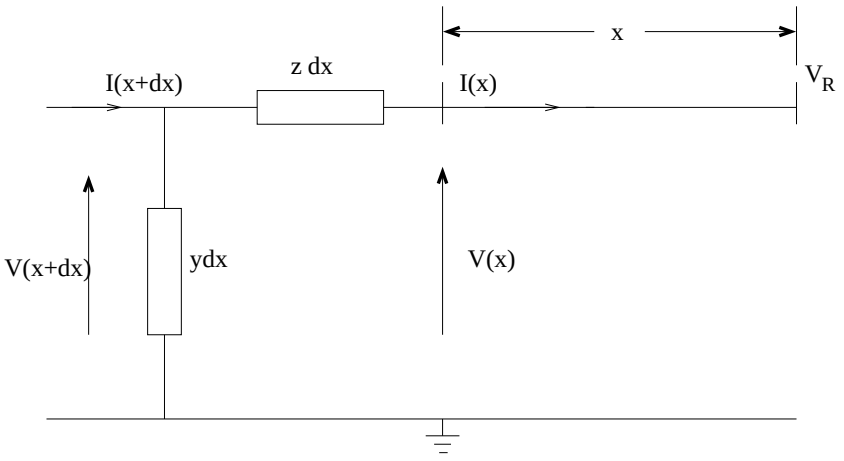

Figure 2.2: Voltage and current variation in a long line

It is to be noted that both V and I are phasors that are functions of x. From the above equations, we get the following differential equations for V and I.

$$\frac{dV}{dx} = zI, \tag{2.3}$$

$$\frac{dI}{dx} = yV \tag{2.4}$$

Taking derivative of both sides of Eq. (2.3), we get

$$\frac{d^2V}{dx^2} = zyV \tag{2.5}$$

Similarly, it can be shown that,

$$\frac{d^2I}{dx^2} = zyI \tag{2.6}$$

The solution of Eq. (2.5) gives

$$V(x) = A_1 e^{\gamma x} + A_2 e^{-\gamma x} \tag{2.7}$$

where

$$\gamma = \sqrt{zy} = \alpha + j\beta \tag{2.8}$$

is termed as the propagation constant. α is called the attenuation constant and β is called the phase constant.

A_1 and A_2 are constants dependent on the boundary conditions. Substituting (2.7) in (2.3), we can derive

$$I(x) = \frac{1}{Z_c}[A_1 e^{\gamma x} - A_2 e^{-\gamma x}] \tag{2.9}$$

where

$$Z_c = \sqrt{\frac{z}{y}} \tag{2.10}$$

is termed as the characteristic impedance.

The constants A_1 and A_2 are determined from

$$V_R = V(x=0) = A_1 + A_2 \tag{2.11}$$

$$I_R = I(x=0) = \frac{(A_1 - A_2)}{Z_c} \tag{2.12}$$

Solving for A_1 and A_2 from the above and substituting in (2.7) and (2.9), we have

$$V(x) = V_R \cosh(\gamma x) + I_R Z_c \sinh(\gamma x) \tag{2.13}$$

$$I(x) = \frac{V_R}{Z_c}\sinh(\gamma x) + I_R \cosh(\gamma x) \tag{2.14}$$

where $\cosh(\gamma x) = \frac{e^{\gamma x}+e^{-\gamma x}}{2}, \sinh(\gamma x) = \frac{e^{\gamma x}-e^{-\gamma x}}{2}$.

Normally, the conductance g of a line can be neglected. The series resistance r has only a secondary effect on the voltage and power flow in the line and hence can be neglected for simplicity. It is to be noted that r is to be considered while computing transmission (active power) loss.

Expressions for a Lossless line

Neglecting r and g, the propagation constant γ is purely imaginary with

$$\gamma = j\beta = j\omega\sqrt{lc} \tag{2.15}$$

and the characteristics impedance Z_c is purely resistive with

$$Z_c = \sqrt{\frac{l}{c}} = Z_n \tag{2.16}$$

In this case the Z_c is termed as surge impedance or natural impedance (Z_n). Substituting (2.15) and (2.16) in (2.13) and (2.14), we get

$$V(x) = V_R \cos(\beta x) + jI_R Z_n \sin(\beta x) \tag{2.17}$$

$$I(x) = j\frac{V_R}{Z_n} \sin(\beta x) + I_R \cos(\beta x) \tag{2.18}$$

For the special case when

$$V_R = Z_n I_R \tag{2.19}$$

we have,

$$V(x) = e^{j\beta x} V_R \tag{2.20}$$

$$I(x) = e^{j\beta x} I_R \tag{2.21}$$

This shows that the magnitude of voltage (and current) at any point on the line is constant but the phase angle varies uniformly as the distance (x) increases. When $x = \lambda$, such that

$$\beta\lambda = 2\pi \tag{2.22}$$

λ is defined as the wavelength, which depends on the frequency f. It can be shown that

$$\lambda = uT = \frac{u}{f} = \frac{u2\pi}{\omega} \tag{2.23}$$

where u is the velocity of propagation of the (voltage or current) wave given by

$$u = \frac{1}{\sqrt{lc}} \tag{2.24}$$

Typically, the value of u for overhead high voltage transmission lines is slightly less than the velocity of light ($u = 3 \times 10^8$ m/sec).

Substituting $x = d$ (where d is the length of the transmission line) in Eqs. (2.17) and (2.18) we have

$$V_S = V_R \cos\theta + jI_R Z_n \sin\theta \tag{2.25}$$

$$I_S = j\frac{V_R}{Z_n}\sin\theta + I_R \cos\theta \tag{2.26}$$

where

$$\theta = \beta d = \omega\sqrt{lc}d = \frac{2\pi}{\lambda}d \tag{2.27}$$

is termed as the electrical length of the line expressed in radians.

Remarks

1. Equations (2.25) and (2.26) can be expressed as

$$\begin{bmatrix} V_S \\ I_S \end{bmatrix} = \begin{bmatrix} A & B \\ C & D \end{bmatrix} \begin{bmatrix} V_R \\ I_R \end{bmatrix} \tag{2.28}$$

where $A = \cos\theta, B = jZ_n \sin\theta$, $C = \frac{j\sin\theta}{Z_n}, D = \cos\theta$ are the A, B, C, D constants of the two port network shown in Fig. 2.3.

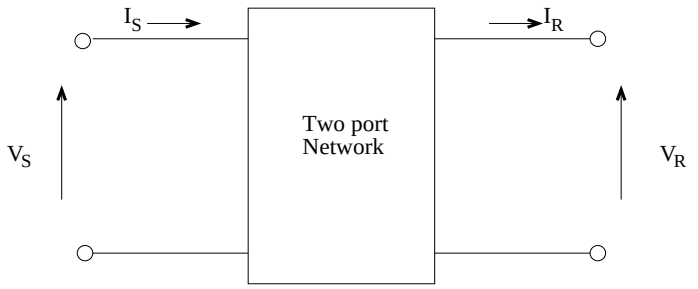

Figure 2.3: Transmission line as a two port network

2. It is to be noted that $D = A$ and $AD - BC = 1$, with the result that V_R and I_R can be expressed as

$$\left.\begin{aligned} V_R &= V_S \cos\theta - jI_S Z_n \sin\theta \\ I_R &= -j\tfrac{V_S}{Z_n}\sin\theta + I_S \cos\theta \end{aligned}\right\} \tag{2.29}$$

2.1.3 Performance of a Line Connected to Unity Power Factor Load

Assuming that the sending end voltage of the line is held constant at V_S, the receiving end voltage V_R varies with the load. It will be assumed that the line is lossless.

It is convenient to represent the line by Thevenin equivalent at the receiving end. The Thevenin voltage is the open circuit voltage at the receiving end given by,

$$V_{Th} = \frac{V_S}{\cos\theta} \tag{2.30}$$

and Thevenin impedance is obtained as

$$Z_{Th} = -\frac{V_R}{I_R}|_{V_S=0} = jZ_n \tan\theta \tag{2.31}$$

The equivalent circuit of the line and the load is shown in Fig. 2.4. The phasor diagram of the voltages V_{Th} and V_R are shown in Fig. 2.5. It can be seen from Fig. 2.5, that

$$V_R = \frac{V_S \cos\delta}{\cos\theta} \tag{2.32}$$

and the power flow in the line, $P = P_R$ is given by

$$P = \frac{V_{Th}V_R \sin\delta}{Z_n \tan\theta} = \frac{V_S^2 \sin 2\delta}{Z_n \sin 2\theta} \tag{2.33}$$

The maximum power (theoretical limit) occurs at $\delta = 45^\circ$ and is given by

$$P_{\max} = \frac{V_S^2}{Z_n \sin 2\theta} \tag{2.34}$$

At this value of power, the receiving end voltage is

$$V_{Rm} = \frac{V_S}{\sqrt{2}\cos\theta} \tag{2.35}$$

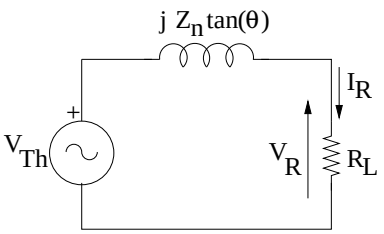

Figure 2.4: Equivalent circuit of the line connected to a unity p.f. load

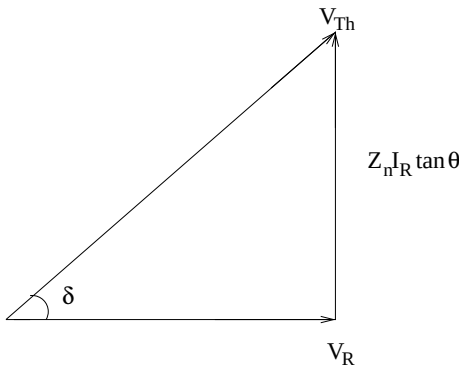

Figure 2.5: Phasor diagram of voltages

At no load ($P_R = 0$), the voltage at the receiving end is higher than the sending due to the line charging. This is termed as Ferranti Effect. The no load voltage at the receiving end is given by

$$V_{R0} = \frac{V_S}{\cos\theta} \tag{2.36}$$

This can be excessive as θ increases. At line lengths approaching quarter wavelength, V_{R0} is very high. Note that V_{R0} is bounded in real lines as the resistance of the line cannot be ignored at high charging currents.

At no load, the sending end current is the charging current of the line and is given by

$$\hat{I}_{S0} = j\frac{\sin\theta\hat{V}_S}{Z_n\cos\theta} = j\frac{\hat{V}_S}{Z_n}\tan\theta \tag{2.37}$$

This also increases as θ increases and can overload the generator. The no load reactive power Q_{S0} is obtained as

$$Q_{S0} = Im[V_S I^*_{S0}] = -\frac{V_S^2\tan\theta}{Z_n}$$

2.1.4 Performance of a Symmetrical Line

To control the receiving end voltage and increase the power transfer capability of the line it is necessary to have a generator or a controlled reactive power source (with fast control) such as a SVC at the receiving end (see Fig. 2.6). The reactive power injected is $-Q_R$. If line is symmetrical ($V_S = V_R = V$), then from symmetry, $Q_S = -Q_R$. Thus, the reactive power requirements of the line are shared equally at both ends of the line.

From Fig. 2.6, it can be derived that if the voltage V_R is controlled using a reactive power source in parallel with R_L, then the power transfer

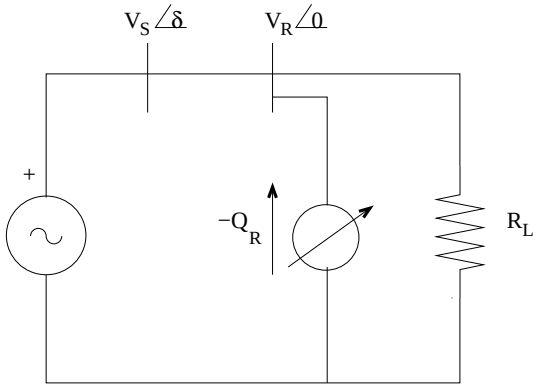

Figure 2.6: A transmission line with dynamic voltage support at the receiving end

on the line is given by

$$P = \frac{V^2}{Z_n \sin\theta} \sin\delta \tag{2.38}$$

This result can be derived also from the transmission line equation. The current I_R is obtained as

$$\hat{I}_R = \frac{\hat{V}_S - \hat{V}_R \cos\theta}{jZ_n \sin\theta} = \frac{V\angle\delta - V\cos\theta}{jZ_n \sin\theta} \tag{2.39}$$

The complex power (S_R) at the receiving end is defined by

$$S_R = P_R + jQ_R = \hat{V}_R I_R^* = \frac{V^2\angle -\delta - V^2\cos\theta}{-jZ_n \sin\theta} \tag{2.40}$$

From the above,

$$P = \frac{V^2 \sin\delta}{Z_n \sin\theta} = \frac{P_n \sin\delta}{\sin\theta} \tag{2.41}$$

where P_n is termed as Surge Impedance Loading (SIL) defined by

$$P_n = \frac{V^2}{Z_n}$$

and

$$Q_R = \frac{V^2}{Z_n \sin\theta}(\cos\delta - \cos\theta) = -Q_S \tag{2.42}$$

The voltage profile along the line varies as the loading varies. For $P = P_n$ (SIL) the voltage profile is flat. The voltage variation at the midpoint is maximum for the symmetrical line as the load varies from zero to the

maximum value. (see Fig. 2.7) To compute the midpoint voltage (V_m) we can divide the line into two equal sections of half the length. For the line section connecting the sending end to the midpoint, we have

$$V_S = V\angle\delta = \hat{V}_m \cos\frac{\theta}{2} + j\hat{I}_m Z_n \sin\frac{\theta}{2} \tag{2.43}$$

where I_m is the current flowing at the midpoint.

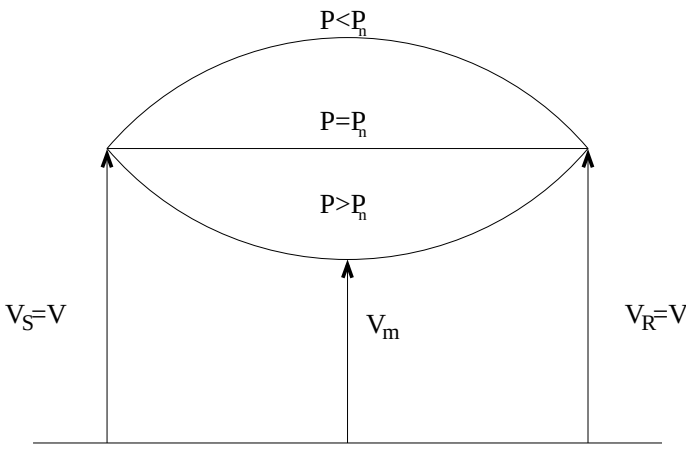

Figure 2.7: Voltage profile along the line

For the line section connecting midpoint to the receiving end, we have

$$V_R = V\angle 0 = \hat{V}_m \cos\frac{\theta}{2} - j\hat{I}_m Z_n \sin\frac{\theta}{2} \tag{2.44}$$

Adding (2.43) and (2.44), we can solve for V_m as

$$\hat{V}_m = \frac{V\cos\delta/2}{\cos\frac{\theta}{2}}\angle\delta/2 \tag{2.45}$$

Subtracting (2.44) from (2.43) we can solve for I_m as

$$\hat{I}_m = \frac{V\sin\delta/2}{Z_n\sin\frac{\theta}{2}}\angle\delta/2 \tag{2.46}$$

Since I_m is in phase with V_m we can obtain the power (P) as

$$P = V_m I_m = \frac{V^2\sin\delta}{Z_n\sin\theta} \tag{2.47}$$

The no load voltage at the midpoint (V_{mo}) is given by

$$V_{mo} = \frac{V}{\cos\theta/2} \tag{2.48}$$

The charging reactive power at no load is given by

$$Q_{So} = -Q_{Ro} = \frac{V^2}{Z_n \sin\theta}(\cos\theta - 1) = -\frac{V^2}{Z_n}\tan\frac{\theta}{2} \tag{2.49}$$

Comparing the expressions for the power, no load voltage and charging reactive power with those given in the previous section (2.1.3) shows that a symmetrical line can be viewed as two line sections of half the length each (see Fig. 2.8). One end of each line section is connected to unity power factor load and at the other end the voltage is regulated. The load is negative for one line section and positive for the other line section. The negative load results in the reversal of power flow.

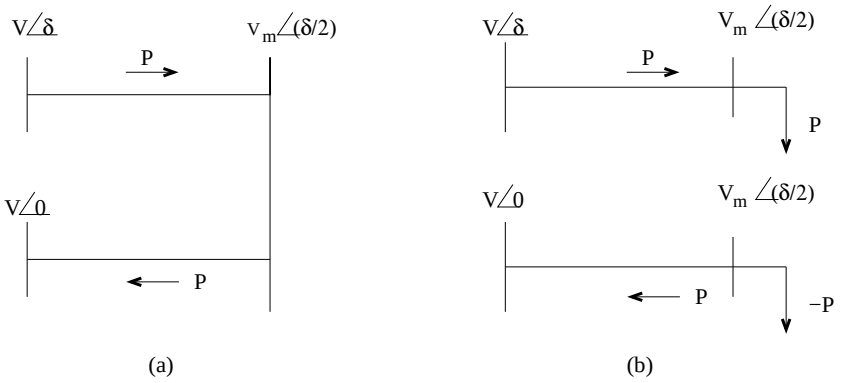

Figure 2.8: Representation of a symmetrical line

In general, it is not possible to consider the voltages at the two ends of the line as constants. It is necessary to consider the effects of the systems connected to the two ends by representing Thevenin equivalents at both ends as shown in Fig. 2.9. The mutual coupling between x_S and x_R is neglected.

Figure 2.9: A transmission line with Thevenin equivalent at both ends

For simplifying the analysis we can consider $E_S = E_R = E$ and $x_S = x_R = x$. In this case, it can be shown that

$$V_m = \frac{E\cos\delta/2}{\cos(\theta/2)(1 - \frac{x}{Z_n}\tan(\theta/2))}\angle\delta/2 \tag{2.50}$$

and

$$I_m = \frac{E\sin\delta/2}{Z_n\sin(\theta/2)(1 + \frac{x}{Z_n}\cot(\theta/2))}\angle(\delta/2) \tag{2.51}$$

The power flow (P) is obtained as

$$P = V_m I_m = \frac{E^2 \sin\delta}{Z_n \sin\theta \left[1 + \frac{2x}{Z_n}\cot\theta - \frac{x^2}{Z_n^2}\right]} \tag{2.52}$$

The effect of source reactances is to reduce the power flow (compared to the case with $x = 0$) when

$$\frac{x}{Z_n} < 2\cot\theta \tag{2.53}$$

and increase it for higher values of x. However increasing values of x result in large values of V_m and high reactive power flows. In practical situations, $\frac{x}{Z_n}$ is generally less than unity.

Performance of uncompensated lines – summary

Based on the analysis given in this and the previous sections, the following points emerge

1. The dynamic regulation of voltage at the receiving (load) end of the line by using a controllable reactive source, improves power transfer and voltage profile along the line.
2. However, even with symmetrical lines (with voltages maintained at both ends), the power transfer capability is decreased as the line length increases. Assuming that a line is operated with $\delta_{\max} = 30^\circ$, the maximum power transfer reduces below SIL for line lengths $\theta > 30^\circ$ (approximately 500 km long line in systems operating at 50 Hz).
3. The problems of voltage control and charging reactive power (at no load) become severe as line length increases. For a symmetric line, the voltage variation is maximum at the mid point of the line.

2.2 Passive Reactive Power Compensation

The transmission line has series inductance which absorbs reactive power while the shunt capacitance releases (generates reactive power). For light loads, the absorption is less than the generation and voltage in the line tends to rise. On the other hand, at loads exceeding Surge Impedance Loading (SIL), the absorption is higher than the generation and the voltage tends to fall. By connecting series capacitors and shunt inductors in the line, we can control the reactive power flow in the line to limit the voltage variations and increase (active) power transfer capability. To study the effects of passive reactive compensation, we will first consider the distributed compensation (which is difficult to arrange, but is easier to analyze) before taking up discrete compensation (which is practical).

2.2.1 Distributed Compensation

Let us consider distributed series compensation (capacitive) whose effect, in steady state, is to counteract the effect of the distributed series inductance of the line. Similarly, by providing distributed shunt (inductive) compensation, the effect of line capacitance is reduced.

The phase constant (β') of a compensated line is given by

$$\begin{aligned} \beta' &= \sqrt{\omega l' \cdot \omega c'} = \sqrt{\omega l(1-k_{se})\omega c(1-k_{sh})} \\ &= \beta\sqrt{(1-k_{se})(1-k_{sh})} \end{aligned} \tag{2.54}$$

where β is the phase constant of the uncompensated line, k_{se} is the degree of series compensation and k_{sh} is the degree of shunt compensation. It is assumed that both k_{se} and k_{sh} are less than unity.

The surge impedance (Z'_n) of the compensated line is obtained as

$$Z'_n = \sqrt{\frac{\omega \ell'}{\omega c'}} = Z_n\sqrt{\frac{(1-k_{se})}{(1-k_{sh})}} \tag{2.55}$$

From Eqs. (2.54) and (2.55) we note that the electrical length (θ') of the compensated line given by

$$\theta' = d\beta' = \theta\sqrt{(1-k_{se})(1-k_{sh})} \tag{2.56}$$

is reduced by both series and shunt compensation. On the other hand, Z_n is reduced by series compensation (capacitive) and increased by shunt compensation (inductive).

For a lossless symmetrical line, the power flow in a compensated line is given by

$$P' = \frac{V^2}{Z'_n \sin\theta'}\sin\delta \simeq \frac{V^2}{Z'_n\theta'}\sin\delta = \frac{V^2\sin\delta}{Z_n\theta(1-k_{se})} \tag{2.57}$$

for small values θ'.

The no load voltage at the mid-point (V'_{mo}) is given by

$$V'_{mo} = \frac{V}{\cos\frac{\theta'}{2}} \tag{2.58}$$

The charging reactive power (Q'_{So}) at no load is given by

$$Q'_{So} = -Q'_{Ro} = -\frac{V^2}{Z'_n}\tan\frac{\theta'}{2} \simeq \frac{V^2}{Z'_n}\frac{\theta'}{2} = \frac{V^2\theta}{2Z_n}(1-k_{sh}) \tag{2.59}$$

From Eqs. (2.57) to (2.59) we can observe that

1. The distributed shunt compensation reduces the no load voltage and charging reactive power, but has little effect on the maximum power flow in the line.
2. The distributed series compensation reduces the no load voltage and increases the power transfer capacity, but less little effect on the no load charging reactive power.

2.2.2 Discrete Passive Compensation

It is not practical to provide distributed compensation. Here, we will consider discrete series and shunt compensation. Before taking this up, it is instructive to derive an equivalent circuit (in steady state) of the distributed parameter, uncompensated line. Figure 2.10 shows the equivalent π circuit of the line.

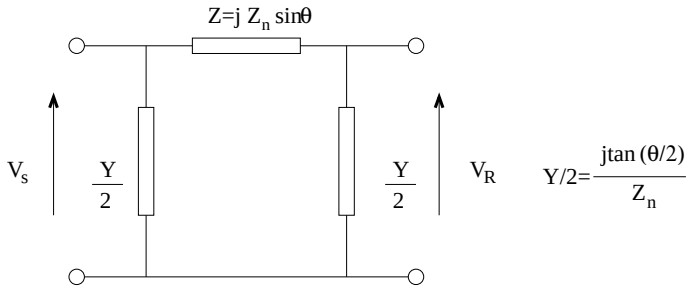

Figure 2.10: The exact π equivalent circuit of a lossless uncompensated line

This is obtained by comparing the A and B constants of the line and the equivalent circuit as given below

$$A = 1 + \frac{YZ}{2} = \cos\theta, \quad B = Z = jZ_n \sin\theta$$

We can also express Z and Y as

$$Z = jX^n \frac{\sin\theta}{\theta}, \quad \frac{Y}{2} = j\frac{B^n}{2}\left(\frac{\tan\frac{\theta}{2}}{\frac{\theta}{2}}\right)$$

where $X^n = \omega ld = Z_n\theta$ the total (nominal) reactance of the line and $B^n = \omega cd = \frac{\theta}{Z_n}$ is the total (nominal) susceptance of the line.

For small values of θ, $\frac{\sin\theta}{\theta} \simeq 1$ and $\tan\frac{\theta}{2} \simeq \frac{\theta}{2}$. Hence $Z \simeq jX^n$, $Y \simeq jB^n$. With this approximation, this equivalent circuit is called as the 'nominal' π circuit of the transmission line.

Note: When we are dealing with single phase equivalent of a balanced symmetric 3 phase network, the parameters of this circuit are the positive

sequence parameters while the voltages and currents are assumed to contain only positive sequence components. As a matter of fact, for symmetric networks with no zero sequence components, the coupled 3 phase network can be reduced to 3 uncoupled single phase networks. For example, from the simple 3 phase network described by

$$\begin{bmatrix} V_a \\ V_b \\ V_c \end{bmatrix} = \begin{bmatrix} Z_s & Z_m & Z_m \\ Z_m & Z_s & Z_m \\ Z_m & Z_m & Z_s \end{bmatrix} \begin{bmatrix} I_a \\ I_b \\ I_c \end{bmatrix} \tag{2.60}$$

the network is decoupled if $I_a + I_b + I_c = 0$ and is described by the equation

$$V_\alpha = (Z_s - Z_m) I_\alpha, \quad \alpha = a, b \text{ or } c \tag{2.61}$$

The positive sequence impedance is $(Z_s - Z_m)$.

For a lossless transmission line, the shunt susceptance is capacitive and results in charging reactive power at no load. The shunt reactors at both ends of the line can be used to fully or partially compensate for this reactive power. With full shunt compensation (by reactors), the lossless line is represented by only a series reactance (X) given by

$$X = Z_n \sin\theta \tag{2.62}$$

2.3 Compensation by a Series Capacitor Connected at the Midpoint of the Line

The two cases of the series compensation are considered.

Case 1: Series compensation accompanied by shunt compensation:

The equivalent circuit of the line with the series and (full) shunt compensation connected at the midpoint in addition to the two ends of the line (see Fig. 2.11(a)) is shown in Fig. 2.11(b).

The power flow in the compensated line is given by

$$P = \frac{V_S V_R}{\left(2Z_n \sin\frac{\theta}{2} - X_c\right)} \sin\delta \tag{2.63}$$

It is to be noted that when $V_S = V_R = V$, the no load voltage at the midpoint of the line is V (and at both terminals of the series capacitor as the current through the capacitor is zero at no load). The Eq. (2.63) can also be expressed as

$$P = \frac{V_S V_R \sin\delta}{Z_n \sin\theta \left[\frac{1}{\cos\frac{\theta}{2}} - \frac{X_c}{Z_n \sin\theta}\right]} = \frac{V_S V_R \sin\delta \cdot \cos\frac{\theta}{2}}{Z_n \sin\theta \left[1 - \frac{X_c}{2Z_n \sin\frac{\theta}{2}}\right]} \tag{2.64}$$

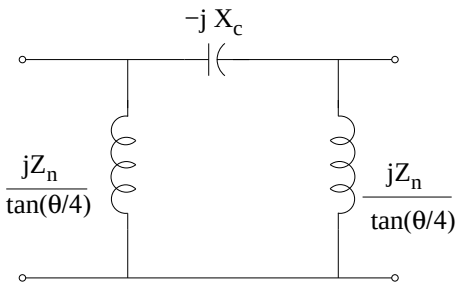

(a) Series capacitor and shunt reactors connected at the midpoint

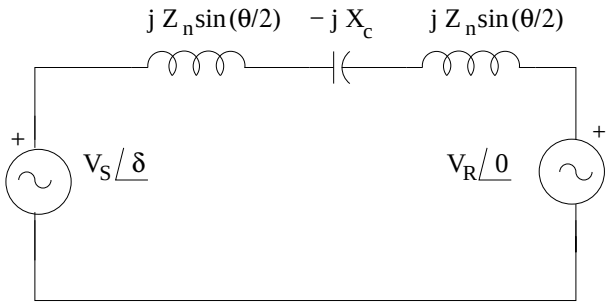

(b) Equivalent circuit of the compensated line

Figure 2.11: Representation of a compensated line

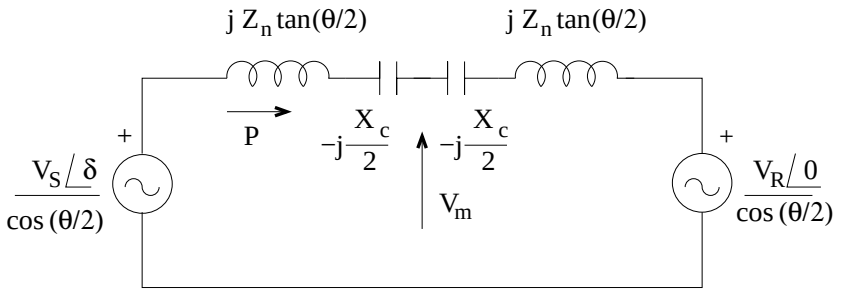

Figure 2.12: Equivalent circuit of a line with pure series compensation

Case 2: With pure series compensation at the midpoint:

If no shunt reactors are used at the terminals the series capacitor, the equivalent circuit of half the line can be obtained – as shown in Fig. 2.4 and the combined equivalent circuit of the series compensated line is shown in Fig. 2.12.

The power flow (P) in the line is given by

$$P = \frac{V_S V_R \sin\delta}{\cos^2\frac{\theta}{2}\left[2Z_n \tan\frac{\theta}{2} - X_c\right]} = \frac{V_S V_R \sin\delta}{Z_n \sin\theta\left[1 - \frac{X_c}{2Z_n \tan\frac{\theta}{2}}\right]} \tag{2.65}$$

It is to be noted that when $V_S = V_R = V$, the midpoint voltage (V_m) is unaffected by the series capacitor while the midpoint current (I_m) is modified (compared to Eq. (2.46)) to

$$I_m^{se} = \frac{V \sin\frac{\delta}{2}}{Z_n \sin\frac{\theta}{2}(1 - k_{se})} \tag{2.66}$$

where

$$k_{se} = \frac{X_c}{2Z_n \tan\frac{\theta}{2}} \tag{2.67}$$

It can be shown that both ($\hat{V}_m$) and ($\hat{I}_m^{se}$) are in phase and the power flow (P) is

$$P = V_m I_m^{se} \tag{2.68}$$

Remarks

Using the equivalent circuits of the uncompensated line sections, the power flow in a series compensated line, where the series capacitor is located at any point in the line, can be obtained as

$$P = \frac{V_S V_R \sin\delta}{Z_n \sin\theta\left[1 - \frac{X_c}{Z_n}\left(\frac{1}{\tan\theta_1 + \tan\theta_2}\right)\right]} \tag{2.69}$$

where $\theta = \theta_1 + \theta_2$.

For small values of θ_1 and θ_2, the degree of series compensation (k_{se}) is independent of the location of the capacitor and is given by

$$k_{se} \simeq \frac{X_c}{Z_n \theta} \tag{2.70}$$

2.4 Shunt Compensation Connected at the Midpoint of the Line

As mentioned earlier, the control of no load voltage requires a shunt reactor. On the other hand, increase in the power flow in a line requires shunt capacitor. Unlike in the case of the series capacitor, the location of the shunt capacitor is very crucial. The best location is at the midpoint of the line to

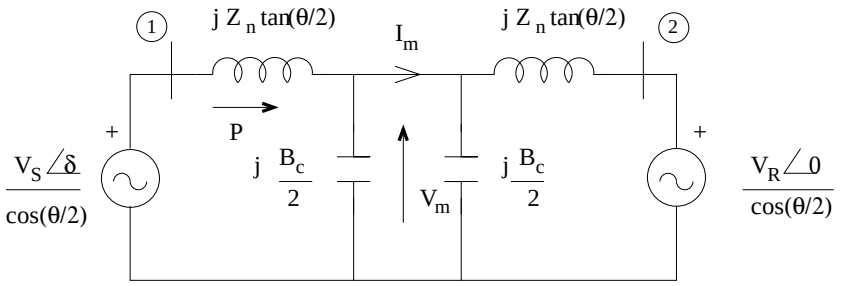

Figure 2.13: Equivalent circuit of a line with shunt capacitor at the midpoint

maximize the power flow in the line. The equivalent circuit of the line with the shunt susceptance connected at the midpoint, is shown in Fig. 2.13.

The transfer reactance (X_t) between the nodes (1) and (2) is given by

$$X_t = 2Z_n \tan\frac{\theta}{2} - B_c Z_n^2 \tan^2\frac{\theta}{2} \tag{2.71}$$

The power flow (P) in the line is given by

$$P = \frac{V_S V_R \sin\delta}{X_t \cos^2\frac{\theta}{2}} = \frac{V_S V_R \sin\delta}{Z_n \sin\theta \left[1 - B_c \frac{Z_n}{2} \tan\frac{\theta}{2}\right]} \tag{2.72}$$

If $V_S = V_R = V$, the midpoint voltage (V_m) is given by

$$V_m^{sh} = \frac{V\cos\frac{\delta}{2}}{\cos\frac{\theta}{2}\left[1 - \frac{Z_n B_c}{2}\tan\frac{\theta}{2}\right]} \tag{2.73}$$

The current ($\hat{I}_m$) at the midpoint is given by the same expression as in Eq. (2.46). It is unaffected by the shunt susceptance. Both $\hat{V}_m^{sh}$ and $\hat{I}_m$ are in phase and hence the power flow is the product of V_m and I_m.

Remarks

In deriving expressions for V_m^{sh} and I_m, the following circuit relations are used.

$$\frac{V}{\cos\frac{\theta}{2}}\angle\frac{\delta}{2} - (\hat{I}_m + j\frac{B_c}{2}\hat{V}_m)jZ_n\tan\frac{\theta}{2} = \hat{V}_m \tag{2.74}$$

$$\frac{V}{\cos\frac{\theta}{2}}\angle 0 + (\hat{I}_m - j\frac{B_c}{2}\hat{V}_m)jZ_n\tan\frac{\theta}{2} = \hat{V}_m \tag{2.75}$$

Adding (2.74) and (2.75) results in (2.73).

2.5 Comparison between Series and Shunt Capacitor

The maximum power flow in the line is given by substituting $\delta = \delta_{\max}$ in the expression for the power flow (P). $\delta_{\max}$ is chosen from considerations of the steady state margin that will not result in the power flow exceeding limits during a contingency.

For the same amount of maximum power transfer, we obtain the following relation (comparing (2.65) with (2.72)).

$$\frac{B_c}{2} Z_n \tan\frac{\theta}{2} = \frac{X_c}{2Z_n \tan\frac{\theta}{2}} \tag{2.76}$$

While transferring maximum power, the reactive power (Q_{se}) supplied by the series capacitor (for a symmetric line with $V_S = V_R = V$) is given by

$$Q_{se} = I_m^2 X_c = \frac{V^2 \sin^2\frac{\delta_{\max}}{2} X_c}{Z_n^2 \sin^2\frac{\theta}{2}(1-k_{se})^2} \tag{2.77}$$

The reactive power (Q_{sh}) supplied by the shunt capacitor (B_c) at $P = P_{\max}$ is obtained as

$$Q_{sh} = V_m^2 B_c = \frac{V^2 \cos^2\frac{\delta_{\max}}{2} B_c}{\cos^2\frac{\theta}{2}(1-k_{sh})^2} \tag{2.78}$$

where

$$k_{sh} = \frac{B_c Z_n}{2} \tan\frac{\theta}{2}$$

Since $k_{se} = k_{sh}$ (from Eq. (2.76)), we get from comparing (2.77) and (2.78),

$$\frac{Q_{se}}{Q_{sh}} = \frac{\tan^2\frac{\delta_{\max}}{2}}{Z_n^2 \tan^2\frac{\theta}{2}} \left(\frac{X_c}{B_c}\right) = \tan^2\frac{\delta_{\max}}{2} \tag{2.79}$$

The above relation shows that the series capacitor is much more effective than the shunt capacitor in increasing power transfer.

Note: The peak voltage (V_p^{sh}) across the shunt capacitor occurs at no load and is given by

$$V_p^{sh} = \frac{V}{\cos\frac{\theta}{2}}$$

If this voltage is used instead of V_m, in determining the rating of the shunt capacitor, then the comparison of the two ratings (of the series and shunt capacitors) is given by

$$\frac{Q_{se}}{Q_{sh}} = \sin^2\frac{\delta_{\max}}{2} \tag{2.80}$$

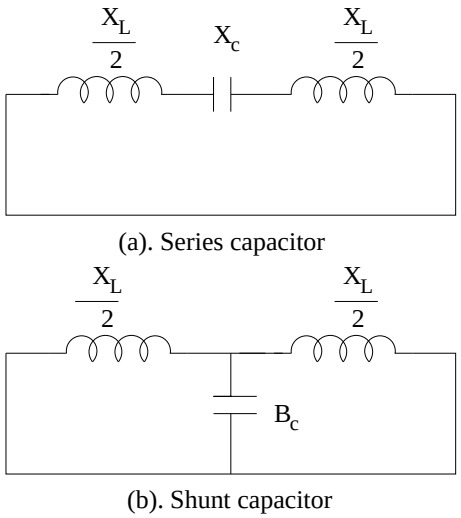

Figure 2.14: Equivalent circuits for determining resonance frequencies

Another factor in the comparison of the series and shunt (capacitor) compensation is the electrical resonance frequency. The comparison can be made from the Fig. 2.14.

The electrical resonance frequency (f_{er}^{se}) for the series capacitor compensation

$$f_{er}^{se} = \frac{1}{2\pi}\sqrt{\frac{1}{LC}} = f_0\sqrt{\frac{X_c}{X_L}} = f_0\sqrt{(1-k_{se})} \tag{2.81}$$

The resonance frequency for the shunt capacitor compensation is obtained as

$$f_{er}^{sh} = f_0\sqrt{\frac{4}{B_c X_L}} = f_0\sqrt{\frac{1}{(1-k_{sh})}} \tag{2.82}$$

where f_0 is the operating system frequency (50 or 60 Hz).Note that in deriving these expression, the equation, $\frac{X_L}{2} = Z_n \tan\frac{\theta}{2}$ is used.

It is shown in reference [3] that oscillations of the generator rotor corresponding to a subsynchronous frequency torsional mode (of frequency, f_m) causes amplitude modulation of the generator voltage. This causes two side bands of frequency $(f_0 - f_m)$ and $(f_0 + f_m)$ of the injected voltage, which result in a subsynchronous frequency and a supersynchronous frequency current components flowing in the generator armature. While the subsynchronous frequency current component results in a negative damping torque, the supersynchronous frequency current results in a positive damping torque. The electrical resonance at frequency, $f_0 - f_m$, increases the negative damping torque while resonance at $f_0 + f_m$, results in increase in the positive damping torque.

Comparing (2.82) with (2.81), it is obvious that $f_{er}^{sh} > f_0$ while $f_{er}^{se} < f_0$. This implies that there is no danger of Subsynchronous Resonance (SSR) with shunt capacitor, while it exists with the series capacitor. On the other hand, the rating of the shunt capacitor required is high unless the lines are substantially long resulting in large operating values of $\delta_{\max}$. The cost of a series capacitor is higher (typically by a factor of 2) as it has to be designed to withstand overvoltages during fault transients.

2.6 Compensation by STATCOM and SSSC

2.6.1 STATCOM at the Midpoint of the Line

The shunt connected STATCOM draws a pure reactive current if losses are neglected. Thus, it has similar effects on the bus voltage and power flow as the shunt connected susceptance. The major difference is that a STATCOM is more effective at low voltages as it can regulate (at constant value) the reactive current drawn.

As mentioned earlier, the location of a STATCOM is optimum when connected at the midpoint.

Fig. 2.15 shows the equivalent circuit of the line with shunt connected STATCOM (constant reactive current source) at the midpoint. It is assumed that $V_S = V_R = V$. The following equations apply.

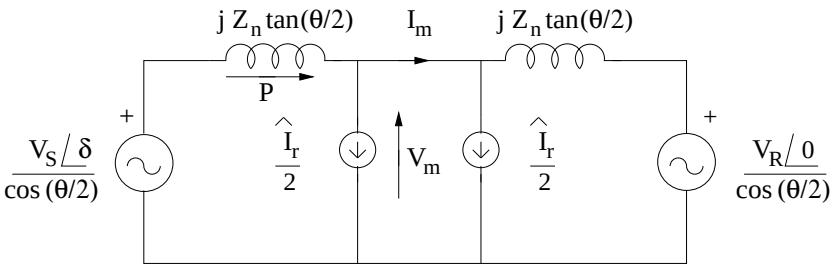

Figure 2.15: Equivalent circuit of a line with STATCOM at the midpoint

$$\frac{V\angle\delta}{\cos\frac{\theta}{2}} - jZ_n \tan\frac{\theta}{2}\left(\hat{I}_m + \frac{\hat{I}_r}{2}\right) = \hat{V}_m \tag{2.83}$$

$$\frac{V\angle 0}{\cos\frac{\theta}{2}} + jZ_n \tan\frac{\theta}{2}\left(\hat{I}_m - \frac{\hat{I}_r}{2}\right) = \hat{V}_m \tag{2.84}$$

where

$$\hat{I}_r = -j\frac{\hat{V}_m}{V_m}I_r \tag{2.85}$$

(*Note:* It is assumed that I_r is positive, when it lags the bus voltage. In other words, inductive reactive current drawn is assumed to be positive).

Adding (2.83) and (2.84) we have

$$\frac{2V\cos\frac{\delta}{2}}{\cos\frac{\theta}{2}}\angle\frac{\delta}{2} - jZ_n\tan\frac{\theta}{2}\hat{I}_r = 2\hat{V}_m$$

Substituting for $\hat{I}_r$, (from Eq. (2.85)), we finally get

$$\hat{V}_m = \left(\frac{V\cos\frac{\delta}{2}}{\cos\frac{\theta}{2}} - \frac{I_r Z_n}{2}\tan\frac{\theta}{2}\right)\angle\frac{\delta}{2}. \tag{2.86}$$

By subtracting (2.84) from (2.83) and simplifying, we get

$$\hat{I}_m = \frac{V\sin\frac{\delta}{2}}{Z_n\sin\frac{\theta}{2}}\angle\frac{\delta}{2} \tag{2.87}$$

From (2.86) and (2.87) we note that $\hat{V}_m$ and $\hat{I}_m$ are in phase and the power flow (P) is given by

$$P = \frac{V^2\sin\delta}{Z_n\sin\theta} - \frac{VI_r\sin\frac{\delta}{2}}{2\cos\frac{\theta}{2}} \tag{2.88}$$

To increase power transfer, I_r should be negative (capacitive) and this is as expected. The major difference between a shunt capacitor and STATCOM is that the maximum power for the latter, occurs at $90^\circ < \delta_p < 180^\circ$ and is a function of I_r in addition to the line length.

Remarks

In general, when the power angle relationship is expressed as

$$P = A\sin\delta + B\sin\frac{\delta}{2}$$

the angle (δ_p) at which the power is maximum is defined by

$$\frac{dP}{d\delta} = 0 = A\cos\delta_p + \frac{1}{2}B\cos\frac{\delta_p}{2}$$

Defining $x = \cos\frac{\delta_p}{2}$, the above equation can be expressed as a quadratic equation in x, namely,

$$A(2x^2 - 1) + \frac{1}{2}Bx = 0$$

The solution of this equation is given by

$$x = -\frac{B}{8A} \pm \frac{\sqrt{\frac{B^2}{4} + 8A^2}}{4A}$$

Only the positive solution for x is selected as relevant. Fig. 2.16 shows a typical power angle curve (for $I_r = -0.5, \theta = 30°$) where P is expressed in per unit of the SIL.

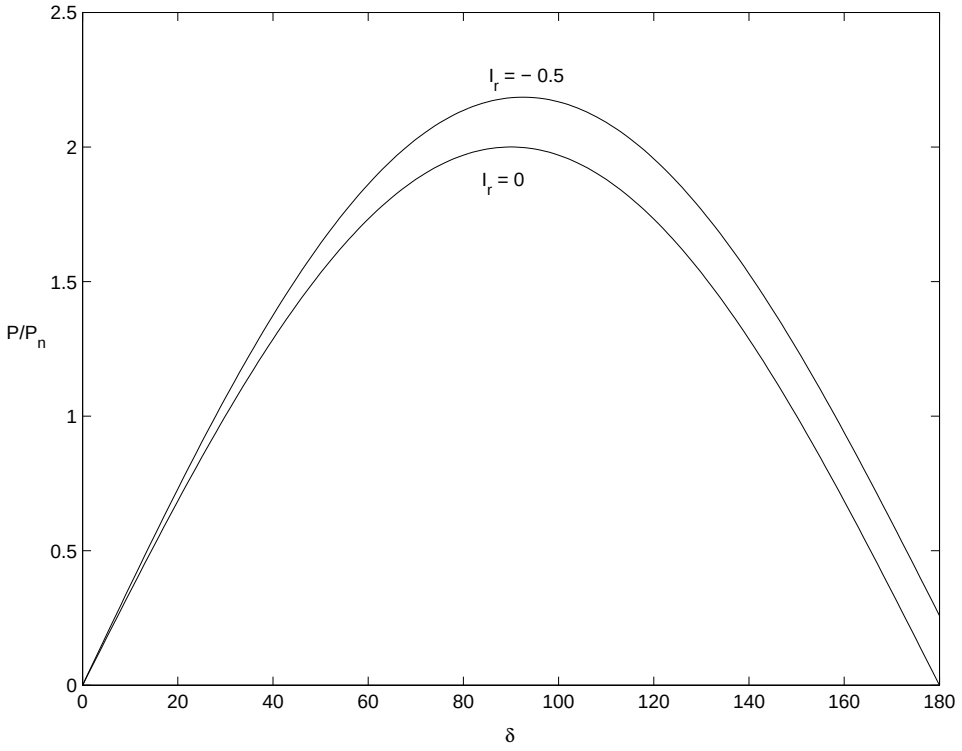

Figure 2.16: Power angle curve with STATCOM

2.6.2 SSSC at the Midpoint of the Line

For simplicity, it is assumed that the SSSC is connected at the midpoint of the line. The SSSC injects a reactive voltage (V_r) in series with the line (neglecting losses). The reactive voltage is considered to be positive when it is capacitive.

Assuming $V_S = V_R = V$, the following equations can be written from the circuit shown in Fig. 2.17.

$$\frac{V}{\cos\frac{\theta}{2}}\angle\delta - jZ_n \tan\frac{\theta}{2}\hat{I}_m = \hat{V}_m - \frac{\hat{V}_r}{2} \tag{2.89}$$

$$\frac{V}{\cos\frac{\theta}{2}}\angle 0 + jZ_n \tan\frac{\theta}{2}\hat{I}_m \quad = \quad \hat{V}_m + \frac{\hat{V}_r}{2} \tag{2.90}$$

where

$$\hat{V}_r = j\frac{\hat{I}_m}{I_m}V_r \tag{2.91}$$

(the voltage ($\hat{V}_r$) leads the current ($\hat{I}_m$) as it is assumed to be a voltage rise in the direction of the current).

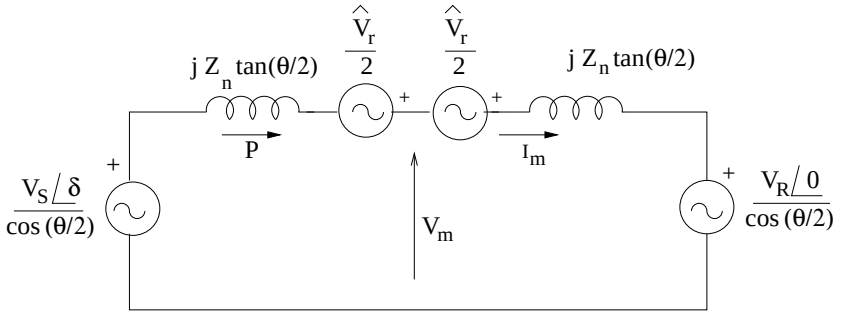

Figure 2.17: Equivalent circuit of a line with SSSC at the midpoint

From the above equations, we can obtain,

$$\hat{V}_m \quad = \quad \frac{V}{\cos\frac{\theta}{2}}\cos\frac{\delta}{2}\angle\frac{\delta}{2} \tag{2.92}$$

$$\hat{I}_m \quad = \quad \left(\frac{V\sin\frac{\delta}{2}}{Z_n\sin\frac{\theta}{2}} + \frac{V_r}{2Z_n\tan\frac{\theta}{2}}\right)\angle\frac{\delta}{2} \tag{2.93}$$

$$P \quad = \quad V_m I_m = \frac{V^2\sin\delta}{Z_n\sin\theta} + \frac{VV_r\cos\frac{\delta}{2}}{2Z_n\sin\frac{\theta}{2}} \tag{2.94}$$

2.6.3 Comparison between STATCOM and SSSC in Enhancing Power Transfer

The power angle expression for a SSSC is given by

$$P = A\sin\delta + B\cos\frac{\delta}{2}$$

It can be shown that P is maximum at $\delta = \delta_p$ and $0 < \delta_p < 90°$. On the other hand, the power is nonzero for $\delta = 0$. A major advantage is that increase in the power transfer is directly proportional to the reactive voltage injected for small values of the operating angle δ.

It can be shown that the rating of SSSC required for the same level of power enhancement as a STATCOM at the midpoint, can be related to the STATCOM rating as

$$Q_{\mathrm{SSSC}} = \tan^2\left(\frac{\delta_{\max}}{2}\right) \cdot Q_{\mathrm{STATCOM}}$$

(Hint: The rating of the STATCOM is given by

$$Q_{\mathrm{STATCOM}} = V_m I_{r\,\max}$$

while the rating of SSSC is given by

$$Q_{\mathrm{SSSC}} = I_m V_{r\,\max})$$

2.7 Some Representative Examples

Example 2.1

Consider the system shown in Fig. 2.18, where a generator feeds power to a load through a line. (Even if there are several lines feeding the load, there is no loss of generality in representing the system in steady state as shown in the Figure). There is a fixed capacitor of susceptance B_C, connected at the load bus. Depending on the size, this can compensate not only the power factor of the load, but also the requirements of the line to boost the load bus voltage to the rated value. For simplifying the analysis, it is assumed that the resistance and shunt capacitance of the line are neglected and the series impedance is assumed to be jX. The normalized voltage ($\bar{V}$) at the load bus and the normalized power flow ($\bar{P}$) in the line are defined by

$$\bar{V} = \frac{V}{E}, \bar{P} = \frac{PX}{E^2}$$

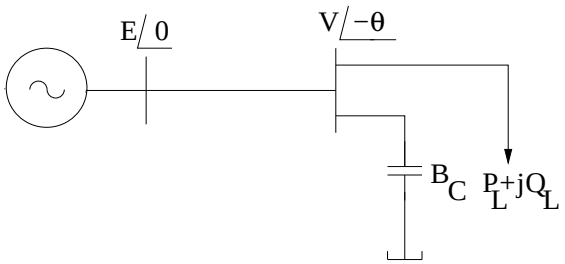

Figure 2.18: A transmission line feeding a load

Thevenin equivalent at the load bus and the phasor diagram are shown in Fig. 2.19. From this, we can derive expressions for V and P as

$$V = \frac{V_{Th}\cos(\theta+\phi)}{\cos\phi}, \quad P = \frac{V_{Th}V\sin\theta}{X_{Th}}$$

Since,

$$V_{Th} = \frac{E}{(1-K)}, \quad X_{Th} = \frac{X}{(1-K)}, \quad K = B_C X,$$

we obtain,

$$\bar{V} = \frac{\cos(\theta+\phi)}{(1-K)\cos\phi}, \quad \bar{P} = \frac{1}{2(1-K)\cos\phi}[\sin(2\theta+\phi) - \sin\phi]$$

where $\phi = \tan^{-1}\frac{Q_L}{P_L}$ (power factor angle). $\bar{P}$ is maximum when $\theta = \theta_m$, such that

$$\frac{d\bar{P}}{d\theta} = 0$$

It can be observed that $\theta_m = \frac{\pi}{4} - \frac{\phi}{2}$. Thus, when $\phi = 30°$, $\theta_m = 30°$.

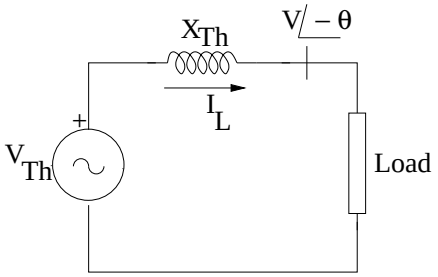

(a) Thevenin equivalent

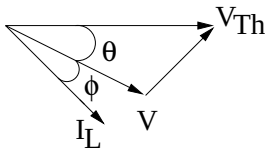

(b) Phasor diagram

Figure 2.19: Equivalent circuit and phasor diagram

It is interesting to note that the provision of fixed capacitor does not affect the value of θ_m which is determined only by ϕ. By providing dynamic voltage regulation, it is possible to increase θ_m to $\frac{\pi}{2}$.

To obtain a specified voltage ($\bar{V}$) at the load bus, the total reactive power required at the load bus is given by

$$Q_C = P_L \tan\phi + \frac{E^2}{X}\bar{Q}$$

where $\bar{Q}$ is the normalized reactive power injected into the line at the load bus and is expressed by

$$\bar{Q} = \cos\alpha[\bar{V}^2\cos\alpha - \bar{V}\cos(\theta+\alpha)]$$

where $\alpha = \tan^{-1} \frac{R}{X}$.

In the above expression, the line losses are also considered as they affect $\bar{Q}$ (which is increased while $\bar{P}$ is reduced). For example, for $\bar{V} = 1.0$, $\theta = 30^\circ$, (i) $\bar{Q} = 0.134$ for $R = 0$ and (ii) $\bar{Q} = 0.182$ for $\frac{R}{X} = 0.1$.

The $\bar{P} - \bar{V}$ curves for the three following cases are shown in Fig. 2.20.

(i) $B_C = 0$

(ii) $B_C = B_L$ where B_L is the inductive susceptance of the load

(iii) B_C is adjusted to keep $\bar{V} = 1.0$ at $\theta = \theta_m$.

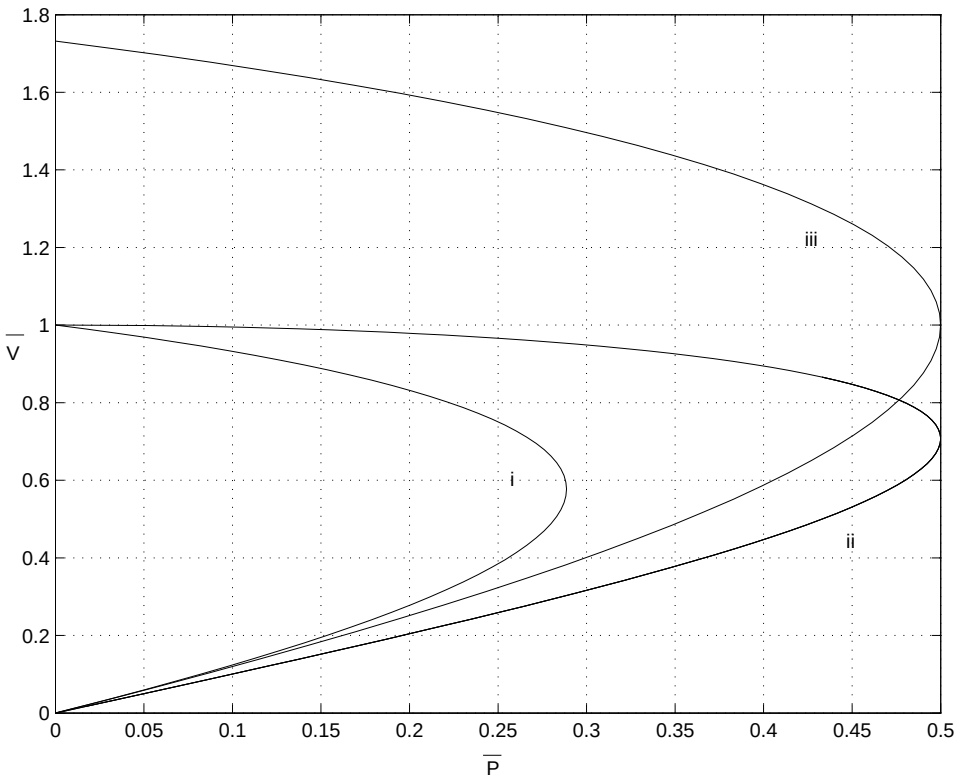

Figure 2.20: Plot of $\bar{V}$ vs. $\bar{P}$

It is assumed that the load power factor is 0.866 lagging ($\phi = 30^\circ$). It is interesting to observe that in case (i) the maximum value of $\bar{P}$ is only 0.289 and the corresponding load bus voltage is 0.577. By compensating the power factor to unity in case (ii), $\bar{P}_{\max}$ is increased to 0.5 and the corresponding $\bar{V} = 0.707$. Although the variation of the load requires variation of B_C to

maintain unity power factor, this can be achieved by slow control (using mechanically switched capacitors) if the load variation is slow. In case (iii) B_C is set at the constant value of

$$B_C = \frac{\sqrt{3}-1}{\sqrt{3}X}$$

since $\phi = 30°$, $\theta_m = 30°$. For case (iii) it is observed that load rejection results in overvoltage of $1.73E$ at the receiving end. Also, $\bar{P}_{\max} = 0.5$ even though $\bar{V} = 1.0$. This shows the limitation of providing fixed capacitors at load bus for voltage support. Although the voltage is normal at the operating point of $\bar{P} = 0.5$, any incremental increase in the load results in voltage collapse.

If fast reactive power control using SVC or STATCOM is employed, $\bar{V}$ can be regulated at $\bar{V} = 1.0$ at all times irrespective of the load. In this case, $\bar{P}_{\max} = 1.0$ which is double of the value corresponding to case (ii) or (iii).

This example highlights the importance of reactive power compensation at a load bus if there are no generators in the vicinity to regulate the bus voltage.

It is interesting to note that reference [4] mentions the possibility of utilizing the excellent voltage control capability of shunt FACTS controllers (such as STATCOM) to replace older, less efficient urban generation that is "must run" for voltage support in that area. This implies importing power from more efficient and less costly generation. This also helps in meeting environmental constraints of maintaining strict air quality standards.

Example 2.2

A 400 kV, 50 Hz, 600 km long symmetrical line is operated at the rated voltage.

(a) What is the theoretical maximum power carried by the line? What is the midpoint voltage corresponding to this condition?

(b) A series capacitor is connected at the midpoint of the line to double the power transmitted. What is its reactance?

(c) A shunt capacitor of value 450 ohms is connected at the midpoint of the line. If the midpoint voltage is 0.97, compute the power flow in the line corresponding to this operating point.

Data: $l = 1$ mH/km, $c = 11.1 \times 10^{-9}$ F/km.

Solution

From the data given

$$\begin{aligned} Z_n &= \sqrt{\frac{l}{c}} = \sqrt{\frac{10^6}{11.1}} = 300 ohms \\ \beta &= \omega\sqrt{lc} = 2\pi \cdot 50\sqrt{1 \times 11.1 \times 10^{-12}} \times \frac{180}{\pi} degrees \\ &= 0.06^\circ/km \\ \theta &= \beta d = 0.06 \times 600 = 36^\circ \\ P_{\max} &= \frac{P_n}{\sin\theta} = \frac{400 \times 400}{300 \sin(36^\circ)} = 907.4 MW \end{aligned}$$

$P_{\max}$ occurs at $\delta = \delta_{\max} = 90^\circ$. The midpoint voltage corresponding to this condition is

$$V_m = \frac{V \cos\frac{\delta}{2}}{\cos\frac{\theta}{2}} = \frac{400 \cos 45^\circ}{\cos 18^\circ} = 297.4 kV$$

(b) Since the power flow with a series capacitor is given by

$$P = \frac{P_n \sin\delta}{\sin\theta(1 - k_{se})}$$

If power is to be doubled, $k_{se} = 0.5$. The expression for k_{se} (when the series capacitor is connected at the midpoint) is given by

$$k_{se} = \frac{X_c}{2Z_n} \cot\frac{\theta}{2}$$

Substituting the values for k_{se}, θ and Z_n, we get

$$X_c = 2k_{se}Z_n \tan\frac{\theta}{2} = 300 \times \tan 18^\circ = 97.48 ohms$$

(c) The midpoint voltage, with a shunt capacitor connected there, is given by

$$V_m = \frac{V \cos\frac{\delta}{2}}{\cos\frac{\theta}{2}(1 - k_{sh})}, k_{sh} = \frac{B_c Z_n}{2} \tan\frac{\theta}{2}$$

Hence,

$$\begin{aligned} \cos\frac{\delta}{2} &= 0.97 \times \cos 18^\circ \left[1 - \frac{300 \tan 18^\circ}{450 \times 2}\right] \\ &= 0.823 \Rightarrow \delta = 69.31^\circ \end{aligned}$$

The power flow in the line is given by

$$\begin{aligned} P &= \frac{VV_m \sin\frac{\delta}{2}}{Z_n \sin\frac{\theta}{2}} = \frac{1 \times 0.97 \times \sin 34.65^\circ}{\sin 18^\circ} \times P_n \\ &= 1.785 P_n = \frac{1.785 \times 400 \times 400}{300} = 952 MW \end{aligned}$$

Example 2.3

A SSSC is connected at the midpoint of the lossless, 600 km long described in example 2.2. At the operating angle of $\delta = 30°$, the current in the line (at the midpoint) is same as the current in the line when a series capacitor of the magnitude calculated in Example 2.2 is connected.

(a) Compute the reactive voltage (V_r) injected

(b) With the constant reactive voltage calculated in (a) what is the maximum power flow in the line? What is the value of δ at which this occurs?

(c) Compute the power flow at $\delta = 0$. What are the line voltages at the two terminals of the SSSC?

Solution

(a) With series capacitor, the current at the midpoint is given by

$$I_m = \frac{V \sin\frac{\delta}{2}}{(1-k_{se})Z_n \sin\frac{\theta}{2}}, \quad k_{se} = 0.5$$

At $\delta = 30°$, I_m in per unit is given by

$$I_m = 2 \times 0.8376 p.u.$$

The current with SSSC is given by

$$\begin{aligned} I_m &= \frac{\sin\frac{\delta}{2}}{\sin\frac{\theta}{2}} + \frac{V_r}{2\tan\frac{\theta}{2}} \\ &= (0.8376 + 0.8376) p.u. \end{aligned}$$

The injected voltage (V_r) in per unit is given by

$$\begin{aligned} \bar{V}_r &= 2 \times 0.8376 \times \tan 18° = 0.5443 p.u. \\ V_r &= 0.5443 \times \frac{400}{\sqrt{3}} = 125.7 kV \end{aligned}$$

(b) The power flow with constant reactive voltage injected is

$$\bar{P} = \frac{P}{P_n} = A \sin\delta + B \cos\frac{\delta}{2}$$

where

$$A = \frac{1}{\sin\theta}, \quad B = \frac{\bar{V}_r}{2\sin\frac{\theta}{2}}$$

Substituting values for $\bar{V}_r$ and θ, we get

$$A = \frac{1}{\sin 36^\circ} = 1.7013, \quad B = \frac{0.5443}{2\sin 18} = 0.8807$$

$\bar{P}$ is maximum when $\frac{d\bar{P}}{d\delta} = 0$

$$\frac{d\bar{P}}{d\delta} = A\cos\delta - B\sin\frac{\delta}{2} = 0$$

If we let $x = \sin\frac{\delta}{2}$, we get a quadratic equation given below.

$$2Ax^2 + Bx - A = 0$$

The solution ($x > 0$) of the equation is

$$x = 0.5894 = \sin\frac{\delta}{2} \Rightarrow \delta = 72.24^\circ$$

$$\begin{aligned} \bar{P}_{\max} &= A\sin(72.24^\circ) + B\cos(36.12^\circ) \\ &= 2.3316 \\ P_{\max} &= 2.3316 \times \frac{400^2}{300} = 1243.52MW \end{aligned}$$

(c) The power flow with SSSC at $\delta = 0$ is

$$\bar{P} = B = 0.8807p.u.(469.7MW)$$

The single line diagram of the line with midpoint connected SSSC is shown in Fig. 2.21. The voltage at the midpoint (V_m) is same as that without SSSC.

$$\bar{V}_m = \frac{\cos\frac{\delta}{2}}{\cos\frac{\theta}{2}} \cdot \text{For } \delta = 0, \quad \bar{V}_m = \frac{1}{\cos 18^\circ} = 1.0515$$

The voltages $\hat{V}_1$ and $\hat{V}_2$ are given by

$$\begin{aligned} \hat{V}_1 = V_m\angle 0 - j\frac{V_r}{2} &= 1.0515\angle 0 - j\frac{0.5443}{2} \\ &= 1.086\angle -14.5^\circ \\ \hat{V}_2 = V_m\angle 0 + j\frac{V_r}{2} &= 1.086\angle 14.5^\circ \end{aligned}$$

Example 2.4

For the line described in Example 2.2, a STATCOM is connected at the midpoint instead of a shunt capacitor of 450 ohms. If the operating point for both cases is same with $V_m = 0.97$, (a) compute the reactive current drawn by the STATCOM. (b) What is the maximum power flow in the line with constant reactive current calculated in (a).

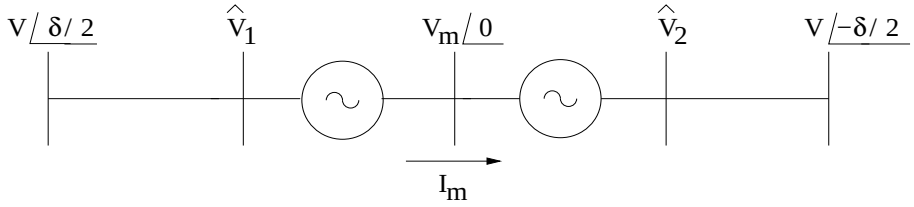

Figure 2.21: A SSSC connected at the midpoint of the line

Solution

With shunt capacitor of 450 ohms, it was calculated that $\delta = 69.31^\circ$ when $V_m = 0.97$.

(a) To get same operating point, the required I_r is calculated from the equation,

$$V_m = \frac{V\cos\frac{\delta}{2}}{\cos\frac{\theta}{2}} - \frac{I_r Z_n \tan\frac{\theta}{2}}{2}$$

In per unit, we calculate I_r as

$$\bar{I}_r = 2\left[\frac{\cos 34.65^\circ}{\cos 18^\circ} - 0.97\right]\frac{1}{\tan 18^\circ} = -0.6466 p.u.$$

Note that $I_r = -V_m B_C = 0.97 \times \frac{300}{450} = -0.6466$

(b) The power flow in the line is given by

$$\bar{P} = \frac{P}{P_n} = A\sin\delta + B\sin\frac{\delta}{2}$$

where

$$A = \frac{1}{\sin\theta}, \quad B = \frac{-\bar{I}_r}{2\cos\frac{\theta}{2}}$$

$$A = \frac{1}{\sin 36^\circ} = 1.7013, B = \frac{0.6466}{2\times\cos 18^\circ} = 0.3399$$

From the analysis given in section 2.6.1, $\bar{P}$ is maximum when

$$2Ax^2 + \frac{B}{2}x - A = 0, \quad x = \cos\frac{\delta}{2}$$

The solution of this equation gives $x = 0.6826$. Hence P is maximum at $\delta = 94^\circ$.

The maximum value of P is given by

$$\begin{aligned} P_{\max} &= \bar{P}\max \times \frac{400^2}{300}, \quad \bar{P}_{\max} = A\sin 94^\circ + B\sin 47^\circ \\ &= 1.9455 \times \frac{400^2}{300} = 1037.6MW \end{aligned}$$

Note that the maximum power flow in the line with a shunt capacitor of 450 ohms (connected at the midpoint) is given by

$$P_{\max} = \frac{V^2}{Z_n \sin\theta(1-k_{sh})}, \quad k_{sh} = \frac{B_c Z_n}{2}\tan\frac{\theta}{2}$$

Substituting the values for B_C, Z_n and θ,

$$\begin{aligned} k_{sh} &= 0.1083, \\ P_{\max} &= \frac{400^2}{300(1-0.1083)\sin 36^\circ} \\ &= 1.9079 \times \frac{400^2}{300} = 1017.6MW \end{aligned}$$

The maximum power with STATCOM is higher than with shunt capacitor. This is due to the fact, the reduction of midpoint voltage (as δ is increased) is less with STATCOM.

References and Bibliography

1. T.J.E. Miller, Ed., **Reactive Power Control in Electric Systems**, John Wiley and Sons, New Work, 1982
2. E.W. Kimbark, "How to improve system stability without risking subsynchronous resonance". Paper F77 125.8, IEEE PES Winter Meeting, 1977
3. K.R. Padiyar, **Analysis of Subsynchronous Resonance in Power Systems**, Kluwer Academic Publishers, Boston, 1999
4. T.W. Cease, A. Edris and T. Lemak, "TVA's ±100 MVAR STATCOM field performance and future developments", EPRI Workshop on "The Future of Power Delivery in the 21st Century", California, U.S.A., 1997.

Chapter 3

Static Var Compensator

In this chapter, the Static Var Compensator (SVC), a first generation FACTS controller is taken up for study. It is a variable impedance device where the current through a reactor is controlled using back to back connected thyristor valves. The application of thyristor valve technology to SVC is an offshoot of the developments in HVDC technology. The major difference is that thyristor valves used in SVC are rated for lower voltages as the SVC is connected to an EHV line through a step down transformer or connected to the tertiary winding of a power transformer.

The application of SVC was initially for load compensation of fast changing loads such as steel mills and arc furnaces. Here the objective is to provide dynamic power factor improvement and also balance the currents on the source side whenever required. The application for transmission line compensators commenced in the late seventies. Here the objectives are:

1. Increase power transfer in long lines [1,3,6]
2. Improve stability with fast acting voltage regulation [7,8]
3. Damp low frequency oscillations due to swing (rotor) modes [9–12]
4. Damp subsynchronous frequency oscillations due to torsional modes [13–15]
5. Control dynamic overvoltages [1,5]

A SVC has no inertia compared to synchronous condensers and can be extremely fast in response (2-3 cycles). This enables the fast control of reactive power in the control range.

3.1 Analysis of SVC

The location of SVC is important in determining its effectiveness. Ideally, it should be located at the electrical centre of the system or midpoint of a transmission line. For example, consider a symmetric lossless transmission

line with SVC connected at the midpoint (see Fig. 3.1). Without SVC, the voltage at the midpoint is given by,

$$V_{mo} = \frac{V \cos \delta/2}{\cos \theta/2} \tag{3.1}$$

where $\theta = \beta l$ is the electrical length of the line, l is the length of the line and β is the phase constant given by

$$\beta = \omega\sqrt{lc} = 2\pi f\sqrt{lc} \tag{3.2}$$

where l and c are positive sequence inductance and capacitance of the line per unit length, f is the operating frequency.

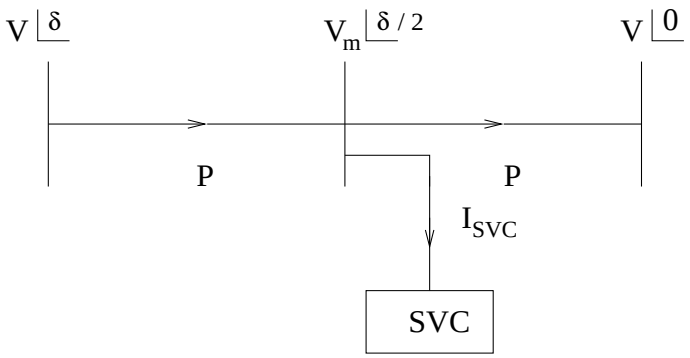

Figure 3.1: A transmission line with SVC connected at midpoint

It can be shown that the voltage variation in the line (due to variation in δ) is maximum at the midpoint. SVC helps to limit the variation by suitable control. The steady state control characteristics of SVC is shown in Fig. 3.2 where ADB is the control range. OA represents the characteristic where the SVC hits the capacitor limit, BC represents the SVC at its inductor limit. Note that SVC current is considered positive when SVC susceptance is inductive. Thus

$$I_{SVC} = -B_{SVC} V_{SVC} \tag{3.3}$$

The slope of OA is B_C (susceptance of the capacitor) and the slope of OBC is B_L (susceptance of the reactor). A positive slope (in the range of 1-5%) is given in the control range to

(a) enable parallel operation of more than one SVC connected at the same or neighboring buses and

(b) prevent SVC hitting the limits frequently.

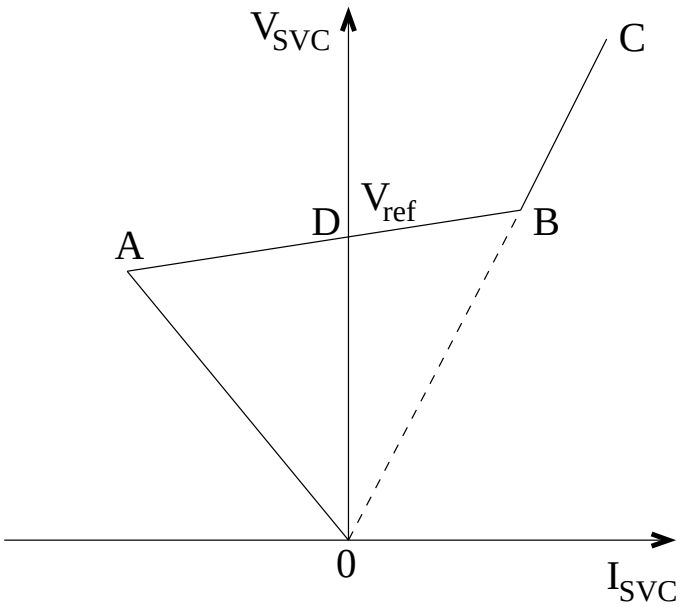

Figure 3.2: Control characteristic of SVC

The steady state value of the SVC bus voltage is determined from the intersection of the system characteristic and the control characteristic (see Fig. 3.3). The system characteristic is a straight line with negative slope and is defined by

$$V_{SVC} = V_{Th} - X_{Th} I_{SVC} \tag{3.4}$$

where V_{Th} and X_{Th} are the Thevenin voltage and reactance viewed from the SVC bus. For the system shown in Fig. 3.1, we have

$$V_{Th} = V_{mo} = \frac{V \cos(\delta/2)}{\cos(\theta/2)} \tag{3.5}$$

$$X_{Th} = \frac{Z_n}{2} \tan(\theta/2) \tag{3.6}$$

where Z_n is the surge impedance defined by

$$Z_n = \sqrt{\frac{l}{c}} \tag{3.7}$$

Expression for Voltage and Power

(a) Control Range: The SVC control range is described by

$$V_{SVC} = V_{ref} + X_s I_{SVC} \tag{3.8}$$

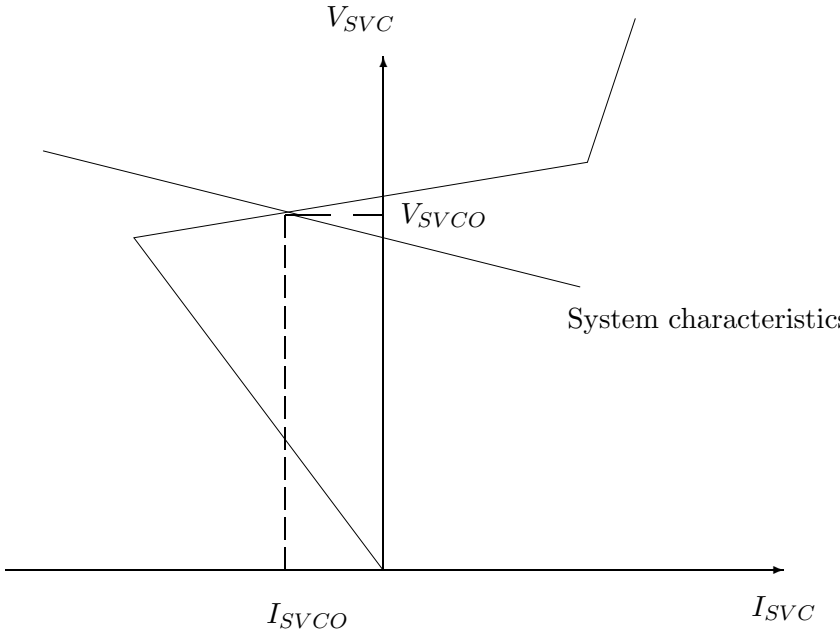

Figure 3.3: Determination of operating point of SVC

where X_s is the slope of the control characteristic. V_{ref} is the SVC voltage (corresponding to point D) when $I_{SVC} = 0$.

Combining eqs (3.4) and (3.8), we get

$$V_{SVC} = V_m = \frac{V_{Th}X_s}{X_s + X_{Th}} + \frac{V_{ref}X_{Th}}{X_s + X_{Th}} \tag{3.9}$$

The expression for power flow in the line is given by

$$P = \frac{V_m V \sin(\delta/2)}{Z_n \sin(\theta/2)} \tag{3.10}$$

With $V_{ref} = V$, it can be shown that P is given by,

$$P = kP_0 + (1-k)P_1 \tag{3.11}$$

where

$$P_0 = \frac{V^2 \sin\delta}{Z_n \sin\theta}, \quad P_1 = \frac{V^2 \sin(\delta/2)}{Z_n \sin(\theta/2)} \tag{3.12}$$

and

$$k = \frac{X_s}{X_s + X_{Th}} \tag{3.13}$$

Remarks

1. P_0 is the power flow in the line without SVC and P_1 is the power flow in the line when SVC maintains a constant voltage V at the midpoint ($X_s = 0$)
2. $k \to 1$ as $X_s \to \infty$
3. For small values of θ, it can be assumed that $\sin\theta \simeq \theta$, $\sin\frac{\theta}{2} \simeq \frac{\theta}{2}$, $\cos\frac{\theta}{2} \simeq 1$.

In this case,

$$P_0 = \frac{V^2}{X_L}\sin\delta, \quad P_1 = 2\frac{V^2}{X_L}\sin\delta/2$$

where $X_L = (\omega l)d$ is the total reactance of the line (d is the length of the line).

(b) At SVC limits: When the SVC hits the limit it can be represented as a fixed susceptance (B_{SVC}) where $B_{SVC} = B_C$ at capacitive limit. At the inductive limit, $B_{SVC} = -B_L$.

Substituting I_{SVC} from eq. (3.3) in eq. (3.4), we get

$$V_{SVC} = \frac{V_{Th}}{(1 - X_{Th}B_{SVC})} = \frac{V\cos(\delta/2)}{(1 - X_{Th}B_{SVC})\cos(\theta/2)} \tag{3.14}$$

The power flow in the line is given by

$$P = \frac{P_0}{(1 - X_{Th}B_{SVC})} = \frac{V^2\sin\delta}{Z_n(1 - X_{Th}B_{SVC})\sin\theta} \tag{3.15}$$

Power Angle Curve for SVC

The power angle curve for SVC is made up of 3 segments corresponding to

(i) $B_{SVC} = -B_L$,

(ii) control range

(iii) $B_{SVC} = B_C$.

For typical value of parameters, the power (expressed in per unit of P_n = Surge Impedance Load) as a function of δ is shown in Fig. 3.4. The power angle curve for the line without SVC is also shown in Fig. 3.4 (curve b).

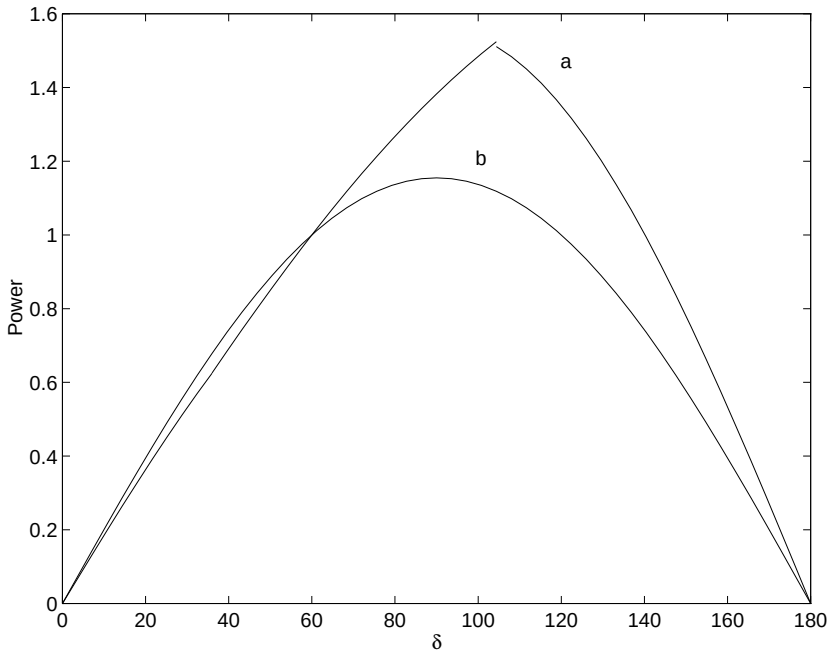

Figure 3.4: Plot of Power Vs δ

Example 3.1

A three phase, 400 kV, 50 Hz, 900 km long line is operating with $V_S = V_R = V = 1.0$ p.u. and $\delta = 60^\circ$. A SVC is planned to be connected at the midpoint of the line to increase power transfer capability. The limits on the control range correspond to $\delta = 30^\circ$ and $\delta = 90^\circ$.

(a) Find the limits of SVC susceptance if the slope (X_s) of the control characteristic is (i) 0.0 and (ii) 0.05 p.u.

(b) What is the maximum power flow in the line for the two cases, (i) $X_s = 0.0$ and (ii) $X_s = 0.05$ (Data : $Z_n = 300$ ohms, $\beta = 0.06^\circ$/km).

Solution

(a) Without SVC

$$V_m = \frac{V \cos\frac{\delta}{2}}{\cos\frac{\theta}{2}} = \frac{\cos 30^\circ}{\cos 27^\circ} = 0.972 p.u.$$

(Note $\theta = 0.06 \times 900 = 54^\circ$).

With SVC, the midpoint voltage (V_m) is given by

$$V_m = V_{m0} - X_{Th} I_r, \quad X_{Th} = \frac{Z_n}{2} \tan \frac{\theta}{2}$$

With Z_n = Base impedance, $X_{Th} = \frac{\tan 27^\circ}{2} = 0.2548$ p.n. The reactive current (I_r) drawn by SVC, also satisfies the equation $V_m = V_{ref} + X_s I_r$. Hence, we can solve for I_r as

$$I_r = \frac{(V_{mo} - V_{ref})}{(X_s + X_{Th})}$$

In Fig. 3.2 showing the control characteristics of a SVC, the limit A corresponds to the higher value of power flow. In this example, the operating angle $\delta = 90^\circ$. Hence, at the capacitive limit, $V_{mo} = \frac{V \cos 45^\circ}{\cos 27^\circ} = 0.7936$ p.u. V_{ref} corresponds to $\delta = 60^\circ$, the operating point in the line for which we assume $I_r = 0.0$. Hence

$$(i) \qquad I_{rmin} = \frac{0.7936 - 0.972}{0.2548} = -0.70 \ p.u.$$

$$(ii) \qquad I_{rmin} = \frac{0.7936 - 0.972}{0.2548 + 0.05} = -0.5853 \ p.u.$$

The value of $B_{max} = \frac{-I_{rmin}}{V_{SVC}}$. For case (i) $V_{SVC} = 0.972$ and (ii) $V_{SVC} = 0.9427$. Hence

$$\begin{aligned} B_{SVCmax} &= 0.72 \ p.u. \text{ for case (i)} \\ &= 0.621 \ p.u. \text{ for case (ii)} \end{aligned}$$

For the inductive limit of SVC corresponding to point B, we have

$$V_{mo} = \frac{V \cos 15^\circ}{\cos 27^\circ} = 1.0841$$

$$\begin{aligned} I_{rmax} &= \frac{1.0841 - 0.972}{0.2548} = 0.4399 \ p.u. \text{ for case (i)} \\ &= \frac{1.0841 - 0.972}{(0.2548 + 0.05)} = 0.3678 \text{ for case (ii)} \end{aligned}$$

The SVC bus voltage (V_{SVC}) is 0.972 for case (i), and 0.99 for case (ii). Hence B_{SVCmin} is given by

$$\begin{aligned} (i) \qquad B_{SVCmin} &= \frac{-I_{rmax}}{V_{SVC}} = -0.453 \ p.u. \text{ and} \\ (ii) \qquad B_{SVCmin} &= -0.372 \ p.u. \end{aligned}$$

Note that a positive slope in the control characteristic reduces the ratings of a SVC.

(b) The maximum power corresponds to $\delta = 90^\circ$ as the SVC behaves like a constant capacitor for $\delta > 90^\circ$. As

$$P_{\max} = P_n \frac{\bar{V}\bar{V}_m \sin\frac{\delta}{2}}{\sin\frac{\theta}{2}},$$

$$(i) \quad \frac{P_{\max}}{P_n} = \frac{0.972 \sin 45^\circ}{\sin 27^\circ} = 1.5139$$

$$(ii) \quad \frac{P_{\max}}{P_n} = \frac{0.9427 \sin 45^\circ}{\sin 27^\circ} = 1.4683$$

Note that $P_{max} = 1.2361\ P_n$ in the absence of SVC. The SVC designed with 0.05 p.u. slope increases the power limit by 124 MW.

3.2 Configuration of SVC

There are two types of SVC:

1. Fixed Capacitor-Thyristor Controlled Reactor (FC-TCR)
2. Thyristor Switched Capacitor - Thyristor Controlled Reactor (TSC-TCR).

The second type is more flexible than the first one and requires smaller rating of the reactor and consequently generates less harmonics.

The schematic diagram of a TSC-TCR type SVC is shown in Fig.3.5. This shows that the TCR and TSC are connected on the secondary side of a step-down transformer. Tuned and high pass filters are also connected in parallel which provide capacitive reactive power at fundamental frequency. The voltage signal is taken from the high voltage SVC bus using a potential transformer.

The TSC is switched in using two thyristor switches (connected back to back) at the instant in a cycle when the voltage across valve is minimum and positive. This results in minimum switching transients. In steady state, TSC does not generate any harmonics. To switch off a TSC, the gate pulses are blocked and the thyristors turns off when the current through them fall below the holding currents. It is to be noted that several pairs of thyristors are connected in series as the voltage rating of a thyristor is not adequate for the voltage level required. However the voltage ratings of valves for a SVC are much less than the voltage ratings of a HVDC valve as a step down transformer is used in the case of SVC. To limit $\frac{di}{dt}$ in a TSC it is necessary to provide a small reactor in series with the capacitor.

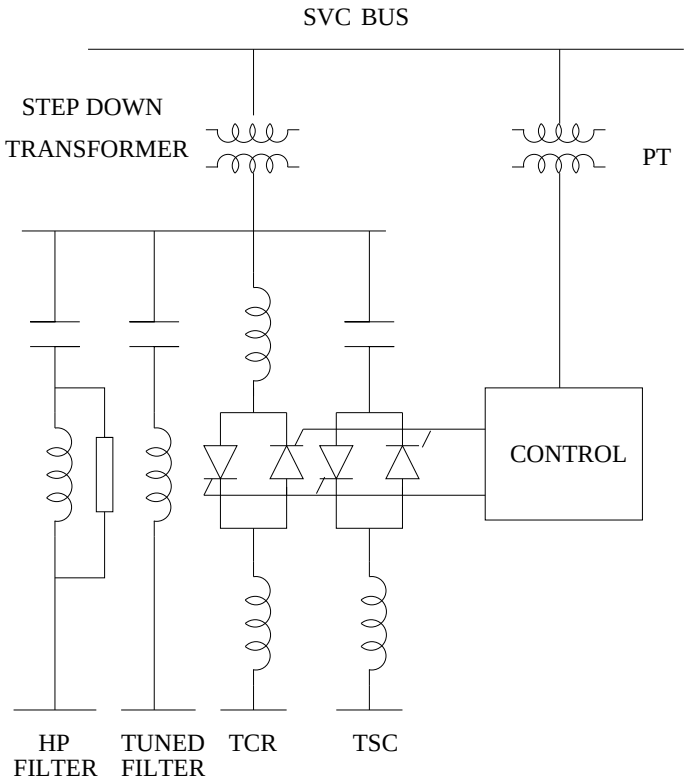

Figure 3.5: A Typical SVC (TSC-TCR) Configuration

Thyristor Controlled Reactor [1,4]

The current in a TCR can be continuously varied from zero (corresponding to zero conduction angle) to maximum (corresponding to conduction angle of 180°) by phase control in which the firing angle α (with respect to the zero crossing of the voltage) is varied from 180° to 90°. The instantaneous current i_{TCR} over half a cycle is given by

$$\left.\begin{array}{ll} i_{TCR} & = \frac{\sqrt{2}V}{X_L}(\cos\alpha - \cos\omega t), \quad \alpha < \omega t < \alpha + \sigma \\ & = 0, \qquad\qquad \alpha + \sigma < \omega t < \alpha + \pi \end{array}\right\} \tag{3.16}$$

where V is the rms voltage applied, X_L is the fundamental frequency reactance of the reactor. The current waveform in a single phase TCR is shown in Fig. 3.6. The current is non-sinusoidal and contains odd harmonics which are functions of the conduction angle σ.

The fundamental component of the TCR current, I_1 is given by

$$I_1 = B_{TCR}(\sigma)V \tag{3.17}$$

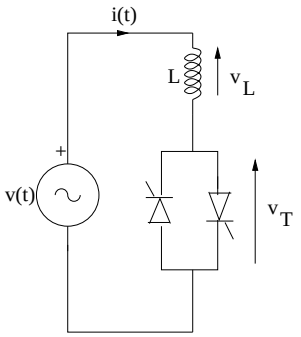

(a) A TCR circuit

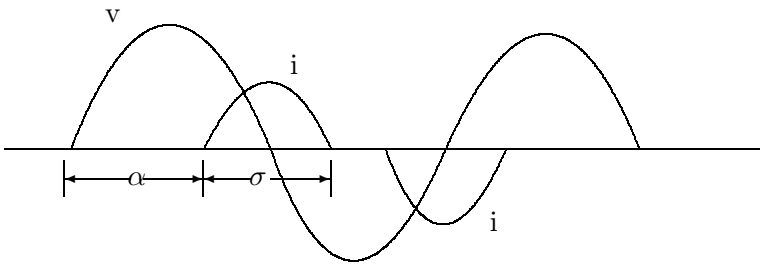

(b) Waveforms of v and i

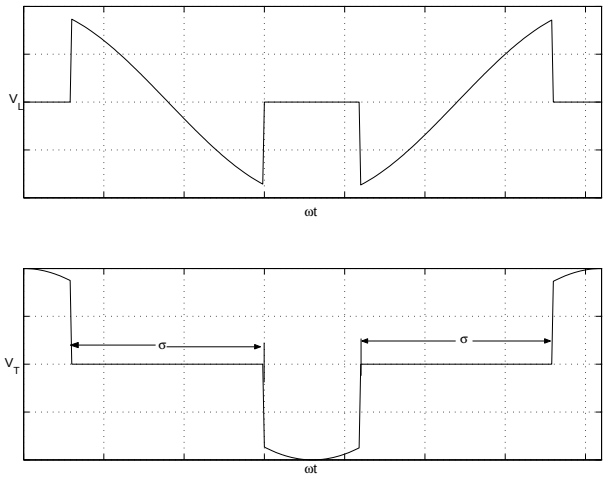

(c) Waveforms of v_L and v_T

Figure 3.6: Voltage and current waveforms in TCR

where

$$B_{TCR} = \frac{\sigma - \sin\sigma}{\pi X_L} \tag{3.18}$$

The conduction angle σ is related to α by

$$\sigma = 2(\pi - \alpha)$$

The TCR current contains odd harmonics. The rms value of the nth harmonic is given by

$$\begin{aligned} I_n &= \frac{V}{X_L} \cdot \frac{2}{\pi} \left[\frac{-2\cos\alpha}{n} \sin(n\alpha) + \frac{\sin(n-1)\alpha}{n-1} + \frac{\sin(n+1)\alpha}{n+1} \right] \\ &= \frac{V}{X_L} \cdot \frac{4}{\pi} \left[\frac{\sin\alpha\cos(n\alpha) - n\cos\alpha\sin(n\alpha)}{n(n^2-1)} \right], \quad n = 2k+1 \end{aligned} \tag{3.19}$$

where k is an integer, 1,2,3,....

The peak values of the individual harmonic currents are shown in Table 3.1. It is to be noted that $I_n = 0$ at both $\alpha = 90^\circ$ and $\alpha = 180^\circ$. The variations of I_1 and I_h, where

$$I_h = \left[\sum_{n=1}^{\infty} I_n^2 \right]^{1/2}, \quad n = 2k+1$$

are shown in Fig. 3.7(a) as functions of α. The variations of I_5 and I_7 as functions of α are shown in Fig. 3.7(b).

By connecting the TCR in delta, the triplen harmonics are eliminated on the line side. The harmonics present in the line current are of the order

$$n = 6k \pm 1 \tag{3.20}$$

where k is an integer.

It is assumed that the TCR currents are identical in waveform and magnitude in the three phases and only phase shifted from each other by 120^o. This is possible only if α is the same in all three phases. To limit the harmonics entering the system, some of the fixed capacitors are connected as series tuned filters. To reduce the harmonics further, it is possible to have twelve pulse configuration of TCR, in which there are two branches of TCR supplied by the two sets of secondaries of the step down transformer. One set of the secondary windings is connected in delta while the other set is connected in star. In this case, the line currents on the primary side will have harmonics of the order

$$n = 12k \pm 1 \tag{3.21}$$

where k is an integer. This happens because the harmonics of the order other than those defined in (3.21) , generated in the two TCR branches cancel each other as they flow on the primary side.

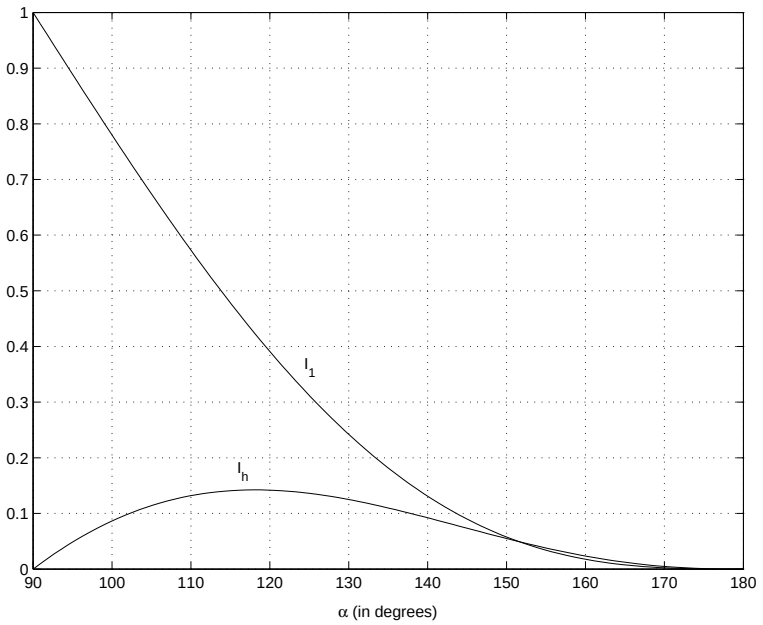

(a) Variation of I_1 and I_h

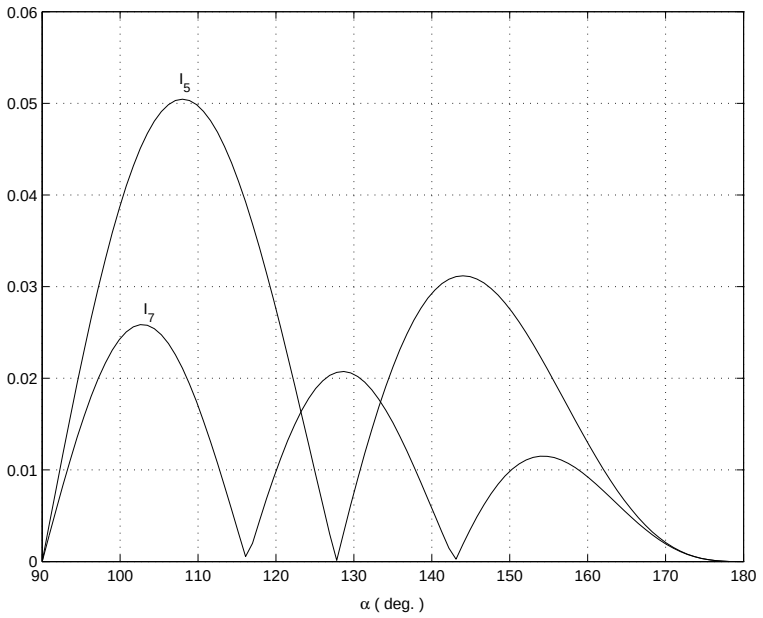

(b) Variation of I_5 and I_7

Figure 3.7: Variation of fundamental and harmonic components with firing angle

Table 3.1: Peak values of harmonic currents

Harmonic order	Peak Value (Percentage)
3	(13.78)
5	5.05
7	2.59
9	(1.57)
11	1.05
13	0.75
15	(0.57)
17	0.44
19	0.35

Note that the peak values of harmonics are expressed as a percentage of peak value of $I_1 \left(\frac{V}{X_L}\right)$

Another way of reducing the harmonics generated by TCR is to segment the TCR into two or more parallel connected branches and operate all except one of the branches as Thyristor Switched Reactors (TSR) which do not contribute any harmonics. The controllability is provided by varying the α (phase control) of one of the TCR branches.

The advantages of TSC-TCR type SVC over FC-TCR type are

(i) the reduction in the reactor size and consequently the harmonics generated

(ii) greater flexibility in control and

(iii) better performance under system fault conditions. The power losses in the quiescent operating condition (with SVC output current close to zero) also tend to be less with TSC-TCR type SVC.

For a FC-TCR type SVC, the rating of TCR covers the entire control range (AB) in the control characteristics of SVC shown in Fig.3.2. On the other hand, the rating of the TCR required for a TCS-TCR type SVC is DB. Although FC-TCR type SVC can generate higher harmonic currents, existing (fixed) capacitor bank can be designed as a filter. This is not feasible in the case of TSC-TCR type SVC.

The speeds of response for both types of SVC are similar. Fast switching of capacitor can be used to reduce overvoltages and for better control response under faulted conditions.

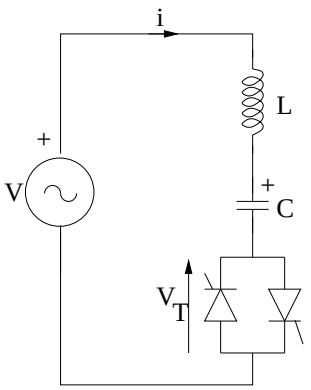

Figure 3.8: A TSC with series reactor

Thyristor Switched Capacitor (TSC)

When a capacitor is switched into a sinusoidal voltage source, a large current surge flows through the capacitor if the initial voltage acrose the capacitor is different than the supply voltage at the instant of switching. The current through the capacitor will be finite (corresponding to the steady state value) if the initial capacitor voltage is equal to the supply voltage at the instant of switching. However the rate of change of current $\left(\frac{di}{dt}\right)$ will be very high, beyond the rating of the thyristor devices (acting as switches). To limit the $\frac{di}{dt}$, it is necessary to insert a reactor in series with the capacitor, as shown in Fig. 3.8.

Let the supply voltage $v(t)$ be defined as

$$v(t) = \sqrt{2}V \sin(\omega_0 t + \alpha) \tag{3.22}$$

and the switch is turned on at $t = 0$ with the initial conditions, $i(0) = 0$ and $v_C(0) = V_{CO}$.

It can be shown that the expression for the current $i(t)$ is given by

$$\begin{aligned} i(t) &= \sqrt{2}I_{AC}\cos(\omega_0 t + \alpha) - nB_C\left[V_{CO} - \frac{n^2}{n^2-1}\sqrt{2}V\sin\alpha\right]\sin\omega_n t \\ &\quad -\sqrt{2}I_{AC}\cos\alpha\cos\omega_n t \end{aligned} \tag{3.23}$$

where

$$\omega_n = n\omega_0 = \sqrt{\frac{1}{LC}}, \quad n = \sqrt{\frac{X_C}{X_L}}, \quad B_C = \omega_0 C = \frac{1}{X_C}$$

$$I_{AC} = \frac{VB_C B_L}{B_L - B_C} = \frac{VB_C n^2}{n^2-1}, \quad B_L = \frac{1}{X_L}$$

The reactor value is chosen such that $n > 3$. In eq. (3.23), the first term in the R.H.S is the steady-state current component, while the other two terms are transient current components. (It is to be noted that for simplicity, the circuit resistance is ignored in the solution for $i(t)$. The presence of the resistance will result in the decay of the transient components).

If the switching has to be transients free, the following conditions have to be met.

$$\cos\alpha = 0 \Rightarrow \sin\alpha = \pm 1 \tag{3.24}$$

$$V_{CO} = \pm\sqrt{2}\frac{Vn^2}{n^2-1} = \pm\sqrt{2}X_C I_{AC} \tag{3.25}$$

In practice, it is not possible to satisfy both conditions. The condition represented by (3.25) implies that the capacitor has to be precharged and this is not realistic. In general, the residual voltage on the capacitor (V_{CO}) can vary from 0 to $\sqrt{2}V(n^2/n^2-1)$. There are two switching strategies depending on the value of V_{CO}.

Switching Strategy 1 ($0 < V_{CO} < \sqrt{2}V$)

$$\alpha = \sin^{-1}\frac{V_{CO}}{\sqrt{2}V} \tag{3.26}$$

The above implies that the capacitor is turned on at the instant when the supply voltage is equal to V_{CO}.

The transient current component (I_{tr}) where

$$\begin{aligned} I_{tr} &= \sqrt{a^2+b^2} \\ a &= nB_C\left[V_{CO} - \frac{n^2}{n^2-1}\sqrt{2}V\sin\alpha\right] \\ b &= \sqrt{2}I_{AC}\cos\alpha \end{aligned} \tag{3.27}$$

can be derived as

$$I_{tr} = I_{AC}\sqrt{1-\left(\frac{V_{CO}}{\sqrt{2}V}\right)^2\left(1-\frac{1}{n^2}\right)} \tag{3.28}$$

Note that $I_{tr} = I_{AC}$ when $V_{CO} = 0$. The variation of $\frac{I_{tr}}{I_{AC}}$ as a function of n for different values of $r\left(=\frac{V_{CO}}{\sqrt{2}V}\right)$ are shown in Fig. 3.9. It is to be noted that $I_{tr} < I_{AC}$ for all values of $\sin\alpha \neq 0$.

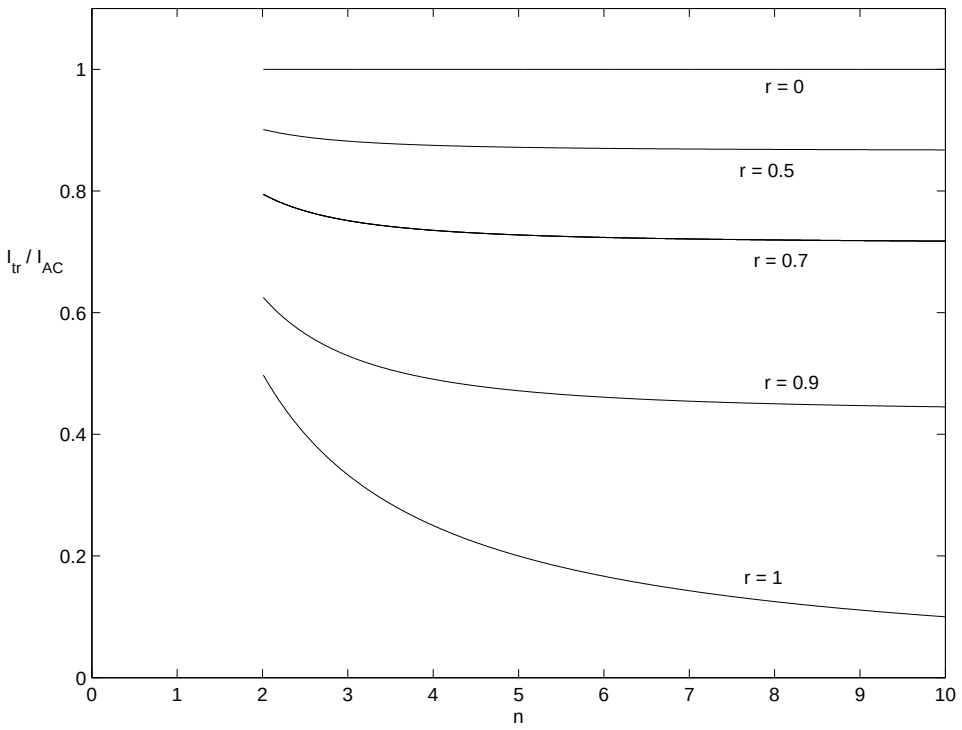

Figure 3.9: Plot of I_{tr}/I_{AC} as a function of n for different values of r

Switching Strategy 2 ($V_{CO} > 0.75\sqrt{2}V$)

Here, the capacitor is switched on when the supply voltage is at peak. At this instant

$$\cos\alpha = 0 \tag{3.29}$$

I_{tr} can be obtained as

$$I_{tr} = n\left[\frac{n^2-1}{n^2}\frac{V_{CO}}{\sqrt{2}V} - 1\right] I_{AC} \tag{3.30}$$

The variation of $\left|\frac{I_{tr}}{I_{AC}}\right|$ as a function of n for different values of r is shown in Fig. 3.10. It is to be noted that the two expressions (3.28) and (3.30) are identical for $V_{CO} = \sqrt{2}V$. Also, for $V_{CO} = \sqrt{2}V\frac{n^2}{n^2-1}$, $I_{tr} = 0$ for strategy 2. For low values of r, the transients are high. As a practical scheme for TSC firing, the two strategies can be combined as follows. If $V_{CO} < \sqrt{2}V$, adopt strategy 1, otherwise adopt strategy 2. This is equivalent to the firing scheme when v_T is minimum. (The thyristor that is forward biased is fired first. The subsequent firings are equidistant).

Although the precharging of capacitors can eliminate the transients,

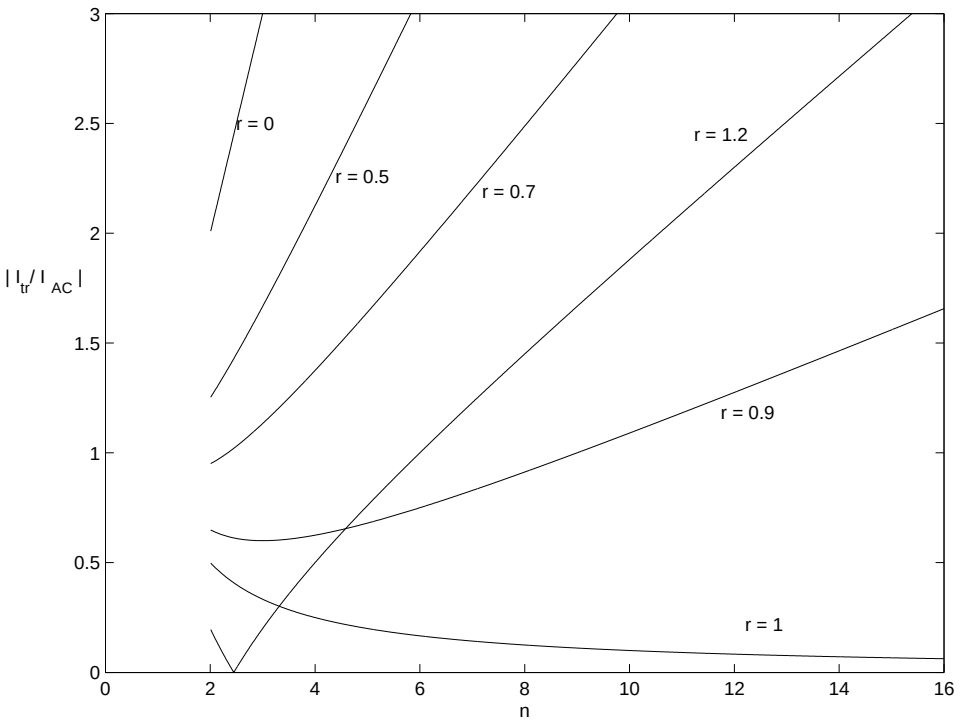

Figure 3.10: Plot of I_{tr}/I_{AC} as a function of n for different values of r

this method is not used in the application of TSC for power transmission lines.

It is to be noted that when the thyristor is switched off, the capacitor has peak value of the supply voltage across it as the capacitor current becomes zero at that instant. The voltage across the thyristor switch reaches a value of twice the peak voltage when the supply voltage reverses its sign and reaches a maximum. The capacitor voltage decays slowly depending on the losses in the circuit. Thus, the thyristors in the TSC have to be rated for twice the peak voltage ($2\sqrt{2}V$) whereas the thyristors in a TCR are rated for the peak voltage ($\sqrt{2}V$).

Since the TSC continues to conduct when the capacitor is on, there is no blocking voltage (across the thyristor) available to energize the thyristor electronics of an optoelectronic gating system (where the gating command from the ground potential is sent through the optical fibres to the thyristor level). However, this is not a problem as a current transformer is provided as the second source of energy.

3.3 SVC Controller

The block diagram of basic SVC Controller incorporating voltage regulator is shown in Fig.3.11. This shows that both voltage (V_{SVC}) and current (I_{SVC}) signals are obtained from potential and current transformers and then rectified. The AC filter is basically a notch filter to eliminate the signal component of frequency corresponding to the parallel resonance in the system viewed from the SVC bus. The line capacitance (in parallel with SVC capacitance) can result in parallel resonance with the line inductance. The SVC voltage regulator has a tendency to destabilize this resonant mode of oscillation and the notch filter is aimed at overcoming this problem. As a matter of fact, any parallel resonance mode (of frequency below second harmonic) can have adverse interaction with SVC voltage regulator. If series capacitors are used along with SVC, then they can cause parallel resonance with a neighbouring shunt reactor. If the second (parallel resonance) mode has a lower frequency (say below 20 Hz), a high pass filter in addition to the notch filter has been suggested [23].

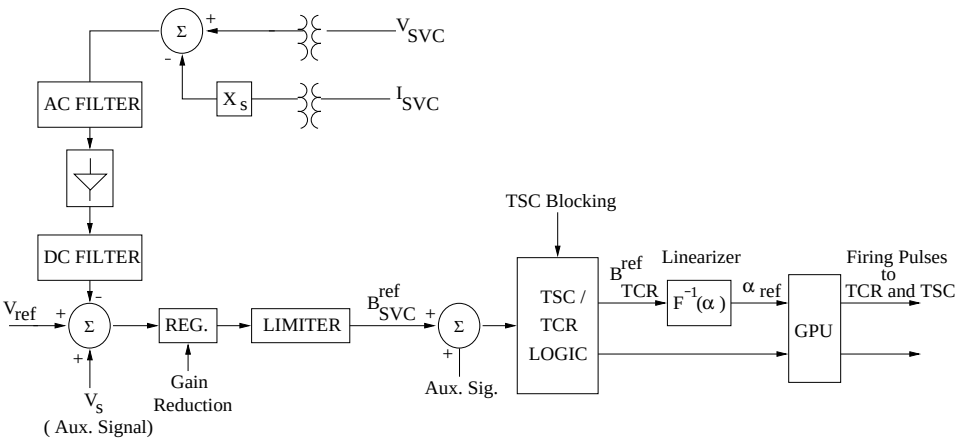

Figure 3.11: SVC Controller

The rectified signal is filtered. The DC side filters include both a low pass filter (to remove the ripple content) and notch filters tuned to the fundamental and second harmonic components. The notch filters are provided to avoid the adverse interactions of SVC caused by second harmonic positive sequence and fundamental frequency negative sequence voltages on the SVC bus. For example, second harmonic positive sequence voltages at the SVC bus cause a fundamental frequency component in the rectified signal that results in the modulation of SVC susceptance at the same frequency. This in turn (due to amplitude modulation) results in two components at side band frequencies (0,2f) in the SVC current. The dc component can result in unsymmetric saturation of the SVC transformer and consequent increase in

the magnetization current containing even harmonics. It has been observed that this adverse harmonic interactions between the SVC and the network can result in large distortion of the SVC bus voltage and impaired operation of SVC (termed as second harmonic instability).

The auxiliary signals mentioned in Fig.3.11 are outputs from the Susceptance (or reactive power) Regulator (SR) and Supplementary Modulation Controller (SMC). The Susceptance Regulator is aimed at regulating the output of SVC in steady state such that the full dynamic range is available during transient disturbances. The output of Susceptance Regulator modifies the voltage reference V_{ref} in steady state. However its operation is deliberately made slow such that it does not affect the voltage regulator function during transients.

In contrast to the Susceptance Regulator, the Supplementary Modulation Controller (SMC) is designed to improve the performance of SVC during transient conditions and not affect the steady state. SMC has control input using appropriate signal obtained from local measurements and provide a limited output at either the summing junction before the voltage regulator or after it. Thus, it modulates directly either the SVC bus voltage or susceptance in order to damp oscillations and improve stability.

The gate pulse unit for SVC produces firing pulses for TCR and TSC. The logic determines whether a TSC is to be switched in or out. B_{TCR}^{ref} is calculated from B_{SVC}^{ref} and if $B_{TCR}^{ref} \leq 0$, then a TSC is switched in. If $B_{TCR}^{ref} \geq B_L$, then a TSC is switched out. In computing B_{TCR}^{ref} from B_{SVC}^{ref} the effect of leakage reactance of the step down transformer is to be considered as B_{SVC} is given by

$$B_{SVC} = -\frac{B_\sigma(B_C - B_{TCR})}{B_C - B_{TCR} - B_\sigma} = \frac{B_C - B_{TCR}}{(1 - \frac{B_C - B_{TCR}}{B_\sigma})} \tag{3.31}$$

where B_C is the capacitance of the fixed capacitor or TSC. $B_\sigma = \frac{1}{X_\sigma}, X_\sigma$ is the leakage reactance of the transformer. If $B_\sigma \gg B_C$ or B_{TCR} then,

$$B_{SVC} \simeq (1 + \frac{B_C}{B_\sigma})B_C - [1 + \frac{(2B_C - B_L)}{B_\sigma}]B_{TCR} = C_1 - C_2 B_{TCR} \tag{3.32}$$

B_L is the reciprocal of X_L and is the maximum value of TCR susceptance. Neglecting leakage reactance of the transformer, the variation of B_{TCR} with variation of B_{SVC} for a case with two identical TSC's is shown in Fig.3.12. This shows that B_L (the rating of TCR) is slightly larger than the rating of either TSC and there is hysteresis in the operation of the TSC. This is desirable as the switching of a TSC is not well defined if B_{C1}(susceptance of a TSC) is exactly equal to B_L. If B_{C1} is greater than B_L, then the operation of the SVC is degraded.

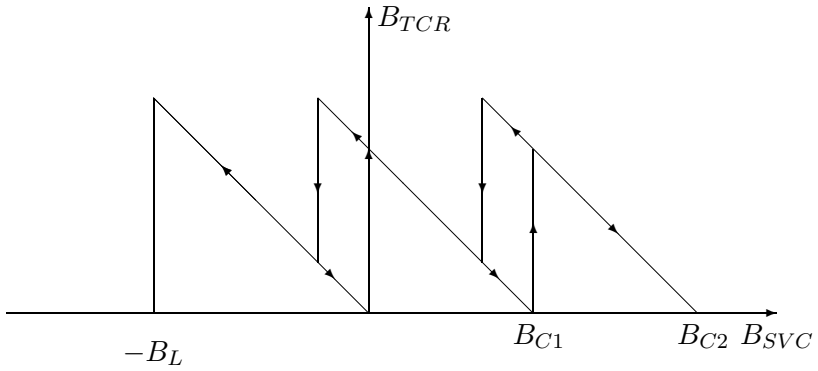

Figure 3.12: Variation of B_{TCR} with B_{SVC} for TSC-TCR type SVC

For stability studies, it is not essential to model GPU. In this case, the modelling of the controller shown in Fig.3.11 can be simplified greatly by also assuming that SVC does not generate harmonics. The block diagram of the controller in this case is shown in Fig.3.13. Here the voltage regulator is typically a PI controller as shown in Fig.3.14. The proportional gain (K_P) may be set zero unless a faster response is required. The transfer function $H_m(s)$ represents a low pass filter as given below:

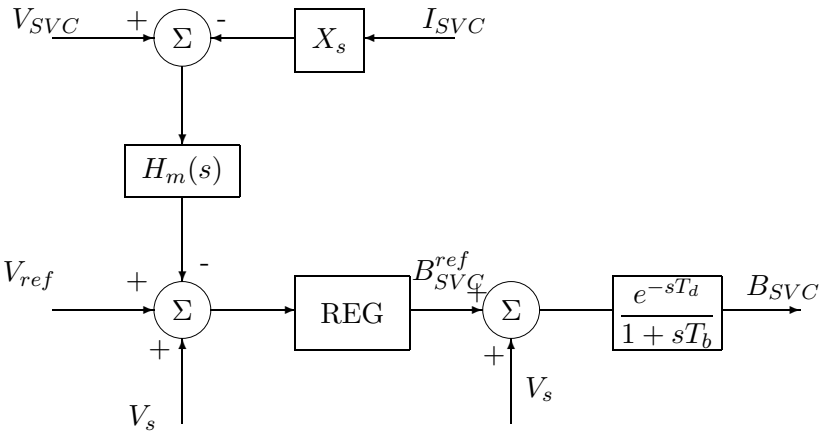

Figure 3.13: Block Diagram of SVC Voltage Control

First order LP filter:

$$H_m(s) = \frac{1}{1 + sT_m} \tag{3.33}$$

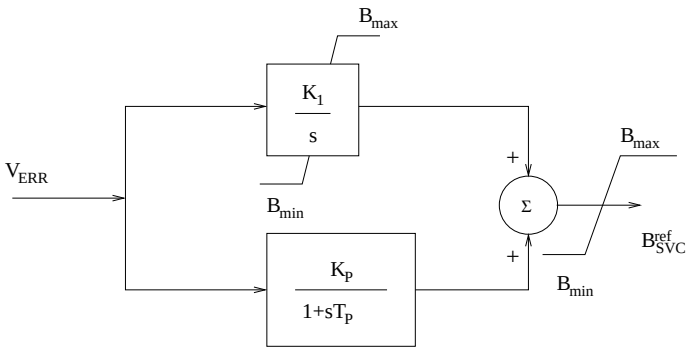

Figure 3.14: Voltage Regulator for SVC

Second order LP filter:

$$H_m(s) = \frac{1}{1 + 2s\zeta T_m + (sT_m)^2} \tag{3.34}$$

T_m is typically 2 to 3 ms and $\zeta = 0.7$.

The transport delay, T_d is typically

$$T_d = \frac{T}{12} \tag{3.35}$$

where T is the period of the supply voltage. T_d arises due to the discrete nature of the firing pulse. T_b represents the average delay in getting B_{SVC} from the instant of delivering the order and is given by

$$T_b = \frac{T}{4} \tag{3.36}$$

It is to be noted that T_b represents maximum (average) delay when the B_{TCR}^{ref} changes from maximum (B_L) to zero.

In Fig.3.11 or Fig.3.13, the current signal I_{SVC} is used to provide a positive slope for the control characteristic of SVC. However the current signal contains harmonics and there are measurement problems particularly when I_{SVC} is close to zero (the normal operating point) . A solution to this problem is to take the signal from B_{SVC}^{ref} instead of I_{SVC}.

In this case, the block diagram of Fig.3.13 can be simplified as shown in Fig.3.15. Here, assuming $K_P = 0$,

$$K_R = \frac{1}{X_s} \tag{3.37}$$

and

$$T_R = \frac{K_R}{K_I} \tag{3.38}$$

K_R (typically) varies from 20 to 100, whereas T_R varies between 20 to 150 ms.

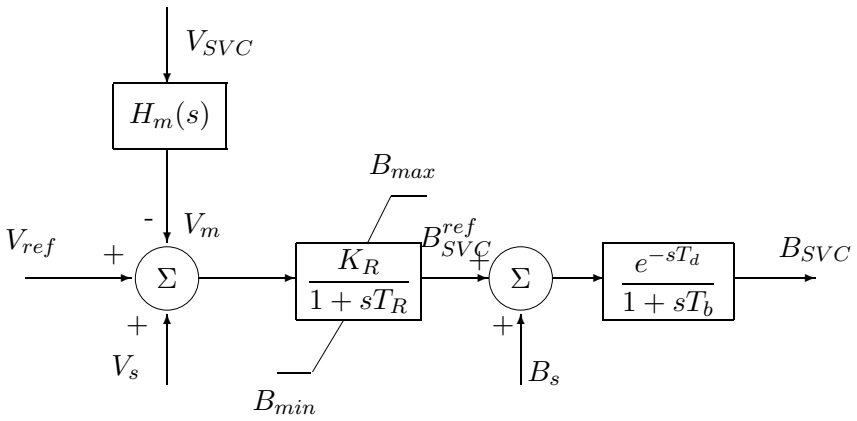

Figure 3.15: Simplified Block Diagram of SVC Voltage Control

Control Instability and Gain Supervisor [21]

The transfer function between change in the SVC susceptance ΔB_{SVC} and the change in the SVC voltage ΔV_{SVC} is independent of frequency if only fundamental component of V_{SVC} is considered. Assuming the operating voltage at SVC bus as unity, then

$$\Delta V_{SVC} \simeq X_{Th} \Delta B_{SVC} \tag{3.39}$$

The loop gain of the control system shown in Fig.3.15 depends on X_{Th}. The speed of the response depends on the loop gain and increases as X_{Th} is increased. However for high values of X_{Th} the system can be unstable. The voltage regulator of SVC is designed to provide the fastest response corresponding to a contingency condition at which X_{Th} is maximum (in the range of operating conditions considered) or the short circuit level at the SVC bus is minimum. However, during abnormal conditions resulting in tripping of several transmission lines in the system, X_{Th} will be higher than the design value and the SVC controller can be unstable. In such cases, it is necessary to reduce the gain of SVC (K_I) automatically by detecting instability. This is called as gain supervisor. The gain is restored to the normal value when the instability is not present. It is to be noted that although instability can be avoided by designing the voltage regulator gain corresponding to the lowest value of short circuit level (highest value of X_{Th}) this is not an optimal choice as the response of SVC will be slower under normal conditions.

The transfer function ($\frac{\Delta V_{SVC}}{\Delta B_{SVC}}$) is in general, a function dependent on frequency if network (electromagnetic) transients are considered. The magnitude of the transfer function is maximum at frequency, f_r defined by

$$f_r = f_{Np} - f_o \tag{3.40}$$

where f_{Np} is the frequency corresponding to the parallel resonance in the network and f_o is the operating frequency.

The controller gain will be severely restricted even under normal conditions if f_r is within the controller bandwidth. Hence the practical solution to this problem is to provide a notch filter in the controller (on the input side) as mentioned earlier.

Susceptance Regulator (SR)

A typical SR is shown in Fig.3.16. Here the output of the voltage regulator, B_{SVC}^{ref} and a set reference B_{SVC}^{set} are compared. If the error exceeds a threshold, it activates an integrator after an adjustable time delay (of the order of several seconds). The integrator output is hard limited by a non-wind up limiter and modifies the voltage reference.

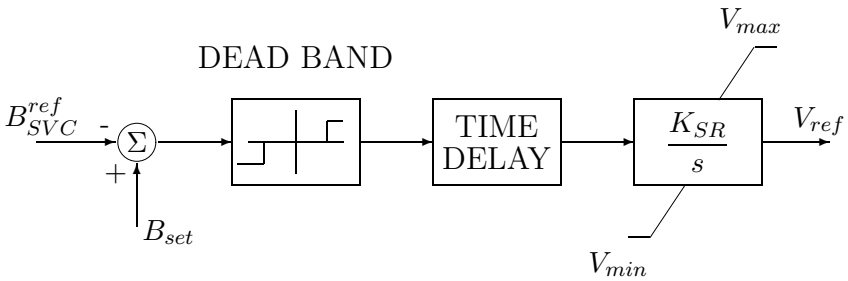

Figure 3.16: Susceptance Regulator

The SR has to be coordinated with other reactive power controllers in the vicinity such as HVDC converter control, switched capacitor and reactor banks, tap changing transformers etc.

Supplementary Modulation Controller (SMC) [11,19,20,25]

This controller modulates either V_{SVC} or B_{SVC} by processing a signal obtained from local measurements. The objective is to damp critical low frequency inter area or local modes that can affect stability during disturbances. The control signals are selected on the basis of following criteria

1. The signal should predominantly contain the mode that needs to be damped.
2. The controller design based on a particular control signal should be simple and reject noise.
3. The controller should not destabilize modes that are otherwise stable.

4. The controller should be effective and robust under widely varying operating conditions.

The control signals that have been used or suggested include: (1) line current (2) active and reactive power (3) bus frequency (4) Computed Rotor Frequency (CRF) and (5) Computed Thevenin voltage. The last two signals are synthesized from current and voltage measurements at the SVC location.

A typical controller configuration of SMC is shown in Fig.3.17. The washout circuit is designed to drive the SMC output to zero during steady state. The gain and phase compensation of SMC are chosen such that it improves the system response under a wide variety of operating conditions and different types of disturbances.

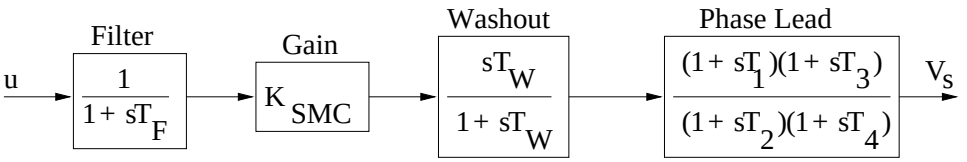

Figure 3.17: Block Diagram of SMC

Protective Functions of SVC control

The SVC control also has functions to provide protection under faulted or overload conditions that may affect the equipment or system response. These are listed below.

1. Undervoltage Strategy

The SVC is ineffective under low voltage conditions due to faults in the system. However, the clearing of the fault can result in temporary overvoltages due to load rejection, particularly under weak system conditions. The response of the SVC required immediately after the fault clearing is opposite of the normal voltage regulator function during a fault. To avoid delay in the required response of the SVC, the normal voltage regulator action is deactivated when voltage falls below a threshold (say 60% of the normal voltage). TSC is blocked and B_{SVC}^{ref} is frozen at the previous value (prior to the voltage dip). The normal SVC regulator action is resumed after the voltage climbs above a certain threshold (say 70%) and remains (above the threshold) there for sometime (say 30 ms). The blocking of TSC also helps in reducing the transient by preventing the capacitor discharge.

2. TCR Overcurrent Limiter

Under high voltage conditions, the SVC will be at its inductive limit and the TCR current may exceed its rated value. To protect the thyristor valves used in TCR, it is necessary to limit the current through it by phase control. To avoid interaction with voltage regulator function, a time delay is introduced (of the order of 100 ms). The overcurrent limiter takes into account the short-term overload capability of the TCR.

3. SVC Control Interactions at Subsynchronous Frequencies [15,26]

The SVC voltage regulator can adversely affect the damping of the subsynchronous frequency torsional modes due to turbine-generator rotors and elastic shafts (constituting a lightly damped mass-spring-damper system). Unlike in the case of fixed series capacitors, the Torsional Interaction (TI) problem with SVC is not very significant. It has been suggested that the use of low pass filter or Transient Gain Reduction (TGR) in conjunction with the voltage regulator is adequate to overcome the problem.

3.4 Voltage Regulator Design – Some Issues

3.4.1 Speed of Response as Function of ESCR

As mentioned in the previous section, the voltage regulator is of PI (Proportional - Integral) type. Neglecting limiters, measurement and transport delays, the voltage regulator loop can be simplified as shown in Fig.3.18. Here, the transfer function $\frac{\Delta V_{SVC}(s)}{\Delta B_{SVC}(s)}$ is assumed to be a static gain (K_N), neglecting the network dynamics.

The expression for K_N is obtained from the equivalent circuit shown in Fig.3.19. It is to be noted that the operating values of the SVC susceptance (B_{SVCO}) is considered as part of the network and X_{Th} is calculated at the operating point. The SVC bus voltage (V_{SVC}) is obtained from Fig.3.19 as

$$V_{SVC} = \frac{V_{Th}}{(1 - X_{Th}\Delta B_{SVC})} \simeq V_{Th}(1 + X_{Th}\Delta B_{SVC})$$

From the above, we get ΔV_{SVC} as

$$\begin{aligned} \Delta V_{SVC} = V_{SVC} - V_{Th} &= V_{Th}X_{Th}\Delta B_{SVC} \\ &= K_N \Delta B_{SVC} \end{aligned} \tag{3.41}$$

where

$$K_N = V_{Th}X_{Th} \tag{3.42}$$

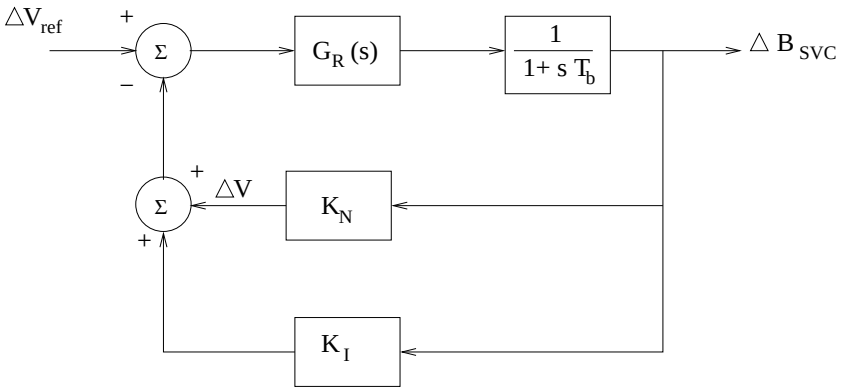

Figure 3.18: Simplified system block diagram

Assuming $V_{Th} \simeq 1.0$, we can also write

$$K_N \simeq X_{Th} = \frac{1}{ESCR} = \frac{Q_{SVC}}{S_C} \tag{3.43}$$

The Effective Short Circuit Ratio (ESCR) is defined as the ratio of the short circuit level to the rating of the SVC. In defining ESCR it is assumed that the operating value of B_{SVC} is merged with the network admittance in computing the short circuit level (in MVA).

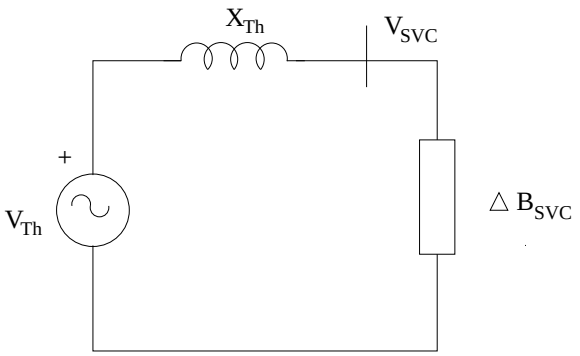

Figure 3.19: An equivalent circuit

In Fig. 3.18, the feedback from I_{SVC} is obtained as $K_I \Delta B_{SVC}$. This follows from the relation

$$-X_s \Delta I_{SVC} = X_s \Delta B_{SVC} = K_I \Delta B_{SVC} \tag{3.44}$$

In deriving (3.44) it is assumed that $V_{SVC} \simeq 1.0$ and $B_{SVCO} = 0$ in linearizing Eq. (3.3).

The transfer function of the voltage regulator (G_R) is assumed as

$$G_R(s) = K_C \left(\frac{1 + sT_C}{sT_C} \right) \tag{3.45}$$

By selecting $T_C = T_b$ and $K_C = \frac{1}{2(K_I + K_{Nmax})}$ where K_{Nmax} corresponds to the operating point with lowest value of ESCR, we get a regulator with fast response with good margin of stability. The closed loop transfer function $[G_c(s)]$ is obtained as

$$G_c(s) = \frac{\Delta V_{SVC}(s)}{\Delta V_{ref}(s)} = \frac{K_N}{K_N + K_I} \left(\frac{1}{1 + sT_w} \right) \tag{3.46}$$

where

$$T_w = \frac{2(K_I + K_{Nmax})}{(K_I + K_N)} T_b \tag{3.47}$$

As K_N increases to K_{Nmax}, T_w reduces to a value of $2T_b = \frac{T}{2}$ (10 ms for the nominal frequency of 50 Hz). For a step input in ΔV_{ref}, the variation in ΔV_{SVC} is given by

$$\Delta V_{SVC}(t) = \frac{K_N}{K_N + K_I} \Delta V_{ref} (1 - e^{-t/T_w}) \tag{3.48}$$

The response time (to reach 95% of the final value) is $3T_w$. The fastest response time for the minimum value of ESCR is 30 ms (for the 50 Hz system).

Remarks

1. The response of the SVC slows down as the ESCR increases. This is fortunately not a major problem as the speed of SVC is not critical for strong systems.

2. The choice of the regulator gain (K_C) is dependent on the minimum value of ESCR considered. If too small a value of ESCR is considered (corresponding to loss of several lines in the network), this can lead to a sluggish response of the SVC in normal operating conditions. It is realistic to choose credible contingencies in determining minimum value of ESCR.

If, under abnormal conditions, the ESCR goes below the design value (selected in the determination of the regulator gain) there is a possibility of the controller instability (as the control delays cannot be ignored in practice and higher gains result in instability with a pair of complex eigenvalues crossing imaginary axis). The controller instability can be avoided by the installation of the gain supervisor which automatically reduces the gain as it detects sustained or growing oscillations in the output of the voltage regulator.

Example 3.2

The voltage regulator of a SVC is designed for an ESCR of 2.0. If the slope of the control characteristics is 0.05 p.u., determine the transfer function of the regulator. If the operating value of ESCR is 5.0, what is the response time (to reach 95% of the final value) and the steady state change in the SVC voltage if V_{ref} is increased by 0.05 p.u. Assume the system frequency to be 50 Hz.

Solution

From Eq. (3.45), the transfer function of the voltage regulator is

$$G_R(s) = \frac{K_C(1 + sT_C)}{sT_C}$$

where $T_C = T_b = \frac{T}{4}$,

$$K_C = \frac{1}{2(K_I + K_{N\max})}, \quad K_N \simeq \frac{1}{ESCR}$$

Since the design value of ESCR is 2.0,

$$K_{N\max} = \frac{1}{2.0} = 0.5, \quad K_C = \frac{1}{2(0.05 + 0.5)} = 0.909 p.u$$

Note that the output of the voltage regulator is B_{SVC}^{ref} in per unit.

The response time is $3T_w$ where T_w is given by Eq. (3.47)

$$T_w = \frac{2(K_I + K_{N\max})}{(K_I + K_N)} T_b$$

For ESCR = 5, $K_N \simeq 0.2$, $K_I = 0.05$, $T_w = 4.4T_b$. For 50 Hz system, $T_b = \frac{T}{4} = 5$ ms. The response time is 66 ms (increased from 30 ms at ESCR = 2.0).

The steady state change in V_{SVC} is given by Eq. (3.48) as

$$\begin{aligned} \Delta V_{SVC} = \frac{K_N}{K_N + K_I} \Delta V_{ref} &= \frac{0.2}{0.25} \times 0.05 \\ &= 0.04 p.u. \end{aligned}$$

3.4.2 Control Interaction with Network Resonance

It was mentioned in the previous section that any parallel resonance mode (of frequency below the second harmonic) can result in adverse interactions with the voltage regulator. In James Bay system involving shunt compensation of

the 735 kV line, a 90 Hz frequency component is critical and a notch filter is provided in the voltage measuring circuit [36]. This problem is generic in all SVC installations used for compensating high voltage transmission lines. A possible explanation for this phenomenon is given in [44] and is reproduced below.

Consider a simplified system as seen from the terminals of the static shunt compensator (shown in Fig. 3.20).

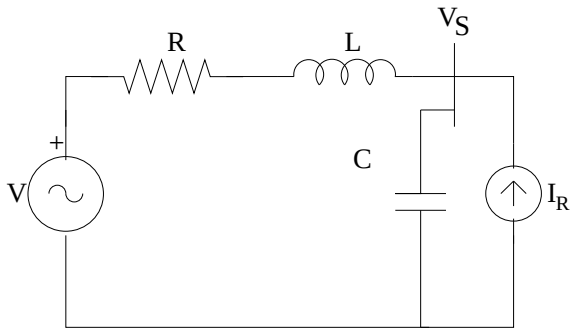

Figure 3.20: A simplified representation for interaction with network resonance

The positive sequence driving point impedance $Z_{Th}(s)$ in the Laplace domain, at the SVC bus is given by

$$Z_{Th}(s) = \frac{(R + sL)}{(s^2LC + sRC + 1)} \tag{3.49}$$

The equations in the D-Q (synchronously rotating reference frame) variables are given by

$$\begin{bmatrix} V_{SD}(s) \\ V_{SQ}(s) \end{bmatrix} = \begin{bmatrix} Z_{DD}(s) & Z_{DQ}(s) \\ Z_{QD}(s) & Z_{QQ}(s) \end{bmatrix} \begin{bmatrix} I_{RD}(s) \\ I_{RQ}(s) \end{bmatrix} \tag{3.50}$$

where

$$Z_{DD}(s) = Z_{QQ}(s) = \frac{Z_{Th}(s + j\omega_0) + Z_{Th}(s - j\omega_0)}{2} \tag{3.51}$$

$$\begin{aligned} Z_{QD}(s) = -Z_{DQ}(s) &= j\frac{Z_{Th}(s + j\omega_0) - Z_{Th}(s - j\omega_0)}{2} \\ &= -Im[Z_{Th}(s + j\omega_0)] \end{aligned} \tag{3.52}$$

The D-Q components of the SVC bus voltage (V_S) and current (I_R) are shown in Fig. 3.21.

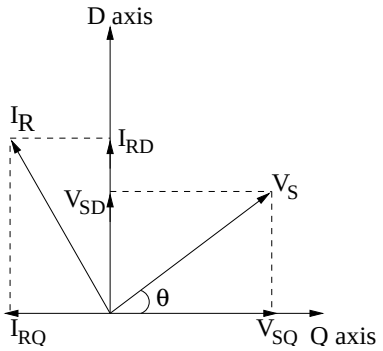

Figure 3.21: A phasor diagram

From Fig.(3.21), we have

$$V_{SD} = V_S \sin\theta, \quad V_{SQ} = V_S \cos\theta \tag{3.53}$$

From Eq. (3.53), we get

$$\Delta V_S = \sin\theta_0 \Delta V_{SD} + \cos\theta_0 \Delta V_{SQ} \tag{3.54}$$

If we assume that the current injected by the SVC is purely reactive, we have

$$I_{RQ} = -I_R \sin\theta, \quad I_{RD} = I_R \cos\theta \tag{3.55}$$

From Eq. (3.55), we get

$$\begin{aligned} \begin{bmatrix} \Delta I_{RD}(s) \\ \Delta I_{RQ}(s) \end{bmatrix} &= \begin{bmatrix} \cos\theta_0 \\ -\sin\theta_0 \end{bmatrix} \Delta I_R(s) + I_{Ro} \begin{bmatrix} -\sin\theta_0 \\ -\cos\theta_0 \end{bmatrix} \Delta\theta(s) \\ &= \begin{bmatrix} \cos\theta_0 \\ -\sin\theta_0 \end{bmatrix} \Delta I_R(s) \end{aligned} \tag{3.56}$$

We have assumed $I_{Ro} = 0$ as before. Linearizing Eq. (3.50), and substituting from (3.54) and (3.56), we get

$$\frac{\Delta V_S(s)}{\Delta I_R(s)} = Z_{QD}(s) = \frac{KN(s)}{D(s)} \tag{3.57}$$

where $N(s)$ and $D(s)$ are the numerator and the denominator polynomials, where

$$\begin{aligned} K &= (\omega_0 L)\omega_n^2 \\ D(s) &= [s + \sigma + j(\omega - \omega_0)][s + \sigma - j(\omega - \omega_0)] \\ &\quad \times [s + \sigma + j(\omega + \omega_0)][s + \sigma - j(\omega + \omega_0)] \\ N(s) &= s^2 + 2\frac{R}{L}s + \frac{R^2}{L^2} + \omega_0^2 - \frac{1}{LC} \\ \sigma &= \frac{R}{2L}, \quad \omega = \sqrt{\omega_n^2 - \sigma^2}, \omega_n = \frac{1}{\sqrt{LC}} \end{aligned}$$

When $R \simeq 0$, then

$$N(s) \simeq s^2 + \omega_0^2 - \frac{1}{LC} = s^2 + \omega_0^2 - \omega_n^2 \tag{3.58}$$

Since $\omega_n > \omega_0$, the numerator polynomial $N(s)$ has a pair of real zeros given by

$$s = \pm\sqrt{\omega_n^2 - \omega_0^2} \tag{3.59}$$

Thus, the transfer function $\frac{\Delta V_s(s)}{\Delta I_r(s)}$ is a non-minimum phase type with a zero in the R.H.P. (on the positive real axis). The control of plants with non-minimum phase type is always problematic and requires compensation to enable the use of P-I control with high gains.

Remarks

1. The four poles of the transfer function $\frac{\Delta V_S(s)}{\Delta I_R(s)}$ all lie in the L.H.P. and are given by

$$p_1, p_2 = -\sigma \pm j(\omega - \omega_0), \quad p_3, p_4 = -\sigma \pm j(\omega + \omega_0)$$

where $-\sigma \pm j\omega$ are the poles of the impedance function $Z_{Th}(s)$.

2. For $R \simeq 0$, it can be shown that the transfer function reduces to

$$\frac{\Delta V_S(s)}{\Delta I_R(s)} \simeq \frac{(\omega_0 L)\omega_n^2(s^2 - \omega_n^2 + \omega_0^2)}{[s^2 + (\omega_n - \omega_0)^2][s^2 + (\omega_n + \omega_0)^2]} \tag{3.60}$$

Substituting for $s = 0$, we get

$$\frac{\Delta V_S}{\Delta I_R} = -X_{Th} \tag{3.61}$$

where

$$X_{Th} = \frac{\omega_0 L}{1 - \omega_0^2 LC} = \frac{(\omega_0 L)}{\omega_n^2 - \omega_0^2}\omega_n^2$$

is the reactance of the parallel combination of L and C, evaluated at the operating frequency ω_0. Eq. (3.61) can be compared with Eq. (3.41) as $I_R = I_{SVC} = -B_{SVC}V_{SVC}$. As it is assumed that $I_{Ro} = 0$, $V_{SVCo} = V_{Th}$ (Note that the subscript 'o' indicates the operating value of the variable).

The adverse control interactions with network resonance are functions of the ESCR and the operating point. The lower value of ESCR and the SVC operation at capacitive region worsen the control stability problem. The controller gain needs to be reduced to overcome the problem. This may not be practical as the response of SVC needs to be fast at lower values of ESCR. One of the solution suggested in [44] is to provide a compensator

in cascade with the voltage regulator, that rejects the complement of the network resonance frequency component. The transfer function of the compensator is assumed to be

$$G_{comp}(s) = \frac{(s+\sigma_1)^2 + \omega_r^2}{(s+\sigma_2)^2 + \omega_r^2} \tag{3.62}$$

where $\sigma_1 < \sigma_2$. This transfer function represents a notch filter that rejects the component of frequency of ω_r. By arranging $\omega_r = \omega_n - \omega_0$, the interaction between the network resonance (of frequency ω_n) and the controller can be avoided. It is to be noted that a frequency of ω_n in the AC voltage is transformed to a frequency of ω_r after demodulation in the voltage measurement circuit.

Example 3.3

A voltage regulator with the transfer function $G_R(s) = -\frac{K_i}{s}$ is used to control the reactive current injected into the static compensator bus. The plant (system) transfer function is given by Eq. (3.57) (Note the gain is assumed to be negative as the reactive current has opposite sign to that of the SVC susceptance).

(a) Plot the root loci as K_i varies from zero to a high value

(b) Repeat (a) if a compensator with a transfer function given in Eq. (3.62) is connected in cascade with the voltage regulator

Data: $\omega_0 = 377$ rad/sec, $\omega_0 L = 0.5$, $R = 0.05$, $\omega_n = 1.5\omega_0$, $\sigma_1 = 30$, $\sigma_2 = 300$.

Solution

The root loci for case (a) is shown in Fig. 3.22(a). The root loci for the case (b) is shown in Fig. 3.22(b).

It is interesting to observe that without the compensator, the system becomes unstable when $K_i > 33.7$. The provision of the compensator increases the value of instability gain to 978. In this case, two complex roots cross imaginary axis at $\omega = 292$ rad/sec.

The provision of the compensator in the voltage control system is an alternative to providing a notch filter (tuned to ω_n) on the AC side, before the voltage input signal is demodulated using a rectifier.

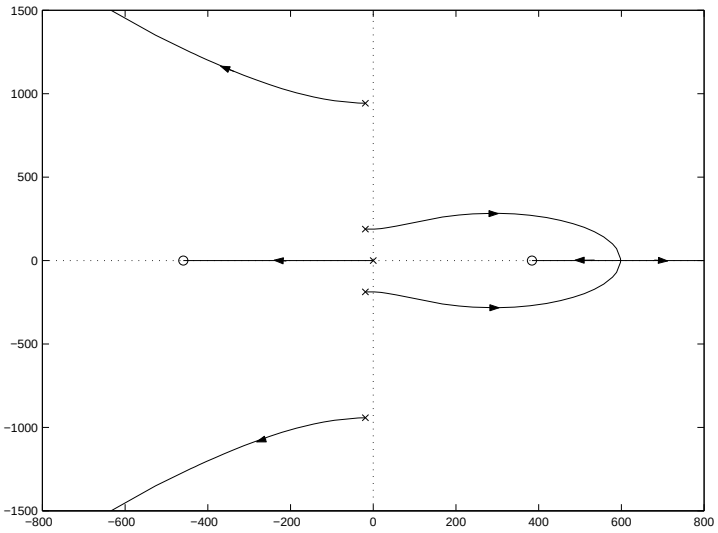

(a) Without compensator

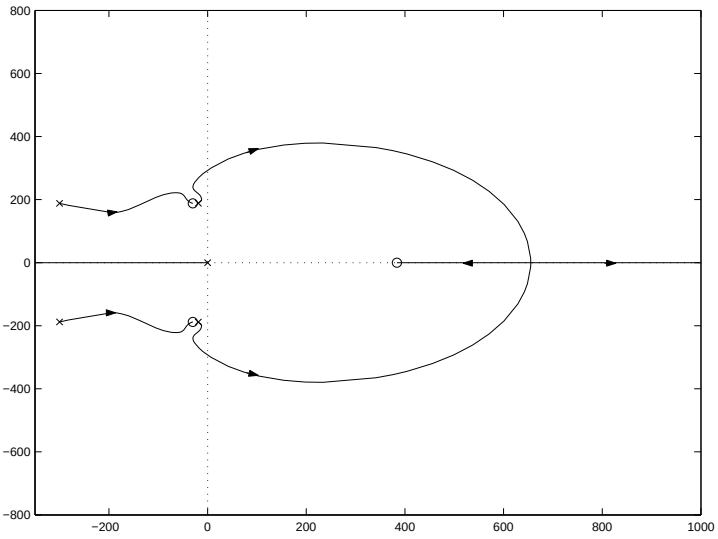

(b) With compensator

Figure 3.22: Root loci

3.5 Harmonics and Filtering

3.5.1 General

The harmonics in a SVC are generated by the TCR. Neither TSC or TSR (Thyristor Switched Reactor) generate harmonics. The current harmonics

generated by TCR can be classified into two categories:

1. Characteristic harmonics which are the harmonics present under ideal conditions such as sinusoidal, balanced AC voltages, equidistant firing pulses, and identical values of impedances in the three phases.
2. Uncharacteristic harmonics are the result of non-ideal conditions such as
   (a) Unbalanced AC voltages, also containing harmonics
   (b) Tolerances of short circuit impedances of the step-down transformer
   (c) Tolerances of reactors
   (d) Asymmetry of the firing angles in the phases
   (e) Asymmetry of the firing angle for positive and negative half cycles of one phase.

The non-characteristic harmonics are usually less than $\frac{1}{10}$ of the characteristic harmonics for $\Delta L = 5\%$, $\Delta\alpha = 1^\circ$ (ΔL is the tolerance in the reactors, $\Delta\alpha$ is the deviation in the firing angle from equidistant pulse control). However, these non-characteristic harmonics cannot be neglected. For example, a small dc component present in the SVC current (due to firing angle asymmetry) can drive the connecting transformer into saturation resulting in large harmonic voltages at the SVC bus.

3.5.2 Harmonic Interactions

A major concern is the possibility of harmonic interactions with the AC network (Note that this is a separate phenomenon from what was discussed in the previous section regarding control instability). The problem of harmonic magnification (of low order such as second or third) has been viewed by some as 'harmonic instability' in the past. The harmonic interactions with the network can arise from the following factors.

(a) Direct: Effects due to the harmonics present in the bus voltage. These harmonics influence the harmonics in the TCR current which in turn affect the harmonic distortion in the bus voltage. Normally such effects are secondary unless the impedance seen by the TCR current is very high.

(b) Through voltage regulation loop: The modulation of the TCR admittance at frequency f_c, results in the frequencies, $f_0 \pm f_c$ at the SVC bus which are picked up by the voltage measuring circuit and may be amplified. This problem can be solved by providing notch filters in the control circuit. To eliminate the possibility of magnification of

(positive sequence) second and third harmonics, filters at the fundamental frequency (f_0) and second harmonic ($2f_0$) are provided. The voltage unbalance can result in second harmonics on the dc side and third harmonic on the ac side.

(c) Through gate pulse synchronization: Although the gate pulses are equidistant in normal steady state, during network faults, there can be firing angle asymmetries that result in harmonics. In general, gate pulse synchronization should be insensitive to the presence of harmonics in the bus voltage.

3.5.3 Harmonic Filters

The presence of harmonics (both current and voltage) is viewed as 'pollution' affecting the operation of power systems. The injection of current harmonics by nonlinear loads also results in the distortion of the voltage waveforms due to the system impedances. The adverse effects of the harmonics include

1. Harmonic over voltages, particularly during a transient which can also be sustained due to inrush current phenomena in transformers.
2. Increased losses in shunt capacitor banks and rotating machines whose impedances are much lower at harmonic frequencies than at system frequency
3. Telephone interference

The single-tuned shunt filters are commonly applied to eliminate harmonic currents injected by SVCs. The configuration of the single tuned filter is shown in Fig. 3.23(a) and its impedance characteristics are shown in Fig. 3.23(b). The normalized impedance $\left(\frac{Z}{X_r}\right)$ magnitude and its phase angle (ϕ) are given by

$$\frac{Z}{X_r} = \left[\left(\frac{R}{X_r}\right)^2 + \left(\frac{f}{f_r} - \frac{f_r}{f}\right)^2\right]^{1/2} \tag{3.63}$$

$$\phi = \tan^{-1}\left[\frac{X_r}{R}\left(\frac{f}{f_r} - \frac{f_r}{f}\right)\right] \tag{3.64}$$

where

$$f_r = \frac{1}{2\pi\sqrt{LC}}, \quad X_r = \sqrt{\frac{L}{C}}$$

In FC-TCR type SVC, the fixed capacitor branches can also be designed to operate as tuned filters by inserting a reactor with appropriate Q factor. Double tuned and damped high pass filters are also used as filters.

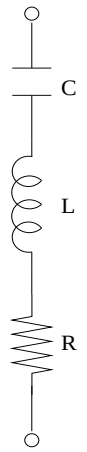

(a) Configuration

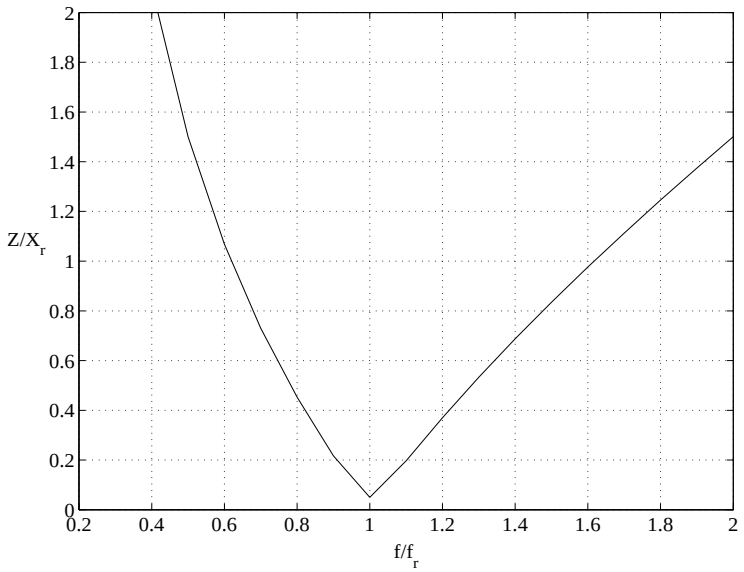

(b) Impedance characteristics

Figure 3.23: Single tuned filter

The filter design is based on the specification of various performance indices.

1. Voltage distortion factor (D_n) at n^{th} harmonic

$$D_n = \frac{V_n}{V_1},$$

where V_n is the rms voltage at frequency $f = nf_0$.

2. Total harmonic (voltage) distortion factor (THD)

$$THD = \frac{1}{V_1}\sqrt{\sum_{n=2}^{N} V_n^2}$$

N is the highest harmonic order considered.

3. IT product

$$IT = \sqrt{\sum_{n=1}^{\infty}(k_f p_f I_n)^2}$$

$k_f = 5nf_0$, p_f = weighing factor.

4. Telephone Interference Factor (TIF)

$$\begin{aligned} TIF &= \frac{1}{V}\sqrt{\sum_{n=1}^{\infty}(k_f p_f V_n)^2} \\ V &= \sqrt{\sum_{n=1}^{\infty} V_n^2} \end{aligned}$$

The equivalent circuit used to evaluate the effectiveness of the filter is shown in Fig. 3.24.

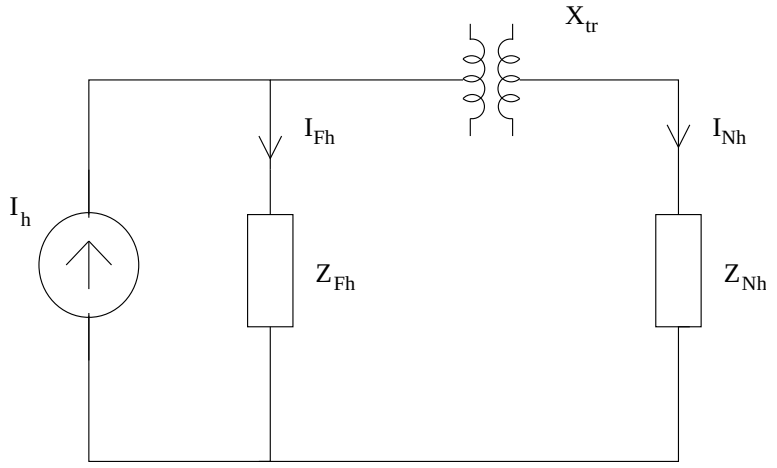

Figure 3.24: Equivalent circuit for the filter design

The ratio $\left(\frac{I_{Nh}}{I_h}\right)$ is given by

$$\frac{I_{Nh}}{I_h} = \frac{Z_{Fh}}{|Z_{Fh} + Z_{Nh} + jX_{tr}|} = \frac{Z}{|Z_{Nh} + jX_{tr}|} \tag{3.65}$$

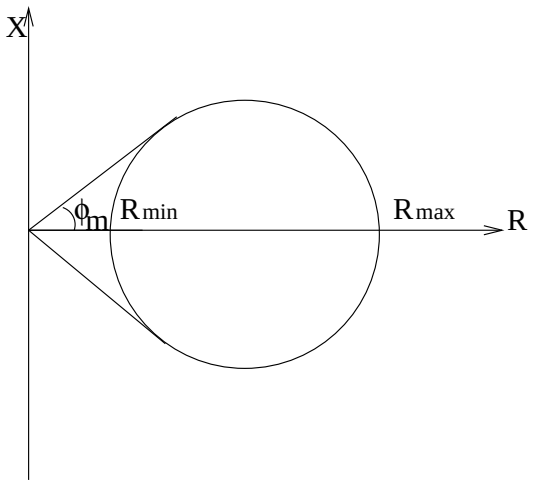

Figure 3.25: Region of system impedance

X_{tr} is the leakage reactance of the step-down transformer and Z in the effective impedance seen by the TCR (the parallel combination of the filter and the network).

The network impedance may not be known exactly at different frequencies. However, the region in which the system impedances (at different operating points and frequencies) are located is assumed to lie in a circle in the R-X plane with centre on the R-axis. The upper limit on the impedance angle is also specified. A typical region is shown in Fig. 3.25.

3.5.4 A Mathematical Model for the Investigation of Harmonic Stability

This is illustrated by considering a single phase SVC as shown in Fig.3.26. The state vector $x(t)$ is defined by

$$x(t) = [i_t \; v_C \; i_s]^T \tag{3.66}$$

The source voltage $v(t)$ is assumed to be periodic with period T. When the thyristors are conducting ($i_t \neq 0$), the system equations are given below.

$$\dot{x}(t) = [A]x(t) + [B]v(t) \tag{3.67}$$

where

$$[A] = \begin{bmatrix} -\frac{R_t}{L_t} & \frac{1}{L_t} & 0 \\ -\frac{1}{C} & 0 & \frac{1}{C} \\ 0 & -\frac{1}{L_s} & -\frac{R_s}{L_s} \end{bmatrix}, \quad [B] = \begin{bmatrix} 0 \\ 0 \\ 1 \end{bmatrix}$$

When the thyristors are off, the system equations are

$$\dot{x}(t) = [PA]x(t) + [PB]v(t) \tag{3.68}$$

where $[P]$ is the projection matrix

$$[P] = \begin{bmatrix} 0 & 0 & 0 \\ 0 & 1 & 0 \\ 0 & 0 & 1 \end{bmatrix} \tag{3.69}$$

Note that $[PB] = [B]$.

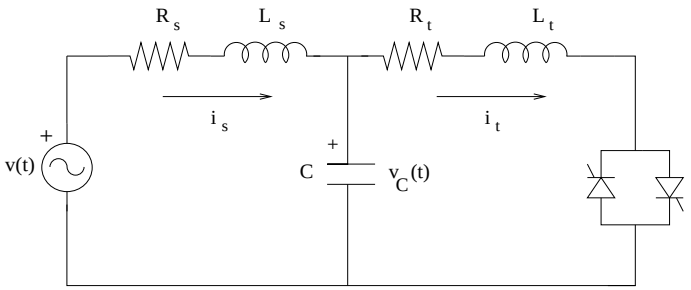

Figure 3.26: A single phase SVC system

Fig. 3.27 shows the evolution of the system dynamics from the state x_0 at t_0 to the state x_1 at $t = t_0 + T$. t_0 is the instant at which the thyristor switch closes and $\frac{\sigma_1}{\omega}$ is the conduction time in the forward (when the supply voltage is positive) direction of the current flow in TCR. Similarly, $\frac{\sigma_2}{\omega}$ is the conduction time of the TCR current in the reverse direction. (Note $\omega = \frac{2\pi}{T}$). t_h is the instant at which the thyristor is fired to allow conduction (Note that $t_h = t_0 + T_1$).

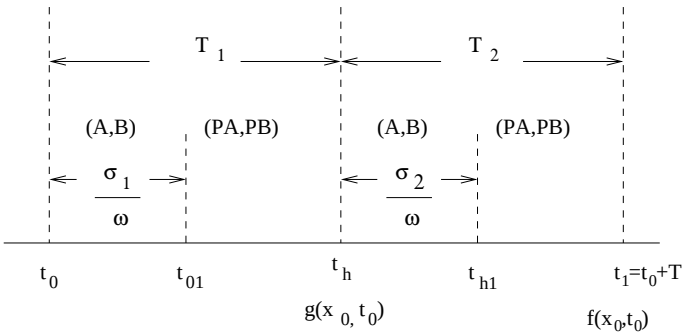

Figure 3.27: System dynamics from t_0 to $t_0 + T$

It is to be noted that normally, $\sigma_1 = \sigma_2 = \sigma$ and $T_1 = T_2 = \frac{T}{2}$ (with half wave odd symmetry).

The Poincare map f for a complete cycle is obtained by applying twice the map g for the half cycle operation from t_0 to t_h. The half cycle map g is obtained by integrating the two linear systems (3.67) and (3.68) in sequence. Thus,

$$\begin{aligned} g(x_0, t_0) &= \exp\left[PA\left(T_1 - \frac{\sigma_1}{\omega}\right)\right] \exp\left(A\frac{\sigma_1}{\omega}\right) \\ &\quad \left\{x_0 + \int_0^{\frac{\sigma_1}{\omega}} e^{-As} B v(s + t_0) ds\right\} \\ &\quad + \int_{\frac{\sigma_1}{\omega}}^{T_1} e^{PA(T_1 - s)} PB v(s + t_0) ds \end{aligned} \tag{3.70}$$

$$f(x_0, t_0, t_h) = g(g(x_0, t_0), t_h) \tag{3.71}$$

It is to be noted that $\frac{\sigma_1}{\omega}$ and $\frac{\sigma_2}{\omega}$ are obtained from the boundary conditions

$$i_t\left(t_0 + \frac{\sigma_1}{\omega}\right) = 0 \tag{3.72}$$

$$i_t\left(t_h + \frac{\sigma_2}{\omega}\right) = 0 \tag{3.73}$$

When the SVC is in steady state with a periodic trajectory of period T, the Poincare map f has a fixed point defined by

$$f(x_0, t_0, t_h) = x_0 \tag{3.74}$$

The stability of a periodic orbit of a nonlinear time-varying system is the same as the stability of the corresponding fixed point of the Poincare map. Thus, the stability of the periodic orbit can be computed from the Jacobian Df of the Poincare map f evaluated at the fixed point. The periodic orbit is stable if the eigenvalues of Df lie inside a unit circle. It can be shown that

$$Df(x_0, t_0, t_h) = e^{PA(T_2 - \frac{\sigma_2}{\omega})} P e^{A\frac{\sigma_2}{\omega}} e^{PA(T_1 - \frac{\sigma_1}{\omega})} P e^{A\frac{\sigma_1}{\omega}} \tag{3.75}$$

An interesting observation is that the Jacobian is identical to that obtained by treating σ_1 and σ_2 as constants. In other words, the Jacobian can also be obtained by considering the circuit shown in Fig. 3.26 described by a linear time-varying equations of the form

$$\dot{x} = [A(t)]x \tag{3.76}$$

$[A(t)]$ is assumed to be periodic with period T. The solution of (3.76) can be expressed as

$$x(t) = \Phi(t, t_0)x_0 \tag{3.77}$$

where

$$\Phi(t, t_0) = [G(t)e^{Kt}] \tag{3.78}$$

$[G(t)]$ is a periodic, bounded matrix. The stability of the system is determined from the location of the eigenvalues of the constant matrix $[K]$.

If $T_1 = T_2 = \frac{T}{2}$ and $\sigma_1 = \sigma_2 = \sigma$, then

$$[Df] = \left[e^{PA(\frac{T}{2}-\frac{\sigma}{\omega})} P e^{A\frac{\sigma}{\omega}}\right]^2 \tag{3.79}$$

The eigenvalues of $[Df]$ are the squares of the eigenvalues of $[Dg]$ which is given by

$$Dg(x_0, t_0) = \left[e^{PA(\frac{T}{2}-\frac{\sigma}{\omega})} P e^{A\frac{\sigma}{\omega}}\right] \tag{3.80}$$

An example given in [40] illustrates the theory described above. The data chosen is such that the system inductance (L_s) and the capacitor (C) has a resonance at $f_r = 4.9 f_0$. The connection of L_t in parallel raises the resonance frequency to 5.18 f_0 where f_0 is the fundamental system frequency (of the source voltage). This indicates that there are values of the conduction angle (σ) for which the circuit will be unstable.

3.6 Protection Aspects

All electrical equipment have to be designed to handle current and voltage stresses when subjected to overloads and faults or any abnormal incidents of transient nature. When the stresses exceed the ratings, it is essential to protect the equipment or the system against damage by providing adequate protection. SVC is no exception and one has to analyze the performance under faulted conditions to evaluate the stresses. In this section, the emphasis is placed on the thyristor valves that are used to switch a capacitor (TSC) or control the current in a reactor (TCR).

The faults that are related to thyristor valves (made up of a series string of bidirectional pair of thyristors) are:

(a) firing at the wrong instant (misfiring)

(b) lack of firing on the entire valve

(c) lack of firing on a single thyristor in a valve

(d) damaged thyristors in the valve.

Fortunately, the thyristors fail by creating a short circuit. Hence a valve (with some redundant thyristors) can continue to operate as long as the voltage rating across a device is not exceeded. Lack of firing in single thyristor can result in voltage stress across the thyristor even under normal conditions. By providing automatic firing of the thyristor using Break Over

Diode (BOD), it is possible to solve this problem. In general, there are monitoring circuits for thyristors which indicate the status of a thyristor.

The layout design of the equipment also helps in minimizing the probability of failures. For example, a TCR is divided into two sections with the thyristor valve connected in the middle of the two sections. This protects the valve against faults involving flash over across the reactor. The probability of both reactors sections being short circuited simultaneously is negligible.

In designing the protection scheme and the selection of component ratings, it is very important to know if the equipment is to be tripped or kept in operation when a certain fault occurs. In general, operation is maintained for:

(i) system faults if the stress encountered is lower than that for a specified worst case fault

(ii) single misfiring

(iii) loss of some thyristors in a valve

(iv) partial loss of auxiliaries.

The rating of an electrical equipment is related to the heating of the materials (primarily the insulation) and the damage caused by the temperature rise. (Actually, the absolute temperature determines the failure, which implies that the ambient temperature and the cooling arrangement affect the ratings). For modern thyristor valves, the circulation of deionized water through the cooling pipes in the heat sinks (normally made of aluminium) is the accepted norm. The water cooling of the thyristor devises is an efficient method that has replaced the air cooling practices in the earlier days. For thyristor devices, the junction temperature in a major parameter which affects its working. For temperatures below 120°C the device can withstand the specified voltage. The voltage withstand capability deteriorates as the junction temperature is increased and above 190°C, the device can fail.

The overload on a SVC occurs when the SVC bus voltage is high and it is operating in the inductive mode. The TCR current increases linearly as the voltage increases (after the conduction angle reaches the limit of 180°). To limit the overload on the thyristors it is necessary to provide a current limiter which implies that the conduction angle is reduced. However, as the junction temperature goes up beyond 120°C, the capacity to withstand voltage (when the thyristor valve is not conducting) decreases. Then it becomes essential to provide protective firing at point D (shown in Fig.3.28) and the V-I characteristics resume along line BC. If there is a possibility of the junction temperature exceeding 190°C, it is necessary to trip the SVC by opening the circuit breaker.

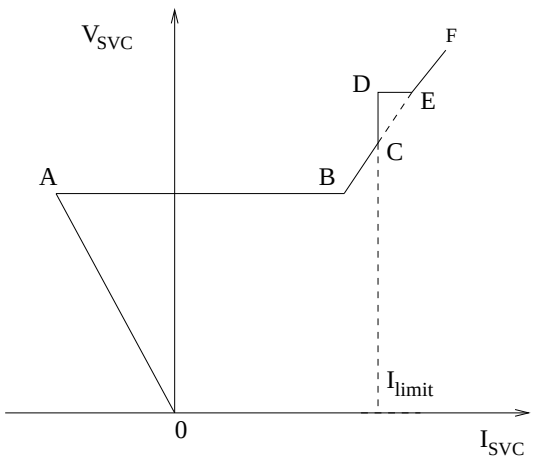

Figure 3.28: V - I characteristics showing current limit

The thyristor device has very limited capacity for temporary overloads. As a matter of fact, this capacity is built into the system by deliberately choosing the junction temperature below 120°C (say 80 to 90°C) at rated loads. The thermal model of the thyristor with the cooling system can be used to reliably predict the junction temperature for transient overloads. For the thyristor with the heat sinks shown in Fig.3.29, it is possible to develop an electrical R-C equivalent circuit shown in Fig.3.30. Here, R_{JC}, R_{CH} and R_{HW} represent the thermal resistances between the junction to case, case to heat sink and heat sink to water respectively. The capacitances represent the storage of heat in the junction, case and the heat sink. The power loss (generating heat) is viewed as a current source while the temperatures are equivalent to the bus voltages in the circuit. It is possible to estimate accurately the junction temperature rise for transient current stresses. The objective is to keep the junction below a maximum temperature limit by adjusting the prefault junction temperature.

The worst case current stress on TCR can be due to the following causes

(a) *Misfiring*: If the TCR is fired at $\alpha = 0^\circ$ (instead of in the range $90^\circ < \alpha < 180^\circ$), the current reaches to a peak of twice the normal value (under full conduction).

(b) *Short circuit across the reactor*: Since the reactor is usually split into two reactors (of equal size), the short circuit current is double the full load current.

(c) *AC system fault and its clearing*: If a three phase or a line to line fault occurs very close to the SVC and the clearing of the fault is accompanied by a temporary overvoltage, it is possible that after the fault

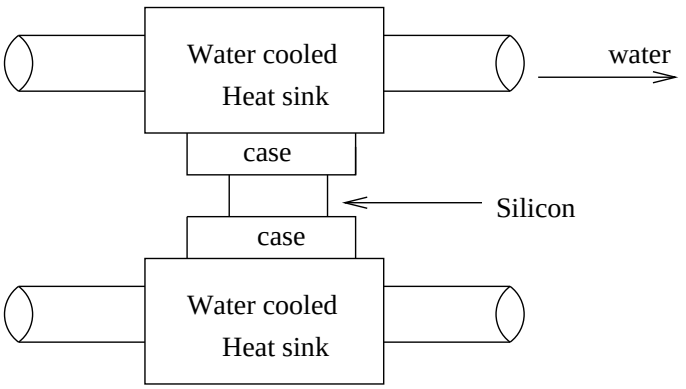

Figure 3.29: A thyristor with heat sink

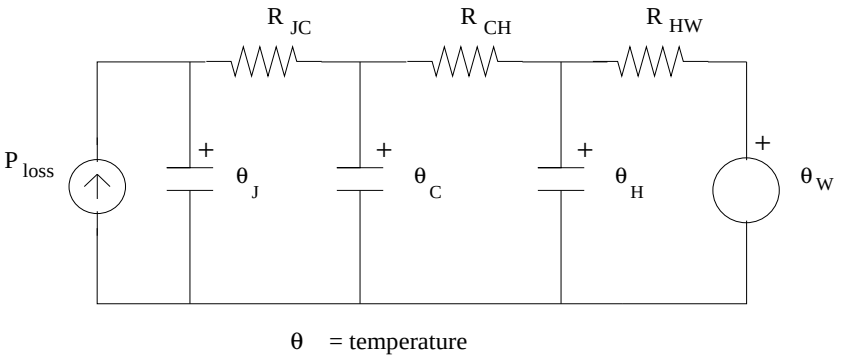

Figure 3.30: An electrical equivalent circuit of the thermal model

clearing, the current may build up to a large magnitude. However, this possibility assumes that the clearing occurs at a voltage zero, which is unlikely (Normally the fault is cleared at current zero). This condition results in the maximum current stress in the TCR.

The worst case current stress in a TSC occurs with misfiring at maximum system voltage. Fig. 3.31 shows the voltage and current waveforms in a TSC (a) under normal operation and (b) the worst case misfiring. A high current results due to the misfiring and the valve voltage rises to 4 times the peak value of the system voltage after blocking.

Voltage Ratings and Protection

The thyristor valve in a TCR is designed to withstand the maximum (specified) system voltage. However, this is not always the need, as TCR is expected to go into full conduction at overvoltages and this will ensure that the valves do not have to block the overvoltage. However, the current limits

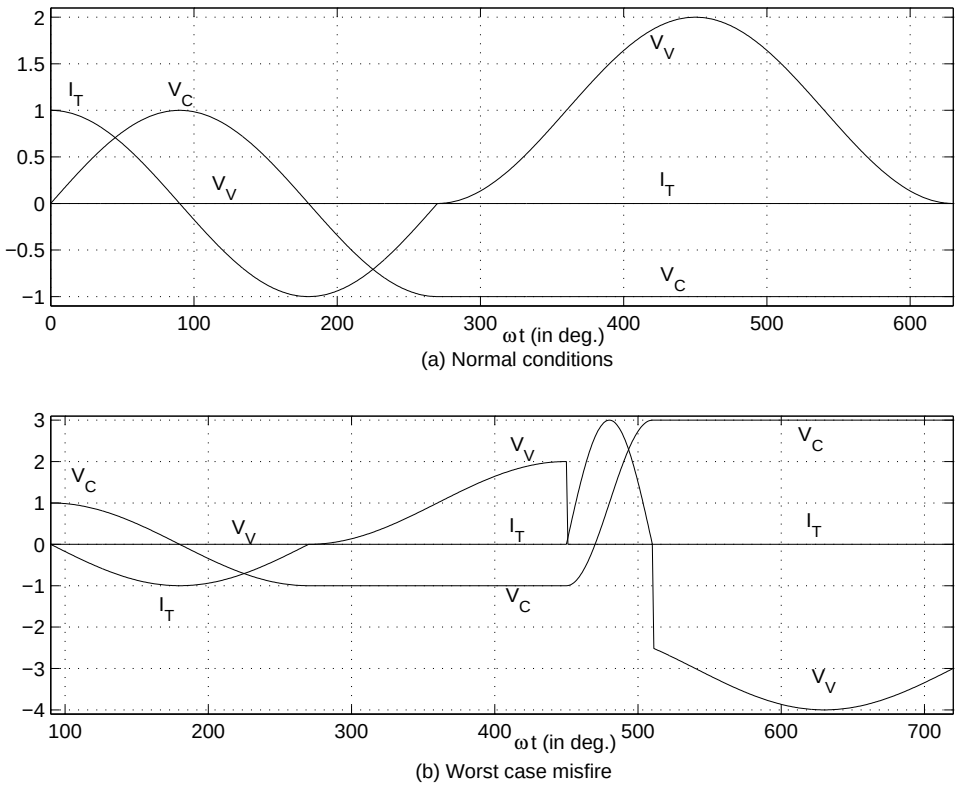

Figure 3.31: Voltage and current waveforms in a TSC

(mentioned earlier) in a TCR implies the necessity to block the system over voltages. A trade off is possible with the thyristor valve designed to withstand higher current stresses rather than higher voltage stresses. The cost and losses in a valve decrease if the voltage ratings are lower. On the other hand, the need for continuous conduction at higher voltages implies loss of controllability.

The TSC valve, in contrast to a TCR valve must be designed to block overvoltages as the TSC conduction will aggravate overvoltages. However, the overvoltage protection above the designed voltage rating is provided by the Metal Oxides Varistor (MOV) which is very effective in clipping the voltage above a certain limit. The energy loss in the surge arrester is an important factor in selecting the ratings.

The protection against overvoltages can be provided by either (a) BOD firing which convert a voltage stress into current stress or (b) MOV arrester absorbing energy.

3.7 Modelling of SVC

For a detailed study of SVC control interactions, it is necessary to perform transient simulation for which SVC is modelled in detail including the switching of the thyristor valves in TCR and TSC. The transient network is modelled by differential equations rather than algebraic equations [27-30].

However for stability study it is not necessary to consider the switching of valves and assume that SVC generates only fundamental current. In addition, the network transients are neglected and represented by algebraic equations of the type:

$$[Y]V = I \tag{3.81}$$

With these simplifications, SVC can be modelled as a variable susceptance which is the output of the control system as shown in Fig.3.13. If SMC is a part of the SVC controller, it should be included in the model. However, susceptance regulator, gain supervisor and the protective functions can be neglected in the model.

For the preliminary studies, it is adequate to ignore the dynamics of SVC control (without SMC) and assume that the SVC is described by its steady state control characteristics. If SMC is present, it can be modelled as shown in Fig. 3.17.

Steady State Model of SVC [32]

The steady state control characteristics are modelled by an equivalent circuit shown in Fig. 3.32. This shows a complex voltage source $\hat{E}_{SVC}$ in series with a reactance X_{SVC}. The losses in the SVC are neglected. The values of $\hat{E}_{SVC}$ and X_{SVC} are given below for the SVC operating in (i) the control range, (ii) capacitive limit and (iii) inductive limit

(i) Control Range

$$\hat{E}_{SVC} = V_{ref}\angle\phi_{SVC} \tag{3.82}$$

$$X_{SVC} = X_s \tag{3.83}$$

where ϕ_{SVC} is the angle of the SVC bus voltage. The control range applies when the SVC bus voltage lies in the range

$$\frac{V_{ref}}{1 + X_s B_{max}} < V_{SVC} < \frac{V_{ref}}{1 + X_s B_{min}} \tag{3.84}$$

where B_{min} and B_{max} are the limits of B_{SVC}. Note that B_{min} is, in general, negative (corresponding to the inductive limit) and $B_{max} = B_C$, where B_C is the total capacitive susceptance. (neglecting the transformer leakage reactance)

(ii) At Capacitive Limit :

$$\hat{E}_{SVC} = 0.0 + j0.0 \qquad X_{SVC} = -\frac{1}{B_{max}} \tag{3.85}$$

(iii)At inductive Limit :

$$\hat{E}_{SVC} = 0.0 + j0.0 \qquad X_{SVC} = -\frac{1}{B_{min}} \tag{3.86}$$

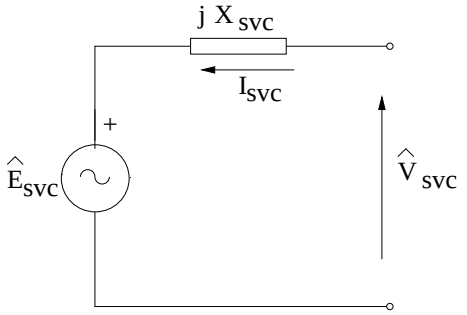

Figure 3.32: Equivalent circuit of SVC

The equivalent circuit of SVC for the control range is nonlinear (since the angle of $\hat{E}_{SVC}$ depends on the bus voltage) and is time varying when the limits are considered. Thus, in general, the inclusion of SVC model in transient stability simulation, involves iterative network solution. However, with nonlinear voltage dependant static load models in the system, the handling of SVC is no more complicated than the handling of nonlinear loads.

If only one SVC is to be considered, the network solution with SVC can be considerably simplified by applying compensation theorem. In this approach, the SVC is treated as a time varying current source which can be computed from the solution of a simple network shown in Fig.3.33. Here, the network external to the SVC is modelled by a time-varying Thevenin equivalent. If the network impedances are constant, Z_{eq} remains constant. Z_{eq} is calculated as the impedance of the network seen at the SVC terminals when all the sources in the network are removed (the voltage sources are shorted and the current sources are open circuited). $\hat{V}_{eq}$ is found as the SVC terminal voltage with the SVC current zero. $\hat{V}_{eq}$ varies with time as the generator voltages vary during a disturbance.

From Fig.3.33, the SVC current can be computed as

$$\hat{I}_{SVC} = \frac{\hat{V}_{eq} - \hat{E}_{SVC}}{Z_{eq} + jX_{SVC}} \tag{3.87}$$

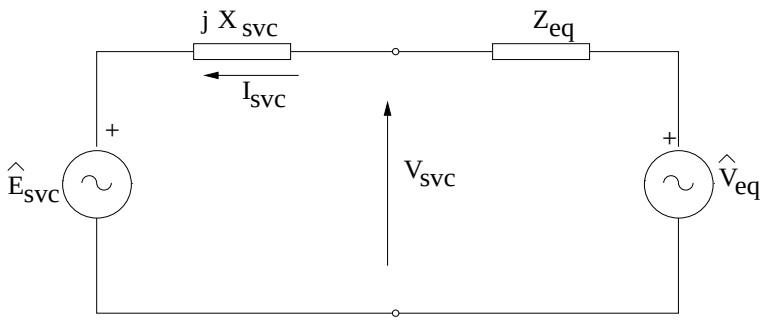

Figure 3.33: SVC connected to Thevenin equivalent

If $\hat{E}_{SVC} = 0.0 + j0.0$,the solution is straight forward. However, in the control range, the angle ϕ_{SVC} needs to be known to apply Eq.(3.87).

It can be shown that $\tan\phi_{SVC}$ is obtained as the solution of a quadratic equation given by

$$a\tan^2\phi_{SVC} + b\tan\phi_{SVC} + c = 0 \tag{3.88}$$

where

$$\begin{aligned} a &= x^2 - z^2\sin^2\alpha, \\ b &= -2xy, \\ c &= y^2 - z^2\sin^2\alpha \\ x &= Re[(1-\hat{A})\hat{V}_{eq}], \quad y = Im[(1-\hat{A})\hat{V}_{eq}] \\ z &= |\hat{A}|V_{ref} \\ \hat{A} &= A\angle\alpha = \frac{Z_{eq}}{Z_{eq} + jX_{SVC}} \end{aligned}$$

Network Solution

The network solution is carried out in two steps. In the first step, the voltage solution is obtained by putting $\hat{I}_{SVC} = 0$. The voltage calculated at the SVC bus, at the end of the first step is same as $\hat{V}_{eq}$. The knowledge of $\hat{V}_{eq}$ and Z_{eq} (which has been calculated in advance and stored) enables the computation of $\hat{I}_{SVC}$ from Eq. (3.87) and Eq.(3.88) (if required).

The network is solved again with the injection of $\hat{I}_{SVC}$ at the SVC bus (all other sources put equal to zero).The second solution requires minimal computations as the current vector is sparse.

The voltage at all the buses are obtained from the addition (superposition) of the two sets of the voltage calculated in the two network solutions.

Remarks

1. It is assumed, in the calculation of Z_{eq}, that the generators have no dynamic saliency. Dynamic saliency results in time varying impedance of the stator (with respect to the network or common synchronously rotating reference frame). Also, the generator impedance needs to be expressed as a $2 * 2$ matrix in D-Q axes. In this case, it can be shown that ϕ_{SVC} is obtained from solving a quartic equation.
2. Z_{eq} changes whenever there is change in the network configuration.
3. If Z_{eq} is purely reactive (inductive) impedance, then ϕ_{SVC} is the phase angle of $\hat{V}_{eq}$, which is known. This eliminates the need for the solution of Eq. (3.88).
4. The appropriate solution of ϕ_{SVC} obtained from Eq. (3.88) is the one which is closer to the phase angle of $\hat{V}_{eq}$.

3.8 Applications of SVC

The major application of SVC is for rapid voltage regulation and control of dynamic (temporary) overvoltages caused by load throw off, faults or other transient disturbances. The dynamic reactive control at the load bus increases power transfer and can solve the problem of voltage instability (collapse) caused by contingency conditions.

It is to be noted that steady state voltage regulation can be achieved by mechanically switched capacitors and reactors (MSC and MSR). However, fast voltage regulation is required to prevent instability under transient conditions. Thus, generally, a SVC is operated with minimum reactive power output under normal conditions. This is achieved by the Susceptance Regulator described earlier which ensures that full dynamic range is available for control under contingency conditions.

The fast controllability provided by the thyristor switches can be also utilized to improve system stability (both transient and small signal). The use of auxiliary damping controllers can help damp low frequency, interarea power oscillations that can appear at stressed operating conditions (involving high loading of tie lines). The design of such damping controllers for shunt and series FACTS controllers will be taken up separately in Chapter 10.

The location of SVC is an important issue. If the objective is to compensate a long transmission line, the SVC is to be located at the midpoint of the line (if a single SVC is to be used). For very long lines, multiple SVC at regular intervals can be applied. For example, if two SVCs are to be used, one is located at a distance $\frac{d}{3}$ from the sending end while the other is located

at a distance, $\frac{d}{3}$ from the receiving end (d is the length of the line). When SVCs are applied to improve the power transfer in a transmission network, the location can be determined by the sensitivity of voltage at the critical buses with respect to the reactive power injection ($\Delta V_i/\Delta Q_j$). In general, it can be stated that a bus with low short circuit level can be a candidate bus. Incidentally a synchronous condenser can raise the fault level while providing controllable reactive power. It is to be noted that a SVC does not raise the fault level which can be a blessing as the requirement of the fault current interruption capability of circuit breakers does not go up. On the other hand, for reactive power control at HVDC converter stations with low Short Circuit Ratios (SCR), the synchronous condenser improves voltage regulation and system performance.

However, a SVC has several advantages over SC (synchronous condenser) namely,

(a) Faster response under transient conditions

(b) There are no moving parts, hence requires less maintenance

(c) There are no problems of loss of synchronism

(d) As mentioned earlier, a SVC doe not contribute to short circuit currents.

The drawbacks of a SVC are mainly related to the injection of current harmonics. These can be minimized by segmented TCR (with several segments/modules of TCR connected in parallel) and operating all except one module in the TSR (Thyristor Switched Reactor) mode.

The preparation of specification of a SVC, the design and testing of the controller requires detailed studies involving power flow, short circuit and stability analysis in addition to studies involving a TNA (Transient Network Analyzer) or RTDS (Real Time Digital Simulator). The steady state control (V-I) characteristics are defined by the SVC rating (in MVAR), range of the reference voltage (V_{ref}) (typically from 0.95 pu to 1.05 pu) and the slope (varying from 2% to 10%). The slopes can be different in the capacitive and inductive modes of operation. The range of short circuit levels at the SVC bus is also an important parameter in the choice of the voltage regulator gain.

In the past, saturable reactors have been applied in situations when temporary overvoltages can be a critical factor. However, in recent times, Thyristor Controlled Transformer (TCT) where the leakage reactance of the step down transformer can be used to replace the reactor has been suggested to provide controllable shunt reactors in long EHV transmission lines. The cost considerations will determine whether such innovations will be applied in practice.

References and Bibliography

1. T.J.E. Miller, **Reactive Power Control in Electric Systems**, John Wiley (New York), 1982.
2. L.Gyugyi, "Power Electronics in Electric Utilities: Static Var Compensators", Proc. IEEE, v. 76, n.4, 1988, pp.483-494
3. A.Olwegard et al, "Improvement of Transmission Capacity by Thyristor Controlled Reactive Power", IEEE Trans., v. PAS-100, 1981, pp.3930-3939.
4. L.Gyugyi, "Reactive Power Generation and Control by Thyristor Circuits" IEEE Trans., v. IA-15, n.5, 1979, pp.521-531
5. R.M. Mathur, Editor, **Static Compensators for Reactive Power Control**, Canadian Electrical Association, Cantext Publications, Winnipeg, 1984
6. K.R.Padiyar and R.K.Varma, "Concepts of Static Var System Control for Enhancing Power Transfer in Long Transmission Lines", Electric machines and Power Systems, v.18, 1990, pp.337-358
7. M. O'Brien and G.Ledwich, "Static Reactive Power Compensator Controls for Improved System Stability", IEEE Proc., v.134, Pt.c, n.1, 1987, pp.38-42
8. A.E.Hammad, "Analysis of Power System Stability Enhancement by Static Var Compensators", IEEE Trans., v.PWRS-1, n.4, 1986, pp.222-227
9. K.R. Padiyar and R.K. Varma, "Damping Torque Analysis of Static Var System Controllers", IEEE Trans., Power Systems, v.6, n.2, 1991, pp.458-465
10. E.Lerch, D.Povh and L.Xu, "Advanced SVC Control for Damping Power Systems Oscillations", IEEE Trans. on Power Systems, vol. 6, n. 2, 1991, pp.524-535
11. K.R.Padiyar and R.K.Varma, "Static Var System Auxiliary Controllers for Improvement of Dynamic Stability", Int. J. of Electrical Power and Energy Systems, v.12, n.4, 1990, pp.287-298
12. R.L.Lee, M.J. Beshir, A.T. Finley, D.R Hayes, J.C. Hsu, H.R. Peterson, G.L.Deshazo and D.W. Gerlach, "Application of Static Var Compensators for the Dynamic Performance of the Mead-Adelanto and Mead-Phoenix Transmission Projects", IEEE Trans. on Power Delivery, v.10, n.1, 1995, pp.459-466
13. T.H.Putman and D.G. Ramey, "Theory of Modulated Reactance Solution for Subsynchronous Resonance", IEEE Trans., v.PAS-101, n.6, 1982, pp.1527-1535

14. O. Wasynczuk, "Damping Subsynchronous Resonance Using Reactive Power Control", IEEE Trans., v. PAS-100, n.3, 1981, pp.1096-1104

15. K.R.Padiyar and R.K.Varma, "Static Var System Auxiliary Controllers for Damping Torsional Oscillations", Int. J. of Electrical Power and Energy Systems, v.12, n.4, 1990, pp.271-286

16. G.Romegialli and H.Beeler, "Problems and Concepts of Static Compensator Control", Proc. IEE, v.128, Pt.C, n.6, 1981, pp.382-388

17. D. Dickmander, B. Thorvaldsson, G. Stromberg, D. Osborn, A. Poitras and D. Fisher, "Control System Design and Performance Verification for the Chester, Maine Static Var Compensator", IEEE Trans. on Power Delivery, v.7, n.3, 1992, pp.1492-1503

18. IEEE Special Stability Controls Working Group, "Static Var Compensator Models for Power Flow and Dynamic Performance Simulation", IEEE Trans. on Power Systems, v.9, n.1, 1994, pp.229-240

19. E.Larsen, N. Rostamkolai, D. Fisher and A. Poitros, "Design of a Supplementary Modulation Control Function for the Chester SVC", IEEE Trans. on Power Delivery, v.8, n.2, 1993, pp.719-724

20. E.V.Larsen, K.Clark, A.T. Hill, R.J. Piwko, M.J. Beshir, M.Bhuiyan, F.J.Hormozi and K. Braun, "Control Design for SVC's on the Mead-Adelanto and Mead-Phoenix Transmission Project", IEEE Trans. on Power Delivery, v.11, n.3, 1996, pp.1498-1506

21. J. Belanger, G. Scott, T. Andersson and S.Torseng, "Gain Supervisor for thyristor Controlled Shunt Compensators", CIGRE, Paper 38-01, 1984

22. E.V.Larsen, D.H. Baker, A.F. Imece and L.Gerin-Lajoie, "Basic Aspects of Applying SVC's to Series-Compensated AC Transmission Lines", IEEE Trans. on Power Delivery , v.5, n.3, 1990, pp.1466-1473

23. L.Gerin-Lajoie, G.Scott, S.Breault, E.V.Larsen, D.H. Baker and A.F Imece, "Hydro-Quebec Multiple SVC Application Control Stability Study", IEEE Trans. on Power Delivery, v.5, n.3, July 1990, pp.1540-1551

24. A.J.P. Ramos and H.Tyll, "Digital Performance of a Radial Weak Power System with Multiple Static Var Compensators", IEEE Trans. on Power Systems, v.4, n.4, 1989, pp.1316-1323

25. K.R.Padiyar and P. Rajashekaram, C. Radhakrishna and M.A. Pai "Dynamic Stabilization of Power Systems through Reactive Power Modulation", Electric Machines and Power Systems, v.11, 1986, pp.281-293

26. N.Rostamkolai et al, "Subsynchronous Torsional Interactions with Static Var Compensators - Concepts and Practical Implications", IEEE Trans. on Power Systems, v.5, n.4, 1990, pp.1324-1332

27. A.M. Gole and V.K Sood , "A Static Compensator Model for Use with Electromagnetic Transients Simulation Programs", IEEE Trans. on Power Delivery, v.5, n.3, 1990, pp-1398-1417

28. S.Lefebvre and L.Gerin-Lajoie, "A Static Compensator Model for the EMTP", IEEE Trans. on Power Systems, v.7, n.2, 1992, pp-477-486

29. S.Y.Lee, S. Bhattacharya, T. Lejonberg, A. Hammad and S.Lefebvre, "Detailed Modelling of Static Var Compensators Using the Electromagnetic Transients Program (EMTP)", IEEE Trans. on Power Delivery, v.7, n.2, 1992, pp.836-847

30. R.H. Lasseter and S.Y. Lee, "Digital Simulation of Static Var Transients", IEEE Trans., v.PAS-101, n.10, 1982, pp.4171-4177

31. D.A. Woodford, "Electromagnetic Design Considerations for Fast Acting Controllers", 95 SM 414-3, PWRD.

32. K.R.Padiyar, **Power System Dynamics -Stability and Control**, John Wiley (Singapore), 1996

33. R.T. Byerly, D.T. Poznaniak and E.R. Taylor Jr. "Static Reactive Compensation for Power Transmission Systems", IEEE Trans. on Power Apparatus and Systems, v. PAS-101, n. 10, October 1982, pp. 3997-4005.

34. M.H. Baker, H.L. Thanawala, D.J. Young and I.A. Erinmetz, "Static Var Compensators Enhance a Meshed Transmission System", Paper 14/37/38-03, CIGRE, 1992.

35. O. Hauge, P. Meringdal, H. Frank and K. Engberg, "The 360 MVAR Static Compensator in Hasle, Norway, Paper 31-10, CIGRE, 1982.

36. D. McGillis, N. Hien Huynh and G. Scott, "Role of Static Compensation Meeting AC System Control Requirements with Particular to the James Bay System", IEE Proc. v. 128, Pt.C. n.6, November 1981, pp. 389–393.

37. M. Nayebzadeh, H.J. Haubrich, D. Povh, G. Guth and W. Dietel, "Applications of Static Var Compensators in Extended Power Systems", Paper 38-105, CIGRE, 1994.

38. L.J. Bohmann and R.H. Lasseter, "Equivalent Circuit for Frequency Response of a Static Var Compensator", IEEE Trans. on Power Systems. v. PWRS-1, n.4, Nov. 1986, pp. 68-74.

39. L.J. Bohmann and R.H. Lasseter, "Harmonic Interactions in Thyristor Controlled Reactor Circuits", IEEE Trans. on Power Delivery, v. 4, n.3, July 1989, pp. 1919-1926.

40. L.J. Bohmann and R.H. Lasseter, "Stability and Harmonics in Thyristor Controlled Reactors", IEEE Trans. on Power Delivery, v.5, n.2, April 1990, pp. 1175-1181.

41. J.D. Rico, E. Acha and T.J.E. Miller, "Harmonic Domain Modelling of Three Phase Thyristor – Controlled Reactors by Means of Switching Vectors and Discrete Convutions", IEEE Trans. on Power Delivery, v. 11, n.3, July 1996, pp. 1678-1684.

42. S.G. Jalali, R.H. Lasseter and I. Dobson, "Instabilities due to bifurcation of switching times in a thyristor controlled reactor", Power Electronics Specialists Conference, Toledo, Spain, July 1992, pp. 546–552.

43. J.D. Ainsworth, "Phase-locked oscillator control system for thyristor - controlled reactors", IEE Proc. v. 135, Pt. C., n.2, March 1988, pp. 146-156.

44. K.R. Padiyar and A.M. Kulkarni, "Design of reactive current and voltage controller of static condenser", Int. J. of Electrical Power and Energy Systems, v.19, n.6, 1997, pp.397-410.

Chapter 4

Thyristor and GTO Controlled Series Capacitor

4.1 Introduction

Series Capacitors have been used in long distance EHV transmission lines for increasing power transfer. The use of series capacitors is generally the most economic solution for enhancing power flow. However, the problem of SSR has deterred system planners from going in a big way for series compensation. While the use of shunt capacitors don't have the problem of SSR, they have drawbacks of their effectiveness being dependent largely on their location. Even when a shunt capacitor is located at the midpoint of a long line, it requires much larger rating to achieve the same level of increase in power transfer as a series capacitor. It was shown in chapter 2 that the ratio of the two ratings is given by

$$\frac{Q_{se}}{Q_{sh}} = \tan^2\left(\frac{\delta_{\max}}{2}\right) \tag{4.1}$$

where Q_{se} and Q_{sh} are the ratings of the series and the shunt capacitor respectively, $\delta_{\max}$ is the maximum angular difference between the two ends of the line. For $\delta_{\max}$ in the range of 30°–40°, Q_{se} varies from 7% to 13% of Q_{sh}. Although the series capacitors tend to be twice as costly as shunt capacitors (per unit var), they are still cheaper to use. In addition, the location of a series capacitor is not critical.

The use of thyristor control to provide variable series compensation makes it attractive to employ series capacitors in long lines. A major advantage is that the SSR problem (Torsional Interaction) is significantly reduced. The feasibility of fast control of thyristor valves enables the improvement of stability and damping of oscillations using appropriate control strategies.

The first demonstration project of TCSC was commissioned in 1991 at a 345 kV Kanawha River Substation in West Virginia, U.S.A. under American Electric Power Company. This was a test installation of thyristor switches in one phase for rapid switching of series capacitor segment and was supplied by ABB, Sweden.

In October 1992, the first three phase TCSC was installed at 230 kV Kayenta Substation in Arizona under Western Area Power Administration (WAPA). Here a 15Ω capacitor bank is connected in parallel with a TCR and permits a smooth and rapid control of (capacitive) reactance between 15 and 60Ω through phase control of TCR.

A larger prototype three phase TCSC was installed in 1993 at 500 kV Slatt Substation in Oregon under Bonneville Power Administration (BPA). The project was sponsored by Electric Power Research Institute (EPRI) and the equipment was developed by General Electric in U.S.A. Here, six modules of TCSC are connected in series and controlled to provide a variation in impedance from $+1.4\Omega$ to -16Ω.

In Sweden, a long, series-compensated 400 kV transmission line connected to a nuclear power station was chosen to install TCSC by splitting the existing series capacitor into two parts – a fixed capacitor and a Thyristor Controlled Series Capacitor at Stode Station [23]. This was necessitated by an SSR problem that caused repeated triggering of protections. The TCSC allowed the existing level of compensation to be continued without any SSR problems.

4.2 Basic Concepts of Controlled Series Compensation

By controlled series compensation, we imply dynamic control of the degree of series compensation in a long line. This can be achieved in two ways as

1. Discrete control using TSSC (Thyristor Switched Series Capacitor)
2. Continuous control using
   (a) TCSC or
   (b) GTO thyristor Controlled Series Capacitor (GCSC)

The configuration using TSSC is shown in Fig. 4.1(a). Here, the thyristor switch is either off or on continuously. To insert the capacitor, the switch is turned off while it is turned on to bypass the capacitor. A major problem with this configuration is that the SSR characteristics of the TSSC are no different from that of the fixed capacitor. Also, the full line current flows through the thyristor switch when it is on. Thus, this configuration is not common.

The configuration using TCSC is shown in Fig. 4.1(b). Here, a TCR is used in parallel with a fixed capacitor to enable continuous control over the series compensation. Although harmonics are present in steady state with

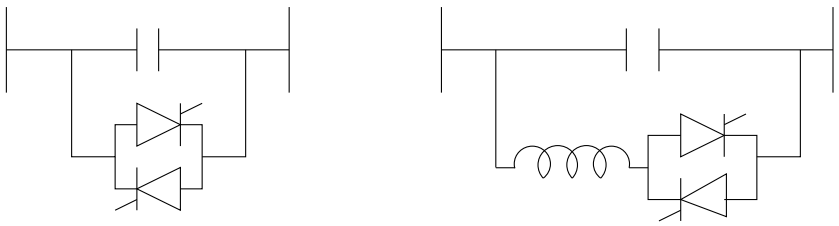

(a). TSSC (b). TCSC

Figure 4.1: Configurations of series compensation

partial conduction of thyristor switches, the TCSC can be used to mitigate SSR. In addition, TCSC provides inherent protection against over voltages.

The configuration of GCSC in similar to what in shown in Fig. 4.1(a) except that the switch is made of GTO thyristors to permit turn off capability when current is flowing through the switch. This enables, phase control to be applied to the capacitor in a similar fashion as in a TCR. As a matter of fact, the GCSC is a dual of the TCR in that the voltage across the capacitor can be controlled by controlling the conduction (or turn-off) angle of the GTO thyristor switch.

Although continuous control of the capacitor is possible in both TCSC and GCSC, the latter is yet to be applied in practice. In comparing TCSC with GCSC, the former has the advantages of (a) lower costs due to the requirements of conventional thyristors as opposed to GTO and (b) boost in the capacitor voltage provided by the discontinuous conduction of the TCR (Note that TCSC is formed by the parallel combination of a fixed capacitor and a TCR in each phase). The TCSC was also labeled as RANI (Rapid Adjustment of Network Impedance) in a paper by Vithayathil *et al.* [6].

TCSC is a mature technology available for application in AC lines of voltage up to 500 kV. This chapter will concentrate mainly on TCSC except for a section on GCSC.

Consider the equivalent circuit of the TCSC modeled as a capacitor in parallel with a variable inductor (as shown in Fig. 4.2(a)). The impedance of TCSC (Z_{TCSC}) is given by

$$Z_{\text{TCSC}} = \frac{-jX_C \cdot jX_{TCR}}{j(X_{TCR} - X_C)} = \frac{-jX_C}{\left(1 - \frac{X_C}{X_{TCR}}\right)} \tag{4.2}$$

The current through the TCR (I_{TCR}) is given by

$$\hat{I}_{TCR} = \frac{-jX_C}{j(X_{TCR} - X_C)}\hat{I}_L = \frac{\hat{I}_L}{\left(1 - \frac{X_{TCR}}{X_C}\right)} \tag{4.3}$$

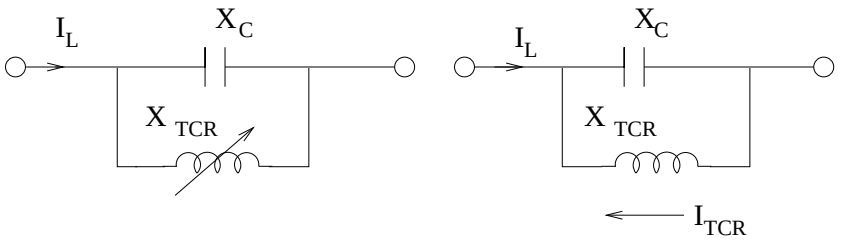

(a). Equivalent circuit of TCSC (b). Capacitive operation

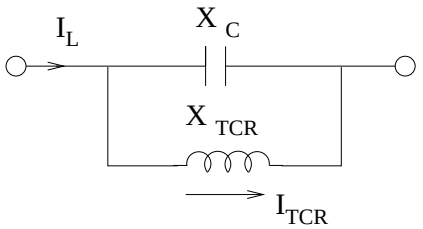

(c). Inductive operation

Figure 4.2: TCSC circuit representation

Since the losses are neglected, the impedance of TCSC is purely reactive. The capacitive reactance of TCSC is obtained from (4.2) as

$$X_{\text{TCSC}} = \frac{X_C}{\left(1 - \frac{X_C}{X_{TCR}}\right)} \tag{4.4}$$

Note that X_{TCSC} is capacitive as long as $X_C < X_{TCR}$. $X_{TCR} = \infty$ when the thyristors are blocked and $I_{TCR} = 0$. For the condition when $X_C < X_{TCR}$, $\hat{I}_{TCR}$ is 180° out of phase with the line current phases $\hat{I}_L$. In other words, $\hat{I}_L$ is in phase with $-\hat{I}_{TCR}$.

For the condition where $X_C > X_{TCR}$, the effective reactance of TCSC (X_{TCSC}) is negative implying that it behaves like an inductor. In this case, $\hat{I}_L$ and $\hat{I}_{TCR}$ are in phase. The capacitive and the inductive operation of TCSC is shown in Fig. 4.2(b) and (c) respectively.

Example 1

Compute $\frac{X_{\text{TCSC}}}{X_C}$ and $\frac{I_{TCR}}{I_L}$ if (a) $X_{TCR} = 1.5X_C$ and (b) $X_{TCR} = 0.75X_C$.

(a) From Eqs. (4.4) and (4.3), we get substituting the values

$$\begin{aligned} \frac{X_{\text{TCSC}}}{X_C} &= \frac{1}{1 - \frac{2}{3}} = 3.0 \\ \frac{I_{TCR}}{I_L} &= \frac{1}{1.5 - 1} = 2.0 \end{aligned}$$

(b) For $X_{TCR} = 0.75 X_C$,

$$\begin{aligned} \frac{X_{\text{TCSC}}}{X_C} &= \frac{1}{1 - \frac{4}{3}} = -3.0 \\ \frac{I_{TCR}}{I_L} &= \frac{1}{1 - 0.75} = 4.0 \end{aligned}$$

It is interesting to observe that even though the magnitude of the TCSC reactance is same in both (capacitive and inductive) cases, the current through the TCR is more for the inductive operation (twice that for the capacitive operation). This indicates that thyristor ratings determine the maximum limit on the X_{TCSC} for the inductive operation.

The TCR injects also harmonics in addition to the fundamental frequency current. This distorts the capacitor voltage which does not remain sinusoidal even though the line current remains approximately sinusoidal. (Note that the presence of harmonics in the capacitor voltage can result in harmonics in the line current, but for long lines, these can be neglected). It is also obvious that inductive operation of the TCSC results in higher voltage harmonics across the capacitor.

The presence of the voltage harmonics invalidate the expression for the susceptance of TCR derived in chapter 3, (assuming sinusoidal voltage). This expression is repeated below for ready reference.

$$B_{TCR} = \frac{\sigma - \sin \sigma}{\pi X_L} \tag{4.5}$$

Eq. (4.5) cannot be used for the calculation of X_{TCSC} as a function of the conduction angle (σ). A new expression for X_{TCSC} will be derived in section 4.4.

It is to be noted that $X_L < X_C$. A typical value of $\frac{X_L}{X_C}$ is 0.16. This results in protection against over-voltages due to fault currents by increasing the conduction angle to 180°. It is obvious that there is a value of the conduction angle (σ_{res}) for which $X_{TCR} = X_C$ and the TCSC reactance is maximum (theoretically infinite when losses are neglected). It is necessary to ensure that the conduction angle stays within limits even during transient operation. The ratio of $\frac{X_{TCSC}}{X_C}$ is kept below a limit (say 3.0 in the capacitive region). The actual value of the limit is also a function of the line current to ensure that the capacitor voltage rating is not exceeded. In general, there are three voltage ratings based on the current ratings.

1. V_{rated} is the maximum continuous voltage across the TCSC. This must be more than $X_C * I_{\text{rated}}$ to allow for continuous modulation with vernier operation (typically with 15 % margin)

2. V_{temp} is the maximum temporary voltage ($X_C I_{\text{temp}}$) where I_{temp} is the temporary line current (typically $1.35 \times I_{\text{rated}}$) that has a typical duration of 30 minutes.
3. V_{tran} is the maximum voltage required during transient swings. This must be equal to or more than $X_C \times I_{\text{tran}}$ where I_{tran} is the maximum line current for which the thyristor control is not affected by protective considerations. Typically, $I_{\text{tran}} = 2 \times I_{\text{rated}}$ and lasts for a duration of 3 to 10 seconds.

4.3 Operation of TCSC

A single line diagram of a TCSC is shown in Fig. 4.3 which shows two modules connected in series. There can be one or more modules depending on the requirement. To reduce the costs, TCSC may be used in conjunction with fixed series capacitors.

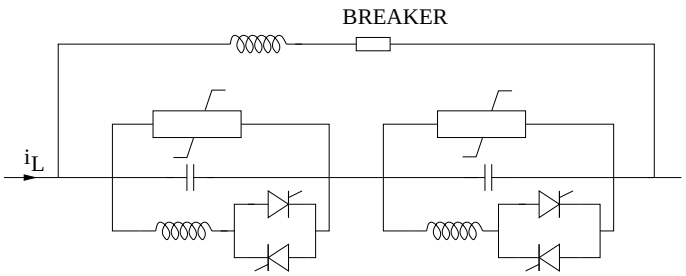

Figure 4.3: Single Line Diagram of a TCSC

Each module has three operating modes (see Fig. 4.4).

(a) Bypassed

Here the thyristor valves are gated for 180° conduction (in each direction) and the current flow in the reactor is continuous and sinusoidal. The net reactance of the module is slightly inductive as the susceptance of the reactor is larger than that of the capacitor. During this mode, most of the line current is flowing through the reactor and thyristor valves with some current flowing through the capacitor. This mode is used mainly for protecting the capacitor against overvoltages (during transient overcurrents in the line). This mode is also termed as TSR (Thyristor Switched Reactor) mode.

(b) Inserted with Thyristor Valve Blocked

In this operating mode no current flows through the valves with the blocking of gate pulses. Here, the TCSC reactance is same as that of the fixed capaci-

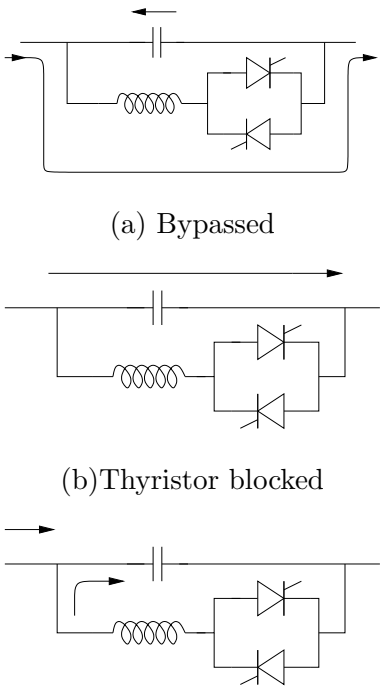

(a) Bypassed

(b)Thyristor blocked

(c)Vernier operation

Figure 4.4: Operating Modes in a TCSC

tor and there is no difference in the performance of TCSC in this mode with that of a fixed capacitor. Hence this operating mode is generally avoided. This mode is also termed as waiting mode.

(c) Inserted with Vernier Control

In this operating mode, the thyristor valves are gated in the region of ($\alpha_{\min} < \alpha < 90°$) such that they conduct for the part of a cycle. The effective value of TCSC reactance (in the capacitive region) increases as the conduction angle increases from zero. $\alpha_{\min}$ is above the value of α corresponding to the parallel resonance of TCR and the capacitor (at fundamental frequency). In the inductive vernier mode, the TCSC (inductive) reactance increases as the conduction angle reduced from 180°.

Generally, vernier control is used only in the capacitive region and not in the inductive region.

4.4 Analysis of TCSC

To understand the vernier control operation of TCSC, it is necessary to analyze the TCSC circuit (see Fig. 4.5).

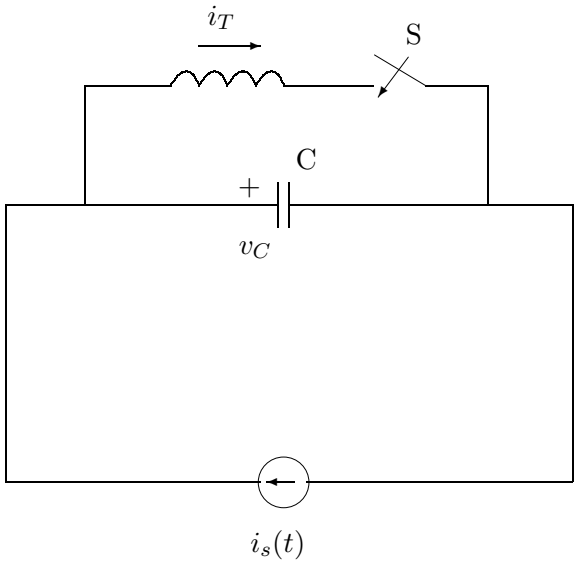

Figure 4.5: The TCSC Circuit

For simplicity, it is assumed that the line current is specified and can be viewed as a current source. The equations are

$$C\frac{dv_C}{dt} = i_s(t) - i_T \tag{4.6}$$

$$L\frac{di_T}{dt} = v_C u \tag{4.7}$$

where $u = 1$ when the switch is closed and $u = 0$ when it is open. The current in the thyristor switch and the reactor (i_T) is zero at the instant when the switch is opened. Note that when $u = 0$, and the initial current $i_T = 0$, it remains at the zero value until S is turned on and $u = 1$. The line current i_s is defined by,

$$i_s(t) = I_m \cos \omega t \tag{4.8}$$

It is convenient to measure the firing angle (α) form the zero crossing instant of the line current. It can be shown that the zero crossing of the capacitor

voltage (v_C) coincides with the peak value of the line current in steady state. The range of α is from 0 to 90° corresponding to the conduction angle varying from 180° to 0°. The angle of advance (β) is defined as

$$\beta = 90^\circ - \alpha \tag{4.9}$$

which also varies from 0 to 90°. Fig. 4.6 shows the waveforms of $i_s(t), i_T(t)$ and $v_C(t)$ with delay angle (α), angle of advance (β) and conduction angle (σ) indicated.

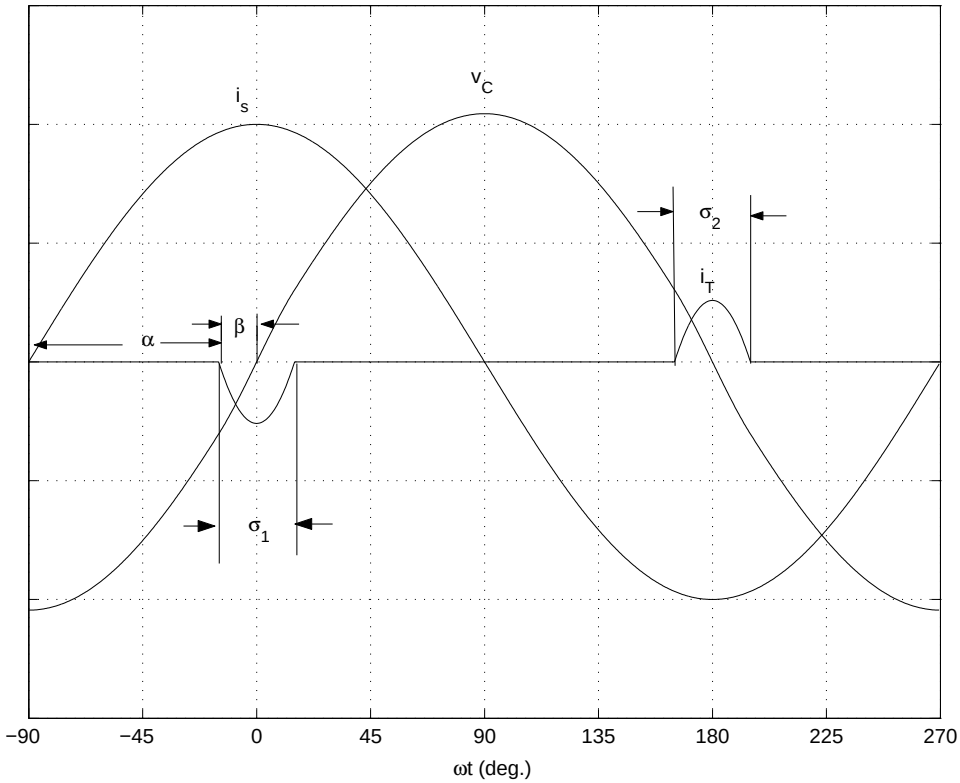

Figure 4.6: Waveforms of $i_s(t)$, $i_T(t)$, $v_c(t)$

The equations (4.6) and (4.7) can be solved if the switching instants are known. The switch, 'S' is turned on twice in a cycle (of the line current) at the instants (assuming equidistant gating pulses)

$$\left.\begin{array}{c} t_1 = \frac{-\beta}{\omega} \\ t_3 = \frac{\pi-\beta}{\omega} \end{array}\right\} \tag{4.10}$$

where $0 < \beta < \beta_{\max}$. The thyristor switch turns off at the instants t_2 and t_4 given by

$$\left.\begin{array}{c} t_2 = t_1 + \frac{\sigma_1}{\omega} \\ t_4 = t_3 + \frac{\sigma_2}{\omega} \end{array}\right\} \tag{4.11}$$

where σ_1 and σ_2 are the conduction angles in the two halves of the cycle. In steady state, $\sigma_1 = \sigma_2 = \sigma$ with half wave symmetry and

$$\sigma = 2\beta \tag{4.12}$$

Solution for the time interval $(-\beta \leq \omega t \leq \beta)$

During this interval, $u = 1$. From Eqs. (4.6) and (4.7) we obtain

$$LC\frac{d^2 i_T}{dt^2} + i_T = i_s(t) \tag{4.13}$$

The solution of this differential equation is given by

$$i_T(t) = \frac{\lambda^2}{\lambda^2 - 1} I_m \cos\omega t + A\cos\omega_r t + B\sin\omega_r t \tag{4.14}$$

where

$$\omega_r = \frac{1}{\sqrt{LC}}, \quad \lambda = \frac{\omega_r}{\omega} = \sqrt{\frac{X_C}{X_L}}, \quad X_C = \frac{1}{\omega C}, \quad X_L = \omega L \tag{4.15}$$

The constants A and B are determined from the boundary conditions. From Eq, (4.7) and (4.14), we obtain

$$v_C(t) = L\frac{di_T}{dt} = -\frac{\lambda^2}{\lambda^2 - 1} I_m X_L \sin\omega t - A\lambda X_L \sin\omega_r t + B\lambda X_L \cos\omega_r t \tag{4.16}$$

In steady state, due to half wave (odd) symmetry,

$$v_C(\omega t = -\beta) = -v_C(\omega t = \beta) \tag{4.17}$$

The above condition leads to the conclusion that the constant $B = 0$. This also shows that the zero crossing of the capacitor voltage occurs at $\omega t = 0$. Since $i_T(t) = 0$ at $\omega t = -\beta$, we get

$$A = -\frac{\lambda^2}{\lambda^2 - 1} I_m \frac{\cos\beta}{\cos\lambda\beta} \tag{4.18}$$

and we can express $i_T(t)$ and $v_C(t)$ as

$$i_T(t) = \frac{\lambda^2}{\lambda^2 - 1} I_m \left[\cos\omega t - \frac{\cos\beta}{\cos\lambda\beta}\cos\omega_r t\right] \tag{4.19}$$

$$v_C(t) = \frac{I_m X_C}{\lambda^2 - 1}\left[-\sin\omega t + \frac{\lambda\cos\beta}{\cos\lambda\beta}\sin\omega_r t\right] \tag{4.20}$$

It can be shown that

$$i_T(\omega t = \beta) = 0 \tag{4.21}$$

and

$$v_{C1} = -v_{C2} \tag{4.22}$$

where

$$v_{C1} = v_C(\omega t = -\beta), \quad v_{C2} = v_C(\omega t = \beta)$$

The expression for v_{C2} is given by

$$v_{C2} = \frac{I_m X_C}{\lambda^2 - 1}[-\sin\beta + \lambda\cos\beta\tan\lambda\beta] \tag{4.23}$$

Solution for the time interval ($\beta < \omega t < \pi - \beta$)

For this interval, $u = 0$. Also $i_T(t) = 0$. The capacitor voltage (v_C) is given by

$$\begin{aligned} v_C(t) &= v_{C2} + \frac{1}{C}\int_{\beta}^{\omega t} i_s(t) d\omega t \\ &= v_{C2} + I_m X_C[\sin\omega t - \sin\beta] \end{aligned} \tag{4.24}$$

Note that the current through the capacitor (i_C) is given by

$$i_C(t) = i_s(t) - i_T(t) \tag{4.25}$$

The waveforms of $i_s(t), i_T(t)$ and $v_C(t)$ over a cycle are shown in Fig. 4.6 for $\lambda = 2.5$, $\beta = 15°$.

Computation of the TCSC Reactance (X_{TCSC})

The TCSC reactance corresponding to the fundamental frequency, is obtained by taking the ratio of the peak value of the fundamental frequency component (V_{C1}) to the peak value of the sinusoidal line current. From Fourier analysis, the fundamental frequency component (V_{C1}) is calculated from

$$V_{C1} = \frac{4}{\pi}\int_0^{\pi/2} v_C(t)\sin\omega t d(\omega t) \tag{4.26}$$

The above equation follows from the fact that v_C has half-wave odd symmetry about the axis $\omega t = 0$. Substituting (4.20) and (4.24) in Eq. (4.26), we get

$$V_{C1} = \frac{4}{\pi}\left[\int_0^{\beta} v_C^1(t)\sin\omega t d\omega t + \int_{\beta}^{\pi/2} v_C^2(t)\sin\omega t d\omega t\right]$$

where

$$v_C^1(t) = \frac{I_m X_C}{\lambda^2 - 1}\left[-\sin\omega t + \frac{\lambda\cos\beta}{\cos\lambda\beta}\sin\omega_r t\right] \tag{4.27}$$

$$v_C^2(t) = v_{C2} + I_m X_C(\sin\omega t - \sin\beta) \tag{4.28}$$

The reactance (X_{TCSC}) is usually expressed in terms of X_C. By defining,

$$X_{TCSC} = \frac{V_{C1}}{I_m} \tag{4.29}$$

we can derive the ratio $\frac{X_{TCSC}}{X_C}$ as

$$\frac{X_{TCSC}}{X_C} = 1 + \frac{2}{\pi}\frac{\lambda^2}{(\lambda^2-1)}\left[\frac{2\cos^2\beta}{(\lambda^2-1)}(\lambda\tan\lambda\beta - \tan\beta) - \beta - \frac{\sin 2\beta}{2}\right] \tag{4.30}$$

The above expression can be simplified as

$$\frac{X_{TCSC}}{X_C} = 1 + \frac{2}{\pi}\frac{\lambda^2}{(\lambda^2-1)}\left[-\left(\frac{\lambda^2+1}{\lambda^2-1}\right)\frac{\sin 2\beta}{2} - \beta + \frac{2\cos^2\beta \cdot \lambda \tan\lambda\beta}{(\lambda^2-1)}\right] \tag{4.31}$$

The capacitor voltage also contains odd harmonics of the order

$$n = 2k-1, \quad k = 1, 2, 3, \ldots \tag{4.32}$$

Remarks

1. The fundamental frequency component and the harmonics in the capacitor voltage can also be obtained from the calculation of harmonics in the TCR current $i_T(t)$.

   The peak value of the fundamental component I_{T1} can be found from

$$\begin{aligned} I_{T1} &= \frac{4}{\pi}\int_0^{\pi/2} i_T(t)\cos\omega t d\omega t \\ &= \frac{4}{\pi}\left[\int_0^{\beta}\frac{\lambda^2}{\lambda^2-1} I_m\left[\cos\omega t - \frac{\cos\beta}{\cos\lambda\beta}\cos\lambda\omega t\right] d\omega t\right] \end{aligned} \tag{4.33}$$

   The fundamental component of the capacitor voltage is obtained from

$$V_{C1} = (I_m - I_{T1})X_C \tag{4.34}$$

   The peak value of the nth harmonic (I_{Tn}) in the TCR current is obtained from

$$I_{Tn} = \frac{4}{\pi}\int_0^{\pi/2} i_T(t)\cos n\omega t d\omega t \tag{4.35}$$

$$\begin{aligned} &= \frac{2}{\pi}\frac{I_m\lambda^2}{(\lambda^2-1)}\left\{\frac{\sin(n-1)\beta}{n-1} + \frac{\sin(n+1)\beta}{n+1}\right. \\ &\quad \left. -\frac{\cos\beta}{\cos\lambda\beta}\left[\frac{\sin(n-\lambda)\beta}{n-\lambda} + \frac{\sin(n+\lambda)\beta}{n+\lambda}\right]\right\} \end{aligned} \tag{4.36}$$

   The peak value of the n^{th} harmonic in the capacitor voltage (V_{Cn}) is given by

$$V_{Cn} = I_{Tn}\frac{X_C}{n} \tag{4.37}$$

   The ratio $\left(\frac{V_{Cn}}{I_m X_C}\right)$ is obtained as

$$\begin{aligned} \frac{V_{Cn}}{I_m X_C} &= \frac{2}{\pi}\frac{\lambda^2}{(\lambda^2-1)}\left[\frac{\sin(n-1)\beta}{n-1} + \frac{\sin(n+1)\beta}{n+1}\right. \\ &\quad \left. -\frac{\cos\beta}{\cos\lambda\beta}\left[\frac{\sin(n-\lambda)\beta}{n-\lambda} + \frac{\sin(n+\lambda)\beta}{n+\lambda}\right]\right], \quad n = 3, 5, 7, \ldots \end{aligned} \tag{4.38}$$

2. $\frac{X_{TCSC}}{X_C} \rightarrow \infty$ at $\beta_{\text{res}} = \frac{(2k-1)\pi}{2\lambda}$ where k is an integer. Since the range of β is limited to 90°, if $\lambda < 3$, there will be only one value of β_{res} at which the TCR and the capacitor will be in resonance at the fundamental frequency. Typically, $\lambda = 2.5$. The variation of $\frac{X_{TCSC}}{X_C}$ as a function of β for $\lambda = 2.5$ is shown in Fig. 4.7. The negative value of $\frac{X_{TCSC}}{X_C}$ indicate that the reactance is inductive.

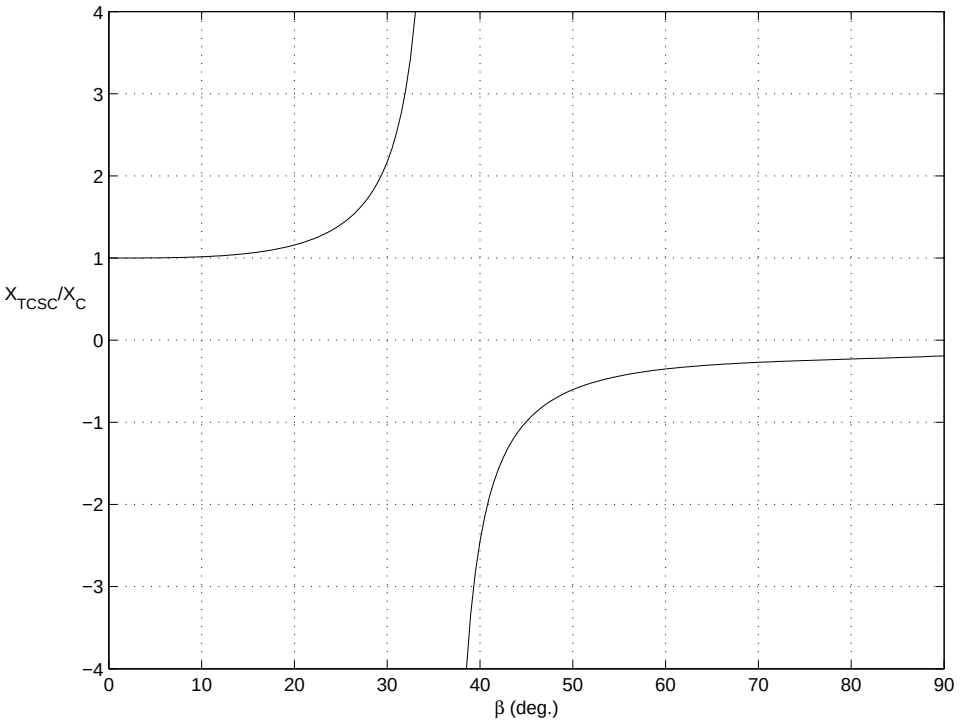

Figure 4.7: Variation of (X_{TCSC}/X_C) as a function of β

The variation of $\left(\frac{|V_{Cn}|}{I_m X_C}\right)$ as a function of β is shown in Fig. 4.8. The capacitor voltage wave forms for (i) $\beta = 20°$ and (ii) $\beta = 70°$ are shown in Fig. 4.9.

3. As the TCSC impedance is very high at resonance (β_{res}) given by

$$\beta_{\text{res}} = \frac{\pi}{2\lambda} \tag{4.39}$$

the operation of TCSC must ensure that the upper limit on $\beta(\beta_{\max})$ should be strictly enforced even under transient conditions. Generally $\frac{X_{TCSC}}{X_C} < 4$ to ensure that the voltage ratings on the capacitor are not exceeded.

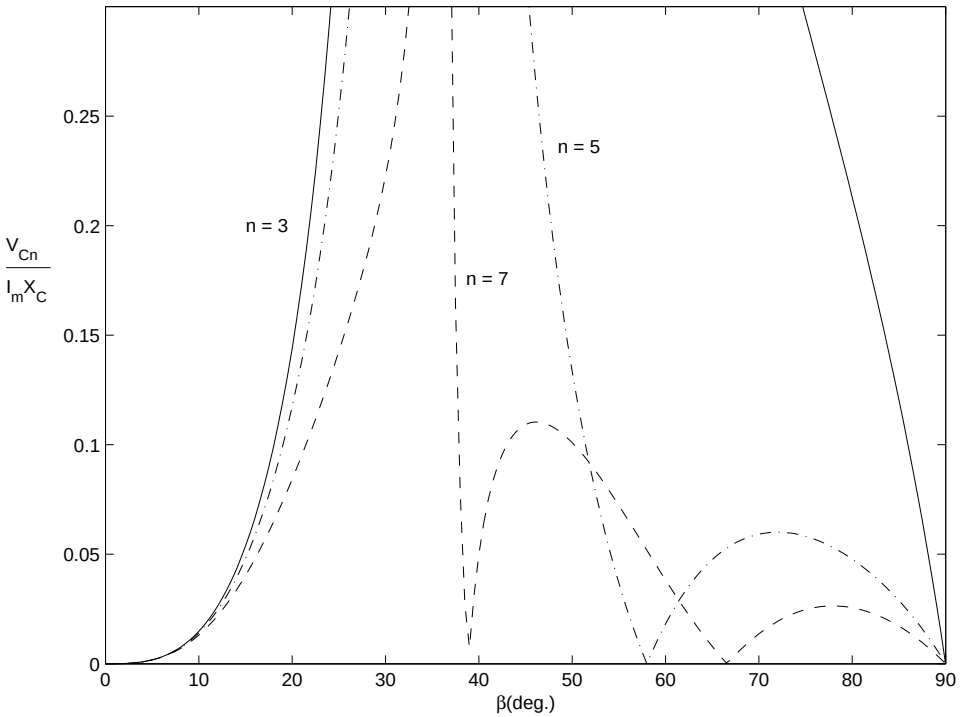

Figure 4.8: Variation of $(V_{cn}/I_m X_c)$ as a function of β

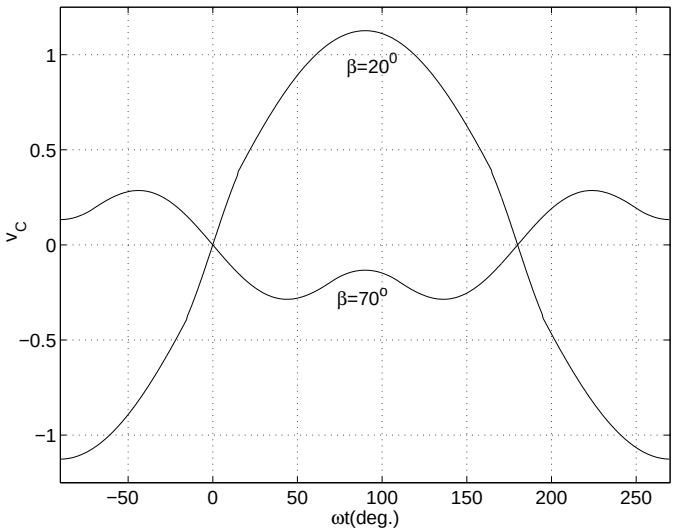

Figure 4.9: Capacitor voltage waveforms for $\beta = 20^0$ $\beta = 70^0$

4.5 Control of TCSC

The control of TCSC also includes protective functions (protective bypass). The control functions are partitioned into two levels - common (to all mod-

ules) and the module (level). Commands for the control flow from the common level to the module levels while the status information is sent back from each module level.

Module Control Functions

There are three basic functions at each module level. These are

(a) reactance control

(b) SSR damping control (involving modulation of the reactance) and

(c) Bypass (for protection)

The controller also ensures that the transients associated with mode transitions are minimized. The module controller executes the ordered change to reactance within one half cycle. This includes bypassing, reinsertion and setting the vernier without overshoot.

The protective bypass (TSR mode) is initiated in response to

(i) line overcurrent

(ii) arrester overcurrent

(iii) arrester energy exceeding a limit.

The line overcurrent protection detects fault currents in the line and rapidly implements thyristor bypass to reduce duty on MOV (metal oxide varistors) and capacitors. The bypass is performed on all the three phases simultaneously. When the line current returns and stays within limits for a preset time, the bypass is removed. The arrester overcurrent protection detects overcurrents in the arrester and implements thyristor bypass in the affected phase(s) to reduce varistor duty. The bypass is removed when the arrester currents reduce and stay below limits for a preset time.

The arrester energy protection initiates a bypass when $\int i^2 dt$ in the arrester exceeds its rating. In this case, the bypass is not removed automatically because of the long thermal time constants associated with excessive arrester energy.

Common Control Functions

The common level receives signals of line current and TCSC voltage to generate feedback signals for closed-loop control functions. It also receives commands from energy management centre for setting power order. The major control functions in a TCSC are described below.

Power Scheduling Control

The simplest type of power scheduling control adjusts the reactance order (or setpoint) slowly to meet the required steady-state power flow requirements of the transmission network. The adjustment may be done manually or by a slow acting feedback loop.

An alternative approach is to use a closed-loop current control in which the measured line current is compared to a reference current (which may be derived from the knowledge of the required power level).

An interesting approach to power scheduling is one where during a transient, the line in which TCSC is situated carries the required power so that the power flow in parallel paths is kept constant. This is equivalent to maintaining the angular difference across the line a constant and has been termed as Constant Angle (CA) control. Assuming the voltage magnitudes at the two ends of the line are regulated, maintaining constant angle is equivalent to maintaining constant voltage difference between two ends of the line.

Both CC (Constant Current) and CA controllers can be of PI type with dynamic compensation for improving the response. The steady state control characteristics of both CC and CA control are shown in Fig.4.10(a) and (b) respectively. Assuming V_{TCSC} to be positive in the capacitive region, the characteristics have three segments OA, AB and BC. The control range is AB. OA and BC correspond to the limits on X_{TCSC}. In Fig.4.10(b), the control range AB is described by the equation

$$V_{TCSC} = I_L X_{LR} - V_{Lo} \tag{4.40}$$

where I_L is the magnitude of the line current, X_{LR} is the net line reactance (taking into account the fixed series compensation if any), V_{Lo} is the constant (regulated) voltage drop across the line (including TCSC). Thus, the slope of the line AB is the reciprocal of X_{LR}. OA in Fig.4.10(b), corresponds to the lower limit on TCSC reactance while BC corresponds to the higher limit on TCSC reactance.

Power Swing Damping Control (PSDC)

This is designed to modulate the TCSC reactance in response to an appropriately chosen control signal derived from local measurements. The objective is to damp low frequency swing modes (corresponding to oscillation of generator rotors) of frequencies in the range of 0.2 to 2.0 Hz. One of the signals that is easily accessible is the line current magnitude. Alternatively, the signal corresponding to the frequency of Thevenin (equivalent) voltage of the system across the TCSC can be used. This signal can be synthesized from the knowledge of voltage and current measurements.

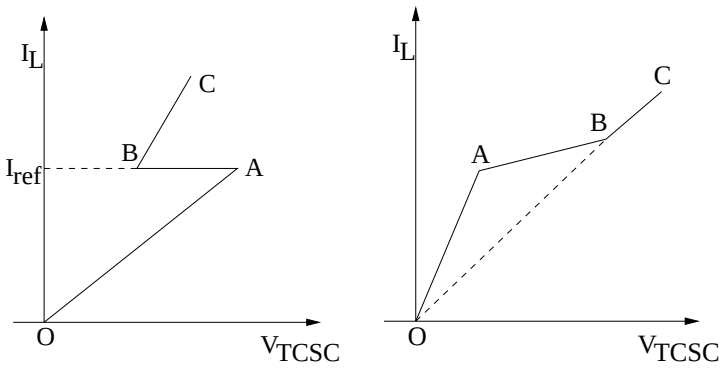

(a) CC Control (b) CA Control

Figure 4.10: Control Characteristics

Transient Stability Control (TSC)

This is generally a discrete control in response to the detection of a major system disturbance.

The discrete or bang-bang control of TCSC in response to signals from locally measured variables is described in [16]. The controller is activated immediately after a major disturbance such as clearing of a fault and is deactivated when the magnitude of frequency deviation is below threshold. This type of control is beneficial not only in reducing the first swing but also for damping subsequent swings.

Subsynchronous Damping Control (SSDC)

The use of vernier control mode at the module level by setting the reactance setpoint at the requisite (minimum) level is often adequate to damp subsynchronous oscillations caused by series resonance in the line and sustained due to torsional interaction. However in some cases, the constant reactance control may not be adequate. In such cases, a damping control is added. The control signal is based on the synthesis of speed of remote turbo-generators. The control signal can be derived from the locally measured current and voltage signals.

The coordination of control actions of all modules in a TCSC is carried out by devising a suitable logic. For example, at Slatt substation, the highest priority is given to the need to tackle SSR, which determines the minimum number of modules to be inserted and their minimum reactance. The power scheduling control has next priority. Even here, there are two options - one based on minimizing the losses and other based on maximizing

smooth operation (avoiding stepped variation in reactance order). It is to be noted that vernier operation results in increased losses in a module.

Power swing damping control has the next priority in modulating the set point for reactance. This can be replaced by TSC whenever required.

Under normal operational conditions, all the modules may not be required. To ensure balanced long term duty for each module in a TCSC, the control logic also incorporates a rotation feature, according to which, the modules in series are rotated if no insert/bypass operations occur for some preset time (say an hour). The rotation is performed without changing the net reactance.

4.6 Modelling of TCSC for Stability Studies

For stability studies it is not necessary to model the gate pulse unit and the generation of gate pulses. It is adequate to assume that the desired value of TCSC reactance is implemented within a well defined time frame. This delay can be modelled by first order lag as shown in Fig.4.11. The value of T_{TCSC} is from 15 to 20 ms. X_{ref} is determined by the power scheduling controller or in its absence, by manual control based on order from load dispatch.

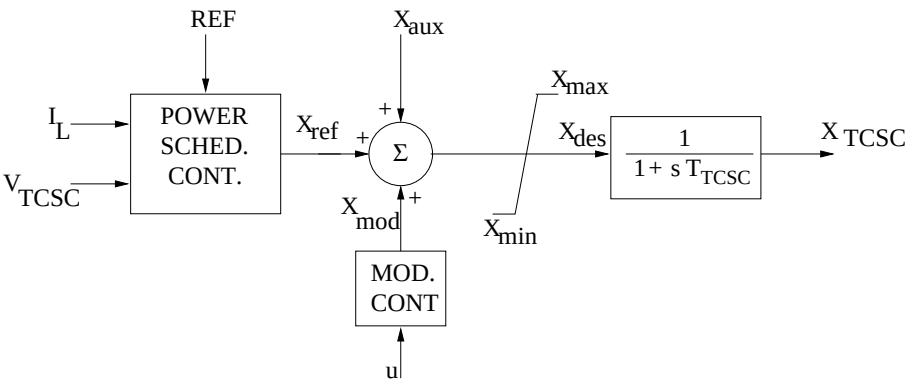

Figure 4.11: Block diagram of TCSC

The block diagram of constant current (CC) or constant angle (CA) controller is shown in Fig.4.12. T_m is the time constant of first order low pass filter associated with the measurement of line current I_L and the TCSC voltage. $S = 0$ for CC control and $S = \frac{1}{X}$ for CA control. X is the net reactance of line given by

$$X = X_{Line} - X_{FC} \tag{4.41}$$

where X_{Line} is the line reactance and X_{FC} is the reactance of the fixed series capacitor if any. Generally, TCSC will be used in conjunction with fixed series capacitor to minimize overall cost of compensation while providing effective control for stability improvement.

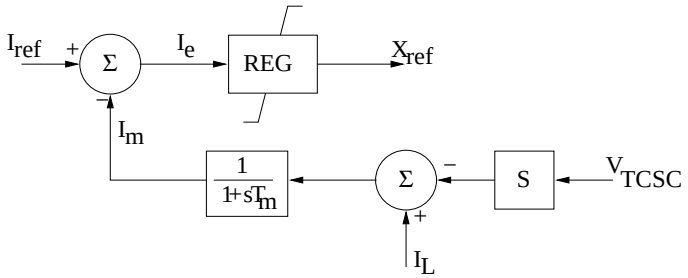

Figure 4.12: Block diagram of CC or CA controller

The regulator block diagram is shown in Fig.4.13. This consists mainly PI controller and phase lead circuit if required. K_P, the proportional gain can be set to zero if only integral control is used. The gain K_I is positive in the case of current control and negative in case of CA control. In the latter case I_{ref} is actually the voltage reference divided by X. Hence positive error signal implies the net voltage drop in the line is less than the reference and X_{TCSC} (assumed to be positive in capacitive region) is to be reduced. On the other hand for current control, if the error is positive, the controller has to increase X_{TCSC} to raise the line current to reduce the error.

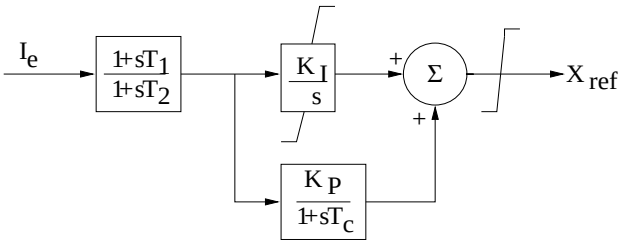

Figure 4.13: Block diagram of the Regulator

The modulation controller is designed to damp power swings in the line by using a control signal derived from local measurement. A convenient signal to use is the magnitude of line current. The control configuration is similar to the SMC used in SVC. X_{aux} could represent the increase in the reactance order required for mitigating SSR or improving transient stability.

The limits on the total reactance order X_{des} are based on the TCSC capability. For a single module, the operational region of TCSC in the

(a) V-I Plane

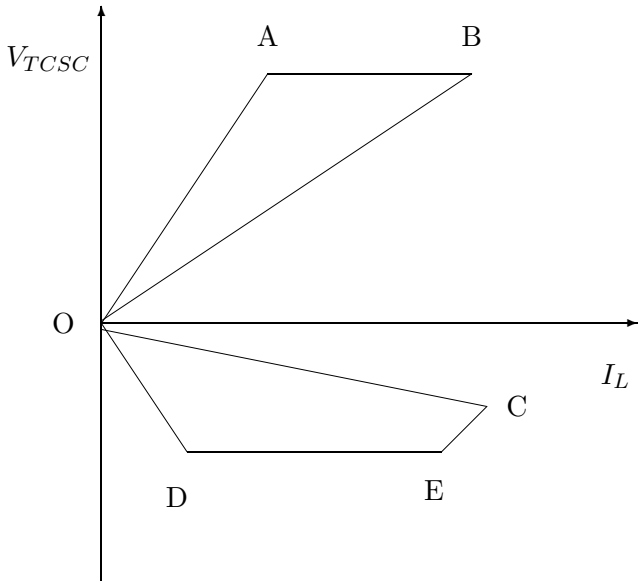

(b) X-I Plane

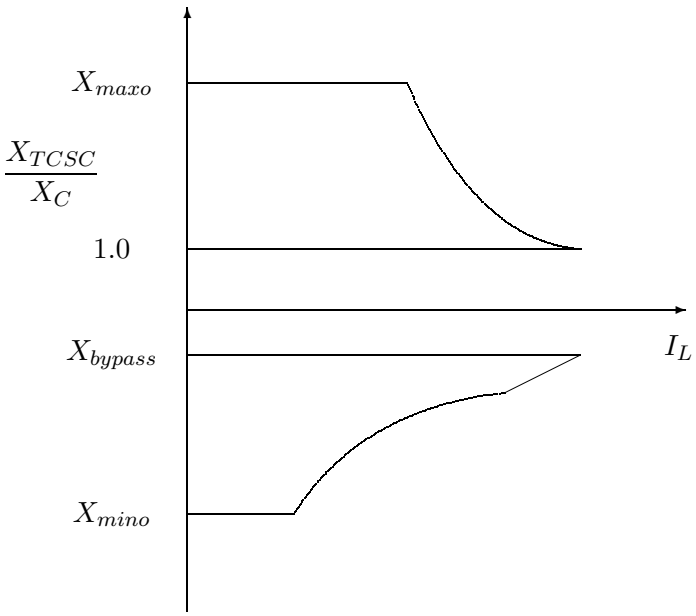

Figure 4.14: TCSC capability curves for a module

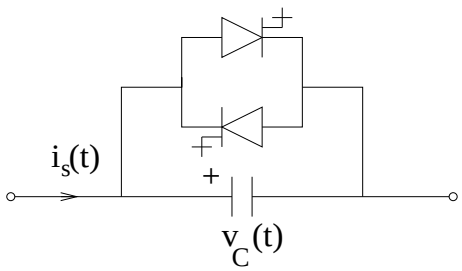

Figure 4.15: GTO Controlled Series Capacitor (GCSC)

$V_{TCSC} - I_L$ plane is shown in Fig.4.14(a). The operation region in $(\frac{X_{TCSC}}{X_C}) - I_L$ plane is shown in Fig.4.14(b). The voltage and reactances are considered to be positive when TCSC is in the capacitive region.

The line OA in Fig.4.14(a) corresponds to the constant reactance of TCSC at its limit X_{max0}. This is selected based on the TCSC design and should be such that the TCSC does not operate close to the resonance point which would be inherently unstable. A typical value of X_{max0} (in pu of X_C) is 3.0. Line AB corresponds to maximum voltage rating of TCSC. Line OB corresponds to the operation of TCSC with thyristors blocked. Here $X_{TCSC} = 1$ pu.

The line OC has negative slope corresponding to X_{bypass} (which is negative) in the bypass mode of TCSC. Line OD corresponds to the upper limit on the inductive reactance (X_{min0}). Line DE corresponds to trhe voltage limit of TCSC in the inductive region. EC corresponds to limit imposed on the thyristor current in the inductive vernier mode. Under normal conditions, the TCSC operates only in the first quadrant of both $V_{TCSC} - I_L$ plane and $X_{TCSC} - I_L$ plane.

The operation at constant maximum voltage (across TCSC) implies that X_{TCSC} is reduced in inverse ratio of the line current.

The equations for TCSC can be written down from the block diagrams shown in Fig.4.11 to Fig.4.13.

4.7 GTO Thyristor Controlled Series Capacitor (GCSC)

A single phase GCSC is shown in Fig. 4.15. It consists of a fixed capacitor in parallel with a bidirectional switch made up of a pair of GTO thyristors. In contrast to a thyristor, a GTO thyristor can be turned off upon command.

A GCSC is a dual of a TCR which is connected across a voltage

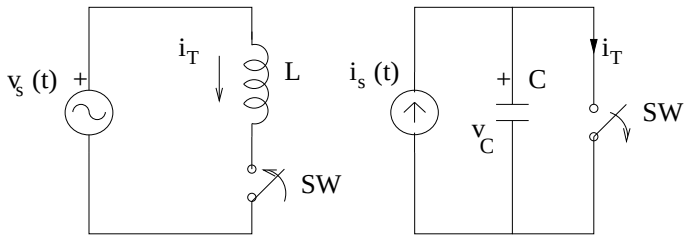

(a). A TCR (b). A GCSC

Figure 4.16: Representation of a TCR and a GCSC

source which is assumed to be sinusoidal. By phase control (varying the delay angle α measured from the instant corresponding to peak value of the source voltage), the current through a TCR can be controlled. See Fig. 4.16 (a) which represents the thyristor valve as a switch that can be turned on at controllable delay angle (α) in the range from 0 to 90°. A GCSC is connected in series with a sinusoidal current source. The controllable switch is connected in parallel with the capacitor (see Fig. 4.16(b)) while the thyristor switch is connected in series with the reactor. The switch in a GCSC is *turned off* at an angle (γ) measured with reference to the peak value of the sinusoidal line current (i_s). When the switch across the capacitor is turned off at an angle γ, the current $i_s(t)$ is forced to flow through the capacitor and the voltage (v_C) starts building up according to the relation given by

$$\begin{aligned} v_C(t) &= \frac{1}{C}\int_{\gamma}^{\omega t} i_s(t)d(\omega t) = \frac{1}{C}\int_{\gamma}^{\omega t} I_m \cos\omega t d(\omega t) \\ &= \frac{I_m}{\omega C}[\sin\omega t - \sin\gamma] \end{aligned} \tag{4.42}$$

The GTO switch is closed when $v_C(t) = 0$ and this occurs at the instant when $\omega t = \pi - \gamma$. The switch remains off for the duration δ given by

$$\delta = \pi - 2\gamma = 2\left(\frac{\pi}{2} - \gamma\right) = 2\beta \tag{4.43}$$

δ may be called the hold off angle (as opposed to the conduction angle in a TCR). β is the angle of advance defined as

$$\beta = \frac{\pi}{2} - \gamma \tag{4.44}$$

Both γ and β vary in the range 0 to 90°. When $\gamma = 0$, the capacitor is continuously conducting and $\delta = 180°$. When $\gamma = \frac{\pi}{2}, \delta = 0$ and the capacitor voltage remains at zero as the capacitor is continuously bypassed by the GTO switch. The instantaneous capacitor voltage is maximum corresponding to

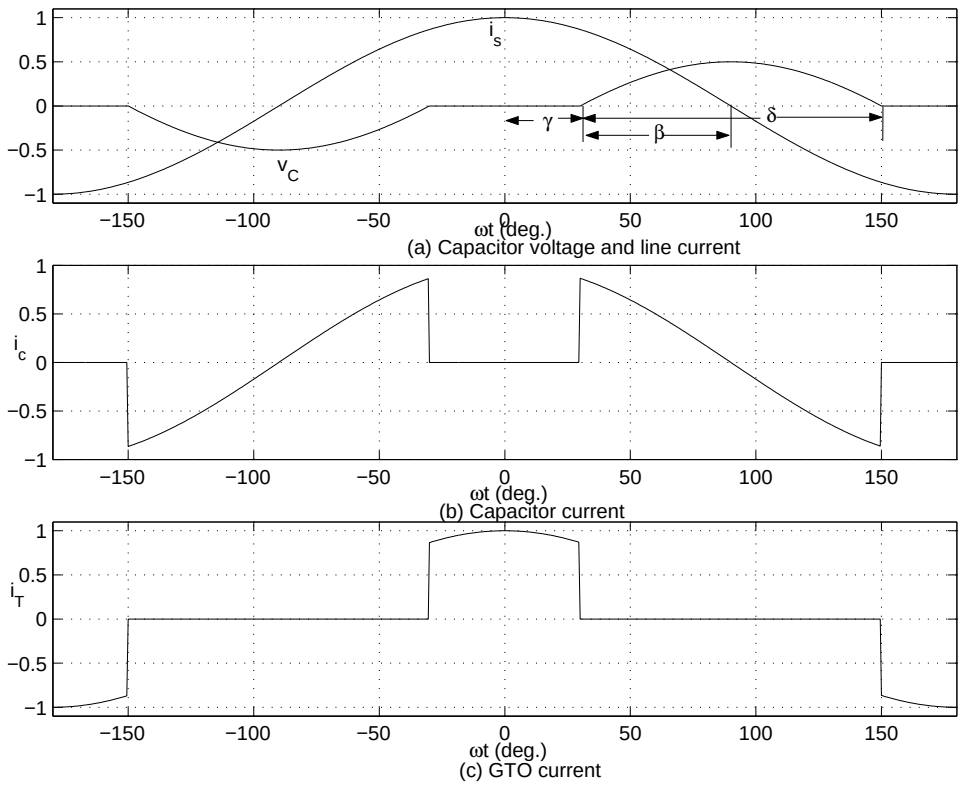

Figure 4.17: Current and voltage waveforms

the instant when the line current is zero. The capacitor voltage and the line current waveforms are shown in Fig. 4.17 along with the currents through the capacitor and the GTO switch. By comparing the TCR quantities (given in chapter 3) with those shown in Fig. 4.17, it can be observed that the TCR current is analogous to the capacitor voltage, the voltage across the thyristor switch (in a TCR) is analogous to the current in the GTO switch and the voltage across the reactor (in a TCR) is analogous to the current through the capacitor. It is to be noted that the firing (delay) angle in a TCR (α) corresponds to the blocking angle (γ) in a GCSC, while the conduction angle (σ) in a TCR corresponds to the hold off angle δ in a GCSC.

The capacitor voltage waveform is not sinusoidal. The fundamental frequency component is given by

$$\begin{aligned} V_{C1} &= \frac{4}{\pi}\int_0^{\pi/2} v_C(t)\sin\omega t d(\omega t) \\ &= \frac{4}{\pi}\frac{I_m}{\omega C}\int_\gamma^{\pi/2}[\sin\omega t - \sin\gamma]\sin\omega t d(\omega t) \end{aligned}$$

$$= I_m X_C \left[1 - \frac{2\gamma}{\pi} - \frac{\sin 2\gamma}{\pi}\right] \quad (4.45)$$

The effective reactance of the GCSC is given by

$$\begin{aligned} X_{GCSC} &= \frac{V_{C1}}{I_m} = X_C \left(1 - \frac{2\gamma}{\pi} - \frac{\sin 2\gamma}{\pi}\right) \\ &= \frac{X_C}{\pi}(\delta - \sin\delta) \end{aligned} \quad (4.46)$$

As δ varies from 0 to 180°, X_{GCSC} varies from 0 to X_C. (Note that in a TCR, B_{TCR} varies from 0 to B_L as σ varies from 0 to 180°.)

The amplitude of the harmonics voltage (V_{cn}) across the capacitor, is given by

$$V_{cn} = I_m X_C \frac{4}{\pi}\left[\frac{\sin\gamma\cos(n\gamma) - n\cos\gamma\sin(n\gamma)}{n(n^2-1)}\right], \quad n = 2k+1, k = 1, 2, 3, \ldots \quad (4.47)$$

The third harmonic component has a peak value of 13.8% of ($I_m X_C$) at a value of γ around 35°. Unlike in a three phase TCR, there is no provision of connecting the GCSC in a delta to eliminate the triplen harmonics (unless an insertion transformer is used). The GCSC would normally be inserted directly (without any magnetics) in series with the line. Fortunately, the line impedance (inductive) would be sufficiently high to limit the triplen (zero sequence) current harmonics to values that would not create problems. Further, just as a segmented TCR (made of multiple modules connected in parallel) can be operated with all (except one module) in the TSR mode, a GCSC made up of multiple, identical modules connected in series, can be operated with all (except one) in a GSSC (GTO Switched Series Capacitor) mode. However, in comparison with TSR operation it should be noted that a GTO switch in a GSSC is called upon to turn-off and on at the instant when the line current is maximum and the capacitor voltage is zero. A thyristor switch in a Thyristor Switched Series Capacitor (TSSC) can be turned on at the voltage zero, but has to wait until the instant of current zero to turn-off. At this instant, the capacitor voltage is maximum and results in dc offset for the capacitor voltage which is 100% of ($I_m X_c$).

4.8 Mitigation of Subsynchronous Resonance with TCSC and GCSC

4.8.1 Description of SSR

The turbo generators have several rotors corresponding to steam turbines (High Pressure, Intermediate Pressure and Low Pressure) in addition to the generator and rotating exciter (if any), all connected by elastic shafts

which can be modelled as springs. Thus, the mechanical system of rotors and shaft sections is a lightly damped mass-spring system analogous to the electrical network of capacitors (analogous to rotor inertias) and inductors (analogous to the springs). This system has as many torsional modes as the number of rotors (masses), of frequencies ranging from 0 to 50 Hz (in the subsynchronous range). These frequencies are computed considering the mechanical system in isolation. The torsional mode corresponding to the zero frequency is turned as 'mode zero' in which all the rotors participate equally. (The eigenvector has identical elements). The external electrical system consisting of the generator stator coils connected to the transmission network can affect the frequency and damping of the torsional modes. While the change in the frequency is significant for mode zero, the changes in the frequencies of the remaining modes are slight and can be neglected. (It is to be noted that the frequency of the 'mode zero' in the combined system varies in the range of 0.2 to 2.0 Hz and the damping of the oscillations corresponding to this low frequency mode has been discussed extensively in the literature since last 40 years and still continues to be important for secure system operation). The damping of the remaining torsional modes is significantly affected by the characteristics of the electrical system. A series compensated transmission line connected to a turbogenerator has a (electrical) resonance frequency (f_{er}) given by

$$f_{er} = f_0 \sqrt{\frac{x_C}{x'' + x_T + x_E}} \tag{4.48}$$

where x'' is the subtransient reactance of the generator, x_T is the leakage reactance of the transformer, x_E and x_C are the external reactances of the series connected inductor and capacitor respectively. Since $x_C < x_E$, $f_{er} < f_0$ (f_0 is the system frequency). When the torsional mode frequency (f_m) is a complement of the electrical resonance frequency (f_{er}), that is

$$f_m = f_0 - f_{er} \tag{4.49}$$

there is a danger of Subsynchronous Resonance (SSR) which has the primary consequence of growing torsional oscillations due to the instability of the torsional mode caused by the large negative damping introduced by the electrical system. This problem has been termed as Torsional Interaction (TI) that results in self excitation (steady state SSR problem). Even if the net damping (due to the mechanical and the electrical system) is positive, there can be high amplitude transient subsynchronous frequency oscillations that can damage the shafts. The transient torque oscillations are induced by large disturbances such as faults followed by their clearing.

An IEEE Committee Report (1985) has defined SSR as follows: "subsynchronous resonance is an electric power system condition where the electric network exchanges energy with a turbine generator at one or more of the

natural frequencies of the combined system below the synchronous frequency of the system". The two aspects of the SSR problem are:

1. Self excitation (also called as steady state SSR)
2. Transient torques (also called as transient SSR)

The self excitation problem includes (a) Induction Generator Effect (IGE). Here the mechanical system is not modelled. The subsynchronous frequency (positive sequence) armature currents produce a rotating mmf which moves slower than the generator rotor. The resistance of the rotor circuits appear to be negative (viewed from the armature terminals) due to the negative slip of the machine (corresponding to the subsynchronous frequency currents). If the net resistance is zero or negative, self excitation occurs. (b) Torsional Interaction (TI). This is due to the interplay between the electrical and mechanical system and is a much more serious problem compared to IGE. The problem was discovered accidentally after the shaft damage experienced at Mohave generating station in 1970 and 1971.

The analysis of steady state SSR or self excitation problem can be carried out by linear system methods of checking for the stability of an operating point (steady state equilibrium). There are two major approaches

1. Damping torque analysis based on frequency domain technique. This is a heuristic, simpler approach for checking for TI and gives reasonably accurate results.
2. Eigenvalue analysis based on the state space model of the linearized system equations. This gives accurate information about the stability of all the system modes including torsional modes.

The damping torque analysis can be used as a screening tool for fast evaluation of a host of system conditions for torsional interactions. Since IGE is not a major problem, it can be neglected. This permits the use of simple 'classical model' of the generator which simplifies the computation of the damping torque.

The analysis of the transient torques requires detailed system simulation based on the nonlinear models. In the presence of FACTS controllers, three phase models considering switching action of the thyristor or other power semiconductor devices are most accurate. However, for SSR analysis, the modelling of a FACTS controller using D-Q variables (based on synchronously rotating reference frame) is found to be adequate. The use of D-Q variables implies that the harmonics generated by the FACTS devices have little effect on the SSR performance. It must be noted that unlike in the case of study of low frequency phenomena involving swing modes, the

analysis of SSR requires representation of the network dynamics (by differential equations rather than algebraic equations involving phasors). Thus, it is not unusual to employ EMTP (Electromagnetic Transients Program) type software which was originally developed for the study of lightning and switching transients.

4.8.2 A Simplified SSR Analysis [32]

Consider the classical model of a generator where the field flux decay, damper circuits and transient saliency are ignored. Assuming that the generator rotor oscillates (about a constant speed of ω_0) sinusoidally, the per unit speed ($\bar{\omega}$) is given by

$$\bar{\omega} = \bar{\omega}_0 + A \sin \omega_m t \tag{4.50}$$

where ω_m is the oscillation frequency of the rotor (about a synchronously rotating axis) in radians per second. The induced voltages in the armature in the $\alpha - \beta$ sequence are given by

$$e_\alpha = \bar{\omega} E' \sin(\omega_0 t + \delta) \tag{4.51}$$

$$e_\beta = \bar{\omega} E' \cos(\omega_0 t + \delta) \tag{4.52}$$

Since

$$\frac{d\delta}{dt} = (\bar{\omega} - \bar{\omega}_0)\omega_B \tag{4.53}$$

we get

$$\delta = \delta_0 - \left(\frac{A\omega_B}{\omega_m}\right) \cos \omega_m t \tag{4.54}$$

If the amplitude (A) of the rotor oscillations is very small, the induced voltages consist of three sinusoidal components, one of frequency f_0 (in Hz), the other two components of frequency, $f_0 \pm f_m$. We can get this by substituting Eqs. (4.50) and (4.54) in (4.51) and (4.52). Thus,

$$\begin{aligned} e_\alpha = {} & \bar{\omega}_0 E' \sin(\omega_0 t + \delta_0) - \frac{AE'}{2\omega_m}(\omega_0 - \omega_m) \cos[(\omega_0 - \omega_m)t + \delta_0] \\ & - \frac{AE'}{2\omega_m}(\omega_0 + \omega_m) \cos[(\omega_0 + \omega_m)t + \delta_0] \end{aligned} \tag{4.55}$$

$$\begin{aligned} e_\beta = {} & \bar{\omega}_0 E' \cos(\omega_0 t + \delta_0) + \frac{AE'}{2\omega_m}(\omega_0 - \omega_m) \sin[(\omega_0 - \omega_m)t + \delta_0] \\ & + \frac{AE'}{2\omega_m}(\omega_0 + \omega_m) \sin[(\omega_0 + \omega_m)t + \delta_0] \end{aligned} \tag{4.56}$$

If the network impedance (in the Laplace domain) is

$$Z(s) = R + Ls + \frac{1}{Cs} \tag{4.57}$$

we can obtain the currents flowing in these α and β sequence networks for the applied voltages given by Eqs. (4.55) and (4.56). These can be converted to the $d-q$ (in Park's reference frame) components from the following equation

$$(i_q + ji_d) = e^{-j(\omega_0 t+\delta)}(i_\beta + ji_\alpha) \tag{4.58}$$

The electrical torque (T_e) is given by

$$T_e = E' i_q \tag{4.59}$$

i_q contains a constant component and two other components (both oscillating sinusoidally at frequency f_m) due to the (i) subsynchronous components and (ii) supersynchronous components of the armature currents. The oscillating component (of frequency, f_m) of the electrical torque consists of two components, T_e^{sub} and T_e^{sup} corresponding to the sub- and supersynchronous components of the armature currents. These can be derived as

$$T_e^{sub} = E' i_q^{sub} = \frac{-A(E')^2}{2\omega_m Z_{sub}}(\omega_0 - \omega_m)\sin(\omega_m t + \phi_{sub}) \tag{4.60}$$

$$T_e^{sup} = E' i_q^{sup} = \frac{A(E')^2}{2\omega_m Z_{sup}}(\omega_0 + \omega_m)\sin(\omega_m t - \phi_{sup}) \tag{4.61}$$

The damping torque coefficient (T_{De}) is given by

$$T_{De} = Re\left[\frac{\Delta T_e(j\omega_m)}{\Delta\bar{\omega}(j\omega_m)}\right] \tag{4.62}$$

where $\Delta T_e = T_e^{sub} + T_e^{sup}$ and $\Delta\omega = A\sin\omega_m t$. It can be shown from Eqs (4.60) to (4.62) that

$$T_{De}(\omega_m) = -\frac{(E')^2}{2\omega_m}\left[\frac{(\omega_0 - \omega_m)}{Z_{sub}}\cos\phi_{sub} - \frac{(\omega_0 + \omega_m)}{Z_{sup}}\cos\phi_{sup}\right] \tag{4.63}$$

It is to be noted that $Z_{sub}\angle\phi_{sub}$ and $Z_{sup}\angle\phi_{sup}$ are the impedances of the network calculated at the sub- and supersynchronous frequencies. That is,

$$Z_{sub}\angle\phi_{sub} = Z[s = j(\omega_0 - \omega_m)]$$
$$Z_{sup}\angle\phi_{sup} = Z[s = j(\omega_0 + \omega_m)]$$

Remarks

1. The damping due to the subsynchronous frequency currents is negative while that due to the supersynchronous frequency currents is positive. This results from the fact that both ϕ_{sub} and ϕ_{sup} can vary in the range -90° to 90° and $\cos\phi$ is positive in this range.

2. If the electrical network is resonant at a frequency (f_{er}) which is close to the frequency, $f_0 - f_m$, then $Z_{sub} \ll Z_{sup}$ for typical values of the network impedances. Actually if $f_{er} = f_0 - f_m$, then $Z_{sub} = R$ and $\phi_{sub} = 0$. Also $\phi_{sup} \simeq 90^\circ$. Thus T_e^{sub} has a much larger magnitude compared to T_e^{sup} and T_{De} tends to be negative. If we make the approximation, $T_e^{sup} \simeq 0$, then,

$$\begin{aligned} T_{De}(\omega_m) &= \frac{-(E')^2}{2\omega_m}\frac{(\omega_0-\omega_m)}{Z_{sub}}\cos\phi_{sub} \\ &\simeq \frac{-(\omega_0-\omega_m)}{2\omega_m}G(\omega_0-\omega_m) \end{aligned} \tag{4.64}$$

where

$$G(\omega_0-\omega_m) = Re[Z^{-1}(j(\omega_0-\omega_m))] \tag{4.65}$$

is the conductance of the network viewed from the generator internal bus.

The significance of the damping torque coefficient (T_{De}) is that with some approximations, it is related to the change in the decrement factor ($\Delta\sigma_e$) brought about by the electrical system. We can show that for negligible mechanical damping, the electrical system results in the decrement factor (for oscillation at frequency, f_m)

$$\sigma_e \simeq \frac{T_{De}(\omega_m)}{4H_m} \tag{4.66}$$

where H_m is the 'modal' inertia constant which is associated with the swing equation in the decoupled modal variables given by

$$\frac{2H_m}{\omega_B}\frac{d^2\Delta\delta^m}{dt^2} + K_m\Delta\delta^m = -\Delta T_e \tag{4.67}$$

(Note that since the damping torque is related to the linearized systems, we are dealing with the linearized swing equation in the modal domain. In deriving (4.67), it is assumed that the mechanical torques are constants). the relationship between the generator rotor angle ($\Delta\delta$) and the modal variables ($\Delta\delta^m, 0, 1, 2, ...(N-1)$) is given by

$$\Delta\delta = \sum_{m=0}^{m=N-1}\Delta\delta^m \tag{4.68}$$

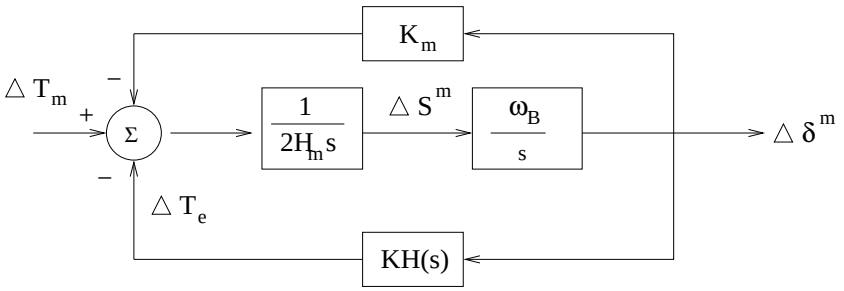

Figure 4.18: Block diagram

where N is the number of rotor masses, $m = 0$ corresponds to mode zero. The modal frequency (f_m) is given by

$$f_m = \frac{1}{2\pi}\sqrt{\frac{\omega_B K_m}{2H_m}} \tag{4.69}$$

For $m = 0, K_m = 0$ and $f_m = 0$

Remarks

1. The concept of modal inertias is quite significant in judging the effect of the electrical system. For large modal inertias, the electrical system has negligible effect (see Eq. (4.66))
2. For mode zero, the modal inertia is the sum of all the rotor inertias.

Fig. (4.18) shows the block diagram depicting the interaction between the electrical and the mechanical (in the modal domain) systems.

Here, $H(s)$ is defined by

$$H(s) = \frac{\Delta T_e(s)}{\Delta \delta^m(s)} \tag{4.70}$$

and K is a parameter introduced for convenience. The value of K is obviously equal to 1. However, $K = 0$ indicates that the electrical system is not considered. In the absence of the electrical system, the eigenvalues of the system are imaginary given by

$$\lambda_m = \pm j\omega_m \tag{4.71}$$

It can be shown that $T_{De}(\omega_m)$ can be expressed as

$$T_{De}(\omega_m) = Re\left[\frac{\omega_B}{j\omega_m} H(j\omega_m)\right] \tag{4.72}$$

The sensitivity of the eigenvalues ($\lambda = -\sigma \pm j\omega$) with respect to the parameter K, evaluated at $K = 0$, is given by

$$\frac{\partial \lambda}{\partial K}|_{K=0} = -RH(s)|_{s=\pm j\omega_m} \tag{4.73}$$

where R is the residue corresponding to the initial eigenvalues $\pm j\omega_m$, given by

$$R = \pm \frac{\omega_B}{4jH_m\omega_m} \tag{4.74}$$

(Note that for $K = 0$, $\lambda = \pm j\omega_m$).

The sensitivity of the decrement factor σ is given by

$$\frac{d\sigma}{dK}|_{K=0} = Re[RH(j\omega_m)] = \frac{T_{De}(\omega_m)}{4H_m} \tag{4.75}$$

If the sensitivity remains constant as K varies from 0 to 1, then Eq. (4.66) applies.

4.8.3 Modelling of TCSC for SSR Analysis

The initial attempts at modelling a TCSC considered the discrete control of the device as the firing of the thyristor valve (switch) in the TCR occurs only twice in a cycle. However, since the frequencies involved in the SSR phenomenon are less than $2f_0$ (f_0 is the fundamental frequency), the continuous time modelling of a TCSC is quite accurate in capturing the sybsynchronous behaviour of a TCSC. We will discuss two models proposed [14,29] in this section and finally present a new model based on switching functions. It is to be noted that the accuracy of a model needs to be validated by detailed simulation considering switching action.

It should be noted that mitigation of SSR with a TCSC is generally possible only through the vernier mode of operation. The partial conduction of the TCR ($\beta < \frac{\pi}{2\lambda}$) results in net increase in the capacitive reactance at the fundamental frequency but results in inductive behaviour at subsynchronous frequencies (below a limit corresponding to a specified value of β). For example, the measured response at 35 Hz for the Kayenta TCSC, showed inductive behaviour for conduction angles ($\sigma = 2\beta$) above 20°. Similar response was also observed for the Slatt TCSC. The inductive behaviour of a TCSC in the critical frequency range is primarily responsible for the mitigation of torsional interaction.

Synchronous Voltage Reversal (SVR) and the TCSC Impedance at Subsynchronous Frequencies

When the thyristor switch (in the TCR connected in parallel with the fixed capacitor) fires, the voltage across the capacitor reverses if there are no losses

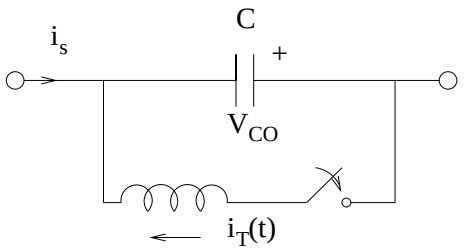

Figure 4.19: TCSC circuit

in the TCSC and the line current magnitude is assumed to be small. For the circuit shown in Fig. 4.19, we can derive (for $i_s \simeq 0$), that

$$\begin{aligned} i_T(t) &= \sqrt{\frac{C}{L}} V_{CO} \sin \omega_r t, \quad 0 \leq t \leq \frac{\pi}{\omega_r} \\ v_C(t) &= L\frac{di_T}{dt} = \sqrt{LC} \cdot \omega_r V_{CO} \cos \omega_r t \\ &= V_{CO} \cos \omega_r t \end{aligned}$$

Since, $\omega_r = \lambda\omega_0$, we can express $i_T(t)$ as

$$i_T(t) = \frac{V_{CO}\lambda}{X_C} \sin(\lambda\omega_0 t)$$

It is obvious that when $\omega_r t = \pi$, the TCR current goes to zero and the capacitor voltage reverses to $-V_{CO}$. The charge passing through the TCR branch is $2CV_{CO}$.

The response of the TCSC circuit can be considered as the superposition of responses due to (i) the line current and (ii) the reversal of the capacitor voltage due to the partial conduction of the TCR. In ref. [14] it is postulated that the impedance characteristics of a TCSC can be approximately calculated even if we assume the conduction angle (σ) approaches zero. This approximation is based on the fact that the peak value of the TCR current is much larger than the peak value of the line current (for a high value of λ).

The frequency characteristics in the subsynchronous frequency range can be derived for small perturbations. Considering that the response is sampled at a frequency $2f_0$, let us select the sampling instants t_k and t_{k+1} as midpoints between voltage reversals. Assuming the voltage reversal is instantaneous (as mentioned earlier), we have, for $t_k \leq t < t_{k+\frac{1}{2}}$

$$C\frac{dv_C}{dt} = i_s(t) \tag{4.76}$$

For $t_{k+\frac{1}{2}} < t \leq t_{k+1}$ also, the above equation applies.

Linearizing Eq. (4.76), we can express

$$\Delta v_C^- \left(k + \frac{1}{2}\right) = \Delta v_C(k) + \frac{1}{C} \int_{t_k}^{t_{k+\frac{1}{2}}} \Delta i_s(t) dt \tag{4.77}$$

$$\Delta v_C(k+1) = \Delta v_C^+ \left(k + \frac{1}{2}\right) + \frac{1}{C} \int_{t_{k+\frac{1}{2}}}^{t_{k+1}} \Delta i_s(t) dt \tag{4.78}$$

where $\Delta v_C^- \left(k + \frac{1}{2}\right)$ and $\Delta v_C^+ \left(k + \frac{1}{2}\right)$ are the perturbations in the capacitor voltage just prior to and immediately after the (instantaneous) voltage reversal. Assuming some losses in the TCR, we can write

$$v_C^+ \left(k + \frac{1}{2}\right) = -D v_C^- \left(k + \frac{1}{2}\right) \tag{4.79}$$

where D is the loss factor ($D < 1$).

Substituting Eq. (4.79) in (4.78) and using Eq. (4.77), we get

$$\Delta v_C(k+1) = -D v_C(k) - D[\Delta q \left(k + \frac{1}{2}\right) - \Delta q(k)] + \Delta q(k+1) - \Delta q \left(k + \frac{1}{2}\right) \tag{4.80}$$

where Δq is the change in charge due to the line current Δi_s.

Taking z transform of Eq. (4.80), we can derive

$$\frac{\Delta V_C(z)}{\Delta Q(z)} = \frac{(z^{1/2} - D)(z^{1/2} - 1)}{(z + D)} \tag{4.81}$$

In continuous time, the transfer function (in Laplace variable) is obtained by substituting $z = e^{sT}$, where $T = \frac{\pi}{\omega_0}$, ω_0 is the operating radian frequency. Noting that,

$$\Delta Q(s) = \frac{1}{sC} \Delta I_s(s) \tag{4.82}$$

we can obtain the frequency response by substituting $s = j\omega$. The final expression for the apparent impedance of TCSC is,

$$\begin{aligned} Z_{app}(j\omega) &= \frac{\Delta V_C(j\omega)}{\Delta I_s(j\omega)} \\ &= -jX_C \frac{\omega_0}{\omega} \frac{(e^{\frac{j\omega\pi}{2\omega_0}} - D)(e^{\frac{j\omega\pi}{2\omega_0}} - 1)}{(e^{\frac{j\omega\pi}{\omega_0}} + D)} \end{aligned} \tag{4.83}$$

If $D = 1.0$ (neglecting losses in the TCR), we can express $Z_{app}(j\omega)$ as

$$Z_{app}(j\omega) = jX_C \frac{\omega_o}{\omega} \frac{(1 - \cos\frac{\omega}{\omega_o}\frac{\pi}{2})}{\cos(\frac{\omega}{\omega_o}\frac{\pi}{2})} \tag{4.84}$$

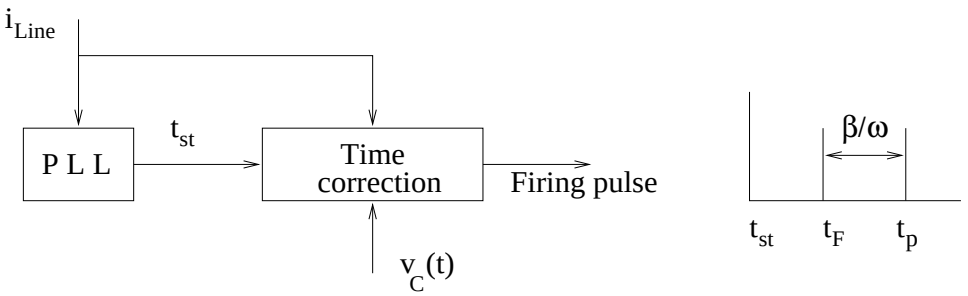

Figure 4.20: TCSC firing control

Eq. (4.84) shows that the apparent impedance is inductive for all $\omega < \omega_0$.

It is to be noted that the above expression ignores the non-zero conduction angle of the TCR which is also a function of $i_s(t)$.

It is common to express the TCSC reactance as a normalized value of $\left(\frac{X_{TCSC}}{X_C} = K_B\right)$. K_B is also termed as the boost [14]. The reference value of K_B is obtained from a higher level control (such as power or current control). Although the firing angle, α, can be directly determined from K_B (in a similar fashion as the susceptance control in a SVC), this type of open loop control is not desirable in a TCSC. The primary reason is the danger of straying close to the resonance $(\beta_{res} = \frac{\pi}{2\lambda})$ and the consequent problem of over voltages. For high values of λ, the K_B is highly nonlinear as K_B increases from unity. Also, the response time with open loop control of K_B is of the order of several hundred ms.

Since the voltage boost can be directly controlled by adjusting the time instant at which the TCR is fired (advancing the firing instant increases the boost while delaying the firing instant reduces the boost), a simple feedback control of the voltage boost is feasible. This is shown in Fig. 4.20.

The firing pulses are synchronized with the line current as it is practically sinusoidal unlike the capacitor voltage. The PLL gives a start pulse to the time correction circuit at t_{st}. The time correction circuit generates firing pulse at t_F which is calculated from measured instantaneous values of $i_{Line}(t)$ and $v_C(t)$. The instant t_F varies depending on the boost level required. However, the instant t_p at which the capacitor voltage crosses zero (also the instant when the thyristor (TCR) current is at its peak) is not disturbed for all operating conditions.

Remarks

1. The presence of DC and subsynchronous frequency components in the capacitor voltage introduces asymmetry in the positive and negative inter-

vals. The synchronous voltage reversal has the property of forcing half-wave symmetry which will reduce the subsynchronous components.

2. The TCSC at Stode substation in Sweden is primarily utilized to mitigate SSR. In such applications, the frequency ratio $\lambda = \frac{\omega_r}{\omega_0}$ can be selected much higher than in situations where TCSC in primarily utilized for power control.

Dynamic Phasor Model of TCSC [28,29]

Neglecting harmonics, the TCR current $i_T(t)$ and the capacitor voltage can be represented as dynamic phasors defined by

$$\begin{aligned} I_T &= I_{TQ} + jI_{TD} \\ V_C &= V_{CQ} + jV_{CD} \\ I_s &= I_{sQ} + jI_{sD} \end{aligned}$$

Eqs. (4.6) and (4.7) can be expressed in terms of dynamic phasors as

$$C\frac{dV_C}{dt} = I_s - I_T - j\omega_0 C V_C \tag{4.85}$$

$$L\frac{dI_T}{dt} = \langle uv_C\rangle_1 - j\omega_0 L I_s \tag{4.86}$$

where $u = 0$ when $i_T(t) = 0$ and $u = 1$ when $i_T(t) \neq 0$, $\langle uv_C\rangle_1$ indicates the fundamental frequency component of the time-varying (periodic) variable $(uv_C(t))$. We can simplify the analysis by assuming that the TCR is in quasi-steady state based on the approximation that I_T has fast dynamics relative to that of V_C. Thus, we can express

$$I_T \simeq \frac{V_C}{j\omega_0 L_{eff}(\sigma)} \tag{4.87}$$

where

$$L_{eff}(\sigma) = \frac{1}{\omega_0^2[C - C_{eff}(\sigma)]}$$

and

$$X_{TCSC}(\sigma) = \frac{1}{\omega_0 C_{eff}(\sigma)}$$

The value of the conduction angle (σ) that is used in the above expression depends on the pulse firing scheme. Assuming that the firing pulses are synchronized with the line current, for constant firing angle control, where $\alpha = \alpha^* = \frac{\pi - \sigma^*}{2}$, under dynamic conditions,

$$\sigma = \sigma^* + 2\phi \tag{4.88}$$

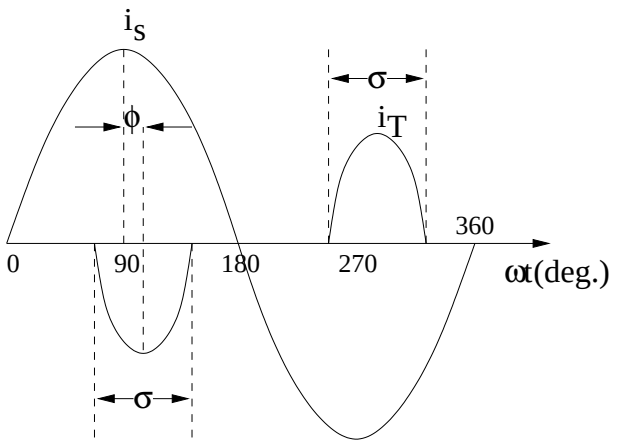

Figure 4.21: Transient waveforms

where ϕ is the phase angle by which the phasor $-\hat{I}_T$ lags the phasor $\hat{I}_S$. (see Fig. 4.21). It is assumed that the peak value of the current in the TCR branch occurs at the midpoint of the conduction period. The angle ϕ can be expressed as

$$\begin{aligned} \phi &= arg[-I_s\bar{I}_T] \\ &= arg[-jI_s\bar{V}_C] \end{aligned} \tag{4.89}$$

where $\bar{I}_T$ and $\bar{V}_C$ indicate complex conjugates of I_T and V_C respectively.

Remarks

The model based on Eqs. (4.85), (4.86) to (4.89) has given accurate results for constant α control of a TCSC. The results predicted from the model were compared with the simulation results [33].

A Case Study

The system considered is based on IEEE First Benchmark Model (FBM) [32,42]. The generator data are identical. The reactance external to the generator terminals is assumed to be 1.0 pu including the leakage reactance of the generator transformer and the system impedance at the receiving end of the line. The series resistance is assumed to be 0.02 pu (which is on the low side). The generator is provided with a static excitation system having data $K_A = 200$, $T_A = 0.025$ s. The operating conditions are $V_g = E_b = 1.0$, $P_b = 1.0$ (V_g and E_b are voltage magnitudes at the generator terminals and the infinite bus respectively). A speed input PSS is provided to damp low frequency rotor oscillations. A torsional filter in the PSS is designed to avoid SSR interactions.

The series compensation consists of a fixed capacitor of 0.28 pu in series with a TCSC ($X_C = 0.1$, $\lambda = 2.0$). The system model is linearized at the operating point and the eigenvalues of the system matrix are computed. The eigenvalues corresponding to the torsional and the network modes are shown in Table 4.1 for the two cases (i) $\sigma = 0$ and (ii) $\sigma = 50°$. For the first case, $X_{TCSC} = X_C$ and for the second case, $X_{TCSC} = 1.19\ X_C$.

Table 4.1: Eigenvalues corresponding to torsional and network modes.

Case (i): $\sigma = 0$	Case (ii): $\sigma = 50°$	Comments
$-1.8504 \pm j298.17$	$-1.8504 \pm j298.17$	Mode 5
$-0.3612 \pm j202.74$	$-0.3036 \pm j202.75$	Mode 4
$0.8260 \pm j160.95$	$-0.3916 \pm j160.58$	Mode 3
$-0.0729 \pm j127.00$	$-0.0563 \pm j127.00$	Mode 2
$-0.2338 \pm j99.18$	$-0.1618 \pm j99.18$	Mode 1
$-0.6739 \pm j9.36$	$-0.6271 \pm j9.53$	Mode 0 (Swing mode)
$-3.5581 \pm j161.39$	$-20.905 \pm j163.44$	Subsynch. Network mode
$-3.4802 \pm j592.18$	$-21.064 \pm j566.41$	Supersynch. Network mode

From the results, it is observed that the third torsional mode (having radian frequency of 161) is unstable for case (i) but stable for the case (ii). Mode 5 is not affected by the external network as it has very high modal inertia. The damping of modes 0, 1, 2 and 4 is reduced for the case (ii) while the damping of the network modes is significantly increased.

The stability of the torsional modes is investigated as the conduction angle is increased from 0° to 80°. It was observed that the system was stable only in the range $32° < \sigma < 72°$. For $\sigma < 32°$, the instability is due to mode 3 while for $\sigma > 72°$, mode zero causes instability. The analytical results were validated by detailed transient simulation [33].

The dynamic phasor model of the TCSC gives reasonably accurate results. It is observed that the network resonance frequency is marginally increased by the vernier operation of TCSC.

4.8.4 A TCSC Model Based on Switching Functions

From Fig. 4.5, the current in the TCR branch is described by Eq. (4.7) given below.

$$L\frac{di_T}{dt} = v_C(t) \cdot u(t) \tag{4.90}$$

where $u(t)$ is a switching function. In steady state it is periodic (of frequency 2 f_0) and is shown in Fig. 4.22.

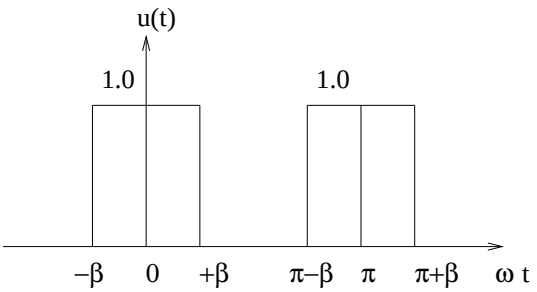

Figure 4.22: Switching function for the TCR

From Fig. 4.22, we have

$$\begin{aligned} u(t) &= 1, \quad -\beta \leq \omega t \leq \beta \\ &= 0, \quad \beta \leq \omega t \leq \pi - \beta \end{aligned}$$

We can approximate $u(t)$, by Fourier analysis

$$u(t) \simeq U_0 + U_1 \cos 2\omega t \tag{4.91}$$

where

$$U_0 = \frac{2\beta}{\pi}, \quad U_1 = \frac{2}{\pi} \sin 2\beta$$

If $v_C(t) = V_1 \sin \omega_0 t + \Delta v_C(t)$, substituting in Eq. (4.90) results in

$$L\frac{di_T}{dt} = (U_0 + U_1 \cos 2\omega t_0)(V_1 \sin \omega_0 t + \Delta v_C(t)) \tag{4.92}$$

Case (i) $\Delta v_C(t) = 0$

$$\begin{aligned} L\frac{di_T}{dt} &= \frac{U_1 V_1 \sin 3\omega_0 t}{2} + V_1 \sin \omega_0 t \left(U_0 - \frac{U_1}{2}\right) \\ i_T(t) &= -\frac{U_1 V_1 \cos 3\omega_0 t}{6X_L} - \frac{V_1 \cos \omega_0 t}{X_L} \left(U_0 - \frac{U_1}{2}\right) \end{aligned}$$

Substituting the above expression in Eq. (4.6), we get

$$\begin{aligned} C\frac{dv_C}{dt} &= I_m \cos \omega_0 t - i_T(t) \\ &= \left[I_m + \frac{V_1}{X_L}\left(U_0 - \frac{U_1}{2}\right)\right] \cos \omega_0 t + \frac{U_1 V_1}{6X_L} \cos 3\omega_0 t \end{aligned}$$

The fundamental component (V_1) can be obtained from substituting $v_C(t) = V_1 \sin\omega_0 t$ in the L.H.S. of the above equation. We get

$$\begin{aligned} \frac{V_1}{X_C}\cos\omega_0 t &= \left[I_m + \frac{V_1}{X_L}\left(U_0 - \frac{U_1}{2}\right)\right]\cos\omega_0 t \\ V_1 &= \frac{I_m X_C}{1 - U_0\lambda^2 + \frac{U_1}{2}\lambda^2} \end{aligned} \tag{4.93}$$

From Eq. (4.93), we obtain X_{TCSC} as

$$X_{TCSC} = \frac{V_1}{I_m} = \frac{X_C}{1 - \left(\frac{2\beta}{\pi} - \frac{\sin 2\beta}{\pi}\right)\left(\frac{X_C}{X_L}\right)} \tag{4.94}$$

Note that the above expression is identical to the one where X_{TCR} is approximated as

$$X_{TCR} \simeq \frac{\pi X_L}{\sigma - \sin\sigma} = \frac{\pi X_L}{2\beta - \sin 2\beta}$$

Case (ii) $\Delta v_C(t) \neq 0$.

As discussed in section 4.8.2, the torsional oscillations (of frequency ω_m) in the rotor lead to the presence of subsynchronous components (of frequency, $(\omega_0 - \omega_m)$) and a supersynchronous (of frequency, $(\omega_0 + \omega_m)$) components in the voltages and currents in the transmission line. Hence, we can assume that

$$\Delta v_C(t) = V_{sub}\sin\omega_{sub}t + V_{sup}\sin\omega_{sup}t \tag{4.95}$$

where, $\omega_{sub} = \omega_0 - \omega_m = \omega_e$, $\omega_{sup} = \omega_0 + \omega_m = 2\omega_0 - \omega_e$.

The Eq. (4.95) represents the response of the TCSC to the presence of the perturbations in the line current given by

$$\Delta i_s(t) = I_{sub}\cos\omega_{sub}t + I_{sup}\cos\omega_{sup}t \tag{4.96}$$

The perturbation in the current flowing in the TCR branch is obtained from

$$L\frac{d\Delta i_T}{dt} = (U_0 + U_1\cos 2\omega_0 t)(V_{sub}\sin\omega_e t + V_{sup}\sin(2\omega_0 - \omega_e)t) \tag{4.97}$$

Neglecting higher frequency components in $\Delta i_T(t)$ and considering only subsynchronous and supersynchronous components, we can obtain

$$\begin{aligned} \Delta i_T(t) &= \frac{1}{L\omega_{sub}}\left[\frac{U_1}{2}V_{sup} - U_0 V_{sub}\right]\cos\omega_{sub}t \\ &\quad + \frac{1}{L\omega_{sup}}\left[\frac{U_1}{2}V_{sub} - U_0 V_{sup}\right]\cos\omega_{sup}t \end{aligned} \tag{4.98}$$

Substituting Eqs. (4.95) and (4.98) in

$$C\frac{d\Delta v_C(t)}{dt} = \Delta i_s(t) - \Delta i_T(t) \tag{4.99}$$

permits us to relate I_{sub}, I_{sup} to V_{sub} and V_{sup}. The final equations are

$$C\omega_{sub}V_{sub} = I_{sub} - \frac{1}{L\omega_{sub}}\left[\frac{U_1}{2}V_{sup} - U_0 V_{sub}\right] \tag{4.100}$$

$$C\omega_{sup}V_{sup} = I_{sup} - \frac{1}{L\omega_{sup}}\left[\frac{U_1}{2}V_{sub} - U_0 V_{sup}\right] \tag{4.101}$$

The above equations can be expressed as,

$$\begin{bmatrix} \bar{\omega}_{sub}B_C\left(1 - \frac{U_0}{\omega_{sub}^2 LC}\right) & \frac{U_1 B_C \bar{\omega}_{sub}}{2\omega_{sub}^2 LC} \\ \frac{U_1 B_C \bar{\omega}_{sup}}{2\omega_{sup}^2 LC} & \bar{\omega}_{sup}B_C\left(1 - \frac{U_0}{\omega_{sup}^2 LC}\right) \end{bmatrix} \begin{bmatrix} jV_{sub} \\ jV_{sup} \end{bmatrix} = \begin{bmatrix} I_{sub} \\ I_{sup} \end{bmatrix} \tag{4.102}$$

where

$$\bar{\omega}_{sub} = \frac{\omega_{sub}}{\omega_0}, \quad \bar{\omega}_{sup} = \frac{\omega_{sup}}{\omega_0}, \quad B_C = \omega_0 C$$

The above equation indicates that a subsynchronous current can result in a supersynchronous voltage and vice versa. This is unlike in a passive linear circuit where the sub- and super-synchronous currents produce only voltages having the same frequency as the line current. The presence of the supersynchronous frequency voltage across the TCSC due to subsynchronous frequency currents has been reported in ref. [34] from SSR studies and TNA (Transient Network Analyzer) test results. However, a mathematical analysis is not presented.

Remarks

1. The determinant of the matrix in Eq. (4.108) can be expressed as

$$Det = \bar{\omega}_{sub}\bar{\omega}_{sup}B_C^2\left[a_1 a_4 - \frac{U_1^2\lambda^4}{4\bar{\omega}_{sub}\bar{\omega}_{sup}^2}\right]$$

where

$$a_1 = 1 - \frac{U_0\lambda^2}{\bar{\omega}_{sub}^2}, \quad a_4 = 1 - \frac{U_0\lambda^2}{\bar{\omega}_{sup}^2}$$

For small values of β, it is obvious that

$$U_1 \simeq 2U_0$$

With the above approximation, we can obtain

$$Det \simeq \bar{\omega}_{sub}\bar{\omega}_{sup}B_C^2\left[1 - U_0\lambda^2\left(\frac{1}{\bar{\omega}_{sub}^2} + \frac{1}{\bar{\omega}_{sup}^2}\right)\right]$$

The determinant is zero for $\beta = \beta_{cr}$ where β_{cr} is defined as

$$\beta_{cr} = \frac{\pi}{4}\frac{(\omega_0^2 - \omega_m^2)^2}{\lambda^2(\omega_0^2 + \omega_m^2)\omega_0^2} \tag{4.103}$$

For $\lambda = 2.5$, $\omega_m = 0.4\omega_0$, we get $\beta_{cr} = 10.43°$.

If $\beta > \beta_{cr}$, the nature of the TCSC reactance changes from capacitive to inductive.

2. If the switching function is represented by more terms in the Fourier series it is possible to get improved accuracy of the results. For example, X_{TCSC} corresponding to the fundamental frequency would be calculated with better accuracy than what is obtained from Eq. (4.94). However, for small values of β, the approximation given by Eq. (4.94) is considered to be adequate [9].

The computation of harmonic voltage across the TCSC can also be obtained from an accurate Fourier analysis of the switching function. In general, the switching function $u(t)$ can be expressed as

$$u(t) = U_0 + U_1\cos 2\omega_0 t + \cdots U_n \cos 2n\omega_0 t$$

where

$$U_n = \frac{2}{\pi}\int_{-\pi/2}^{\pi/2}\cos 2n\theta d\theta = \frac{2}{\pi}\frac{\sin 2n\beta}{n}$$

3. The analysis has assumed that the sub- and supersynchronous currents are in phase. However, this assumption does not affect the critical nature of β at which the determinant changes sign (as it goes through zero).

It is to be noted that the calculation of sub- and supersynchronous currents would depend also on the passive elements of the network. If it is assumed that $I_{sup} \simeq 0$, then Eq. (4.102) can be approximated as

$$\frac{-j\omega_{sub}(B_C)}{Det}\left(1 - \frac{U_0}{\bar{\omega}_{sup}LC}\right)I_{sub} = V_{sub}$$

It is obvious that there is a value (β_z) of β at which the reactance is zero. This value for the data given is $\beta_z = 20.2°$.

4.8.5 A Discrete Control Strategy for TCSC to Damp Subsynchronous Oscillations

It was mentioned earlier, that the TCSC has to be operated in the (capacitive) vernier mode to enable mitigation of SSR. In this subsection, we discuss the possibility of using discrete control of TCSC by using Thyristor Switched Series capacitors (TSSC). The control strategy is based on the concept of phase imbalance proposed by Edris in [35] and [36].

The damping torque coefficient T_{De} can be approximately evaluated as (Eq. 4.64)

$$T_{De}(\omega_m) \simeq \frac{-(\omega_0 - \omega_m)}{2\omega_m} G_p(\omega_0 - \omega_m)$$

Here G_p is the conductance of the positive sequence network, evaluated at the frequency $(\omega_0 - \omega_m)$. When there is phase imbalance, the admittance (Y_p) of the positive sequence network is given by

$$Y_p = \frac{1}{3}(Y_{aa} + Y_{bb} + Y_{cc}) \tag{4.104}$$

where Y_{aa}, Y_{bb} and Y_{cc} are the self admittances of the phases a, b, and c respectively. For simplicity, mutual admittances are neglected.

Assuming that all three phases are balanced and the electrical resonance frequency (ω_r) is $(\omega_0 - \omega_m)$, then we get

$$G_p(\omega_0 - \omega_m) = \frac{1}{R} \tag{4.105}$$

In deriving the above, we have assumed that

$$\begin{aligned}
Y_{aa} &= Z_{aa}^{-1}, \quad Z_{aa} = R + j\left(\omega L - \frac{1}{\omega C_a}\right) \\
Y_{bb} &= Z_{bb}^{-1}, \quad Z_{bb} = R + j\left(\omega L - \frac{1}{\omega C_b}\right) \\
Y_{cc} &= Z_{cc}^{-1}, \quad Z_{cc} = R + j\left(\omega L - \frac{1}{\omega C_c}\right)
\end{aligned}$$

Note that the imbalance is introduced by unequal capacitance in the three phases. This results in unequal resonance frequencies in the three phases.

If we assume that only phase b has a resonance frequency of $(\omega_0 - \omega_m)$, we can calculate G_p as

$$G_p = G_{pu} = \frac{1}{3}\left[\frac{R}{R^2 + (\omega_0 - \omega_m)^2 L^2 \left(1 - \frac{\omega_{ra}^2}{\omega_r^2}\right)^2} + \frac{1}{R} + \frac{R}{R^2 + (\omega_0 - \omega_m)^2 L^2 \left(1 - \frac{\omega_{rc}^2}{\omega_r^2}\right)^2}\right]$$

where

$$\omega_{ra}^2 = \frac{1}{LC_a}, \quad \omega_{rc}^2 = \frac{1}{LC_c}, \quad \omega_r = \frac{1}{LC_b} = \omega_0 - \omega_m$$

Obviously, we have $G_{pu} < \frac{1}{R}$. Thus, phase imbalance can reduce the negative damping introduced by series capacitors. In general, phase imbalance can mitigate torsional interaction (Note that TI is maximum when $\omega_r = \omega_0 - \omega_m$).

A case study based on IEEE SBM (Second Benchmark Model) [32] is presented in ref. [37]. With a 55% balanced compensation in the series compensated line, it was observed that the torsional mode 1 (at 24.6 Hz) becomes unstable. However, with zero compensation in phase a, 75% compensation in phase c without altering the level of compensation in phase b (55%) stabilizes the system with minimum value of the (negative) T_{De}. The analytical results have been validated by detailed transient simulation. It was also observed that the torsional mode is equally damped when the compensation levels in phases a and c are reduced from 55% to 10% (without altering compensation of phase b).

4.8.6 Analysis of SSR with GCSC

The analysis is based on similar lines as that given in section 4.8.4. Consider the circuit of GCSC shown in Fig. 4.23.

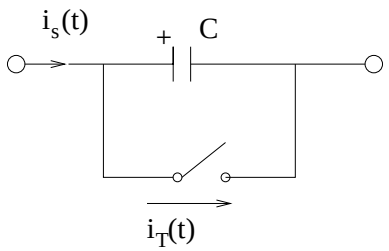

Figure 4.23: GCSC circuit

The equation for the capacitor voltage $v_c(t)$ is given by

$$C\frac{dv_C}{dt} = i_s(t) - i_T(t)$$

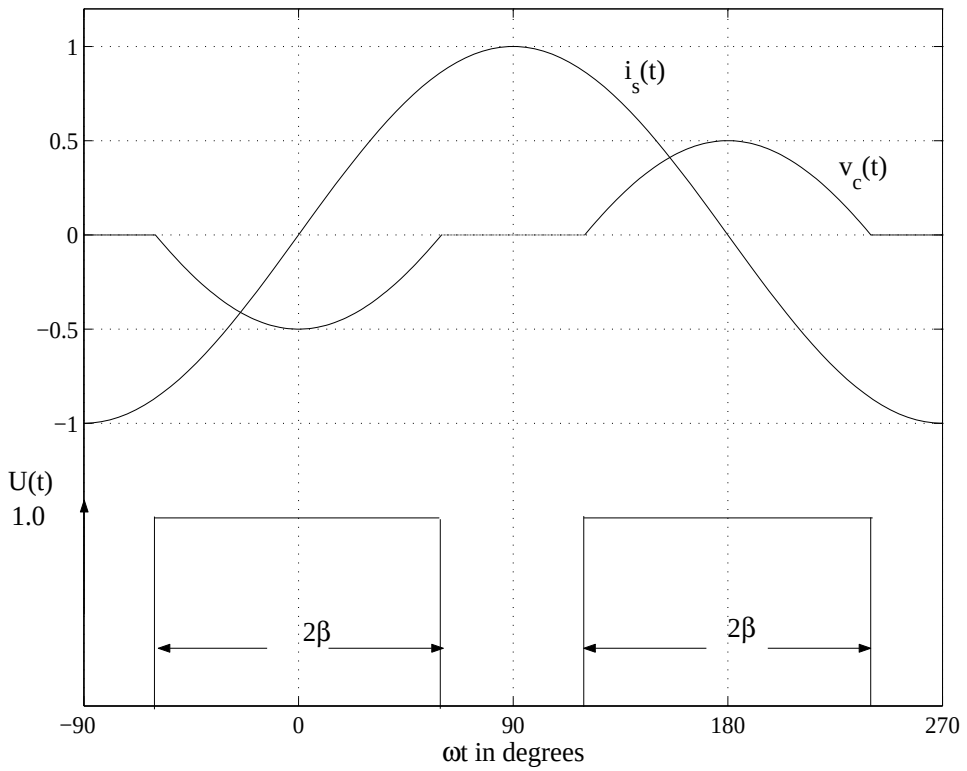

Figure 4.24: Line current, capacitor voltage and switching function waveforms in a GCSC

where

$$i_T(t) = (1 - u(t))i_s(t)$$

Hence,

$$C\frac{dv_c}{dt} = u(t)i_s(t) \tag{4.106}$$

We can approximate $u(t)$ (as before) as

$$u(t) \simeq U_0 + U_1 \cos 2\omega_0 t$$

The line current, $i_s(t)$ is defined by

$$i_s(t) = -I_s \sin \omega_0 t + \Delta i_s(t) \tag{4.107}$$

Fig. 4.24 shows the line current, capacitor voltage and switching function waveforms. Note that the period of the switching function is $\frac{\pi}{\omega_0}$ as before.

Case (i) $\Delta i_s(t) = 0$

Substituting Eq. (4.107) in (4.106), we obtain the fundamental component of $v_C(t)$ as

$$v_{C1}(t) = V_1 \cos \omega_0 t$$

where

$$V_1 = I_s X_C \frac{(2\beta - \sin 2\beta)}{\pi} \tag{4.108}$$

Note that the blocking angle (measured from the instant of the peak of the line current) is $\gamma = \frac{\pi}{2} - \beta$ and the hold off angle (δ) is 2β.

Case (ii)

$$\Delta i_s(t) = -I_{sub} \sin \omega_{sub} t - I_{sup} \sin \omega_{sup} t \tag{4.109}$$

Substituting Eq. (4.109) in (4.108) and simplifying we can derive the following equation

$$v_C(t) = V_1 \cos \omega_0 t + V_{sub} \cos \omega_{sub} t + V_{sup} \cos \omega_{sup} t \tag{4.110}$$

where V_{sub} and V_{sup} are related to I_{sub} and I_{sup} by the equation

$$\begin{bmatrix} V_{sub} \\ V_{sup} \end{bmatrix} = \begin{bmatrix} \frac{U_0}{C\omega_{sub}} & \frac{-U_1}{2C\omega_{sub}} \\ \frac{-U_1}{2C\omega_{sup}} & \frac{U_0}{C\omega_{sup}} \end{bmatrix} \begin{bmatrix} -jI_{sub} \\ -jI_{sup} \end{bmatrix} \tag{4.111}$$

The determinant of the 2×2 matrix can be expressed as

$$Det = \frac{1}{C^2 \omega_{sub} \omega_{sup}} \left(U_0 - \frac{U_1}{2}\right) \left(U_0 + \frac{U_1}{2}\right) \tag{4.112}$$

Since,

$$U_0 = \frac{2\beta}{\pi}, \quad U_1 = \frac{2}{\pi} \sin 2\beta$$

we note that

$$Det = \frac{X_C X_{GCSC} (2\beta + \sin 2\beta)}{\bar{\omega}_{sub} \cdot \bar{\omega}_{sup} \pi}$$

where

$$\bar{\omega}_{sub} = \frac{\omega_{sub}}{\omega_0}, \quad \bar{\omega}_{sup} = \frac{\omega_{sup}}{\omega_0}$$

and

$$X_{GCSC} = X_C \frac{(2\beta - \sin 2\beta)}{\pi}$$

It is obvious that Det is always positive and no change of sign occurs. Thus a GCSC (unlike a TCSC) has capacitive response.

If $I_{sup} \simeq 0$, then we obtain

$$V_{sub} = \frac{2\beta}{\pi C \omega_{sub}} I_{sub} = \frac{1}{C' \omega_{sub}} I_{sub} \tag{4.113}$$

where C' can be expressed as

$$C' = C_{eq} \left(1 - \frac{\sin 2\beta}{2\beta}\right) \tag{4.114}$$

where

$$C_{eq} = \frac{\pi C}{2\beta - \sin 2\beta} \tag{4.115}$$

If a fixed capacitor of value C_{eq} is used instead, we would obtain,

$$V_{sub} = \frac{1}{\omega_{sub} C_{eq}} I_{sub} \tag{4.116}$$

Thus the effect of GCSC is to modify the effective value of the capacitance from C_{eq} to C' which results in determining the resonance. It is to be noted that we have assumed that the hold off angle is held constant by the GCSC firing controls.

The mitigation of SSR by a GCSC is limited to changing the resonance frequency as compared to a fixed capacitor. This may not be adequate and Subsynchronous Damping Controller (SSDC) may have to be used as a supplementary controller to damp subsynchronous oscillations.

4.9 Applications of TCSC

The major objective in applying TCSC is to increase power transfer capacity in critical transmission lines (typically tie lines) under contingency conditions. Under normal steady state conditions, series compensation using fixed capacitors may be adequate unless SSR becomes a problem. A TCSC may be used in such cases to damp (mitigate) SSR by converting a part of the fixed compensation to controllable series compensation.

Often, the contingency conditions are also accompanied by low frequency oscillations that can threaten dynamic security. Sometimes, transient stability may be affected. Thus, it becomes necessary to provide Power Oscillation Damping (POD) using appropriate control signals synthesized from local measurements. Typically active power or line current have been suggested as input to POD [27].

In the restructured electricity supply regime, the problem is to increase the Available Transfer Capability (ATC) which is defined as a measure of transfer capability for transfers of power for further commercial activity, over and above already committed uses [38]. The reference [39] has discussed the application of SVC and TCSC to maximize ATC. The optimal size of a FACTS controller such as a TCSC is defined as that which results in the minimum cost of enhancing ATC.

An important consideration in the application of TCSCs is their location. Based on DC power flow analysis, a technique is suggested in [40] that ranks the effectiveness of the location of a TCSC. The norm of the

sensitivity vector $\left[\frac{\Delta P_L}{\Delta X_j}\right]$ when the i^{th} element of the vector is given by $\frac{\Delta P_{Li}}{\Delta X_j}$, determines the rank. Here, ΔP_{Li} is the change in the power flow in i^{th} line when there is a change in the reactance of line j. The sum norm of a vector v is defined by

$$Norm[v] = \sum_{i=1}^{n} |v(i)|$$

is suggested as a convenient measure. The line which results in maximum value of the norm is the most effective location. It is to be noted that within a line, the location of the controller is not significant.

The ratings of the TCSC are determined from power flow, SSR and transient stability studies [24].

The choice of $\lambda\left(\frac{\omega_r}{\omega_0}\right)$ is important in the design of a TCSC. Higher values require increased thyristor currents and ratings of the TCR. In Kayenta TCSC, λ was reduced by doubling the value of the inductance from 3.4 to 6.8 mH. As mentioned earlier, λ should be less than 3 to ensure that only one resonance occurs in the range $0 \leq \beta \leq 90^\circ$ (Note that $\beta_{res} = 90^\circ/\lambda$).

In India, the first (commercial) TCSC was commissioned on 400 kV Raipur-Rourkela double circuit link in September 2004. A combination of 40% fixed series compensation and 5-15% variable compensation (TCSC) is used to provide dynamic power control during a HVDC pole outage of Talcher-Kolar HVDC link.

References and Bibliography

1. L. Angquist, B. Lundin and J. Samuelsson, "Power Oscillation Damping Using Controlled Reactive Power Compensation - A Comparison between Series and Shunt Approaches", IEEE Trans. on Power Systems, v.8, n.2, 1993, pp.687-700
2. F.P deMello, "Exploratory Concepts on Control of Variable Series Compensation in Transmission Systems to Improve Damping of Intermachine/System Oscillations", IEEE Trans. on Power Systems, v.9, n.1, 1994, pp.102-108
3. R. Johnson, P. Krause, A. Montoya, N. Christl and R. Hedin, "Power System Studies and Modelling for the Kayenta 230 kV Substation Advanced Series Compensation", IEE Fifth Int. Conf. on AC and DC Power Transmission, Sept.17-20, 1991, London, UK.
4. N. Christl, R. Hedin, K. Sadek, P. Lutzelburger, P.E. Krause, S.M. McKenna, A.H. Montoya and D. Torgerson, "Advanced Series Compensation(ASC) with Thyristor Controlled Impedance", CIGRE , Paper 14/37/38-05, 1992

5. A.J.F. Keri, B.J. Ware, R.A. Byron, A.S. Mehraban, M. Chamia, P. Halverson and L. Angquist, "Improving Transmission System Performance Using Controlled Series Capacitors", CIGRE , Paper 14/37/38-07, 1992

6. J.Vithayathil, C. Taylor, M, Klinger and W. Mittelstadt, "Case Studies of Conventional and Novel Methods of Reactive Power Control on AC Transmission Systems", CIGRE, SC 38-02, 1988

7. J. Urbanek, R.J. Piwko, E.V. Larsen, B.L. Damsky, B.C. Furumasu, W. Mittelstadt and J.D. Eden, "Thyristor Controlled Series Compensation Prototype Installation at the Slatt 500 kV Substation", IEEE Trans. on Power Delivery, v.8, n.3, 1993, pp.1460-1469

8. R.J. Piwko, C.A. Wegner, B.C. Furumasu, B.L. Damsky and J.D. Eden, "The Slatt Thyristor-Controlled Series Capacitor Project-Design, Installation, Commissioning and System Testing", CIGRE, Paper 14-104, 1994

9. S.G. Helbing and G.G. Karady, "Investigations of an Advanced Form of Series Compensation", IEEE Trans. on Power Delivery, v. 9, n. 2, 1994, pp.939-947

10. J.J Paserba, N.W. Miller, E.V Larsen and R.W. Piwko, "A Thyristor Controlled Series Compensation Model for Power System Stability Analysis", IEEE Trans. on Power Delivery, v.10, n.3, 1995, pp.1471-1478

11. M. Noroozian and G. Andersson, "Power Flow Control by Use of Controllable Series Components", IEEE Trans. on Power Delivery , v.8, n.3, 1989, pp. 12-18

12. M. Noroozian and G. Andersson, "Damping of Power System Oscillations by Controllable Components", IEEE Trans. on Power Delivery , v.9, n.4, 1994, pp. 2046-2054

13. J.F Gronquist, W.A Sethares, F.L Alvarado and R.H. Lasseter, "Power Oscillation Damping Control Strategies for FACTS Devices Using Locally Measurable Quantities", IEEE Trans. on Power Systems, v.10, n.3, 1995, pp.1598-1605

14. L.Angquist, G. Ingestrom and H.A. Jonsson, "Dynamical Performance of TCSC Schemes", CIGRE, Paper 14-302, 1996

15. K.R.Padiyar, M.K.Geetha and K. Uma Rao, "A Novel Power flow controller for Controlled Series Compensation"IEE Conf. Publication No.423, Sixth Int Conf on AC and DC transmission,London, May 1996,pp.329-334

16. K.R.Padiyar and K.Uma Rao, "Discrete Control of Series Compensation for Stability Improvement in Power System",to appear in Int.J. of Electrical Power and Energy Systems, v.19, n.5, 1997, pp.311-319

17. E. Larsen, C. Bowler, B. Damsky and S. Nilsson, "Benefits of Thyristor Controlled Series Compensation", Paper 14/37/38-04, CIGRE 1992.

18. H.A. Othman and L. Angquist, "Analytical modeling of Thyristor-Controlled Series Capacitors for SSR studies", IEEE Trans. on Power Systems, v. 11, n. 1, February 1996, pp. 119-127.

19. R. Rajaraman and I. Dobson, "Damping estimates of subsynchronous and power swing oscillations in power systems with thyristor switching devices", IEEE Trans. on Power Systems, v. 11, n.4, November 1996, pp. 1926-1930.

20. R. Rajaraman, I. Dobson, R.H. Lasseter and Y. Shern, "Computing the damping of subsynchronous oscillations due to a Thyristor Controlled Series Capacitor", Paper 95 SM 403-6 PWRD, IEEE PES Summer Meeting, Portland, Oregon, July 1995.

21. W. Zhu, R. Spee, R. Mohler, G.C. Alexander, W.A. Mittelstadt and D. Maratukulam, "An EMTP study of SSR mitigation using Thyristor Controlled Series Capacitor", Paper 94 SM 477-0, PWRD IEEE PES Summer Meeting, San Francisco, California, 1994.

22. S. Nyati, et al, "Effectiveness of Thyristor Controlled Series Capacitor in enhancing power system dynamics: an analog simulator study", IEEE Trans. on Power Delivery, v.9, n.2, April 1994, pp. 1018-1027.

23. D. Holmberg, M. Danielsson, P. Halvarsson and L. Angquist, "The Stode Thyristor Controlled Series Capacitor", Paper No. 14-105, CIGRE, 1998.

24. D.N. Kosterev, W.A. Mittelstadt, R.R. Mohler and W.J. Kolodziej, "An application study for sizing and rating controlled and conventional series compensation", paper 95 SM 401-0 PWRD, IEEE PES Summer Meeting, Portland, Oregon, 1995.

25. E.V. Larsen, K. Clark, S.A. Miske Jr. and J. Urbanek, "Characteristics and rating considerations of Thyristor Controlled Series Capacitor", IEEE Trans. on Power Delivery, v. 9, n.2, April 1994.

26. H. Okamoto, A. Kurita, K. Clark, E.V. Larsen and N.W. Miller, "Modeling and performance of multi-module TCSCs in ATP", paper 14-307, CIGRE, 1996.

27. C. Gama, L. Angquist, G. Ingestrom and M. Noroozian, "Commissioning and operative experience of TCSC for damping power oscillation in Brazilian North-South interconnections", Paper 14-104, CIGRE, 2000

28. P. Mattavelli, G.C. Verghese and A.M. Stankovic, "Phasor dynamics of Thyristor-Controlled Series Capacitor", IEEE Trans. on Power Systems, v. 12, n.3, August 1997, pp. 1259-1267.

29. P. Mattavelli, A.M. Stankovic and G.C. Verghese, "SSR analysis with dynamic phasor model of Thyristor - Controlled Series Capacitor", IEEE Trans. on Power Systems, v. 14, n.1, February 1999, pp. 200-208.

30. L.F.W. De Souza, E.H. Watanabe and M. Aredes, "A GTO Controlled Series Capacitor for distribution lines", Paper 14-201, CIGRE, 1998.

31. G.G. Karady, T.H. Ortmeyer, B.R. Pilvelait and D. Maratukulam, "Continuously regulated series capacitor", IEEE Trans. on Power Delivery, v. 8, n.3, July 1993, pp. 1348-1355.

32. K.R. Padiyar, **Analysis of Subsynchronous Resonance in Power Systems**, Kluwer Academic Publishers, Boston, 1999.

33. Venkatesh Prabhu, 'Modelling and simulation of TCSC and GCSC for SSR Studies' M.E. Project Report, Dept. of Elec. Engg., I.I.Sc., Jan. 2001.

34. R.A. Hedin, S. Weiss, D. Torgerson and L.E. Eilts, "SSR characteristics of alternative types of series compensation schemes", IEEE Trans. on Power Systems, v. 10, n.2, May 1995, pp. 845-852.

35. A. Edris, "Series compensation schemes reducing the potential of subsynchronous resonance", IEEE Trans. on Power Systems, v.5, n.1, Feb. 1990, pp. 219-226.

36. A. Edris, "Subsynchronous resonance countermeasure using phase imbalance", IEEE Trans. on Power Systems, v. 8, n.4, Nov. 1993, pp. 1438-1444.

37. Sujatha Subhash, B.N. Sarkar and K.R. Padiyar, "A novel control strategy for TCSC to damp subsynchronous oscillations", Conf. Publication No. 485, AC-DC Power Transmission, IEE, November 2001, London.

38. G.C. Ejebe, J. Tong, J.G. Waight, J.G. Frame, X. Wang and W.F. Tinney, "Available Transfer Capability Calculations", IEEE Trans. in Power Systems, v. 13, n.4, 1998, pp. 1521-1527.

39. C.A. Canizares, A. Berizzi and P. Marannino, "Using FACTS controllers to maximize Available Transfer Capability", Bulk Power Systems Dynamics and Control IV-Restructuring, Conference, August 1998, Greece.

40. Sujatha Subhash, B.N. Sarkar and K.R. Padiyar, "Sensitivity based determination of suitable locations for controlled series compensation for enhancement of steady state stability in a large power system", IFAC Symposium on "Control of Power Systems and Power Plants", Beijing, August 1997.

41. A.K. Datta, P.C. Garg and A. Dubey, "Operational experience of TCSC on 400 kV Raipur-Rourkela D/C line", Conference on Power Transmission, Central Power Research Institute, Bangalore, December 2005.

42. IEEE Committee Report, "First benchmark model for computer simulation of subsynchronous resonance", IEEE Trans., v. PAS-96, n. 5, 1977, pp. 1565-1570.

This page intentionally left blank

Chapter 5

Static Phase Shifting Transformer

5.1 General

Phase shifting transformers (PST) have been in use since 1930s for control of power flows in transmission lines in steady state. The primary objective is to control loop flows and ensure the power flow in the contracted path. They are not meant to increase power transfer in a line and hence not intended to be used in long lines. By applying power electronic controllers, the operation of PSTs can be made fast which enables dynamic regulation of power flow and improvement of system stability and dynamic security. These are called Static Phase Shifting Transformers (SPST) or Thyristor Controlled Phase Angle Regulator (TCPAR) as thyristor devices have been primarily suggested to achieve the objective. However, with the advent of Voltage Source Converter (VSC) based FACTS controllers it is also possible to apply a UPFC type device for SPST.

5.2 Basic Principle of a PST

Consider an ideal phase shifting transformer shown in Fig. 5.1. This also shows Thevenin's equivalents connected at the two ports of PST.

The turns ratio of the transformer is a complex quantity of magnitude unity ($a = e^{j\phi}$) where ϕ is the phase angle shift (positive or negative). From

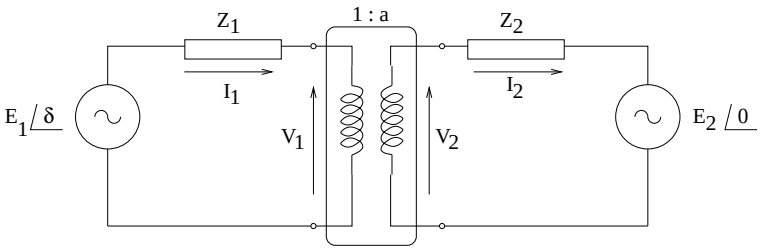

Figure 5.1: A PST connected in a network

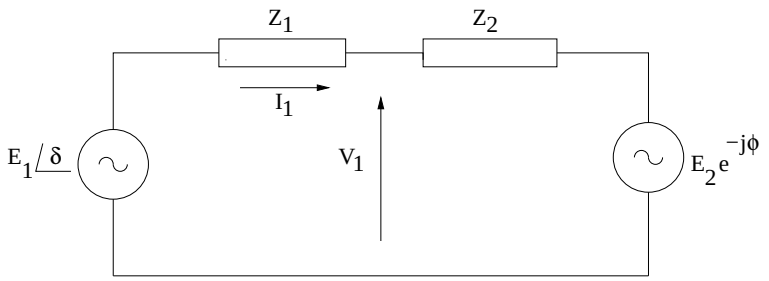

Figure 5.2: The equivalent circuit referred to primary

Fig. 5.1, we have

$$V_2 = aV_1, \quad I_1 = a^* I_2 = e^{-j\phi} I_2 \tag{5.1}$$

Note that Eq. (5.1) results from the fact that there is no power (both active and reactive) losses in an ideal transformer. That is

$$V_1 I_1^* = V_2 I_2^* \tag{5.2}$$

Since,

$$I_2 = \frac{V_2 - E_2}{Z_2} \tag{5.3}$$

we get from Eq. (5.1),

$$I_1 = \frac{a^*(aV_1 - E_2)}{Z_2} = \frac{V_1 - a^* E_2}{Z_2} \tag{5.4}$$

Eq. (5.4) represents the equivalent circuit shown in Fig. 5.2.

If the losses are neglected in the circuit, i.e.,

$$Z_1 = jx_1, \quad Z_2 = jx_2 \tag{5.5}$$

we can derive the power flow in the circuit as

$$P = \frac{E_1 E_2 \sin(\delta + \phi)}{(x_1 + x_2)} \tag{5.6}$$

Note that ϕ can be adjusted in the range

$$\phi_{\min} < \phi < \phi_{\max} \tag{5.7}$$

Typically the limits on ϕ are symmetric about zero, i.e. $\phi_{\min} = -\phi_{\max}$. The limits are directly related to the rating of the PST.

The question that arises now is how do we arrange for the phase shift? Noting that

$$e^{j\phi} \simeq 1 + j\phi \tag{5.8}$$

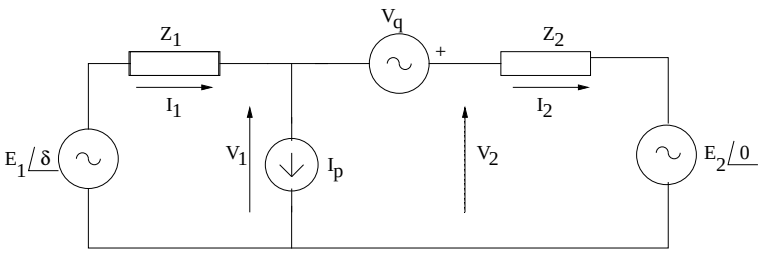

Figure 5.3: A representation for PST

for small values of ϕ, we get

$$V_1 - V_2 = (1 - a)V_1 = -j\phi V_1 = -V_q \tag{5.9}$$

Similarly,

$$I_1 - I_2 = (a^* - 1)I_2 = -j\phi I_2 = I_p \tag{5.10}$$

From Eq. (5.9) and (5.10) we can derive a representation of PST shown in Fig. 5.3.

Hence the voltage V_q injected in series is a voltage in quadrature with V_1. The current I_p is the shunt current drawn by the PST. It is obvious that

$$V_1 I_p^* = V_q I_2^* \tag{5.11}$$

indicating that the complex power drawn by the shunt current source (I_p) supplies the power supplied by the series quadrature voltage (V_q).

In a three phase system with a balanced set of source voltage applied to the primary windings of the PST (connected in delta), the voltage $V_{cb}(V_c - V_b)$ leads V_a by 90°. Similarly V_{ac} leads V_b and V_{ba} leads V_c by 90° each. This indicates a scheme to construct a PST as shown in Fig. 5.4. Here the secondary windings of the excitation transformer (ET), connected in shunt, supply the Boost Transformer (BT) connected in series with the line. In Fig. 5.4, only one phase of the ET and BT is shown in detail for clarity. The arrangement in other two phases is similar. The converter shown in Fig. 5.4 is connected between the ET and BT for controlling the magnitude and polarity of the quadrature voltage injected in series.

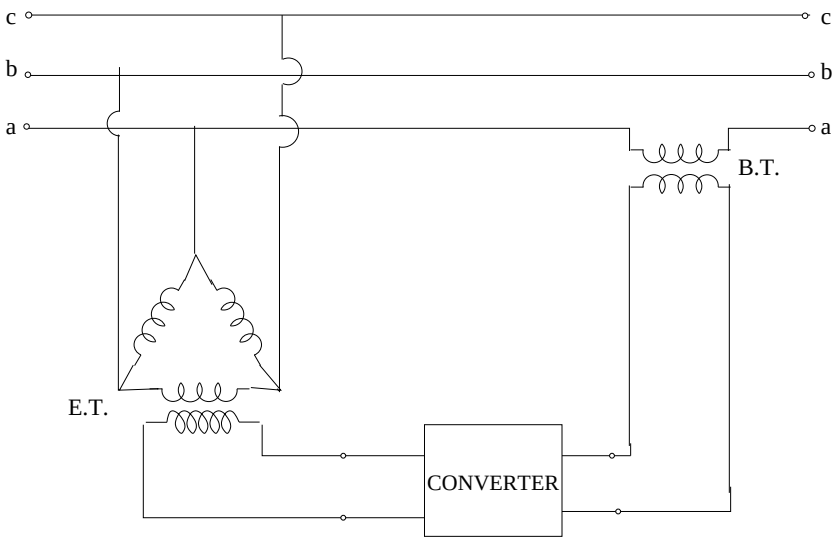

Figure 5.4: Schematic diagram of a SPST

Remarks

1. Typically bidirectional thyristor switches are used in the converter for control. These can be used for phase control (for continuous control of the phase shift) or switching in a step wise manner (for discrete control of the phase shift).

2. The loss of synchronism between the two power systems connected to the two ports of the SPST will result in δ not remaining constant in steady state. It may continuously increase or decrease. If ϕ can vary over 360° and can track the variation in δ, it is obvious (from Eq. (5.6)), that the power flow in the line can be held constant even if the SPST interconnects two asynchronous power systems. Thus a 360° SPST can be an alternative to BTB (Back to Back) HVDC link. However, BTB HVDC link is cheaper than a 360° SPST.

   An interesting concept suggested in reference [13] is to control a BTB HVDC link to operate as a SPST to provide some degree of synchronizing power. If all existing BTB links between two asynchronous systems (operating with identical, nominal frequency, for e.g. Western and Eastern U.S.A) provided synchronizing power, then there is a possibility of having additional interconnections to be AC.

3. While the use of semiconductor (solid state) switches such as thyristors enable fast control of the phase angle (ϕ) and can be used to damp low frequency and higher frequency subsynchronous oscillations, the direct control over ϕ is more suited to improving transient stability.

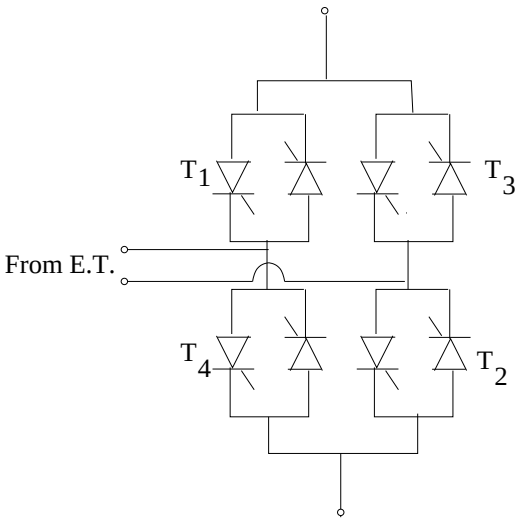

Figure 5.5: A bridge circuit using bidirectional thyristor switches

5.3 Configurations of SPST

While a detailed review of various configurations is presented in reference [8], we will consider here only 3 configurations given below

1. Point-on-wave controlled phase angle regulator
2. Discrete step controlled phase angle regulator
3. Using voltage source converter (VSC)

The first two configurations can be obtained using a single phase bridge circuit using four bi-directional thyristor switches (see Fig. 5.5). There are other configurations proposed in [1–3] which we will not take up as, in general, the use of continuous control of the phase angle (ϕ) is not desirable as it generates harmonics which are difficult to filter. (Note that zero sequence triplen harmonics are not eliminated).

For configuration 1, a single secondary winding (per phase) of the excitation transformer (E.T) is adequate as the control of the phase angle is provided by controlling the firing (delay) angle of the thyristor switch in relation to the applied voltage. The switches T_1 and T_2 are used for injecting the series voltage with positives polarity (boost), whereas T_3 and T_4 are used to inject the series voltage with negative or reverse polarity (buck). Thus, the phase shift of positive or negative angle can be achieved. If switches T_1 and T_4 (or T_2 and T_3) conduct, the output voltage remains zero.

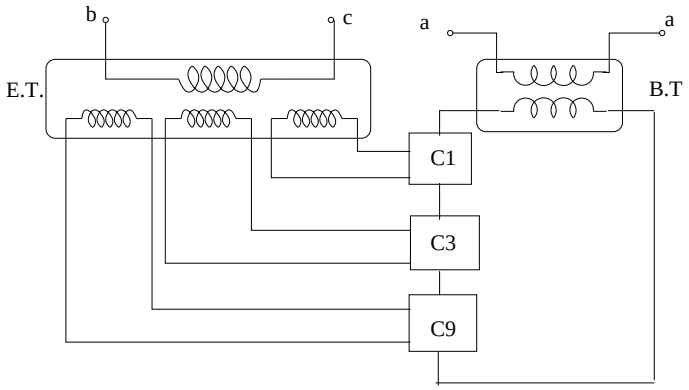

Figure 5.6: Simplified single phase representation of a discrete step SPST

For configuration 2 with discrete control, the conduction angle (σ) of the thyristor switches is maximum at 180°. The advantage is that the harmonic generation is eliminated. On the other hand, several secondary windings have to be provided on E.T. to have discrete control of the phase angle. With three secondary windings whose voltages (number of turns) are in the ratios of 1:3:9, it is possible to have 13 steps for each polarity. This requires a converter in one phase to have 3 sub-converters (each connected to its individual winding) connected in series (see Fig. 5.6).

Note that the voltage ratings of the thyristor valves (made up of series connection of thyristor pairs connected back to back) in converter C3 and C9 are three times and nine times respectively, the voltage rating of valves in converter C1.

Each subconverter can have three states – (i) with zero output voltage, (ii) with output voltage ($V_{ck} = kV_{step}$) and (iii) with output voltage ($V_{ck} = -kV_{step}$), where V_{step} is the quadrature voltage per step injected by the SPST. We can associate a control variable (u_{ck}) with each subconverter ck, which can take 3 values of 0, 1 or -1 and express the output voltage of the subconverter (ck) as

$$V_{ck} = u_{ck} \cdot kV_{step} \tag{5.12}$$

For a SPST with K subconverters, (supplied by K secondary windings of the E.T. whose voltages are in ratios of 1:3:9 . . . 3^{K-1}) we can have a total of M steps for each polarity (positive and negative) where M is given by

$$M = \sum_{i=0}^{K-1} 3^i \tag{5.13}$$

Thus, with $K = 4$, we get 40 steps which are quite adequate. For example, if we want to inject a quadrature voltage of 0.25 pu, the voltage corresponding to a single step is $V_{step} = \frac{0.25}{40} = 0.00625$ which is small enough. Thus, even though the control is discrete, it is reasonably smooth due to the adequate number of steps.

For $K = 3$, the values of the control variables for individual subconverters for all possible values of the step ($S = i$, which i ranges from 13 to -13) are shown in Table 5.1. It is to be noted that the quadrature voltage (V_q) injected by the SPST is given by

$$V_q = SV_{step} \tag{5.14}$$

where $S = 0, \pm i, i = 1, 2, \ldots, 13$.

It should be noted that for a given value of ($S = i$) , the control variables u_{ck}, are related to the values corresponding to $S = -i$. Thus,

$$u_{ck}^{(i)} = -u_{ck}^{(-i)}, \quad k = 1, 3, 9 \tag{5.15}$$

The switching of a subconverter from one state to another takes place when the current passes through zero. The converter output voltage can be adjusted within one half cycle of the system frequency.

When the variation of the quadrature voltage (V_q) is required only in one direction, (say from zero to a positive maximum) this can be achieved with a simplified converter circuit: two of the four bi-directional switches in each subconverter can be omitted. Also, a geometric progression with a factor of 2 can be chosen. With 4 secondary windings in the ratio of 1:2:4:8, 16 steps are obtained while with 3 windings in the ratio 1:2:4, there are 8 steps.

SPST Based on Voltage Source Converter

The converter shown in Fig. 5.4 can be made up of two, three phase Voltage Source Converters (VSC) connected to each other on the DC side as shown in Fig. 5.7. The equivalent circuits of this type of SPST is shown in Fig. 5.8. The injected series voltage (V_q) can be arranged to have the relation with V_1 as

$$V_q = V_1 e^{j\phi} \simeq jV_1\phi \tag{5.16}$$

Neglecting losses in the SPST (made up of the excitation and boost transformers, VSC1 and VSC2 and the DC capacitor), the power balance in the DC side requires

$$Re[V_1 I_p^*] = Re[V_q I_2^*] \tag{5.17}$$

Table 5.1: Control variables with 3 subconverters.

S	u_{c9}	u_{c3}	u_{c1}
13	1	1	1
12	1	1	0
11	1	1	−1
10	1	0	1
9	1	0	0
8	1	0	−1
7	1	−1	1
6	1	−1	0
5	1	−1	−1
4	0	1	1
3	0	1	0
2	0	1	−1
1	0	0	1
0	0	0	0
−1	0	0	−1
−2	0	−1	1
−3	0	−1	0
−4	0	−1	−1
−5	−1	1	1
−6	−1	1	0
−7	−1	1	−1
−8	−1	0	1
−9	−1	0	0
−10	−1	0	−1
−11	−1	−1	1
−12	−1	−1	0
−13	−1	−1	−1

This is to be contrasted with Eq. (5.11) which indicates two real constraints. Actually, the SPST configuration shown in Fig. 5.7 is a special case of the Unified Power Flow Controller where the series voltage injected is controlled according to Eq. (5.16) to provides variable phase shift within the limitations of its rating.

If V_1 is in phase with the line current I_2, V_q is the reactive voltage in quadrature with the current. In this case, the shunt converter can be dispensed with and only the series converter is retained. This is a Static

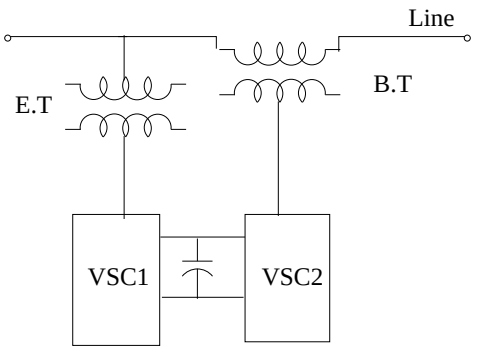

Figure 5.7: A single line diagram of VSC based SPST

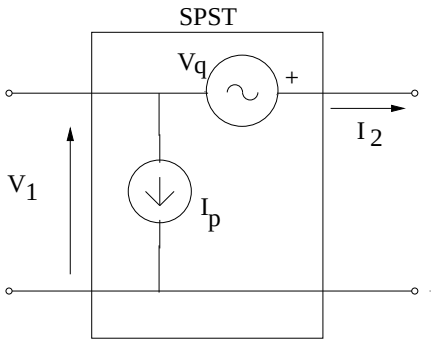

Figure 5.8: Equivalent circuit of a VSC based SPST

Synchronous Series capacitor (SSSC) mentioned in chapter 1. It has no real power exchange with the line in steady state except to meet the losses in the converter.

As discussed in chapter 2, the power factor at the midpoint of a symmetrical line is unity. Thus a SSSC connected at the midpoint can work as a SPST with varying magnitude of V_q. The negative value of V_q implies inductive operation with reduction in the power flow in the line (analogous to the negative phase angle shift).

It is interesting to compare a SSSC with a series capacitor also connected at the midpoint of the symmetric line. In this case also, the series capacitor can be viewed as providing a phase shift, however the magnitude of which is dependent on the line current. Also, while a fixed capacitor can provide only capacitive reactive voltage (assumed to be positive), SSSC has symmetric capability of positive and negative reactive voltage insertion.

Although a TCSC can be operated in the inductive vernier mode, this is normally not utilized. In any case, it has no symmetric capability in both directions.

5.4 Improvement of Transient Stability Using SPST

Although the general topic of improving transient stability with FACTS controllers will be taken up separately in chapter 11, this section will describe briefly the possibility of improving the transient stability by a simple control algorithm. This will be illustrated using a Single Machine connected to an Infinite Bus (SMIB) system and from equal area criterion.

Consider the SMIB system shown in Fig. 5.9. Here, the generator transformer is configured to work also as a SPST. Assuming a 3 phase fault occurs at the sending end of one of the transmission lines which is cleared by tripping the faulted line section. The power angle curves for (i) prefault and the (ii) postfault cases are shown in Fig. 5.10 for the case without SPST. If the area $A_2 < A_1$, then the system will be unstable. Since, the electrical power output (P_e) changes to

$$P_e = \frac{E_g E_b}{X} \sin(\delta \pm \phi) \tag{5.18}$$

in the presence of the SPST; the power angle curves for this case are shown in Fig. 5.11. Here, it is assumed that,

(a) The SPST is activated when (i) the electrical power output is maximum and $\frac{dP_e}{dt}$ changes from positive to negative

(b) The control algorithm is given by

$$\frac{d\phi}{dt} = \frac{d\delta}{dt} \tag{5.19}$$

The decelerating area (A_2) available now is (shown in Fig. 5.11) much larger than A_2 shown in Fig. 5.10.

Fig. 5.11 shows only the condition for the first (forward swing). The control algorithm of Eq. (5.19) can also be applied during the back swing to improve system stability.

Of course, this simple explanation indicates the capability of the fast control of the phase angle shift of the SPST in improving the first swing stability of a power system. In practice, different control algorithms can be used to realize the benefits while taking into account the various control constraints.

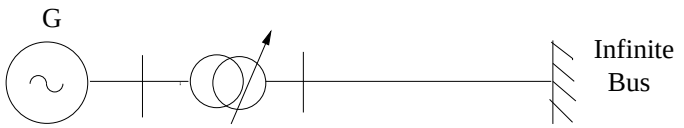

Figure 5.9: A SMIB system with SPST

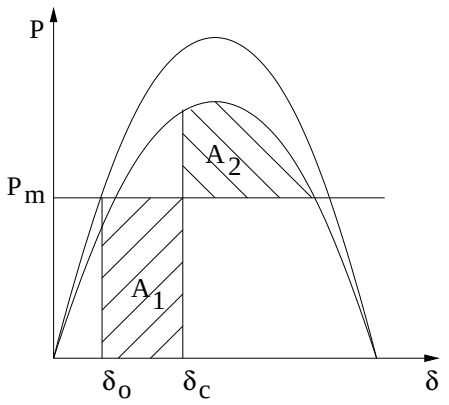

Figure 5.10: Power angle characteristics of a SMIB system

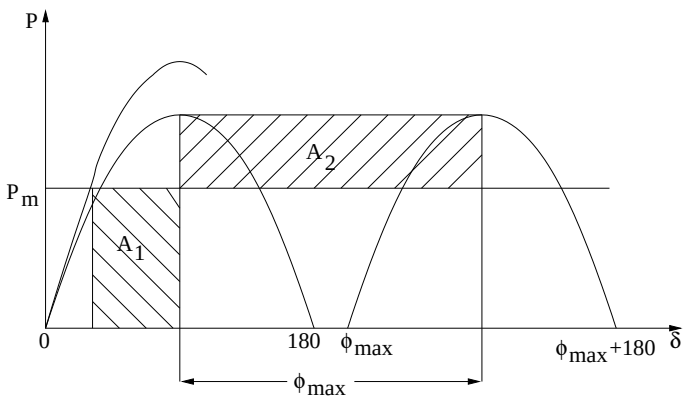

Figure 5.11: Power angle characteristics with the controlled SPST

5.5 Damping of Low Frequency Power Oscillations

Although the various issues involving the design of the Power Oscillation Damping (POD) will be taken up separately in chapter 10, a brief discussion of stabilizing the low frequency oscillations using a SPST is taken up here.

The problem of low frequency oscillations involving rotor swings is an old one, observed for the first time in the 1960s after the introduction of the fast acting exciters and electronic AVRs (Automatic Voltage Regulator). The development of Power System Stabilizer (PSS) which modulates the terminal voltage of the generator in response to the rotor swings, was a major milestone in the solution of the problem of small signal instability. With the advent of the power electronic controllers such as HVDC converters and SVC, an auxiliary damping controller could be easily implemented as a Supplementary Modulation Controller (SMC) to the power or voltage scheduling controller. A major feature of such SMC is that they utilize signals obtained from local measurements to synthesize the control signal to damp critical interarea modes which have the lowest frequencies and have the participation from many generators that are geographically separated. The outputs of such SMCs are generally limited to lie in narrow band such that they dont interfere with the basic control objectives.

There are several issues that are important in the application of SMCs. The location of the SMC, control signals used and the control algorithms are the basic issues while the concerns about adverse interaction with other controllers and their effect on subsynchronous torsional oscillations are other factors that need to be considered. Generally, damping controllers for low frequency (0.2 to 2.0 Hz) oscillations can destabilize subsynchronous frequency (10–50 Hz) oscillations due to the torsional modes.

Coming to the problem of design of SMC for SPST in a SMIB system, consider the system shown in Fig. 5.9. The small signal model for the system is obtained by linearizing the system equations at an operating point (equilibrium). Neglecting damper windings for simplicity, the block diagram representing the small signal stability model is shown in Fig. 5.12. The transfer functions use Heftron-Phillips constants evaluated at the operating point. The diagram of Fig. 5.12 can be simplified as shown in Fig. 5.13 where the transfer function $K_{1e}(s)$ is defined as

$$K_{1e}(s) = \frac{\Delta T_e(s)}{\Delta \delta(s)} \tag{5.20}$$

The damping torque (T_D) and synchronizing torque (T_S) coefficients are defined as

$$T_S(\omega) = Re[K_{1e}(j\omega)], T_D(\omega) = \frac{\omega_B}{\omega} Im[K_{1e}(j\omega)] \tag{5.21}$$

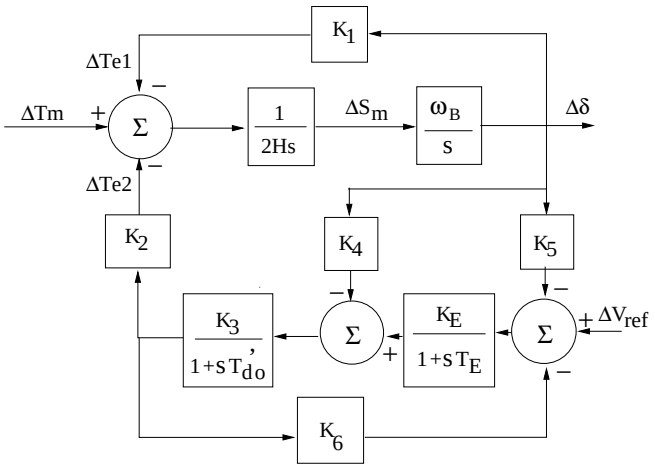

Figure 5.12: Block diagram representing small signal stability of a SMIB system

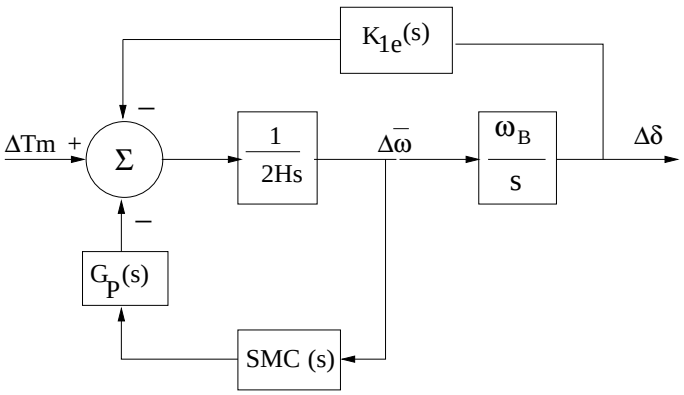

Figure 5.13: Block diagram with SMC of SPST

Generally, an AVR enhances synchronizing torque, but can reduce damping torque in stressed conditions (involving maximum power transfer and weak transmission network). By designing a SMC for the SPST based on the rotor speed signal, it is possible to enhance the damping torque and stabilize the swing mode. Fig. 5.13 also shows the SMC acting through the plant transfer function ($G_P(s)$) defined by

$$G_P(s) = \frac{\Delta T_e(s)}{\Delta\phi(s)} \tag{5.22}$$

It can be shown that

$$G_P(s) = K_{1e}(s) \tag{5.23}$$

The transfer function for SMC is chosen as

$$SMC(s) = \frac{sT_w}{1+sT_w} K_S \left[\frac{(1+sT_1)}{(1+sT_2)}\right]^n \tag{5.24}$$

where T_1, T_2 and n are chosen to provide the required phase compensation to give the necessary damping without affecting the synchronizing torque. If no phase compensation is required, then $T_1 = T_2$ (the value of n is immaterial). The gain (K_S) of the SMC is selected from root loci to provide adequate damping for the critical modes. T_w is the washout circuit time constant. The typical value for T_w varies from 10 to 20 s for damping interarea modes. The objective of the washout circuit is to remove any dc offsets in the output of SMC in steady state. The SMC is expected to act only during dynamic conditions involving oscillations.

5.6 Applications of SPST

Although work on static phase shift transformers is reported since more than 25 years, it is yet to be applied for transmission line applications. The introduction of any technology depends essentially on the cost-benefit analysis. A major drawback of SPST is the cost of the two transformers (Excitation and Boost) in addition to the power semiconductor switches. In contrast, a TCSC has no such limitations and has found wide acceptance commercially (depending on the control requirements). Although some applications of SPST were considered for enhancing the transfer capability of AC ties (interconnecting two systems) they have not been implemented.

An interesting new technology introduced recently is the Variable Frequency Transformer (VFT) developed by General Electric (U.S.A) to transfer power between two asynchronous networks [17]. The first installation of this new technology is located at Langlois substation, interconnecting the New York (USA) and the Hydro-Quebec (Canada) system. The technology is based on a rotary transformer (continuously variable phase-shifting transformer) with three phase windings on both rotor and stator. A drive system adjusts the VFT rotor in order to control the phase shift between the networks through the action of a fast power controller. The first installation at Langlois controls power transfer up to 100 MW in both directions. The development of VFT shows that a 360° PST is feasible with a rotary device which is essentially based on old technology. However, the control and drive system for VFT are based on modern technology. It is to be noted that by regulating torque applied to the rotor, through a motor drive system, the power transfer through the VFT is controlled. The rotor will rotate continuously if the two grids operate at different frequencies.

Incidentally, the principle of phase shifting transformer can also be applied to in-phase regulators for controlling the voltage magnitude. For example, the boost transformer is used to inject a voltage in phase with the line voltage (which can be in positive or negative direction). Alternately, thyristor switched tap changers are used to vary the turns ratio and control the magnitude of the secondary voltage. These devices are not covered in this book as alternate means of regulating the bus voltage by shunt reactive power controllers are used extensively.

References and Bibliography

1. J. Arrillaga and R.M. Duke, "Thyristor-controlled quadrature boosting", Proc. IEE, v. 126, n. 6, June 1979, pp. 493–498
2. C.P. Arnold, R.M. Duke and J. Arrillaga, "Transient stability improvement using thyrister controlled quadrature voltage injection", IEEE Trans., v. PAS-100, n. 3, March 1981, pp. 1382–1388
3. R.M. Mathur and R.S. Basati, "A thyristor controlled static phase-shifter for AC power transmission", IEEE Trans., v. PAS-100, n. 5, May 1981, pp. 2650– 2655
4. H. Stemmler and G. Guth, "A thyristor controlled static phase shifter, a new tool for power flow control in AC transmission systems", Brown Boveri Review, v. 69, n. 2, 1982, pp. 73–78
5. R. Baker, G. Guth, W. Egli and P. Eglin, "Control algorithm for a static phase shifting transformer to enhance transient and dynamic stability of large power systems", IEEE Trans., v. PAS-101, n. 9, September 1982, pp. 3532–3542
6. A. Edris, "Enhancement of first-swing stability using a high-speed phase shifter", IEEE Trans., Power Systems, v. 6, n. 3, August 1991, pp. 1113–1118
7. M.R. Iravani and D. Maratukulam, "Application of static phase shifter in power systems", IEEE Trans., Power Delivery, v. 9, n. 3, July 1994, pp. 1600– 1608
8. M.R. Iravani and D. Maratukulam, "Review of semiconductor-controlled (static) phase shifters for power system applications", IEEE Trans., Power Systems, v. 9, n. 4, November 1994, pp. 1833–1839
9. B.T. Ooi, S.Z. Dia and F.D. Galiana, "A solid state PWM phase shifter", IEEE Trans., Power Delivery, v. 8, n. 2, April 1993, pp. 573–579
10. J.D. Kappenman, S.R. Norr, M, Klein and D. Maratukulam, "An evaluation of a thuristor controlled phase angle regulator in the Minnesota

power transmission system", Electric Power Research Institute, U.S.A. TR-101932, May 1993

11. B.K. Johnson and G. Venkataramanan, "A hybrid solid state phase shifter using PWM AC converters", IEEE Trans., Power Delivery, v. 13, n. 4, October 1998, pp. 1316–1321

12. S. Nyati, M. Eitzmann, J. Kappenman, D. VanHouse, N. Mohan and A. Edris, "Design issues for a single core transformer thyristor controlled phase-angle regulator", IEEE Trans., Power Delivery, v. 10, n. 4, October 1995, pp. 2013– 2019

13. D.A. Woodford and R.W. Menzies, "Controlling a back-to-back DC link to operate as a phase shift transformer", Paper No. 14-202, CIGRE, 1994

14. M.R. Iravani and R.M. Mathur, "Damping subsynchronous oscillations in power systems using a static phase-shifter", IEEE Trans., Power Systems, v. 1, n. 2, May 1986, pp. 76–83

15. F. Jiang, S.S. Choi and G. Shrestha, "Power system stability enhancement using static phase shifter", IEEE Trans., Power Systems, v. 12, n. 1, February 1997, pp. 207–214

16. A. Ishigame, J. Zhao and T. Taniguchi, "Representation and control of high speed phase shifter for an electric power system", IEE Proc. GTD, v. 145, n. 3, May 1998, pp. 308–314

17. D. Mc Nabb, D. Nadeau, A. Nantel, E. Pratico, E. Larsen, G. Sybille, V.Q. Do and D. Pare, "Transient and dynamic modeling of the new Langlois VFT asynchronous tie and validation with commissioning tools", Paper presented at the Int. Conf. on Power Systems Transients (IPST-05), Montreal, Canada, June 2005

Chapter 6

Static Synchronous Compensator (STATCOM)

6.1 Introduction

This shunt connected static compensator was developed as an advanced static VAR compensator where a voltage source convertor (VSC) is used instead of the controllable reactors and switched capacitors. Although VSCs require self-commutated power semiconductor devices such as GTO, IGBT, IGCT, MCT, etc (with higher costs and losses) unlike in the case of variable impedance type SVC which use thyristor devices, there are many technical advantages of a STATCOM over a SVC. These are primarily:

(a) Faster response

(b) Requires less space as bulky passive components (such as reactors) are eliminated

(c) Inherently modular and relocatable

(d) It can be interfaced with real power sources such as battery, fuel cell or SMES (superconducting magnetic energy storage)

(e) A STATCOM has superior performance during low voltage condition as the reactive current can be maintained constant (In a SVC, the capacitive reactive current drops linearly with the voltage at the limit (of capacitive susceptance). It is even possible to increase the reactive current in a STATCOM under transient conditions if the devices are rated for the transient overload. In a SVC, the maximum reactive current is determined by the rating of the passive components - reactors and capacitors.

A ± 80 MVA STATCOM using 4.5 kV, 3000 A GTO devices was developed in Japan in 1991. A ±100 MVA STATCOM, also based on GTOs (4.5 kV and 4000 A (peak turn off)) was commissioned in late 1995 at Sullivan substation of Tennessee Valley Authority (TVA) in U.S.A. The major objective of the prototype installation is to regulate the 161 kV bus voltage

during daily load variations so that the duty on the tap changers on the transformer banks is minimized. (The failure of tap changers is a common problem when they are forced to act continuously).

The STATCOM was originally called as advanced SVC and then labelled as STATCON (STATic CONdenser).

6.2 Principle of Operation of STATCOM

A STATCOM is comparable to a Synchronous Condenser (or Compensator) which can supply variable reactive power and regulate the voltage of the bus where it is connected. The equivalent circuit of a Synchronous Condenser (SC) is shown in Fig.6.1, which shows a variable AC voltage source (E) whose magnitude is controlled by adjusting the field current. Neglecting losses, the phase angle (δ) difference between the generated voltage (E) and the bus voltage (V) can be assumed to be zero. By varying the magnitude of E, the reactive current supplied by SC can be varied. When $E = V$, the reactive current output is zero. When $E > V$, the SC acts as a capacitor whereas when $E < V$, the SC acts as an inductor. When $\delta = 0$, the reactive current drawn (I_r) is given by

$$I_r = \frac{V - E}{X'} \tag{6.1}$$

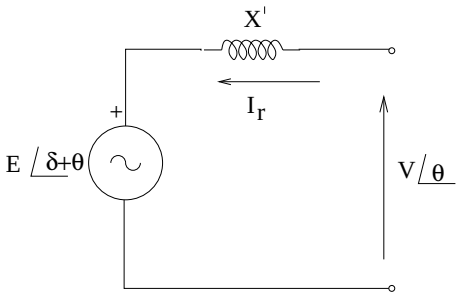

Figure 6.1: A synchronous condenser

A STATCOM (previously called as static condenser (STATCON)) has a similar equivalent circuit as that of a SC. The AC voltage is directly proportional to the DC voltage (V_{dc}) across the capacitor (see Fig. 6.2 which shows the circuit for a single phase STATCOM)

If an energy source (a battery or a rectifier) is present on the DC side, the voltage V_{dc} can be held constant. The self-commutated switches

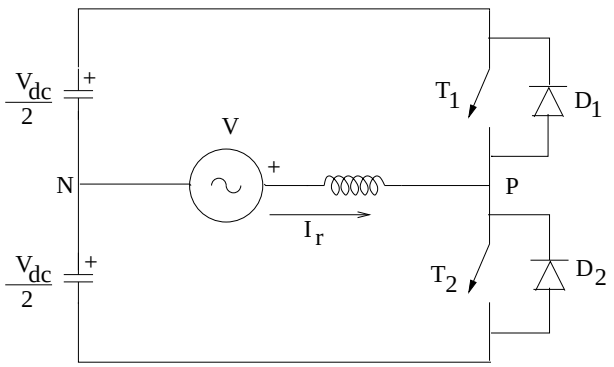

Figure 6.2: A single phase STATCOM

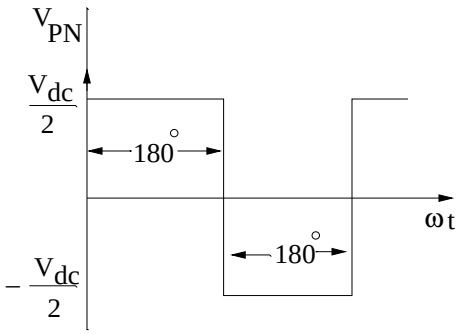

Figure 6.3: The waveform of v_{PN}

T_1 and T_2 (based on say GTOs) are switched on and off once in a cycle. The conduction period of each switch is 180° and care has to be taken to see that T_1 is off when T_2 is on and vice versa. The diodes D_1 and D_2 enable the conduction of the current in the reverse direction. The charge on the capacitors ensure that the diodes are reverse biased. The voltage waveform across PN is shown in Fig. 6.3. The voltage $V_{PN} = \frac{V_{dc}}{2}$ when T_1 is conducting (T_2 is off) and $V_{PN} = -\frac{V_{dc}}{2}$ when T_2 is conducting (and T_1 is off).

The switches are synchronized with the supply voltage (V) which is assumed to be sinusoidal of frequency ω. The fundamental component, rms value (E_1) is obtained as

$$E_1 = \frac{\sqrt{2}}{\pi} \int_0^{\pi} \frac{V_{dc}}{2} \sin\theta d\theta = \frac{\sqrt{2}}{\pi} V_{dc} \tag{6.2}$$

When $E_1 > V$, the STATCOM draws a capacitive reactive current, whereas it is inductive if $E_1 < V$. Note that, to be compatible with the convention used for SVC, the inductive current drawn is assumed to be positive.

At the instant when T_1 is switched on and I_r is inductive, the current (I_r) flowing through the circuit is negative (as it is a lagging current) and flows through T_1 (as i_{T1} is negative of I_r). After 90°, the current through T_1 becomes zero and as I_r rises above zero and becomes positive, the diode D_1 takes over conduction. Similar events occur when T_2 turns on and off. Thus, both T_1 and T_2 cease conduction before they are turned off. On the other hand, when I_r is capacitive, the current I_r is positive at the instant of turning on T_1 and flows through the diode D_1. After 90°, the current reverses its sign and flows through T_1. At the time of switching off T_1, the current through it is at its peak value. Thus, we need self commutated devices such as GTOs when the STATCOM draws capacitive reactive current. In contrast, T_1 and T_2 carry peak current at turn on when I_r is inductive.

Note that diode D_1 or D_2 turns off automatically when the parallel device (T_1 or T_2) turns off. Also, the capacitors can be charged from the source through the diodes.

In comparing SC and STATCOM, we note that while rotation of the DC field winding on the rotor results in the generation of AC voltages in the stator windings through magnetic induction, the synchronous operation of the switches in a STATCOM results in the AC voltage at the output. Unlike in a SC, this output voltage also contains many harmonics and some solution has to be found to eliminate them. These will be discussed later.

Unlike in the case of a SC, the capacitors can be charged from the AC side and there is no need of an energy source on the DC side if only reactive current is to be provided in steady state. The losses in the STATCOM can be met from the AC source. The advantages of a STATCOM over a SC are:

(a) The response is much faster to changing system conditions.

(b) It does not contribute to short circuit current.

(c) It has a symmetric lead-lag capability.

(d) It has no moving parts and hence the maintenance is easier.

(e) It has no problems of loss of synchronism under a major disturbance.

The steady state control characteristics of a STATCOM are shown in Fig. 6.4. The losses in the STATCOM are neglected and $I_{STATCOM}$ is assumed to be purely reactive. As in the case of a SVC, the negative current indicates capacitive operation while positive current indicates inductive operation. The limits on the capacitive and inductive currents are symmetric ($\pm$ I_{max}). The positive slope BC is provided for the V-I characteristic to (i) prevent the STATCOM hitting the limits often and (ii) to allow parallel operation of two or more units. The reference voltage (V_{ref}) corresponds to zero current output and generally, the STATCOM is operated close to zero

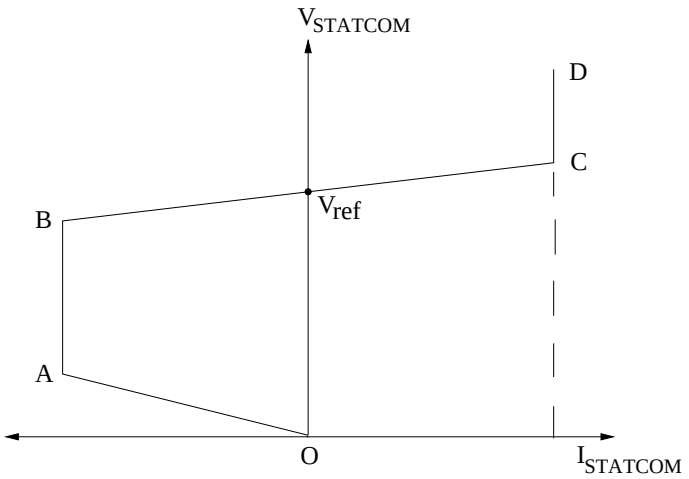

Figure 6.4: Control characteristics of a STATCOM

output during normal operating conditions, such that full dynamic range is available during contingencies. This is arranged by controlling the mechanically switched capacitors/reactors connected in parallel with a STATCOM.

6.3 A Simplified Analysis of a Three Phase Six Pulse STATCOM

The basic building block of a high power GTO based STATCOM is a six pulse circuit shown in Fig. 6.5. The circuit consists of six switches, made

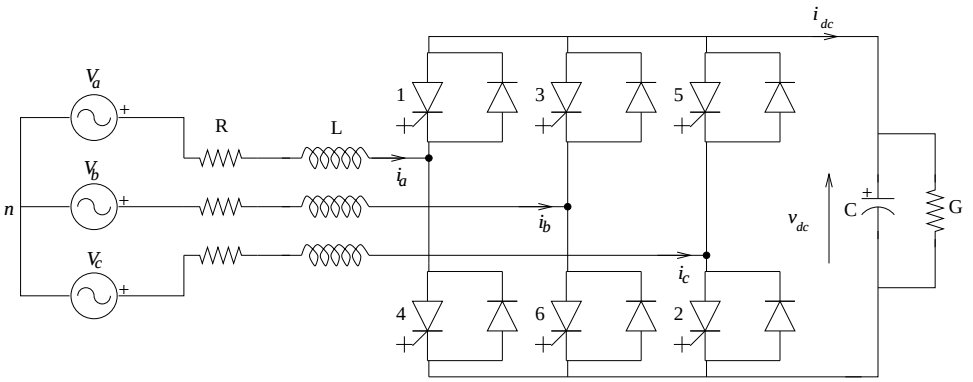

Figure 6.5: A six pulse VSC circuit

up of six GTO thyristors with antiparallel diodes connected as a six pulse Graetz bridge. The analysis of the circuit assumes that each switch is turned on only once in a cycle of supply voltage and conducts for 180° each. The

switches (or valves) are numbered in the sequence in which they are turned on (fired). Also, the two switches connected in series in each leg operate in a complementary fashion. Only one of the switches is conducting at any given time to prevent short circuit of the capacitor. Thus, before switch 4 is turned on, the switch 1 must be turned off and vice versa.

To simplify the analysis, to derive the equations describing the steady-state performance, we assume (initially) that

(i) the capacitor size is infinite (very large) and therefore the DC side voltage is constant

(ii) the losses in the circuit are neglected.

The waveform of the voltage (E_{aN}) is as shown in Fig.6.3. The waveforms of E_{bN} and E_{cN} are also similar except that they are displaced from one another by 120°. (E_{bN} lags E_{aN} by 120° and E_{cN} lags E_{bN} by 120°).

The voltages E_{an}, E_{bn} and E_{cn} (measured with respect to the source neutral) can be obtained from the following equations

$$E_{an} = E_{aN} + V_{Nn} \tag{6.3}$$
$$E_{bn} = E_{bN} + V_{Nn} \tag{6.4}$$
$$E_{cn} = E_{cN} + V_{Nn} \tag{6.5}$$

From the symmetry of the circuit, it can be shown that

$$E_{an} + E_{bn} + E_{cn} = 0 \tag{6.6}$$

Substituting Eq. (6.6) in (6.3) to (6.5), we get

$$V_{Nn} = -\frac{E_{aN} + E_{bN} + E_{cN}}{3} \tag{6.7}$$

and

$$E_{an} = \frac{2E_{aN}}{3} - \frac{E_{bN}}{3} - \frac{E_{cN}}{3} \tag{6.8}$$
$$E_{bn} = \frac{2E_{bN}}{3} - \frac{E_{cN}}{3} - \frac{E_{aN}}{3} \tag{6.9}$$
$$E_{cn} = \frac{2E_{cN}}{3} - \frac{E_{aN}}{3} - \frac{E_{bN}}{3} \tag{6.10}$$

The waveform of E_{an} is shown in Fig. 6.6 (which also shows the supply voltage v_a). The fundamental frequency component (rms value) of E_{an} is obtained as

$$E_{a1} = \frac{4}{\pi\sqrt{2}} \int_0^{\pi/2} E_{an} \sin\theta d\theta \tag{6.11}$$
$$= \frac{\sqrt{2}}{\pi} V_{dc} = 0.45 V_{dc} \tag{6.12}$$

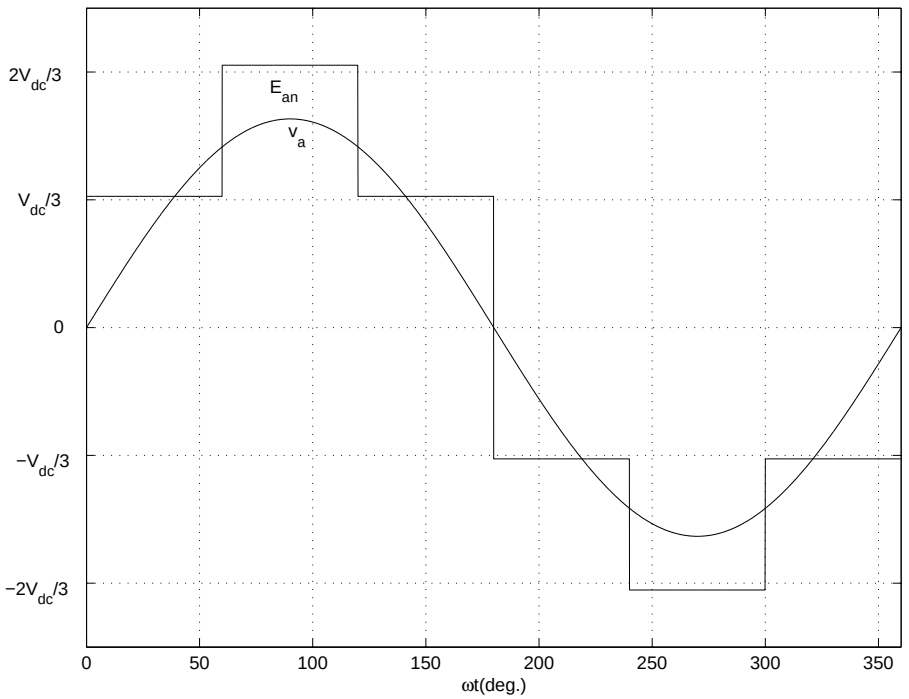

Figure 6.6: Waveforms of E_{an} and v_a

The harmonic component (E_{ah}) is obtained as

$$\begin{aligned} E_{ah} &= \frac{E_{a1}}{h} = \frac{0.45V_{dc}}{h}, \\ h &= 6k \pm 1, \quad k = 1, 2, 3. \end{aligned} \tag{6.13}$$

The rms value of the fundamental component of (reactive) current, I_r is calculated from

$$I_r = \frac{V - 0.45V_{dc}}{\omega L} \tag{6.14}$$

The harmonic current (rms) is obtained as

$$I_h = \frac{0.45V_{dc}}{h^2 \omega L} \tag{6.15}$$

AC Current Waveform

The instantaneous current in phase a (i_a) is obtained from

$$L\frac{di_a}{dt} = v_L(t) = v_a(t) - E_{an}(t) \tag{6.16}$$

since $E_{an}(t)$ varies depending on the interval in which ωt lies, we get different expressions for $i_a(t)$ depending on the interval. However, in all intervals, $v_a(t) = \sqrt{2}V \sin \omega t$.

Interval 1, $0 \leq \omega t \leq 60^\circ$,

$$i_a(t) = \frac{V}{\omega L}\left[-\sqrt{2}\cos\omega t + \frac{V_{dc}}{V}\left(\frac{2\pi}{9} - \frac{\omega t}{3}\right)\right] \tag{6.17}$$

Interval 2, $60^\circ \leq \omega t \leq 120^\circ$

$$i_a(t) = \frac{V}{\omega L}\left[-\sqrt{2}\cos\omega t + \frac{V_{dc}}{V}\left(\frac{\pi}{3} - \frac{2\omega t}{3}\right)\right] \tag{6.18}$$

Interval 3, $120^\circ \leq \omega t \leq 180^\circ$

$$i_a(t) = \frac{V}{\omega L}\left[-\sqrt{2}\cos\omega t + \frac{V_{dc}}{V}\left(\frac{\pi}{9} - \frac{\omega t}{3}\right)\right] \tag{6.19}$$

The current in the interval, $180^\circ \leq \omega t \leq 360^\circ$ is given by

$$i_a(t) = -i_a\left(t - \frac{\pi}{\omega}\right) \tag{6.20}$$

Fig. 6.7 shows the AC current waveforms (as calculated from Eqs (6.17) to (6.20) for $V = 1.0$, $\omega L = 0.2$, $I_r = \pm 1.0$). Both leading and lagging current waveforms are shown. As discussed earlier, the lagging current flows through the GTO thyristor switch 1 till $\omega t = 90^\circ$ and the reverse current flows through the anti-parallel diode. Thus, the current flowing through the switch 1 is zero when it is turned off. On the other hand, switch 1 current starts from zero at $\omega t = 90^\circ$ when it is leading and is at a peak value when it is turned off. The peak GTO thyristor turn-off current (in the capacitive mode) is obtained from Eq. (6.17) (substituting $\omega t = 0$) as,

$$I_{Tpeak} = \frac{1}{\omega L}\left[\frac{2\pi V_{dc}}{9} - \sqrt{2}V\right] \tag{6.21}$$

DC Capacitor Current and Voltage

The current flowing through the DC capacitor (i_{dc}) is dependent on the switch currents. If we consider the interval, $0 \leq \omega t < 60^\circ$, the switches 5, 6 and 1 are conducting. In general, for any combination of switches, the following equation applies (neglecting losses in the switches).

$$V_{dc} i_{dc} = E_{an} i_a + E_{bn} i_b + E_{cn} i_c \tag{6.22}$$

The above is applicable at all times. Since E_{an}, E_{bn} and E_{cn} are linearly dependent on V_{dc} (see Fig. 6.6), we can express them as

$$E_{an}(t) = S_a(t)V_{dc} + S_b(t)V_{dc} + S_c(t)V_{dc} \tag{6.23}$$

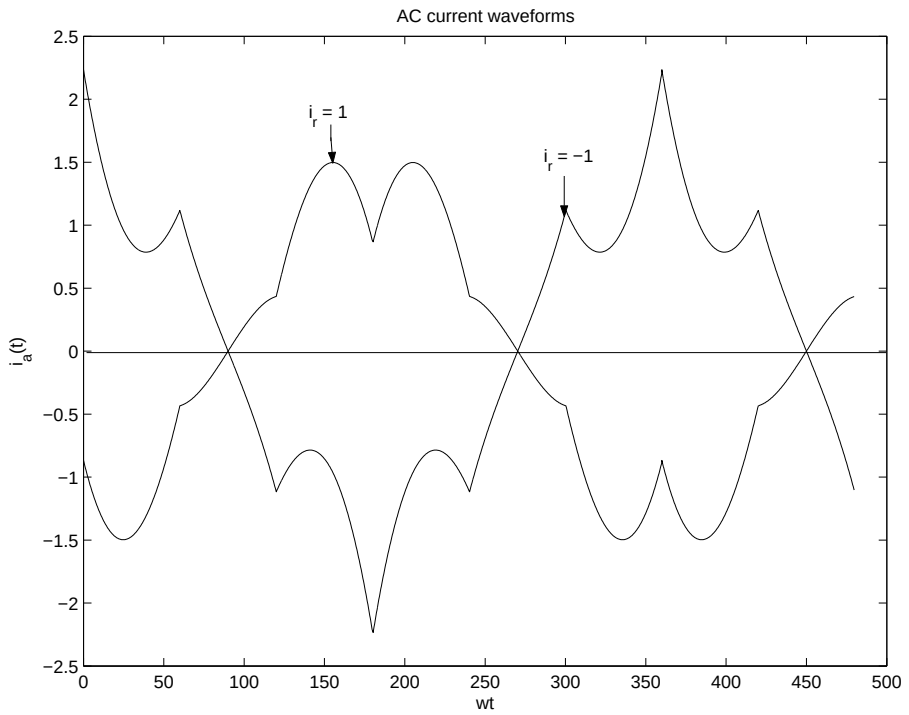

Figure 6.7: AC current waveforms

where $S_a(t)$, $S_b(t)$ and $S_c(t)$ are termed as switching functions with constant values dependent on the interval considered. The switching functions are shown in Fig. 6.8. For the interval, $0 \leq \omega t < 60^\circ$, the values of the switching functions are

$$S_a = \frac{1}{3}, \quad S_b = -\frac{2}{3}, \quad S_c = \frac{1}{3} \tag{6.24}$$

If we substitute Eq. (6.23) in (6.22), we get

$$i_{dc}(t) = S_a(t)i_a(t) + S_b(t)i_b(t) + S_c(t)i_c(t) \tag{6.25}$$

For the interval, $0 \leq \omega t \leq 60^\circ$, we get

$$i_{dc}(t) = \frac{1}{3}i_a - \frac{2}{3}i_b + \frac{1}{3}i_c = \frac{1}{3}(i_a + i_b + i_c) - i_b \tag{6.26}$$

As the sum of phase currents, i_a, i_b and i_c is zero by Kirchchoff's Current Law (KCL), we can simplify Eq. (6.26) as

$$i_{dc}(t) = -i_b(t), \quad 0 \leq \omega t \leq 60^\circ \tag{6.27}$$

It can be shown that (from symmetry)

$$\begin{aligned} -i_b(\omega t) &= i_{a2}(\omega t + 60^\circ) \\ &= \frac{V}{\omega L}\left[\sqrt{2}\sin(\omega t - 30^\circ) + \frac{V_{dc}}{V}\left(\frac{\pi}{9} - \frac{2\omega t}{3}\right)\right] \end{aligned} \tag{6.28}$$

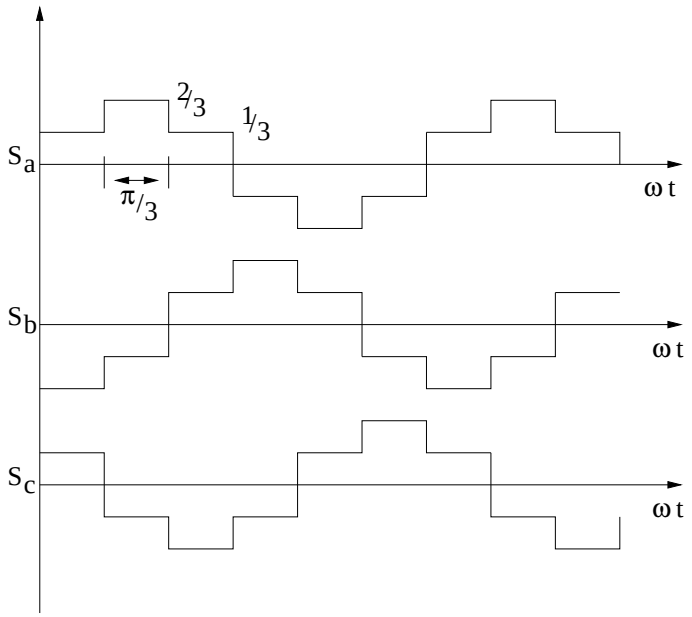

Figure 6.8: Switching functions for six pulse STATCOM

where $i_{a2}(\omega t)$ is the expression for $i_a(\omega t)$ in the interval 2, $60^\circ \leq \omega t \leq 120^\circ$, given in Eq. (6.18).

The capacitor current waveform in a cycle is obtained as the repetition of the waveform (from $0 \leq \omega t \leq 60^\circ$) over the remaining 5 intervals. It can be shown that the average value of the capacitor current is zero in steady state. (Otherwise the capacitor voltage cannot remain a constant). The fundamental component of this periodic waveform has the frequency of 6ω.

The capacitor voltage (v_c) was assumed as constant in the above analysis (due to infinite capacitance). However, with finite capacitance, the capacitor voltage will have ripples. Assuming that the capacitor current (i_{dc}) is not affected by the voltage ripple, v_c can be obtained from

$$v_c(t) = V_0 + \frac{1}{C}\int i_{dc}(t)dt \tag{6.29}$$

where V_0 is the value of $V_{dc}(t)$ at $t = 0$.

Substituting Eq. (6.28) in (6.29), we get (for $0 \leq \omega t \leq 60^\circ$)

$$\begin{aligned} v_c(t) &= V_0 - \frac{\sqrt{2}V\cos(\omega t - 30^\circ)}{\omega^2 LC} + \frac{V_{dc}\pi t}{9\omega LC} \\ &\quad -\frac{2V_{dc}t^2}{6LC} + \frac{\sqrt{6}V}{2\omega^2 LC} \end{aligned} \tag{6.30}$$

The average value of $v_c(t)$ is V_{dc}. This enables the calculation of V_0 as,

$$V_0 = V_{dc} - 0.061\frac{V_{dc}}{\omega^2 LC} + \frac{0.126V}{\omega^2 LC} \tag{6.31}$$

The waveform of $v_c(t)$ for the interval, $0 \leq \omega t \leq 60^\circ$ is obtained after substituting Eq. (6.31) in (6.30). The waveform of $v_c(t)$ over the entire cycle is a repetition of the waveform for the interval $0 \leq \omega t \leq 60^\circ$. The waveforms of $i_{dc}(t)$ and $v_c(t)$ over a complete cycle are shown in Fig. 6.9 for $V = 1.0$ pu, $I_r = -1.0$, $\omega L = 0.2$, $\omega C = 0.6$.

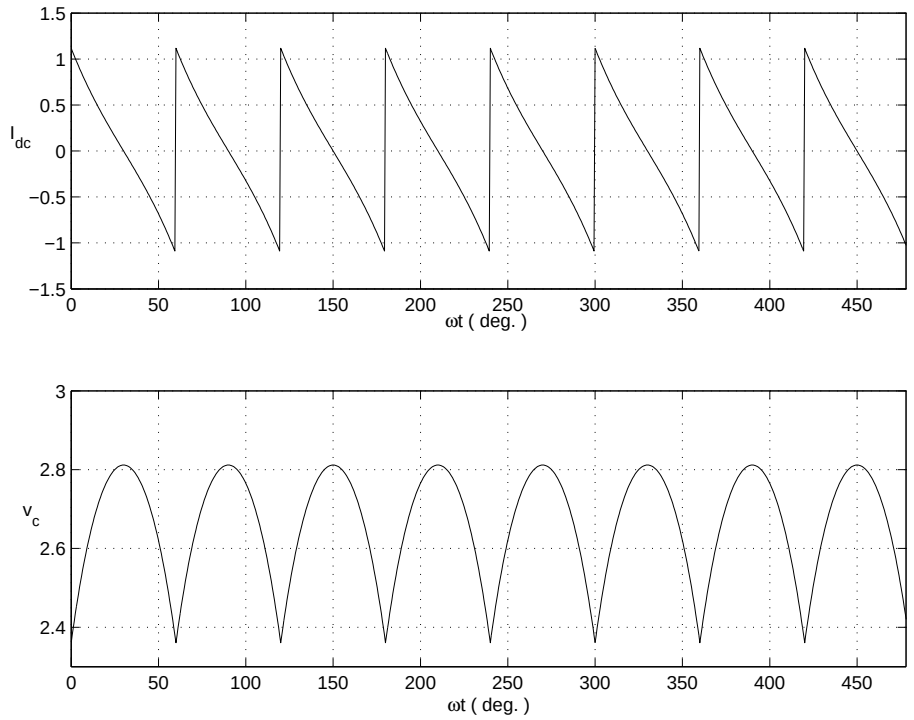

Figure 6.9: Waveforms of i_{dc} and v_C

The peak value of the capacitor voltage (V_{pk}) is obtained by substituting $\omega t = 30^\circ$ in the expression given by Eq. (6.30). We get,

$$V_{pk} = V_{dc} + \frac{0.03V_{dc}}{\omega^2 LC} - \frac{0.063V}{\omega^2 LC} \tag{6.32}$$

The value of V_{pk} determines the voltage ratings of the GTO thyristors and diodes.

Remarks

1. The presence of the capacitor voltage ripple also alters the AC current waveform. However, the errors in the expressions (6.17) to (6.19) can be assumed to be not very significant. The objective in deriving these analytical expressions is to gain insight. Such approximate analysis is quite common in power electronics as the first step towards a detailed analysis based on more exact models.
2. The constraint expressed by Eq. (6.6) is valid if (a) the source voltages have no zero sequence components and (b) the impedances in all the three phases are identical. In the simplified analysis we have assumed that the source voltages contain only positive sequence, fundamental frequency (sinusoidal) voltages. We have also assumed that $R = 0$.

The impedances could be either due to series reactor inserted between the source and VSC or the leakage impedances of the connecting transformer.

A detailed analysis of the VSC based on switching functions and relaxing the assumptions made earlier is taken up in the next section. This is valid both during steady state and transient conditions.

6.4 Analysis of a Six Pulse VSC Using Switching Functions

Here, the assumptions made in the previous section are relaxed. The capacitor is considered to be finite and the losses in the reactor and the capacitor are considered. Only the losses in the switches are ignored and the switches are assumed to be ideal. The source voltages are assumed to be balanced and sinusoidal (We will consider the effects of harmonics in a separate section). A six pulse VSC shown in Fig. 6.5 is described by the differential equations:

$$L\frac{di_a}{dt} + Ri_a = v_a - e_a \tag{6.33}$$

$$L\frac{di_b}{dt} + Ri_b = v_b - e_b \tag{6.34}$$

$$L\frac{di_c}{dt} + Ri_c = v_c - e_c \tag{6.35}$$

$$C\frac{dv_{dc}}{dt} + Gv_{dc} = i_{dc} \tag{6.36}$$

Note that we are using lower case letters for instantaneous quantities. All the voltages are with reference to the source neutral 'n'. As described in the previous section, we can express the voltages injected by the six pulse VSC as

$$e_a(t) = S_a^6(t)v_{dc}(t), e_b(t) = S_b^6(t)v_{dc}(t), e_c(t) = S_c^6(t)v_{dc}(t) \tag{6.37}$$

where the switching functions in steady state are periodic and are shown in Fig. 6.8. From the principle of energy conservation, we get

$$v_{dc}(t)i_{dc}(t) = e_a(t)i_a(t) + e_b(t)i_b(t) + e_c(t)i_c(t) \tag{6.38}$$

From Eqs (6.37) and (6.38), we can derive

$$i_{dc}(t) = S_a^6(t)i_a(t) + S_b^6(t)i_b(t) + S_c^6(t)i_c(t) \tag{6.39}$$

The switching functions in steady state are related by

$$S_a^6(\omega t) = S_b^6(\omega t + 120^\circ) = S_c^6(\omega t + 240^\circ) \tag{6.40}$$

Substituting Eqs (6.37) and (6.39) in (6.33) to (6.36) makes the system time-varying. If the switching functions are approximated by their fundamental frequency components only we obtain

$$e_a \simeq v_{dc}\frac{2}{\pi}\sin(\omega_0 t + \theta + \alpha) \tag{6.41}$$

$$e_b \simeq v_{dc}\frac{2}{\pi}\sin\left(\omega_0 t + \theta + \alpha - \frac{2\pi}{3}\right) \tag{6.42}$$

$$e_c \simeq v_{dc}\frac{2}{\pi}\sin\left(\omega_0 t + \theta + \alpha - \frac{4\pi}{3}\right) \tag{6.43}$$

In deriving the above equations we have assumed that the injected voltages lead the source voltages by an angle α, which can be controlled. θ is the angle of the source voltage whose line to line magnitude is V_s. We can express $v_a(t)$ as

$$v_a(t) = \sqrt{\frac{2}{3}}V_s\sin(\omega_0 t + \theta) \tag{6.44}$$

The expressions for $v_b(t)$ and $v_c(t)$ are obtained from the fact that the source voltages are balanced and contain only positive sequence components. The system frequency is assumed to be ω_0 and a constant (or varies very slowly).

Equations in D-Q Reference Frame

The voltages and current is the AC circuit can be transformed to a synchronously rotating reference frame by Kron's transformation defined by

$$f_{abc} = C_K f_{DQO} \tag{6.45}$$

where f_{abc} can be voltage or current vector defined by

$$f_{abc} = [f_a \ f_b \ f_c]^t$$

similarly,

$$f_{DQO} = [f_D \ f_Q \ f_O]^t$$

and C_K is the transformation matrix defined by

$$C_K = \sqrt{\frac{2}{3}} \begin{bmatrix} \cos\omega_0 t & \sin\omega_0 t & \frac{1}{\sqrt{2}} \\ \cos\left(\omega_0 t - \frac{2\pi}{3}\right) & \sin\left(\omega_0 t - \frac{2\pi}{3}\right) & \frac{1}{\sqrt{2}} \\ \cos\left(\omega_0 t + \frac{2\pi}{3}\right) & \sin\left(\omega_0 t + \frac{2\pi}{3}\right) & \frac{1}{\sqrt{2}} \end{bmatrix} \tag{6.46}$$

The subscript 'O' indicates zero sequence variable. C_K is an orthogonal matrix with the property,

$$[C_K]^{-1} = [C_K]^t \tag{6.47}$$

The advantage of the above is that the transformation is power invariant. We can derive

$$v_a i_a + v_b i_b + v_c i_c = v_D i_D + v_Q i_Q + v_O i_O \tag{6.48}$$

By applying Kron's transformation, we can derive the circuit equations in D-Q variables. These are given below

$$L\frac{di_D}{dt} + Ri_D + \omega_o L i_Q = v_D - k\sin(\alpha+\theta)v_{dc} \tag{6.49}$$

$$L\frac{di_Q}{dt} + Ri_Q - \omega_o L i_D = v_Q - k\cos(\alpha+\theta)v_{dc} \tag{6.50}$$

$$C\frac{dv_{dc}}{dt} + Gv_{dc} = k[\sin(\alpha+\theta)i_D + \cos(\alpha+\theta)i_Q] \tag{6.51}$$

where $k = \frac{\sqrt{6}}{\pi}$ for a square wave converter with no control over the magnitude of the injected voltage. The only control is assumed to be through the change of α. The converters where both k and α are controlled are termed as type 1 converters while they are termed as type 2 if only α can be controlled.

Remarks

1. In a high power VSC with GTO thyristor switches, the switch is turned on and off only once in a cycle to minimize switching losses. Here, k is a constant.

   The magnitude of the injected voltage can be controlled by Pulse Width Modulation (PWM). There are many variations in PWM. PWM converters requires several switchings in a cycle.

2. In a STATCOM with an energy source on the DC side, it is advisable to control both the magnitude and phase angle of the injected voltage by the VSC in order to control the power and reactive power output.

3. It is possible to express Eqs (6.49) and (6.50) in terms of current and voltage phasors. By multiplying Eq. (6.49) by j on both sides and adding to Eq. (6.50), we get,

$$L\frac{d\hat{I}}{dt} + (R + j\omega_0 L)\hat{I} = \hat{V} - \hat{E} \tag{6.52}$$

where

$$\hat{I} = I_Q + jI_D, \quad \hat{V} = V_Q + jV_D$$

and

$$\hat{E} = kV_{dc}\angle(\theta + \alpha) \tag{6.53}$$

Equation (6.52) represents the simple circuit shown in Fig.6.10. The phasor diagram is also shown here. Note that, since v_D and v_Q are the components of the (dynamic) phasor, they become constants in steady state (corresponding to an operating point). Generally, we use upper case to denote phasors. On the other hand, the D-Q components are also instantaneous values. Thus, to simplify the notation we will use both lower and upper cases symbols interchangeably.

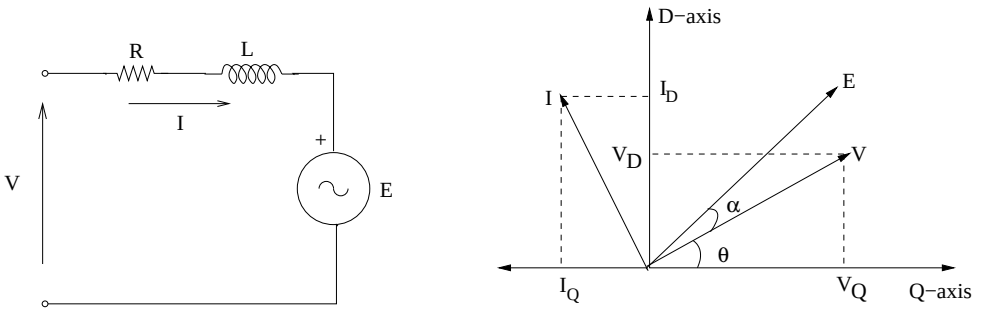

(a) Equivalent circuit (b) Phasor diagram

Figure 6.10: Equivalent circuit and phasor diagram of a STATCOM

4. For type II converters (with control only over the phase angle of the injected voltage), the elimination of voltage harmonics requires multi-pulse configuration of the VSC. Twelve pulse operation can be arranged with two six pulse converter bridges connected in series or parallel on the AC side and in parallel on the DC side. The output voltages of the two converters are summed up by a 'summing transformer' or an 'interphase magnetics'. For connection to high voltage AC lines, it is necessary to also use a coupling transformer (as in the case of a SVC).

For type I converters, one could consider multilevel converters or a combination of multilevel and multi-pulse topologies. At the prototype installation at Sullivan substation of TVA, a 48 pulse operation is used with 8 three phase converters each with a nominal rating of 12.5 MVA. The converter is coupled to the 161 kV transmission line by a single step down transformer having a Y (primary) and a delta secondary. The nominal secondary voltage is 5.1 kV line to line. The nominal voltage across the DC capacitor is 6.6 kV. The converter valves employ five GTO thyristor modules in series, one being redundant. The series connected devices share the

applied voltage. The GTO thyristors are rated for 4500 V and 4000 A (peak turn-off) and are water cooled. The total number of GTO thyristors is 240 ($6 \times 5 \times 8$).

The second installation of a ±160 MVA STATCOM (as a part of UPFC) at Inez substation of American Electric Power (AEP) in 1997 uses a quasi 24 pulse, 3 level converters. The converter output is nearly sinusoidal (48 pulse) quality that is coupled to the 138 kV transmission line by a conventional (main) coupling transformer. The secondary windings are rated at 37 kV (line to line). The nominal, maximum DC voltage is 24 kV. The converter output voltages are fed to an intermediate transformer (magnetics) to eliminate voltage harmonics. The rating of the intermediate transformer is approximately 50% of the main transformer rating. Here also, 4.5 kV, 4000 A GTO devices are used. Each GTO module consists of a GTO thyristor, its associated anti-parallel diode, snubber circuits and heat sinks. Snubber circuits are required for both $\frac{di}{dt}$ and $\frac{dv}{dt}$ protection. Each 3 level converter pole has 4 valves and each valve has 8 or 9 GTO module connected in series. Each valve contains a redundant GTO module so that the equipment can continue to operate safely under all conditions with one failed module in every valve.

It is to be noted that no harmonic filters are required with 48 pulse converters.

6.5 Multi-pulse Converters

As mentioned earlier, a six pulse converter contains voltage harmonics of the order given by

$$h = 6k \pm 1, \quad k = 1, 2, 3...$$

A 12 pulse converter circuit is shown in Fig. 6.11. This consists of two 6 pulse bridges connected in series on the AC side with an intermediate (summing) transformer. The two bridges are connected in parallel on the DC side. The summing transformer adds the phase to neutral voltage of bridge 1 to the phase to phase voltage of bridge 2. The transformer requires a $1{:}\sqrt{3}$ turns ratio so that the magnitude of the current flowing into each bridge is equal. The firing angles in bridge 2 are delayed by 30° with respect to the firing angles in bridge 1. This is required as the phase to phase voltage (v_{ab}) for bridge 2 is leading the phase voltage (v_a) for bridge 1 by 30°. To ensure that the fundamental frequency components of the voltages of bridge 1 and bridge 2 are in phase, it is essential to provide for a phase shift of 30° in the firing angles of the two bridges.

The output voltage waveforms (phase to neutral) for the two bridges are shown in Fig. 6.12.

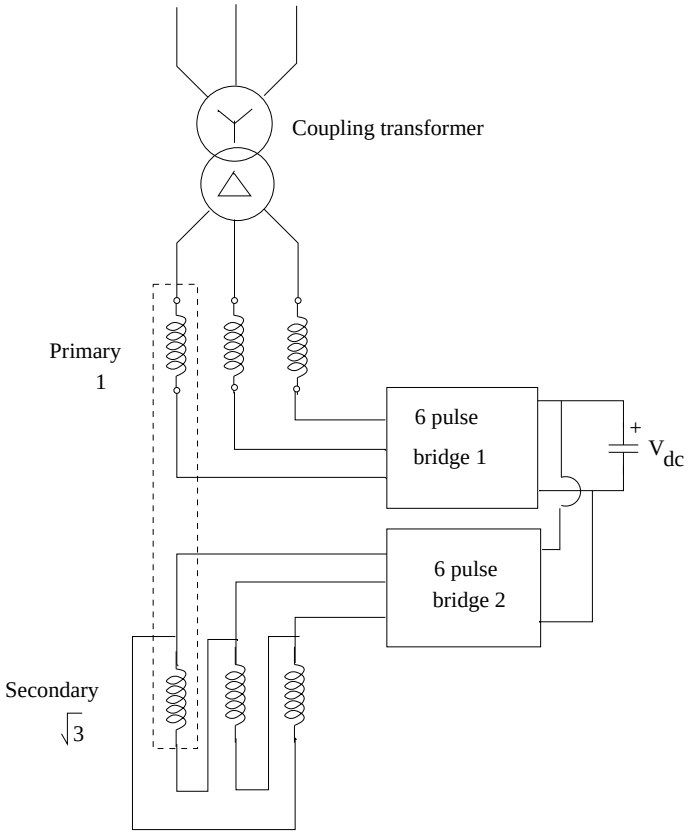

Figure 6.11: A twelve pulse STATCOM

This also shows the sum of the two voltage waveforms ($e_a = e_{a1}+e_{a2}$). It can be shown that the rms values of the phase to neutral voltage for the 12 pulse converters are given by

$$E_1^{12} = \frac{2\sqrt{2}}{\pi}V_{dc}, \quad E_h^{12} = \frac{E_1}{h}, \quad h = 12k \pm 1, \quad k = 1, 2, 3. \tag{6.54}$$

where E_1 is the magnitude of the fundamental component and E_h is the (rms) value of the harmonic component. The lowest harmonic order is now 11 as 5th and 7th harmonics are eliminated.

The current and the voltage waveforms in a 12 pulse converter for (i) capacitive and (ii) inductive operation are shown in Fig. 6.13. These waveforms are obtained by simulation of equations (6.33) to (6.39). For a 12 pulse converter, the switching functions are defined by

$$S_a^{12}(\omega_0 t) = S_a^6(\omega_0 t) + \frac{1}{\sqrt{3}}[S_a^6(\omega_0 t - 30^\circ) - S_b^6(\omega_0 t - 30^\circ)] \tag{6.55}$$

$$S_b^{12}(\omega_0 t) = S_b^6(\omega_0 t) + \frac{1}{\sqrt{3}}[S_b^6(\omega_0 t - 30^\circ) - S_c^6(\omega_0 t - 30^\circ)] \tag{6.56}$$

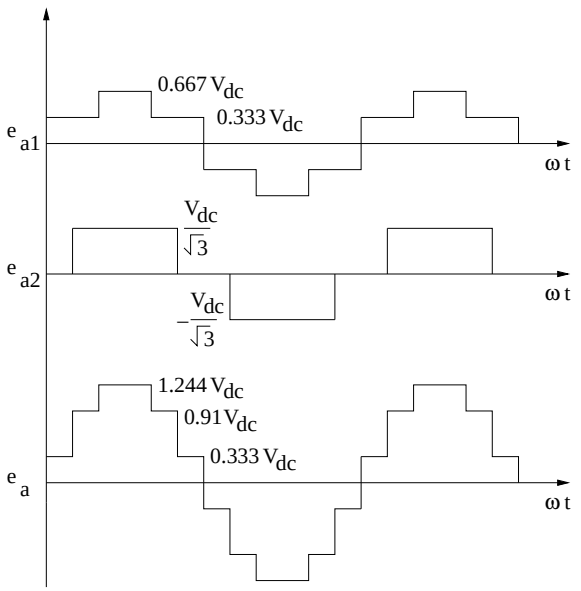

Figure 6.12: Output voltage waveforms of a 12 pulse converter

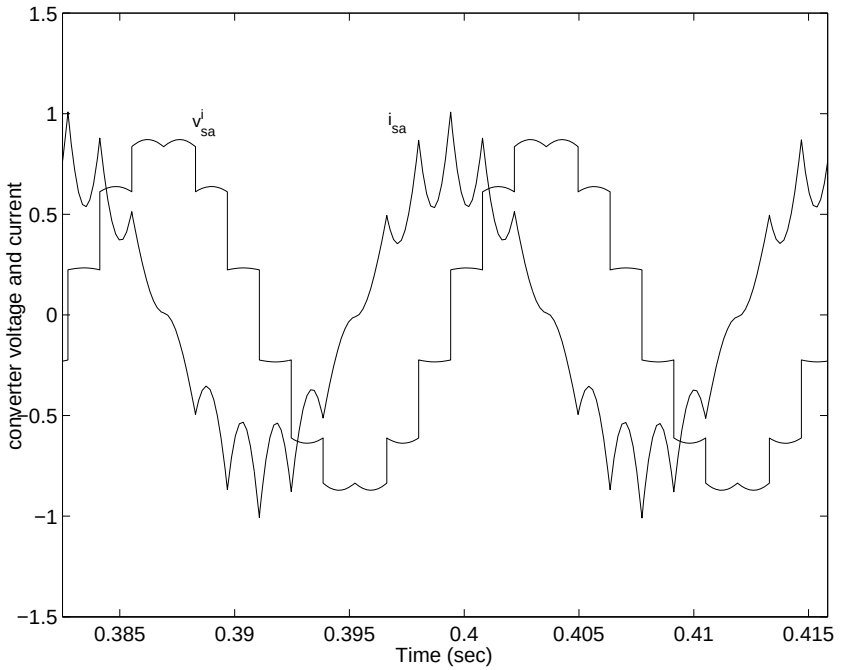

Figure 6.13: Voltage and current waveforms in a 12 pulse converter

$$S_c^{12}(\omega_0 t) \quad = \quad S_c^6(\omega_0 t) + \frac{1}{\sqrt{3}}[S_c^6(\omega_0 t - 30^\circ) - S_a^6(\omega_0 t - 30^\circ)] \quad (6.57)$$

A 24 pulse converter can be obtained by the series connection (on the AC side) of four 6 pulse bridge converters and fed by four transformers that can provide 15° phase shift between the voltages of two adjacent transformers. However, such an arrangement of transformer windings is complex and not practical. What is feasible is to connect two 12 pulse converters in series on the AC side and in parallel on the DC side. The firing angles of the two corresponding bridges (say connected to the star connected windings of the intermediate (summing) transformer) are phase shifted by 15° (see Fig. 6.14).

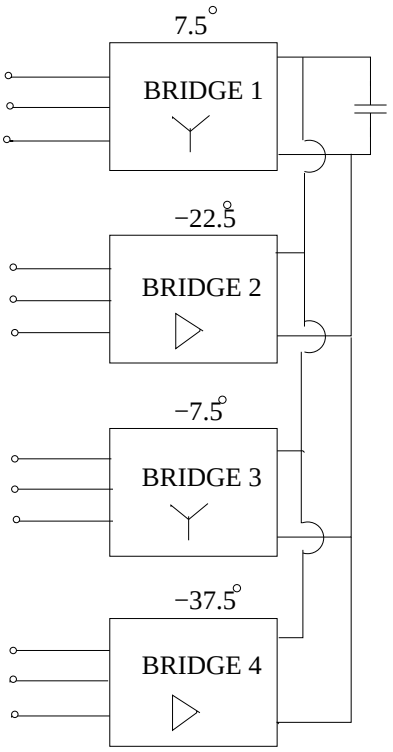

(a) Configuration

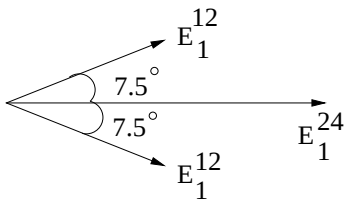

(b) Phasor diagram

Figure 6.14: A (quasi) 24 pulse converter

The rms values of the fundamental and harmonic components for a quasi 24 pulse converter are given by

$$E_1^{24} = 2E_1^{12}\cos\frac{\pi}{24}, \quad E_h^{24} = 2E_h^{12}\cos\frac{h\pi}{24}, \quad h = 12k \pm 1 \tag{6.58}$$

It can be observed that the 11th and 13th harmonics are not zero for the quasi 24 pulse converter. However, both these harmonics will be about 13% of their values of the 12-pulse converter.

A quasi 48 pulse converter can be built by connecting two quasi 24 pulse converters in series with a phase displacement of 7.5°. It can be shown that the fundamental component of the output voltage of a quasi 48 pulse converter is given by

$$E_1^{48} = 4E_1^{12} \cos\frac{\pi}{24} \cos\frac{\pi}{48} \tag{6.59}$$

The harmonic component of order 'h' is given by

$$E_h^{48} = 4E_h^{12} \cos\frac{h\pi}{24} \cos\frac{h\pi}{48} \qquad h = 12k \pm 1, \quad k = 1, 2, 3... \tag{6.60}$$

6.6 Control of Type 2 Converters

As mentioned earlier, in a Type 2 converter we can control only the phase angle of the injected voltage relative to the supply voltage. The reactive current (I_r) drawn by the STATCOM is controlled by adjusting the firing angle α. Before discussing the control aspects, we will first examine how the active (I_p) and reactive current (I_r) flowing into the STATCOM vary with the control and other parameters in steady-state. The active current (I_p) is in phase with the source voltage (with magnitude V_S) and the positive reactive current (I_r) lags the source voltage by 90°. We can express the relationship between D-Q and p-r variables by the following:

$$i_Q + ji_D = (i_p - ji_r)e^{j\theta} \tag{6.61}$$

Substituting Eq. (6.61) in (6.52) we get,

$$L\frac{d\hat{I}'}{dt} + j\dot{\theta}L\hat{I}' + (R + j\omega_0 L)\hat{I}' = V_S + j0 - kV_{dc}e^{j\alpha} \tag{6.62}$$

where $\hat{I}' = i_p - ji_r$.

We can express the transformed equations as

$$L\frac{di_p}{dt} + Ri_p + \omega Li_r = V_S - kv_{dc}\cos\alpha \tag{6.63}$$

$$L\frac{di_r}{dt} + Ri_r - \omega Li_p = kv_{dc}\sin\alpha \tag{6.64}$$

$$C\frac{dv_{dc}}{dt} + Gv_{dc} = k(i_p\cos\alpha - i_r\sin\alpha) \tag{6.65}$$

where $\omega = \omega_0 + \frac{d\theta}{dt}$.

In steady state, i_p, i_r and v_{dc} are constants if V_S and α are constants. From Eqs. (6.63) to (6.65) we can derive,

$$V_{dco} = \frac{k}{G}(i_{p0}\cos\alpha_0 - i_{r0}\sin\alpha_0) \tag{6.66}$$

$$i_{p0} = \frac{\left(R + \frac{k^2}{G}\sin^2\alpha\right)}{\left(\omega L + \frac{k^2}{2G}\sin 2\alpha\right)} i_{r0} \tag{6.67}$$

and finally,

$$i_{r0} = \frac{V_{S0}\left(\omega L + \frac{k^2}{2G}\sin 2\alpha_0\right)}{R^2 + k^2\frac{R}{G} + \omega^2 L^2} \tag{6.68}$$

Note that α_0 is negative for the capacitive mode of operation (as i_r is assumed to be negative). The slope of the line OA, (X_{ST}) in Fig. 6.4 is given by

$$X_{ST} = \frac{R^2 + \frac{k^2 R}{G} + \omega^2 L^2}{\omega L - \frac{k^2}{2G}}$$

corresponding to $\alpha_0 = -45°$. If $G = 0$, then

$$X_{ST} = -2R$$

From Eq. (6.68) it is obvious that i_{r0} is positive for $\alpha > 0$ and can be negative for $\alpha < 0$. V_{dc0} is given by

$$V_{dc0} = \frac{k}{G}\frac{(R\cos\alpha_0 - \omega L\sin\alpha_0)V_{S0}}{(R^2 + \frac{k^2 R}{G} + \omega^2 L^2)} \tag{6.69}$$

For low values of α, both V_{dc0} and i_{r0} vary linearly with α_0. The operating values of V_{dc0}, i_{r0} and i_{p0} as functions of α are shown in Fig. 6.15 for $V_{S0} = 1.0$, $\omega L = 0.2$, $R = 0.01$, $G = 0.02$, $k = 1.56$. It is to be noted for a 'p' pulse converter, the line to line voltage injected by the STATCOM can be expressed as

$$E_S = kV_{dc}, \quad k = \frac{p}{6} \cdot \frac{\sqrt{6}}{\pi}$$

The per unit system for a STATCOM is discussed in Appendix C.

The Eqs. (6.63) to (6.65) can be linearized about the operating point to derive the transfer functions. For reactive current control, the (plant) transfer function of interest is $\frac{\Delta I_r(s)}{\Delta\alpha(s)}$. It can be shown that this transfer function can be obtained as (for typical values of parameters)

$$\frac{\Delta I_r(s)}{\Delta\alpha(s)} = \frac{K[(s+\sigma_z)^2 + \omega_{nz}^2]}{(s+p_1)[(s+\sigma_p)^2 + \omega_{np}^2]} \tag{6.70}$$

where p_1, σ_z, σ_p and K are positive values. There is a real and a complex pair of poles, all in the left half plane. It can also be shown that the poles are independent of the operating point. However, the complex pair of zeros are function of the operating point. It will be shown that a P-I controller with

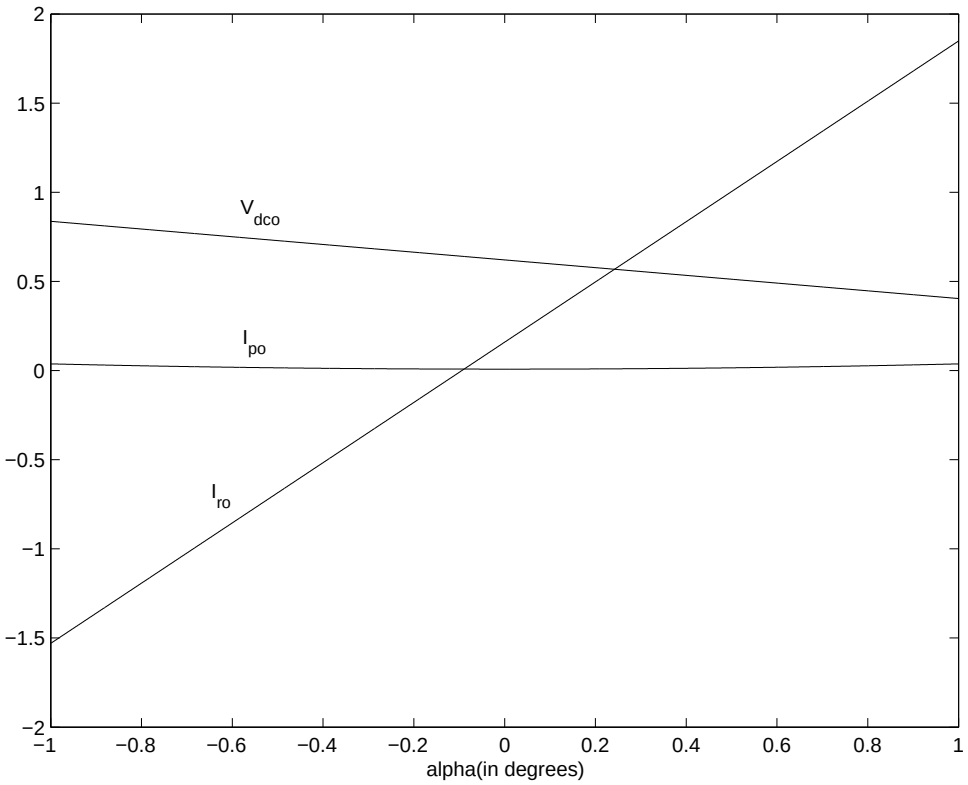

Figure 6.15: Variation of V_{dc0}, i_{r0}, i_{p0}

feedback (from the reactive current) can destabilize the system depending on the relative location of the poles and zeros of the transfer function.

To simplify the analysis, let us assume that $R = 0$ and $G = 0$ (there are no losses in converter circuit). In this case, the transfer function reduces to

$$\frac{\Delta I_r(s)}{\Delta \alpha(s)} = \frac{kV_{dc0}}{Ls} \frac{\left[s^2 + \frac{k^2}{LC} + \frac{\omega k}{CV_{dc0}} i_{r0}\right]}{s^2 + \frac{k^2}{LC} + \omega^2} \tag{6.71}$$

There are 3 poles all on the imaginary axis. There are also two zeros on the imaginary axis. From root locus analysis, it can be shown (see Fig. 6.16) that if the magnitude of the zeros is less than the magnitude of the (imaginary) poles, the angle of departure at the pole will be such as to stabilize the system. On the other hand, the closed loop poles will move to the R.H.P. if the imaginary zero is above the pole.

The condition for stability can be expressed as

$$i_{r0} < \frac{\omega C}{k} V_{dc0} \tag{6.72}$$

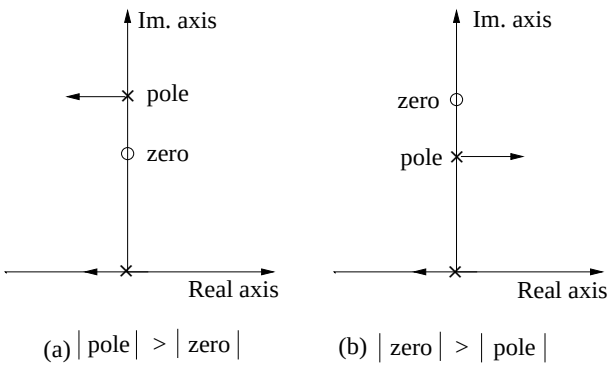

Figure 6.16: Root locus based on pole zero location

Note that the above condition is always satisfied when $i_{r0} < 0$ (when the converter is operating in the capacitive mode). Thus, the problem of instability can arise only while operating in the inductive mode.

Schauder and Mehta [4] propose a nonlinear feedback controller to overcome the problem of instability in the inductive mode of operation. The block diagram of the controller is shown in Fig. 6.17. It is to be noted that the nonlinear controller is active only when $i_{r0} > \frac{\omega C}{K} V_{dc}$ and also only during a transient. In steady state, (when V_{dc} is a constant), the output of the multiplier, $(\Delta\alpha)$ is zero.

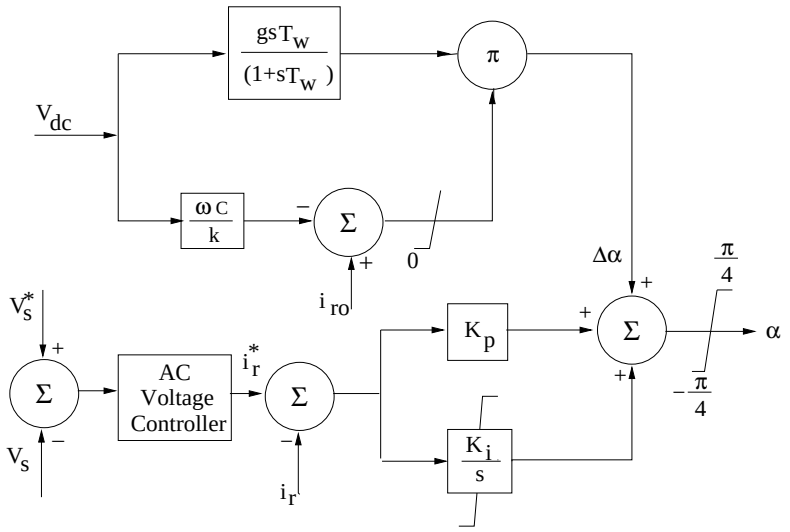

Figure 6.17: Block diagram of the reactive current controller

In reference [3], a fuzzy logic controller has been applied which is more robust than the controller shown in Fig. 6.17. In the presence of the

external network (the modelling of which has not been considered in [4]), the fuzzy logic controller performed better than the nonlinear controller.

The firing pulses for the GTO thyristor switches have to be synchronized to the bus voltage such that, in steady state, the fundamental component of the voltage injected by the converter leads the supply (sinusoidal) voltage by the control angle (α). This synchronization is achieved by a Phase Locked Loop (PLL) which produces the phase angle of the bus voltage as an output. Actually, the output is (θ_t) which is defined as

$$\theta_t = \omega_0 t + \theta \tag{6.73}$$

where ω_0 is the operating frequency (in radians/sec) and θ is relative phase of the bus voltage with respect to a synchronously rotating reference. The block diagram of the PLL is shown in Fig. 6.18. The PLL consists of a P-I

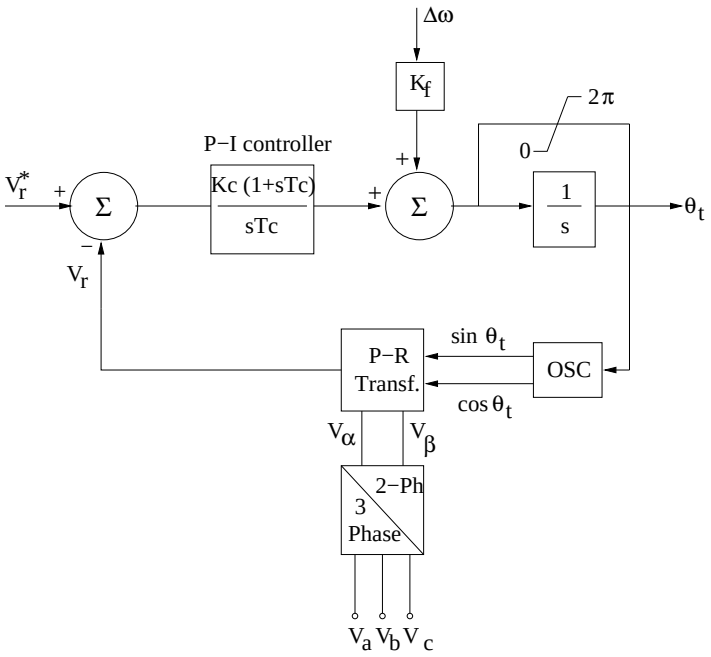

Figure 6.18: Block diagram of the PLL

controller, a saw tooth generator (whose output is θ_t which is restricted in the range of $0 \leq \theta_t \leq 2\pi$) and an oscillator that produces the output, $\sin\theta_t$ and $\cos\theta_t$, which are used to compute the quantities V_p and V_r according to the relationship given by,

$$\left.\begin{array}{rcl} V_p &=& V_\alpha \sin\theta_t + V_\beta \cos\theta_t \\ V_r &=& V_\alpha \cos\theta_t - V_\beta \sin\theta_t \end{array}\right\} \tag{6.74}$$

where

$$\left.\begin{array}{rcl} V_\alpha & = & \sqrt{\frac{2}{3}}[v_a - 0.5v_b - 0.5v_c] \\ V_\beta & = & \frac{1}{\sqrt{2}}[v_c - v_b] \end{array}\right\} \tag{6.75}$$

In steady state,

$$V_\alpha = V_S \sin\theta_t, \quad V_\beta = V_S \cos\theta_t \tag{6.76}$$

which will result in

$$V_p^* = V_S, V_r^* = 0 \tag{6.77}$$

where V_S is the line to line voltage at the converter bus. Thus, PLL tracks the phase of the voltage by feedback control of V_r and driving it to zero (the reference quantity).

The PLL should operate satisfactorily under distorted utility conditions such as voltage unbalance, dips, harmonics and frequency variations. The speed of response is also an important factor. The controller parameters, K_c and T_c are selected to satisfy both requirements. The feedforward of frequency variation ($\Delta\omega$) compensates for the change in frequency. If the change in frequency is not predictable, an additional integral term may be used in the controller to achieve the same result.

6.7 Control of Type 1 Converter

If an energy source (say a battery) is connected on the DC side, the capacitor voltage (V_{dc}) is held constant. The control of α in this case only regulates the active power exchange with the system. In order to regulate the reactive power, it is necessary to control the magnitude of the AC voltage injected by the converter. This is achieved by varying k through modulation. There are different ways in which the modulation can be achieved depending on the converter topology and the system requirements. In general, it can be stated that

$$k_{var} = k_{fix} \cdot m$$

where m is the modulation index (with $0 \leq m \leq 1$) and k_{fix} is the highest value of k that can be realized. For a twelve pulse converter,

$$k_{fix} = \frac{2\sqrt{6}}{\pi}$$

It is possible to use two Type 1 converters in series, such that the total voltage magnitude can varied by having different α for the two converters. This is shown in Fig. 6.19. The control angles of VSC1 and VSC2 are selected as

$$\alpha_1 = \alpha + \beta, \quad \alpha_2 = \alpha - \beta$$

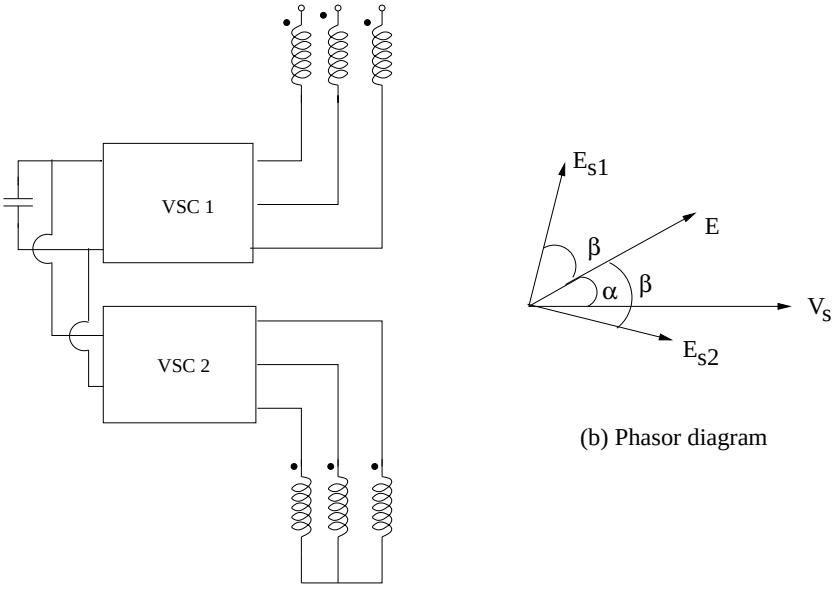

Figure 6.19: Series connection of two VSC for voltage magnitude control

The resultant voltage outputs of the two converters is given by

$$E_S = k_{fix} V_{dc} \cos\beta$$

If each converter is a 12 pulse converter, then

$$k_{fix} = \frac{4\sqrt{6}}{\pi}$$

Hence, the modulation index is $\cos\beta$ which is determined by the controller. By defining the components of the voltage injected by the converter as

$$e_p = kV_{dc}\cos\alpha, \quad e_r = -kV_{dc}\sin\alpha \tag{6.78}$$

we can express Eqs. (6.63) and (6.64) as

$$\frac{d}{dt}\begin{bmatrix} i_p \\ i_r \end{bmatrix} = \begin{bmatrix} \frac{-R\omega_B}{X} & 0 \\ 0 & \frac{-R}{X}\omega_B \end{bmatrix}\begin{bmatrix} i_p \\ i_r \end{bmatrix} + \begin{bmatrix} u_p \\ u_r \end{bmatrix} \tag{6.79}$$

where $X = \omega_B L$ and ω_B is the rated (nominal) frequency. u_p and u_r are control inputs obtained as outputs from the P-I controller, as given below.

$$u_p = G_{ci}(s)(i_p^* - i_p) \tag{6.80}$$

$$u_r = G_{ci}(s)(i_r^* - i_r) \tag{6.81}$$

where $G_{ci}(s)$ is defined by

$$G_{ci}(s) = \frac{K_{ci}(1 + sT_{ci})}{sT_{ci}} \tag{6.82}$$

Comparing Eq. (6.79) with Eqs. (6.63) and (6.64), we get

$$e_p = -\frac{\omega}{\omega_B} X i_r + V_S - \frac{X}{\omega_B} u_p \tag{6.83}$$

$$e_r = \frac{\omega X}{\omega_B} i_p - \frac{X}{\omega_B} u_r \tag{6.84}$$

From e_p and e_r, one can calculate for k and α as $k = \frac{\sqrt{e_p^2+e_r^2}}{V_{dc}}$, $\alpha = -\tan^{-1}\frac{e_r}{e_p}$.

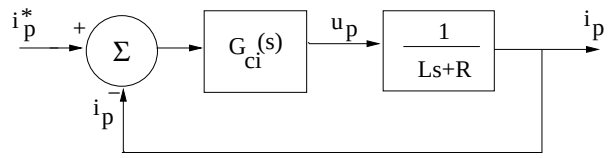

(a) Active current controller

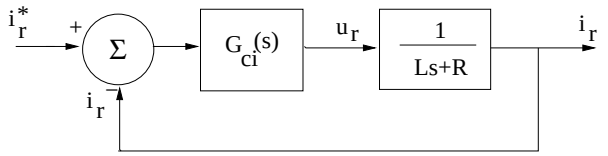

(b) Reactive current controller

Figure 6.20: Block diagram of current controller

Fig. (6.20) shows the Type 1 controller for Type 1 VSC. The feedback current controller is based on the decoupling strategy outlined above. The two current controllers (for i_p and i_r) are decoupled with the introduction of feedforward terms from i_p, i_r and V_S as given in Eqs. (6.83) and (6.84). The P-I controller time constant T_{ci} can be chosen to cancel the poles introduced by the current flow in the inductive circuit. If

$$T_{ci} = \frac{L}{R}$$

and the gain K_{ci} is chosen as

$$K_{ci} = \frac{L}{T_r}$$

it can be shown that (see Fig. 6.20),

$$i_p = \frac{1}{1+sT_r} i_p^*, \quad i_r = \frac{1}{1+sT_r} i_r^* \tag{6.85}$$

The value of T_r can be chosen to provide a specified response time for the current controllers. In general, the response time is a fraction of a cycle

(about 10 ms). It is to be noted that in Fig. 6.20, the time delays introduced by the discrete control in a VSC are neglected.

The reference for the active current (i_p^*) is obtained as the output of a DC voltage regulator (or a power controller in case the STATCOM supplies active power). The reference for the reactive current (i_r^*) is either held constant or obtained as the output of the AC voltage controller. The AC voltage controller is designed in a similar fashion as the voltage controller for a SVC. This is already discussed in chapter 3.

6.8 Multilevel Voltage Source Converters

The multi-pulse converters are generally of type II with no control over the magnitude of the injected voltage by the converter. In other words, the value of $k = \frac{E_S}{V_{dc}}$ is fixed. The multi-pulse converters also have the drawbacks of

1. Need for an intermediate transformer or harmonic neutralizing magnetics which is quite expensive and also occupies space. The rating of this magnetics is about 50% of the rating of the main transformer and also contributes to the total losses of the system.
2. The magnetics can cause difficulties in control due to DC magnetizing and overvoltage problems resulting from saturation of the transformers during a transient.
3. These transformers are prone to failure.

An alternative to multi-pulse converter is a multilevel converter. The objective is to reduce the harmonics generated by the converter while not increasing the switching losses in the power semiconductor devices. In general, the switches employed in a multilevel converter turn on and off only once in a cycle.

The general structure of the multilevel converter is designed to synthesize a near sinusoidal voltage source from several (multi) levels of voltages obtained from the DC capacitor voltages. The six pulse Graetz bridge discussed earlier is a two level converter where the phase voltage (V_{aN}, V_{bN} or V_{cN}) measured with respect to the midpoint (N) of the DC capacitor has only two levels $\left(\pm\frac{V_{dc}}{2}\right)$. In a three level converter, there will be three levels. In general, a M-level converter will have M levels of the phase voltage. There are three types of multilevel converters.

1. Diode-clamped
2. Flying capacitors or capacitor clamped

3. Cascaded or chain cell converters

These are described next.

6.8.1 Diode-clamped Multilevel Converter

A M level diode-clamped converter has (M-1) capacitors on the DC bus. In each phase leg, there are 2(M-1) switches, with each switching device required to block a voltage level of $V_{dc}/(M-1)$. However, with the same rating, there will be (M-1)(M-2) clamping diodes required for each phase. Thus as M increases, there is a quadratic increase in number of clamping diodes which puts a practical limit on the number of levels (not exceeding 9).

A special case is a three level converter which is also termed as Neutral Point Clamped (NPC) converter. This is now used extensively for high power applications.

Three Level (NPC) Converter

The circuit of a three level (NPC) converter is shown in Fig. 6.21. There are 4 switches in each phase leg out of which only two are turned on at any time. Each of the switches has to block only one-half of the DC link voltage (as also the six clamping diodes). Thus, although the number of switches is doubled, the voltage rating is also doubled. In contrast, in a two level converter, the doubling of the rating involves doubling of the GTO devices connected in series to form a switch. However, a special problem (that does not arise with two level converter) is the need to ensure voltage balance across the two series connected capacitors in the DC link. One method is to connect the capacitors to its own isolated DC source. The other method is to balance the two capacitor voltages by feedback control to regulate the average current into the centre (mid) point to be zero.

The voltage of phase a with respect to the mid point (N), E_{aN} can have 3 levels. When switches 1 and 1A are turned on, $E_{aN} = \frac{V_{dc}}{2}$. When 1A and 4A are turned on, $E_{aN} = 0$, when 4A and 4 are turned on, $E_{aN} = -\frac{V_{dc}}{2}$. In general, we can write,

$$\begin{aligned} E_{aN}(t) &= P_a(t)\frac{V_{dc}}{2} \\ E_{bN}(t) &= P_b(t)\frac{V_{dc}}{2} \\ E_{cN}(t) &= P_c(t)\frac{V_{dc}}{2} \end{aligned}$$

where $P_a(t)$, $P_b(t)$ and $P_c(t)$ are switching functions that are periodic in steady state. The duration of the time when E_{aN} is zero, is equal to $\frac{2\beta}{\omega_0}$ in

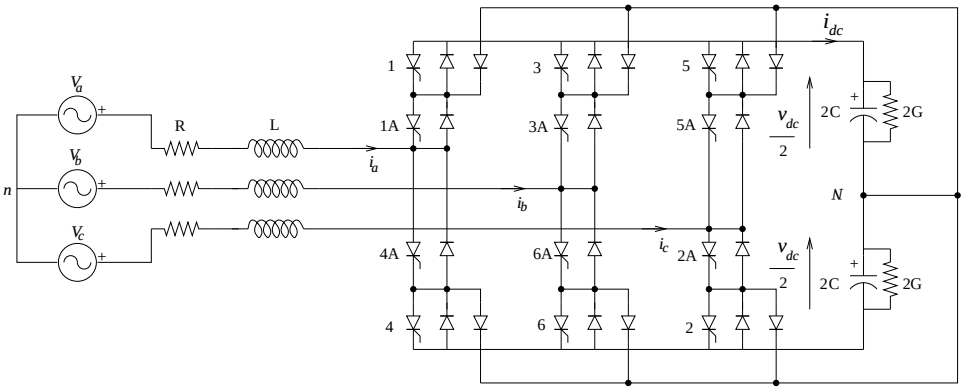

Figure 6.21: Three level NPC converter

a half cycle. β is termed as the 'dead angle' which can be controlled to vary the magnitude of the injected voltage.

It can be shown that E_{an} (the voltage of phase a with reference to the source neutral) can be expressed as,

$$E_{an}(t) = S_a(t)V_{dc}$$

where

$$S_a(t) = \frac{P_a(t)}{2} - \left[\frac{P_a(t) + P_b(t) + P_c(t)}{6}\right]$$

From Fourier analysis, the harmonic components of $E_{an}(t)$ can be obtained. It can be shown that the (rms) value of E_{ah} is given by

$$E_{ah} = \frac{\sqrt{2}}{h\pi} V_{dc} \cos(h\beta), \quad h = 6k \pm 1$$

The fundamental component (for $h = 1$) is given by

$$E_{a1} = \frac{\sqrt{2}}{\pi} V_{dc} \cos\beta$$

The line to line voltage E_{ab} and E_{an} are shown in Fig. 6.22, along with E_{aN} for comparison.

Remarks

1. When $\beta = 15°$, the 3 level converter, behaves like a quasi 12 pulse converter with low values of 5th and 7th harmonic. The fundamental component, for $\beta = 15°$ is

$$E_1 = \frac{\sqrt{2}}{\pi} \cos\left(\frac{\pi}{12}\right) V_{dc} = 0.435 V_{dc}$$

This is to be compared with the value of 0.45 for the two level converter.

2. For the same voltage ratings of the switches used in a two level converter, the capacitor voltage (V_{dc}) can be doubled in a three level converter. Thus, the value of E_1 rises to 0.870 V_{dc2} (for $\beta = 15°$) where $V_{dc2} = \frac{V_{dc}}{2}$ is the capacitor voltage in a two level converter.
3. The combination of a 12 pulse and three level converter is analogous to a quasi 24 pulse converter when $\beta = 7.50°$. Here two three level converters are connected in series on the AC side and in parallel on the DC side. The current and voltage waveforms for a 12 pulse, three level converter ($\beta = 7.5°$) are shown in Fig. 6.23. These can be compared with the waveforms in a 12 pulse converter (shown in Fig. 6.13).
4. Note that the series connection of two 2-level Type 2 converters with control angles displaced by 2β, also result in the modulation ratio of $m = \cos\beta$, same as that obtained in a 3 level converter, where β is termed as the dead angle.

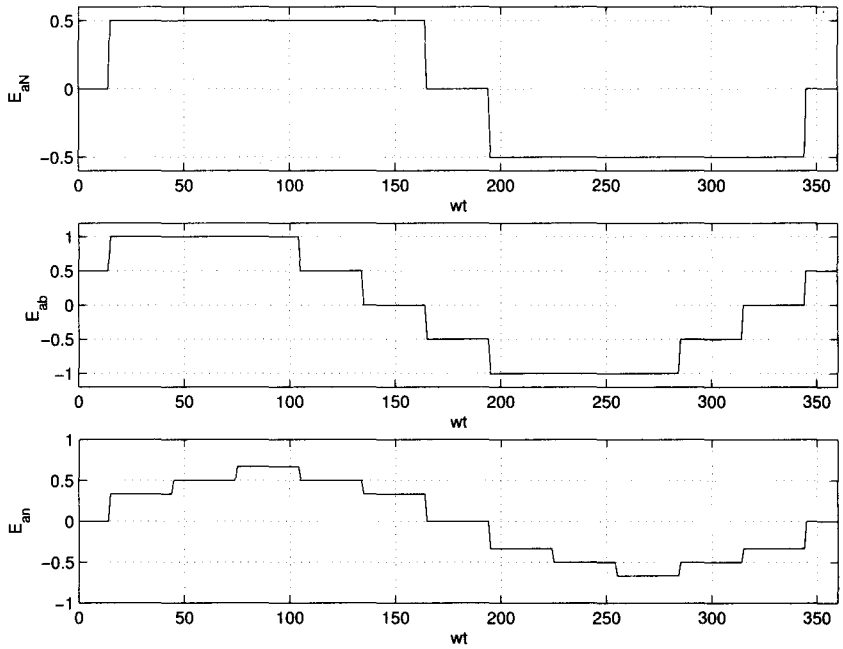

Figure 6.22: Waveforms of E_{aN}, E_{ab} and E_{an}

6.8.2 Capacitor Clamped Multilevel Converter

Here, the clamping diodes are replaced by the 'flying capacitors'. For a M-level converter, the number of capacitors (each with the voltage rating, identical to that of the main switches) is equal to (M-1)(M-2)$\frac{3}{2}$ + (M-1). In contrast, an M-level diode damped convertor requires (M-1) capacitors.

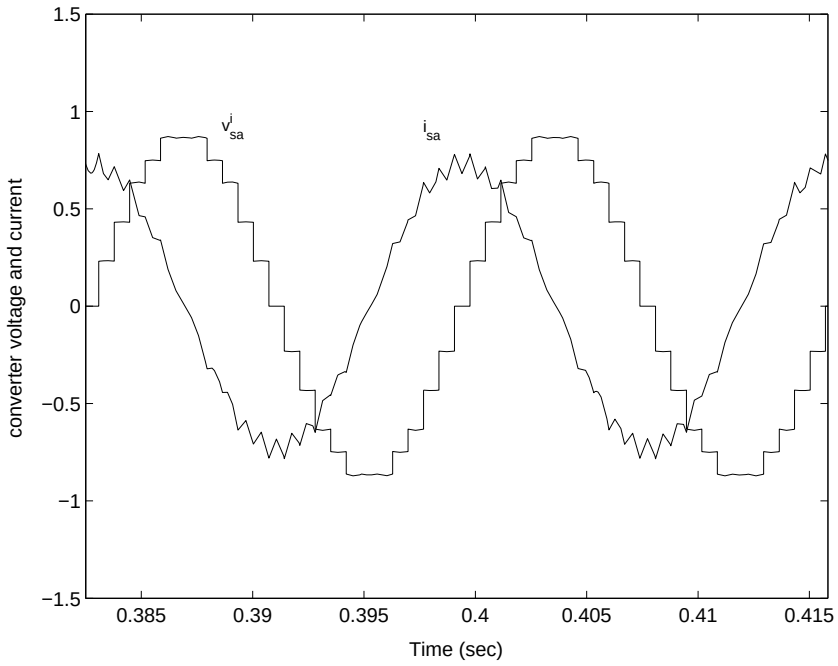

Figure 6.23: Converter voltage and current waveforms in a 12-pulse 3-level converter

The control gets complicated and a higher switching frequency is required to balance each capacitor voltage.

A three level, capacitor clamped converter is shown in Fig. 6.24. Only one leg (phase) is shown here.

6.8.3 Cascaded (Chain Cell) Multilevel Converter

This multilevel converter has the advantage of eliminating extra clamping diodes or voltage balancing capacitors. In this configuration, each phase comprises a chain of independent single phase, full bridge converters connected in series as shown in Fig. 6.25. A M-level converter is made up of (M-1)/2 SFB (Single phase, Full Bridge) converters. Fig. 6.25 shows a 3 link (cell) converter with 7 levels. The voltage waveforms (across each link and the total are shown in Fig.6.26. The control (switching) angle α_1, α_2 and α_3 of the three SFBS are chosen so that the summed voltage is a good approximation to a sine wave.

The control of individual SFB (cell) can be explained with reference to Fig. 6.27. Out of the 4 switches, only two switches are turned on at any given time. Depending on the pair (of switches) that are on, there can be 4 states of the SFB or chain cell. The voltage across the cell can be $+V_{dc}$, $-V_{dc}$

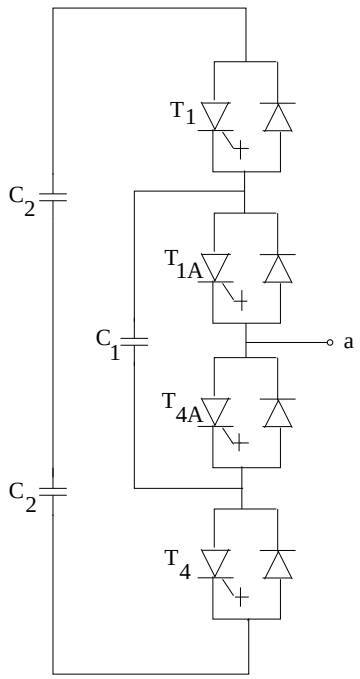

Figure 6.24: A three level capacitor clamped converter

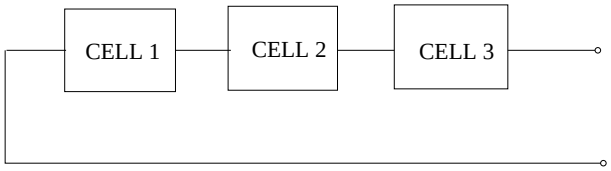

(a) Series connection of cells

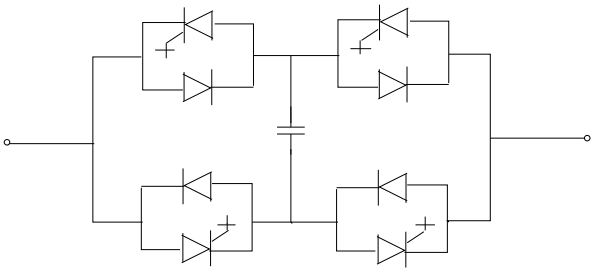

(b) A cell circuit (single phase full bridge)

Figure 6.25: Single phase chain cell converter

or 0. The two states (2 and 4) result in the same output (of zero voltage across the cell). The voltage required is positive during the positive half of the cycle (of fundamental component) and negative during the negative

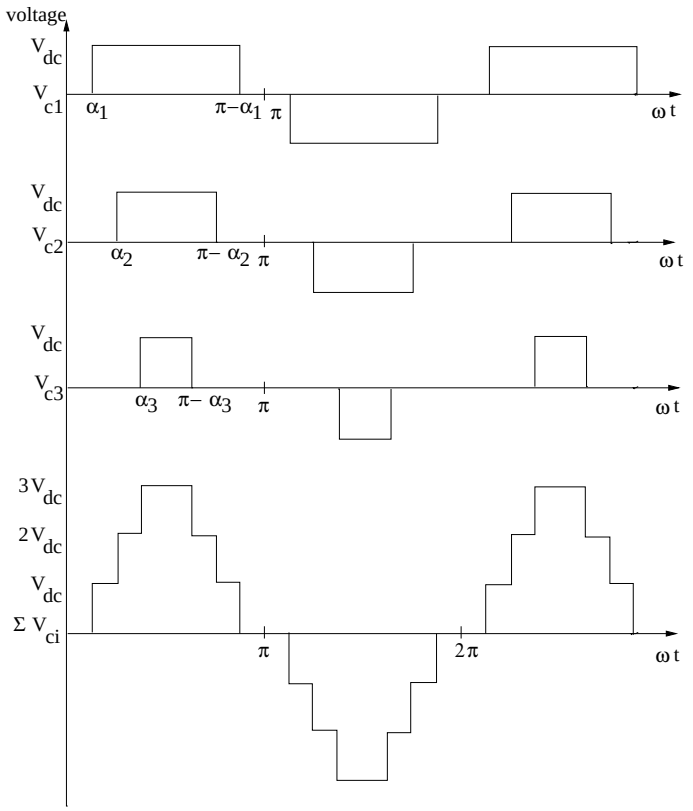

Figure 6.26: Voltage waveforms for a 7-level chain cell converter

half cycle. The duration of $+V_{dc}$ and $-V_{dc}$ voltage states are identical for a cell in steady state. However, the duration varies depending on the cell. Thus, the step variation in the converter output voltage during the switch commutation is limited to V_{dc}, as there is only a single commutation taking place in the converter at any instant.

A STATCOM with 8 SFBs per phase can eliminate harmonic voltages up to the 25th for balanced operating condition. By providing an extra SFB in each phase, redundancy can be built into the design. In the event of GTO failures a SFB can operate continuously in the bypass mode (short circuit) until the next planned maintenance outage. If all the SFBs are identical, the control system can be programmed to change over to a new switching pattern for the remaining SFBs to minimize the harmonic voltages.

The cascaded (chain cell converters) have several advantages in addition to what have been mentioned earlier. These are listed below [16]

1. Modular construction as SFBs are designed to have the same voltage and current ratings

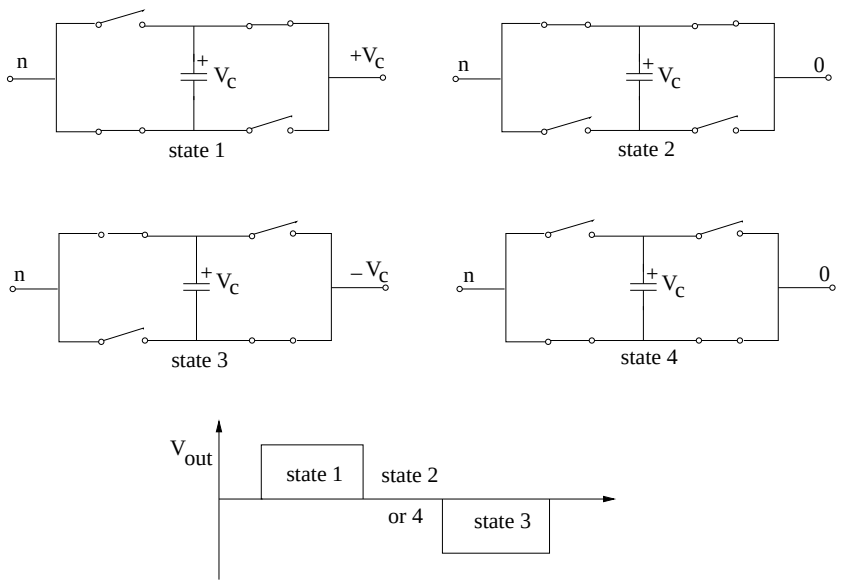

Figure 6.27: Control of a cell (SFB) by switching

2. As the control of each phase is independent, there is scope for compensating for the phase unbalance
3. As each SFB switch in a sequence, the maximum instantaneous voltage excursion (of the converter waveform) is limited (to about 2 kV). Therefore, radio interference is minimized.
4. There is no need for harmonic filters. With a suitable choice of switching angles, the generation of low order (particularly triplen) harmonics can be eliminated during unbalanced AC system conditions, which is not feasible with circuits using 3 phase Graetz bridge.
5. The problems and limitations of direct series connection of GTO thyristors are avoided.
6. The replacement of capacitors in SFBs by energy storage elements such as batteries or fuel cells enable the exchange of real power with the AC system.

A ±75 MVA STATCOM based on cascaded (chain cell) converter has been commissioned by National Grid Company, U.K. in 1999. This is a part of a 225 MVA relocatable SVC.

Control of Cascaded Converter

Since, the currents in the three phases of a cascaded (chain cell) converter can be controlled independently, there could be different approaches to the

control of a cascaded converter. However, in transmission applications, it is acceptable to neglect unbalanced operation. Thus, it is possible to apply the Type 1 controller discussed in the previous section. The modulation index (m) is calculated from

$$m = \frac{k_{var}}{k_{fix}}$$

where

$$k_{var} = \frac{E_S^*}{V_{dc}^*}, \quad k_{fix} = \frac{\sqrt{6}}{\pi} n_c$$

where E_S^* and V_{dc}^* are the line to line AC voltage (desired) and the (reference) voltage across the individual capacitor (the voltage across all the capacitors are assumed to be same in steady state). n_c is the number of SFBs connected in series in each phase.

The modulation index is used to determine the switching angle (calculated off line to minimize harmonics for the particular value of the modulation index). However, the control angle (δ) that determines the phase shift between the source voltage and the fundamental component of the injected voltage (E_S) is not identical for individual SFB. To ensure, that the voltage across each capacitor is same it is necessary to apply a correction, using feedback control [13]. Here, V_{dc} is calculated as

$$V_{dc} = \frac{\sum_i V_{ci}}{n_c}$$

It is to be noted that the values of capacitances for individual SFBs are not identical (although voltage ratings are identical). The value of the capacitance (C_i) is determined from considerations of voltage ripple [13]. An improved voltage balancing control is suggested in [30]. In this approach, the voltage pulses, $P_1, P_2 \ldots P_{n_c}$ produced by n_c SFBs are rotated every half cycle among the SFBs. This ensures that all DC capacitors are charged equally and balanced over n_c half cycles. Thus, to regulate all DC capacitor's average voltages, only one DC capacitor's voltage needs to be monitored and fed back for DC voltage control. The block diagram of the controller is shown in Fig. 6.28. In the duty cycle lookup table, the switching angles, $\alpha_1, \alpha_2 \ldots \alpha_{n_c}$ are stored. A duty cycle swapping circuit rotates pulses every half cycle.

This approach also ensures that the size of all capacitors are equal. This fact improves reliability as redundancy can be in-built easily.

If the SFBs are rated for different voltage ratings in the ratio of 1:2:4:...2^{n_c-1}, then it is possible to have $(2^{n_c+1}-1)$ levels in the phase voltage [14]. For example with $n_c = 3$, it is possible to have 15 levels. However, the issues of redundancy and modularity can pose problems.

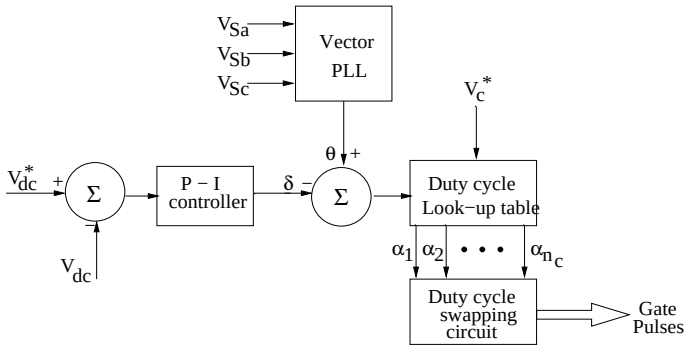

Figure 6.28: Control of a cell considering correction for capacitor voltage

6.9 Harmonic Transfer and Resonance in VSC

The DC capacitor and the series inductor can cause resonance at low order harmonics that can be present in the system under contingency conditions or due to any harmonic source in the vicinity (nonlinear loads). For example, unbalance due to faults results in negative sequence voltage (of fundamental frequency) which in turn results in second harmonic components on the DC side. A second harmonic voltage on the DC capacitor results in both negative sequence (fundamental) component and a positive sequence third harmonic component. Depending on the value of the DC capacitor, it is possible that the negative sequence (fundamental) current and positive sequence third harmonic current in the AC are magnified.

Analysis

To simplify the analysis, we will neglect the losses in the converter. Also, the switching functions are approximated by their fundamental frequency components. This is a major assumption that enables the use of the converter model in $p-r$ variables, given in Eqs. (6.63) to (6.65). Since the losses are neglected, $R = G = 0$ and $\alpha = 0$ in steady state. The simplified equations (with these approximations) for the converter are,

$$L\frac{di_p}{dt} + \omega_0 L i_r = V_p - kV_{dc} \tag{6.86}$$

$$L\frac{di_r}{dt} - \omega_0 L i_p = V_r \tag{6.87}$$

$$C\frac{dV_{dc}}{dt} = ki_p \tag{6.88}$$

There is no loss of generality in assuming θ as a constant (say $\theta = 90^\circ$). Let us consider that the source voltages include a harmonic voltage of order (n)

in addition to the fundamental. The phase voltages can be expressed as

$$\begin{bmatrix} v_a(t) \\ v_b(t) \\ v_c(t) \end{bmatrix} = \sqrt{\frac{2}{3}} \left\{ V_s \begin{bmatrix} \cos\omega_0 t \\ \cos\left(\omega_0 t - \frac{2\pi}{3}\right) \\ \cos\left(\omega_0 t + \frac{2\pi}{3}\right) \end{bmatrix} + V_n \begin{bmatrix} \cos n\omega_0 t \\ \cos\left(n\omega_0 t - \frac{2\pi}{3}\right) \\ \cos\left(n\omega_0 t + \frac{2\pi}{3}\right) \end{bmatrix} \right\} \tag{6.89}$$

The in-phase (V_p) and quadrature phase (V_r) components are calculated as

$$V_p = V_s + V_n \cos(n-1)\omega_0 t \tag{6.90}$$

$$V_r = 0 - V_n \sin(n-1)\omega_0 t \tag{6.91}$$

Note that a negative sequence component of harmonic order (n) can be treated by taking n as negative.

Since Eqs. (6.86) to (6.88) are linear, we can apply superposition theorem and consider the response to the following inputs

$$V_{pn}(t) = V_n \cos(n-1)\omega_0 t$$
$$V_{rn}(t) = -V_n \sin(n-1)\omega_0 t$$

In the Laplace domain, Eqs (6.86) to (6.88) can be expressed as

$$V_{dc}(s) = \frac{k}{C} I_{pn}(s) \tag{6.92}$$

$$\begin{bmatrix} Ls + \frac{k^2}{Cs} & \omega_0 L \\ -\omega_0 L & Ls \end{bmatrix} \begin{bmatrix} I_{pn}(s) \\ I_{rn}(s) \end{bmatrix} = \begin{bmatrix} V_{pn}(s) \\ V_{rn}(s) \end{bmatrix} \tag{6.93}$$

We can solve Eq. (6.93) to obtain

$$I_{pn}(s) = \frac{LsV_{pn}(s)}{\Delta(s)} - \frac{\omega_0 L}{\Delta(s)} V_{rn}(s) \tag{6.94}$$

$$I_{rn}(s) = \frac{\omega_0 L V_{pn}(s)}{\Delta(s)} + \frac{\left(Ls + \frac{k^2}{Cs}\right) V_{rn}(s)}{\Delta(s)} \tag{6.95}$$

where

$$\Delta(s) = L^2 \left[s^2 + \frac{k^2}{LC} + \omega_0^2 \right] \tag{6.96}$$

Since, the inputs $V_{pn}(t)$ and $V_{rn}(t)$ are sinusoidal quantities of frequency $(n-1)\omega_0$, the state variables are also sinusoidal in steady state and we can solve for them using phasor notation and substituting $s = j(n-1)\omega_0$. From the expressions for $V_{pn}(t)$ and $V_{rn}(t)$, we can write (taking $V_{pn}(j\omega)$ as the reference phasor)

$$V_{pn}(j\omega) = V_n + j0, \quad V_{rn}(j\omega) = jV_n \tag{6.97}$$

The solutions for $I_{pn}(t)$ and $I_{rn}(t)$ can be derived as

$$I_{pn}(t) = V_n A \sin(n-1)\omega_0 t, \quad I_{rn}(t) = V_n B \cos(n-1)\omega_0 t \tag{6.98}$$

where

$$\begin{aligned} A &= \frac{-(n-2)}{D}, \quad B = \frac{-1}{D}\left[(n-2) - \frac{\omega_r^2}{\omega_0^2(n-1)}\right] \\ D &= X_L\left[\frac{\omega_r^2}{\omega_0^2} - n(n-2)\right], \quad X_L = \omega_0 L \\ \omega_r &= \frac{k^2}{LC} \end{aligned}$$

From Eq. (6.98) we can derive $i_a(t)$ as

$$\begin{aligned} i_a(t) &= \sqrt{\frac{2}{3}}[A\sin(n-1)\omega_0 t\cos\omega_0 t + B\cos(n-1)\omega_0 t\sin\omega_0 t]V_n \\ &= \sqrt{\frac{2}{3}}\left[\frac{A+B}{2}\sin(n\omega_0 t) + \frac{A-B}{2}\sin[(n-2)\omega_0 t]\right]V_n \end{aligned} \tag{6.99}$$

From the above equation, we note that a harmonic component (of order n) in the source voltages result in two harmonic components of order n and $(n-2)$. If $n = -1$, then we get both a negative sequence fundamental and third harmonic component. The capacitor voltage (V_{dc}) also contains a harmonic component of order $(n-1)$ given by

$$V_{dc}(t) = \frac{kV_n(n-2)}{D(n-1)\omega_0 C}\cos[(n-1)\omega_0 t] \tag{6.100}$$

From Eq. (6.99) we get

$$i_{an}(t) = \frac{\sqrt{\frac{2}{3}}V_n\left[(n-2) - \frac{\omega_r^2}{2\omega_0^2(n-1)}\right]}{X_L\left[\frac{\omega_r^2}{\omega_0^2} - n(n-2)\right]}\sin n\omega_0 t \tag{6.101}$$

$$i_{a(n-2)}(t) = \frac{\sqrt{\frac{2}{3}}V_n\left[\frac{\omega_r^2}{2\omega_0^2(n-1)}\right]}{X_L\left[\frac{\omega_r^2}{\omega_0^2} - n(n-2)\right]} \tag{6.102}$$

All the quantities shown above tend to infinity when

$$\frac{\omega_r^2}{\omega_0^2} = n(n-2).$$

where

$$\frac{\omega_r^2}{\omega_0^2} = \frac{k^2}{LC} = \frac{X_{Ce}}{X_L}, \quad X_{Ce} = \frac{1}{\omega_0 C_e}, \quad C_e = \frac{C}{k^2}$$

When the losses are considered, the magnitudes of the current and capacitor voltage are limited at resonance, but will be magnified. The resonance condition is given by

$$X_{Ce} = n(n-2)X_L \tag{6.103}$$

For $n = -1$, this corresponds to $X_{Ce} = 3X_L$. It is interesting to observe that when

$$X_{Ce} = 2(n-1)(n-2)X_L \tag{6.104}$$

the harmonic current $i_{an}(t)$ is zero. For $n = -1$, this corresponds to $X_{Ce} = 12X_L$. Actually for higher values of X_{Ce}, the harmonic current remains small. However, there is an upper limit on X_{Ce} determined by the voltage ripple on the capacitor that can be tolerated.

The value of $(\frac{I_n X_L}{V_n})$ as a function of $(\frac{X_{Ce}}{X_L})$ is shown in Fig. 6.29 for $n = -1$ and $n = 3$.

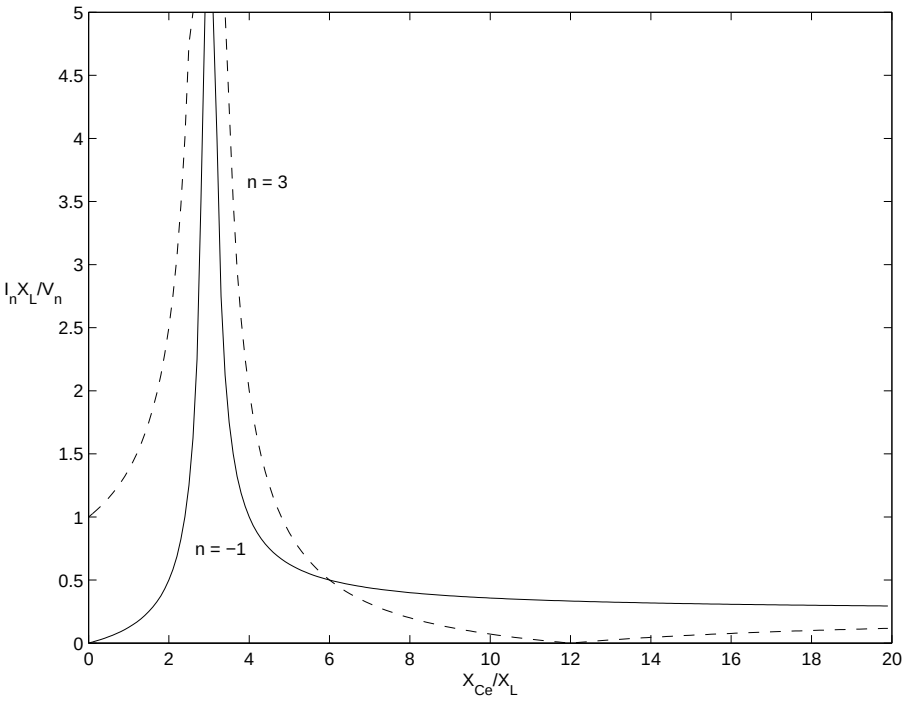

Figure 6.29: Variation of $\left(\frac{I_n X_L}{V_n}\right)$ as a function of $\left(\frac{X_{Ce}}{X_L}\right)$

Remarks

1. Note that the analysis considers only the harmonic components (using superposition theorem which applies for linear systems). The exact analysis considering losses and controller modelling would be quite

complex. However, the simplified analysis indicates the problem areas and can act as a guide in the choice of the DC capacitor ratings.

2. It is interesting to observe that the harmonic component in the DC voltage is zero for $n = 2$. This indicates that the second harmonic instability problem that affects a SVC, would not be present in a STATCOM.

   Note that the second harmonic instability problem arises due to the presence of a positive sequence second harmonic component in the source voltage which can be magnified also due to the presence of DC components in the SVC currents.

3. If the capacitor voltage (V_{dc}) has a sinusoidal component of frequency, ω_d, such that

   $$V_{dc} = V_{dco} + A \sin \omega_d t$$

   the AC voltages will contain 2 components, (i) of frequency $(\omega_0 + \omega_d)$ and (ii) of frequency $(\omega_d - \omega_0)$. The former is always a positive sequence component, while the latter is of negative sequence if $\omega_d > \omega_0$. On the other hand, if $\omega_d < \omega_0$, the component of frequency $(\omega_d - \omega_0)$ is also a positive sequence component.

Note that ω_d can have any value, not necessarily a multiple of ω_0. For example, subsynchronous frequency currents flowing in the converter can result in the presence of a subsynchronous frequency component in the DC capacitor voltage.

6.10 Applications of STATCOM

Since a STATCOM is an advanced type of SVC (based on VSC), the motivations for the applications are similar to that of a SVC, discussed in chapter 3. A STATCOM has several advantages over a SVC, namely (i) better performance under low voltage conditions, (ii) faster response that is independent of the system conditions and (iii) reduced space requirement (smaller footprint). Also, a STATCOM can be built up in a modular fashion which will reduce the engineering costs.

The primary objective of applying a STATCOM in transmission networks is the fast regulation of voltage at a load or an intermediate bus. This will also increase the power transfer capacity of the network and thus enhance ATC (Available Transfer Capacity). The design of a voltage regulator is similar to that in a SVC which is discussed in chapter 3. The problems caused by interactions (electromagnetic) with the network also affect the design of voltage regulator in a STATCOM.

The smaller footprint and faster response of a STATCOM provides an opportunity to import power (for an urban area) from distant economic generators while the voltage is stabilized with a local STATCOM (older, uneconomic generators have been used in urban areas primarily for voltage regulation).

The use of multi-pulse and/or multilevel converters eliminates the need for harmonic filters in the case of a STATCOM. However, the costs increase not only due to the increased costs of magnetics and self-commutated devices (such as GTO thyristors), but also resulting from increased losses. (The total losses can vary from 0.5 to 1.0%). The new developments in power semiconductor technology are expected to bring down the costs and losses. The voltage and power ratings are expected to increase. At present, the use of STATCOM in distribution systems has become attractive, not only for voltage regulation, but also for eliminating harmonics and improving power quality.

Utilizing an auxiliary controller with Thevenin Voltage signal as input, it it possible to damp both low frequency oscillations [28] and subsynchronous oscillations [29]. In the latter case, the objective is to provide adequate damping torque in the critical range of torsional frequencies.

References and Bibliography

1. N.G. Hingorani and L. Gyugyi, '**Understanding FACTS - Concepts and Technology of Flexible AC Transmission Systems**', New York, IEEE Press 2000
2. D.R. Trainer, S.B. Tennakoon and R.E. Morrison, "Analysis of GTO-based static VAR Compensators", IEE Proc. Eletr. Power Appl., v. 141, n.6, November 1994, pp. 293-302
3. K.R. Padiyar and A.M. Kulkarni, "Design of reactive current and voltage controller of static condenser", Int. J. of Electrical Power & Energy Syst., v. 19, n.6, 1997, pp. 397-410
4. C. Schauder and H. Mehta, "Vector analysis and control of advanced static VAR compensators", IEE Proc.-C, v. 140, n.4, July 1993, pp. 299-306
5. C. Schauder, M. Gernhardt, E. Stacey, T. Lemak, L. Gyugyi, T.W. Cease and A. Edris, "Development of a ±100 MVAR Static Condenser for voltage control of transmission systems", IEEE Trans. on Power Delivery, v.10, n.3, July 1995, pp. 1486-1496.
6. S. Mori et al, "Development of a large static VAR generator using self commutated inverters for improving power system stability", IEEE Trans. on Power Systems, v.8, n.1, Feb. 1993, pp. 371-377

7. C.W. Edwards et al, "Advanced Static VAR generator employing GTO thyristors", IEEE Trans. on Power Delivery, v.3, n.4, Oct. 1988, pp. 1622-1627

8. P.J. Fritz, D.R. Trainer, G.A. Ferry and S.B. Tennakoon, "Converter topologies for advanced static VAR compensator", EPRI FACTS Conference, Boston, USA, 1992

9. V. Blasko and V. Kaura, "A new mathematical model and control of a three-phase AC-DC voltage source converter", IEEE Trans. on Power Electronics, v.32, n.1, January 1997, pp. 116-122

10. V. Kaura and V. Blasko, "Operation of a phase locked loop system under distorted utility conditions", IEEE Trans. on Industry Applications, v.33, n.1, 1997, pp. 58-63.

11. A. Gole, V.K. Sood and L. Mootoosamy, "Validation and analysis of a grid control scheme using d-q-z transformation for static compensator systems", Canadian Conf. on Elec. and Computer Engg., Montreal, Cananda, Sept. 1989

12. J.S. Lai and F.Z. Peng, "Multilevel converters – a new breed of power converters", IEEE Trans. on Industry Applications, v. 32, n.3, 1996, pp. 509-517

13. F.Z. Peng et al, "A multilevel voltage source inverter with separate DC sources for static VAR generation", IEEE Trans. on Industry Applications, v.32, n.5, 1996, pp. 1130-1138

14. K.V. Patil, R.M. Mathur, J. Jiang and S.H. Hosseini, "Distribution system compensation using a new binary multilevel voltage source inverter", IEEE Trans. on Power Delivery, v.14, n.2, April 1999, pp. 459-464

15. C. Hochgraf and R.H. Lasseter, "A transformer-less Static Synchronous Compensator employing a multi-level Inverter", IEEE Trans. on Power Delivery, v.12, n.2, April 1997, pp. 881-887

16. J.D. Ainsworth, M. Davies, P.J. Fitz, K.E. Owen and D.R. Trainer, "Static VAR compensator (STATCOM) based on single phase chain circuit converters" IEE Proc. GTD, v. 145, n.4, July 1998, pp. 381-386

17. D.W. Sandells, T.C. Green, M. Osborne and A. Power, "Power system applications for the chain-cell converter", IEE Conf. on AC-DC Power Transmission, November 2001

18. S. Dong, W. Zhonghong, J.Y. Chen and Y.H. Song, "Harmonic resonance phenomena in STATCOM and relationship to parameters selection of passive components", IEEE Trans. on Power Delivery, v.16, n.1, January 2001, pp. 46-52

19. Y. Jiang and A Ekstrom, "General analysis of harmonic transfer through converters", IEEE Trans. on Power Electronics, v.12, n.2, March 1997, pp. 287-293

20. A.K. Jain et al, "Nonlinear controllers for fast voltage regulation using STATCOMs", IEEE Trans. on Control Systems Technology, v.12, n.6, Nov. 2004, pp. 827-842

21. L.H. Walker, "Force-commutated reactive power compensator", IEEE Trans. on Industry Applications, v.22, Nov/Dec 1986, pp. 1091-1104

22. M. Hagiwara, H. Fujita and H. Akagi, "Performance of a self-commutated BTB HVDC link system under a single line-to-ground fault condition", IEEE Trans. on Power Electronics, v.18, n.1, January 2003, pp. 278-282

23. G.E. Valderrama, P. Mattavelli and A.M. Stankovic, "Reactive power and unbalance compensation using STATCOM with dissipativity-based control", IEEE Trans. on Control Systems Technology, v.9, n.5, Sept. 2001, pp. 718-727

24. P.W. Lehn and M.R. Iravani, "Experimental evaluation of STATCOM closed loop dynamics", IEEE Trans. on Power Delivery, v.13, n.4, October 1998, pp. 1378-1384

25. J.B. Ekanayake and N. Jenkins, "A three level advanced static VAR compensator", IEEE Trans on Power Delivery, v. 11, n.1, April 1996, pp. 540-545

26. J.B. Ekanayake and N. Jenkins, "Mathematical models of a three level advanced static VAR compensator", IEE Proc. -GTD, v. 144, n.2, March 1997

27. C. Schauder et al, "AEP UPFC Project: Installation, commissioning and operation of the ±160 MVA STATCOM (Phase 1)", IEEE Trans. on Power Delivery, v.13, n.4, October 1998, pp. 1530-1535

28. K.R. Padiyar and V. Swayam Prakash, "Tuning and performance evaluation of damping controller for a STATCOM", Int. J. of Electr. Power and Energy Syst., v.25, 2003, pp.155-166

29. K.R. Padiyar and Nagesh Prabhu, "Design and Performance Evaluation of Subsynchronous damping controller with STATCOM", IEEE Trans. on Power Delivery, v.21, 2006

30. F.Z. Peng, J.W. McKeever and D.J. Adams, "A power line conditioner using cascade multilevel inverters for distribution systems", IEEE Trans. Industry Appl., v. 34, n.6, 1998, pp. 1293-1298

Chapter 7

Static Synchronous Series Compensator

7.1 Introduction

The Static Synchronous Series Compensator (SSSC) is a series connected FACTS controller based on VSC and can be viewed as an advanced type of controlled series compensation, just as a STATCOM is an advanced SVC. A SSSC has several advantages over a TCSC such as (a) elimination of bulky passive components – capacitors and reactors, (b) improved technical characteristics (c) symmetric capability in both inductive and capacitive operating modes (d) possibility of connecting an energy source on the DC side to exchange real power with the AC network.

However, a SSSC is yet to be installed in practice except as a part of UPFC or Convertible Static Compensator (CSC). An example of the former is a 160 MVAR series connected converter as part of the Unified Power Flow Controller installed at Inez station of American Electric Power (AEP). An example of the latter are the two, 100 MVA series connected converters at Marcy 345 kV substation in Central New York belonging to NYPA. In both cases, 24 pulse three-level converters are used. This topology reduces the injected harmonic voltages considerably and there is no need for harmonic filters.

7.2 Operation of SSSC and the Control of Power Flow

7.2.1 Description

The schematic of a SSSC is shown in Fig. 7.1(a). The equivalent circuit of the SSSC is shown in Fig. 7.1(b).

The magnitude of V_C can be controlled to regulate power flow. The winding resistance and leakage reactance of the connecting transformer appear is series with the voltage source V_C. If there is no energy source on

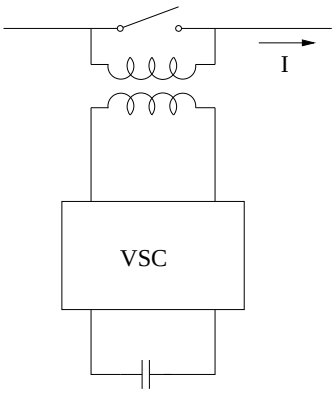

(a) Schematic of SSSC

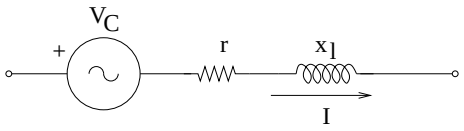

(b) Equivalent circuit

Figure 7.1: Schematic of SSSC

the DC side, neglecting losses in the converter and DC capacitor, the power balance in steady state leads to

$$Re[V_C I^*] = 0 \tag{7.1}$$

The above equation shows that V_C is in quadrature with I. If V_C lags I by 90°, the operating mode is capacitive and the current (magnitude) in the line is increased with resultant increase in power flow. On the other hand, if V_C leads I by 90°, the operating mode is inductive, and the line current is decreased. Note that we are assuming the injected voltage is sinusoidal (neglecting harmonics).

Since the losses are always present, the phase shift between I and V_C is less than 90° (in steady state). In general, we can write

$$\begin{aligned} \hat{V_C} &= V_C(\cos\gamma - j\sin\gamma)e^{j\phi} \\ &= (V_{Cp} - jV_{Cr})e^{j\phi} \end{aligned} \tag{7.2}$$

where ϕ is the phase angle of the line current, γ is the angle by which $\hat{V_C}$ lags the current. V_{Cp} and V_{Cr} are the in-phase and quadrature components of the injected voltage (with reference to the line current). We can also term them as active (or real) and reactive components. The real component is required to meet the losses in the converter and the DC capacitor.

We use the convention that the reactive voltage lagging the current by 90° as positive (Note that for a SVC or STATCOM, we used the convention of lagging reactive current as positive.) According to this convention, the positive reactive voltage implies capacitive mode of operation while negative reactive voltage implies inductive mode of operation. Since γ is close to ±90°, we can write

$$\gamma = sgn(V_{Cr})[-90^\circ + \alpha^\circ] \tag{7.3}$$

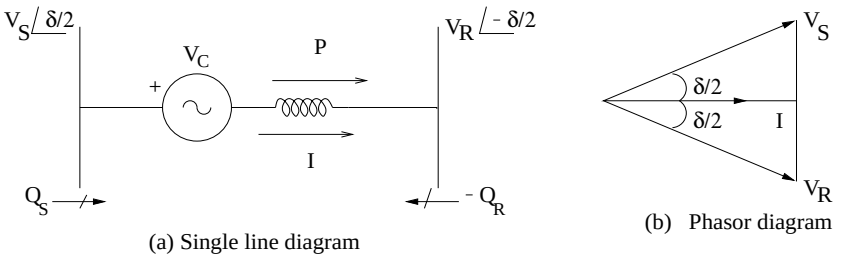

Figure 7.2: Representation of SSSC in a transmission line

where $sgn(.)$ indicates the signum function whose value is $+1$ if the argument is positive and -1 if the argument is negative. Substituting Eq. (7.3) in (7.2) we can write,

$$V_{Cp} = V_C \sin\alpha, \quad V_{Cr} = V_C \cos\alpha \tag{7.4}$$

Since the losses are expected to be small (typically below 1%) the magnitude of V_{Cp} is very small and may be neglected to simplify the analysis. V_{Cp} will vary during a transient to increase or decrease the voltage across the DC capacitor (particularly in the case of type 2 converter where the ratio between the AC voltage and the DC capacitor voltage is constant, with no modulation).

7.2.2 Comparison between Variable Series Compensation and SSSC

For comparing the characteristics of a variable series compensation (say TCSC) and a SSSC, let us consider a simple system with a transmission line (with the compensator) connected to constant voltage sources at the two ends (see Fig. 7.2). The transmission line is represented only by a series reactance (X) in which x_1 (shown in Fig. 7.1 (b)) is merged.

If the magnitudes of V_S and V_R are equal to V, the voltage drop across the line (see phasor diagram) is given by

$$IX - V_C = 2V \sin\frac{\delta}{2} \tag{7.5}$$

The magnitude of the current is obtained as

$$I = \frac{V_C}{X} + \frac{2V \sin\frac{\delta}{2}}{X} \tag{7.6}$$

The power flow (P) in the line is given by

$$P = VI\cos\frac{\delta}{2} = \frac{VV_C}{X}\cos\frac{\delta}{2} + \frac{V^2\sin\delta}{X} \tag{7.7}$$

The reactive power supplied at the two ends of the line are equal (Q). The expression for Q is given by

$$Q = VI \sin\frac{\delta}{2} = \frac{V_C V}{X} \sin\frac{\delta}{2} + \frac{V^2}{X}(1 - \cos\delta) \tag{7.8}$$

From Eq. (7.6), it is observed that I varies linearly with V_C for a specified value of δ. If V_C is negative (inductive), it is possible to reverse the line current phasor which leads to power reversal in the line. The property of reversal of power is not feasible with variable series compensation as shown below.

The line current with variable series compensation is given by

$$I = \frac{2V \sin\frac{\delta}{2}}{X(1 - k_{se})} \tag{7.9}$$

This shows that only way of power reversal is by increasing the compensation level, k_{se} above 1.0 (overcompensation). However, this is not practical for two reasons. (1) As k_{se} approaches 1, the current in the line increases without limit due to resonance at the fundamental frequency. (Inclusion of the line resistance in the model puts an upper limit on the current which can still be dangerously high). (2) The power angle curve for a line with overcompensation ($k_{se} > 1$) is shown in Fig. 7.3. The operating value of δ is assumed to be 30°. The system is not stable at this operating point as synchronizing torque is negative ($\frac{dP}{d\delta}$ is negative). The operating point corresponding to $\delta = 180° - 30°$ is stable, but the current in the line is much higher which gives rise to increased losses in the line when resistance is considered.

The above arguments shows that while power reversal in a transmission line is feasible with a SSSC injecting the desired value of inductive reactive voltage; the power reversal with a TCSC (for positive δ) is not feasible. Also, in a TCSC, the inductive vernier operation is rarely used (due to increased thyristor currents, losses and harmonic voltages). Only during the TCSC bypass mode, the net reactance is small inductive. This mode is used to protect the capacitor against overvoltages caused by high currents in the line due to faults.

The variation of power (P) and reactive power (Q) as a function of δ is shown in Fig. 7.4 for different values of V_C. It is assumed that $V = 1.0$, $X = 0.5$. The reactive power (Q_C) supplied by the SSSC is given by $Q_C = V_C I$ whereas for a fixed compensation, $Q_C = I^2 X(I - k_{se})$ also shown as a function of δ. These quantities for $V_C = 0.25$ are compared with those for a fixed compensation ($k_{se} = 0.5$) and the results are shown in Fig. 7.5. Note that for rated current, both compensations result in identical operating conditions ($\delta = 15.96°$, $P = 0.992$, $Q = 0.125$).

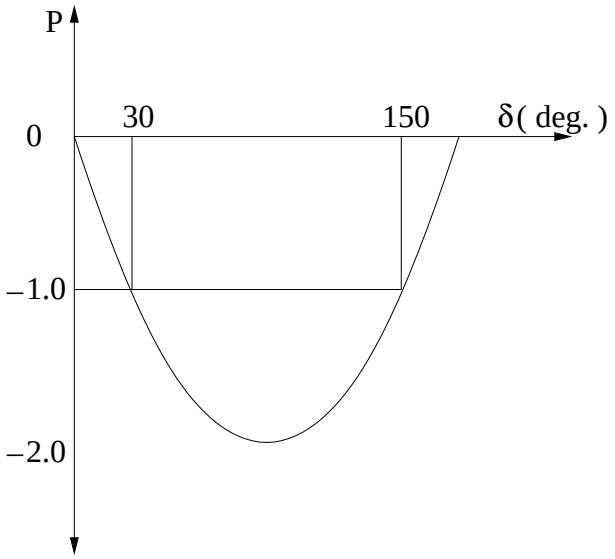

Figure 7.3: Power angle curve with $k_{se} > 1$ (overcompensation)

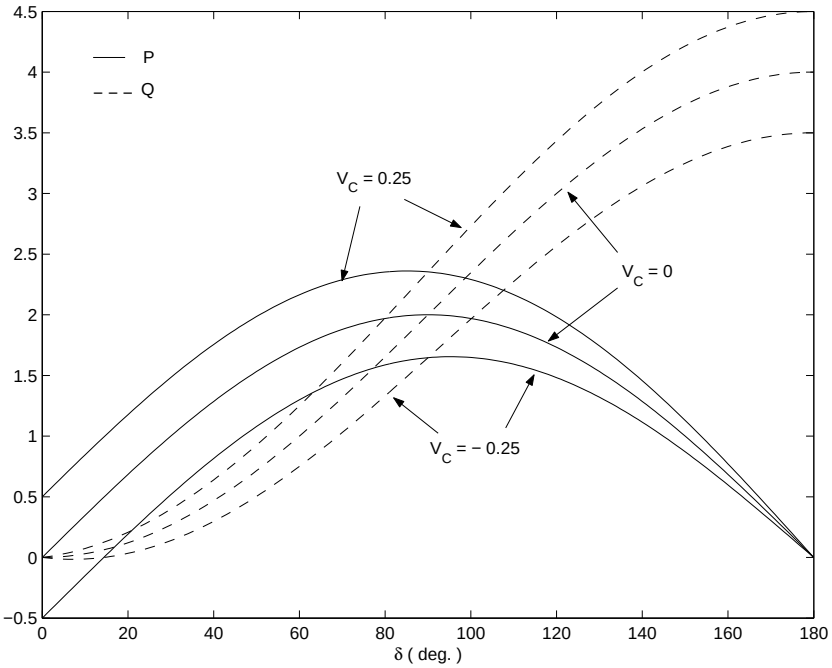

Figure 7.4: Variation of P and Q with δ

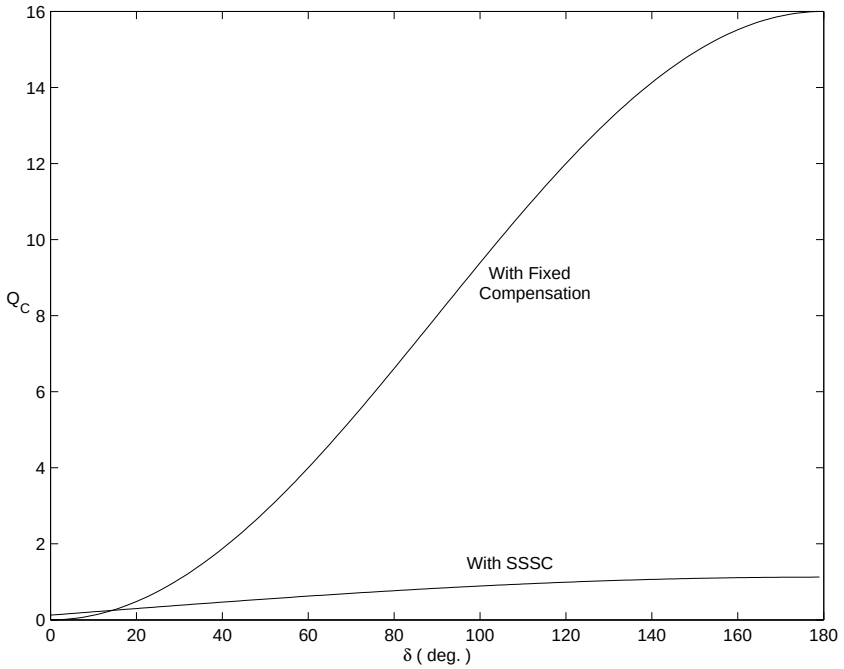

Figure 7.5: Reactive power supplied by SSSC with $V_C = 0.25$

Remarks

1. The property of a SSSC that results in the reversal of power by injecting required magnitudes of inductive reactive voltage (for $\delta > 0$) is similar to that of a phase shifter. Thus, a Static Phase Shifting Transformer (SPST) or Phase Angle Regulator (PAR) can be made up of series and shunt connected VSCs.

2. The DC capacitor is initially charged by the currents flowing in the anti-parallel connected diodes which function as a rectifier that draws energy from the current flowing in the transmission line. The steady state operation of a SSSC when the line current is very low may be problematic unless separate DC sources are used to charge the capacitor.

   The advantage of power reversal in the transmission line for $\delta > 0$, is intended to be useful mainly under dynamic conditions. The full dynamic range of operation of a SSSC is utilized during contingency conditions to improve stability

3. The SSR characteristics of a SSSC are quite different from that of a TCSC. Theoretically, if the capacitor voltage can be held constant, or the variations minimized by selecting a large value of the capacitance, then the SSR can be claimed to be SSR neutral. Under such conditions,

the resonance at subsynchronous frequencies is determined by the rest of the electrical network-line inductance and fixed capacitors if any (Note that because of cost considerations, the total compensation in a line will be made up of fixed and variable type).

The SSR characteristics of a SSSC will be discussed separately.

7.2.3 Power Flow Control Characteristics

A SSSC controls the power flow in a transmission line by varying the magnitude and polarity of the reactive voltage injected in series with line. In this section, we will study the control characteristics of a SSSC in the $P-Q$ plane where P and Q are the power and reactive power at the receiving end. In deriving the control characteristics we will relax the assumptions about losses in the line and the equality of sending end and receiving end voltage magnitudes.

If $Z = R + jX$ represents the series impedance of the line shown in Fig. 7.2, the complex power at the receiving end (S_R) is given by

$$S_R = P_R + jQ_R = \frac{\hat{V}_R(\hat{V}_S - \hat{V}_C - \hat{V}_R)^*}{Z^*} \tag{7.10}$$

If $V_C = 0$, then S_R is defined as

$$S_R = S_0 = P_0 + jQ_0 = \frac{\hat{V}_R(\hat{V}_S - \hat{V}_R)^*}{Z^*} \tag{7.11}$$

Substituting Eq. (7.11) in (7.10), we get

$$S_R = S_0 - \frac{\hat{V}_R V_C^*}{Z^*} \tag{7.12}$$

Assuming V_C is purely reactive voltage, then

$$\hat{V}_C = -jA\hat{I}, \quad A = \frac{V_C}{|I|} \tag{7.13}$$

Substituting Eq. (7.13) in (7.12) and noting that

$$I^* = \frac{S_R}{V_R} \tag{7.14}$$

we obtain,

$$S_R = S_0 - \frac{\hat{V}_R(jAI^*)}{Z^*} = S_0 - j\frac{AS_R}{Z^*} \tag{7.15}$$

From the above, we can solve for S_R as,

$$S_R = \frac{S_0 Z^*}{Z^* + jA} = \frac{S_0 Z^*}{R + j(A - X)} \tag{7.16}$$

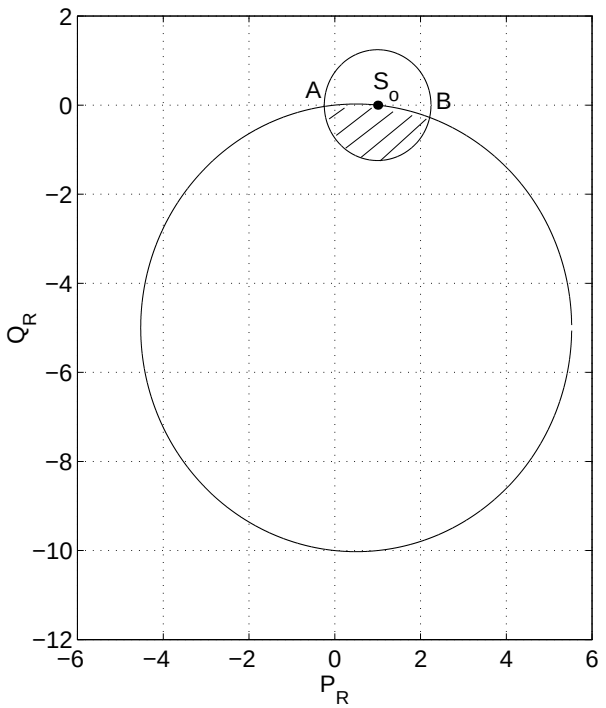

Figure 7.6: Operating region and control characteristics of a SSSC in the $P_R - Q_R$ plane

As A varies from $-\infty$ to ∞, the locus of $R + j(A - X)$ in the $R - X$ plane is a straight line parallel to the X axis and passing through the point $(R, 0)$. The locus of the reciprocal of $R+j(A-X)$ is a circle with the center $\left(\frac{1}{2R}, 0\right)$ and radius $\frac{1}{2R}$. From Eq. (7.15), it can be seen that S_R describes a circle in the $P - Q$ plane with $\frac{S_0 Z^*}{2R}$ as center and radius of $\left|\frac{S_0 Z^*}{2R}\right|$.

Note that this circle passes through the origin as well as the point S_0 (corresponding to $V_C = 0$). The locus of P_R and Q_R lie on the circumference of the circle which is a function of S_0 and the ratio $\frac{X}{R}$. The value of S_0 (P_R and Q_R in the absence of SSSC) is a function of δ and the line impedance Z (for specified V_S and V_R). However, different combinations of Z and δ can give a specified value of S_0.

If $|S_0| = 1.0$ and $\frac{X}{R} = 10$, then the radius of the circle is 5.025 pu. Fig. 7.6 shows the control characteristics for $P_0 = 1.0$, $Q_0 = 0.0$, with $|S_0| = 1.0$.

The range of operation of a SSSC is only a part of the circle around the operating point S_0. This is due to the limitations imposed by the rating

of SSSC. Fig. 7.6 also shows the range of operation of a SSSC which is bounded by a circle with $\hat{S}_0$ as centre and radius = $|\frac{V_{C\max}V}{Z}|$.

7.3 Modelling and Control of SSSC

7.3.1 Modelling of SSSC

Neglecting harmonics, we can express the system equations (including SSSC) in D–Q variables (referred to a synchronously rotating axis). The advantage of using these variables is that in steady state, the D–Q components are constants and can be expressed as rectangular coordinates of phasors. For stability studies involving phenomena of frequency below 5 Hz, it is adequate to express the network equations using phasors by neglecting network transients. However, for phenomena involving higher frequencies, one cannot ignore network transients (even for studies involving subsynchronous frequency oscillations).

We can illustrate the derivation of the network equations by considering the single line containing a SSSC shown in Fig. 7.2.

Neglecting, zero sequence components, we can express the network equations (using two phase variables, α and β) in the complex form given below.

$$L\frac{d\hat{i}}{dt} + R\hat{i} = \hat{v}_S - \hat{v}_C - \hat{v}_R \tag{7.17}$$

where

$$\begin{aligned} \hat{i} &= (i_\beta + ji_\alpha), \quad \hat{v}_S = v_{S\beta} + jv_{S\alpha}, \\ \hat{v}_C &= v_{C\beta} + jv_{C\alpha}, \quad \hat{v}_R = v_{R\beta} + jv_{R\alpha}, \end{aligned}$$

Transforming from α, β to $D-Q$ components which are related as,

$$\begin{bmatrix} i_\alpha \\ i_\beta \end{bmatrix} = \begin{bmatrix} \cos\theta & \sin\theta \\ -\sin\theta & \cos\theta \end{bmatrix} \begin{bmatrix} i_D \\ i_Q \end{bmatrix} \tag{7.18}$$

where $\theta = \omega_0 t + \theta_0$. There is no loss of generality in assuming $\theta_0 = 0$. Similar transformation as given above applies to the variables $v_{S\alpha}, v_{S\beta}$ and v_{SD}, v_{SQ} and so on.

We can also express Eq. (7.18) as a complex equation given below.

$$(i_\beta + ji_\alpha) = (i_Q + ji_D)e^{j\omega_0 t} = \hat{I}e^{j\omega_0 t} \tag{7.19}$$

Utilizing Eq. (7.18) and similar equations for other variables in Eq. (7.17), the latter can be expressed as

$$L\frac{d(\hat{I}e^{j\omega_0 t})}{dt} + R(\hat{I}e^{j\omega_0 t}) = (\hat{V}_S - \hat{V}_C - \hat{V}_R)e^{j\omega_0 t} \tag{7.20}$$

Simplifying, we get,

$$L\frac{d\hat{I}}{dt} + j\omega_0 L\hat{I} + R\hat{I} = \hat{V}_S - \hat{V}_C - \hat{V}_R \tag{7.21}$$

where

$$\begin{aligned} \hat{I} &= I_Q + jI_D, \quad \hat{V}_S = V_{SQ} + jV_{SD}, \quad \hat{V}_C = V_{CQ} + jV_{CD}, \\ \hat{V}_R &= V_{RQ} + jV_{RD} \end{aligned}$$

In steady state, $\hat{I}$ is a constant and $\frac{d\hat{I}}{dt} = 0$. Hence, we get (in steady state),

$$(R + j\omega_0 L)\hat{I} = \hat{V}_S - \hat{V}_C - \hat{V}_R \tag{7.22}$$

Remarks

1. The advantages of writing a complex equation such as Eq. (7.20) for a network element (such as a transmission line) are two fold
   (a) The extension to a complex network consisting of inductors, capacitors, resistors etc is straightforward.
   (b) The derivation of phasor equations in steady state (such as Eq. (7.21)) is, again, simplified.
2. Both lower case and upper case letters are used for $D-Q$ components as they are both instantaneous quantities as well as components of phasors (in steady state).

Actually, the term 'dynamic phasors' can be used when the derivatives are not zero. (under dynamic conditions).

The voltage injected by SSSC can be expressed as

$$V_{CQ} + jV_{CD} = (V_{Cp} - jV_{Cr})e^{j\phi} \tag{7.23}$$

where,

$$\tan\phi = \frac{I_D}{I_Q} \tag{7.24}$$

The equation for the DC capacitor voltage is

$$C\frac{dv_{dc}}{dt} + Gv_{dc} = i_{dc} \tag{7.25}$$

From the power balance considerations,

$$Re(\hat{V}_C\hat{I}^*) = v_{dc}i_{dc} \tag{7.26}$$

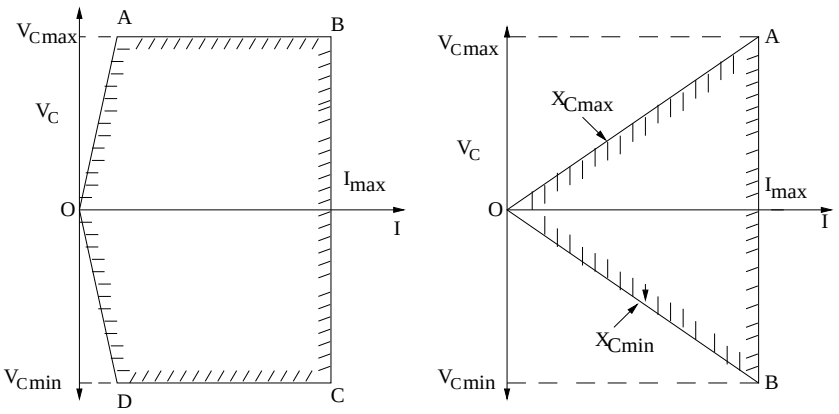

Figure 7.7: Operating region of SSSC in $V_C - I$ plane

The L.H.S is expressed as

$$IV_{Cp} = IV_C \sin\alpha = IkV_{dc} \sin\alpha \tag{7.27}$$

From the above, we get

$$i_{dc} = kI \sin\alpha \tag{7.28}$$

where, $I = \sqrt{I_D^2 + I_Q^2}$, α is defined in Eq. (7.3).

In steady state, we can express V_C as

$$V_C = \frac{k^2 I}{G} \sin\alpha \tag{7.29}$$

Note that $\alpha > 0$ in steady state.

The operating region in the $V_C - I$ plane is shown in Fig. 7.7 where SSSC is operated in voltage control. This figure also shows the operating region when the SSSC is operated in the reactance control mode (which has also been proposed in the literature). However, as discussed earlier, the voltage control model is more advantageous than the reactance control mode.

The operating region in the voltage control mode is OABCD. The slope of OA and OD are obtained from Eq. (7.29) as

$$\frac{dV_C}{dI} = \pm\frac{k^2}{G} \tag{7.30}$$

corresponding to $\alpha = 90°$. V_C is assumed to be positive when it is capacitive and negative when it is inductive. Note that $V_{C\,\min} = -V_{C\,\max}$. Similarly X_C is assumed to be positive (when capacitive) and negative (when inductive). Also $X_{C\,\min} = -X_{C\,\max}$. The operating region in the reactance control mode is OAB.

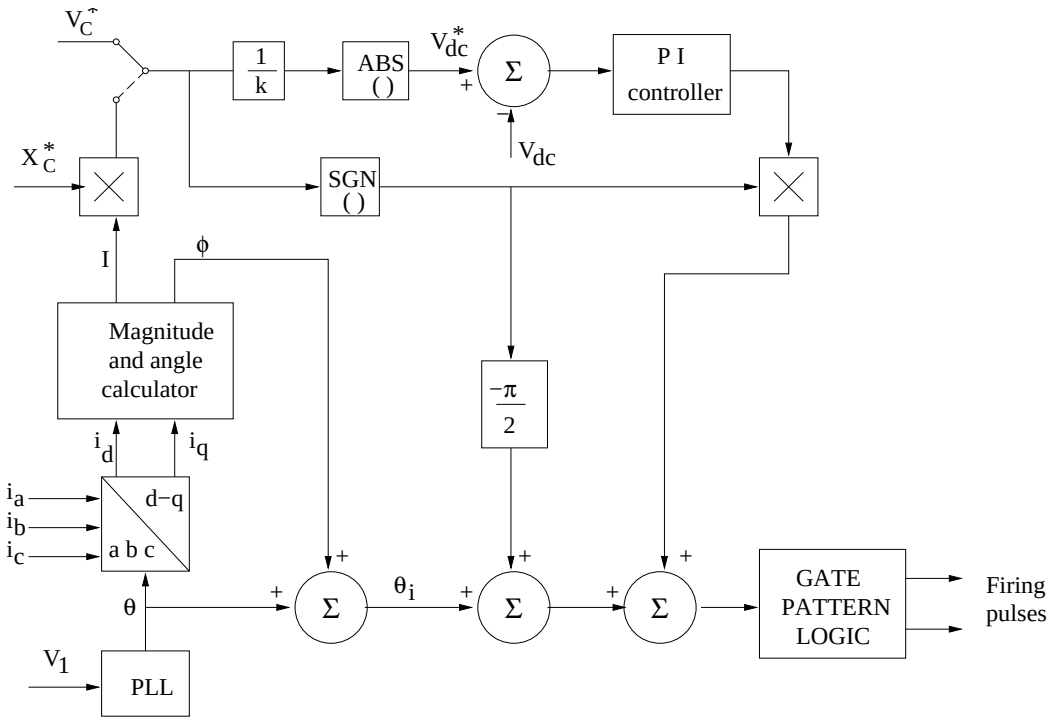

Figure 7.8: Block diagram of controller for type 2 VSC

7.3.2 Control Scheme for SSSC Using Type 2 Converter

When the ratio of the magnitude of the injected voltage to the DC capacitor voltage $\left(\frac{V_C}{V_{dc}} = k\right)$ is held constant, the only control variable is α that is used to regulate the magnitude of V_C. The block diagram of the controller is shown in Fig. 7.8.

The voltage reference (V_C^*) injected by SSSC is obtained as the output of higher level controls - power scheduling, power oscillation damping and transient stability (enhancement) controls. These issues are discussed in chapter 4 when dealing with the control of a TCSC. There is no essential difference between a TCSC or a SSSC in the matter of higher level controls. The power scheduling control can be either Constant Current (CC) type or Constant Angle (CA) type. The control strategies for the improvement of transient stability are based on the discrete or bang-bang control. This will be discussed in detail in chapter 11. It is also possible to provides an auxiliary (supplementary) control for damping subsynchronous oscillations.

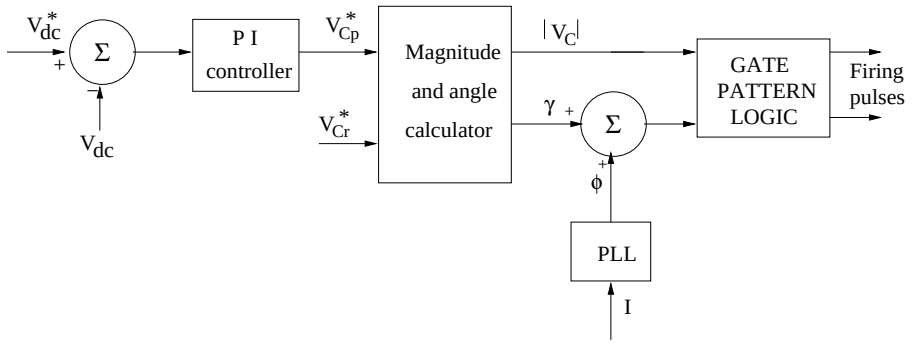

Figure 7.9: Block diagram of controller for type 1 VSC

7.3.3 Controller of SSSC Using Type 1 Converter

It is very likely that a practical SSSC will utilize Type 1 converters. The existing SSSCs at Inez and Marcy substations in USA use 24 pulse, 3 level converters. Here, k is variable in addition to α. The gating pulses are based on the computation of k and α as follows.

$$\begin{aligned} k_{var} &= \frac{V_C}{V_{dc}}, \quad V_C = \sqrt{V_{Cp}^2 + V_{Cr}^2} \\ \alpha &= \tan^{-1} \frac{V_{Cp}}{|V_{Cr}|} \end{aligned}$$

For a three level converter, the dead angle (β) required can be obtained from

$$\cos\beta = \frac{k_{var}}{k_{fix}}, \quad k_{fix} = \frac{p}{6}\frac{\sqrt{6}}{\pi} \tag{7.31}$$

where p is the pulse number.

The block diagram of the controller for type 1 converter is shown in Fig. 7.9.

7.4 SSSC with an Energy Source

If an energy source such as battery or fuel cell is provided on the DC side of the VSC, it is possible to exchange real (active) power with the AC network. Here, the real (active) voltage component can be controlled in addition to the reactive voltage. This enables two degrees of freedom to control active and reactive power flow in the line. Alternately, it is possible to compensate for the line resistance to increase the power transfer capacity in the line.

Instead of an energy source, it is possible to provide the real power from a shunt connected VSC which is connected to the series connected

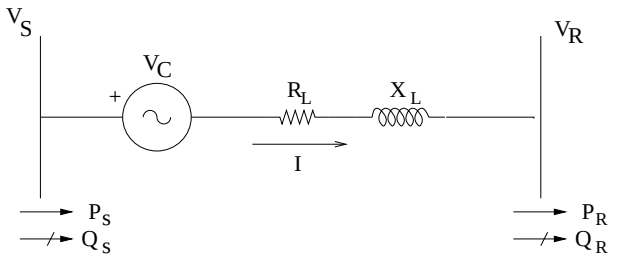

Figure 7.10: A SSSC in a lossy transmission line

SSSC on the DC side. This arrangement is known as Unified Power Flow Controller (UPFC) which is described in the next chapter in detail. Here, we will discuss two different control strategies which also apply to UPFC.

7.4.1 Emulation of Resistance and Reactance

Consider a transmission line with a SSSC as shown in Fig. 7.10. The SSSC injects active voltage (V_{Cp}) in addition to the reactive voltage (V_{Cr}). Assuming the reactive voltage is controlled to compensate for the line reactance, V_{Cp} can be controlled to introduce a negative resistance (by injecting active power in the line) to raise the $\frac{X}{R}$ ratio in the line. The compensation for the line reactance reduces the $\frac{X}{R}$ ratio, which can be raised by the compensation of the line resistance [2]. For a given value of X, raising the $\frac{X}{R}$ ratio increases the power transfer in the line.

For the line shown in Fig. 7.10, the resistance and reactance emulation control in the SSSC, result in

$$V_{Cp} = -IR_C, \quad V_{Cr} = IX_C \tag{7.32}$$

The net resistance (R) and reactance (X) in the line are given by

$$R = R_L - R_C, \quad X = X_L - X_C \tag{7.33}$$

Power Flow in the Line

The equivalent series impedance in the line is given by

$$Z = R + jX \tag{7.34}$$

Assuming $|V_S| = |V_R| = V$, for simplicity, we get

$$I = (G - jB)(\hat{V}_S - \hat{V}_R) = \hat{I}_G + \hat{I}_B \tag{7.35}$$

where

$$G - jB = \frac{1}{R + jX}$$

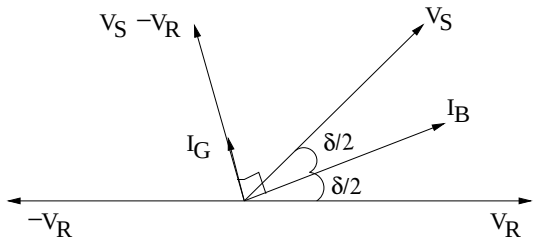

Figure 7.11: Phasor diagram for circuit in Fig. 7.10

Referring to the phasor diagram shown in Fig. 7.11, we have,

$$\hat{V}_S - \hat{V}_R = 2V \sin\frac{\delta}{2} \angle \left(\frac{\pi}{2} + \frac{\delta}{2}\right) \tag{7.36}$$

$$\hat{I}_G = 2GV \sin\frac{\delta}{2} \angle \left(\frac{\pi}{2} + \frac{\delta}{2}\right), \quad \hat{I}_B = 2BV \sin\frac{\delta}{2} \angle \frac{\delta}{2} \tag{7.37}$$

$$P_S + jQ_S = \hat{V}_S(\hat{I}_G^* + \hat{I}_B^*) \tag{7.38}$$
$$P_R + jQ_R = \hat{V}_R(\hat{I}_G^* + \hat{I}_B^*) \tag{7.39}$$

Substituting $\hat{V}_S = V\angle\delta, \hat{V}_R = V\angle 0$ and Eq. (7.37) in (7.38) and (7.39), we get the following expressions

$$P_S = BV^2 \sin\delta + GV^2(1 - \cos\delta) \tag{7.40}$$
$$Q_S = BV^2(1 - \cos\delta) - GV^2 \sin\delta \tag{7.41}$$
$$P_R = BV^2 \sin\delta - GV^2(1 - \cos\delta) \tag{7.42}$$
$$-Q_R = BV^2(1 - \cos\delta) + GV^2 \sin\delta \tag{7.43}$$

It is interesting to observe that the conductance (G) of a line results in the transmission of reactive power from the receiving end to the sending end, without any loss.

G and B are defined from

$$G = \frac{R}{R^2 + X^2} = \frac{h^2}{(h^2+1)R} = \frac{h}{(h^2+1)X}$$
$$B = \frac{X}{R^2 + X^2} = \frac{h}{(h^2+1)R} = \frac{1}{(h^2+1)X}$$

where $h = \frac{R}{X}$.

P_R is maximum at $\delta = \delta_m$ defined by $\frac{dP_R}{d\delta} = 0$. For a specified value of h, we can derive

$$\cos\delta_m = h \sin\delta_m \tag{7.44}$$

Case (i): R is held constant, X is variable.

For this case, we can show that the maximum received power (corresponding to $\delta = \delta_m$) can be expressed as

$$P_m = \frac{V^2}{R}\cos\delta_m - \frac{V^2h^2}{R(1+h^2)} = \frac{V^2}{R}\cos\delta_m(1-\cos\delta_m) \tag{7.45}$$

If h is a controllable parameter (which also determines δ_m), we can maximize P_m by letting

$$x = \cos\delta_m = 0.5 \Longrightarrow \delta_m = 60^\circ \tag{7.46}$$

Note that we obtain this result by the condition $\frac{dP_m}{d\delta_m} = 0$. Also, the optimum value of h is obtained from Eq. (7.40) as

$$h_{opt} = \cot\delta_m = \frac{1}{\sqrt{3}} \tag{7.47}$$

Note that this is a well-known result. The maximum value of the series reactive compensation is determined from the (optimum) $\frac{X}{R} = \sqrt{3}$. Thus, if $\frac{X_L}{R_L} = 10$, maximum series reactive compensation is limited to 82.7%.

The line current for the optimum value of h, is given by

$$\begin{aligned} \hat{I} &= \frac{4}{\sqrt{3}}BV\sin\frac{\delta_m}{2}\angle 60^\circ \\ \hat{I} &= \sqrt{3}\frac{V}{X}\sin 30^\circ\angle 60^\circ \end{aligned} \tag{7.48}$$

It is interesting to observe that $\hat{V}_S$ and $\hat{I}$ are in phase and the reactive power at the sending end is zero. The maximum power at the receiving end is given by

$$P_{R\max} = \frac{V^2}{4R} = \frac{\sqrt{3}V^2}{4X} = \frac{0.433V^2}{X} \tag{7.49}$$

It can be shown that Q_S=0 and $-Q_R = \frac{3V^2}{4X}$. Also, $P_S = 2P_R$ implying that half the sending end power is consumed by SSSC.

Case (ii): X is held constant, R is variable.

It is assumed that the SSSC regulates X_C which is held constant. This implies that X is a constant. R_C is made variable. The objective is to solve for the optimum value of R which maximizes P_R. We proceed as before. While Eq. (7.44) applies, P_m is now expressed as

$$\begin{aligned} P_m &= \frac{V^2}{X}\sin\delta_m - \frac{V^2}{X}\,\frac{h}{(1+h^2)} \\ &= \frac{V^2}{X}\left[\sin\delta_m - \frac{\sin 2\delta_m}{2}\right] \end{aligned} \tag{7.50}$$

P_m is maximized by letting $\frac{dP_m}{d\delta_m} = 0$. We get

$$\cos\delta_m - \cos 2\delta_m = 0 \tag{7.51}$$

Denoting $x = \cos\delta_m$, we get a quadratic equation in x, from Eq. (7.51), given by

$$2x^2 - x - 1 = 0 \tag{7.52}$$

and the relevant solution for $x = -\frac{1}{2}$. This gives $\delta_m = 120^\circ$ and $h_{opt} = -\frac{1}{\sqrt{3}}$. Note that the net resistance is now negative and optimum value of R_C is given by

$$R_C^{opt} = \frac{-X}{\sqrt{3}} - R_L \tag{7.53}$$

It can be shown that $P_{R\max}$ is given by

$$P_{R\max} = \frac{V^2 3\cdot\sqrt{3}}{4X} = 1.299\frac{V^2}{X} \tag{7.54}$$

Note that this is three times the value given by Eq. (7.49). The line current for this condition can be expressed as

$$\hat{I} = \sqrt{3}\frac{V}{X}\sin 60^\circ \angle 30^\circ \tag{7.55}$$

It is interesting to observe that the line current lags the sending end voltage by 90°. This implies that the sending end power is zero and the entire power flow comes from the SSSC. The reactive power injected by the sending end is maximum and is given by

$$Q_S = \frac{3V^2}{2X} \tag{7.56}$$

The reactive power injected at the receiving end ($-Q_R$) is only half of the value of Q_S. The value of $-Q_R$ is same as that in case (i).

Remarks

1. By injecting active power from SSSC and resistance emulation, the maximum power at the receiving end exceeds the theoretical maximum of $\frac{V^2}{X}$ (for $R = 0$) (see Eq. (7.49). The sending end supplies only reactive power.
2. The magnitude of the line current in case (ii) (with negative R) is $\sqrt{3}$ times the current in case (i). However, the power factor at the receiving end for case (ii) is 0.866 while it is 0.5 for case (i). Thus, the maximum power is three times that for case (i).
3. The negative resistance emulation can destabilize oscillations in power. Thus, the practical use of this strategy appears to be limited.

7.4.2 Active and Reactive Voltage Control

If, instead of emulating resistance and reactance, we control directly active and reactive voltage (within the constraints imposed by the ratings), it is possible to control and regulate the power and reactive power flow in the line. If the power and reactive power at the receiving end can be held at their command values independent of the normal variations in the operating conditions in the system; this would be a remarkable achievement for systems control.

Referring to Fig. 7.10 and Eq. (7.12) reproduced below,

$$S_R = P_R + jQ_R = S_0 - \frac{V_C^* V_R}{Z^*} \tag{7.57}$$

Assuming that the rating of SSSC only limits the magnitude of V_C (the voltage injected), but the phasor V_C can lie in any of the four quadrants, the Eq. (7.57) describes a circle in the $P_R - Q_R$ plane with the center (P_0, Q_0) and a radius of $\left|\frac{V_C V_R}{Z}\right|$. We can rewrite Eq. (7.57) as follows.

$$(P_R - P_0)^2 + (Q_R - Q_0)^2 = \left|\frac{V_C V_R}{Z}\right|^2 \tag{7.58}$$

Assuming that $|V_C| < V_{C\max}$, the circle corresponding to the radius of $\left|\frac{V_{C\max} V_R}{Z}\right|$ circumscribes the region in $P - Q$ plane, that is controlled by the SSSC.

For $Z = 0.02 + j0.2, V_{C\max} = 0.25, V_R = 1.0,\ P_0 = 1.0, Q_0 = 0.0$, the region of operation is shown in Fig. 7.6 as bound by a circle with $\hat{S}_0$ as centre. This figure also shows the circle corresponding to the SSSC operating without an energy source (injecting only a reactive voltage). The overlapping region of the two circles correspond to the operation when the SSSC absorbs power from the transmission line. The rest of the circular region described by Eq. (7.58) corresponds to the operation of SSSC when it supplies power to the transmission line. (Note that the SSSC circle with reactive voltage injection maps the line (parallel to y- axis) passing through the point $(R, 0)$ in the $R-X$ plane to a circle in the $P-Q$ plane. The inside of the circle corresponds to the region in the $R-X$ plane to the right of the line passing through $(R, 0)$. This region corresponds to the net resistance of the transmission line exceeding R).

It is obvious that it is possible to regulate P_R and Q_R in the line with the injection of V_C (of required magnitude and phase angle) as long as the desired values of P_R and Q_R lie in the region defined by the circle with (P_0, Q_0) as center and a radius of $\left|\frac{V_{C\max} V_R}{Z}\right|$.

7.4.3 Power Flow with Constant Active and Reactive Voltage Injection in the Line

It is possible to derive expressions for the power flow in the line if we consider the control strategy is to regulate the magnitude of the active (V_{Cp}) and reactive (V_{Cr}) voltage injected by the SSSC. To simplify the analysis, we will neglect the line resistance (R_L) in the line (shown in Fig. 7.10). If $V_{Cp} = 0$, then the current phasor ($\hat{I}$) has the phase angle of $(\delta_S + \delta_R)/2$ if $|V_S| = |V_R| = V$ and $R_L = 0$. If we assume $\delta_S = \frac{\delta}{2}, \delta_R = \frac{-\delta}{2}$, the phase angle of the current is zero if $V_{Cp} = 0$.

The presence of V_{Cp} alters the phase angle of the line current. If we assume

$$\hat{I} = I\angle -\phi$$

we can express $\hat{V}_C$ as

$$\hat{V}_C = (V_{Cp} - jV_{Cr})\angle -\phi = (-V_p + jV_r)\angle -\phi$$

Note that we are assuming V_{Cp} as negative which implies that $\phi > 0$. This can be deduced from the analysis given in section 7.4.1.

From the equivalent circuit of the line shown in Fig. 7.12, we can express $\hat{I}$ (by applying superposition principle) as

$$I\angle -\phi = \frac{2V\sin\frac{\delta}{2}}{X_L} + \frac{V_p\angle -\phi}{jX_L} + \frac{jV_r\angle -\phi}{jX_L} \tag{7.59}$$

Separating the real and imaginary components, we get

$$I\cos\phi = \frac{2V\sin\frac{\delta}{2}}{X_L} - \frac{V_p\sin\phi}{X_L} + \frac{V_r}{X_L}\cos\phi \tag{7.60}$$

$$I\sin\phi = \frac{V_p\cos\phi}{X_L} + \frac{V_r}{X_L}\sin\phi \tag{7.61}$$

By multiplying both sides of Eq. (7.60) and Eq. (7.61) by $\cos\frac{\delta}{2}$ and $\sin\frac{\delta}{2}$ respectively and adding, we can derive

$$\left(I - \frac{V_r}{X_L}\right)\cos\left(\frac{\delta}{2} - \phi\right) = \frac{V\sin\delta}{X_L} + \frac{V_p}{X_L}\sin\left(\frac{\delta}{2} - \phi\right) \tag{7.62}$$

Since,

$$P_R = VI\cos\left(\frac{\delta}{2} - \phi\right),$$

we get the final expression for P_R as

$$P_R = \frac{V^2\sin\delta}{X_L} + \frac{VV_p}{X_L}\sin\left(\frac{\delta}{2} - \phi\right) + \frac{VV_r}{X_L}\cos\left(\frac{\delta}{2} - \phi\right) \tag{7.63}$$

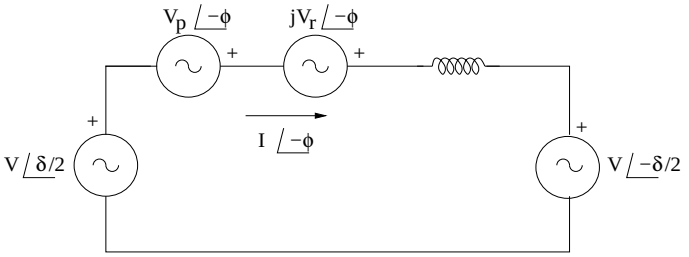

(a) Equivalent circuit

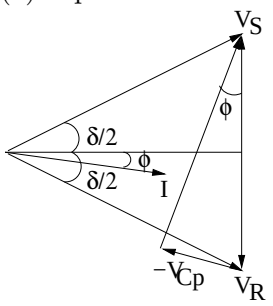

(b) Phasor diagram

Figure 7.12: SSSC with constant active and reactive voltage injection

From the phasor diagram (also shown in Fig. 7.12) we can express ϕ as a function of V_p and δ as follows

$$\sin\phi = \frac{V_p}{2V\sin\frac{\delta}{2}} \tag{7.64}$$

The above equation also shows that $\phi > 0$ if $V_{Cp} = -V_p$ is negative implying that SSSC is supplying power to the line from the energy source connected on the DC side.

It is also possible to express Q_R defined as $-Q_R = VI\sin\left(\frac{\delta}{2} - \phi\right)$.

The final expression for the reactive power injected into the line at the receiving end can be derived from Eqs (7.60)and (7.61). This is given by

$$-Q_R = \frac{V^2}{X_L}(1-\cos\delta) - \frac{VV_p}{X_L}\cos\left(\frac{\delta}{2} - \phi\right) + \frac{VV_r}{X_L}\sin\left(\frac{\delta}{2} - \phi\right) \tag{7.65}$$

Note that $\phi = 0$ if $V_p = 0$. The role of real power transfer from SSSC is to reduce the reactive power supplied at the receiving end in addition to enhance the active power received (P_R). While pure reactive voltage injection increases P_R, it is also accompanied by the increase in $(-Q_R)$.

7.5 Analysis of SSR with a SSSC

As mentioned earlier, the SSSC is strictly SSR neutral if the DC capacitor has large size and the controller regulates the capacitor voltage with no perturbations caused by perturbations in the line current.

To simplify the analysis, we assume that the perturbations in the line currents can be expressed as

$$\begin{aligned}
\Delta i_a(t) &= \sqrt{\frac{2}{3}}\left[I_{sub}\cos\omega_{sub}t + I_{sup}\cos\omega_{sup}t\right] \\
\Delta i_b(t) &= \sqrt{\frac{2}{3}}\left[I_{sub}\cos\left(\omega_{sub}t - \frac{2\pi}{3}\right) + I_{sup}\cos\left(\omega_{sup}t - \frac{2\pi}{3}\right)\right] \\
\Delta i_c(t) &= \sqrt{\frac{2}{3}}\left[I_{sub}\cos\left(\omega_{sub}t + \frac{2\pi}{3}\right) + I_{sup}\cos\left(\omega_{sup}t + \frac{2\pi}{3}\right)\right]
\end{aligned}$$

The perturbations in the capacitor voltage (ΔV_{dc}) is given by the equation,

$$\begin{aligned}
C\frac{d\Delta V_{dc}}{dt} &= \Delta i_{dc} \\
&= \sqrt{\frac{2}{3}}k\left[\Delta i_a \cdot \sin\omega_0 t + \Delta i_b \cdot \sin\left(\omega_0 t - \frac{2\pi}{3}\right) + \Delta i_c \cdot \sin\left(\omega_0 t + \frac{2\pi}{3}\right)\right]
\end{aligned} \tag{7.66}$$

The above equation can be simplified as

$$C\frac{d\Delta V_{dc}}{dt} = k(I_{sub} - I_{sup})\sin\omega_m t \tag{7.67}$$

where $\omega_m = \omega_0 - \omega_e = \omega_0 - \omega_{sub} = \omega_{sup} - \omega_0$.

From Eq. (7.67), we can derive,

$$\Delta V_{dc}(t) = -\frac{k}{C\omega_m}(I_{sub} - I_{sup})\cos\omega_m t \tag{7.68}$$

The perturbation in the injected voltage (ΔV_{Ca}) is given by

$$\Delta V_{Ca}(t) = -\frac{k^2}{2C\omega_m}\sqrt{\frac{2}{3}}[(I_{sub} - I_{sup})\sin\omega_{sub}t + (I_{sub} - I_{sup})\sin\omega_{sup}t] \tag{7.69}$$

The L.H.S. can be expressed as

$$\Delta V_{Ca}(t) = \sqrt{\frac{2}{3}}[-V_{sub}\sin\omega_{sub}t - V_{sup}\sin\omega_{sup}t] \tag{7.70}$$

The expressions for ΔV_{Cb} and ΔV_{Cc} are similarly obtained. Relating $\Delta V_{Ca}(t)$ to $\Delta i_a(t)$, we can drive the following matrix equation.

$$\begin{bmatrix} V_{sub} \\ V_{sup} \end{bmatrix} = jX_{Cm}\begin{bmatrix} 1 & -1 \\ 1 & -1 \end{bmatrix}\begin{bmatrix} I_{sub} \\ I_{sup} \end{bmatrix} \tag{7.71}$$

where

$$X_{Cm} = \frac{k^2}{2C\omega_m}, \quad \omega_m = \omega_0 - \omega_e$$

Eq. (7.71) shows the coupling between subsynchronous and supersynchronous frequency networks. Generally, $|I_{sub}| > |I_{sup}|$, and hence a SSSC appears as a capacitive impedance at the subsynchronous frequency.

A Case Study [6]

The system considered is adapted from IEEE FBM Model [11]. The generator data is identical except that it is also equipped with a static excitation system and a speed input PSS. The line impedance is assumed to be 0.04 + j1.0 pu. The transformer leakage impedance (0.14 pu) and the system impedance (0.06 pu) at the receiving end are same as given in [11]. The operating conditions are $P_g = 0.9, V_g = 1.0$ and $E_b = 1.0$. Following cases are considered for series compensation

1. With a fixed capacitor of reactance 0.6 pu.
2. With a fixed capacitor of reactance 0.4 pu.
3. With a SSSC in series with a fixed capacitor of 0.4 pu. The SSSC provides a compensation of 0.2 pu at the operating point. That is, $\frac{V_{ro}}{I_o} = 0.2$ where V_{ro} is the injected reactive voltage at the operating point and I_o is the line current magnitude at the operating point.

The SSSC controller regulates the magnitude of the reactive voltage injected. The system model is linearized about the operating point and the eigenvalues corresponding to the torsional and network modes are shown in Table 7.1 for the three cases. It is observed that the system is unstable (due to mode 2) for case 1 while it is stable for case 3, even though the compensation levels are same for both cases. The introduction of a SSSC for series compensation is not strictly SSR neutral as it is observed that the damping of the third torsional mode is significantly reduced.

It has been suggested that a SSSC with an energy source on the DC side can be used to compensate for the line resistance drop also [2]. However, this can destabilize the critical torsional mode (No. 3). See the first column of Table 7.2 which shows the eigenvalues for the case 3 with line resistance reduced from 0.04 pu to 0.02 pu.

It is observed from the comparison of the results of the cases 2 and 3, that a SSSC offers a capacitive reactance. The network resonance frequency for case 2 ($X_C = 0.40$) is $\omega_{er} = 204$ rad/sec while for case 3 it is 218 rad/sec. The resonance frequency for case-1 is 250 rad/sec. This is in accordance

Table 7.1: Eigenvalues for Cases 1, 2 and 3

Case 1 ($X_C = 0.6$)	Case 2 ($X_C = 0.4$)	Case 3 ($X_C = 0.4$, $X_{SSSC} = 0.2$)	Comments
-1.790 ± j6.281	-1.054 ± j5.786	-1.348 ± j5.901	TM0
-0.184 ± j99.137	-0.268 ± j98.853	-0.235 ± j98.908	TM1
0.190 ± j127.000	-0.075 ± j127.020	-0.070 ± j127.030	TM2
-0.644 ± j160.440	-0.562 ± j160.780	-0.128 ± j160.200	TM3
-0.367 ± j202.830	-0.352 ± j202.720	-0.372 ± j202.800	TM4
-1.850 ± j298.170	-1.850 ± j298.170	-1.850 ± j298.170	TM5
-4.222 ± j127.640	-4.773 ± j172.800	-5.046 ± j158.400	Network Sub. Mode
-5.740 ± j626.740	-5.714 ± j580.890	-4.884 ± j566.900	Network Sup. Mode

Table 7.2: Eigenvalues with and without SSDC for Case 3

Without SSDC	With SSDC	Comments
-1.311 ± j5.936	-1.312 ± j5.935	Torsional Mode 0
-0.239 ± j98.914	-0.247 ± j98.917	Torsional Mode 1
-0.072 ± j127.030	-0.075 ± j127.030	Torsional Mode 2
0.259 ± j159.590	-0.503 ± j160.070	Torsional Mode 3
-0.376 ± j202.790	-0.374 ± j202.790	Torsional Mode 4
-1.850 ± j298.170	-1.850 ± j298.170	Torsional Mode 5
-2.478 ± j159.020	-1.969 ± j153.750	Network Subsynchronous Mode
-2.330 ± j567.050	-2.458 ± j567.280	Network Supersynchronous Mode

with the relation that ω_{er} is directly proportional to the square root of the fixed series capacitor in the line (without any active series compensation).

Unlike in the case of a TCSC, there is no significant damping introduced by a SSSC unless an auxiliary controller (termed as Subsynchronous Damping Controller (SSDC)) is introduced. The mitigation of SSR by a SSSC with constant reactive voltage control works mainly by detuning the network resonance.

Design of SSDC

The SSDC is designed with line current (magnitude) as the input signal. The structure of the transfer function is assumed as

$$SSDC(s) = \frac{\Delta V_r(s)}{\Delta I(s)} = \frac{as + b}{s^2 + cs + d}$$

with the constraints that $c > 0, d > 0$ and $(c^2 - 4d) < 0$. The first two constraints ensure that the poles are in left half of the s plane. The third constraint ensures that the poles are complex. The parameters a, b, c and d are determined from a constrained optimization technique to minimize the deviations in the specified damping torque in the frequency range of interest. Thus, the objective function to be minimized is selected as

$$J(a, b, c, d) = \sum_{\omega=\omega_{\min}}^{\omega=\omega_{\max}} [T^*_{De}(\omega) - T_{De}(\omega)]^2$$

where $T_{De}(\omega)$ is the damping torque (coefficient) which is a function of frequency (of oscillation of the rotor) and T^*_{De} is the desired value of T_{De}.

By selecting $\omega_{\min} = 120$ rad/sec., $\omega_{\max} = 180$ rad/sec. and $T^*_{De} = 1.0$ pu, we get the transfer function of the SSDC as

$$SSDC(s) = -\frac{(100s + 75)}{s^2 + 50s + 26000}$$

The eigenvalues for the case-3 ($R_L = 0.02$) with SSDC modulating the output of the SSSC, are shown in the second column of Table 7.2. It is observed that the SSDC is effective in damping the torsional mode 3 without destabilizing other modes. The coupling between the subsynchronous frequency network mode and the torsional mode results in the reduction of the damping of the former mode, but this is not a problem.

The results obtained from the damping torque analysis and detailed transient simulation are in agreement with the eigenvalue results [6].

7.6 Applications of SSSC

A SSSC is an advanced version of controlled series compensation, that is based on VSC and the use of GTOs instead of thyristors. There are many technical advantages of a SSSC over a TCSC. However, the application of a SSSC would depend on the techno-economic evaluation and proven reliability based on operating experience. A major drawback with SSSC is the need for a coupling transformer (and an intermediate transformer if multipulse converters are used). In contrast, TCSCs don't require any magnetic devices

or coupling transformers. However, the harmonics are better controlled with a SSSC.

A SSSC requires protection against overcurrents. A high speed electronic Thyristor Bypass Switch (TBS) is installed in parallel with the converter terminals [9]. When an overcurrent is detected, it operates quite fast. In case the system fault is not cleared by primary protection, then, the TBS is protected by a parallel connected low voltage breaker (LVB) which bypasses the TBS in about 6 cycles. If LVB fails to close when required, then its breaker failure protection closes the high side breaker (HSB) that bypasses the SSSC. After the fault is cleared, the SSSC is reinserted into the line by opening the LVB.

The improvements in the power (semiconductor) device characteristics and the reduction in the costs would spur the applications of SSSC in place of TCSCs.

References and Bibliography

1. L. Gyugyi, "Dynamic compensation of AC transmission lines by solid-state synchronous voltage sources", IEEE Trans. on Power Delivery, v. 9, n. 2, 1994, pp. 904–911
2. L. Gyugyi, C.D. Schauder and K.K. Sen, "Static synchronous series compensator: a solid state approach to the series compensation of transmission lines", IEEE Trans. on Power Delivery, v. 12, n. 1, 1997, pp. 406–417
3. K.K. Sen, "SSSC-static synchronous series compensator: theory, modeling and applications", IEEE Trans. on Power Delivery, v. 13, n. 1, 1998, pp. 241–246
4. C. Hatziadoniu and A.T. Funk, "Development of a control scheme for a series connected solid state synchronous voltage source", IEEE Trans. on Power Delivery, v. 11, n. 2, April 1996, pp. 1138–1144
5. K.R. Padiyar and Nagesh Prabhu, "Analysis of subsynchronous resonance with three level twelve pulse VSC based SSSC", IEEE TENCON-2003, October 2003, Bangalore
6. K.R. Padiyar and Nagesh Prabhu, "A comparative study of SSR characteristics of TCSC and SSSC", 14th PSCC, 2005, Liege, Belgium
7. R.J. Nelson, J. Bian and S.L. Williams, "Transmission series power flow control", IEEE Trans. on Power Delivery, v. 10, n. 1, 1995, pp. 504–510
8. R.J. Nelson, "Transmission power flow control: electronic vs. electromagnetic alternatives for steady state operation", IEEE Trans. on Power Delivery, v. 9, n. 3, 1994, pp. 1678–1684

9. B. Fardanesh, M. Henderson, B. Shperling, S. Zelinger, L. Gyugyi, B. Lam, R. Adapa, C. Schauder, J. Mountford and A. Edris, "Convertible static compensator application to the New York transmission system", CIGRE 14–103, 1998

10. J. Sun, L. Hopkins, B. Shperling, B. Fardanesh, M. Graham, M. Parisi, S. Macdonald, S. Bhattacharya, S. Berkovitz and A. Edris, "Operating characteristics of the convertible static compensator on the 345 kV network". IEEE-PSCE, Nov. 2004, New York, U.S.A.

11. IEEE Committee Report, "First Benchmark Model for computer simulation of subsynchronous resonance", IEEE Trans., v. PAS-96, n.5, 1977, pp. 1565-1572.

Chapter 8

Unified Power Flow Controller and other Multi-Converter Devices

8.1 Introduction

The Unified Power Flow Controller (UPFC) proposed by Gyugyi [1] is the most versatile FACTS controller for the regulation of voltage and power flow in a transmission line. It consists of two voltage source converters (VSC) one shunt connected and the other series connected. The DC capacitors of the two converters are connected in parallel (see Fig. 8.1). If the switches 1 and 2 are open, the two converters work as STATCOM and SSSC controlling the reactive current and reactive voltage injected in shunt and series respectively in the line. The closing of the switches 1 and 2 enable the two converters to exchange real (active) power flow between the two converters. The active power can be either absorbed or supplied by the series connected converter.

As discussed in the previous chapter, the provision of a controllable power source on the DC side of the series connected converter, results in the

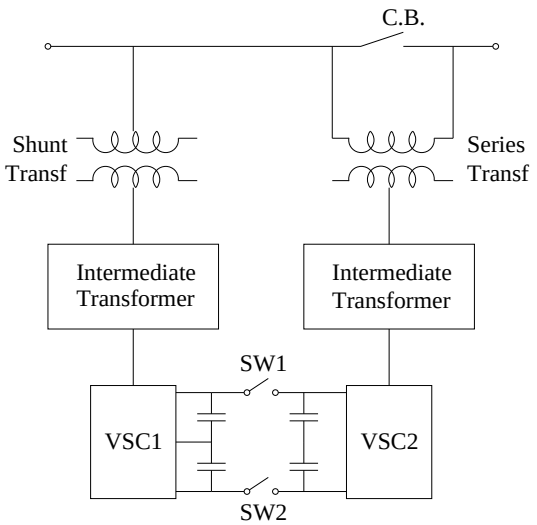

Figure 8.1: A UPFC schematic

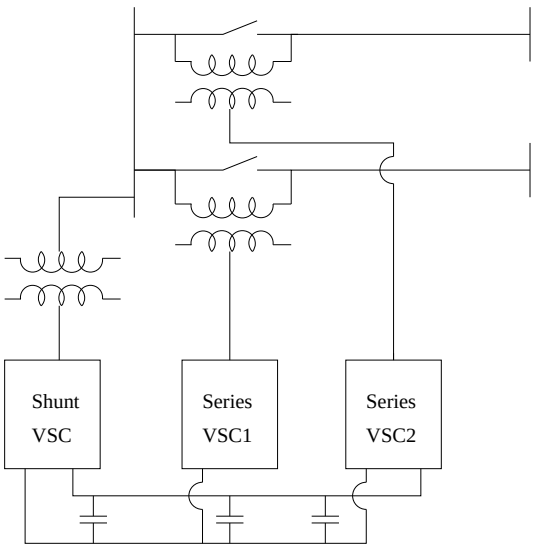

Figure 8.2: A three converter GUPFC

control of both real and reactive power flow in the line (say, measured at the receiving end of the line). The shunt connected converter not only provides the necessary power required, but also the reactive current injected at the converter bus. Thus, a UPFC has 3 degrees of freedom unlike other FACTS controllers which have only one degree of freedom (control variable).

The concept of combining two or more converters can be extended to provide flexibility and additional degrees of freedom. A Generalized UPFC (GUPFC) refers to 3 or more converters out of which one is shunt connected while the remaining converters are series connected [16]. (see Fig. 8.2). An Interline Power Flow Controller (IPFC) refers to the configuration of two or more series connected converters sharing a common DC bus (see Fig. 8.3).

Even when only two converters are used, they may be designed to operate in the shunt or series mode. Depending on the requirement, there can be up to 11 configurations of the two converters resulting in (i) one or two STATCOMs (ii) one or two SSSCs (iii) combinations of a STATCOM and SSSC (iv) UPFC with series converter connected in either of the two lines and (v) IPFC. Such flexible configuration of the two converters is termed as the Convertible Static Compensator (CSC) and has been installed at New York Power Authority's (NYPA) Marcy 345 kV substation. The CSC which consists of two 100 MVA, three-level VSCs, a 200 MVA shunt transformer and two 100 MVA series transformers was commissioned in 2002.

The American Electric Power (AEP) has installed the world's first UPFC rated at $\pm$ 320 MVA (combined) at Inez 138 kV substation in Ken-

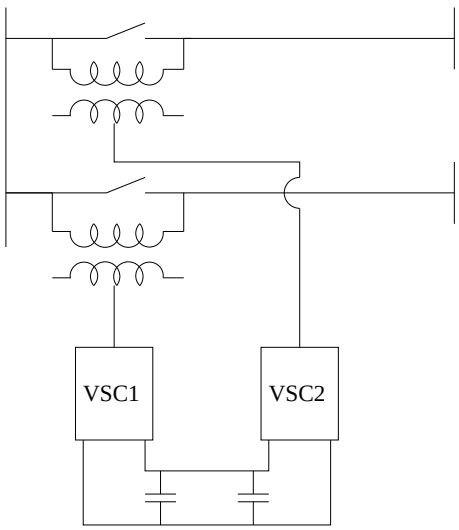

Figure 8.3: A two converter IPFC

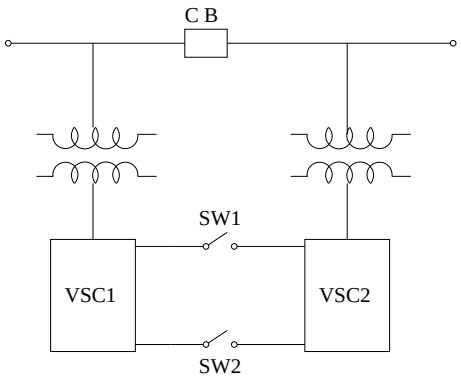

Figure 8.4: A BTB HVDC link

tucky.

If two STATCOMs are provided in the middle of a long transmission line, the parallel connection of the two DC capacitors of the two shunt connected converters enable the power flow through the DC bus. The two STATCOMs now work as Back to Back (BTB) connected VSC based HVDC system. This is particularly useful when it becomes necessary to have asynchronous interconnection. In Fig. 8.4, the closing of the switches 1 and 2 followed by opening the circuit breaker (CB) in the line results in the configuration of a BTB, asynchronous HVDC link. Unlike in BTB links using Line Commutated Converters (LCC) with thyristor valves, the VSC converters are self-commutated and provide reactive power to the AC network (subject to the constraints imposed by the converter ratings). Thus, a HVDC link

using VSC can be used to supply passive loads.

8.2 Operation of a UPFC

8.2.1 A UPFC Connected at the Sending End

It was mentioned in the previous chapter (section 7.4), that the provision of an energy or power source at the DC bus of a SSSC enables the control of not only active power but also reactive power flow in the line. As a matter of fact, both active and reactive power flow in the line can be controlled independently by the injection of both active (real) and reactive voltages. Fig. 8.5 shows the SSSC connected at the sending end of the line. If the power required at the DC bus is fed by a shunt connected converter, then the objectives of independently controlling the active and reactive power in the line are achieved. In addition, the shunt-connected converter can also generate/absorb reactive power such that it can relieve the load on the generator(s) connected to the sending end. As a matter of fact, if the ratings of the shunt-connected converter are adequate, then the UPFC can be connected at any location in the network and the voltage at the bus (where the shunt converter is connected) can be held constant (regulated).

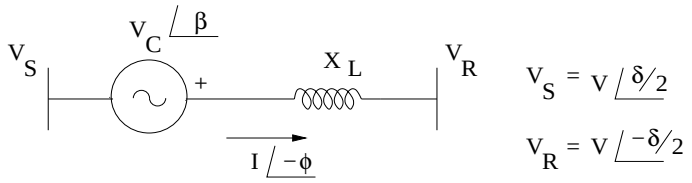

Figure 8.5: A SSSC with a power source connected at the sending end

Let the injected voltage ($\hat{V}_C$) be expressed as

$$\hat{V}_C = V_C \angle \beta = (V_p + jV_r) \angle -\phi \tag{8.1}$$

where $I \angle -\phi$ is the current in the line.

From Eqs. (7.63) and (7.65), we can write

$$P_R = P_0 + \frac{VV_p}{X_L} \sin\left(\frac{\delta}{2} - \phi\right) + \frac{VV_r}{X_L} \cos\left(\frac{\delta}{2} - \phi\right) \tag{8.2}$$

$$-Q_R = Q_0 - \frac{VV_p}{X_L} \cos\left(\frac{\delta}{2} - \phi\right) + \frac{VV_r}{X_L} \sin\left(\frac{\delta}{2} - \phi\right) \tag{8.3}$$

where P_0 and Q_0 are the active and reactive power (at the receiving end) in the absence of the series converter, given by

$$P_0 = \frac{V^2}{X_L} \sin\delta, \quad Q_0 = \frac{V^2}{X_L}(1 - \cos\delta) \tag{8.4}$$

The phase angle (ϕ) of the current is related to V_p from Eq. (7.64) as

$$\sin\phi = \frac{V_p}{2V\sin\frac{\delta}{2}} \tag{8.5}$$

From Eq. (8.1), we have

$$V_p = V_C\cos(\beta+\phi) \tag{8.6}$$

$$V_r = V_C\sin(\beta+\phi) \tag{8.7}$$

Substituting Eqs. (8.6) and (8.7) in (8.2) and (8.3) we get

$$P_R = P_0 + \frac{VV_C}{X_L}\sin\left(\frac{\delta}{2}+\beta\right) \tag{8.8}$$

$$-Q_R = Q_0 - \frac{VV_C}{X_L}\cos\left(\frac{\delta}{2}+\beta\right) \tag{8.9}$$

From Eqs. (8.8) and (8.9), we can express,

$$P_R - jQ_R = (P_0 + jQ_0) + \frac{VV_C}{X_L}e^{j(\frac{\delta}{2}+\beta-\frac{\pi}{2})} \tag{8.10}$$

For a constant value of V_C and β varying over 360°, the locus of $(P_R - jQ_R)$ describe a circle of radius $\frac{VV_C}{X_L}$ and having centre at (P_0, Q_0) in the $P-Q$ plane. The operating region is the inside of the circle bound by the circle having the maximum radius corresponding to $V_C = V_{C\max}$ (based on the series converter ratings. Typical range of $V_{C\max}$ is 0.15 to 0.25 p.u. (of the line, phase to neutral voltage).

For a specified value of δ, P is maximum when

$$\beta = \frac{\pi}{2} - \frac{\delta}{2} \tag{8.11}$$

and $P_{\max}$ is given by

$$P_{\max} = P_0 + \frac{VV_C}{X_L} \tag{8.12}$$

The equivalent circuit of the UPFC is shown in Fig. 8.6. The shunt converter draws both active (I_p) and reactive current (I_r). The active current (I_p) is not independent and is related to V_p by the relation

$$VI_p = IV_p \tag{8.13}$$

in steady-state. The above equation represents power balance on the DC bus neglecting losses in the converter. The reactance x_l in series with the injected voltage represents the leakage reactance of the coupling transformer.

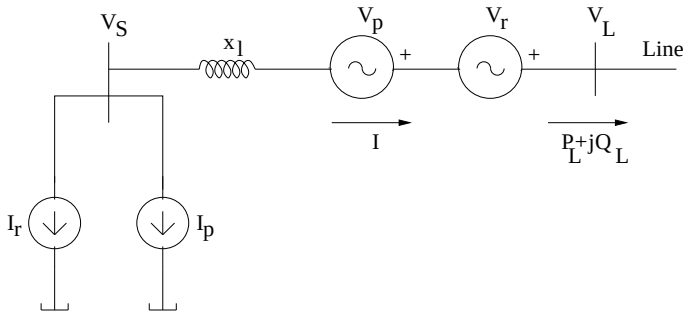

Figure 8.6: Equivalent circuit of a UPFC

In Fig. 8.6, the equivalent circuit of the UPFC can be viewed as a two port network. The shunt converter is connected at one port while the series converter is connected in series with the line at the other port. The voltage at the latter port is denoted by V_L. If the series injected voltages, V_p and V_r are controlled to regulate the power and reactive power in the line, these quantities are conveniently measured at the line side port of the UPFC. Since the voltage V_L is normally uncontrolled, the complex power (P_L+jQ_L) need not describe a circle for constant (magnitude) V_C. Actually, it can be shown that $(P_L + jQ_L)$ describes an ellipse in the P-Q plane. The complex power S_L is given by

$$\begin{aligned} S_L &= P_L + jQ_L = I^* V_L = \frac{V_L^* - V_R^*}{-jX_L} \cdot V_L \\ &= \frac{V_L^2 - V_R^* V_L}{-jX_L} \end{aligned} \tag{8.14}$$

Since $V_R = V\angle -\frac{\delta}{2}$, $\hat{V}_L = \hat{V}_S + \hat{V}_C = V\angle\frac{\delta}{2} + V_C\angle\beta$ we can express P_L and Q_L as

$$P_L = P_0 + \frac{VV_C}{X_L}\sin\left(\frac{\delta}{2} + \beta\right) \tag{8.15}$$

$$Q_L = Q_0 + \frac{V_C^2}{X_L} - \frac{VV_C}{X_L}\cos\left(\frac{\delta}{2} + \beta\right) + \frac{2VV_C}{X_L}\cos\left(\frac{\delta}{2} - \beta\right) \tag{8.16}$$

where P_0 and Q_0 are defined by Eq. (8.4). Defining Q_0' as

$$Q_0' = Q_0 + \frac{V_C^2}{X_L} \tag{8.17}$$

we can finally obtain the equation involving P_L and Q_L after eliminating β. The final equation is

$$\begin{aligned} (P_L - P_0)^2(5 - 4\cos\delta) + (Q_L - Q_0')^2 - 4(P_L - P_0)(Q_L - Q_0')\sin\delta \\ = \frac{V^2V_C^2}{X_L^2}(2\cos\delta - 1)^2 \end{aligned} \tag{8.18}$$

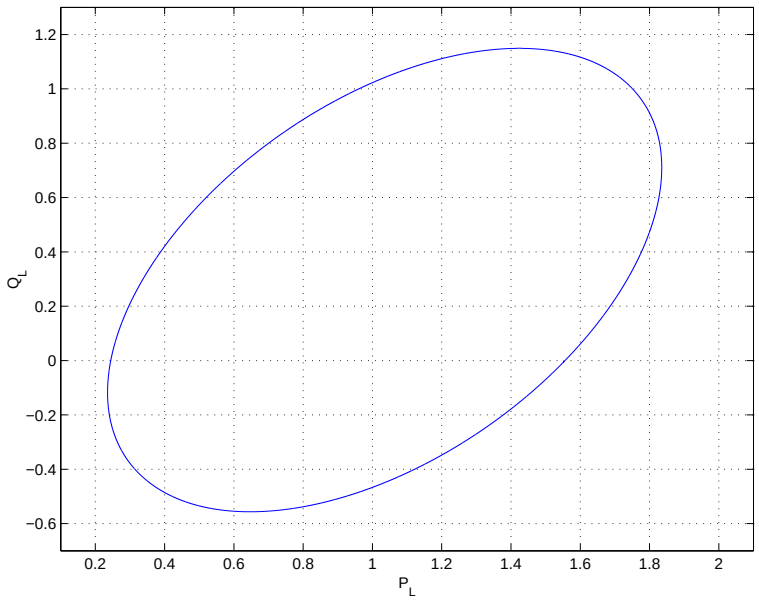

Figure 8.7: Operating region in the $P_L - Q_L$ plane

The above is an equation for ellipse with the centre $\left(P_0, Q_0 + \frac{V_C^2}{X_L}\right)$. For a $\delta = 15°$, $V_C = 0.20$, $X_L = 0.25$, $V = 1.0$, the locus of S_L in the $P - Q$ plane is shown in Fig. 8.7.

It is to be noted that I_r can be controlled to regulate the voltage V_S if it is not regulated by the generator connected at the sending end. Thus, three variables, V_S, P_L and Q_L can be regulated by controlling I_r, V_C and β. It is assumed that there are no constraints imposed by the equipment ratings that will limit the control objectives.

The assumption is valid if the settings or the reference values for the controlled variables (V_S, P_L and Q_L) lie in the feasible region. With this assumption, the analysis of the UPFC is applicable even when the location of the UPFC is not exactly at the sending end.

8.2.2 A Special Case

Here, the line current, which is same as the sending end current (I) is assumed to be in phase with the sending end voltage (V_S). In this case, $\hat{I}_p$ and $\hat{V}_p$ are in phase with $\hat{V}_S$. To simplify the analysis, x_l is either neglected or merged with the series line reactance. The reactive current (I_r) can be either assumed to be zero or being controlled to regulate the magnitude of V_S. The power flow in the line depends essentially on V_p and V_r as before.

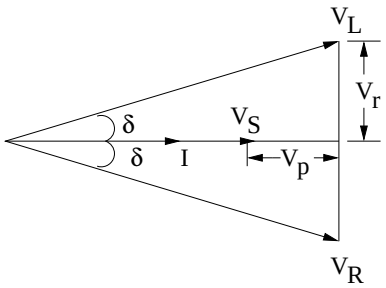

Figure 8.8: Phasor diagram

The phasor diagram of the voltage and line current is shown in Fig.8.8.

The voltage (V_L) is given by

$$\hat{V}_L = \hat{V}_S + \hat{V}_p + \hat{V}_r \tag{8.19}$$

If it is assumed that $|V_R| = |V_L|$, then the line current magnitude (I) is given by

$$I = \frac{2(V_S + V_p)\tan\delta}{X} \tag{8.20}$$

The power flow in the line is given by

$$\begin{aligned} P &= V_R I \cos\delta \\ &= \frac{2V_S V_R n \sin\delta}{X} \\ &= 2nP_0, \quad P_0 = \frac{V_S V_R}{X}\sin\delta \end{aligned} \tag{8.21}$$

where

$$n = \frac{V_S + V_p}{V_S} = 1 + \frac{V_p}{V_S} \tag{8.22}$$

If power is injected into the line from the series converter ($V_p > 0$) then $n > 1$. On the other hand, if the series converter draws power from the line ($V_p < 0$) then $n < 1$. It is obvious that injecting positive V_p has the advantage of increasing the power flow. Since V_r is half the line voltage drop across the line reactance, the current magnitude is doubled and the power flow is doubled.

Remarks

The combination of the shunt active current I_p and the series active voltage (V_p) can be viewed as the representation of an ideal transformer of turns ratio $1 : n$; when the line current is in phase with the voltage. Consider the ideal transformer shown in Fig. 8.9(a). If I_2 is in phase with V_2, I_1 is also in

phase with V_1. The ideal transformer can be represented by the equivalent circuit shown in Fig. 8.9(b). Here,

$$V_p = (n-1)V_1, \quad I_p = (n-1)I_2 \tag{8.23}$$

Obviously,

$$V_p I_2^* = V_1 I_p^* \tag{8.24}$$

The equivalence of the ideal transformer with the circuit representing the power transfer through the two converters of the UPFC (flowing through the DC bus) is valid only when the power factor is unity (V_2 in phase with I_2). The reactive current injected by the shunt converter can be controlled to bring about unity power factor at the sending end (V_S in phase with I in Fig. 8.6). For this special case, we can represent the UPFC by the equivalent circuit shown in Fig. 8.10.

Here, the turns ratio n is variable as V_p varies with the control. Thus, (for this special case, when V_2 is in phase with I_2) the UPFC is made up of a STATCOM, SSSC and variable turns ratio ideal transformer in between the two.

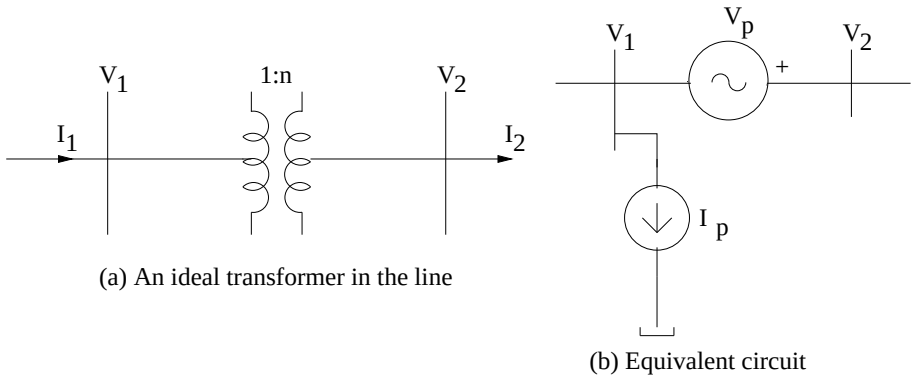

Figure 8.9: Representation of an ideal transformer in the line

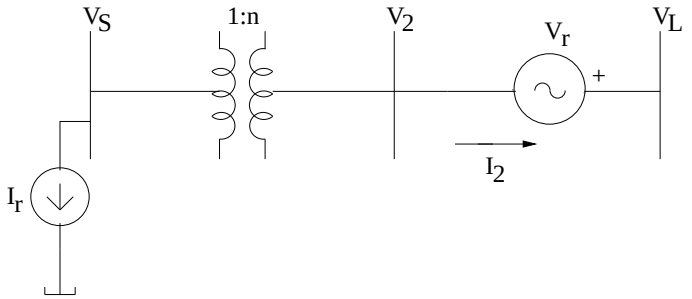

Figure 8.10: Equivalent circuit of a UPFC in the special case

UPFC Connected at the Receiving End

If we assume that a UPFC is connected at the receiving end of a line supplying a load (as shown in Fig. 8.11), we can further assume that the reactive current supplied by the shunt converter improves the power factor of the apparent load (including I_r) to unity. In other words, I is in phase with V.

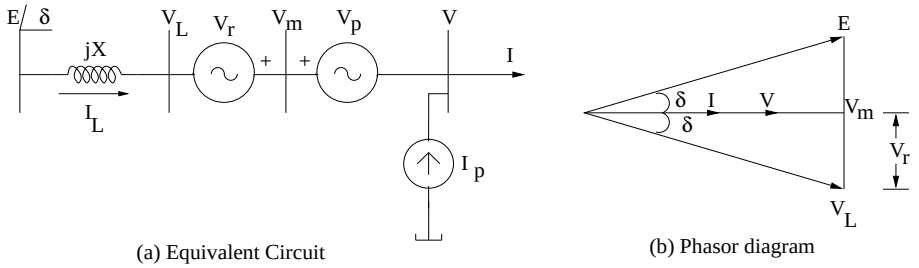

Figure 8.11: A line supplying a load through UPFC

The power transmitted over the line is given by

$$P = VI = V(I_L + I_p) \tag{8.25}$$

V and I_L are obtained (from the phasor diagram) as

$$V = V_m - V_p = E\cos\delta - V_p = nE\cos\delta \tag{8.26}$$

$$I_L = \frac{2E\sin\delta}{X} \tag{8.27}$$

where $n = \frac{V}{V_m} = \frac{V_m - V_p}{V_m}$ and $n < 1$. Note that we have considered V_p as a voltage drop so that $n < 1$. It can be shown that

$$I = \frac{I_L}{n} \tag{8.28}$$

Hence, we can derive

$$P = \frac{E^2}{X}\sin 2\delta = 2P_0 \tag{8.29}$$

Note that the power flow is double the value without the injection of V_r (for a unity power factor load).

The above discussion shows clearly that there is no advantage of the power exchanged between the two converters. The UPFC in this case can be replaced by a SSSC injecting V_r (to enhance line current) and a STATCOM injecting I_r to compensate for the reactive current drawn by the load.

8.2.3 UPFC Connected at the Midpoint

Let us assume that a UPFC is connected at the midpoint of a symmetrical lossless line. The UPFC can be represented by the two port network shown in Fig.8.12. The shunt converter draws a current represented by the phasor $I_C\angle\psi$ and the series converter injects a voltage ($V_C\angle\beta$). It can be shown that the two port network in Fig.8.12 is also equivalent to the two port networks shown in Fig. 8.13.

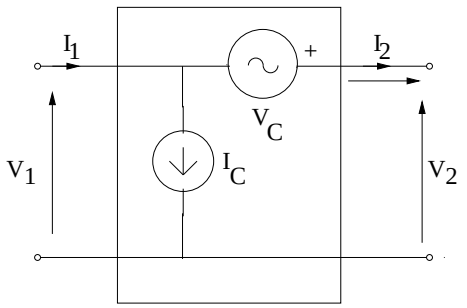

Figure 8.12: Two port network representing a UPFC

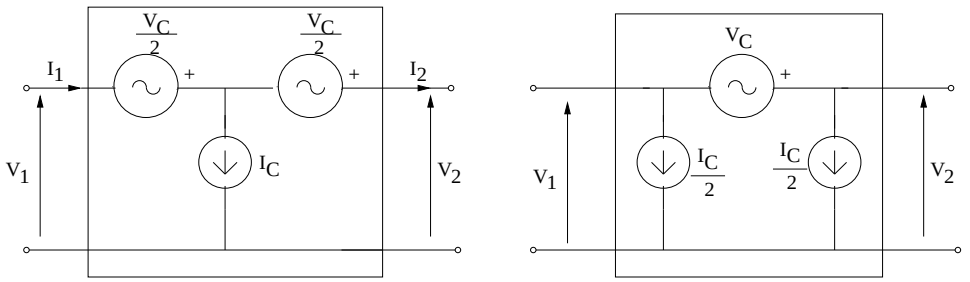

(a) Equivalent network 1 (b) Equivalent network 2

Figure 8.13: Alternative representations for UPFC

It is more convenient to represent the UPFC by any one of the two equivalents shown in Figure 8.13. The analysis is simplified as shown below.

Analysis

The equivalent circuit of a symmetrical lossless line with a UPFC connected at the midpoint is shown in Fig. 8.14. Here, we are representing the UPFC by the equivalent network I shown in Fig. 8.13(a). The current source $I_C\angle\psi$

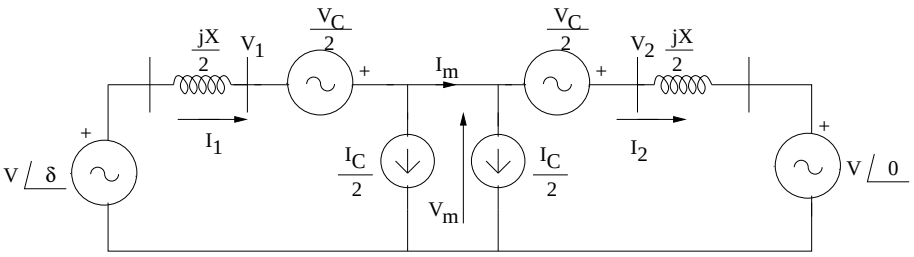

Figure 8.14: System equivalent circuit

is represented as two parallel current sources, for convenience. (Note that we are using the same symbols for the phasor and its magnitude, for simplicity)

For the circuit shown in Fig. 8.14, we can write

$$V\angle\delta - j\frac{X}{2}\left(I_m + \frac{I_C}{2}\right) + \frac{V_C}{2} = V_m \tag{8.30}$$

$$V\angle 0 + j\frac{X}{2}\left(I_m - \frac{I_C}{2}\right) - \frac{V_C}{2} = V_m \tag{8.31}$$

Adding Eqs. (8.30) and (8.31), we can solve for V_m as

$$\hat{V}_m = V_m\angle\delta_m = V\cos\frac{\delta}{2}\angle\frac{\delta}{2} - \frac{jX}{4}I_C\angle\psi \tag{8.32}$$

Subtracting Eq. (8.30) from (8.31), we can solve for I_m as

$$\hat{I}_m = \frac{2V\sin\frac{\delta}{2}}{X}\angle\frac{\delta}{2} + \frac{V_C\angle\beta}{jX} \tag{8.33}$$

The power and reactive power outputs at the port 2 of the UPFC are given by

$$\begin{aligned} P + jQ &= \left(V_m + \frac{V_C}{2}\right)\left(I_m - \frac{I_C}{2}\right)^* \\ &= V_m I_m^* + \frac{1}{2}(V_C I_m^* - V_m I_C^*) - \frac{V_C I_C^*}{4} \end{aligned} \tag{8.34}$$

From power balance equation in steady state, we have

$$\begin{aligned} Re[I_C^* V_m] &= Re\left[\frac{V_C}{2}\left(I_m^* - \frac{I_C^*}{2}\right) + \frac{V_C}{2}\left(I_m^* + \frac{I_C^*}{2}\right)\right] \\ &= Re[V_C I_m^*] \end{aligned} \tag{8.35}$$

Substituting Eq. (8.35) in (8.34), we get the expression for the power flow (P) in the line as

$$P = Re[V_m I_m^*] - Re\left[\frac{V_C I_C^*}{4}\right] \tag{8.36}$$

Substituting for V_m and I_m from Eq. (8.32) and (8.33) in (8.36), we get

$$\begin{aligned} P &= \frac{V^2}{X}\sin\delta + \frac{V_C V}{X}\cos\frac{\delta}{2}\cos\left(\frac{\delta}{2}-\beta+90^\circ\right) \\ &\quad -\frac{I_C V}{2}\sin\frac{\delta}{2}\cos\left(\psi-\frac{\delta}{2}+90^\circ\right) \end{aligned} \tag{8.37}$$

The power is maximized when

$$\beta = \frac{\delta}{2}+90^\circ \tag{8.38}$$

$$\psi = \frac{\delta}{2}+90^\circ \tag{8.39}$$

and $P_{\max}$ is given by

$$P_{\max} = \frac{V^2}{X}\sin\delta + \frac{V_C V}{X}\cos\frac{\delta}{2} + \frac{I_C V}{2}\sin\frac{\delta}{2} \tag{8.40}$$

Note that Eq. (8.40) applies for constant values of V_C and I_C. For maximizing P for a given value of δ, we need to set

$$V_C = V_{C\max}, \quad I_C = I_{C\max} \tag{8.41}$$

where the maximum values of V_C and I_C correspond to the limits on the magnitude of the series voltage and the shunt current.

Remarks

1. For the maximum power transfer, we have

$$\hat{V}_m = \left(V\cos\frac{\delta}{2} + \frac{X}{4}I_C\right)\angle\frac{\delta}{2} \tag{8.42}$$

$$\hat{I}_m = \frac{\left(2V\sin\frac{\delta}{2}+V_C\right)}{X}\angle\frac{\delta}{2} \tag{8.43}$$

and

$$Re[V_m I_C^*] = 0, \quad Re[V_C I_m^*] = 0 \tag{8.44}$$

This indicates that the shunt converter draws only reactive current and operates as a STATCOM. However, the two halves of the series converter exchange real power as the power generated by the series converter (half) near port 2 is,

$$P_{DC} = Re\left[\frac{V_C}{2}\left(I_m^* - \frac{I_C^*}{2}\right)\right] = -\frac{V_C I_C^*}{4} = -\frac{V_C I_C}{4} \tag{8.45}$$

It is interesting to observe that for the condition of maximum power flow in the line, the DC power (at the DC bus) is a constant. The series converter half on the right, absorbs this power from the network and supplies it to the series converter (half) on the left.

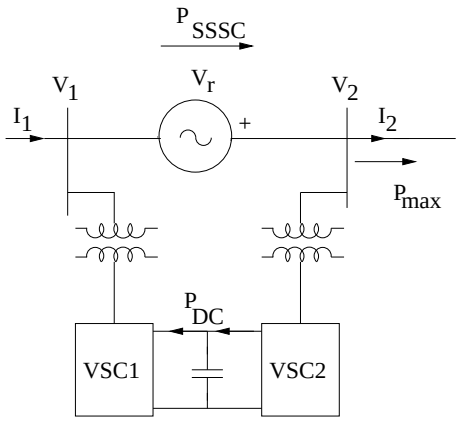

Figure 8.15: A BTB HVDC link across a SSSC

2. From the above discussion, it is obvious that for maximum power flow conditions in the line, a UPFC is equivalent to a combination of (i) STATCOM and (ii) IPFC. In the latter, the two series converters exchange real power in addition to injecting reactive voltages.

3. It is also possible to derive the conditions for the maximum power (Eqs. (8.38) and (8.39)) and the expression for the maximum power (Eq. (8.40)) directly [17], but the approach given here is simpler.

4. From Eq. (8.34), it is possible to compute Q for the maximum power condition. This is given by the expression

$$Q = \frac{VV_C \sin\frac{\delta}{2}}{X} + \frac{I_C V}{2}\cos\frac{\delta}{2} + \frac{V_C^2}{2X} + \frac{I_C^2 X}{8} \tag{8.46}$$

5. The equivalent network of the UPFC shown in Fig. 8.13(b) can also be used to derive the conditions for the maximum power along with the power expressions. Since $\hat{V}_C$ is in quadrature with $\hat{I}_m$ for the maximum power transfer, a series connected SSSC is adequate. However the two halves of the shunt connected converter exchange power through the DC bus. Thus a UPFC can be represented by a SSSC connected across a VSC based HVDC BTB (Back to Back) link. This is shown in Fig. 8.15.

In steady state, the DC power flows from VSC2 to VSC1 and the magnitude is $\frac{V_C I_C}{4}$. The power flow through the SSSC is

$$P_{SSSC} = P_{\max} + \frac{V_C I_C}{4}$$

where $P_{\max}$ is given by Eq. (8.40).

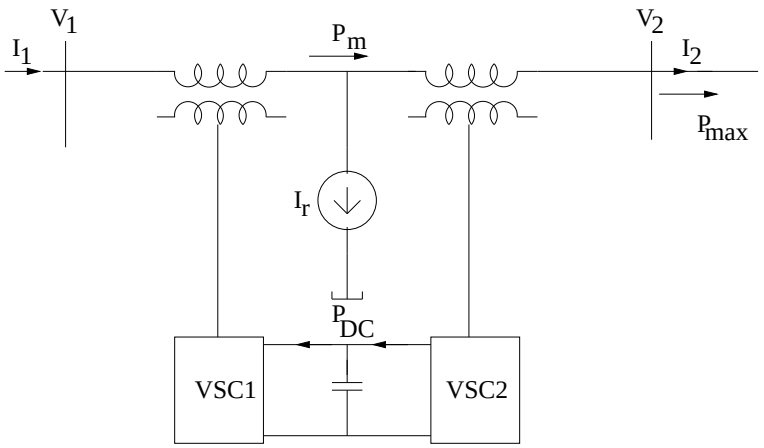

Figure 8.16: A STATCOM connected between IPFC

In comparison with the circuit shown in Fig. 8.15, the alternate circuit that is equivalent to UPFC (discussed earlier) is shown in Fig. 8.16. This circuit consists of a STATCOM that injects reactive current in the middle of an IPFC. The power P_m at the midpoint is also equal to $P_{\max} + \frac{I_C V_C}{4}$.

8.3 Control of UPFC

As the UPFC consists of two converters that are coupled on the DC side, the control of each converter is taken up individually.

8.3.1 Control of the Shunt Converter

The shunt converter draws a controlled current from the system. One component of this current is I_p which is automatically determined by the requirement to balance the real power supplied to the series converter through the DC link. This power balance is enforced by regulating the DC capacitor voltage by feedback control.

The other component of the shunt converter current is the reactive current, I_r which can be controlled in a similar fashion as in a STATCOM. There are two operating (control) modes for a STATCOM or the shunt converter. These are,

1. VAR control mode where the reactive current reference is determined by the inductive or capacitive VAR command. The feedback signals are obtained from current transformers (CT) typically located on the bushings of the coupling (step down) transformer.

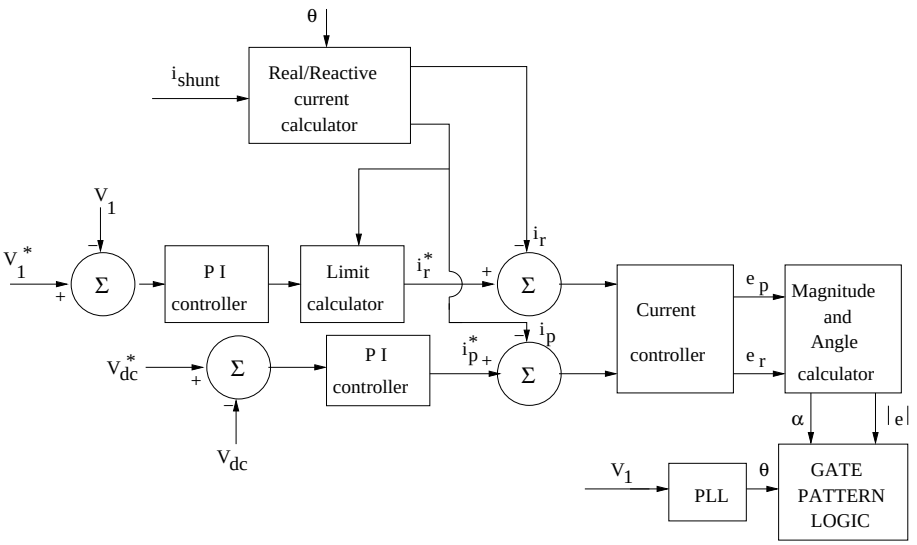

Figure 8.17: Block diagram of shunt VSC controller

2. Automatic voltage control mode where the reactive current reference is determined by the output of the feedback voltage controller which incorporates a droop characteristic (as in the case of a SVC or a STATCOM). The voltage feedback signals are obtained from potential transformers (PT) measuring the voltage V_1 at the substation feeding the coupling transformer.

The block diagram of the shunt converter controller is shown in Fig. 8.17.

8.3.2 Control of the Series Converter

The series converter control is aimed at injecting a series voltage of the required magnitude and angle. These are different control modes for the series voltage listed below.

1. Direct voltage injection mode where the converter simply generates a voltage phasor in response to the reference input. A special case is when the desired voltage is a reactive voltage in quadrature with the line current.

2. Phase Angle Shifter Emulation mode where the injected voltage $\hat{V}_C$ is phase shifted relative to the voltage V_1 by an angle specified by the reference input.

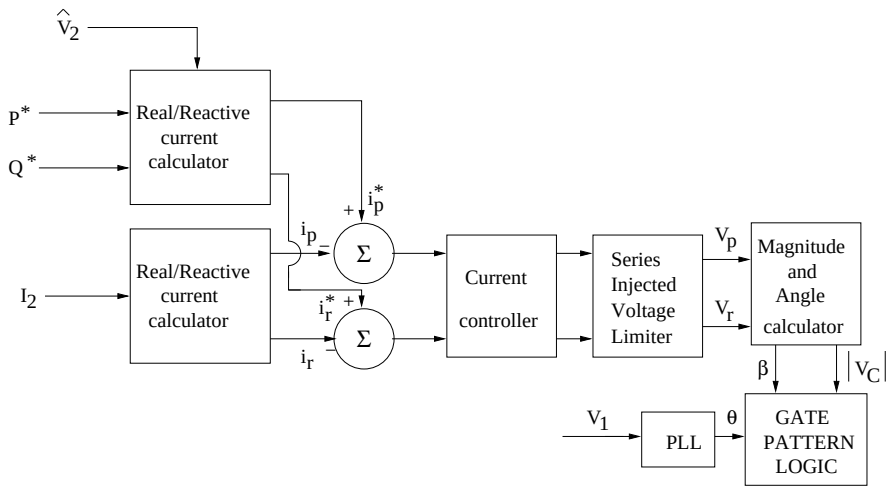

Figure 8.18: Block diagram of series VSC controller

3. Line impedance emulation mode where the series injected voltage is controlled in proportion to the line current. The complex impedance (the injected voltage divided by the line current) seen by the line current is determined by the reference inputs. It is essential to take care (in employing this control mode) to avoid instability or resonance. For example, negative values of the resistance can cause instability. A large value of the capacitive (negative) reactance can result in resonance.
4. Automatic power flow control mode where the reference inputs determine the required real power (P) and the reactive power (Q) at a specified location in the line. Both P and Q can be controlled independently of each other in a feasible region determined by the satisfaction of various constraints that will be discussed later.

In this control mode, the series injected voltage is determined by a vector control system to ensure the flow of the desired current (phasor) which is maintained even during system disturbances (unless the system control dictates the modulation of the power and reactive power). Although the normal conditions dictate the regulation of the complex power flow in the line, the contingency conditions require the controller to contribute to system stability by damping power oscillations.

The feedback signals for the series converter control come from CT and PTs where the line current and the voltages at the two ports of the UPFC are measured. The block diagram of the series converter control is shown in Fig. 8.18.

The automatic power flow control is implemented utilizing the vector control scheme that regulates the line current based on Synchronous

Reference Frame (SRF). Here the controlled quantities are the in-phase and quadrature components (relative to the voltage at port 1 of the UPFC). Neglecting harmonics, these components are constants in steady state and depend on the desired reference values of P and Q. The feedback control of the in-phase and quadrature components of the line current is utilized to determine the magnitude and angle of the series injected voltage.

8.3.3 Operating Constraints

There are basically six major constraints that must be satisfied in scheduling the control of a UPFC in steady-state. These are

1. Upper limit on the magnitude of the shunt converter current, namely
$$|I_C| < I_{C\,\max} \tag{8.47}$$
2. Upper limit on the magnitude of the voltage injected by the shunt converter
3. Upper limit on the magnitude of the voltage injected by the series converter
$$|V_C| < V_{C\,\max} \tag{8.48}$$
4. Upper limit on the magnitude of the line current flowing through the series converter
5. Maximum and minimum limits on the line side voltage, V_L given by
$$V_{L\,\min} \leq |V_L| \leq V_{L\,\max} \tag{8.49}$$
6. Upper limits on the magnitude of the power flow (P_{DC}) in the DC link.

The limits on the voltages injected by the shunt and series converter depend not only on the voltage ratings of the converters (and the coupling transformers), but also on the magnitude of the DC bus voltage. This implies that $V_{C\,\max}$ (for the series converter) is not constant but varies with the operating conditions. In general, whenever $V_C \leq V_{C\,\max}$, the phase angle (β) of the voltage can vary over 360° (in all 4 quadrants). See Fig. 8.19 which shows the boundary of the achievable range for V_L ($V_1 + V_C$). However, due to the leakage reactance (x_l) of the coupling transformer (see Fig. 8.6) the voltage appearing across the primary winding of the coupling transformer is ($V_C - jI_{Line}x_l$) rather than V_C. Hence boundary of the achievable range of V_L shifts for a specified line current.

The complete range for V_L cannot be fully utilized as the line side voltage magnitude has to satisfy limits (Eq. (8.49)) imposed by the voltage

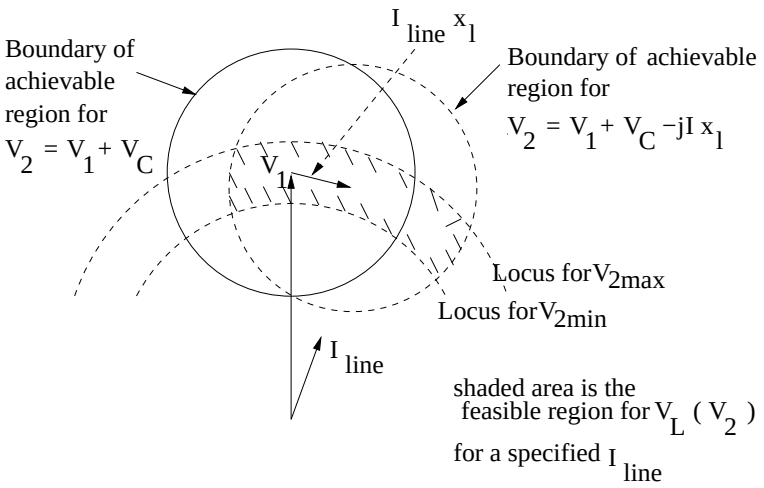

Figure 8.19: Feasible region for V_L or V_2

ratings of the line and requirements of acceptable voltage levels if the line is tapped. The loci of the maximum and minimum allowable V_L are shown in Fig. 8.19 which also shows the feasible region (shaded).

The reference [8] suggests a new control scheme where the magnitude of the line side voltage (V_L or V_2) is regulated instead of controlling the reactive power flow in the line. Actually, the two specifications ($Q = Q_{spec}$ and $|V_2| = V_{2spec}$) are related. However, if $|V_2| = V_{2spec}$ is used, this control scheme would eliminate the need to monitor the constraints imposed by Eq. (8.49). An interesting observation is that with the regulation of the two port voltage magnitudes and if

$$|V_1| = |V_2| = V$$

then, the UPFC behaves like an ideal phase shifter. (Note that the automatic voltage control mode of the shunt converter can be used to regulate $|V_1| = V$).

In the automatic power flow control mode for the series converter, it is possible for some operating conditions that the specified P and Q may be outside the feasible region (see Fig. 8.20). In such cases, the limits on V_C can be imposed in two ways: (i) both P and Q are reduced while retaining the requested angle for β (of the injected voltage) or (ii) the reactive power is reduced while the active power (P) is maximized. This latter strategy requires change in β while the magnitude of the injected voltage maintains maximum magnitude.

If the injected voltage V_p is used to regulate the line side (port) voltage of the UPFC, and if the feedback controller for P sets the reference

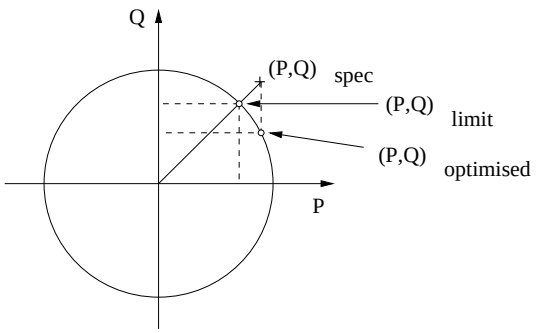

Figure 8.20: $P - Q$ diagram showing handling of limits

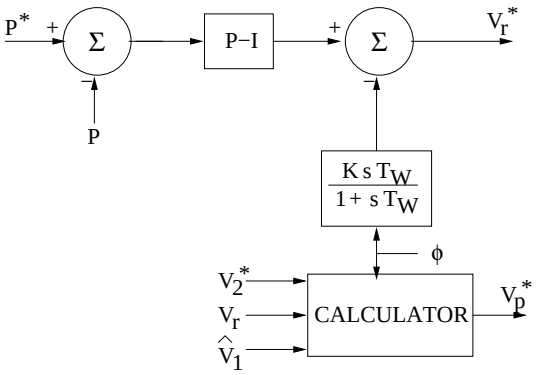

Figure 8.21: An alternative series VSC controller

of V_r, the block diagram of the series converter control is shown in Fig. 8.21 [8]. The reference voltage V_p^* is calculated directly from the equation

$$V_2^2 = (V_{1r} + V_r)^2 + (V_{1p} + V_p)^2$$

where V_{1p} and V_{1r} are the components of the voltage V_1, in phase and quadrature with the line current. These components can be computed if the phase angle (ϕ) of the line current is obtained from PLL. The real power controller also uses feedforward from the phase angle ϕ to improve the phase margin in the controller design.

8.4 Protection of UPFC

There is an upper limit on the current flowing through the GTOs which can be turned-off by applying a gate pulse. This limit is generally much higher than the nominal current rating of the converter. The latter is associated with continuous operation.

When the line current increases rapidly above the critical level, under fault conditions, it is necessary to divert the current from the series converter. The bypassing of the converter may be achieved within microseconds by means of thyristor bypass switch on the secondary side of the coupling transformer. The switch must be designed to carry the maximum fault current for short periods of time. If the fault is a transient fault, the thyristor bypass switch opens when the current drops and the normal operation can be resumed. If the fault is of long duration, it is necessary to initiate the closing of a mechanical bypass switch (breaker) which is located across the primary winding of the coupling transformer, in order to relieve the loading on the thyristor bypass switch.

Once the primary bypass switch is closed, the re-insertion of the series transformer requires the same procedure of startup. The series converter, during the startup has to drive a current through the primary winding of the series transformer, that matches the line current. When the match is achieved, the current in the mechanical bypass switch reduces to zero and it can be opened without creating any transients. The startup can be achieved in a few cycles after the fault clearing.

Although the current through the shunt connected converter is carefully controlled under normal operating conditions, it could exceed the critical level under fault condition. The protective action under such conditions is to interrupt the normal gating sequence. Generally, under transient conditions, it is possible to return to normal operation within a cycle (after the interruption of the normal gating sequence). In most cases, there is no need to trip the shunt breaker. However, a major internal failure may necessitate the opening of the shunt breaker.

8.5 Interline Power Flow Controller

The objective of introducing this controller is to address the problem of compensating a number of transmission lines connected at a substation. While pure series reactive (controllable) compensation (in the form of a TCSC or SSSC) can be used to control or regulate the active power flow in a line, the control of reactive power is not feasible unless active (real) voltage in phase with the line current is not injected. The application of a TCSC (or SSSC with impedance emulation) results in the reduction of net series reactance of the line. However, $\frac{X}{R}$ ratio is reduced significantly and thereby increases the reactive power flow (injected at the receiving end) and losses in the line.

The Interline Power Flow Controller (IPFC) provides, in addition to the facility for independently controllable reactive (series) compensation of each individual line, a capability to directly transfer or exchange real

power between the compensated lines. This is achieved by coupling the series connected VSCs in individual lines on the DC side, by connecting all the DC capacitors of individual converters in parallel. Since all the series converters are located inside the substation in close proximity, this is feasible.

An IPFC with two converters compensating two lines (as shown in Fig. 8.3) is similar to a UPFC in that the magnitude and phase angle of the injected voltage in the prime system (or line) can be controlled by exchanging real power with the support system (which is also a series converter in the second line). The basic difference with a UPFC is that the support system in the latter case is the shunt converter instead of a series converter. The series converter associated with the prime system (of one IPFC) is termed as the master converter while the series converter associated with the support system is termed as the slave converter. The master converter controls both active and reactive voltage (within limits) while the slave converter controls the DC voltage (across the capacitor) and the reactive voltage magnitude.

For the system shown in Fig. 8.22 we can express the received power and the injected reactive power at the receiving end of the prime line (# 1) by the following expressions.

$$P_1 = P_{10} + \frac{VV_{p1}}{X_1}\sin\left(\frac{\delta_1}{2} - \phi_1\right) + \frac{VV_{r1}}{X_1}\cos\left(\frac{\delta_1}{2} - \phi_1\right) \tag{8.50}$$

$$Q_1 = Q_{10} - \frac{VV_{p1}}{X_1}\cos\left(\frac{\delta_1}{2} - \phi_1\right) + \frac{VV_{r1}}{X_1}\sin\left(\frac{\delta_1}{2} - \phi_1\right) \tag{8.51}$$

where

$$\delta_1 = \theta_1 - \theta_2, \quad \sin\phi_1 = \frac{V_{p1}}{2V\sin\frac{\delta_1}{2}}$$

P_{10} and Q_{10} are the power and reactive power in the line 1 (at the receiving end) when both V_{p1} and V_{r1} are zero. These are given by

$$P_{10} = \frac{V^2\sin\delta_1}{X_1}, \quad Q_{10} = \frac{V^2}{X_1}(1 - \cos\delta_1) \tag{8.52}$$

Similar equations also apply to the support line (# 2) except that V_{p2} is not independent. It is related to V_{p1} by the equation

$$V_{p1}I_1 + V_{p2}I_2 = 0 \tag{8.53}$$

The above equation shows that V_{p2} is negative if V_{p1} is positive.

With resistance emulation, we have

$$V_{p1} = -R_1I_1, \quad V_{p2} = -R_2I_2 \tag{8.54}$$

Substituting Eq. (8.54) in (8.53) we get the constraint involving R_1 and R_2 as

$$R_1I_1^2 = -R_2I_2^2 \tag{8.55}$$

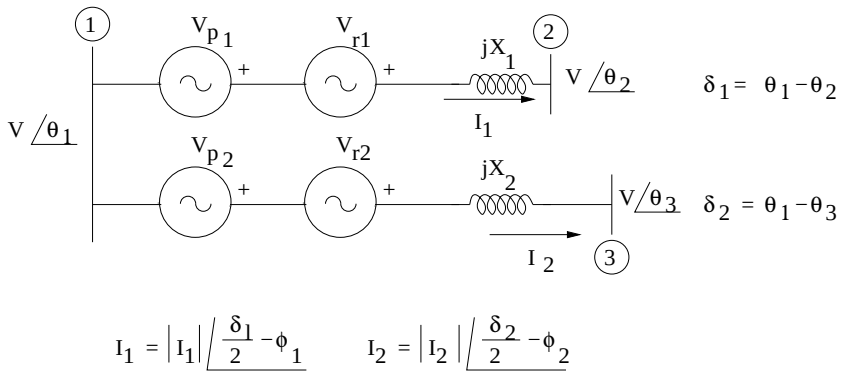

Figure 8.22: Representation of IPFC

The constraint equation (8.53) or (8.55) can limit the utility of IPFC. In such a case, an additional shunt converter (forming a GUPFC) will be useful (see Fig. 8.2).

8.6 Convertible Static Compensator

Using Voltage Source Converters that can be connected in shunt or series, it is possible to develop a versatile and reconfigurable FACTS controller. The first CSC consisting of two 100 MVA VSCs was commissioned at 345 kV Marcy substation of NYPA system in U.S.A. Each converter can be connected to a shunt transformer or a series transformer. There are two series transformers coupling the two converters to two separate lines connected at the substation. The shunt transformer has two secondary windings. Each of the two windings can be connected to any particular converter. The CSC can be operated with one or both converters. Depending on the connection of the converters, the CSC can be operated as one or two STATCOMs (connected in parallel), one or two SSSCs (connected in the two lines). If the DC capacitors are connected in parallel, we can get two configurations of UPFC or an IPFC. These possibilities are listed in Table 8.1 with reference to the Fig. 8.23. There are 10 different FACTS controllers possible. It is to be noted that 1(a) and 1(b) are equivalent as a single STATCOM can be configured using either of the two converters.

One can extend the concept of CSC to a system consisting of over two converters that can lead to a large number of configurations of FACTS controllers. The basic idea behind a CSC is the provision of flexibility to deploy the required type of the controller depending on the requirements that can vary with the operating conditions.

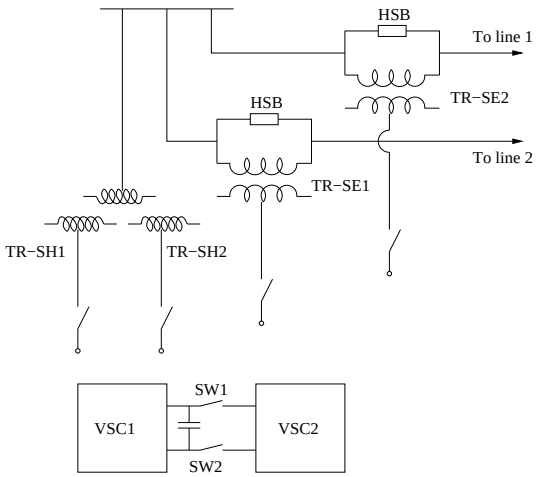

Figure 8.23: Single line diagram of CSC

Table 8.1: CSC Configurations.

Sr. No.	VSC 1 Connected to	VSC 2 Connected to	Status of SW1 and SW2	Controller type
1(a)	TR-SH1	-	NA	1 STATCOM
1(b)	-	TR-SH2	NA	1 STATCOM
2	TR-SH1	TR-SH2	off	2 STATCOM
3	TR-SE1	-	NA	1 SSSC
4	-	TR-SE2	NA	1 SSSC
5	TR-SE1	TR-SE2	off	2 SSSC
6	TR-SH1	TR-SE2	off	1 STATCOM, 1 SSSC
7	TR-SE1	TR-SH1	off	1 STATCOM, 1 SSSC
8	TR-SH1	TR-SE2	on	UPFC1
9	TR-SE1	TR-SH2	on	UPFC2
10	TR-SE1	TR-SE2	on	IPFC

8.7 Modelling of UPFC, IPFC and other Multi-Converter FACTS

There are different types of studies associated with UPFC and other multi-converter FACTS controllers. The studies are carried out from objectives of planning or operational analysis. The broad spectrum of the required studies are listed below with increasing order of complexity

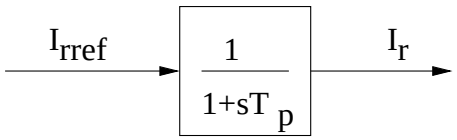

Figure 8.24: Simplified model of reactive current controller

1. Power flow studies
2. Dynamic stability
3. Transient analysis neglecting harmonics
4. Detailed transient analysis considering switching action in the converters

The power flow studies involve the computation of solution of nonlinear algebraic equations that relate the specifications to the system state variables. The constraints are usually handled by modifying the specifications. For example, limits on the reactive current/power are handled by changing the voltage (magnitude) specification. There are many production type computer programmes for power flow analysis of large power systems. These can be modified to include models of multi-converter FACTS.

The dynamic stability refers to the stability of a power system influenced by various controllers (AVR, PSS and network controllers including HVDC and FACTS). There are different mechanisms of system instability. One involves slow growth of undamped low frequency oscillations that are excited by small disturbances that are always present. The growing low frequency oscillations can result in loss of synchronism or voltage collapse. Sometimes, torsional oscillations in subsynchronous frequency range can arise and result in torsional interactions with disastrous effect on the generator shafts.

Both power flow and dynamic stability analysis are based on the single phase model of the network. Since dynamic stability analysis involves phenomena of frequency below 5 Hz, the network variables (voltages and currents) are represented by phasors that vary slowly. Under such circumstances, it is adequate to model the fast FACTS controllers by simplified performance type models that do not require detailed models of the controllers. For example, the reactive current controller in a shunt converter is modelled as shown in Fig. 8.24. Here, the reactive current output of the converter is assumed to follow the reference with a specified delay.

However, it is essential to test the controller performance using detailed three phase models to validate the simplified analysis. For example, the design of AC voltage regulator for the shunt converter requires the study

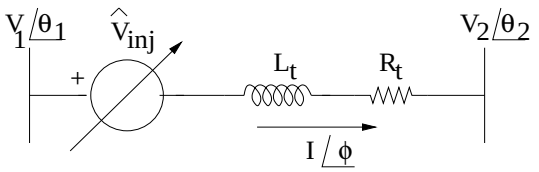

Figure 8.25: Model of a VSC

of electromagnetic interactions that result from the network transients (see chapter 3 for details). In general, this is true for all fast acting controllers. The detailed transient simulation considers three phase nonlinear models of all relevant components.

For the analysis and simulation of SSR, network transients (below third harmonic) need to be modelled by approximate models. For example, a transmission line can be modelled by a single π equivalent network. There is no need to consider the switching action in the converters and the resulting harmonics. The FACTS controllers can be modelled using dynamic phasors or $d-q$ variables referred to a synchronously rotating reference frame.

It would be desirable to employ a common model for all types of studies. For multi-converter circuits, a converter can be modelled by a variable voltage source in series with an inductive impedance as shown in Fig. 8.25. Here, the voltage source is related to the voltage across the DC capacitor based on the converter topology and control action. For three phase models, the voltage source is defined instantaneously and contains harmonics. Neglecting harmonics, we can represent the voltage by $d-q$ components (dynamics phasors) that are determined by exact controller models. The controller models are already described earlier.

The phasor $\hat{V}_{inj}$ is expressed differently for the shunt and series converters. For the shunt converter, $\hat{V}_{inj} = |V_{sh}|\angle(\theta_1 + \alpha)$. For the series converter, $\hat{V}_{inj} = |V_{se}|\angle(\phi - \gamma)$

For transient or dynamic stability analysis, the converter model shown in Fig. 8.25 can be represented conveniently by Norton equivalents that simplifies the network solution using the admittance matrix. For power flow analysis, a shunt converters (in isolation) can be modelled as synchronous condenser with the specification of bus voltage (magnitude). The two control variables $|V_{sh}|$ and α are calculated from the specified voltage magnitude and the constraint equation that relates the power drawn to the losses in the converter. For the series converter, the specification is the line power flow (P) and the constraint is the power supplied by the series converter which may be assumed as zero.

For coupled converters such as a UPFC, the four control variables, $|V_{sh}|, |V_{se}|$. α and γ can be computed from the three specified variables, (say V_1, P_2, Q_2) and the constraint that relates the power balance in the DC circuit.

8.8 SSR Characteristics of UPFC

It was mentioned in chapter 6 that a STATCOM has limited influence on the SSR characteristics of the network. It was mentioned in chapter 7 that a SSSC is generally SSR neutral if the DC capacitance is large. The major advantage of controllable compensation such as a combination of fixed capacitor and SSSC is to dynamically avoid resonance by the proper choice of the fixed series capacitor and meeting the required compensation using SSSC. It was also mentioned that the provision of a well designed Subsynchronous Damping Controller (SSDC) as an auxiliary controller (with a STATCOM or SSSC) can be used to damp Subsynchronous Oscillations (SSO).

The UPFC can be viewed as a combination of STATCOM and SSSC with an additional degree of freedom (of injecting a real voltage). If this voltage is controlled to emulate positive resistance, it was observed from a case study based on IEEE First Benchmark Model (FBM), the critical torsional mode can be damped adequately [19]. The shunt converter of the UPFC is connected at the electrical center of the line (considering the series injected reactive voltage). The eigenvalues for the cases (i) $V_p = 0$ and (ii) $V_p = 0.065$ are shown in Table 8.2. It is assumed that the shunt converter regulates the bus voltage while the series converter injects a constant reactive voltage in addition to positive resistance emulation (The real power flows from the series converter to the shunt converter). It is observed from Table 8.2, that the critical torsional mode (# 3 corresponding to radian frequency of 160) is undamped for case (i) and gets damped for case (ii). Thus a UPFC provides an inherent control for damping SSR without any SSDC.

Similar results are also obtained with an IPFC [21]. However, IPFC connected in two parallel lines results in positive resistance in one line and a negative resistance in the other line (with resistance emulation). If the net resistance in the loop is positive that can be controlled, it is possible to damp the critical mode using IPFC.

8.9 Applications of UPFC

A UPFC may be required whenever the problems of voltage and power flow are present. The planning studies are required to determine the need of a UPFC.

Table 8.2: Eigenvalues corresponding to the torsional and network modes.

Case (i): $V_p = 0.0$	Case (ii): $V_p = 0.065$	Comments
$-1.6923 \pm j8.438$	$-1.5863 \pm j8.121$	Mode 0 (Swing Mode)
$-0.1993 \pm j99.107$	$-0.1749 \pm j99.039$	Mode 1 (Torsional Mode)
$-0.0686 \pm j127.040$	$-0.0621 \pm j127.030$	Mode 2 (Torsional Mode)
$0.8427 \pm j159.930$	$-0.3876 \pm j160.480$	Mode 3 (Torsional Mode)
$-0.3850 \pm j202.790$	$-0.3669 \pm j202.810$	Mode 4 (Torsional Mode)
$-1.8504 \pm j298.170$	$-1.8504 \pm j298.170$	Mode 5 (Torsional Mode)
$-2.7931 \pm j160.070$	$-11.9020 \pm j159.920$	Subsynch. Network Mode
$-1.3266 \pm j560.190$	$-16.8880 \pm j545.270$	Supersynch. Network Mode

A major advantage with multi-converter FACTS controller is the versatility and flexibility afforded by more than one degree of freedom. With a UPFC or IPFC, there are 3 degrees of freedom which can be utilized to regulate 3 quantities in the network - bus voltage and/or power and reactive power flows in the line(s). Such flexibility is of importance in the operation of restructured power systems. The concept of CSC is a first step in this direction.

References and Bibliography

1. L. Gyugyi, "A Unified Power Flow Controller concept for flexible AC transmission systems", IEE Proceedings-C, v. 139, n.4, 1992, pp. 323-331
2. L. Gyugyi, "The Unified Power Flow Controller: A new approach to power transmission control", IEEE Trans. on Power Delivery, v.10, n.2, April 1995, pp. 1085-1099
3. R. Mihalic, P. Zunko and D. Povh, "Improvement of transient stability using unified power flow controller", IEEE Trans. on Power Delivery, v. 11, n. 1, January 1996, pp. 485–492
4. E. Lerch, D. Povh, R. Witzmann, B. Hlebear and R. Mihalic, "Simulation and performance analysis of unified power flow controller", Paper 14-205, CIGRE 1994
5. C. Schauder, E. Stacey, M. Lund, L. Gyugyi, L. Kovalsky, A. Keri, A. Mehraban and A. Edris, "AEP UPFC Project: Installation, commissioning and operation of the ±160 MVA STATCOM (Phase I)" IEEE Trans. on Power Delivery, v.13, n. 4, October 1998, pp. 1530-1535

6. C. Schauder, L. Gyugyi, M.R. Lund, D.M. Hamai, T.R. Rietman, D.R. Torgerson and A. Edris, "Operation of the Unified Power Flow Controller (UPFC) under practical constraints", IEEE Trans. on Power Delivery, v.13, n.2, April 1998, pp. 630-639

7. I. Papic, P. Zunko and D. Povh, "Basic Control of Unified Power Flow Controller", IEEE Trans. on Power Systems, v.12, n.4, November 1997, pp. 1734-1739

8. K.R. Padiyar and A.M. Kulkarni, "Control design and simulation of Unified Power Flow Controller", IEEE Trans. on Power Delivery, v. 13, n. 4, October 1998, pp. 1348-1354

9. K.K. Sen and E.J. Stacey, "UPFC-Unified Power Flow Controller: Theory, modelling and applications", IEEE Trans. on Power Delivery, v. 13, n.4, October 1998, pp.1453-1460.

10. J. Bian, D.G. Ramey, R.J. Nelson and A. Edris, "A Study of equipment sizes and constraints for a unified power flow controller", IEEE Trans. on Power Delivery, v. 12, n.3, July 1997, pp. 1385-1391

11. A. Nabavi-Niaki and M.R. Iravani, "Steady-state and dynamic models of unified power flow controller (UPFC) for power system studies, IEEE Trans. on Power Systems, v. 11, n.4, November 1996, pp. 1937-1943

12. X. Lombard and P.G. Therond, "Control of Unified Power Flow Controller: Comparison of methods on the basis of a detailed numerical model", IEEE Trans. on Power Systems, v. 12, n. 2, May 1997, pp. 824-830

13. B.A. Renz, A. Keri, A.S. Mehraban, C. Schauder, E. Stacey, L. Kovalsky, L. Gyugyi and A. Edris, "AEP Unified Power Flow Controller Performance", IEEE Trans. on Power Delivery, v. 14, n.4, October 1999, pp. 1348-1354

14. L. Gyugyi, K.K. Sen and C.D. Schauder, "The Interline Power Flow Controller Concept: A new approach to power flow management in transmission systems", IEEE Trans. on Power Delivery, v. 14, n.3, July 1999, pp. 1115-1123

15. B. Fardanesh et al, "Convertible Static Compensator application to the New York transmission system", Paper 14-103, CIGRE, 1998

16. B. Fardanesh, B.R. Shperling, E. Uzunovic and S. Zelingher, "Multi-Converter FACTS devices - The Generalized Unified Power Flow Controller (GUFC)", IEEE PES Summer Meeting 2000, Seattle, Washington

17. S. Krishna and K.R. Padiyar, "Discrete Control of unified power flow controller for stability improvement", Electric Power System Research, 75, 2005, pp. 178-189

18. K.R. Padiyar and K. Uma Rao, "Modelling and control of unified power flow controllers for transient stability", Int. J. of Elect. Power & Energy Syst., v. 21, 1999, pp. 1-11

19. K.R. Padiyar and Nagesh Prabhu, "Investigation of SSR characteristics of unified power flow controller", Electric Power Systems Research 74 (2005) pp. 211-221

20. S. Arabi and P. Kundur, "A versatile FACTS device model for power flow and stability simulations", IEEE Trans. on Power Systems, v. 11, n. 4, Nov. 1996, pp. 1944-1950

21. K.R. Padiyar and Nagesh Prabhu, "Analysis of SSR interactions with Interline Power Flow Controller", Presented at National Power Systems Conference, IIT Madras, Chennai, December 2004

22. X. Wei, B. Fardanesh and A. Edris, "A common modelling framework of voltage-sourced converters for load flow, sensitivity and dispatch analysis", IEEE Trans., Power Systems, v.19, n.2, May 2004, pp. 934-941

23. X. Wei, J.H. Chow, B. Fardanesh and A. Edris, "A dispatch strategy for a Unified Power Flow Controller to maximize voltage stability limited power transfer", IEEE Trans., Power Delivery, v. 20, n.3, July 2005, pp. 2022-2029

Chapter 9

Interphase Power Controller and other FACTS Devices

In this chapter, we discuss some of the special purpose FACTS controllers and their applications. In particular, we consider the following devices:

1. Interphase Power Controller (IPC)
2. NGH-SSR Damping Scheme
3. Thyristor Controlled Braking Resistor (TCBR)
4. Fault Current Limiter (FCL)
5. Thyristor Controlled Voltage Limiter (TCVL)

Each of the above is a special purpose device designed for specific applications.

9.1 Interphase Power Controller (IPC)

9.1.1 Introduction

The original concept of IPC was first described in reference [1] and the practical design aspects of a 200 MW prototype for the interconnection of the 120 kV networks, was described in [2]. However, the original concept proposed in [1] has undergone modifications that are described in [3–7]. The installation of world's first IPC at the New York Power Authority (NYPA) Plattsburgh substation on the 115 kV tie that interconnects the NYPA and VELCO systems, is described in [8]. This IPC belongs to the category of IPCs called as the Assisted Phase Shifting Transformers (APST) where the major objective is to provide a passive solution for the control of steady state and post-contingency power flows [6]. The basic principle of the APST is to add a high impedance in parallel with an existing PST. The impedance carries a portion of the power flow such that the capabilities of the installation are increased.

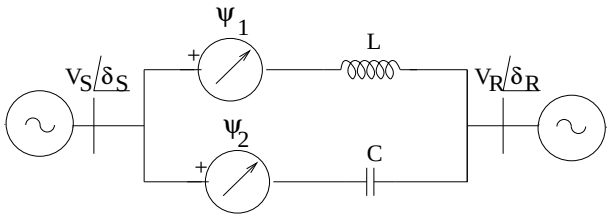

Figure 9.1: IPC equivalent circuit

9.1.2 Initial Concept of IPC

The FACTS controllers based on power electronic devices offer both flexibility and high speed (of operation). There are applications where the speed is not so important, but flexible operation is required. For example, in networks that are sensitive to daily or seasonal load variations, problems can arise in the regulation of power flows in steady state.

The IPC concept involves the series connection of impedances between different phases of the two (synchronous) subnetworks that are to be interconnected, hence the name: the Interphase Power Controller [1].

The IPC proposed in [1] acts as a current source with the following characteristics:

1. The power flow is nearly constant (within 10%) for a wide range of ($\pm 25^\circ$) of angle between the two subnetworks.
2. There is no significant contribution to the short circuit level by the interconnection between the two subnetworks.
3. Major contingencies on one side of the IPC have negligible impact on the voltages of the other side.
4. As no power electronic controllers are required, harmonics are not generated.

The IPC consists of three phase reactors and capacitors each installed in series between the two subnetworks that are to be interconnected (see Fig. 9.1).

However, unlike in the conventional series compensation schemes, the phase A reactor and capacitor of the first subnetwork (or network) could be connected to phases B and C of the second subnetwork (network). This implies that some components are always subjected to voltage even if the angle $\delta_{SR} = (\delta_S - \delta_R)$ is zero. Hence the current and consequently the power flow is nonzero at $\delta_{SR} = 0$.

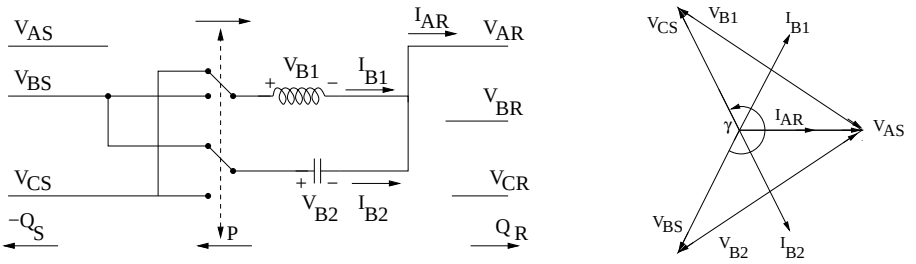

Figure 9.2: IPC 240 equipped with switches to invert the direction of the active power flow

Reference [1] describes two IPC schemes: a) IPC 240 and b) IPC 120. The first scheme is shown in Fig. 9.2. This figure shows only two of the total six susceptances ($B = -\frac{1}{X}$). The susceptances are connected to a set of switches that enable the direction of the active (real) power P to be reversed. The power flow is defined as positive when the flow is from S to R. When the flow is positive, susceptances B_1 and B_2 are connected to voltages V_{CS} and V_{BS} respectively as shown in Fig. 9.2. The power reversal is achieved by connecting B_1 and B_2 to V_{BS} and V_{CS} respectively. The IPC in Fig. 9.2 is designated as IPC 240 as the voltages of connection points of B_1 and B_2 are phase shifted by an angle $\gamma = 240°$. The phase current I_{AR} is the sum of I_{B1} and I_{B2} (the currents in the two susceptances). The phasor diagram for $\delta_{SR} = 0$ is also shown in Fig. 9.2. I_{B1} leads V_{AR} by 60° while I_{B2} lags V_{AR} by 60°.

To improve the power factors of the two currents (I_{B1} and I_{B2}), IPC120 is proposed which involves the use of a Y-y6 (180° phase shift) transformer (see Fig. 9.3). Here, $\gamma = 120°$, hence the name IPC120.

The phasor diagram in Fig. 9.3 shows that I_{B1} leads V_{AR} by 30° while I_{B2} lags V_{AR} by −30°. If the transformer shown in Fig. 9.3 is assumed to be ideal and $n = 1$, the values for P, Q_S and Q_R are given by

$$P = (-V_S V_R \sin\delta_{B1})B_1 + (-V_S V_R \sin\delta_{B2})B_2 \quad (9.1)$$

$$-Q_S = (V_S^2 - V_S V_R \cos\delta_{B1})B_1 + (V_S^2 - V_S V_R \cos\delta_{B2})B_2 \quad (9.2)$$

$$Q_R = (V_R^2 - V_S V_R \cos\delta_{B1})B_1 + (V_R^2 - V_S V_R \cos\delta_{B2})B_2 \quad (9.3)$$

where the angles δ_{B1} and δ_{B2} are the phase angles across the admittances B_1 and B_2 respectively. Hence,

$$\delta_{B1} = \delta_{SR} - \psi_1 \quad (9.4)$$

$$\delta_{B2} = \delta_{SR} - \psi_2 \quad (9.5)$$

For IPC 120, $\psi_1 = -60°$ and $\psi_2 = 60°$. (Note that B_1 is negative while B_2 is positive.)

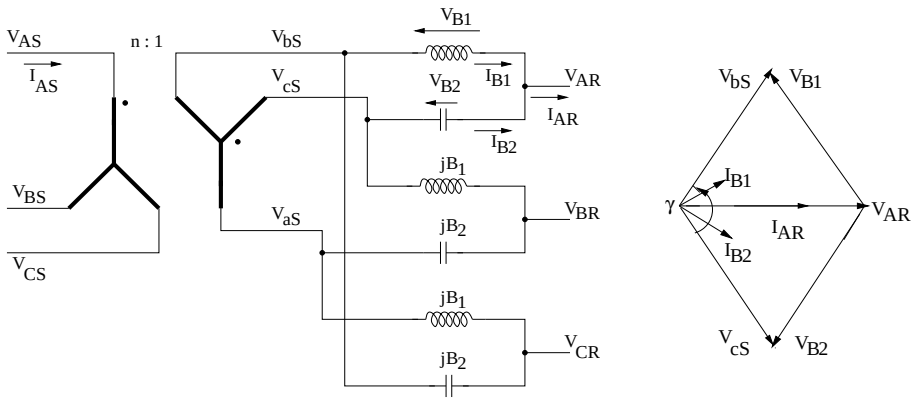

(a) Three phase diagram (b) Phasor diagram

Figure 9.3: IPC 120

Eqs. (9.1) to (9.3) relate P, Q_S and Q_R to the two susceptances B_1 and B_2. It is possible to regulate two variables (say P and Q_R) by adjusting the values of the susceptances B_1 and B_2.

The solutions for B_1 and B_2 for specified P and Q_R are given below.

$$B_1 = \frac{P(2V_R - V_S\cos\delta_{SR} - \sqrt{3}V_S\sin\delta_{SR}) - Q_R V_S(\sqrt{3}\cos\delta_{SR} - \sin\delta_{SR})}{\sqrt{3}V_S V_R(V_S - 2V_R\cos\delta_{SR})} \tag{9.6}$$

$$B_2 = \frac{-P(2V_R - V_S\cos\delta_{SR} + \sqrt{3}V_S\sin\delta_{SR}) - Q_R V_S(\sqrt{3}\cos\delta_{SR} + \sin\delta_{SR})}{\sqrt{3}V_S V_R(V_S - 2V_R\cos\delta_{SR})} \tag{9.7}$$

From Eqs. (9.2) and (9.3), we get,

$$-Q_S = (B_1 + B_2)(V_S^2 - V_R^2) + Q_R \tag{9.8}$$

This shows that $Q_S = -Q_R$ if $B_1 = -B_2$, irrespective of V_S and V_R. The variations of P and $Q_R(-Q_S)$ are shown for $B_1 = -B_2 = -1$ as δ_{SR} is varies from -25° to 25° are shown in Fig. 9.4. This figure also shows the variations of P and Q_R for $|B_1| = |B_2| = 0.5$. In the calculation of P and Q_R, V_R and V_S are assumed to be equal to 1.0 p.u.

9.1.3 Improvements in IPC

To reduce the ratings of IPC and thus their costs and losses, improvements in the original concept were introduced. A major innovation is to use phase shifting transformers (PST) to apply phase shifted voltages to the two susceptances. This is termed as injection IPC as phase shifts are introduced by

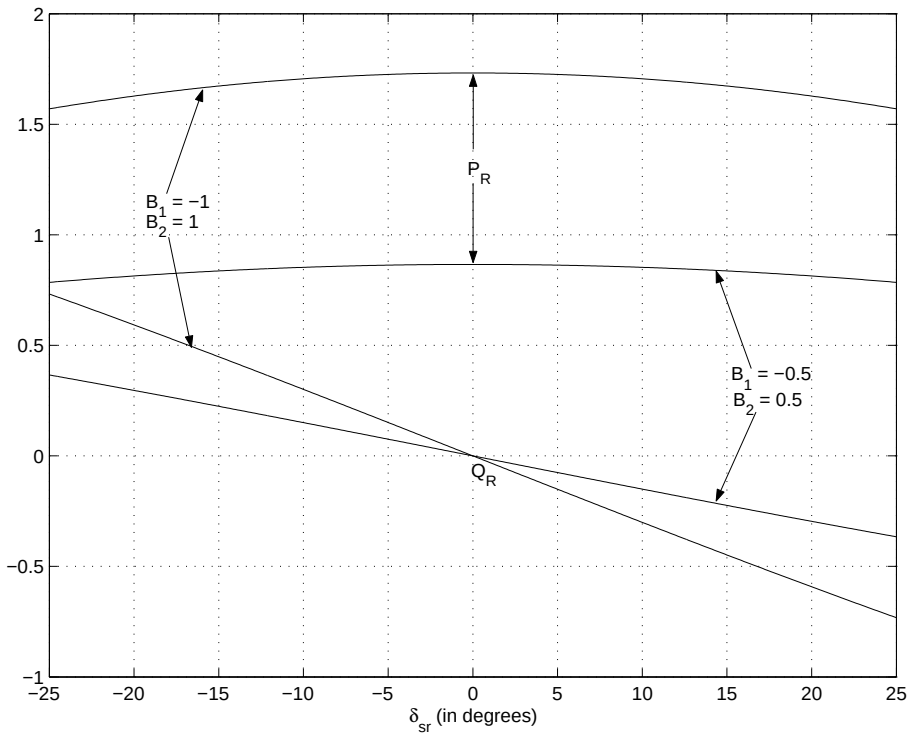

Figure 9.4: Plot of P_R and Q_R as a function of δ_{SR}

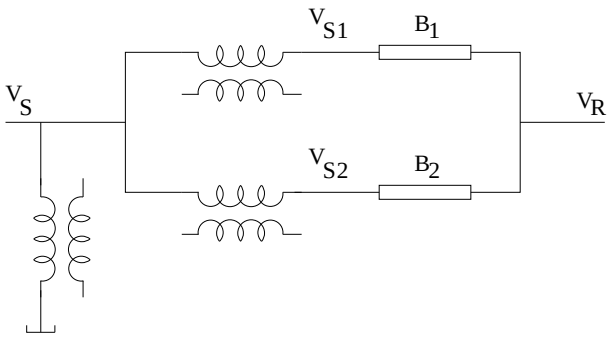

Figure 9.5: A voltage injection IPC

injection of quadrature voltages in series with the two susceptances [3]. (see Fig. 9.5). In the injection of IPC, the phase shift angles ψ_1 and ψ_2 can be varied while they are fixed at $\pm 60^\circ$ in the IPC120. In the injection IPC, the voltages V_{B1} and V_{B2} are substantially smaller because ψ_1 and ψ_2 can be as small as $\pm 20^\circ$ for the same useful range of δ_{SR} ($\pm 25^\circ$). Thus, the ratings are reduced which in turn results in the reduction of costs, space requirement and losses. These are important issues in higher voltage transmission lines.

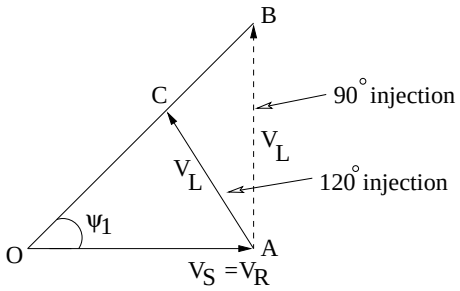

Figure 9.6: Comparison of 120^o and 90^o injection

In conventional PST, the excitation transformer (ET) is normally equipped with on-load tap changer (LTC) to adjust the power set point. In an IPC, the power flow is maintained constant in a passive manner by its inherent characteristics and the power level is adjusted by switching the desired susceptance values. Thus, the ET and LTC can be dispensed with when PST is used for voltage injection. This is possible by injecting the voltage with an angle of 120° (instead of 90° in a conventional PST). See Fig. 9.6 for comparison of the 120° and 90° voltage injections. A 120° angle of injection is easily achieved by taking the phase to neutral voltage from another phase. Also, a 120° angle of injection limits the magnitudes of the voltages V_{B1} and V_{B2} as the angles ψ_1 and ψ_2 increase in magnitude. Fig. 9.7 shows an injection IPC without ET and angle of injection of 120°. Typically, $\psi_1 = -\psi_2 = \psi$.

The equivalent circuit for the injection IPC is shown in Fig. 9.8. The major differences compared to the equivalent circuit shown in Fig. 9.1 are the presence of the ideal transformers in the two parallel branches. The turns ratios for quadrature (90°) voltage injection are given by

$$n_1 = n_2 = \frac{OA}{OB} = \cos\psi \tag{9.9}$$

For injection at 120° (as shown in Fig. 9.7), the turns ratios are:

$$n_1 = n_2 = \frac{OA}{OC} = \sin[120^\circ - |\psi|]/\sin 60^\circ \tag{9.10}$$

Power Characteristics

In deriving the expressions for P, Q_S and Q_R, we assume that $|B_1| = |B_2|$. Also, we assume that B_1 is an inductive susceptance ($B_1 = -\frac{1}{X}$) and B_2 is a capacitive susceptance. The expressions for the active and reactive power can be derived from the following equations for I_{B1} and I_{B2}

$$I_{B1} = \frac{V_{B1}}{jX} = \frac{[V'_S\angle(\delta_S - \psi_1) - V_R\angle\delta_R]}{jX} \tag{9.11}$$

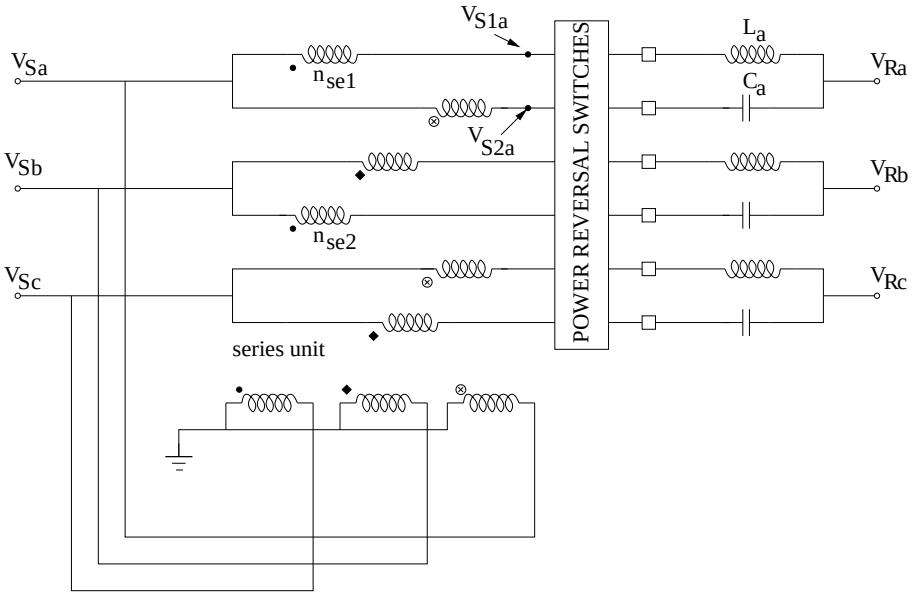

(a) Three phase diagram

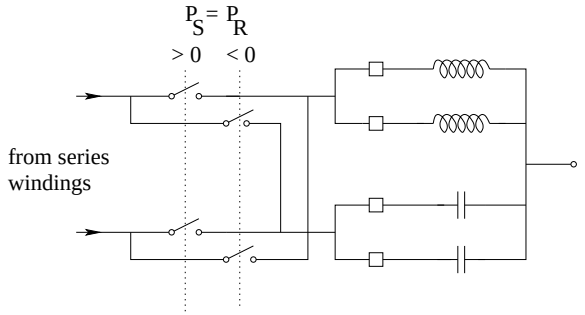

(b) Power reversal switches in one phase

Figure 9.7: A 120^o injection IPC without excitation unit

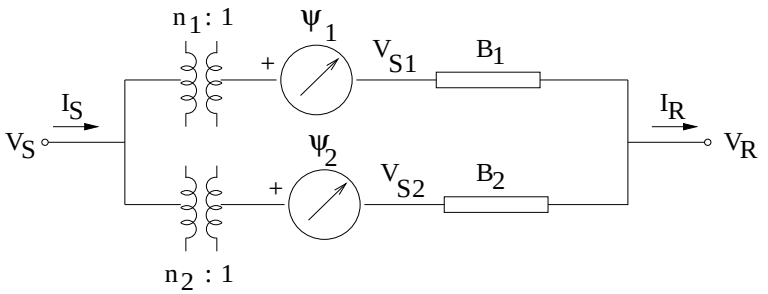

Figure 9.8: Equivalent circuit for the injection IPC

$$I_{B2} = \frac{V_{B2}}{-jX} = \frac{[V'_S \angle(\delta_S - \psi_2) - V_R \angle \delta_R]}{-jX} \tag{9.12}$$

where $V'_S = \frac{V_S}{n}$.

Since,

$$(P_S - jQ_S) = V'_S(I^*_{B1} + I^*_{B2}) \tag{9.13}$$

$$(P_R + jQ_R) = V_R(I^*_{B1} + I^*_{B2}) \tag{9.14}$$

Note that the direction of Q_S is opposite to that of P_S and P_R. We can obtain the expressions for P_S, Q_S, P_R and Q_R which are given below:

$$P_S = P_R = P_{\max} \cos\left(\delta_{SR} - \frac{\psi_1 + \psi_2}{2}\right) \sin\left(\frac{\psi_2 - \psi_1}{2}\right) \tag{9.15}$$

$$-Q_S = Q_R = -P_{\max} \sin\left(\delta_{SR} - \frac{\psi_1 + \psi_2}{2}\right) \sin\left(\frac{\psi_2 - \psi_1}{2}\right) \tag{9.16}$$

where $P_{\max} = \frac{2V'_S V_R}{X}$ is the maximum (theoretical) power flow in the IPC. $\delta_{SR} = \delta_S - \delta_R$. In practice, the rated power of IPC is limited by the maximum voltages across the inductive and capacitive susceptances.

9.1.4 Further Simplifications

We can simplify the topology of IPC if we used voltage injection in the reactor branch only. ($\psi_2 = 0$). If $\psi_1 = -30°$, $P_S = P_R$ is maximum if $\delta_{SR} = -15°$ (from Eq. (9.15)). For this condition, the line current I_{RA} is in phase with voltage V_{RA}. (To simplify analysis, we assume $n = 1$). For this example, the power factor is unity on both sides of the IPC. We can also observe that P_R is maximum when $\delta_{SR} = 15°$ if $\psi_1 = 30°$ and the power factor is unity on both sides. The range of operation of the IPC in the $P_R - \delta_{SR}$ plane is shown in Fig. 9.9. Here, we observe that the region of operation is a parallelogram (ABCD) bound by the lines AB and CD corresponding to the maximum power flow through the IPC. The width of the parallelogram depends on the changes in the angle δ_{SR} resulting from credible contingencies.

The power levels are adjusted by changing the values of susceptances and the offset is fixed by selecting the internal phase shift angle ψ_1.

The region of operation of the IPC can be obtained by considering the IPC connected to the AC network as shown in Fig. 9.10.

Assuming that $V_1 = |V_S| = |V_R| = V_2 = 1.0$, we can express the active power flow (P_R) as

$$P_R = \frac{1}{X_1} \sin(\delta - \delta_S) = \frac{1}{X_2} \sin(\delta_R)$$

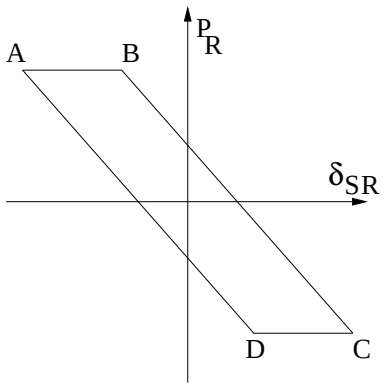

Figure 9.9: Operating region of IPC

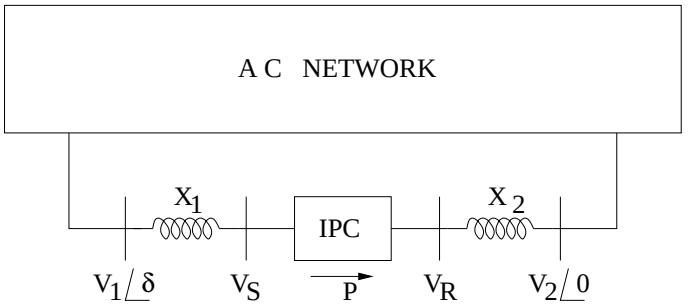

Figure 9.10: IPC connected to a AC network

If the differences in the angles are small, then

$$P_R \simeq \frac{1}{X_1}(\delta - \delta_S) = \frac{1}{X_2}(\delta_R) = \frac{\delta - \delta_{SR}}{(X_1 + X_2)} \tag{9.17}$$

The above equation can be expressed as

$$P_R = m\delta_{SR} + d \tag{9.18}$$

where

$$m = -\frac{1}{X_L}, \quad d = \frac{\delta}{X_L}, \quad X_L = X_1 + X_2$$

This shows that the slope of the lines AD and BC is $-\frac{1}{X_L}$. The width of the parallelogram is given by $(\delta_{\max} - \delta_{\min})$. We have assumed (in Fig. 9.9) that $\delta_{min} = -\delta_{\max}$.

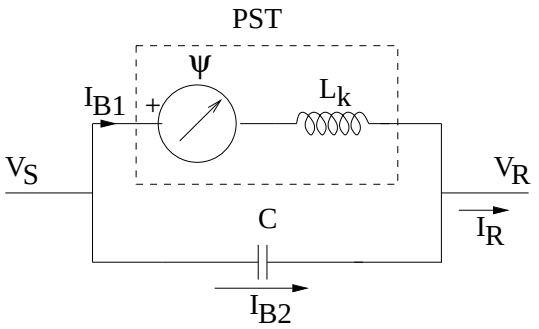

Figure 9.11: IPC as a modified PST

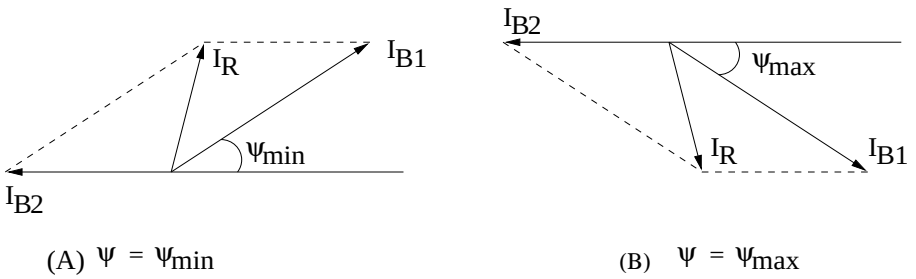

Figure 9.12: Phasor diagram showing I_{B1}, I_{B2} and I_R

9.1.5 Retrofitting of Existing Phase Shifting Transformers

Phase Shifting Transformers are utilized to control power flow in a tie line interconnecting two networks. There are about 90 PST in N. America [8]. By connecting a capacitive impedance in parallel with a PST, it is possible to increase the capability of the PST in the boost position [6]. In this configuration (shown in Fig. 9.11), the inductive impedance X_T is the leakage impedance of the PST. A capacitive impedance X_C of appropriate rating is connected in parallel to enhance the control range of the phase shift and thereby the operating region. The current phasors I_{B1}, I_{B2} and I_R for $\psi = \psi_{\max}$ and $\psi = \psi_{\min}$ are shown in Fig. 9.12. It is obvious that the effective phase shift produced by the IPC is greater than the produced by PST alone.

The region of operation of PST in the $P_R - \delta_{SR}$ plane is shown in Fig. 9.13(a). The operating region is bound by ABCDEFA. The lines BC and EF have the slope of $m = -\frac{1}{X_L}$ and pass through the points $(\delta_{\max}, 0)$ and $(\delta_{\min}, 0)$ respectively (similar to what is shown in Fig. 9.9). Since P_R is

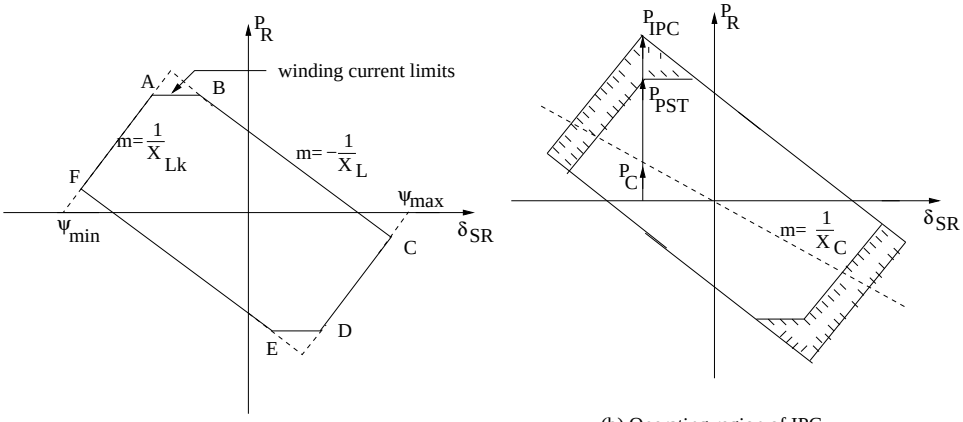

(a) Operating region for a PST

(b) Operating region of IPC

Figure 9.13: Comparison of PST and IPC

also given by

$$P_R = \frac{\delta_{SR} - \psi}{X_T}, \quad X_T = \omega L_k \tag{9.19}$$

the lines CD and FA have the slope of $\frac{1}{X_T}$ and pass through the points $(\psi_{\max}, 0)$ and $(\psi_{\min}, 0)$ respectively. The lines CD and FA form the boundary of the region of operation, imposed by the tap changer limits of the PST. The lines AB and DE relate to the constraints imposed by the PST winding current limits. The lines BC and EF reflect the network limits as mentioned earlier.

The operating region of IPC is shown in Fig. 9.13(b). The power characteristic of the capacitor is shown by the dashed line passing through the origin and having a negative slope of $\frac{1}{X_C}$.

The capacitor can be selected such that the current in the PST (line current - capacitor current) is never exceeded. Thus, the impedance X_C is chosen such that the power flow in the capacitor is equal to the difference between the network limit and the capacity of the PST at its maximum tap position.

The shaded regions in Fig. 9.13(b) correspond to the enhancement of the power flow control capability provided by the IPC over and above that given by the PST working alone. The capacitor also results in reduced losses and provides voltage support.

If the operating point A happens to lie in the first quadrant, then the PST requires an inductive impedance (instead of the capacitive impedance) to be connected in parallel. The size of the inductor can be chosen in a similar fashion (as the capacitor) to enhance the capability of the PST. The

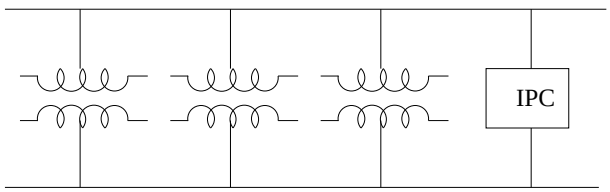

Figure 9.14: An IPC as a FCLT

IPC installed at Plattsburgh substation has an inductive impedance of 75 ohms connected in parallel with the existing PST. To compensate for the reactive losses caused by the inductor, two 25 MVAR shunt capacitor banks are also included on the line side of the IPC. Although the shunt capacitors are not part of the IPC, they are required for its proper operation. The inductors are connected via 115 kV underground cables as there was not enough space for implementing aerial busbar connections to the PST [8].

9.1.6 Application of IPC as Fault Current Limiting Transformer (FCLT)

In reference [7], Fault Current Limiting Transformers (FCLT) have been proposed as a special case of IPC technology. A FCLT involves a phase shifted voltage to be applied in series with a capacitive impedance. Consider a transformer substation in which several transformers are connected in parallel to supply load. If additional load is to be met by adding a new transformer, there is a danger of increased fault level. This can be controlled by connecting an IPC as a FCLT (see Fig. 9.14).

In reference [26], a feasibility study for converting a 345/138 kV auto-transformer into a FCLT is reported. By connecting one winding of a two winding transformer across the B phase of auto-transformer's 13.8 kV delta connected tertiary winding and other winding in series with A phase of auto-transformer's 138 kV terminal (see Fig. 9.15) a phase shifted voltage V_{seA} is obtained. Fig. 9.15 shows the FCLT in parallel with three auto-transformers. A series capacitor of $-$j33.2 ohms is connected in series with the FCLT.

The leakage impedance of the autotransformer (X_{ps}) is 8.4 ohms while that of the series connected two winding transformer is 1 ohm. Under normal operating conditions, the power flow in a FCLT (IPC) is a function of the injected voltage (V_{se}) which can be adjusted by controlling the tap position of the series connected transformer. Thus, the FCLT has similar characteristics as the voltage injection type of IPC described earlier.

During faults, the current flow through FCLT is limited by the high series (capacitive) impedance. The FCLT has about 3 times the impedance

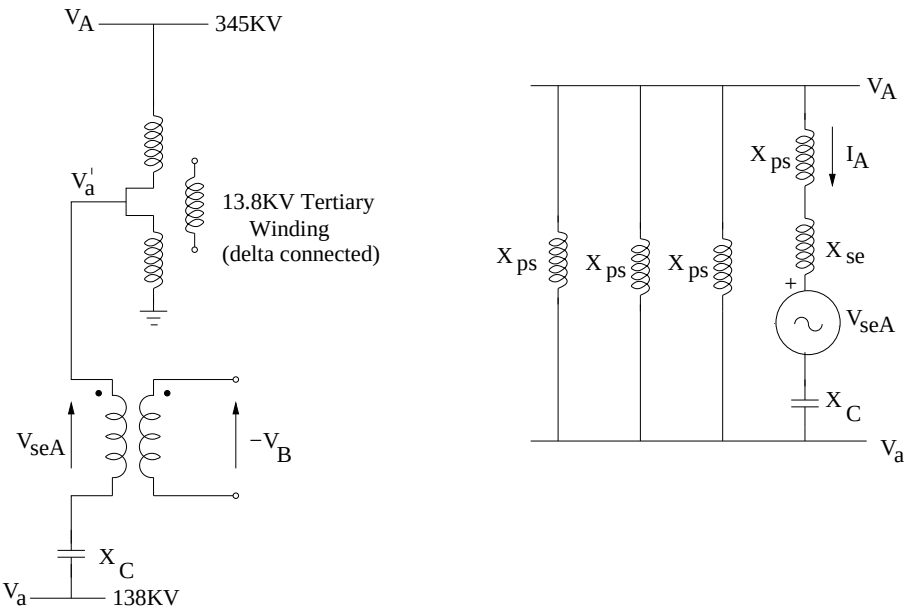

(a) FCLT with an auto transformer (Phase A)

(b) Equivalent circuit

Figure 9.15: A FCLT in parallel with autotransformer

of the autotransformer and hence will contribute only about 1/3 of the fault current provided by an autotransformer.

9.1.7 Applications of IPC

The power flows in transmission lines connected to a generating station or a load centre are determined by the outputs of the generators or load demands which are known in advance. In case of contingencies involving tripping of line(s), the power flow in the remaining lines is regulated by tripping of generators or loads.

In contrast, if a tie line is to connect two networks (or subnetworks) the power flow can vary widely depending on the phase angle (δ) difference across the two buses to which the tie line is connected. To prevent frequent tripping of the tie line, it becomes essential to modify the power characteristics of the line. An Interphase Controller (IPC) uses only passive reactive impedances and a phase shifting transformer to adjust the power flow characteristics of the line such that over the range of δ (determined by network contingencies), the active power remains practically constant. The authors of references [1] to [7] mention a variation of less than 10% in power flow even when δ varies over the range of $\pm 20^\circ$.

Actual implementation of a technology depends on the cost-benefit

aspects and comparison with competitive technologies. For example, if speed is not essential, a phase shifting transformer (PST) which is manually controlled, may be adequate. Introduction of passive impedances (capacitive or inductive) can improve the capability of existing PST. Thus, the first installation of IPC in Plattsburgh station belongs to this category.

References [7] and [26] describe applications of IPCs as FCLTs. However, it is not obvious whether this concept will be implemented in practice.

It is possible to use Static PSTs as parts of IPCs. This provides fast speed of response in addition to flexibility of operation (under credible contingencies). However the use of SPST as new installation is generally not considered due to cost considerations.

Reference [5] reports on simulator studies of IPC technology. There are several issues that affect the design of IPC such as overvoltage (caused by opening one end of the IPC), voltage unbalance, variation of the system frequency and operation with one or two phases out of service. It is claimed in [5], that in a strong system, the IPC can be operated with one or two phases open on one side, provided that all three phases of the PST remain energized on the other side.

9.2 NGH SSR Damping Scheme

This scheme was proposed by N.G. Hingorani [9,10] to damp subsynchronous frequency currents in transmission lines and was first installed at Southern California Edison's Lugo substation in U.S.A. in 1984 [11,12].

The basic concept of NGH-SSR damping scheme can be explained with reference to Fig. 9.16. If a sinusoidal voltage of frequency f_0 is combined with a DC voltage, it is seen that, for the combined voltage, some half cycles are longer than the nominal half cycle period of $\frac{1}{2f_0}$. If a sinusoidal voltage of frequency $f_e < f_0$ is considered instead of the DC voltage, again it is observed that the combined voltage has some half cycles which are longer than $\frac{1}{2f_0}$. Similarly, any combination of a base signal of frequency f_0 with DC and subsynchronous frequencies would result in some half cycles longer than the nominal half cycle period.

The voltage across the series capacitor is a combination of fundamental frequency, DC and subsynchronous frequency components. The basic principle of NGH damping scheme is to dissipate capacitor charges whenever the measured half cycle period exceeds the nominal. This is done by inserting a resistor across the capacitor through thyristor switches (see Fig. 9.17). The thyristor stops conducting whenever the capacitor voltage (and the thyristor current) reaches zero. Therefore, the measurement of half cy-

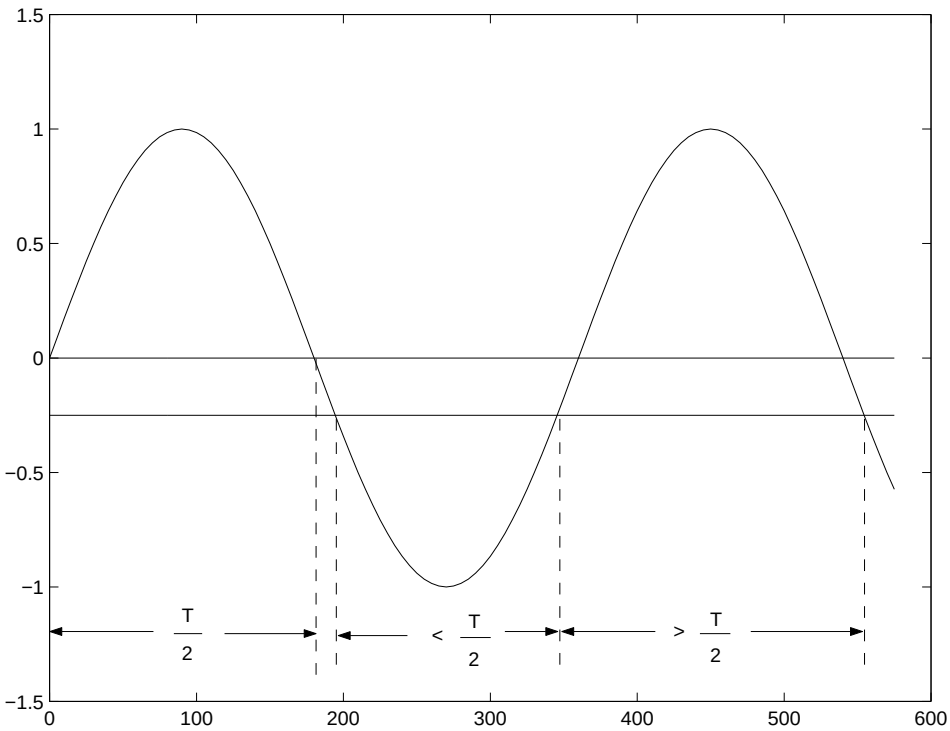

(a) Fundamental frequency combined with DC

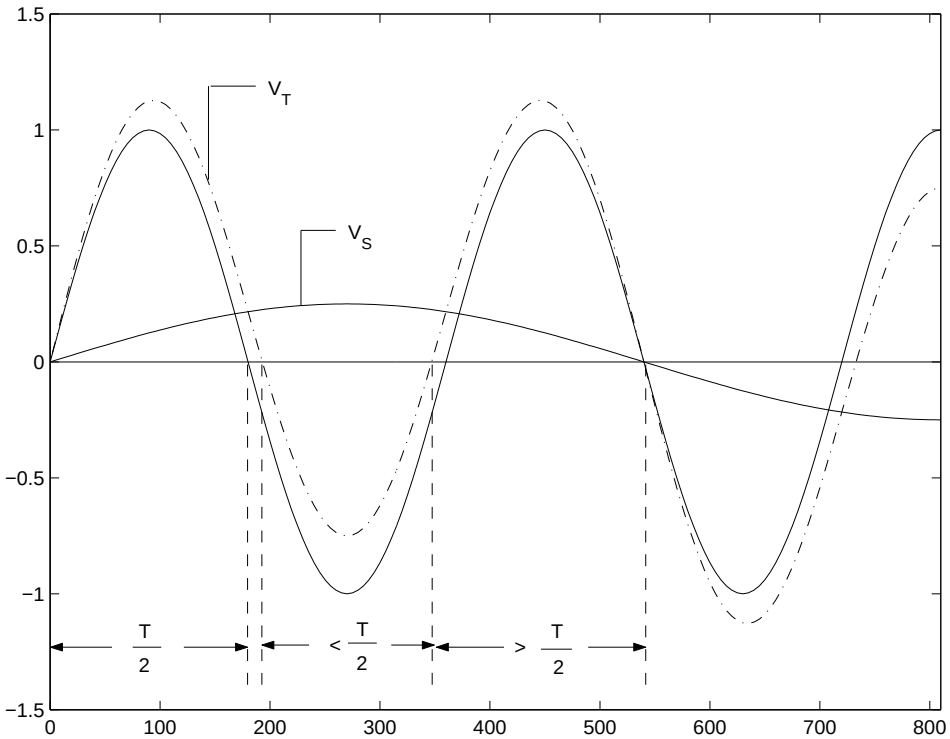

(b) Fundamental frequency combined with subsynchronous frequency

Figure 9.16: Effect of presence of DC and subsynchronous frequency

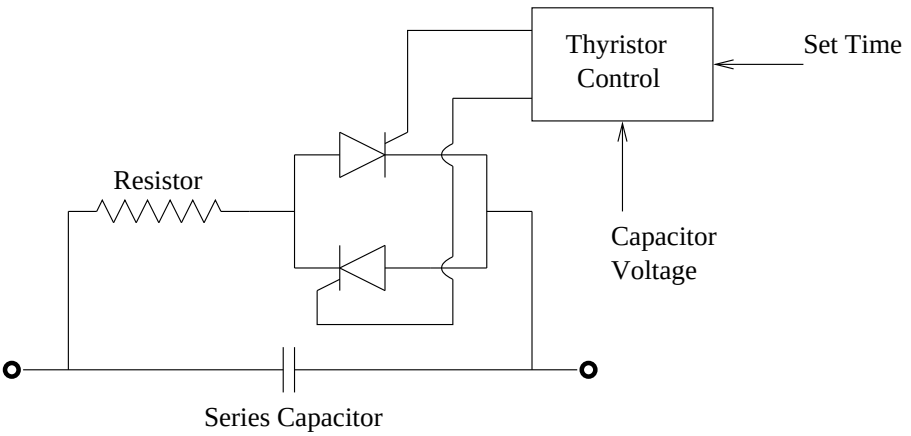

Figure 9.17: Basic NGH-SSR damping scheme

cle period restarts from a new voltage zero. No thyristor fires for half cycles which are shorter than the set period. Two thyristors are needed for the two polarities. For high voltages, the thyristor shown in Fig. 9.17 actually represent a series string of thyristors. The resistor value is not critical although lower its ohmic value, the more effective it is (except when it is too low). It is recommended that the resistor's ohmic value within 5 to 10 percent of the capacitor ohmic value will give satisfactory results. A small series reactor is used to limit the rate of change of current in thyristors.

Thyristor Control

A conceptual firing control scheme for thyristors is shown in Fig. 9.18. A pulse generator continuously generates a train of pulses at a rate high enough so that pulse count can be used as a measure of the half cycle period. A signal proportional to the capacitor voltage is fed into an amplifier/clamp which produces a square wave signal between two zero crossings for one polarity of the input wave, thus representing the length of each half wave. The gate allows the pulses to go through for the duration of the half wave. The counter, which is reset by the square wave, counts the number of pulses from voltage zero so that whenever the count exceeds the set value, the counter releases the firing pulse to its thyristor string. A common pulse generator may be used for the two thyristor strings in each phase.

The operation of the controller is independent for each phase. The controller is simple and does not require detection of specific subsynchronous signals. The control signal can be obtained at the platform level. Alternately, it can be generated as the difference of two voltage signals from the measuring devices (on each side of the capacitor) of the voltage with respect to ground.

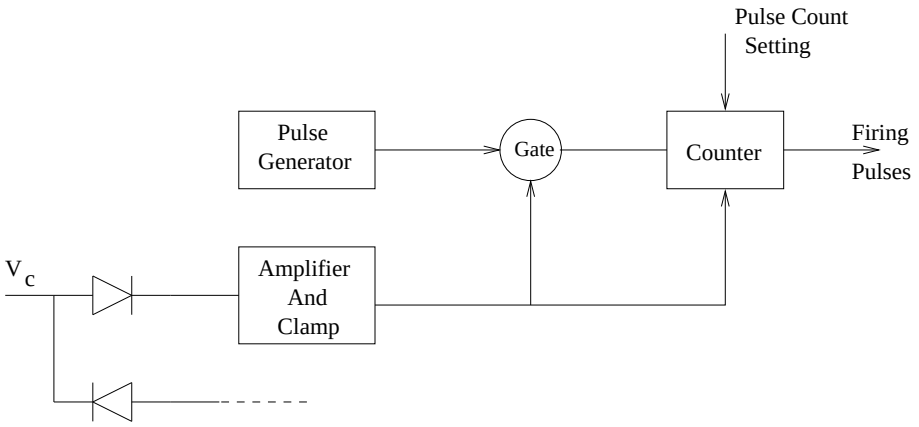

Figure 9.18: Thyristor control for NGH-SSR damping scheme

In this case, the control circuitry could be located at the ground level and firing pulses transmitted through optical links.

The objectives of the NGH damping scheme are

1. reduce transient torques
2. suppress steady state (self excitation) SSR problem
3. suppress offset of series capacitors
4. protect the series capacitors

The scheme may be designed for any or all of the above purposes. If transient torque control is of major concern, the set period can be larger than the nominal half cycle periods so that in steady state and with small perturbations the thyristors will not fire. The thyristors will fire only during large disturbances such as faults followed by clearing. If steady state SSR problem is of major concern, the set period can be slightly less than the nominal half period; then the thyristor will conduct during steady state at the tail end of each half cycle of the capacitor voltage; this will provide detuning effect against gradual build up of oscillations. There will be continuous power loss in this case, but is very small and of minor consequence.

The thyristors can help to protect the capacitors (and themselves) by firing if the instantaneous forward voltage exceeds a set level. The resistor limits the discharge current from the capacitor. The capacitor and thyristor protection can also be implemented by employing nonlinear zinc oxide resistors across the thyristors (see Fig. 9.19). The protection level of the zinc oxide resistor can be selected such that it (in series with the linear

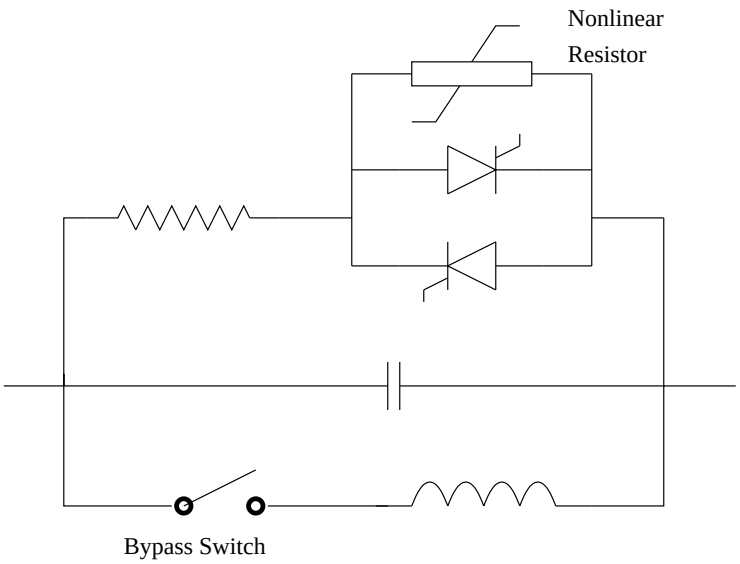

Figure 9.19: Thyristor and capacitor protection

resistor) provides adequate protection for the capacitor. The bypass switch helps to relieve the thyristor/resistor when their duty exceeds safe limits. The bypass switch is also required when capacitor is to be bypassed and reinserted under normal operating conditions.

NGH scheme is a passive scheme-it does not require feedback signals. The requirement of thyristors are well within the state of the art. For example, a 1000 A, 30 ohm capacitor may require a 80 kV thyristor string with a resistor duty of 20-50 MJ per phase.

The studies carried out on NGH scheme [10] indicate that it is an effective countermeasure for both steady state and transient SSR problems. However it was found that some undamping can result for torsional modes which are 'off tune' (not in resonance with the electrical system). It is suggested that the use of SEDC (Supplementary Excitation Damping Control) can help to overcome this problem. In summary, the studies show that NGH scheme with appropriate SEDC is beneficial in applying series compensation over a wider range (0-75%) whereas SSR problem limited the compensation level to 15%.

Reference [13] compares the SSR characteristics of the NGH scheme with the TCSC. Whereas in a TCSC, the thyristor current pulse completely reverses the initial capacitor voltage, in a NGH scheme, the thyristor current pulse reduces the capacitor voltage from the initial value to zero. The design parameters of NGH scheme and TCSC are significantly different. For a 15 ohm capacitor (per phase), with 1000 A line current, the NGH scheme has

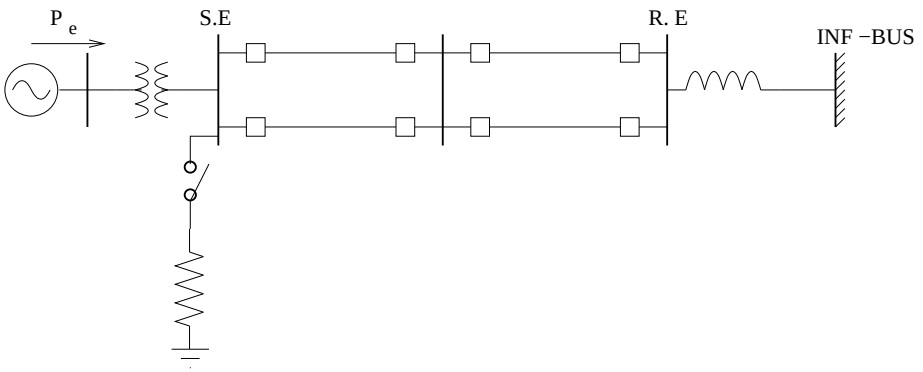

Figure 9.20: Application of shunt braking resistor

R = 4.25 ohms and the reactor size in 0.820 mH. For the same value of capacitive impedance, the reactor size is 6.8 mH which has a resistance of 0.03 ohm.

While the major benefit of NGH scheme is to provide transient (electrical) damping, the characteristics of the TCSC results in inductive impedance at subsynchronous frequencies. See chapter 4 for more details on TCSC.

9.3 Thyristor Controlled Braking Resistor (TCBR)

This is also termed as Dynamic Brake and involves the use of braking resistors, mostly connected in shunt, which are switched in, following a fault clearing, to correct the temporary imbalance between the mechanical power input and electrical power output of generators. In principle, the use of braking resistors of suitable size and appropriate logic to implement controllable duration of resistor insertion can overcome the problem of transient instability. However, the cost of resistor capable of dissipating the required amount of energy and associated switching equipment is a deterrent as there have been very few applications so far. Peace River in British Columbia, Canada [27] and Chief Joseph Substation of Bonneville Power Administration in Western USA [16] are few of the modern applications of the concept.

Fig. 9.20 shows typical location of shunt connected resistors at the sending end of a long double circuit transmission line.

When the inertia of the sending end generator is small compared to that of the receiving end, series braking resistors are also effective in

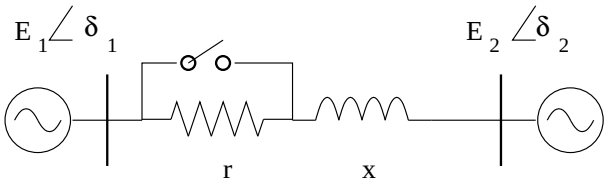

Figure 9.21: Application of series connected brake

controlling the relative angle. See Fig. 9.21.

Series braking resistors can be inserted by connecting them between the neutral and ground on the high voltage (line) side of the step-up transformers. This simplifies the design of the resistors from the insulation point of view. The other advantages of series connected dynamic brake are [28]

1. Speed of insertion is related to opening of a circuit breaker across the resistor as opposed to the closing of a breaker as in the case of the shunt resistor. This permits faster action of the brake and is effective in reducing the severity of the fault in case of prolonged faults by stuck breakers. It is to be noted that series braking resistors are inserted as soon as the fault is detected while shunt resistors are switched on as soon as the fault is cleared.
2. The peak value of the electrical power (in an equivalent single machine system) occurs when $(\delta_1 - \delta_2) > 90°$. This is beneficial as it allows more time for the synchronizing torques to act.
3. The size and cost of series braking resistor tend to be smaller than that of the shunt resistor because of factors listed above.

The effectiveness of the series braking resistors is considerably reduced if M_1 and M_2 (inertias of the two equivalent generators shown in Fig. 9.21) are comparable. This is due to the fact that both machines are decelerated equally when $M_1 = M_2$ and the relative deceleration is zero.

The application of 1400 MW shunt dynamic brake at BPA's Chief Joseph substation resulted in the increase in the transient stability limit of power flow on Pacific Northwest - Southwest (PNW-SW) intertie [16]. Mechanically switched dynamic brake is designed as a discrete controller that acts for a short time after the fault clearing in systems with hydro plants. The replacement of mechanical switches by thyristor switches not only increases the speed of response, but also permits continuous control in response to a locally generated control signal. Thus, a TCBR can be used for a variety of functions [14] in addition to prevention of transient instability during the first swing. These are:

1. Improve damping of low frequency oscillations.
2. Damping of Subsynchronous Resonance (SSR) that can result from fixed series compensation
3. Reduce and damp subsynchronous frequency shaft torques to enable high speed reclosing of lines near a power plant. This is significant even in the absence of fixed series compensation.
4. Facilitate synchronizing a turbine generator. Out-of-phase synchronizing can produce more severe shaft torques compared to a bolted three phase fault at the generator.

The case study reported in reference [18] led to the following conclusions.

1. The proportional control using the speed deviation of the generator (on which the dynamic brake is acting) gives good result in damping of torsional oscillations of the turbogenerator shafts.

   The control signal of speed deviation contains primarily the torsional modes and little of the modes belonging to the electrical network. This results in robust control action which is independent of the network configuration or fault type.
2. A high pass filter acting on the control signal can provide better damping of the torsional modes at the expense of the low frequency swing mode (mode zero). However, for high-speed reclosing applications, this is advantageous as the transient shaft torques are better damped.
3. Simulation results on multimachine systems show that identical generators can be controlled by a single dynamic brake. In most cases, a brake acting on one generator does not affect the torsional modes of a nearby non-identical generator, unless the two generators share a common (torsional) mode frequency.

9.4 Fault Current Limiter (FCL)

With expansion in generation and system interconnections, the fault levels increase. The dynamic loads such as synchronous and induction motors also contribute to fault levels. The interruption capacity of circuit breakers (CB) is less than 80 kA and 63 kA is a widely used CB level. The replacement of switch gear to accommodate increased fault levels is not very practical solution. Other solutions involve bus splitting (which can reduce reliability) and/or the use of reactors and high impedance transformers. The latter is also not desirable on account of increased losses, voltage regulation and

stability problems. The use of low impedance transformers can eliminate the need for on load tap changers.

Sometimes it becomes necessary to protect equipment against destructive effects of fault currents even though the breaker capacity is adequate. An example is a transformer in underground vaults or cables which are very expensive to replace. To reduce the destructive effects of high fault currents, circuit breakers with faster interrupting times have appeared. The clearing times have reduced from 5 cycles to 2 cycles or even 1 cycle. However, all AC circuit breakers require current zero passage in order to interrupt the fault.

It would be desirable to interrupt or limit fault current at well below its first peak in order to limit the fault current magnitude to a fairly low predetermined value. This is a very difficult problem as it requires a very short functioning time of less than 2 milliseconds. There are two types of Fault Current Limiters (FCL) that have been proposed and are being developed. These are:

1. High Temperature Superconductor (HTS) FCL
2. Solid State Current Limiter (SSCL)

The development of HTS in 1986 enables the development of economical FCL. The HTS require cooling by liquid nitrogen at 77°K unlike low temperature superconductors (LTS) that are cooled by liquid helium, which is expensive and difficult to handle. Although earlier designs of FCL based on LTS were studied over 25 years ago, they were not implemented. There is renewed interest in Superconducting Fault Current Limiter (SFCL) with the advent of HTS.

HTS materials such as YBCO lose all resistance at temperatures below 85°K. However, if the current in the material exceeds a critical level of the superconductor, it transits from its normal superconducting state to a resistive state; thereby introducing the required current limiting impedance. Typically, the superconductor would be designed to have a critical current of 2 or 3 times the full load current. The superconductor in its resistive state can also be used as a trigger coil, pushing the bulk of the fault current through a resistor or inductor (see Fig. 9.22). The advantage of this configuration is that it limits the energy that must be absorbed by the superconductor. The FCL is a short across the copper inductive or resistive element Z, under the normal conditions. During a fault, the resistance developed in the limiter shunts the current through Z which absorbs most of the energy.

Another concept is to use a resistive limiter on a transformer secondary, with the primary in series with the circuit. One phase of the SFCL

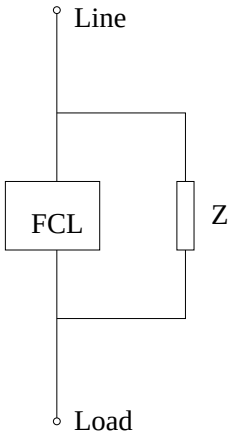

Figure 9.22: Fault Current Limiter with HTS trigger coil

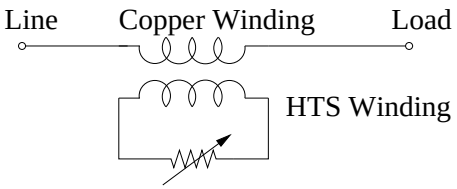

Figure 9.23: Inductive SFCL

is shown in Fig. 9.23. Here a copper winding is inserted in the circuit and is coupled to the HTS winding. During normal operation, a zero impedance is reflected to the primary. Resistance developed in HTS winding during a fault is reflected to the primary and limits the fault current.

The advantages of a SFCL are:

1. Passivity - detection of fault and insertion of current limiting impedance without active monitoring and control mechanisms.
2. Transparency - no substantial I^2R losses or voltage drop across the device during steady state operation. The SFCL is basically invisible to the grid.
3. Modularity and Scalability - A number of basic current limiting modules are arranged in an $m \times n$ matrix to form the current limiting matrix. The nominal grid current level where the FCL is connected determines the number of rows of the matrix and the required current limiting impedance determines the number of columns.
4. Reliability - redundancy can be easily provided due to the matrix configuration.

There are several countries such as USA, Canada, France, Germany and Japan, trying to develop SFCL at EHV levels. It is anticipated that transmission level SFCLs may be available by 2010.

Solid State Current Limiter (SSCL)

A SSCL is made up of several identical modules connected in series to achieve a specified voltage rating. A solid state circuit module can consist of GTO or conventional thyristor switches with commutating circuit to interrupt the current flow in the main circuit and divert the flow into a parallel connected resistor. The circuit is designed to sense and initiate current limiting in a millisecond if the fault current is high. This is similar to the action of a current limiting fuse which ensures that the first current peak is never seen by the line. At present medium voltage current limiters are under development and it is anticipated that transmission class current limiter may undergo field trials in 2008.

The cost of a SSCL is expected to be around six times the cost of conventional mechanical circuit breakers and relays. A SSCL can also operate as a circuit breaker when the thyristor switches can interrupt at the first current zero. It is to be noted that GTO switches have very limited overload capability even though they can interrupt current with negligible delay. A SSCL can also improve power quality for unfaulted lines by limiting the duration and magnitude of the voltage sag.

9.5 Thyristor Controlled Voltage Limiter (TCVL)

Metal Oxide Varistors (MOV) are widely used to provide overvoltage protection of equipment in power systems. MOVs made of gapless Zinc Oxide (ZnO) composition are voltage dependent resistors with highly nonlinear characteristics. ZnO arresters can absorb energy surges (up to 1 kJ/cc) and hence they can be used for fast voltage limiting to protect electrical equipment from excessive voltage stresses caused by switching or lightning induced transients. The use of ZnO arresters in general lead to reduced insulation requirements as the voltage across the equipment is limited to the clamping voltage level of ZnO. This results in reduced costs and improved reliability.

However, the clamping voltage level of MOV arresters is about 1.7 times the normal operating voltage peak. This characteristic can be modified by connecting an anti-parallel connected thyristor switch across a part of the arrester to dynamically lower the voltage limiting level as and when required. See Fig. 9.24 which shows one phase of the TCVL.

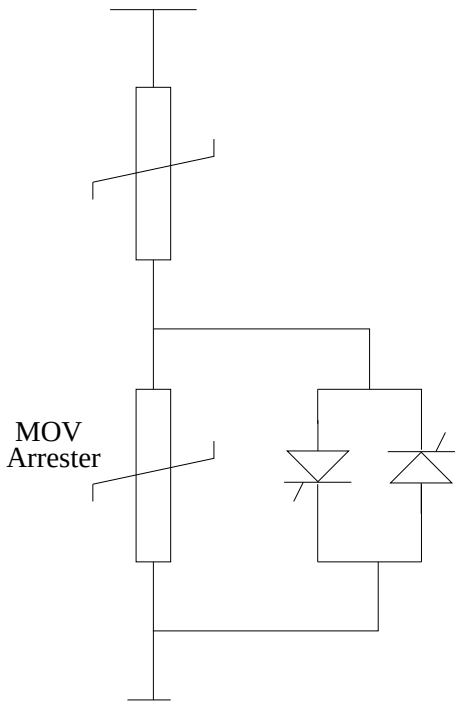

Figure 9.24: A Thyristor Controlled Voltage Limiter (TCVL)

Mechanically switched capacitors can contribute to power quality problems by generating over voltages caused by high inrush currents when closing or possible restrike immediately after opening. Also, after opening the mechanical switch, a five minute discharge time delay is required before reenergizing. Thyristor switched capacitor can overcome these problems under normal conditions, however the cost is more than doubled. The use of TCVL can reduce the overvoltages caused by mechanical switching during energization and also enable fast reenergization without having to replace existing breakers.

References and Bibliography

1. J. Brochu, P. Pelletier, F. Beauregard and G. Morin, "The Interphase Power Controller: A new concept for managing power flow within AC networks", IEEE Trans. on Power Delivery, v. 9, n. 2, 1994, pp. 833-841

2. K. Habashi et al, "The design of a 200 MW Interphase Power Controller prototype", IEEE Trans. on Power Delivery, v. 9, n. 2, 1994, pp. 1041-1048

3. F. Beauregard, J. Brochu, G. Morin and P. Pelletier, "Interphase Power

Controller with voltage injection", IEEE Trans. on Power Delivery, v. 9, n. 4, 1994, pp. 1956-1962

4. J. Brochu, F. Beauregard, G. Morin and P. Pelletier, "Interphase Power Controller adapted to the operating conditions of networks", IEEE Trans. on Power Delivery, v. 10, n. 2, 1995, pp. 961-969
5. G. Sybille et al, "Simulator demonstration of the Interphase Power Controller technology", IEEE Trans. on Power Delivery, v. 11, n. 4, 1996, pp. 1985-1992
6. J. Brochu et al, "Application of the Interphase Power Controller technology for transmission line power flow control", IEEE Trans. on power Delivery, v. 12, n. 2, 1997, pp. 888-894
7. J. Brochu et al, "The IPC technology – A new approach for substation uprating with passive short-circuit limitation", IEEE Trans. on Power Delivery, v. 13, n. 1, 1998, pp. 233-240
8. J. Lemay et al, "The Plattsburgh Interphase Power Controller", IEEE T & D Conference and Exposition, New Orleans, April 1999
9. N.G. Hingorani, " A new scheme for subsynchronous resonance damping of torsional oscillations and transient torque – Part I", IEEE Trans., v. PAS-100, n. 4, 1981, pp. 1852-1855
10. R.A. Hedin, K.B. Stump and N.G. Hingorani, "A new scheme for subsynchronous resonance damping of torsional oscillations and transient torque – Part II, "IEEE Trans., v. PAS-100, n. 4, 1981, pp. 1856-1863
11. N.G. Hingorani et al, "Prototype NGH subsynchronous resonance damping scheme – Part I - Field installation and operating experience", IEEE Trans. on Power Systems, v. 2, n. 4, 1987, pp. 1034-1039
12. I.S. Benko, B. Bhargava and W.N. Rothenbuhler, "Prototype NGH subsynchronous resonance damping scheme - Part II - switching and short circuit tests", IEEE Trans. on Power Systems, v. 2, n. 4, 1987, pp. 1040-1049
13. R.A. Hedin et al, "SSR characteristics of alternative types of series compensation schemes", IEEE Trans. on Power Systems, v. 10, n. 2, 1995, pp. 845-852
14. N.G. Hingorani and L. Gyugyi, **Understanding FACTS – Concepts and Technology of Flexible AC Transmission Systems**, New York, IEEE Press, 2000
15. K.R. Padiyar, **Analysis of Subsynchronous Resonance in Power Systems**, Boston: Kluwer Academic Publishers, 1999
16. M. L. Shelton, W.A. Mittelstadt, P.F. Winkleman and W.L. Bellerby, "Bonneville Power Administration 1400 MW braking resistor", IEEE Trans., v. PAS-94, March 1975, pp. 602-611

17. K.R. Padiyar, **Power System Dynamics - Stability and Control**, Second Edition, Hyderabad: BS Publications, 2002

18. M.K. Donnelly et al, "Control of a dynamic brake to reduce turbine-generator shaft transient torques", IEEE Trans. on Power Systems, v. 8, n. 1, 1993, pp. 67-73

19. O. Wasynczuk, "Damping shaft torsional oscillations using a dynamically controlled resistor bank", IEEE Trans., v. PAS-100, n. 7, 1981, pp. 3340-3349

20. R.K. Smith et al, "Solid state distribution current limiter and circuit breaker: application requirements and control strategies", Paper 92 SM 572-8 PWRD presented at IEEE summer power meeting 1992

21. E. Thuries et al, "Towards the superconducting fault current limiter", IEEE Trans. on Power Delivery, v. 6, n. 2, 1991, pp. 801-808

22. L. Salasoo et al, "Comparison of superconducting fault current limiter concepts in electric utility applications", IEEE Trans. on Applied Superconductivity, v. 5, n. 2, 1995, pp. 1079-1082

23. T. Verhaege et al, " Investigations on HV and EHV superconducting fault current limiters", IEEE Trans. on Applied Superconductivity, v. 5, n. 2, 1995, pp. 1063-1066

24. M. Sarkozi et al, "Thyristor switched ZnO voltage limiter", Paper 14-302, CIGRE, 1994

25. D. J. Christofersen, P.S.S. Holenarsipur and N. Mohan, "Capacitor Dynamic Voltage Suppression (CDVS)", Paper 14-201, CIGRE, 2000

26. D.F. Menzies et al, "A feasibility study for conversion of 345/138 kV auto-transformers into fault current limiting transformers", Int. Conf. on Power System Transients (IPST'05), Montreal, Canada, June 2005

27. H.M. Ellis et al, "Dynamic stability of Peace River transmission system", IEEE Trans., v. PAS-85, June 1966, pp. 586-600

28. F.P. DeMello, "The effects of control", Modern Concepts of Power System Dynamics, IEEE Tutorial Course 70 M62-PWR, 1970

This page intentionally left blank

Chapter 10

Power Oscillation Damping

10.1 Introduction

While the major advantage of FACTS controllers is flexible power scheduling under various (changing) operating conditions, the fast controllability also ensures improvement of (dynamic) security of power systems under contingency conditions where system stability is threatened. In this chapter, we take up the problem of low frequency oscillations and their damping by appropriate auxiliary or supplementary modulation controllers. The problem of transient stability will be taken up in the next chapter.

The transmission network and the generator rotors together act as mass-spring system (the synchronizing torques acting in a manner analogous to the restoring forces in springs) which is lightly damped. The frequency of oscillations of the rotor (swing) modes varies from 0.2 to 4 Hz. The higher frequencies correspond to intra-plant modes involving oscillations among parallel connected generators in a power station. The intra-plant modes are normally well damped by the amortisseur circuits on the salient pole generators or solid rotor in a turbogenerator. (The eddy currents induced in the solid rotor when there is a slip or relative motion between the rotating magnetic field and the rotor introduce a damping torque on the rotor). The lower end of the frequency spectrum corresponds to inter-area modes in which a large number of generators participate and their damping is difficult. The 'local' modes refer to the modes in which only the generators in a local area participate and the typical frequency is in the neighbourhood of 1 Hz. However, the distinction between local modes and interarea modes is somewhat artificial. In general, we can say that lower the frequency of a swing mode, more widespread is the participation.

The power system stabilizer (PSS) with rotor speed/frequency and or power signal as input was the first damping controller applied [1,2]. The PSS used in the excitation control acts through the AVR and modulates the generator bus voltage to provide a damping torque on the generator rotor. With the advent of fast acting power electronic controllers such as HVDC converter and SVC controls, it was possible to damp low frequency oscillations by the modulation of active power and/or reactive power. The

introduction of TCSC allowed the provision of power oscillation damping (POD) with supplementary control that modulates the line reactance in response to the control signal synthesized from local measurements. With emerging FACTS controllers based on VSC, the concept of POD can be extended. Thus the network controllers in HVDC and AC lines supplement the action of PSS in damping critical electromechanical modes.

In this chapter, the modelling, control design and application of POD in FACTS controllers are discussed. Based on a L-C network analogue of the mass-spring system, the control signals and control laws for both series and shunt FACTS controller are proposed [14,15].

10.2 Basic Issues in the Damping of Low Frequency Oscillations in Large Power Systems

The interconnected power systems can have hundreds of generators. Each generator (including the excitation and turbine-governor controls) can be represented by nonlinear differential equations. The number of equations depend on the degree of detail considered and can vary from 5 to 20 per generator. The network transients are normally ignored in analyzing low frequency (below 5 Hz) behaviour. However, the loads may have to be represented by dynamic models in addition to network controllers such as HVDC and FACTS. Thus, a large power system is represented by a large set of Differential Algebraic Equations (DAE) given by

$$\dot{X} = f(X, Y, p) \tag{10.1}$$

$$0 = g(X, Y, p) \tag{10.2}$$

where X is the state vector, Y is the vector of non-state variables, p is the parameter vector. The equilibrium (operating) point is obtained by letting $\dot{X} = 0$ and solving the nonlinear algebraic equations,

$$\left.\begin{aligned} 0 &= f(X_0, Y_0, p) \\ 0 &= g(X_0, Y_0, p) \end{aligned}\right\} \tag{10.3}$$

We can linearize the system represented by equations (10.1) and (10.2) by letting

$$X = X_0 + x, \quad Y = Y_0 + y \tag{10.4}$$

The linearized equations are given by

$$\begin{bmatrix} \dot{x} \\ 0 \end{bmatrix} = \begin{bmatrix} F_1 & F_2 \\ F_3 & F_4 \end{bmatrix} \begin{bmatrix} x \\ y \end{bmatrix} \tag{10.5}$$

where

$$F_1 = \left[\frac{\partial f}{\partial X}\right], \quad F_2 = \left[\frac{\partial f}{\partial Y}\right]$$
$$F_3 = \left[\frac{\partial g}{\partial X}\right], \quad F_4 = \left[\frac{\partial g}{\partial Y}\right]$$

Eq. (10.5) can be simplified eliminating y and we get,

$$\dot{x} = [A(p)]x \tag{10.6}$$

where

$$A = [F_1 - F_2 F_4^{-1} F_3]$$

If the linear system represented by Eq. (10.6) is asymptotically stable, the equilibrium point (X_0, Y_0) is stable. The stability of the linear system is guaranteed if all the eigenvalues of the system matrix $[A]$ have negative real parts. (Note that the eigenvalues of a real matrix can be real or complex. The complex eigenvalues occur in pairs. If $\lambda = \sigma + j\omega$ is an eigenvalue, then $\lambda^* = \sigma - j\omega$ is also an eigenvalue). The complex eigenvalues correspond to the oscillatory modes as the time response of the linear system has the components involving $e^{\sigma t}\sin(\omega t + \phi)$ where ϕ depends on the initial conditions. The imaginary part (ω) of the complex eigenvalue is the radian frequency of the oscillations and the real part (σ) is the decrement rate (assuming it is negative). The damping ratio (ζ) is a dimensionless number defined by

$$\zeta = \frac{-\sigma}{\sqrt{\sigma^2 + \omega^2}} \tag{10.7}$$

If $\sigma \ll \omega$, then $\zeta \simeq -\frac{\sigma}{\omega}$.

Before considering the introduction of damping controllers, it is necessary to analyze the small signal stability characteristics of the power system as the operating conditions represented by the parameter vector 'p' vary. As 'p' varies over the specified region (in the parameter plane), the stability of the equilibrium point can be lost by either (i) a complex pair of eigenvalues or (ii) a real eigenvalue crossing over to the right half of 's' plane at the critical value of $p = p_c$. In the former ease, we say that there is a Hopf bifurcation and in the latter case, there is a saddle-node bifurcation (It is to be noted that a bifurcation results in a drastic change in the system behaviour). Hopf bifurcations are generic particularly for the loss of angle stability under small disturbances (such as minor variations in the load). These bifurcations often lead to undamped oscillations that grow in magnitude until loss of synchronism occurs. Thus, low frequency electromechanical oscillations can lead to dynamic insecurity threatening loss of system integrity and widespread blackout.

In some cases, characterized by the reduction of reactive power reserves, increased loading on lines, the loss of stability by either Hopf or

saddle-node bifurcation can lead to voltage collapse. In such cases, the generators remain in synchronism, but the blackout occurs due to voltage collapse. The protective action can result in tripping of loads (including induction motors).

The operating conditions change not only due to variation of p, but also due to changes in the system structure by tripping of some lines by protective relays. This complicates the stability analysis which is also affected by the system size. For a large system, the size of the matrix $[A]$ can be of the order of a few thousand. For example, a system with 400 dynamic devices, with an average of five state variables per device results in 2000 state variables (total) and as many eigenvalues. Fortunately, it is not necessary to compute all these eigenvalues, but only critical modes. There are efficient algorithms to calculate these critical modes [3,4,5,23].

For designing damping controllers, it is necessary to reduce the order of system model that captures all the important features. It is a challenging job to arrive at an accurate reduced order dynamic model under varying conditions. There are many methods for model reduction-some empirical. There are two major approaches - one based on identifying coherency among generators so that a group of coherent generators can be replaced by an equivalent generator [24]. The other approach is based on Prony analysis or its variations wherein the critical modes and the reduced model are directly obtained from nonlinear time response simulations or from field measurements [18,21,22].

Some of the major issues in the design of damping controllers are,

1. The location of the controller
2. The choice of the control signal
3. Control law or algorithm
4. Robustness of the controller under varying system conditions
5. Coordination among controllers

The location of the controller in damping a specified mode is very important Arbitrary placement of the controller may be ineffective. The criteria for the location of the controller is usually based on participation factors, residues or eigenvalue sensitivities.

The control signal should be synthesized from local measurements to avoid telemetering. The signal should mainly contain the modal components that are to be damped and should not contain any noise which may be amplified. The control law is closely related to the choice of the control signal. The controller should not amplify higher frequency noise.

For designing damping controllers, the linear control theory is invariably used although some attempts have been made to apply nonlinear, adaptive control techniques (including fuzzy logic and neural network based controllers). However, most of these are of academic interest and have not been adopted in practice. The situation may change in future. In general, it is to be noted that what matters most in a practical application, is the robust and trouble free operation of a controller. It would appear that some degree of adaptation would be required in a controller that has to operate under widely varying conditions. Restricting the controller to have a fixed structure with constant parameters may reduce the effectiveness of a controller. However, a major factor is reliability coupled with stable operation.

A single controller at a given location is not adequate to damp all the critical modes. Multiple controllers at different locations would be required to do the job. In such cases, the tuning of individual controllers in isolation may not be feasible. The interactions among controllers is an important phenomenon that requires coordinated control of more than one controller.

10.3 System Modelling for Small Signal Stability

In this section, the development of the system model including the FACTS controllers, for small signal stability analysis is taken up. A power system can be represented as a collection of various dynamical subsystems that are interconnected by the transmission network as shown in Fig. 10.1. The transmission network also includes equivalent circuits of transformers, shunt and series capacitors/reactors. The network is assumed to be in quasi-steady state and is modelled by algebraic equations based on the admittance matrix. The voltages and currents (assumed to be sinusoidal) are represented by slowly varying phasors (with rectangular coordinates). The dynamical subsystems are divided into three categories as follows:

1. Shunt connected. This includes generators, dynamic loads, SVC and STATCOM
2. Series connected subsystems such as TCSC and SSSC
3. Shunt and series connected such as UPFC and TCPAR.

The various component models are described below.

Transmission Network

The linearized network equations can be expressed in terms of the bus admittance matrix or by Jacobian matrix obtained from the real and reactive

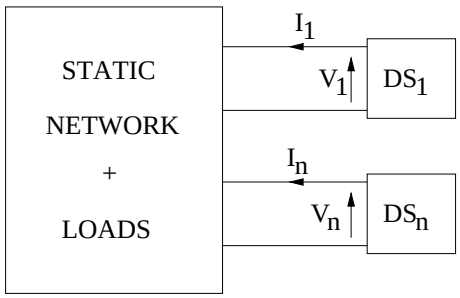

Figure 10.1: Representation of power system

power balance equations. The former is simpler as the network equations are linear given by

$$[Y]V = I \tag{10.8}$$

where V is a $2n$ dimensional vector defined by

$$V^t = [\ V_1^t \quad V_2^t \quad \ldots \quad V_i^t \quad \ldots \quad V_n^t\ ], \quad V_i^t = [\ V_{Qi} \quad V_{Di}\ ]$$

Similarly, I is a $2n$ dimensional vector defined by

$$I^t = [\ I_1^t \quad I_2^t \quad \ldots \quad I_j^t \quad \ldots \quad I_n^t\ ], \quad I_j^t = [\ I_{Dj} \quad I_{Qj}\ ]$$

n is the number of buses in the network. The matrix $[Y]$ can be defined as a composite matrix made up of sub-matrices as elements. The element Y_{ij} is defined as

$$Y_{ij} = \begin{bmatrix} B_{ij} & G_{ij} \\ G_{ij} & -B_{ij} \end{bmatrix}$$

Note that Y_{ij} is symmetric. This is true in general, unless phase shifting transformers are present.

Static Loads

These are also connected in shunt. The load model can be assumed as

$$\begin{aligned} P_L &= P_{Lo}\left(\frac{V_L}{V_{Lo}}\right)^{m_p} \\ Q_L &= Q_{Lo}\left(\frac{V_L}{V_{Lo}}\right)^{m_q} \end{aligned}$$

where V_L is the magnitudes of the load bus voltage. The subscript 'o' refers to the operating value (in steady state).

The load current is given by

$$I_{QL} + jI_{DL} = \frac{P_L - jQ_L}{V_{QL} - jV_{DL}}$$

If we express,

$$\Delta V_L = [\Delta V_{QL}\ \Delta V_{DL}]^t, \quad \Delta I_L = [\Delta I_{DL}\ \Delta I_{QL}]^t$$

then they can be related by the equation [1]

$$\Delta I_L = [Y_L]\Delta V_L \tag{10.9}$$

where $[Y_L]$ is a 2×2 matrix defined by

$$[Y_L] = \begin{bmatrix} B_{Lo} & G_{Lo} \\ G_{Lo} & -B_{Lo} \end{bmatrix} + \begin{bmatrix} b_1 & g_1 \\ g_2 & -b_2 \end{bmatrix} \tag{10.10}$$

where

$$\begin{aligned} b_1 &= \frac{V_{QLo}}{V_o^3}[(m_p - 2)P_{Lo}\sin\theta_o - (m_q - 2)Q_{Lo}\cos\theta_o] \\ g_1 &= b_1\left(\frac{V_{DLo}}{V_{QLo}}\right) \\ g_2 &= \frac{V_{QLo}}{V_o^3}[(m_p - 2)P_{Lo}\cos\theta_o + (m_q - 2)Q_{Lo}\sin\theta_o] \\ b_2 &= -g_2\left(\frac{V_{DLo}}{V_{QLo}}\right) \end{aligned}$$

θ_o is the initial angle of the load bus voltage with respect to Q-axis (chosen as reference). Note that the second term in the R.H.S. of Eq. (10.10) vanishes if $m_p = m_q = 2$ (the load is linear represented by a constant admittance).

Each static load can be represented by Eq. (10.10). All the static load equations can be combined with the linearized network equation (10.8) to give

$$[Y']\Delta V = \Delta I \tag{10.11}$$

where $[Y']$ is the modified admittance matrix including the effects of static loads. Only the diagonal elements of $[Y]$ are modified as follows

$$Y'_{ii} = Y_{ii} + Y_{Li} \tag{10.12}$$

The current sources ΔI are the outputs of various dynamical subsystems described below.

Generator

The linearized equations of a generator can be expressed as

$$\dot{x}_g = [A_g]x_g + [B_g]\Delta V_g + [E_g]u_g \tag{10.13}$$

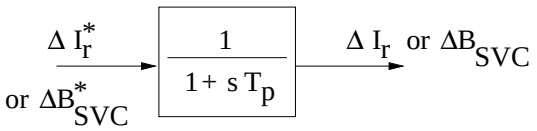

Figure 10.2: A simplified model of the plant

where x_g are the small perturbations in the state variables of the generator including synchronous machine, excitation system and turbine-governor. Neglecting the latter and considering a static exciter with a two-axis model of the machine, we can express x_g as

$$\begin{aligned} x_g &= [\Delta\delta\ \Delta S_m\ \Delta E'_q\ \Delta E'_d\ \Delta E_{fd}]^t \\ u_g &= \Delta V_{ref} \end{aligned}$$

The output variables are the generator currents which can be expressed as

$$\Delta I_g = [C_g]x_g + [D_g]\Delta V_g \tag{10.14}$$

Shunt FACTS Controllers

The shunt FACTS controllers are (a) SVC and (b) STATCOM. While the output of SVC is a variable susceptance, the output of STATCOM is a variable reactive current. (Note that we are neglecting losses). The controller for a shunt FACTS controller consists of primarily the voltage regulator that determines the reference value of the SVC susceptance or STATCOM (reactive) current in conjunction with a supplementary modulation controller. In modelling the plant (SVC or STATCOM), it is adequate to represent it by a single time constant transfer function as shown in Fig. 10.2. The controller diagram is shown in Fig. 10.3. Here $x_{sh}(1) = \Delta B_{SVC}$ for a SVC and $x_{sh}(1) = \Delta I_r$ for a STATCOM. It is possible to combine the plant and controller models to obtain the linearized state space model of a shunt FACTS controller as

$$\dot{x}_{sh} = [A_{sh}]x_{sh} + [B_{sh}]\Delta V_{sh} + [E_{sh}]u_{sh} \tag{10.15}$$

u_{sh} is the vector of input signals to the voltage regulator and SMC. The output equations for a shunt FACTS controller are given by

$$\Delta I_{sh} = [C_{sh}]x_{sh} + [D_{sh}]\Delta V_{sh} \tag{10.16}$$

where

$$\Delta I_{sh} = [\Delta I_{Dsh}\ \Delta I_{Qsh}]^t$$

The above equation can be derived from the equation (10.17) or (10.18)

$$\begin{aligned} \Delta I_{Qsh} + j\Delta I_{Dsh} &= -jB_{SVCo}(\Delta V_{Qsh} + j\Delta V_{Dsh}) \\ &\quad -j(V_{Qsho} + jV_{Dsho})\Delta B_{SVC} \end{aligned} \tag{10.17}$$

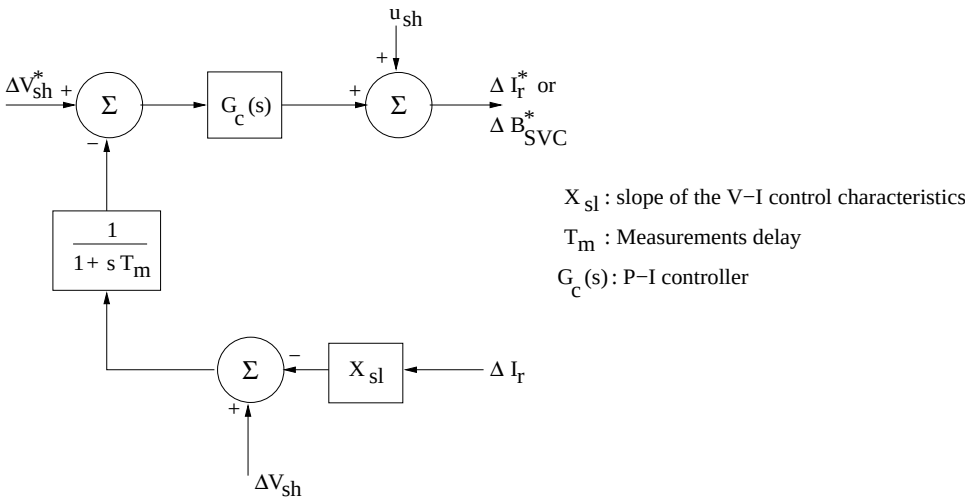

Figure 10.3: STATCOM/SVC Voltage Regulator

$$\begin{aligned} \Delta I_{Qsh} + j\Delta I_{Dsh} &= j(\cos\theta_{sho} + j\sin\theta_{sho})\Delta I_r \\ &\quad + jI_{ro}(-\sin\theta_{sho} + j\cos\theta_{sho})\Delta\theta \end{aligned} \tag{10.18}$$

where

$$\theta_{sh} = \tan^{-1}\left(\frac{V_{Dsh}}{V_{Qsh}}\right)$$

Note that I_{sh} is assumed to be the phasor of the injected current by the shunt controllers.

Series FACTS Controllers

The series FACTS controllers are (a) TCSC and (b) SSSC. While a TCSC can be represented by a variable reactance device, SSSC is a variable reactive voltage device. In general, a series FACTS controller is represented by a functional (control) block diagram as shown in Fig. 10.4. Here, the power scheduling controller can be either a (i) constant current (CC) type or (ii) constant angle (CA) type as discussed in chapter 4. Actually the latter is strictly a constant line (voltage) drop controller which regulates currents in the parallel paths. The CC and CA controllers are shown in Fig. 10.5.

The plant transfer functions for the series FACTS controllers are also represented by a single time constant transfer functions. $x_{se}(1)$ for a TCSC is ΔX_{TCSC} whereas it is equal to ΔV_r for a SSSC. The state and output equations for a series FACTS controller can be written as

$$\dot{x}_{se} = [A_{se}]x_{se} + [B_{se}]\Delta I_{se} + [E_{se}]u_{se} \tag{10.19}$$

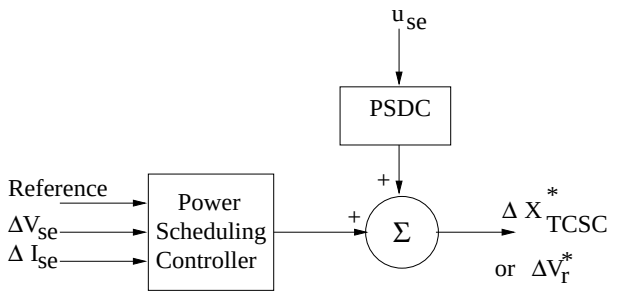

Figure 10.4: Functional block diagram of series FACTS controller

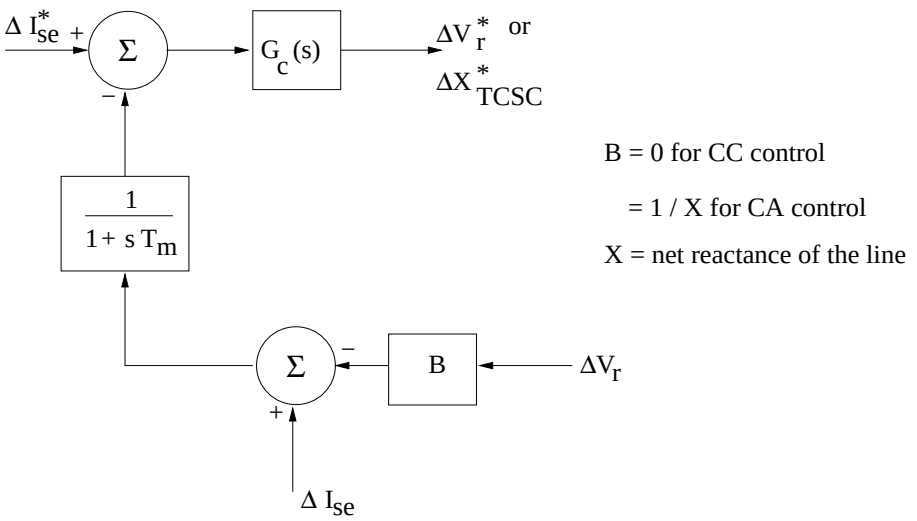

Figure 10.5: CC/CA controller for series FACTS

$$\Delta V_{se} = [C_{se}]x_{se} + [D_{se}]\Delta I_{se} \tag{10.20}$$

where

$$\Delta V_{se} = [\Delta V_{Qse}\ \Delta V_{Dse}]^t, \quad \Delta I_{se} = [\Delta I_{Dse}\ \Delta I_{Qse}]^t$$

The output equation can be derived from the complex equation given by
(a) For a TCSC:

$$\begin{aligned}(\Delta V_{Qse} + j\Delta V_{Dse}) &= -jX_{TCSCo}(\Delta I_{Qse} + j\Delta I_{Dse}) \\ &\quad -j\Delta X_{TCSC}(V_{Qseo} + jV_{Dseo})\end{aligned} \tag{10.21}$$

(b) For a SSSC:

$$\begin{aligned}(\Delta V_{Qse} + j\Delta V_{Dse}) &= -jV_{ro}(-\sin\phi_{seo} + j\cos\phi_{seo})\Delta\phi_{se} \\ &\quad -j\Delta V_r(\cos\phi_{seo} + j\sin\phi_{seo}) \\ &\quad +jX_t(\Delta I_{Qse} + j\Delta I_{Dse})\end{aligned} \tag{10.22}$$

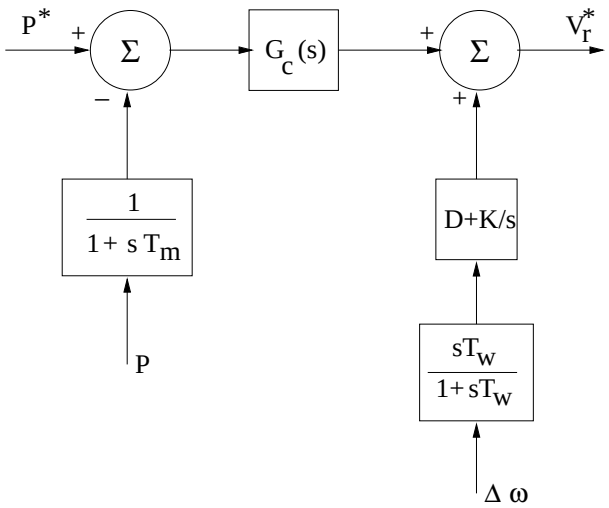

Figure 10.6: Power flow and modulation controller of UPFC

Note that a positive value of V_r implies that the SSSC is operating in the capacitive mode. ΔV_{se} is defined as a voltage drop in the direction of current flow. X_t is the leakage reactance of the coupling transformer of SSSC.

Modelling of UPFC

As discussed in chapter 8, a UPFC can inject real voltage (V_p), reactive voltage (V_r) in series with the line in addition to controlling the shunt reactive current (I_r) as in a STATCOM. However, unlike in a STATCOM, a real current (I_p) also flows in the shunt branch of the UPFC to meet the power requirements of the series branch.

For small signal stability studies, it is adequate to represent the UPFC by the following equations.

$$V_p = \frac{1}{1+sT_p} \cdot V_{pref} \tag{10.23}$$

$$V_q = \frac{1}{1+sT_p} \cdot V_{rref} \tag{10.24}$$

$$I_r = \frac{1}{1+sT_p} \cdot I_{rref} \tag{10.25}$$

The reference variables, in general, are the outputs of a Multi-Input Multi-Output (MIMO) controller, although decoupled controllers can also be used [33]. For example, controller for V_r that regulates the power flow in the line in addition to providing modulation for the damping of power swings, is shown in Fig. 10.6.

It is possible to express the linearized state and output equations of a UPFC as follows

$$\begin{aligned}
\dot{x}_{UPFC} &= [A_U]x_{UPFC} + [B_U^1]\Delta V_U^1 + [B_U^2]\Delta I_U^{se} + [E_U]u_{UPFC} && (10.26)\\
\Delta I_U^{sh} &= [C_U^{sh}]x_{UPFC} + [D_U^{sh}]\Delta V_U^1 + [D_U^{se}]\Delta I_U^{se} && (10.27)\\
\Delta V_U^{se} &= [C_U^{se}]x_{UPFC} + [D_U^{se}]\Delta I_U^{se} && (10.28)
\end{aligned}$$

The above equations are derived from the controller transfer functions in addition to the following algebraic equations

$$\begin{aligned}
(V_{QU}^{se} + jV_{DU}^{se}) &= jX_t(I_{QU}^{se} + jI_{DU}^{se}) \\
&\quad -(V_p + jV_r)(\cos\phi_{se} + j\sin\phi_{se}) && (10.29)\\
(I_{QU}^{sh} + jI_{DU}^{sh}) &= -(I_p - jI_r)(\cos\theta_{sh} + j\sin\theta_{sh}) && (10.30)\\
I_p &= \frac{V_p I^{se}}{V_1} && (10.31)
\end{aligned}$$

where

$$\begin{aligned}
V_1 &= \sqrt{(V_{DU}^{sh})^2 + (V_{QU}^{sh})^2} \\
I^{se} &= \sqrt{(I_{DU}^{se})^2 + (I_{QU}^{se})^2} \\
\phi_{se} &= \tan^{-1}\left(\frac{I_{DU}^{se}}{I_{QU}^{se}}\right), \quad \theta_{sh} = \tan^{-1}\left(\frac{V_{DU}^{sh}}{V_{QU}^{sh}}\right)
\end{aligned}$$

In obtaining the linearized equations of the above algebraic equations, the following symbols are used.

$$\begin{aligned}
\Delta V_U^1 &= [\Delta V_{QU}^{sh}\ \Delta V_{DU}^{sh}]^t, \quad \Delta V_U^{se} = [\Delta V_{QU}^{se}\ \Delta V_{DU}^{se}]^t, \\
\Delta I_U^{sh} &= [\Delta I_{DU}^{sh}\ \Delta I_{QU}^{sh}]^t, \quad \Delta I_U^{se} = [\Delta I_{DU}^{se}\ \Delta I_{QU}^{se}]^t,
\end{aligned}$$

Interfacing of Component Models with the Network Model

Note that each dynamic component (shunt or series connected) is modelled individually and expressed in terms of a pair of differential and algebraic equations. The equations for the individual components are separate (decoupled) and they are interconnected only through the network (algebraic) equations (10.8) or (10.11) (including the static loads). In interfacing the shunt dynamical devices with the network, we use an interconnection matrix P_{sh} which has $2n \times 2n_{sh}$ scalar elements where n_{sh} is the number of shunt devices. Actually, if we assume that each element of P_{sh} as a 2×2 submatrix, then there are $n \times n_{sh}$ elements in P_{sh}. If j^{th} shunt device is connected to i^{th} bus, then the $(i,j)^{th}$ submatrix of P_{sh} is defined as

$$P_{sh}(i,j) = \begin{bmatrix} 1 & 0 \\ 0 & 1 \end{bmatrix} \qquad (10.32)$$

Also,

$$\Delta V_{sh} = P_{sh}^t \Delta V \tag{10.33}$$

If a series connected dynamic device j is connected between f_j^{th} and t_j^{th} node, we can define the $(f_j, j)^{th}$ and $(t_j, j)^{th}$ submatrices of an interconnection matrix P_{se} which has $n \times n_{se}$ submatrices (n_{se} is the number of series devices). We define

$$P_{se}(f_j, j) = -P_{se}(t_j, j) = \begin{bmatrix} 1 & 0 \\ 0 & 1 \end{bmatrix} \tag{10.34}$$

We also have,

$$\Delta V_{se} = P_{se}^t \Delta V \tag{10.35}$$

Note that UPFC contributes to both shunt and series dynamical components.

The total injected current vector at the network buses is given by

$$\Delta I = [P_{sh}]\Delta I_{sh} - [P_{se}]\Delta I_{se} \tag{10.36}$$

Note that the currents (ΔI_{sh}) in the shunt dynamical devices are treated as injections. In series devices, the current flows away from the bus f.

If we ignore the coupling between the shunt and series (converter) devices in UPFC (if the matrix $[D_U^{se}]$ in Eq. (10.26) is assumed to be a null matrix), we can derive the final state equation for the combined system as

$$\dot{X} = [A_T]X + [E]U \tag{10.37}$$

where X is a collection of state variables given by

$$\begin{aligned} X &= [x_{sh1}^t \; x_{sh2}^t \; \cdots \; x_{shn_{sh}}^t \; x_{se1}^t \; x_{se2}^t \; \cdots \; x_{sen_{se}}^t]^t \\ &= [X_{sh}^t \; X_{se}^t]^t \end{aligned}$$

$$\begin{aligned} [A_T] &= [A] + [B][P]^t[W]^{-1}[P][C] \\ [A] &= Diag[A_{sh}^1 \; A_{sh}^2 \; \cdots \; A_{sh}^{n_{sh}} \; A_{se}^1 \; A_{se}^2 \; \cdots \; A_{se}^{n_{se}}] \\ &= Diag[A_{SH} \; A_{SE}] \\ [B] &= \begin{bmatrix} B_{SH}P_{sh}^t \\ B_{SE} \end{bmatrix}, \quad [C] = \begin{bmatrix} P_{sh}[C_{SH}] & [0] \\ [0] & [C_{SE}] \end{bmatrix} \\ [B_{SH}] &= Diag[B_{sh}^1 \; B_{sh}^2 \; \cdots \; B_{sh}^{n_{sh}}], \quad [C_{SH}] = Diag[C_{sh}^1 \; \cdots \; C_{sh}^{n_{sh}}] \\ [B_{SE}] &= Diag[B_{se}^1 \; B_{se}^2 \; \cdots \; B_{se}^{n_{se}}], \quad [C_{SE}] = Diag[C_{se}^1 \; \cdots \; C_{se}^{n_{se}}] \\ [W] &= \begin{bmatrix} [Y_m] & [P_{se}] \\ [P_{se}]^t & [Z] \end{bmatrix} \\ [Y_m] &= [Y'] + [P_{sh}][Y_{sh}][P_{sh}]^t \\ [Y_{sh}] &= Diag[-D_{sh}^1 \; \cdots \; -D_{sh}^{n_{sh}}] \\ [Z] &= Diag[-D_{se}^1 \; \cdots \; -D_{se}^{n_{se}}] \\ [E] &= Diag[E_{sh}^1 \; \cdots \; E_{sh}^{n_{sh}} \; E_{se}^1 \; \cdots \; E_{se}^{n_{se}}] \end{aligned}$$

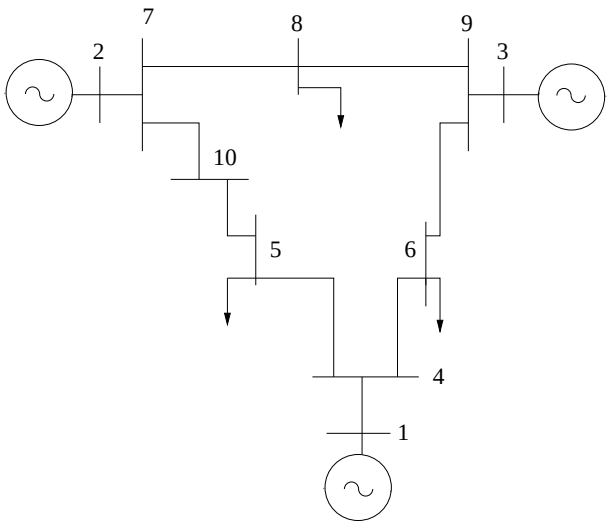

Figure 10.7: Three machine system

U is a collection of all the control variables

$$U^t = [u_{sh}^{1t} \ \cdots \ (u_{sh}^{n_{sh}})^t \ u_{se}^{1t} \ \cdots \ (u_{se}^{n_{se}})^t]$$

If there are no series FACTS controllers in the system, then $[A_{SE}]$ is a null matrix and the system state equation reduces to

$$\dot{X}_{SH} = [A_{SH}]X_{SH} + [B_{SH}][P_{sh}]^t[Y_m]^{-1}[P_{sh}][C_{SH}]X_{SH} \tag{10.38}$$

Note that the matrices $[A_{SH}]$, $[B_{SH}]$ and $[C_{SH}]$ are block diagonal in structure. $[P_{sh}]$ is a sparse matrix with elements 0 and 1. $[Y_m]$ is also a sparse matrix which is a modified bus admittance matrix due to the presence of the shunt dynamical systems. The inclusion of a new shunt FACTS controller can be easily handled with minimum computations. Similar comments apply even if series controllers are considered.

Example 1 [30]

Consider the case study of a 3 machine system [43] shown in Fig. 10.7. All the 3 generators are represented by two-axis model with one damper winding on the q-axis. Turbine governors are neglected and the excitation systems are represented by single time constant models. The loads are assumed to be constant power type. It is possible to refer the generator rotor angles with respect to a reference machine. For the three machine system there are two state variables corresponding to the two relative angles. The total number of state variables for the 3 generators is 14.

A TCSC or a SSSC is connected in series with the line connecting bus 5 to bus 7, and located near bus 5. Note that bus 10 is the midpoint of

Table 10.1: Eigenvalues for swing modes.

Case	Eigenvalue for Mode 1	Eigenvalue for Mode 2
Fixed series compensation	$-0.8459 \pm$ j12.7771	$-0.2808 \pm$ j8.6648
TCSC (CC Control)	$-0.8579 \pm$ j12.7616	$-1.6473 \pm$ j6.9240
TCSC (CA Control)	$-0.8416 \pm$ j12.7856	$-0.0788 \pm$ j9.1971
SSSC (CC Control)	$-0.8572 \pm$ j12.7606	$-1.5570 \pm$ j6.8530
SSSC (CA Control)	$-0.8419 \pm$ j12.7858	$-0.0926 \pm$ j9.2032

line 7-5. The results are also compared with the case when the series compensation is provided by a fixed capacitor. The system initial conditions are chosen to be same for all the three types of compensation (i.e. the quiescent compensating reactance is assumed to be same for the three cases). The SSSC is used with a fixed capacitor and the quiescent value of the reactive voltage output of SSSC is assumed to be zero. Both CC and CA controllers are considered for TCSC and SSSC. The data for the series compensation schemes are:

$$X_{FC} = X_{TCSCo} = 0.0644, \quad T_m = 0.02, \quad T_p = 0.02, \quad B = \frac{1}{0.1610}$$

The eigenvalues corresponding to the three cases (i) fixed capacitor, (ii) TCSC, (iii) SSSC are shown in Table 10.1. For TCSC and SSSC, the results are shown for both CC and CA controls. The integral gain of 5 is assumed for CC control while it is assumed to be -5 for CA control. Note that in the latter case, the capacitive compensation is to be reduced when the error is positive (when the voltage drop across the line is less than the reference value).

The results shown in Table 10.1 indicate that the CC controller increases damping torque while reducing the synchronizing torque. The reverse is true for CA control. There are no significant differences between the results of TCSC and SSSC although the latter gives slightly better damping for the CA control. For CC control, TCSC results in better damping compared to SSSC. In all cases it is observed that a TCSC or SSSC located in line 5-7 has effect primarily on mode 2. The influence of location of the series controller on a particular swing mode is discussed in section 10.6.

10.4 Design of Damping Controllers

We will primarily consider methods that are based on eigenvalue sensitivities [12,19,20,27]. To simplify the presentation, we will consider the design of a single controller with one input and output. We essentially impose a constraint of decentralized control with individual controllers that utilize signals synthesized from local measurements. The problem of coordinated control with multiple controllers will be taken up later.

Consider a linear system expressed in the state space form:

$$\dot{x} = [A]x + bu \tag{10.39}$$
$$y = cx + du \tag{10.40}$$

where u and y are scalars. b is a column vector, c is a row vector and d is a scalar.

We wish to design a feedback controller with input signal y and output of u. For example, if we consider a Power Oscillation Damping (POD) control for a TCSC, the signal y could be the line current, power or any other signal based on local measurements. The system input u (sum of the output of the feedback controller and reference input r) is the modulated value (ΔX_{TCSC}) of the TCSC reactance. It is convenient to express the transfer function (in the Laplace domain) of the controller (with $r = 0$) as

$$\frac{U(s)}{Y(s)} = H(s, q) \tag{10.41}$$

where q is the vector of tunable controller parameters. The block diagram of the system with feedback controller is shown in Fig. 10.8.

The sensitivity of a closed loop eigenvalue (pole) λ_i with respect to a parameter q_j is given by

$$\frac{\partial \lambda_i}{\partial q_j} = R_i \left. \frac{\partial H(s, q)}{\partial q_j} \right|_{s=\lambda_i} \tag{10.42}$$

where R_i is the residue of the closed loop transfer function corresponding to λ_i defined by

$$R_i = (w_i^t b) \frac{1}{[1 - H(\lambda_i, q)d]^2} (cv_i) \tag{10.43}$$

where v_i and w_i are the right and left eigenvectors associated with λ_i and satisfy the following constraint.

$$w_i^t v_i = 1 \tag{10.44}$$

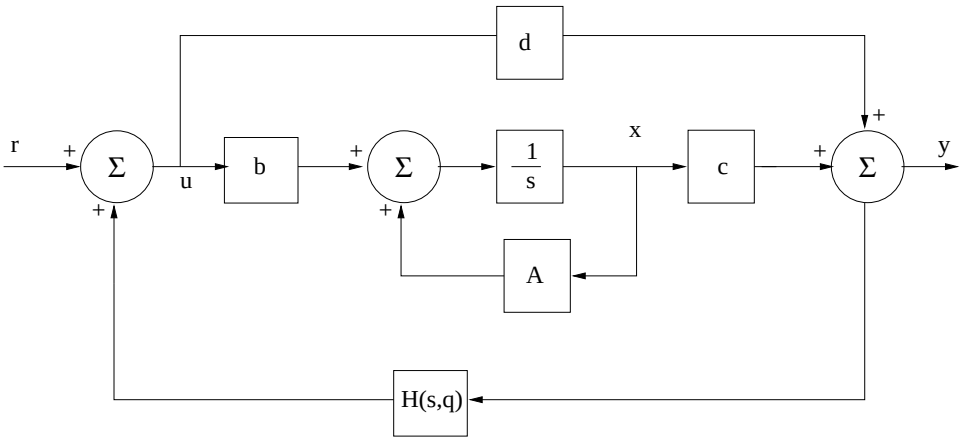

Figure 10.8: Block diagram of the system

$(w_i^t b)$ is termed as the modal controllability factor while (cv_i) is termed as the observability factor. The residue R_i is simply the product of these two factors if either $d = 0$ or $H(s, q) = 0$ (there is no feedback control).

A specific transfer function of a damping controller (used for PSS design) is

$$H(s,q) = K\frac{sT_W}{1+sT_W}\left[\frac{1+sT_1}{1+sT_2}\right]^m \tag{10.45}$$

where m is usually 1 or 2. T_W is called as the washout circuit time constant. The transfer function of the washout circuit is $\frac{sT_W}{1+sT_W}$ and it is used primarily to eliminate steady state bias in the output of the controller. The washout circuit can be generally ignored in the controller design. Thus, there are only 3 tunable parameters in the controller transfer function of Eq. (10.45) if m is specified. The controller essentially consists of m stages of lead-lag network. The objective of a lead-lag network is to introduce a phase advance (ϕ) at the centre frequency (ω_c) given by [1]

$$\phi = \tan^{-1}\sqrt{n} - \tan^{-1}\left(\frac{1}{\sqrt{n}}\right) \tag{10.46}$$

where $n = \frac{T_1}{T_2}$. The centre frequency (ω_c) is defined as $\omega_c = \frac{1}{\sqrt{T_1 T_2}}$ and the phase lead of the transfer function $\left(\frac{1+sT_1}{1+sT_2}\right)$ is maximum at this frequency. Generally, ω_c is chosen as the frequency of the critical electromechanical mode that requires damping.

The objective of the lead-lag network is to ensure that the eigenvalue sensitivity $\frac{d\lambda_i}{dK}$ is negative real (and has no imaginary component). This will result in the locus of the critical eigenvalue moving to the left in the complex plane (providing pure damping without affecting the frequency of

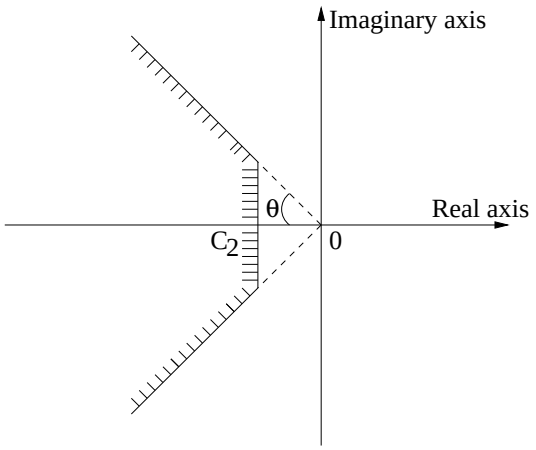

Figure 10.9: Permissible region for the closed loop eigenvalues in the complex left half plane

the oscillation). Thus, we get the requirement,

$$\phi = [\pm 180^\circ - \arg(R_i)]/m \tag{10.47}$$

We can show that, (from Eq. (10.46))

$$\tan\phi = \frac{(n-1)}{2\sqrt{n}} \tag{10.48}$$

The solution of the above equation gives

$$n = \frac{(1+\sin\phi)^2}{\cos^2\phi} = \frac{(1+\sin\phi)^2}{1-\sin^2\phi} = \frac{1+\sin\phi}{1-\sin\phi} \tag{10.49}$$

Remarks

1. As $K \to 0$, the eigenvalue λ_i is obtained as the open loop pole which can be easily calculated. As K is increased from zero, the sensitivity changes along with λ_i. Thus, it would be necessary to track the root locus as K is varied. The optimal value of K is one when $Re[\frac{d\lambda_i}{dK}] = 0$ assuming that the remaining eigenvalues lie in the permissible region in the complex left half plane. A typical permissible region is shown in Fig. 10.9.

   Assuming there are N eigenvalues, the constraints defining the permissible region are,

$$\sigma_i \le C_2 \quad i = 1, 2, N$$
$$D_i = \frac{-\sigma_i}{\sqrt{\sigma_i^2 + \omega_i^2}} \ge C_1 = \cos\theta$$

   where D_i is damping ratio.

2. When a system is described by Differential-Algebraic Equations (DAE), we can express the linearized equations as

$$\begin{bmatrix} \dot{x} \\ 0 \end{bmatrix} = \begin{bmatrix} A_{11} & A_{12} \\ A_{21} & A_{22} \end{bmatrix} \begin{bmatrix} x \\ \Delta V \end{bmatrix} + \begin{bmatrix} 0 \\ b_2 \end{bmatrix} u \tag{10.50}$$

where $\Delta V = [\Delta V_Q \Delta V_D]^t$

$$y = [0 \; c_2] \begin{bmatrix} x \\ \Delta V \end{bmatrix} + du \tag{10.51}$$

The residue R_i is now computed as

$$R_i = (w_{i,\Delta V}^t b) \frac{1}{[1 - H(\lambda_i, q).d]^2} (c_2 v_{i,\Delta V}) \tag{10.52}$$

where $v_{i,\Delta V}$ and $w_{i,\Delta V}$ are the components of the right and left eigenvectors corresponding to the non-state variables, ΔV. (Note that the concept of eigenvectors can be extended to the system described by DAE).

3. The location of a damping controller can be chosen based on the criterion of $|R_i|$. The residue is a function of the location (say k). If $|R_{ik^*}|$ is maximum among all values of k considered, then k^* is the optimal location.

4. The participation factor is a measure of participation of a state variable x_j in a mode corresponding to λ_i and is defined as

$$p_{ji} = v_{ij} w_{ij}$$

with the property $\sum_i p_{ji} = 1$. Also p_{ji} is the sensitivity of the eigenvalue λ_i with respect to $A(j, j)$, the diagonal element of the $[A]$ matrix.

Tuning of Supplementary Modulation Controllers

When multiple SMCs are considered for the damping of several critical swing modes in a power system, the tuning of the SMCs has to be coordinated. An optimal method for this is described next.

The control parameters to be tuned are obtained as the solutions to a constrained optimization problem defined as follows:

$$\min_q \sum_{j=1}^{m} W_j \sigma_j \tag{10.53}$$

subject to

$$D_i = \frac{-\sigma_i}{\sqrt{\sigma_i^2 + \omega_i^2}} \geq C_1 \tag{10.54}$$

$$\sigma_i \leq C_2, \quad i = 1, 2, 3, \ldots, N \tag{10.55}$$

where m = total number of modes of interest, σ_i = real part of λ_i (i^{th} eigenvalue), ω_i = imaginary part of λ_i, D_i = damping ratio of λ_i, W_j = a positive weight associated with j^{th} swing mode, q = vector of control parameters. q is bound both from below and above. The lower bounds are usually positive or zero.

Arbitrary choices of C_1 and C_2 can result in infeasible solution. The problem can also be solved by successive Linear Programming (LP) after linearizing Eqs (10.53) to (10.55) and expressing $\Delta\sigma$ in terms of Δq (perturbations in the control parameters) using eigenvalue sensitivities.

An Alternative Approach [12,17]

We have earlier considered the design of SMC based on eigenvalue sensitivities. The computations of residues of the critical modes determines not only the best locations of SMC, but also the phase compensation required (if any). The gains of SMCs can be obtained by tuning using the procedure outlined. The control parameters can also include other parameters in addition to the gains.

An alternative approach is outlined here. The system dynamics (described in Eqs (10.39) and (10.40) is separated into two connected components - the first one captures the critical mode(s) of interest. The rest of the system dynamics forms the second component. Thus, we can rewrite the system equations as follows:

$$\begin{aligned} \dot{x}_1 &= [A_1]x_1 + b_1 u_1 \\ y_1 &= c_1 x_1 \end{aligned} \tag{10.56}$$

$$\begin{aligned} \dot{x}_2 &= [A_2]x_2 + b_2 u_2 + b_{2c} u \\ y_2 &= c_2 x_2 \end{aligned} \tag{10.57}$$

$$y = c_{1c} x_1 + c_{2c} x_2 \tag{10.58}$$

The simplest model of subsystem 1 describes a single swing mode described by

$$x_1 = [\Delta\delta_{mi} \ \Delta\bar{\omega}_{mi}]^t, \quad u_1 = \Delta T_{mi} \tag{10.59}$$

$$[A_1] = \begin{bmatrix} 0 & \omega_B \\ \frac{-k_{mi}}{2H_{mi}} & \frac{-D_{mi}}{2H_{mi}} \end{bmatrix}, \quad b_1 = \begin{bmatrix} 0 \\ -1 \end{bmatrix}$$

when δ_{mi} and $\bar{\omega}_{mi}$ are the i^{th} modal angle and (per unit) rotor speed respectively. D_{mi} is the modal damping and H_{mi} is the modal inertia (of mode i).

ω_B is the base (rated) speed in radians/second. The modal frequency (ω_i) is approximately given by

$$\omega_i = \sqrt{\frac{\omega_B k_{mi}}{2H_{mi}}} \text{ rad/sec}$$

ΔT_{mi} is the perturbation in the modal torque.

In Eqs. (10.56) and (10.57), the input u_2 is the output y_1 of subsystem 1. Similarly, u_1 is the output y_2 of the subsystem 2. We can define 4 transfer functions for the special case where x_1 contains two variables as defined earlier. Assuming $y_1 = \Delta\delta_{mi}$ and $c_{1c}x_1 = r_i\Delta\omega_{mi}$, we can derive four transfer functions defined below:

$$K_{ci}(s) = \frac{Y_2(s)}{U(s)} = c_2[sI - A_2]^{-1}b_{2c} \tag{10.60}$$

$$K_{oi}(s) = \frac{Y(s)}{\Delta\omega_{mi}(s)} = r_i + c_{2c}[sI - A_2]^{-1}b_2\omega_B \tag{10.61}$$

$$K_{mi}(s) = \frac{Y_2(s)}{\Delta\delta_{mi}(s)} = k_{mi} + c_2[sI - A_2]^{-1}b_2 \tag{10.62}$$

$$K_{ILi}(s) = \frac{Y(s)}{U(s)} = c_{2c}[sI - A_2]^{-1}b_{2c} \tag{10.63}$$

The transfer function of the Power Swing Damping Control (PSDC) or SMC is defined as

$$PSDC(s) = \frac{U(s)}{Y(s)} \tag{10.64}$$

The block diagram of the system including PSDC is shown in Fig. 10.10. In reference [12], the authors have proposed three indices to evaluate the effectiveness of a feedback signal. They are the controller phase influence (CPI), the maximum damping influence (MDI) and the natural phase influence (NPI) which are defined as

$$\begin{aligned} CPI(i) &= -[Arg[K_{ci}(j\omega_i)] + Arg[K_{oi}(j\omega_i)] \\ MDI(i) &= \frac{|K_{ci}(j\omega_i)||K_{oi}(j\omega_i)|}{2\sqrt{10}|K_{ILi}(j\omega_i)|} \\ NPI(i) &= -[CPI(i) + Arg[K_{ILi}(j\omega_i)]] \end{aligned}$$

where ω_i is the frequency of the i^{th} mode. The effective transfer function in the control loop is given by

$$K_{ei}(s) = \frac{K_{ci}(s)PSDC(s)K_{oi}(s)}{(1 - PSDC(s)K_{ILi}(s))} \tag{10.65}$$

When the controller gain is sufficiently small such that $|PSDC(j\omega_i)K_{ILi}(j\omega_i)| \ll 1$, then pure damping of the mode i is obtained

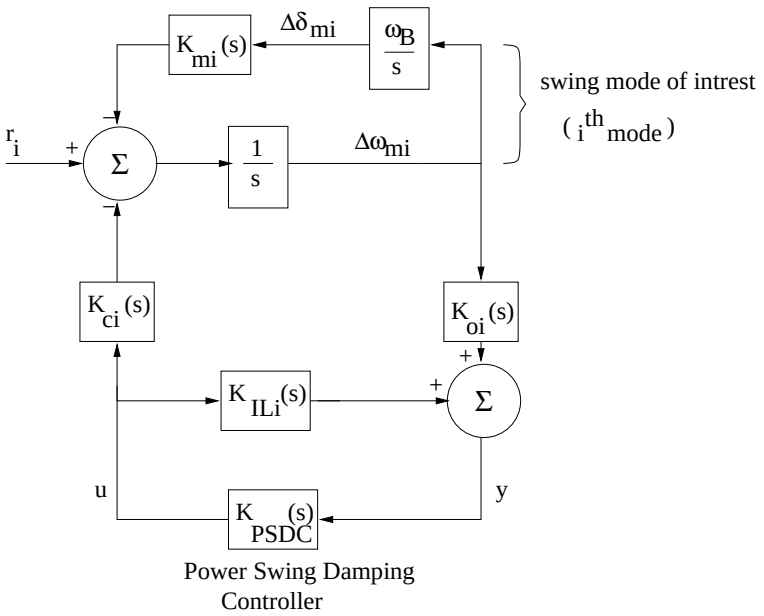

Figure 10.10: System block diagram with PSDC to damp a swing mode i

if the phase of PSDC ($j\omega_i$) is set equal to CPI. The MDI index is a measure of the maximum eigenvalue shift achievable assuming the controller gain is limited to $\frac{|K_{ILi}(j\omega_i)|}{\sqrt{10}}$. The $\sqrt{10}$ factor assures a gain margin of 10 dB. The NPI index gives the phase information on the eigenvalue shift due to the controller. For $0 > NPI > -90°$, the effect of the controller is to increase both damping and synchronizing torques.

10.5 Modal Transformation of Swing Equations

In the previous section, we introduced modal quantities such as modal inertia, frequency etc. These are obtained by transformation of the swing equations of all the generators in the system. Neglecting damping, we can express the swing equations in the matrix form as

$$[M]\frac{d^2\delta}{dt^2} = T_m - T_e \tag{10.66}$$

Linearizing the above equation, we get

$$[M]\frac{d^2\Delta\delta}{dt^2} = -[K]\Delta\delta - \Delta T_e' \tag{10.67}$$

where $[K] = \left[\frac{\partial T_e}{\partial \delta}\right]$ evaluated at the equilibrium point. Note that in steady state, $T_e = P_e$ (in per unit). The mechanical torque (T_m) is assumed to be

constant such that $\Delta T_m = 0$. The change in the electrical torque ($\Delta T'_e$) is a function of other variables.

Defining a transformation matrix $[Q]$ such that $\Delta\delta = [Q]\Delta\delta_m$, it is possible to simultaneously diagonalize matrices $[M]$ and $[K]$ if we select

$$[Q] = [M]^{-1/2}[P] \tag{10.68}$$

where $[P]$ is a matrix whose columns are eigenvectors of the real symmetric matrix $[K'] = [M]^{-1/2}[K][M]^{-1/2}$. Substituting Eq. (10.68) in (10.67) and pre-multiplying both sides by $[Q]^t$, we get

$$[M_m]\frac{d^2\Delta\delta_m}{dt^2} + [K_m]\Delta\delta_m = -[Q]^t\Delta T'_e \tag{10.69}$$

where

$$[K_m] = [Q]^t[K][Q], \quad [M_m] = [Q]^t[M][Q]$$

$[M_m]$ is termed as the modal inertial matrix. However, the elements of the matrix are not unique unless we put constraints on the choice of $[P]$ (eigenvectors of K'). (Note that the eigenvectors are not unique). If we assume that each eigenvector of $[Q]$ has the element 1 corresponding to the generator j, then we can say that the modal inertias are defined with reference to generator j. Note that the matrix $[Q]$ becomes unique with the constraint that the jth row has all the elements equal to unity. This concept has been explained in [42] and utilized to locate the PSS for damping of swing modes since the change in the decrement factor of a mode is approximately equal to

$$\Delta\sigma_i = \frac{T_{Di}}{4H_{mi}} \tag{10.70}$$

where T_{Di} is the damping torque (coefficient) introduced by a damping controller (such as PSS). The eigenvalue shift is maximum when H_{mi} is minimum. Hence, the best location for PSS is the generator where H_{mi} is minimum.

Example 2

Consider the three machine system shown in Fig. 10.7. At the operating point (without PSS), the eigenvalues corresponding to the two swing modes are $\lambda_{1,2} = -0.4510 \pm j13.157$ and $\lambda_{3,4} = -0.0394 \pm j\ 8.585$. The values of the modal inertias of the two swing modes are shown in Table 10.2.

It is interesting to note that the mode M1 is best damped by PSS at generator 3. The PSS at generator 1 has practically no effect on M1. The lower frequency mode (M_2) is best damped by PSS at generator 2.

Table 10.2: Modal inertias for 3-machine system.

Modal Frequency (rad/sec)	Gen. 1	Gen. 2	Gen. 3
12.664 (M1)	3300.90	31.92	3.80
8.313 (M2)	85.17	10.56	25.81

Table 10.3: Modal inertias for 4-machine system.

Modal Frequency (rad/sec)	Gen. 1	Gen. 2	Gen. 3	Gen. 4
7.53 (M1)	0.615	0.538	209.16	20227
6.91 (M2)	174.73	7746	0.634	0.709
4.14 (M3)	0.949	1.212	1.653	1.289

Example 3

The modal inertias of the 4 machine system (shown in Fig. 10.18) described in [11,1] are shown in Table 10.3 for all the 3 swing modes.

Here, M_1 and M_2 are the two local modes corresponding to the areas 1 and 2 respectively. M3 is the interarea mode. It is interesting to observe that PSS for damping a local mode must be located at the generators belonging to the area (G1 and G2 for area 1, and G3 and G4 for area 2). On the other hand, the low frequency interarea mode (M3) can be damped by PSS located at any of the four generators (as the modal inertias for all the generators lie within a narrow range).

Remarks

1. The matrix $[K]$ is singular matrix with an eigenvalue of zero. This corresponds to a mode (of frequency zero) in which all generators participate equally. The modal inertia for this mode zero is the sum of the inertias of all the generators. This is unaffected by the choice of the reference generator.
2. Unless the network is assumed to be lossless, the matrix $[K]$ is not strictly symmetric. However, it was found adequate to approximate $[K]$ by its symmetrical component $\frac{[K]+[K]^t}{2}$ and modify the elements to ensure that the elements of each row add up to zero.
3. The concept of modal inertia is adopted from the analysis of SSR which

considers a multimass model of the generator mechanical system where the elastic shaft sections are modelled as springs. Here, each machine is modelled as a single mass, but is connected to the neighbouring masses by equivalent springs represented by synchronizing torque coefficients. In extending the concept to the study of low frequency oscillations, it is necessary to make some minor approximations (about the nature of $[K]$ matrix) while the modal inertias for the torsional modes are defined exactly. Also note that the $[K]$ matrix for the shaft system is constant while it varies as the operating point changes for the transmission network.

It would be interesting to pose the question whether the concept of modal inertias can be extended further. By using a network analogy for modelling the system dynamics of a lossless network connected to generators modelled by classical models, it is possible to get an insight into the problem of identifying best locations for both shunt and series FACTS controllers. It is also possible to postulate general control laws for both series and shunt FACTS controllers based on appropriate control signals. This is taken up in the next section.

10.6 Damping of Power Oscillations Using Series FACTS Controllers

The objectives of the analysis presented in this section are to present a unified framework for the design of damping controllers on series FACTS devices such as TCSC, SSSC and series converters in UPFC. The analysis is based on a simplified model that enables the derivation of control laws and formulation of indices to evaluate the effectiveness of location of the controllers. The analysis can be validated using case studies with detailed system models [15,33].

The following assumptions are made in the analysis:

1. A synchronous generator is represented by the classical model of a constant voltage source behind (constant) transient reactance.
2. The real power drawn by loads is independent of the bus voltage magnitude, but varies linearly with bus frequency.
3. The electrical network is assumed to be lossless.
4. The mechanical torques acting on the generator rotors are constant and the mechanical damping is neglected.
5. The bus voltage magnitudes are assumed to be constants.

6. There is only one line connected between a pair of specified nodes (say i and j). Note that the parallel lines can be clubbed together and represented by an equivalent line.

Let us consider the electrical network made up of only series elements including the transient reactances of the n_g number of generators. We will assume that there are n number of nodes in the network excluding n_g internal buses of the generators. Let there be n_b number of series elements including the n_g transient reactances. If we consider a branch k connected across nodes i and j, the power flow in steady state is given by

$$\begin{aligned} P_k &= \frac{V_i V_j}{x_k} \sin(\phi_i - \phi_j) \\ &= P_k(\phi_k, u_k) \end{aligned} \tag{10.71}$$

where x_k is the effective reactance of the branch k, ϕ_k is the angle across the branch k given by

$$\phi_k = \phi_i - \phi_j$$

u_k is the control variable which may be a reactance in the case of a TCSC connected in the line (or branch) k. It could be reactive voltage if a SSSC is connected in the line. Due to assumption 5, the power flow P_k in line k is a function of two variables ϕ_k and u_k. If no series FACTS controller is connected, then $u_k = 0$.

When we linearize Eq. (10.71), we get

$$\Delta P_k = \frac{\partial P_k}{\partial \phi_k} \Delta\phi_k + \frac{\partial P_k}{\partial u_k} \Delta u_k \tag{10.72}$$

The term $\frac{\partial P_k}{\partial \phi_k}$ can be viewed as a spring constant K_{ij} of a linear spring defined by

$$\Delta T_{ij} = K_{ij}(\Delta\phi_i - \Delta\phi_j) \tag{10.73}$$

With $u_k = 0$, then,

$$K_{ij} = \frac{V_i V_j}{x_k} \cos\phi_{k0} \tag{10.74}$$

where ϕ_{k0} is the operating value of ϕ_k. It is obvious that $K_{ji} = K_{ij}$.

From assumption 1, the generators are modelled by the swing equations given by

$$\begin{aligned} M_i \frac{d^2\delta_i}{dt^2} &= T_{mi} - T_{ei} \\ &= T_{mi} - \frac{E_{gi} V_i \sin(\delta_i - \phi_i)}{x'_{di}}, i = 1, 2, \ldots, n_g \end{aligned} \tag{10.75}$$

where $M_i = \frac{2H_i}{\omega_B}$ is the inertia, δ_i is the rotor angle, E_{gi} is the generated voltage, V_i and ϕ_i are the magnitude and angle of the terminal bus voltage, x'_{di} is the transient reactance of the generator i. It is assumed that the generator buses are numbered first before the load buses. We will also assume that the generator and load buses are mutually exclusive and the load buses include those nongenerator buses with zero loads.

The linearized equation (10.75) is given by,

$$\begin{aligned} M_i \frac{d^2\Delta\delta_i}{dt^2} &= -\frac{E_{gi}V_i}{x'_{di}} \cos(\delta_i - \phi_i)(\Delta\delta_i - \Delta\phi_i) \\ &= -K_{gi}(\Delta\delta_i - \Delta\phi_i) \end{aligned} \tag{10.76}$$

where

$$K_{gi} = \frac{E_{gi}V_i}{x'_{di}} \cos(\delta_i - \phi_i)$$

From assumption 2) we can express the equations corresponding to load buses as follows.

$$0 = T_{ei} - T_{li}, i = 1, 2, \ldots n \tag{10.77}$$

where $T_{li} = \frac{P_{li}}{\bar{\omega}_i}$ is a constant. $\bar{\omega}_i$ is the per unit frequency at bus i. From Eq. (10.77), T_{ei} = constant.

It is possible to express the linearized system equations as,

$$\begin{bmatrix} M\frac{d^2\Delta\delta}{dt^2} \\ 0 \end{bmatrix} = -\begin{bmatrix} K_{gg} & K_{gl} \\ K_{lg} & K_{ll} \end{bmatrix} \begin{bmatrix} \Delta\delta \\ \Delta\phi \end{bmatrix} \tag{10.78}$$

where

$$\begin{aligned} [M] &= Diag[M_1 M_2 \quad M_{n_g}] \\ [K_{gg}] &= Diag[K_{g1} K_{g2} \quad K_{gn_g}] \\ [K_{gl}] &= [-K_{gg}\ 0] = [K_{lg}]^t \end{aligned}$$

$[K_{gl}]$ has dimensions $n_g \times n$. The matrix $[K_{ll}]$ is a symmetric matrix with elements given by

$$K_{ll}(i,j) = -K_{ij}, \quad K_{ll}(i,i) = \sum_{j=1}^{n} K_{ij}$$

It is possible to eliminate $\Delta\phi$ from Eq. (10.78) and derive,

$$[M]\frac{d^2\Delta\delta}{dt^2} = -[K]\Delta\delta \tag{10.79}$$

where,

$$[K] = [K_{gg}] - [K_{gl}][K_{ll}]^{-1}[K_{lg}]$$

It can be shown that $[K]$ is a singular matrix. The system eigenvalues are the square roots of the matrix $[A_2]$ given by

$$[A_2] = -[M]^{-1}[K]$$

The eigenvalues of $[A_2]$ are real negative, except for one eigenvalue which is zero. Note that Eq. (10.79) can be expressed in the state space form given by

$$\begin{bmatrix} \Delta\dot{\delta} \\ \Delta\dot{\omega} \end{bmatrix} = [A_1] \begin{bmatrix} \Delta\delta \\ \Delta\omega \end{bmatrix} = \begin{bmatrix} 0 & I \\ A_2 & 0 \end{bmatrix} \begin{bmatrix} \Delta\delta \\ \Delta\omega \end{bmatrix} \tag{10.80}$$

where I is identity matrix of order n_g. The eigenvalues of $[A_1]$ are $\pm j\omega_i^m$, $i = 0, 1, 2, \ldots (n_g - 1)$. For $i = 0$, $\omega_i^m = 0$ which corresponds to the frequency of Centre of Inertia (COI) defined by

$$\delta_{COI} = \frac{1}{M_T} \sum M_i \delta_i, \quad \omega_{COI} = \frac{1}{M_T} \sum M_i \omega_i \tag{10.81}$$

where $M_T = \sum M_i$.

The eigenvector v_i of the matrix $[A_1]$ corresponding to the eigenvalue $\lambda_i = j\omega_i^m$ can be expressed as

$$v_i = [v_{i\delta}^t \; v_{i\omega}^t]^t$$

It can be shown that

$$v_{i\omega} = j\omega_i^m v_{i\delta} \tag{10.82}$$

A Network Analogy

Equation (10.78) or its reduced form (10.79) represent a mass-spring system. It can be shown that an R-L-C electrical network is analogous to the mechanical system consisting of viscous dampers, mass and springs. Mass is analogous to a capacitance and spring is analogous to an inductor. This is based on analogy between voltage and $\Delta\omega$ (or $\Delta\dot{\phi}$), current and torque. $\Delta\delta$ (or $\Delta\phi$) is analogous to flux linkage. The spring constant K_{ij} is analogous to the reciprocal of inductance.

Neglecting mechanical or load damping, Eq. (10.78) represents an L-C circuit. For a one-port LC network, having the impedance function $Z(s)$ of the form

$$Z(s) = \frac{N(s)}{D(s)} = \frac{(s^2 + \omega_{z1}^2)(s^2 + \omega_{z2}^2)\ldots}{s(s^2 + \omega_1^2)(s^2 + \omega_2^2)\ldots} \tag{10.83}$$

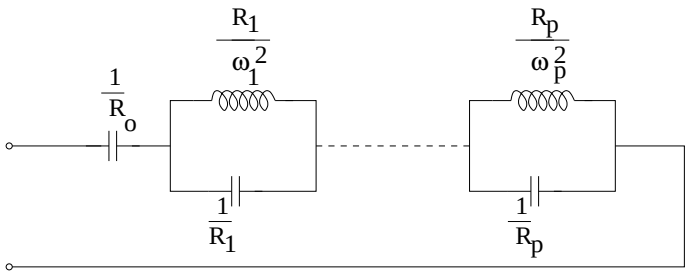

Figure 10.11: One port equivalent circuit of a L-C network

it is possible to represent the impedance function by an equivalent circuit shown in Fig. 10.11. This follows from the partial fraction expansion of $Z(s)$ in the form given by

$$Z(s) = \frac{R_0}{s} + \frac{R_1 s}{s^2 + \omega_1^2} + \cdots \frac{R_p s}{s^2 + \omega_p^2} \tag{10.84}$$

where $R_0, R_2, \ldots, R_p$ are all positive. This follows from the properties of the function $Z(s)$:

1. The degrees of $N(s)$ and $D(s)$ differ exactly by 1
2. $Z(s)$ is an odd function of s, that is $Z(-s) = -Z(s)$.
3. $Z(s)$ has only simple poles and zeroes; all are located interlaced on the imaginary axis (Between any two poles there is a zero and vice versa).
4. The residues at all poles are real and positive.

From the network properties, we note that for the electromechanical system made up of masses and springs, there is an equivalent circuit across any node pair. If we consider a lossless transmission line connected across nodes i and j, we have an equivalent circuit for the one port shown in Fig. 10.12 that takes into account only one swing mode m_i. Since capacitance is analogous to mass, we can define modal inertias for a transmission line (Earlier, we had defined modal inertias at a generator).

In Fig. 10.12, L_k is the equivalent inductance given by

$$L_k = \frac{x_k}{V_i V_j \cos\phi_{ko}} \tag{10.85}$$

Note that L_k is the reciprocal of K_{ij} defined by Eq. (10.74). If $V_i = V_j = 1.0$ and $\cos\phi_{ko} \simeq 1.0$, then $L_k \simeq x_k$. The inductance L_k^{th} is the Thevenin inductance of network (without L_k) viewed from the port i-j when the capacitors in the network (representing the generator rotor masses) are shorted. Note

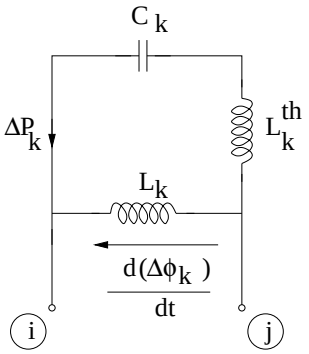

Figure 10.12: An equivalent circuit across port i-j (for swing mode m_i)

that the capacitances in the network can be represented by voltage sources (bus frequency deviations). In Fig. 10.12, the voltage across the equivalent (modal) capacitance is $\frac{d\Delta\phi_k^{th}}{dt}$ assuming that the voltage vector across the capacitances (representing generator masses) is $v_{i\omega}$ which is defined by Eq. (10.82).

In case a damping controller is connected in line k (connected across nodes i and j), there is an additional component in the line current (ΔP_k) given by (see Eq. (10.72)),

$$\Delta P_{kc} = \frac{\partial P_k}{\partial u_k}\Delta u_k = B_k \Delta u_k \tag{10.86}$$

where Δu_k is either ΔX_{TCSCk} or ΔV_{rk} depending on whether a TCSC or SSSC is connected in the line k. Since we have assumed that X_{TCSC} or V_r is considered as positive if it is capacitive, $\frac{\partial P_k}{\partial u_k}$ is also positive.

The constant B_k (assumed to be positive) in Eq. (10.86) is given by

(a) $B_k = \frac{P_{k0}}{x_k}$ for a TCSC and

(b) $B_k \simeq \frac{1}{x_k}$ for a SSSC

If we propose a control law given by

$$\Delta u_k = G_k \frac{d\Delta\phi_k^{th}}{dt} \tag{10.87}$$

where G_k (the proportional gain), is equivalent to a conductance (G_k) across the capacitance as shown in Fig. 10.13. For simplicity, the dependence of C_k on the specific mode (m_i) is not shown in this figure. It is to be noted that L_k and L_k^{th} are independent of the mode and are invariant.

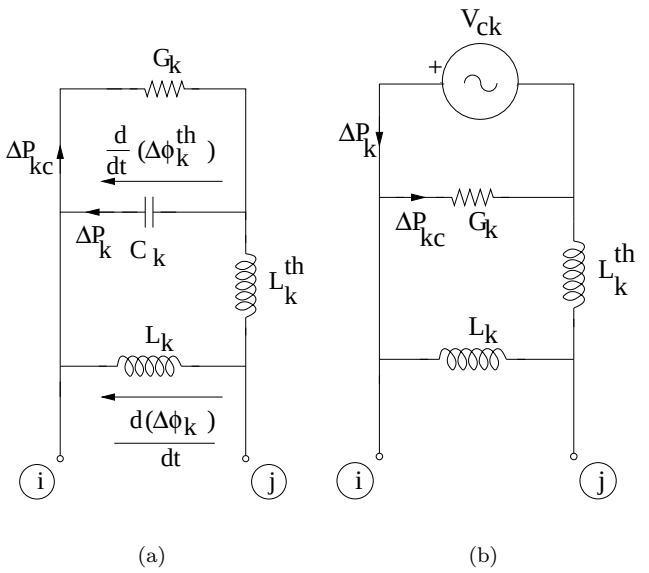

Figure 10.13: An equivalent circuit across port i-j considering damping action

As the value of capacitance C_k is related to the voltage across it by the equation

$$V_{Ck} = \frac{1}{\omega_i^m C_k} \Delta P_k \tag{10.88}$$

where ΔP_k is the equivalent Norton's equivalent current source viewed from the port $i-j$ (after removing L_k). Note that we have replaced the capacitors (corresponding to generator rotor masses) by the voltage sources $v_{i\omega}$ (which are sinusoidal). Thus, V_{Ck} which is also sinusoidal can also be obtained as Thevenin voltage across port $i-j$ (with line k removed). See Fig. 10.13(b).

As discussed earlier, lower modal inertia (equivalent to C_k) is beneficial for damping action. Hence, we can state that a line k for which the modal inertia (C_k) is minimum, is the best location for damping a particular mode m_i. Note that the optimal location depends on the mode considered. In general, out of the $(n_g - 1)$ swing modes in a power system with n_g generators, only a few modes (at lower frequency) are critical. Hence one needs to check for the best locations of damping controllers only for a limited number of the critical modes that are usually the lower frequency modes.

Note that for a particular mode (m_i), the decrement factor (σ_i) is given by $\frac{G_k}{2C_k}$. Hence, the lower the value of C_k, the gain of the controller required for a specified damping is lower. Alternately, for a specified gain, the damping achieved is maximum for the lowest value of C_k.

Since it is convenient to compute Thevenin voltage for a line k, from Eq. (10.88), we can observe that the best location for a series damping controller is one for which $|V_{Ck}|$ is maximum. It is convenient to define a normalized location factor (NLF) as follows

$$NLF(m_i) = \frac{|V_{Ck}|}{|v_{i\omega}|} \tag{10.89}$$

where $|v_{i\omega}|$ is a norm of the eigenvector component v_{iw} corresponding to mode i. We can use Euclidean norm or sum norm. The NLF defined here is different from what is given in [15].

The procedure for computing NLF (m_i) is simpler and is given below.

1. For a specified critical mode (m_i), compute v_{iw}
2. Treating v_{iw} vector as the vector of sinusoidal voltage sources at the generator internal buses, compute Thevenin voltage across different lines.

It is convenient to consider the original network (of series elements) in which the reactances are calculated (in pu) at the base system frequency. Since $L_k \simeq x_k$ and although the equivalent network (made up only of series elements) impedances have to evaluated at the modal frequency ω_i^m, the calculation of Thevenin voltage is unaffected even if we use x_k instead of $\omega_i^m L_k$.

Another approximation is to compute Thevenin voltages across the lines (under consideration) from the original network including all the lines.

Synthesis of the Control Signal

From the network analogy we have identified the appropriate control signal as $\frac{d\Delta\phi_k^{th}}{dt}$ which can be synthesized from the locally measured quantities. If the voltage magnitudes V_i and V_j are assumed to be equal to unity and $\sin\phi_k \simeq \phi_k$, we have

$$\Delta\phi_k = \Delta P_k x_k, \quad \Delta\phi_k^{th} = \Delta P_k(x_k + x_k^{th}) \tag{10.90}$$

A practical scheme for the damping controller is shown in Fig. 10.14. This shows a washout circuit (which will result in zero offset in steady state) and a practical derivative controller. The washout circuit time constant (T_W) can be chosen as 10 s and T_m can be set as 0.01 s.

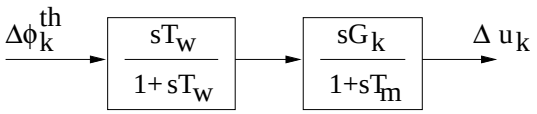

Figure 10.14: Damping controller for a series FACTS device

Remarks

1. The nominal value of x_k^{th} can be obtained from the electrical networks of series elements. However, since there are approximations made in computing x_k^{th}, it is convenient to treat this as a tunable parameter.
2. The gain G_k of the controller is usually obtained from the root locus. This is similar to the tuning of a PSS.
3. There is no need for phase compensation in the controller although the control scheme is obtained based on a simplified system model using classical models of generators. This will be evident when we present a case study on the design of damping controllers for a UPFC [33].
4. It can be shown that the use of the control signal $\frac{d\Delta\phi_k}{dt}$ instead of $\frac{d\Delta\phi_k^{th}}{dt}$ limits the effectiveness of the controller as gain G_k is increased beyond a limit. If $\Delta u_k = G_k s\Delta\phi_k$, then, since $\Delta\phi_k = \Delta\phi_k^{th} - \Delta P_k x_k^{th}$, we have

$$\Delta u_k = \frac{G_k s\Delta\phi_k^{th}}{1 + sG_k B_k x_k^{th}}$$

   by substituting for $\Delta P_k = B_k\Delta u_k$. s is the Laplace operator. The damping will increase as G_k is increased from zero and reach a maximum when $G_k = G_{k\max}$ given by

$$G_{k\max} = \frac{1}{B_k x_k^{th}\omega_i^m}$$

   If $G_k > G_{k\max}$ the damping will reduce. There is no limit on the gain if $\Delta\phi_k^{th}$ is used as the control signal (unless limited by the unmodelled dynamics).
5. In Eg. (10.90), one could use also the line current as measured signal instead of the power flow.

Example 4

Consider the 3 machine system shown in Fig. 10.7. The data is essentially same as in [43] except for the following modifications. All generators are equipped with static exciters with $K_E = 200, T_E = 0.05$. A shunt susceptance of 0.5 pu is provided at bus 5 for voltage support. The loads are

assumed to be constant impedance type and mechanical damping is assumed to be zero.

The eigenvalues for the swing modes at the operating point are calculated as

$$\begin{aligned} \lambda_{1,2} &= -0.4510 \pm j13.1570(Mode1) \\ \lambda_{3,4} &= -0.0392 \pm j8.5809(Mode2) \end{aligned}$$

The computation of location factors gave line 5-4 as the best line for damping the swing mode 2. The series FACTS controller considered is SSSC.

The tuning of the two parameters associated with a damping controller (G and x^{th}) was done using Sequential Linear Programming (SLP) optimization technique to maximize the damping of mode 2 subject to the following constraints: (a) the damping ratio of all the eigenvalues is greater than 0.02 and (b) the real part of all eigenvalues is less than -0.65. The optimal values of the controller parameters are $x^{th} = 0.3391$ and $G = 0.2698$ for the damping controller in line 5–4. The eigenvalues for the two swing modes, with the controller are:

$$\begin{aligned} \lambda_{1,2} &= -0.6631 \pm j13.1510(Mode1) \\ \lambda_{3,4} &= -4.6609 \pm j7.4558(Mode2) \end{aligned}$$

This clearly shows the role of the controller in damping mode 2.

With multiple controllers there is a need for coordinated control, that is simultaneous tuning of all the control parameters.

10.7 Damping of Power Oscillations Using Shunt FACTS Controllers

In the previous section, we assumed that the bus voltage magnitudes are constants. This assumption is essential to relate the linearized model of the network to a linear L–C network with bus frequency deviation analogous to voltage and power (torque) analogous to the current. In this section, we will relax the assumption as a shunt FACTS controller injects reactive current to control the voltage. We need to take a different approach in deriving the control law for the damping controller associated with a shunt FACTS device. The other assumptions mentioned in section 10.6 also apply here. In addition, we will also neglect the presence of a series FACTS controller unless the series controller is used only to regulate constant impedance (inserted) by the controller.

The network analogy described in section 10.6 also applies here. However, we will first consider the nonlinear system before the linearization.

The lossless network with classical models of the generator can be viewed as a network with nonlinear inductors and linear capacitors (corresponding to the generator rotor masses). The equations of the nonlinear reactor representing the series impedance of the line 'k' is given by Eq. (10.71) which is reproduced below.

$$P_k = \frac{V_i V_j}{x_k} \sin \phi_k \Rightarrow i_k = f(\psi_k) \tag{10.91}$$

where i_k is current in the inductor (corresponding to P_k in the line) and ψ_k is the flux linkage of inductor 'k'.

The energy stored in the inductor described by Eq. (10.91) is given by

$$W_k = \int i_k d\psi_k = \int f(\psi_k) d\psi_k \tag{10.92}$$

Substituting Eq. (10.91) in (10.92) and noting that $\psi_k = \phi_k$, we get the following result after integration by parts.

$$\int P_k d\phi_k = \frac{-V_i V_j \cos \phi_k}{x_k} + \int \frac{\cos \phi_k}{x_k} (V_i dV_j + V_j dV_i). \tag{10.93}$$

Adding and subtracting $\frac{V_i^2 + V_j^2}{2x_k}$ to the R.H.S., we can write Eq. (10.93) as

$$\int P_k d\phi_k = \frac{V_k^2}{2x_k} - \int I_{ri}^k \mathrm{d}V_i - \int I_{rj}^k dV_j \tag{10.94}$$

where $V_k^2 = V_i^2 + V_j^2 - 2V_i V_j \cos \phi_k$ is the square of the voltage drop in the line k. I_{ri}^k and I_{rj}^k are the reactive currents injected in line k at the two ends of the line. These are defined as

$$I_{ri}^k = \frac{V_i - V_j \cos \phi_k}{x_k}, \quad I_{rj}^k = \frac{V_j - V_i \cos \phi_k}{x_k} \tag{10.95}$$

When we add the energy in all the inductors (lines and transient reactances of the generators), we get

$$W_L = \sum_{k=1}^{n_b} W_k = \sum_{k=1}^{n_b} \left(\frac{V_k^2}{2x_k} \right) - \sum_{j=1}^{N} \int I_{rj} dV_j \tag{10.96}$$

where I_{rj} is the reactive current injected from bus j in the network which has N buses $(n + n_g)$. n_b is the total number of branches in the network.

The total energy stored in the capacitors (representing generator masses) is obtained as

$$W_C = \frac{1}{2} \sum_{i=1}^{n_g} C_i \left(\frac{d\delta_i}{dt} \right)^2 \tag{10.97}$$

We can express the reactive current (I_{rj}) at bus j as the sum of three components

$$I_{rj} = I_{rjo} + \frac{\partial I_{rj}}{\partial V_j}\Delta V_j + \Delta I_{rj} \tag{10.98}$$

where the second term represents the voltage dependent component of I_{rj} (for small perturbations) and the third current represents the contribution of the SMC (Supplementary Modulation Controller). For conservative system of L–C network, we can show that

$$\frac{d}{dt}(W_L + W_C) = 0. \tag{10.99}$$

However when $\Delta I_{rj} \neq 0$ and is controlled as

$$\Delta I_{rj} = -K_{rj}\left(\frac{dV_j}{dt}\right) \tag{10.100}$$

the total energy does not remain constant and we get,

$$\frac{d}{dt}(W_L + W_C) = -\sum K_{rj}\left(\frac{dV_j}{dt}\right)^2 \tag{10.101}$$

For positive K_{rj}, the average value of the R.H.S. in the above equation is negative. Hence, we introduce dissipation in the system if the reactive current injection at bus j is controlled as given by Eq. (10.100). However this control law is not optimum. For deriving the optimum control law, we need to express $\Delta V_j = (V_j - V_{jo})$ in terms of the perturbations in state variables $\Delta\delta$ and $\Delta\dot{\delta}$. For this, we need to model the system to relate ΔV_j with $\Delta\delta_j$.

Linear Network Model for Reactive Current

Since we are essentially dealing with small perturbations, a linear model is adequate. At the generator internal buses, we have

$$\Delta\hat{E}_{gi} = j\hat{E}_{gio}\Delta\delta_i \tag{10.102}$$

where $\hat{E}_{gio} = |E_{gi}|e^{j\delta_{io}}$. (Note that $|E_{gi}|$ is a constant as the generator is represented by classical model).

Since we are considering only reactive currents injected at various buses and their effect on voltage magnitudes, we can introduce the approximation of $\phi_k = 0$ (the bus angles are all equal for the lossless network). With this assumption, we get $\Delta I^k_{ri} = -\Delta I^k_{rj}$ and described by

$$\Delta I^k_{ri} = b_k(\Delta V_i - \Delta V_j) \tag{10.103}$$

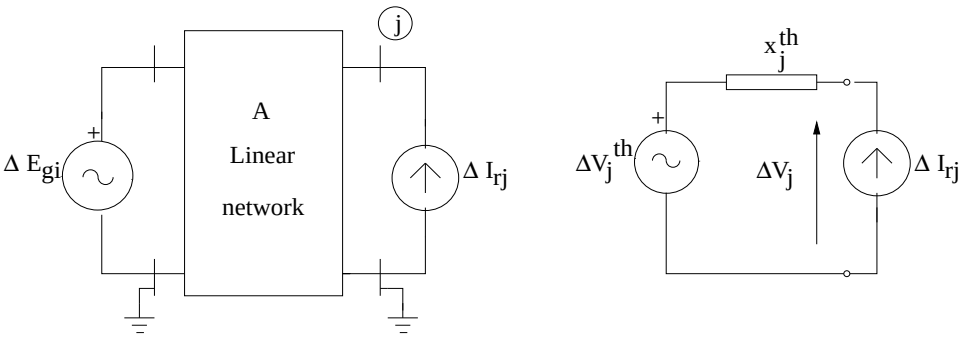

Figure 10.15: An equivalent network relating voltage magnitudes to reactive current injections

where $b_k = \frac{1}{x_k}$. Eq. (10.103) represents the current flow through an equivalent conductance (b_k) which is connected between nodes i and j. At node j, there is one equivalent conductance (b_j) connected between the node j and the reference (ground) node, given by

$$b_j = -\frac{\partial I_{rj}}{\partial V_j} \tag{10.104}$$

The linear network relating the voltage magnitudes and the reactive currents is shown in Fig. 10.15(a). The Thevenin equivalent at node j is shown in Fig. 10.15(b).

For simplicity, we will consider only one modulation controller at bus j. Thevenin voltage V_j^{th} at bus j is a function of the state variables $\Delta\delta$. If we substitute $\Delta\delta = v_{i\delta}$ where $v_{i\delta}$ is the component of the eigenvector corresponding to mode (m_i), we get the equivalent circuit for mode m_i described by the equation

$$\Delta V_j^{th} + x_j^{th}\Delta I_{rj} = \Delta V_j \tag{10.105}$$

From Eq. (10.105) we can obtain the optimal control law for the modulation of the reactive current at bus j as

$$\Delta I_{rj} = -K_{rj}\frac{d}{dt}(\Delta V_j^{th}) \tag{10.106}$$

Note that ΔV_j^{th} is a function of mode m_i. In computing Thevenin voltage, we assume $\Delta E_{gi} = |E_{gi}v_{.\delta}(i)|$ where $v_{.\delta}(i)$ is the component of the eigenvector $v_{.\delta}$ corresponding to the generator i. If we assume $|E_{gi}| = 1.0$, then $\Delta E_{gi} = |v_{.\delta}(i)|$.

Just as in the case of the series FACTS controllers, we define an index (NLF) to evaluate the effectiveness of the location of the damping controller,

based on Thevenin voltage as follows.

$$\text{Normalised Location Factor (NLF)} = \frac{|\Delta V_j^{th}|}{|v_{.\delta}|} \tag{10.107}$$

where $|v_{.\delta}|$ is the norm of eigenvector $v_{.\delta}$ computed for a specified (critical) mode m_i. The best location for the modulation controller for mode m_i is the bus j for which $|\Delta V_j^{th}|$ is maximum.

Remarks

1. Although x_j^{th} can be obtained from the linear network, it is convenient to treat it as a tunable parameter in addition to the proportional gain K_{rj}.
2. The linear network used to compute ΔV^{th} and x^{th} has both series and shunt elements. The series elements correspond to the (constant) reactances of the lines and generators. The shunt elements correspond to the shunt susceptances at various buses.

   In contrast, L–C network representation used for deriving the control law for the series damping controllers, consists of only series elements.
3. The use of the control signal $\left(\frac{dV_j}{dt}\right)$ instead of $\left(\frac{dV_j^{th}}{dt}\right)$ limits the effectiveness of the modulation control of shunt FACTS controllers as the gain K_{rj} is increased.

Example 5

Here we consider the same 3 machine system considered in Example 4. The best location for damping the mode 2 is bus 4. By selecting $K_r = 5.789$ and $X^{th} = 0.0450$, we get the closed loop eigenvalues for the swing modes, after installing the SMC at a STATCOM connected to bus 4, as

$$\begin{aligned} \lambda_{1,2} &= -0.3641 \pm j13.1610 \quad \text{and} \\ \lambda_{3,4} &= -0.5006 \pm j8.1286 \end{aligned}$$

It was observed that installing a SMC leads to the reduction of damping of an exciter mode (EM). For example, the root loci of the critical swing mode (SM) and an exciter mode as the gain K_r is varied from 0 to 1.2 is shown in Fig. 10.16 for a STATCOM (with SMC) connected at bus 9 which is close to the generator # 3. From the analysis of the participation factors, the exciter mode was traced to belong to generator # 3.

The phenomenon observed in Fig. 10.16 is termed as strong resonance [41] in which change in parameters lead to interaction or coupling

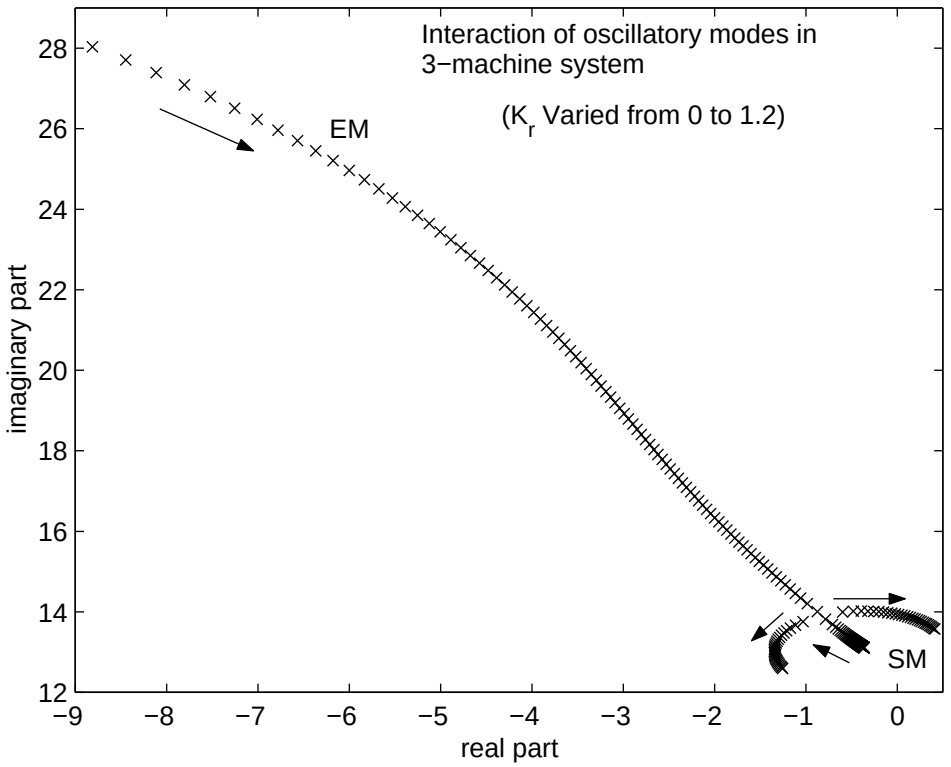

Figure 10.16: Root loci showing interaction of two complex modes in three machine system when K_r is increasing

between two oscillatory modes. The modes that are far away initially move close to each other and collide in such a way that one of the modes may subsequently become unstable. If the system matrix is not diagonalizable at the point of collision of the eigenvalues, the phenomenon is termed 'strong resonance' and 'weak resonance' if it is diagonalizable. Using multi-modal decomposition and a reduced model it is possible to predict the behaviour of the interacting modes near a strong resonance [41]. The asymptotic behaviour of eigenvalues (of the reduced system) when K_r is increased is shown in Fig. 10.17. This shows that there is an upper limit on K_r which results in maximum damping of the critical mode. Depending on the value of x^{th}, the critical mode can be the swing mode or the exciter mode. Even a small change in x^{th} can affect the critical mode. This clearly shows the importance of strong resonance in the design of damping (modulation) controllers.

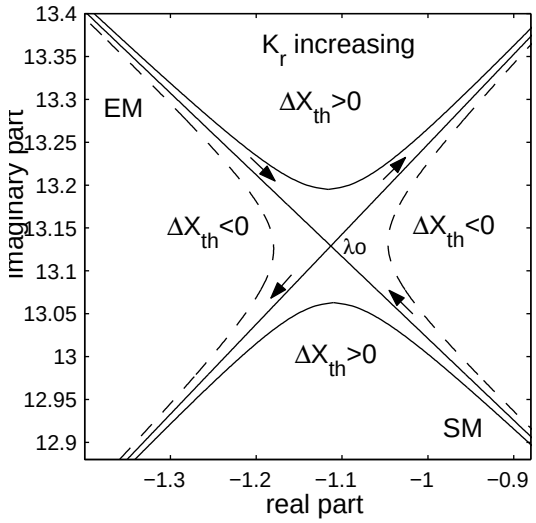

Figure 10.17: Asymptotic behavior of eigenvalues of reduced system when K_r is increasing

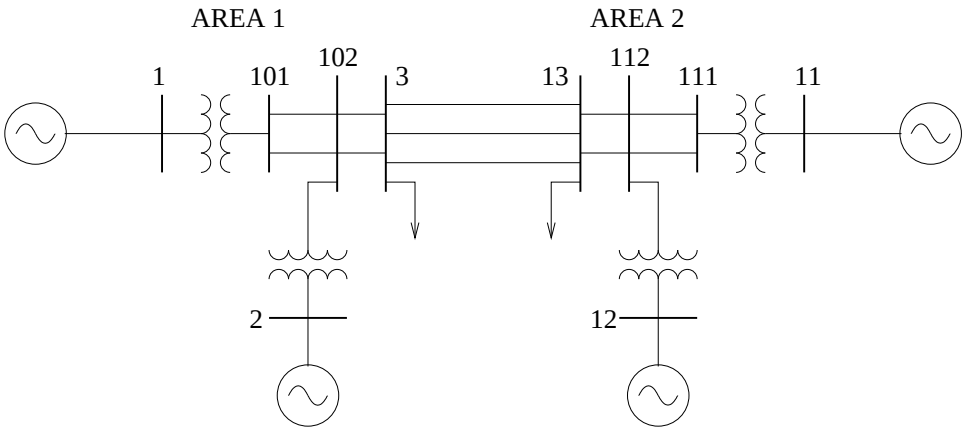

Figure 10.18: A 4 machine 2 Area System

10.8 A Case Study of Damping Controllers in UPFC

A 4-machine, 2 area system is selected for the case study. The single line diagram of the system is shown in Fig. 10.18. This system is same as that described in [1,11] except that the damping of all the generators is assumed to be 1.0 pu (instead of zero) and the armature resistance is neglected. The generators are represented by two-axis models and loads are modelled as constant impedances. The UPFC is installed in one of the three tie lines

connecting the two areas (between buses 3 and 13) with the shunt branch connected at bus 3.

The UPFC has 3 independent control variables - real (series) voltage (V_p), reactive (series) voltage (V_r) and reactive (shunt) current (I_r). We can apply modulation controllers for all the three variables. The block diagram of these controllers is shown in Fig. 10.19. The two series voltage modulation

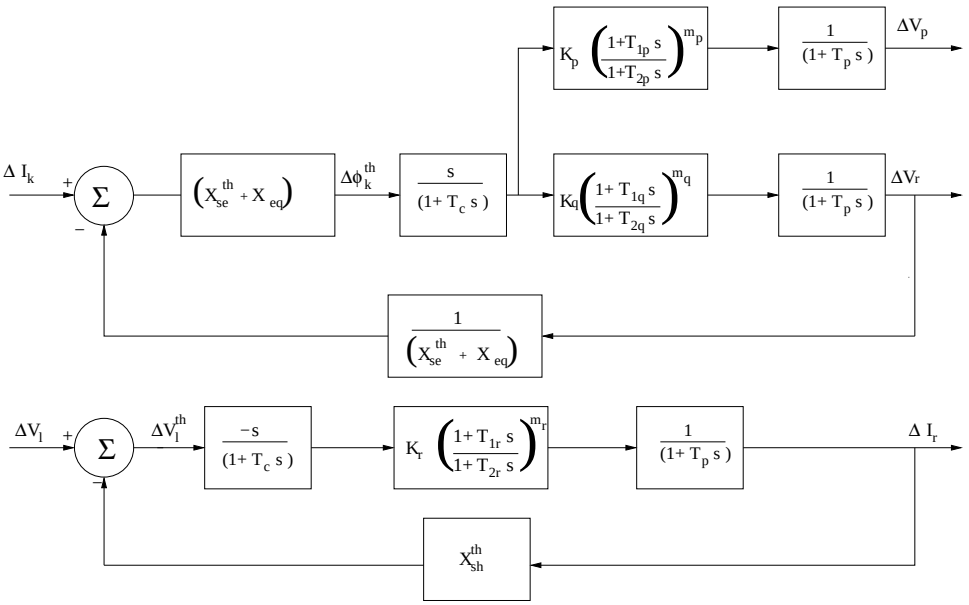

Figure 10.19: Block diagram of UPFC modulation controllers

controllers use Thevenin angle as the control signal while the shunt reactive current modulation controller uses Thevenin voltage (ΔV^{th}) as control signal which is synthesized as follows

$$\Delta V^{th} = \Delta V - x_{sh}^{th} \Delta I_r \tag{10.108}$$

It is to be noted that ΔI_r is the reactive current *injected* at the specified bus, whose voltage magnitude deviation is ΔV. The control signal for the series modulation controllers is synthesized as

$$\Delta \phi^{th} = \Delta I (x_{eq} + x_{se}^{th}) - \Delta V_r \tag{10.109}$$

where x_{eq} is the equivalent line reactance, taking into account the fixed series compensation (if any) and the operating value of reactive voltage injected. Note that x_{se}^{th} is different from x_{sh}^{th}. Both are viewed as tunable controller parameters.

There are 5 control parameters (two Thevenin reactances and 3 gains) associated with the 3 modulation controllers. This is in addition to the

Table 10.4: Details of Phase Compensation.

Controller	Phase of Residue	Reqd. Phase Comp.	T_1 (in seconds)	T_2	No. of Stages m
V_p	128.5°	51.5°	0.6449	0.0785	1
V_r	179.6°	0.0°	–	–	0
I_r	−107.4	−72.6°	0.1139	0.4445	2

three parameters (T_1, T_2 and m) associated with each phase compensation circuit. The parameters of the phase compensation circuits are computed from the knowledge of the phase angle of the residue corresponding to the critical mode (as described in section 10.4). The selection of the controller parameters is based on a constrained optimization technique whose objective is to maximize the damping of the low frequency interarea mode while satisfying constraints on the location of other eigenvalues.

The eigenvalues for the 3 swing modes for the system without modulation controllers is given below. The operating values of V_p, V_r and I_r are assumed to be zero

$$\begin{aligned} \lambda_{1,2} &= -0.0088 \pm j4.4450(InterareaMode) \\ \lambda_{3,4} &= -0.7644 \pm j7.2940(LocalMode1) \\ \lambda_{5,6} &= -0.7410 \pm j6.6904(LocalMode2) \end{aligned}$$

It is obvious that the interarea mode is very lightly damped (having a damping ratio of 0.002). The details of the phase compensation circuits required are given in Table 10.4.

It is to be noted that no phase compensation is required for the series reactive voltage modulation controller. The requirements of phase compensation for other 2 controllers indicate the influence of the unmodelled dynamics on the control law derived in the previous section. The eigenvalues corresponding to the interarea mode for different combinations of the controllers with and without phase compensation are shown in Table 10.5. These indicate that phase compensation improves the damping (as expected). It was also observed that the optimal gains of the controllers was less for the case with phase compensation compared to that without phase compensation.

Table 10.5 shows that the modulation controller for the series reactive voltage is most effective. The influence of the active voltage (V_p) modulation controller is to improve both damping and synchronizing torques. It is more effective than the shunt reactive current modulation.

Table 10.5: Eigenvalues of Interarea Mode.

Modulated Variables	Eigenvalues without phase comp.	Eigenvalues with comp.
I_r	$-0.5392 \pm j4.4632$	$-0.5909 \pm j4.4583$
V_r	$-1.9455 \pm j4.8991$	$-1.9455 \pm j4.8991$
$V_r + I_r$	$-2.1033 \pm j4.8613$	$-3.0892 \pm j4.2701$
$V_r + V_p$	$-2.8736 \pm j5.4176$	$-3.4847 \pm j5.2239$
$V_r + V_p + I_r$	$-3.6951 \pm j5.8982$	$-3.9056 \pm j4.2940$

Discussion

The case study illustrates the effects of coordinated control of the three supplementary modulation controllers associated with a UPFC. The interarea mode is damped very substantially (the damping ratio is increased from 0.002 to 0.673 when all the three controllers are active).

An important characteristics of the control strategy of the UPFC modulation controllers used here, is that the three controllers are decoupled which also makes them robust. Although the control laws are obtained from theoretical analysis based on simplified models, the effectiveness of the modulation controllers is tested on systems with details models.

References and Bibliography

1. K.R. Padiyar, **Power System Dynamics - Stability and Control**, Second Edition, B.S. Publications, Hyderabad, 2002

2. F. P. Demello and C. Concordia, "Concepts of synchronous machine stability as affected by excitation control", IEEE Trans. on Power Apparatus and Systems, v. PAS-88, 1969, pp. 316–329

3. P. Kundur, G. J. Rogers, D. Y. Wong, L. Wang and M. G. Lauby, "A comprehensive computer program package for small signal stability analysis of power systems", IEEE Trans. on Power Systems, v. 5, 1990. pp. 1076-1083

4. D. Y. Wong, G. J. Rogers, B. Poretta and P. Kundur, "Eigenvalue analysis of very large power systems", IEEE Trans. on Power Systems", v. 3, May 1988, pp. 472–480

5. A. Semlyen and L. Wang, "Sequential computation of the complete eigensystem for the study zone in small signal stability analysis of large power systems", IEEE Trans. on Power Systems, v. 3, May 1988, pp. 715–725

6. Nelson Martin and L. T. G. Lima, "Determination of suitable locations for power system stabilizers and static var compensators for damping electromechanical oscillations in large scale power systems", IEEE Trans. on Power Systems, v. 5, n. 4, 1990, pp. 1455–1467

7. K. R. Padiyar and R. K. Varma, "Damping torque analysis of static var system controllers", IEEE Trans. on Power Systems, v. 6, n. 2, 1991, pp. 458–465

8. E. V. Larsen, N. Rostamkolai, D. A. Fisher and A. E. Poitras, "Design of supplementary modulation control function for the chester SVC", IEEE Trans. on Power Systems, v. 8, April 1993, pp. 719–724

9. E. V. Larsen, K. Clark, M. J. Beshir, M. Bhuiyan and K. Braun, "Control design for SVC's on the Mead-Adelanto and Mead-Phoenix transmission project", IEEE Trans. on Power Delivery v. 11, n. 3, 1996, pp. 1498–1506

10. K. R. Padiyar and V. Swayam Prakash, "Tuning and performance evaluation of damping controller for a STATCOM", Int. J. of Elect. Power and Energy Syst., v. 25, 2003, pp. 155-166

11. M. Klein, G. J. Rogers and P. Kundur, "A fundamental study of inter-area oscillations in power systems", IEEE Trans. on Power Systems, v. 16, n. 3, 1991, pp. 914–921

12. E.V. Larsen, J.J, Sanchez-Gasca and J.H. Chow, "Concepts for design of FACTS controllers to damp power swings", IEEE Trans. on Power Systems, v. 10, n. 2, May 1995, pp. 948–955

13. K. Clark, B. Fardanesh and R. Adapa, "Thyristor controlled series compensation application study-control interaction considerations", IEEE Trans. on Power Delivery, v. 10, n. 2, 1995, pp. 1031–1037

14. A. M. Kulkarni and K. R. Padiyar. "Damping of power swings using shunt FACTS controllers", Fourth Workshop on EHV Technology, Bangalore, July 1998

15. A. M. Kulkarni and K. R. Padiyar, " Damping of power swings using series FACTS controllers", Int. J. of Elect. Power and Energy Syst., 1999 (21), pp. 475– 495

16. M. Noroozian and G. Andersson, "Damping of power system oscillations by the use of controllable components", IEEE Trans. on Power Delivery, v. 9, n. 4, 1994, pp. 2046–2054

17. A.B. Leirbukt, J.H. Chow, J.J. Sanchez-Gasca and E. V. Larsen, "Damping control design based on time-domain identified models", IEEE Trans. on Power Systems, v. 14, n. 1, 1999, pp. 172–178

18. J. F. Hauer, C. J. Demure and L. L. Scharf, "Initial results on Prony analysis for power system response signals", IEEE Trans. on Power Systems, v. 5, n. 1, 1990, pp. 80–89
19. N. Yang, Q. Liu and J. D. McCalley, "TCSC controller design for damping interarea oscillations", IEEE Trans. on Power Systems, v. 13, n. 4, 1998, pp. 1304– 1310
20. L. Rouco and F. L. Pagola, "An eigenvalue sensitivity approach to location and controller design of controllable series capacitors for damping power system oscillations", IEEE Trans. on Power Systems, v. 12, n. 4, 1997, pp. 1660–1666
21. J. J. Sanchez–Gasca and J. H. Chow, "Computation of power system low- order models from time domain simulations using a Hankel matrix", IEEE Trans. on Power Systems, v. 12, n. 4, 1997, pp. 1461–1467
22. D. J. Trudnowski, "Order reduction of large-scale linear oscillatory system models", IEEE Trans. on Power Systems, v. 9, n. 1, 1994, pp. 454–458
23. N. Martins, "The dominant pole spectrum eigensolver", IEEE Trans. on Power Systems, v. 12, n. 1, 1997, pp. 245–254
24. L. Wang, M. Klein, S. Yirga and P. Kundur, "Dynamic reduction of large power systems for stability studies", IEEE Trans. on Power Systems, v. 12, n. 2, 1997, pp. 889–895
25. M. Noroozian, L. Angquist, M. Gandhari and G. Andersson, "Improving power system dynamics by series-connected FACTS devices", IEEE Trans. on Power Delivery, v. 12, n. 4, 1997, pp. 1635–1641
26. J. F. Gronquist, W. A. Sethares, F. L. Alvarado and R. H. Lasseter, "Power oscillation damping control strategies for FACTS devices using locally measurable quantities", IEEE Trans. on Power Systems, v. 10, n. 3, 1995, pp. 1598–1605
27. F. Pagola, I. J. Perez-Arriaga and G. C. Verghese, "On sensitivities, residues and participations: applications to oscillatory stability analysis and control", IEEE Trans. on Power Systems, v. 4, n. 1, Feb. 1989, pp. 278–285
28. H. Okamoto, A. Kurita and Y. Sekine, "A method for identification of effective location of variable impedance apparatus on enhancement of steady-state stability in large scale power systems". IEEE Trans. on Power Systems, v. 10, n. 3, 1995, pp. 1401–1407
29. A.M. Stankovic, P.C. Stefanov, G. Tadmore and D.J. Sobajic, "Dissipativity as a unifying control design framework for suppression of low frequency oscillations in power systems", IEEE Trans. on Power Systems, v. 14, n. 1, 1999, pp. 192–198

30. K. R. Padiyar and A. M. Kulkarni, "Modelling of FACTS devices for small signal stability studies", Paper presented at NPSC, 1998, Baroda

31. K. R. Padiyar and K. Bhaskar, "An integrated analysis of voltage and angle stability of a three node power system", Elect. Power and Energy Syst., 2002 (24), pp. 489–501

32. K. R. Padiyar and Kalyani Bhaskar, "Analysis of small signal voltage stability in multimachine systems using detailed and reduced formulations", Elect. Power and Energy Syst., 2005 (27), pp. 301–317

33. K. R. Padiyar and H. V. Saikumar, "Coordinated design and performance evaluation of UPFC supplementary modulation controllers", Elect. Power and Energy Syst., 2005 (27), pp. 101–111

34. M. Klein, L. X. Lei, G. J. Rogers, S. Farrokpay and N. J. Balu, "H_∞ damping controller design in large power systems", IEEE Trans. on Power Systems, v. 10, n. 1, 1995, pp. 158–166

35. I. Kamwa, R. Gondin and Y. Hebert, "Wide-area measurement based stabilizing control of large power systems - A decentralized/hierarchical approach", IEEE Trans. on Power Systems, v. 16, n. 1, 2001, pp. 136–153

36. C. Gama, L. Angquist, G. Ingestrom and M. Noroozian, "Commissioning and operative experience of TCSC for damping power oscillations in the Brazilian North-South interconnection", CIGRE Paper 14-104, 2000

37. G.N. Taranto and J.H. Chow, "A robust frequency domain optimization technique for tuning series compensation damping controllers", IEEE Trans. on Power Systems, v. 10, n. 3, 1995, pp. 1219–1225

38. G.N. Taranto, J.K. Shiau, J.H. Chow and H.A. Othman, "Robust decentralized design for multiple FACTS damping controllers", IEE. Proc., GTD, v. 144, n. 1, 1997, pp. 61–67

39. R. Adapa, K. Madajewski and B. Sobczak, "Improvement of inter-area oscillation damping in UCTE/CENTREL system as a supplementary benefit of FACTS technology application to the Polish power grid", GIGRE Paper 14–108, 2000

40. M. Noroozian, M. Gandhari, G. Andersson, J. Gronquist and I. Hiskens, "A robust control strategy for shunt and series reactive compensators to damp electromechanical oscillations", IEEE Trans. on Power Delivery, v. 16, n. 4, 2001, pp. 812–817

41. K. R. Padiyar and H. V. Sai Kumar, "Investigations of strong resonance in multimachine power systems with STATCOM supplementary modulation controller", IEEE Trans. on Power Systems, v. 21, n. 2, 2006, pp. 754–762

42. K. R. Padiyar and H. V. Sai Kumar, "Modal inertia- a new concept for the location of PSS in multimachine systems", 27th National Systems Conference, December 2003, IIT Kharagpur, India

43. P. M. Anderson and A. A. Fouad, **Power System Control and Stability**, Iowa State University Press, Ames, Iowa, 1977

44. I. Dobson et al., "Is strong resonance a precursor to power system oscillations?", IEEE Trans. Circuits Syst. I, Fundam. Theory Appl., v. 48, n. 3, March 2001, pp. 340–349

45. A. P. Seiranyan, "Collision of eigenvalues in linear oscillatory systems", J. Appl. Math. Mech., v. 58, n. 5, 1994, pp. 805–813

This page intentionally left blank

Chapter 11

Improvement of Transient Stability

11.1 Introduction

In the previous chapter, we considered the application of FACTS controllers for damping power oscillations in transmission lines caused by low frequency rotor swings in generators. The objective is to improve small signal stability of power systems that implies the ability of the power systems to maintain synchronism under small disturbances that are always present (due to small perturbations in the system load). It is essential to maintain small signal stability for all normal operating conditions that a power system is subjected to.

In this chapter, we consider transient stability of power systems and its improvement by suitable control of FACTS controllers. Transient stability is concerned with the stability of power systems when subjected to a severe or large disturbance such as a fault in a line followed by its clearing. Transient stability depends on the location and nature of the disturbance in addition to the initial operating point. Instability results in loss of synchronism leading to separation of generators that are protected by out-of-step relays. Large excursions in the rotor angles imply it is not possible to apply linear system theory. Since nonlinear system analysis is not generally feasible, numerical methods are used to simulate the system to predict system stability for accurate results. However, transient energy function methods have been developed in last 30 years that are fast, reasonably accurate and can handle the presence of FACTS and HVDC controllers by preserving the structure of the system network.

In this chapter, we will look into control strategies that will not only improve first swing stability but also damp the oscillations until their magnitude is reduced below a threshold. The control action is of bang-bang type and is activated on the detection of a disturbance and will be discontinued as the system approaches the post disturbance, stable equilibrium point. Thus, the transient stability controller is a 'discrete' controller as opposed to the continuous controller used for power oscillation damping. Here the term 'discrete' refers to the control action that is not continuous. The assumption here is that the damping controller is not suited for improving transient

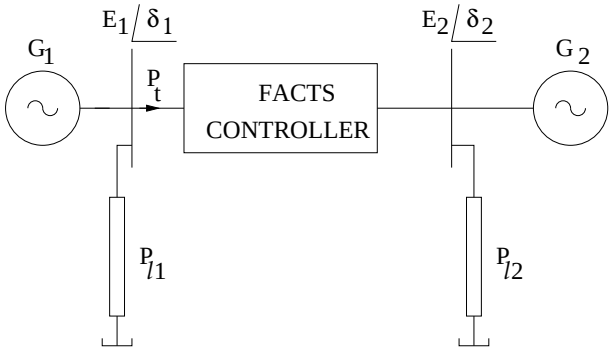

Figure 11.1: A two machine system

stability. This is a valid assumption as the output of the damping controller is limited so as not to interfere with power scheduling controller. Also the control strategy for improving transient stability is quite different from that required for damping of oscillations.

11.2 Transient Stability of a Two Machine System

Consider a two machine system as shown in Fig. 11.1. We can consider each machine as an equivalent representing all the generators in a specified area. The two machines are interconnected by a AC tie line that is used to exchange power between the two areas. For simplicity we will consider the line to be lossless. Also, the generator internal impedances can be neglected in comparison with the impedance of the line. A FACTS controller (series, shunt or a combination) is connected in the line to enhance power transfer in the line.

For simplicity, we will consider classical models of generators described by swing equations:

$$M_1 \frac{d^2\delta_1}{dt^2} = P_{a1} - P_{e1} \tag{11.1}$$

$$M_2 \frac{d^2\delta_2}{dt^2} = P_{a2} - P_{e2} \tag{11.2}$$

where $P_{a1} = P_{m1} - P_{l1}, P_{a2} = P_{m2} - P_{l2}$ are the accelerating powers of the machines 1 and 2 respectively in the absence of power flow in the tie line. Note that $M_1 = \frac{2H_1}{\omega_B}, M_2 = \frac{2H_2}{\omega_B}$ if δ is expressed in radians and time in seconds. H_1 and H_2 are the inertia constants, expressed on a common base.

We can combine Eqs (11.1) and (11.2) by multiplying (11.1) by M_2,

(11.2) by M_1 and subtracting (11.2) from (11.1). We get,

$$M_1 M_2 \frac{d^2\delta_{12}}{dt^2} = M_2 P_{a1} - M_1 P_{a2} - (M_2 P_{e1} - M_1 P_{e2}) \tag{11.3}$$

If $P_{e1} = -P_{e2} = P_t$, we can rewrite (11.3) and follows.

$$M_{eq} \frac{d^2\delta_{12}}{dt^2} = P_m^{eq} - P_e^{eq} \tag{11.4}$$

where

$$M_{eq} = \frac{M_1 M_2}{M_1 + M_2}, \quad P_m^{eq} = \frac{M_2 P_{a1} - M_1 P_{a2}}{M_1 + M_2}, \quad P_e^{eq} = P_t, \quad \delta_{12} = \delta_1 - \delta_2$$

Equation (11.4) shows that a two machine system can be reduced to an equivalent single machine system with the equivalent inertia of $\frac{M_1 M_2}{M_1 + M_2}$. Note that $M_{eq} \simeq M_1$ if $M_2 \gg M_1$. In steady state, $P_m^{eq} = P_t$.

If there is a major disturbance in area 1 or area 2 such that P_m^{eq} suddenly increases to a high value (P_{mf}^{eq}) the angular difference δ_{12} increases as the equivalent machine accelerates. When $\delta = \delta_{cl}$, the P_m^{eq} assumes nominal value. If there is no FACTS controller in the line, the power angle curve is defined by

$$P_t = \frac{E_1 E_2}{X} \sin\delta \tag{11.5}$$

where X is the reactance of the tie line and $\delta = \delta_{12}$. From equal area criterion, we can state the system is transiently stable if area A_2 shown in Fig. 11.2 is not less than A_1. We can derive this result by noting that

$$\frac{d}{dt} W_{KE} = -\frac{d}{dt} W_{PE} \tag{11.6}$$

where

$$W_{KE} = \frac{1}{2} M \left(\frac{d\delta}{dt}\right)^2, \quad W_{PE} = \int_{\delta_0}^{\delta} (P_e - P_m) d\delta$$

where W_{KE} is termed as the kinetic energy and W_{PE} is termed as the potential energy. Note that we have dropped the subscripts and superscripts for convenience. From Eq. (11.6) we get

$$W_T = W_{KE} + W_{PE} = \text{ constant} \tag{11.7}$$

Assuming that the system is initially in equilibrium before the occurrence of a disturbance, at $t = t_0, W_T = 0$. The disturbance lasts from t_0 to t_{cl}. At time $t = t_{cl}$, $W_{KE} =$ Area A_1. For the system to be stable, $\frac{d\delta}{dt}$ should go to zero as δ increases. This is possible only if $\delta_{\max} \leq \delta_u$ where $P_m = P_e(\delta_u)$. The angle δ_u corresponds to the unstable equilibrium point as increase in the angle beyond δ_u leads to loss of synchronism (if $\frac{d\delta}{dt}$ continues to increase

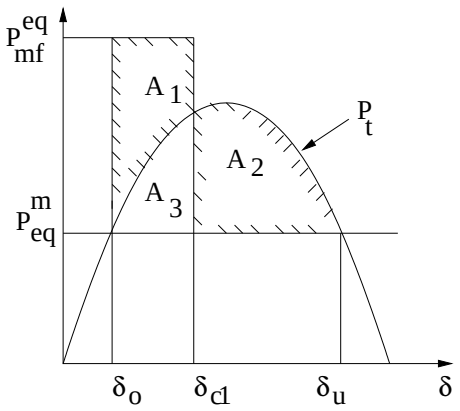

Figure 11.2: Application of equal area criterion

beyond δ_u). The area A_2 is equal to the increase in potential energy that is possible. If $A_2 > A_1$ then the kinetic energy gained during the disturbance gets converted into the potential energy and the system is stable. If all the kinetic energy is not converted before $\delta = \delta_u$, then the system is unstable.

The criterion for transient stability can be stated as follows

$$W_T(t_{cl}) \leq W_{cr} \tag{11.8}$$

where W_{cr} is termed as the critical energy defined by

$$W_{cr} = W_{PE}(\delta_u) = \int_{\delta_o}^{\delta_u} (P_e - P_m) d\delta \tag{11.9}$$

Note that $W_{cr} = A_2 + A_3$ (see Fig. 11.2) and $W_T(t_{cl}) = A_1 + A_3$. Hence the criterion (11.8) is equivalent to the equal area criterion.

For a specified power angle relationship, both δ_0 and δ_u are functions of P_m. For a specified P_m, W_{cr} can be increased by adjusting one or more of the parameters that affects the power flow in the line. For the power angle expression shown in Eq. (11.5), we can reduce X by using switched series capacitors. (The availability of TCSCs enables fast and repetitive switching). While we will discuss the control algorithm for improving stability later, we can note here that increase in power flow (P_t) effected soon after detecting a major disturbance (such as clearing of a fault) will improve first swing stability (by increasing the area A_2).

11.3 Extension to Multimachine Power Systems

We saw in the previous section, relationship between the energy function and equal area criterion in a two machine system. While the equal area criterion

can not be extended to multimachine systems it is possible to extend energy function methods, under some assumptions. These are given below.

1. The electrical network is lossless.
2. The active power loads are constant at all buses.
3. For simplicity, we assume that mechanical damping is zero for all generators (although this can be relaxed)

We will consider structure-preserving network model. This implies that all the buses in the network are retained. In the early applications of Transient Energy Functions (TEF), load buses were eliminated by assuming constant impedance load models and only the generator internal buses were retained. This simplification (apart from the inaccurate representation of loads) resulted in complications arising from transfer conductances in the reduced network which cannot be neglected (even with lossless transmission lines) as they arise from the elimination of the load buses.

A major advantage of using structure-preserving network model is the inclusion of network controllers such as HVDC and FACTS controllers. While HVDC converter controls and SVC control characteristics have been considered in [18] and [19], SSSC and UPFC have been included in the formulation of SPEF (Structure Preserving Energy Function) in [32] and [33]. The detailed two-axis generator models are considered in [17].

There is a large body of literature on Transient Energy Functions (see books by Pai [14] and Pavella, Ernst, Ruiz-Vega [15] for recent developments). Mathematically, TEF is a Lyapunov Function which has a non-positive derivative along the post-fault system trajectory. For accurate results, it is necessary that there are no path-dependent terms in the energy function. (Path-dependent terms require numerical integration based on assumed trajectories which introduce errors). Also, an energy function with path dependent terms is not strictly a Lyapunov Function that guarantees theoretical results on system stability following a disturbance.

In this section, we will derive a SPEF from a network analogy. As discussed in the previous chapter, a lossless electrical network can be viewed as a collection of nonlinear inductors in which current and voltage are analogous to active power (or torque) and frequency deviation respectively.

Derivation of Potential Energy Function

The total energy in the system (W_T) is the sum of the kinetic energy (W_{KE}) and the potential energy (W_{PE}). Here, we will derive an expression for W_{PE} from network analogy [25,28].

The swing equations for the 'm' number of synchronous generators are given by

$$M_i\frac{d^2\delta_i}{dt^2} = M_i\frac{d\omega_i}{dt} = P_{mi} - P_{ei}, \quad i = 1, 2, \ldots, m \tag{11.10}$$
$$= -\frac{\partial W_{PE}}{\partial \delta_i}$$

where W_{PE} is defined as

$$W_{PE} = \sum_{i=1}^{m}\int_{t_0}^{t}(P_{ei} - P_{mi})\frac{d\delta_i}{dt}dt = \sum_{i=1}^{m}\int_{\delta_{io}}^{\delta_i}(P_{ei} - P_{mi})d\delta_i \tag{11.11}$$

Theorem

For lossless systems with constant power loads, we can prove that

$$W_{PE} = \sum_{k=1}^{nb}\int_{t_0}^{t}(P_k - P_{ko})\frac{d\phi_k}{dt}dt = \sum_{k=1}^{nb}\int_{\phi_{ko}}^{\phi_k}(P_k - P_{ko})d\phi_k \tag{11.12}$$

where nb is the total number of series branches in the network (consisting of transmission line and generator reactances).

Proof:

In a lossless network, the active power injection at a bus and the bus frequency $\left(\frac{d\phi}{dt}\right)$ satisfy Kirchhoff's current and voltage laws respectively. Hence, the active powers (or torque) can be considered analogous to currents, bus frequencies to the voltages and bus angles to the flux linkages in an equivalent electrical network [28]. The power (P_k) flowing in the network branch k (connected across buses i and j) is given by

$$P_k = \frac{V_i V_j}{x_k}\sin\phi_k, \quad \phi_k = \phi_{ij}$$

This equation is similar to the equation of a nonlinear inductor given by $i = f(\lambda)$. Thus the power system is analogous to the electrical network with nonlinear inductors (representing series reactances of the transmission lines and generators) (see Fig. 11.3).

For any electrical network, Tellegen's theorem can be applied which states that at any time, the sum of powers delivered to each branch of the network is zero [35]. Separating the (current) sources from other (passive) branches, we can apply Tellegen's theorem for the network shown in Fig. 11.3 and obtain the following result.

$$\sum_{i=1}^{m}P_{ei}\frac{d\delta_i}{dt} - \sum_{j=1}^{n}P_{Lj}\frac{d\phi_j}{dt} = \sum_{k=1}^{nb}P_k\frac{d\phi_k}{dt} \tag{11.13}$$

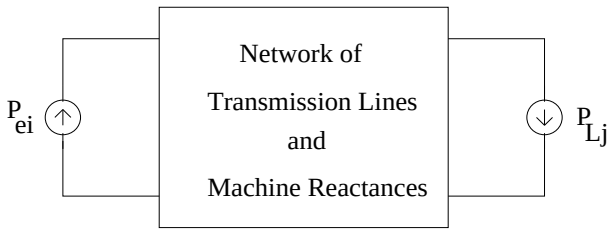

Figure 11.3: Equivalent network for a lossless power system

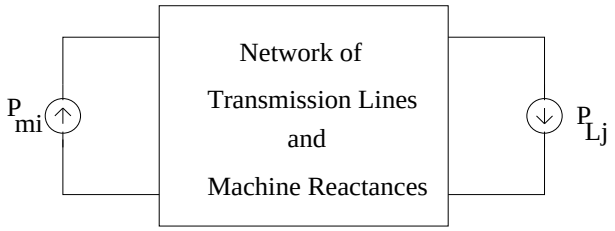

Figure 11.4: Equivalent network in steady state

where P_{Lj} is the load (active) power at bus j. There are n buses in the network (excluding the generator internal buses).

Tellegen's theorem is also valid when branch voltage of one network and branch currents of another network are considered, provided the two networks have the same graph. If we consider the network shown in Fig. 11.3 in steady state we get the source currents as P_{mi} as $P_{ei} = P_{mi}$ (see Fig. 11.4). The currents corresponding to loads remain unchanged in steady state as P_{Lj} is assumed to be constant for $j = 1, 2, \cdots n$.

Considering branch currents in the (steady-state) network of Fig. 11.4 and branch voltages of the network in Fig. 11.3, we get the following result.

$$\sum_{i=1}^{m} P_{mi} \frac{d\delta_i}{dt} - \sum_{j=1}^{n} P_{Lj} \frac{d\phi_j}{dt} = \sum_{k=1}^{nb} P_{ko} \frac{d\phi_k}{dt} \tag{11.14}$$

where P_{ko} is the steady state power flow in branch k. Subtracting Eq. (11.14) from (11.13), we get

$$\sum_{i=1}^{m} (P_{ei} - P_{mi}) \frac{d\delta_i}{dt} = \sum_{k=1}^{nb} (P_k - P_{ko}) \frac{d\phi_k}{dt} \tag{11.15}$$

Integrating the above equation, we get the expression for W_{PE} given by Eq. (11.12).

Remarks

1. It would appear from Eq. (11.12) that the potential energy is path dependent. However, we can show that W_{PE} is also equal to

$$W_{PE} = W_{PE1} + W_{PE2} + W_{PE3} \tag{11.16}$$

where,

$$W_{PE1} = -\sum_{i=1}^{m} P_{mi}(\delta_i - \delta_{io}) + \sum_{j=1}^{n} P_{Lj}(\phi_j - \phi_{jo}) \tag{11.17}$$

$$W_{PE2} = \frac{1}{2}\sum_{k=1}^{nb}(Q_k - Q_{ko}) \tag{11.18}$$

$$W_{PE3} = \sum_{j=1}^{n}\int_{V_{jo}}^{V_j}\frac{Q_{Lj}}{V_j}dV_j + \sum_{i=1}^{m}\int_{t_0}^{t}\left[-i_{qi}\frac{dE'_{di}}{dt} + i_{di}\frac{dE'_{qi}}{dt}\right]dt \tag{11.19}$$

where Q_k is the reactive power absorbed by the branch k. Q_{Lj} is the reactive power load at bus j. i_{di} and i_{qi} are the d- and q-axis components of the armature currents in the generator i·E'_{di} and E'_{qi} are the d- and q-components of the induced voltages in the stator windings of the generator i. Note that if we consider the simplified (classical) model of the generator, then the second term in the R.H.S. of Eq. (11.19) is zero.

Since $\sum Q_k$ must be equal to the net injection of reactive power in the network, we get an alternative expression for W_{PE2} as follows.

$$W_{PE2} = \frac{1}{2}\left[\sum_{i=1}^{m}(Q_{Gi} - Q_{Gio}) - \sum_{j=1}^{n}(Q_{Lj} - Q_{Ljo})\right] \tag{11.20}$$

Note that the subscript 'o' indicates the operating (steady state) value of the variable. Q_{Gi} is the reactive power injected at the internal bus of generator i and is calculated as

$$Q_{Gi} = E'_{di}i_{qi} - E'_{qi}i_{di}$$

Proof of Equation (11.16)

The first term in the potential energy results from applying Eq. (11.14) in the integral $-\int_{\phi_{ko}}^{\phi_k} P_{ko}d\phi_k$. The assumption here is that P_{mi} is also a constant in addition to P_{Lj}. Non-constancy of P_{mi} and P_{Lj} would result in path-dependent terms.

The second and third term in the potential energy can be obtained from noting that

$$\int P_k d\phi_k \;=\; \int \frac{V_i V_j}{x_k}\sin\phi_k d\phi_k$$

$$= -\frac{V_i V_j \cos\phi_k}{x_k} + \int \frac{\cos\phi_k}{x_k}(V_i dV_j + V_j dV_i) \quad (11.21)$$

Adding $\left(\frac{V_i^2+V_j^2}{2x_k}\right)$ and subtracting the same quantity, we can show that

$$\int P_k d\phi_k = \frac{V_i^2 + V_j^2 - 2V_i V_j \cos\phi_k}{2x_k} - \int (I_{ri}^k dV_i + I_{rj}^k dV_j) \quad (11.22)$$

where I_{ri}^k and I_{rj}^k are the reactive currents into the branch k at nodes i and j respectively and are given by

$$I_{ri}^k = \frac{V_i - V_j \cos\phi_k}{x_k}, \quad I_{rj}^k = \frac{V_j - V_i \cos\phi_k}{x_k} \quad (11.23)$$

The first term in the R.H.S. of Eq. (11.22) is $\frac{Q_k}{2}$. The summation over all branches and noting that integral gives the increment over the steady state values, we get the expression for W_{PE2} as given in Eq. (11.18).

Summing the second term in the R.H.S. of Eq. (11.22) gives,

$$-\sum_{k=1}^{nb} \int (I_{ri}^k dV_i + I_{rj}^k dV_j) = \sum_{j=1}^{n} \int_{V_{jo}}^{V_j} \frac{Q_{Li}}{V_j} dV_j \quad (11.24)$$

if we assume classical models for generators. In deriving Eq. (11.24), we note that

$$\frac{Q_{Lj}}{V_j} = -\sum_{k \in j} I_{rj}^k \quad (11.25)$$

where the summation is over the branches that are incident on the bus j.

Note that Eq. (11.24) includes the components corresponding to the generator terminal buses. The reactive current injected to stator (reactance) branch also contributes to the (R.H.S) of Eq. (11.24). However, the reactive current injected into the generator internal bus does not contribute to the term W_{PE3} as the generator voltage is assumed to be a constant for the classical model.

Potential Energy Contributed by Considering the Two-Axis Model of the Synchronous Generator

If we consider the detailed two-axis model for the synchronous generators, W_{PE3} is no longer given by the R.H.S. of Eq. (11.24).

The stator equations for a generator i are [1] given by

$$E'_{qi} + x'_{di} i_{di} = v_{qi} = V_i \cos(\delta_i - \phi_i) \quad (11.26)$$

$$E'_{di} - x'_{qi} i_{qi} = v_{di} = -V_i \sin(\delta_i - \phi_i) \tag{11.27}$$

The electrical power output (P_{ei}) of the generator i is given by

$$P_{ei} = v_{di} i_{di} + v_{qi} i_{qi} \tag{11.28}$$

Substituting from Eqs. (11.26) and (11.27) in (11.28), we get

$$\begin{aligned} P_{ei} &= \frac{E'_{di} V_i \cos(\delta_i - \phi_i)}{x'_{qi}} + \frac{E'_{qi} V_i \sin(\delta_i - \phi_i)}{x'_{di}} \\ &\quad + \frac{V_i^2 \sin\{2(\delta_i - \phi_i)\}}{2} \left(\frac{1}{x'_{qi}} - \frac{1}{x'_{di}} \right) \end{aligned} \tag{11.29}$$

We can show that [36],

$$\begin{aligned} \int_{t_0}^{t} P_{ei} \frac{d(\delta_i - \phi_i)}{dt} dt &= \int_{t_0}^{t} \left(i_{di} \frac{dE'_q}{dt} - i_{qi} \frac{dE'_{di}}{dt} \right) dt \\ &\quad + \int_{t_0}^{t} \frac{Q_{gi}}{V_i} dV_i + \frac{1}{2}(Q_{mi} - Q_{mio}) \end{aligned} \tag{11.30}$$

where Q_{gi} is the reactive output of the generator given by

$$Q_{gi} = v_{di} i_{qi} - v_{qi} i_{di} \tag{11.31}$$

Q_{mi} is the reactive power loss in the stator, given by

$$Q_{mi} = x'_{di} i_{di}^2 + x'_{qi} i_{qi}^2 \tag{11.32}$$

When we sum the potential energy in machine stator reactances, using the expression (11.30), the second term in the R.H.S. of Eq. (11.30) contributes to the first term in the R.H.S. for Eq. (11.19). The third term in the R.H.S. of Eq. (11.30) contributes to W_{PE2}. The only additional term contributing to the potential energy (by the two axis models of the generators) is the second component of W_{PE3} given by

$$W_{PE3}^{m} = \sum_{i=1}^{m} \int_{t_0}^{t} \left(i_{di} \frac{dE'_{qi}}{dt} - i_{qi} \frac{dE'_{di}}{dt} \right) dt \tag{11.33}$$

The above expression is path-dependent. However, this includes the effect of the AVR and the excitation system control.

Kinetic Energy and the Total Energy

The kinetic energy can be derived from Eq. (11.10) (the swing equations of the generators) as

$$W_{KE} = \frac{1}{2} \sum M_i \omega_i^2, \quad \omega_i = \frac{d\delta_i}{dt} \tag{11.34}$$

The total energy (W_T) is the sum of the kinetic and potential energies and it can be observed that

$$\frac{dW_T}{dt} = 0 \tag{11.35}$$

along the post fault trajectory which implies that W_T remains constant. The criterion for transient stability remains the same as for a two machine system, namely (see Eq. (11.8))

$$W_T(t_{cl}) \leq W_{cr}$$

However there are two complications with a multimachine system. Firstly, the calculation of W_{cr} is not simple. There are a number of unstable equilibrium points (UEP) for a multimachine system. It is now accepted that there is a controlling UEP for a specified disturbance, that lies on the boundary of the stability region (that surrounds the stable equilibrium point (SEP) of the post-disturbance system). However, the determination of this controlling UEP (CUEP) is not straightforward. Typically, one has to search for the CUEP in the vicinity of the exit point (where the post fault trajectory leaves the stability boundary) which is predicted from the Potential Energy Boundary Surface (PEBS) method. Some of the theoretical issues are discussed in references [37–39].

The second complication regarding the direct stability evaluation using energy functions, is the accurate determination of the kinetic energy that is responsible for system separation. It can be easily shown that W_{KE} defined in Eq. (11.34) is larger than the energy required for transient instability. If frequency of all the generators increase uniformly, this does not lead to transient instability. Hence, we need to define kinetic energy using generator rotor frequencies relative to the frequency of the Centre of Inertia (COI) defined by

$$\omega_{COI} = \frac{\sum M_i \omega_i}{M_T} \tag{11.36}$$

where $M_T = \sum M_i$. The kinetic energy expression is modified to

$$W'_{KE} = \frac{1}{2} \sum_{i=1}^{m} M_i \tilde{\omega}_i^2 \tag{11.37}$$

where $\tilde{\omega}_i = (\omega_i - \omega_{COI})$. Although, we can express all the angles relative to that of the COI, there is no change in the computation of W_{PE}.

Even the reduced value of W_{KE} given by the expression (11.37) does not represent the kinetic energy responsible for system separation. If we know the mode of instability (MOI) which implies the knowledge of the group of (advanced) machines that separate from the rest, the kinetic energy (W_{KE}^{mod}) responsible for the system separation is calculated from,

$$W_{KE}^{mod} = \frac{1}{2} M_{eq} (\omega_I - \omega_{II})^2 \tag{11.38}$$

where,

$$M_{eq} = \frac{M_I M_{II}}{M_I + M_{II}}, \quad M_I = \sum_{i \in I} M_i, \quad M_{II} = \sum_{i \in II} M_j,$$

$$\omega_I = \frac{\sum_{i \in I} M_i \omega_i}{M_I}, \quad \omega_{II} = \frac{\sum_{j \in II} M_j \omega_j}{M_{II}}$$

The fast determination of MOI and other practical issues are discussed in the literature (see [40]).

Remarks

1. The energy function methods have been used to predict system stability from the knowledge of system variables computed at the fault clearing time. It is also possible to compute critical clearing time (CCT) and use it an index for the evaluation of dynamic security.
2. If is possible to define energy margin as the difference between the critical energy (W_{cr}) and the energy at the fault clearing (W_{cl}). The sensitivity of the energy margin can be used for preventive control by redispatch and reducing power transfer in critical lines (or across interfaces)
3. Energy function methods can be used as screening tool for fast evaluation of transient stability and ranking of contingencies (that can affect dynamic security of power systems).
4. For the two-axis models of generators, with constant E_{fd}, it is possible to define a potential energy function which is path independent. Instead of the term W_{PE3}^m defined in Eq. (11.33), if we use the following term,

$$\begin{aligned} W_{PE4} &= \sum_{i=1}^{m} \left[\frac{(E_{qi}'^2 - E_{qio}'^2)}{2(x_{di} - x_{di}')} + \frac{(E_{di}'^2 - E_{dio}'^2)^2}{2(x_{qi} - x_{qi}')} \right. \\ &\quad \left. - \frac{E_{fdi}(E_{qi}' - E_{qio}')}{(x_{di} - x_{dio}')} \right] \end{aligned} \tag{11.39}$$

we can show that

$$\begin{aligned} \frac{dW_T}{dt} = \frac{dW_{KE}}{dt} + \frac{dW_{PE}}{dt} &= -\sum_{i=1}^{m} \left[\frac{T_{doi}'}{(x_{di} - x_{di}')} \left(\frac{dE_{qi}'}{dt} \right)^2 \right. \\ &\quad \left. + \frac{T_{qoi}'}{(x_{qi} - x_{qi}')} \left(\frac{dE_{di}'}{dt} \right)^2 \right] \end{aligned} \tag{11.40}$$

This implies that W_T is a Lyapunov function.

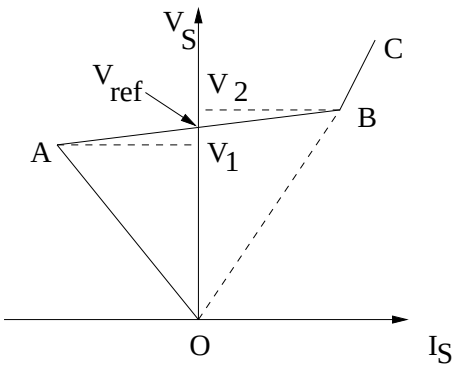

Figure 11.5: SVC steady state control characteristics

5. The integral $\int \frac{Q_{Lj}}{V_j} dV_j$ is a path-independent term if Q_{Lj} is modelled as voltage dependent. If Q_{Lj} is defined as

$$Q_{Lj} = b_0 + b_1 V_j + b_2 V_j^2 \tag{11.41}$$

then,

$$\int_{V_{jo}}^{V_j} \frac{Q_{Lj}}{V_j} dV_j = b_0 \ln\left(\frac{V_j}{V_{jo}}\right) + b_1(V_j - V_{jo}) + \frac{b_2}{2}(V_j^2 - V_{jo}^2) \tag{11.42}$$

11.4 Potential Energy Function for SVC, SSSC and UPFC

11.4.1 Static Var Compensator (SVC)

The energy function for a SVC can be derived from its steady-state control characteristics shown in Fig. 11.5. There are three modes of operation of SVC based on the operating value of V_S. These are given below.

Mode 1 : $V_S < V_1$

Mode 2 : $V_1 \leq V_S \leq V_2$

Mode 3 : $V_S > V_2$

The SVC can be modelled as a voltage-dependent reactive load. Assuming a SVC is connected at bus j, we can express the contribution to the potential energy from SVC as

$$W_{SVC} = \int_{V_{So}}^{V_S} I_S dV_S \tag{11.43}$$

In the above expression, we are considering the SVC current (I_S) as the reactive current flowing from the bus j to the SVC. (I_S is assumed to be positive when it is inductive). The losses in the SVC are neglected. For the three modes of operation, I_S and the energy functions are as follows:

Mode 1:

$$\begin{aligned} I_S &= -B_C V_S \\ W_{SVC1} &= \int_{V_{So}}^{V_S} I_S dV_S = -\frac{B_C}{2}(V_S^2 - V_{So}^2) \end{aligned}$$

Mode 2:

$$I_S = \frac{V_S - V_{ref}}{X_S}$$

where X_S is the slope of the line AB.

$$\begin{aligned} W_{SVC2} &= \int_{V_1}^{V_S} I_S dV_S + W_{SVC1}(V_1) \\ &= \frac{1}{2X_S}[(V_S - V_{ref})^2 - (V_1 - V_{ref})^2] + W_{SVC1}(V_1) \end{aligned}$$

Model 3:

$$\begin{aligned} I_S &= (B_L - B_C)V_S \\ W_{SVC3} &= \int_{V_2}^{V_S} I_S dV_S + W_{SVC2}(V_2) \\ &= \frac{1}{2}(B_L - B_C)(V_S^2 - V_2^2) + W_{SVC2}(V_2) \end{aligned}$$

In expressing I_S for mode 3, we have assumed that the SVC is a FC-TCR type. If the SVC is a TSC-TCR type, $B_C = 0$ as the capacitor is switched off in mode 3.

11.4.2 Static Synchronous Series Compensator

Consider a SSSC connected in line k connected between buses i and j as shown in Fig. 11.6. The SSSC is modelled as a constant reactive voltage V_r which is assumed to be capacitive (V_r leads the line current by 90°).

The expression for the phasor current I_k in the line is given by

$$I_k \angle \gamma_k = \frac{V_i \angle \phi_i - V_j \angle \phi_j}{j x_k} + \frac{j V_r \angle \gamma_k}{j x_k} \tag{11.44}$$

The power flow (P_k) in the line is obtained as,

$$\begin{aligned} P_k &= Re[V_i I_k^*] = Re[V_j I_k^*] \\ &= \frac{V_i V_j \sin(\phi_i - \phi_j)}{x_k} + \Delta P_k \end{aligned} \tag{11.45}$$

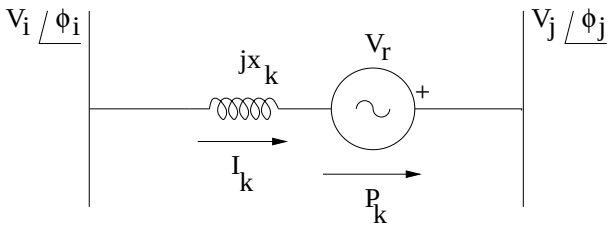

Figure 11.6: A SSSC connected in line k

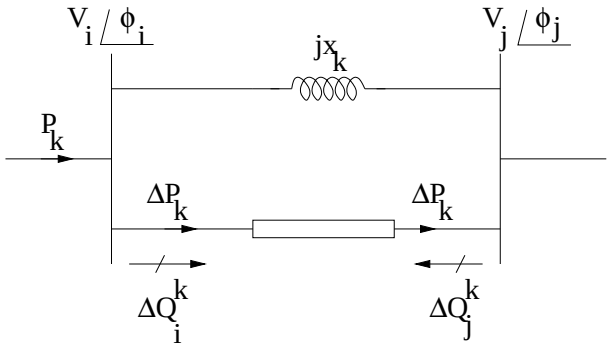

Figure 11.7: SSSC (power) injection model

where

$$\Delta P_k = \frac{V_i V_r \cos(\phi_i - \gamma_k)}{x_k} = \frac{V_j V_r \cos(\phi_j - \gamma_k)}{x_k} \tag{11.46}$$

We can represent the effect of SSSC on the power flow in the line as a incremental flow ΔP_k flowing in a path, parallel with the line k. (See Fig. 11.7).

The incremental reactive power injections at bus i and j due to the SSSC are given by

$$\Delta Q_i^k = \frac{V_i V_r \sin(\phi_i - \gamma_k)}{x_k} \tag{11.47}$$

$$\Delta Q_j^k = -\frac{V_j V_r \sin(\phi_j - \gamma_k)}{x_k} \tag{11.48}$$

The energy function for the SSSC is obtained from

$$W_{SSSC} = \int_{\phi_{k0}}^{\phi_k} \Delta P_k d\phi_k = \int \Delta P_k[(d\phi_i - d\gamma_k) - (d\phi_j - d\gamma_k)] \tag{11.49}$$

$$= \int \frac{V_i V_r \cos(\phi_i - \gamma_k)}{x_k} d(\phi_i - \gamma_k) - \int \frac{V_j V_r \cos(\phi_j - \gamma_k)}{x_k} d(\phi_j - \gamma_k) \tag{11.50}$$

Integrating the R.H.S by parts, we can obtain

$$W_{SSSC} = \Delta Q_i^k + \Delta Q_j^k - \int \frac{\Delta Q_i^k}{V_i} \Delta V_i - \int \frac{\Delta Q_j^k}{V_j} \Delta V_j \tag{11.51}$$

In deriving the above equation, we have assumed that V_r is a constant (which is a realistic assumption as the reactive voltage will be controlled to be at the extremum value immediately after detecting a major disturbance).

The third and fourth term in the R.H.S of Eq. (11.51) can be merged in the expressions $\int \frac{Q_{Li}}{V_i} dV_i$ and $\int \frac{Q_{Lj}}{V_j} dV_j$ which are already present in the energy function. Hence the only term that needs to be added to the energy function on account of the SSSC is

$$W'_{SSSC} = \frac{V_r}{x_k} [V_i \sin(\phi_i - \gamma_k) - V_j \sin(\phi_j - \gamma_k)] \tag{11.52}$$

From Eq. (11.44), we can derive that the R.H.S of Eq. (11.52) is equal to $V_r \left(I_k - \frac{V_r}{x_k} \right)$. Since the voltage drop across the line (V_k) is given by

$$V_k = I_k x_k - V_r = V_i^2 + V_j^2 - 2 V_i V_j \cos \phi_{ij} \tag{11.53}$$

we can finally express W'_{SSSC} as

$$W'_{SSSC} = \frac{V_r V_k}{x_k} = \frac{V_r \sqrt{V_i^2 + V_j^2 - 2 V_j V_j \cos \phi_{ij}}}{x_k} \tag{11.54}$$

In reference [32], there is a sign reversal in the energy function as V_r is assumed to be positive when inductive.

11.4.3 Unified Power Flow Controller

Consider a UPFC connected in line k near the sending end as shown in Fig. 11.8(a). the injection model of the UPFC is shown in Fig. 11.8(b).

It is assumed that the thee independent parameters of the UPFC, V_C, α and I_r are assumed to be constants. The UPFC is assumed to be lossless.

The power flow (P_k) in the line k can be obtained as

$$P_k = Re[I_j^* V_j]$$

where I_j is given by

$$I_j = \frac{V_i \angle \phi_i + V_C \angle (\phi_i + \alpha) - V_j \angle \phi_j}{j x_k} \tag{11.55}$$

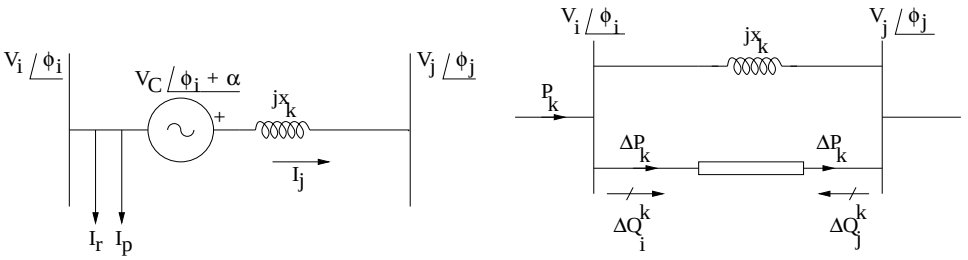

(a) Basic model of a UPFC (b) Injection model

Figure 11.8: A UPFC connected in line k

The incremental power flow in the line (ΔP_k) due to UPFC is given by

$$\Delta P_k = \frac{V_j V_C \sin(\phi_i + \alpha - \phi_j)}{x_k} \tag{11.56}$$

since $Re[V_C I_j^*] = V_i I_p$, we have the constraint

$$V_i I_p + \frac{V_i V_C \sin\alpha}{x_k} = \frac{V_j V_C \sin(\phi_i + \alpha - \phi_j)}{x_k} = \Delta P_k \tag{11.57}$$

The incremental injections of the reactive power at the buses i and j are given by

$$\Delta Q_i^k = V_i I_r + \frac{V_i V_C \cos\alpha}{x_k} \tag{11.58}$$

$$\Delta Q_j^k = -\frac{V_j V_C \cos(\phi_i + \alpha - \phi_j)}{x_k} \tag{11.59}$$

The energy function due to the UPFC is given by

$$W_{UPFC} = \int \Delta P_k d\phi_k = \int \frac{V_j V_C \sin(\phi_i + \alpha - \phi_j)}{x_k} d\phi_{ij} \tag{11.60}$$

Integrating the above expression by parts, we can obtain

$$W_{UPFC} = \Delta Q_i^k + \Delta Q_j^k - \int \frac{\Delta Q_i^k}{V_i} dV_i - \int \frac{\Delta Q_j^k}{V_j} dV_j \tag{11.61}$$

Since the last two terms in the R.H.S of the above expression can be clubbed together with $\int \frac{Q_{Li}}{V_i} dV_i$ and $\int \frac{Q_{Lj}}{V_j} dV_j$, we get the additional term to be added in the energy function due to the UPFC as

$$W'_{UPFC} = \frac{V_i V_C}{x_k} \cos\alpha - \frac{V_j V_C \cos(\phi_i + \alpha - \phi_j)}{x_k} + V_i I_r \tag{11.62}$$

Note that we have assumed V_C, α and I_r as constants in deriving the above expression. It is interesting to observe that the energy function contribution by SSSC or UPFC is ΔQ_k and not $\frac{\Delta Q_k}{2}$ as in the case of line reactances.

11.5 A New Control Algorithm for Improving Transient Stability and Damping of Oscillations

The use of switched series capacitors or TCSC for improving transient stability and time-optimal control of power systems has been considered in [20-23, 25-26]. The nature of the control action is of bang-bang type where a single control variable (series compensation) is switched between two limits. The control strategy is not obvious in the case of a UPFC which has three independent control variables. In this section, we will introduce a general control algorithm which is valid for all FACTS controllers including UPFC. Before presenting this algorithm we will briefly review some concepts on time-optimal control involving switchings.

11.5.1 Time-Optimal Control

Time-optimal control is based on Pontryagin's Minimum Principle [41] and involves bang-bang control. Its application to a single machine system, considered the series capacitor control to transfer the system from a disturbed state to a stable state by a single capacitor switching. Although the concept has been proposed as early as in 1970 [22], the introduction of TCSC has enabled such control strategies to be applied in practice.

To illustrate time-optimal control, consider a Single Machine Infinite Bus (SMIB) system in which series capacitors are used. The swing equations, neglecting damping, are given by

$$\left.\begin{aligned} \dot{\delta} &= \omega = f_1(\omega) \\ \dot{\omega} &= \tfrac{1}{M}\left[P_m - \tfrac{E_g E_b \sin\delta}{(X - X_C)}\right] = f_2(\delta, \omega, X_C) \end{aligned}\right\} \tag{11.63}$$

where E_g and E_b are generator internal voltage and infinite bus voltage respectively. X is the fixed reactance (between the generator internal bus to the infinite bus) and X_C is the reactance of the switchable capacitor. It has a nominal value of X_{Co} and is constrained by $X_{C\,\min} \le X_C \le X_{C\,\max}$.

Let Eq. (11.63) represent the post-fault system and t_{cl} be the initial time of the post- fault system (the fault clearing time). Let T be the final time at which the system trajectory reaches stable equilibrium point $(\delta_{sep}, 0)$ of the post-fault system.

The objective of the time optimal control is to minimize the performance index

$$J = T - t_{cl} = \int_{t_{cl}}^{T} f_0 dt, \quad f_0 = 1 \tag{11.64}$$

To develop the conditions for optimality, we define the Hamiltonian for the system of (11.63) as

$$H = f_0 + p_1 f_1 + p_2 f_2 = 1 + p_1\omega + \frac{p_2}{M}\left(P_m - \frac{E_g E_b \sin\delta}{(X - X_C)}\right) \tag{11.65}$$

where the co-states p_1 and p_2 satisfy

$$\left.\begin{array}{l} \dot{p}_1 = -\frac{\partial H}{\partial \delta} = \frac{p_2}{M}\frac{E_g E_b \cos\delta}{(X - X_C)} \\ \dot{p}_2 = -\frac{\partial H}{\partial \omega} = -p_1 \end{array}\right\} \tag{11.66}$$

From the Minimum Principle, the optimal control satisfies the conditions:

$$X_C = \begin{cases} X_{C\max}, \text{ if } p_2 \sin\delta > 0 \\ X_{C\min}, \text{ if } p_2 \sin\delta < 0 \end{cases} \tag{11.67}$$

If $p_2 \sin\delta = 0$, the control cannot be determined. Eq. (11.67) suggests bang-bang control.

The stability region of the post fault system with $X_C = X_{C\max}$, in the $\delta - \omega$ plane is shown in Fig. 11.9. This figure also shows the system trajectory starting from δ_0 (the stable equilibrium point for the prefault system). At point P_1 the fault is cleared and X_C in switched to $X_{C\max}$. The trajectory with $X_C = X_{C\max}$ intersects a trajectory (S) that passes through δ_{sep} (the stable equilibrium point of the post-fault system) and has $X_C = X_{C\min}$. At the point of intersection P_2, the capacitor is switched to $X_{C\min}$ and the system reaches δ_{sep} in minimum time. The capacitor is switched to the nominal value X_{Co} when the equilibrium point is reached.

The trajectory S is defined by the equation,

$$\begin{aligned} W_T &= W_{KE} + W_{PE} = \frac{1}{2}M\omega^2 - P_m(\delta - \delta_{sep}) - \frac{E_g E_b(\cos\delta - \cos\delta_{sep})}{(X - X_{C\min})} \\ &= 0 \end{aligned} \tag{11.68}$$

Note that the equation is based on the energy function defined for the post-fault system with $X_C = X_{C\min}$ [23].

Complications arise if the assumption that S_1 intersects the trajectory P_1P_2 is not true (particularly when the difference between $X_{C\max}$ and $X_{C\min}$ is small). In such situations, multiple switchings of series capacitor are required [26]. The reference [26] also mentions several issues that may affect the robustness of the time-optimal control in realistic power systems. These relate to the complexity of models, dependence of capacitor switching on the post-fault equilibrium point, control signals that are required for the implementation of the control scheme and the effects of noise present in these signals. The authors of [26] also state. "Suboptimal schemes applicable to a range of power transfer conditions have to be developed. Because

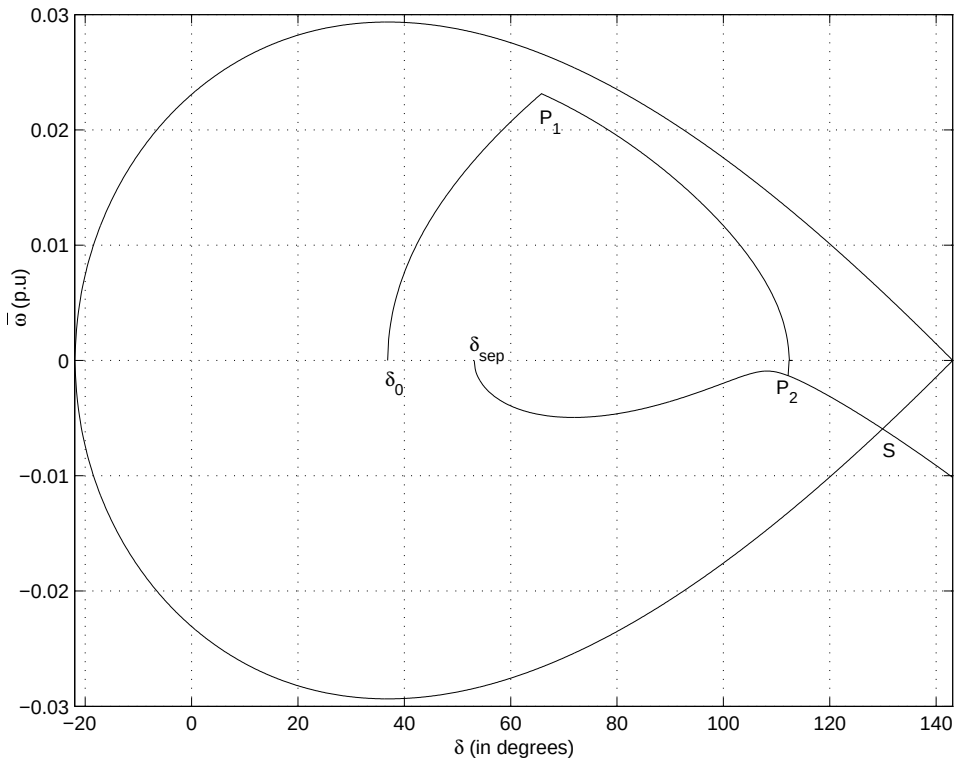

Figure 11.9: System trajectory with single switching

time-optimal is an open-loop control, its integration with a feedback control to achieve small-signal stability should be investigated."

The control strategy developed in the next subsection addresses some of these issues. In the first place, the strategy is a sub-optimal in that the stable equilibrium point is not necessarily reached in minimum time. The strategy is seamlessly integrated with the functioning of the damping controller described in chapter 10. The discrete control scheme that is described in the next subsection, ceases to function when the energy in the system falls below a threshold and then allows the damping controller to act.

11.5.2 Control Strategy for a Two Machine System

Consider a two machine system shown in Fig. 11.1. This can be reduced an equivalent single machine described by Eq. (11.4) reproduced below.

$$M_{eq}\frac{d^2\delta_{12}}{dt^2} = P_m^{eq} - P_e^{eq}$$

where $P_e^{eq} = P_t(\delta_{12}, u_c)$ where u_c is the control vector associated with the FACTS controller connected in the tie line. u_c can be a single variable such as X_{TCSC} or V_r if a TCSC or SSSC is connected in series with the line. It can be B_{SVC} or I_r if a SVC or a STATCOM is connected in shunt at an appropriate location. It can be a vector of 3 variables (V_C, β and I_r) if a UPFC is connected (where $V_C\angle\beta$ is the injected series voltage and I_r is the reactive current drawn by the shunt converter).

The objective of the control strategy is to steer the system to a state in the vicinity of post-fault stable equilibrium point. The control scheme is independent of the size of the FACTS controller and is designed to work reliably.

If the reactances of the two machines are neglected in comparison with the reactance of the tie line, we can express the potential energy of the system (W_{PE}) as the potential energy associated with the tie line. This follows from,

$$W_{PE} = \int_{\delta_o}^{\delta} (P_e - P_m) d\delta = \int_{\delta_o}^{\delta} (P_t - P_{to}) d\delta$$

For convenience, we can assume that δ_0 is also the post-fault stable equilibrium point. (This is not a restriction and can be relaxed). As mentioned in section 11.2, the first swing stability can be optimized by maximizing the power flow in the line (P_t) as soon as the large disturbance is detected. This is achieved by selecting $u_c = u_{cm}$ that corresponds to maximum power. If we assume that this will stabilize the system, then δ_{max} will be less than or equal to the unstable equilibrium point (δ_{um}) that results from $u_c = u_{cm}$.

If $\delta_{\max} \leq \delta_u$ (where δ_u is the unstable equilibrium point with $u_c = u_{co}$ where u_{co} is the (nominal) control vector for the post-fault system) then setting $u = u_{co}$ when $\delta = \delta_{max}$ will ensure that the system will reach the stable equilibrium point due to the inherent damping in the system. However, if we wish to damp the oscillations by the discrete control where u_c can take three values - u_{co}, u_{cm} and u_{cl} (where u_{cl} corresponds to the minimum power flow in the line), the following control strategy is proposed.

1. As soon as a large disturbance is detected (such as a fault followed by its clearing), the control variables are selected such that the power flow (P_t) is maximized.
2. The control variables are switched to their nominal operating values (u_{co}) when $W_{PE}(u_{co})$ is maximum and $\frac{d\delta}{dt} \leq 0$.
3. The control variables are selected ($u_c = u_{cl}$) such that the power flow is minimized when $\frac{d\delta}{dt}$ is minimum and $\frac{d\delta}{dt} < -\varepsilon$.
4. The control variables are switched to their nominal operating values when $\frac{d\delta}{dt} = 0$.

5. The control variables are selected such that the power flow is maximized when $\frac{d\delta}{dt}$ is at a maximum value and $\frac{d\delta}{dt} > \varepsilon$.
6. Go to step 2.

The control action is disabled when the magnitude of $|\frac{d\delta}{dt}| < \varepsilon$. (where ε is appropriately specified).

The step 2 needs clarification. Since,$W_{PE} = \int_{\delta_o}^{\delta}(P_t - P_{to})d\delta$, $\frac{dW_{PE}}{dt} = 0$ wherever $\delta = \delta_{max}$ or $P_t = P_{t0}$. If $\delta_{\max} > \delta_u$, then although $\frac{dW_{PE}}{dt} = 0$ at $\delta = \delta_u$, $\frac{d\delta}{dt} > 0$ at that point. The switching of the control variables has to be delayed until $\delta = \delta_u$ in the reverse swing when $\frac{d\delta}{dt} < 0$. Thus, the condition for switching covers both cases (i) $\delta_{\max} < \delta_u$ and (ii) $\delta_u < \delta_{\max} \leq \delta_{um}$.

Note that $W_{PE}(u_c = u_{co})$ is maximum when $\delta = \delta_u$ or $\delta = \delta_{\max}$ ($\delta_{\max} \leq \delta_u$). $W_{PE}(u_{co})$ starts decreasing as δ increases beyond δ_u.

The control strategy can be explained with the help of power angle curves shown in Fig. 11.10. If we consider a major disturbance such as three phase fault at the generator terminals (of the single machine system), the angle δ increases during the fault from δ_0 to δ_{cl} (when the fault is cleared). The accelerating area is 'abcd'. Due to the kinetic energy stored in the rotor, it swings beyond δ_{cl} and reaches a peak of $\delta_{\max}$ when the decelerating area 'defg' is equal to the area 'abcd'. In order to minimize $\delta_{\max}$, it is necessary to maximize the power flow. Assuming $\delta_{\max} \leq \delta_u$, switching the control variables to the nominal operating values at the instant when $\delta = \delta_{\max}$, results in steering the rotor angle δ to the stable equilibrium value of δ_0. When $\delta = \delta_0$, $\frac{d\delta}{dt}$ is negative and is at the minimum. Selecting the control variables such that power flow is minimum, results in reducing the undershoot in the angle. The rotor angle reaches a minimum value of $\delta_{\min}$ such that the accelerating area 'aijk' is equal to the decelerating area 'gha'. At $\delta = \delta_{\min}$, $\frac{d\delta}{dt} = 0$ and switching the control variables to the nominal operating values at this instant results in steering the rotor angle to δ_0. When $\delta = \delta_0$, $\frac{d\delta}{dt}$ is maximum and the control variables are selected such that the power flow in the line is maximum. To summarize our discussion, both overshoot and undershoot of the rotor angle can be minimized if (a) the power flow is maximized when $\delta > \delta_0$, $\frac{d\delta}{dt} > 0$ and (b) the power flow is minimized when $\delta < \delta_0$, $\frac{d\delta}{dt} < 0$.

The variations of the total energy (W_T) and the potential energy (W_{PE}) with time for the two cases (a) $\delta_{\max} \leq \delta_u$, and (b) $\delta_u < \delta_{\max} \leq \delta_{um}$, over the time period of one swing (as δ increases from δ_0 to $\delta_{\max}$, then decreases to $\delta_{\min}$ and reaches δ_0 in the forward swing) are shown in Fig. 11.11. It is to be noted that during the fault ($0 \leq t \leq t_{c1}$) the total energy increases to reach a value of W_1 (which is likely to be higher than W_{cr} and will result in instability unless the control strategy is applied). The energy $W_1 =$

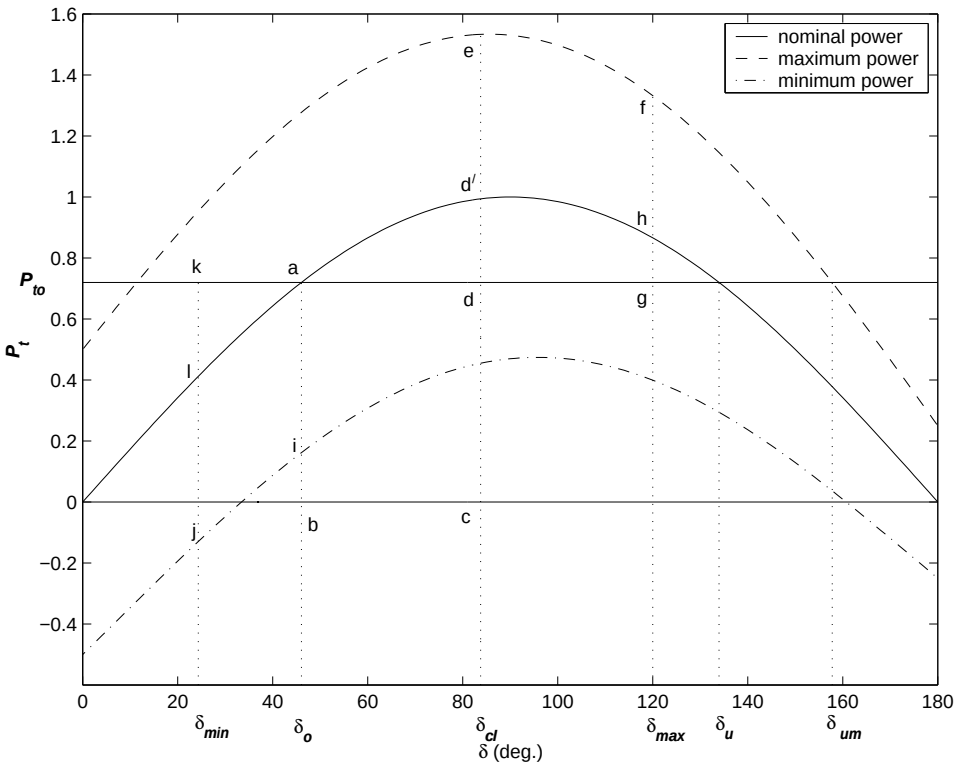

Figure 11.10: Power angle curves

area 'abcdd′' in Fig. 11.10. The control strategy (of maximizing the power flow) at $t = t_{cl}$ results in decrease of W_T to W_2 at $t = t_1$ when $\delta = \delta_{\max}$. The potential energy increases from zero at $t = 0$ to W_2 at $t = t_1$. At the instant $t = t_1$, the kinetic energy is zero. Switching the control variables to nominal operating values at $t = t_1$ (for case (a)) results in W_T remaining constant at W_2 till $t = t_2$ when $\delta = \delta_0$. At this instant $W_{PE} = 0$ and the control variables are switched to the minimum power flow condition. The total energy decreases to W_3 at $t = t_3$ when $\delta = \delta_{\min}$. At this instant, the control variables are switched back to the nominal values and W_T remains constant at W_3 until δ reaches δ_0 at $t = t_4$ when W_{PE} becomes zero. The difference between W_1 and W_2 is the area 'd′efh' in Fig. 11.10. Similarly the difference between W_2 and W_3 is the area 'aijl' in Fig. 11.10.

For case (b) when $\delta_u < \delta_{max} \leq \delta_{um}$, the total energy decreases to W_2 at the instant, $t = t_1$ when $\delta = \delta_{\max}$. At this instant $W_{PE} = W_2$ which is less than W_{cr} given by

$$W_{cr} = \int_{\delta_0}^{\delta_u} [P_t(u_{co}) - P_{to}] d\delta$$

The control variables are switched back to the nominal variables at the

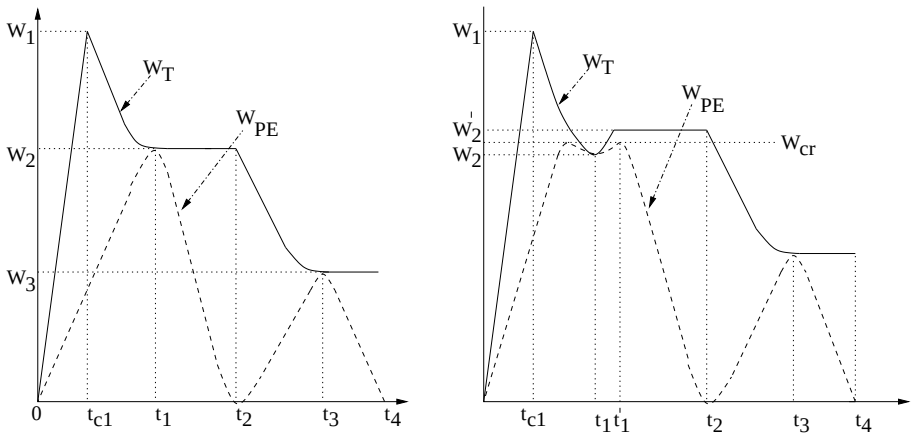

Figure 11.11: Variation of W_T and W_{PE} with time

instant t_1' when $\delta = \delta_u$ when $W_{PE} = W_{cr}$. At this instant, $W_T = W_2'$ (Note that $W_2' > W_2$) and the total energy remains constant till $t = t_2$ when $\delta = \delta_0$. Note also that at $t = t_1'$, the kinetic energy is not zero and $\frac{d\delta}{dt} < 0$.

The application of the control strategy requires the control signal $\delta_{12} = \delta$ and the nominal power flow in the line which can be computed (with the knowledge of the nominal control variables u_{co}). The angle δ_{12} is the difference in the bus angle of the line which can be computed from the local measurements of voltage and current in the line. The knowledge of P_{to} and u_{co} enables the computation of $W_{PE}(u = u_{co})$. Since the switching (from nominal power to maximum (or minimum) power and back) is performed at the instants when $\frac{d\delta}{dt}$ or W_{PE} is at their peak values (or when $\frac{d\delta}{dt}$ is minimum), the exact computation of these control signals is not essential.

11.5.3 Extension of the Control Strategy to Multimachine Power Systems

Whenever a power system becomes transiently unstable, it initially splits into two groups of generators that separate from each other. In addition, for a specified disturbance, there is a unique cutset known as the critical cutset consisting of series elements (transmission lines), connecting the two areas, across which the angle becomes unbounded [31]. It is obvious that if FACTS controllers are located in one or more of the lines forming the critical cutset, the transient stability of the system can be improved apart from damping of the oscillations.

The system can be represented as shown in Fig. 11.12. As derived

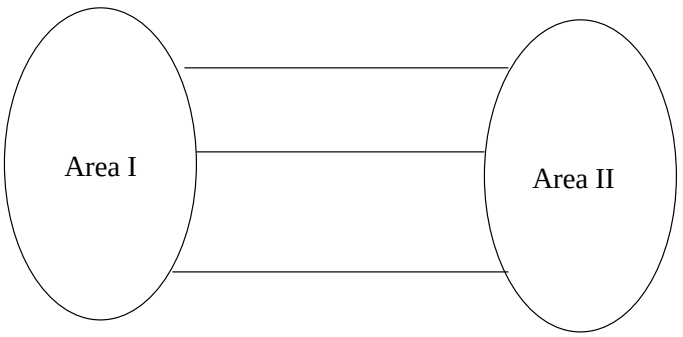

Figure 11.12: Power system divided into two areas connected by the critical cutset

in the section 11.3, the potential energy of the system can be expressed as

$$W_{PE} = \sum_{k=1}^{nb} \int_{t_0}^{t} (P_k - P_{ko}) \frac{d\phi_k}{dt} dt \tag{11.69}$$

where P_k is the power flow in the line k. P_{ko} is the post-fault steady state value ϕ_k is the phase angle across the line. P_k is defined for the post-fault system.

The potential energy can be decomposed into the energy within the two areas and the energy along the critical cutset. Assuming coherent areas, the potential energy within an area is zero as all the buses in that area have the same frequency (and $\frac{d\phi_k}{dt} = 0$ for all the series elements in that area). Hence the potential energy given by Eq. (11.69) can be expressed as follows:

$$W_{PE} = \sum_{k=1}^{nc} \int_{t_0}^{t} (P_k - P_{ko}) \frac{d\phi_k}{dt} dt \tag{11.70}$$

where nc is the number of lines in the critical cutset. Assuming that the variation of energy in all the lines in the critical cutset is similar, we can express W_{PE} as,

$$W_{PE} = A_k \int_{t_0}^{t} (P_k - P_{ko}) \frac{d\phi_k}{dt} dt \tag{11.71}$$

where A_k is a constant for the chosen line k in which we intend to connect FACTS controller.

The approximation given in Eq. (11.71) is used to extend the control strategy for multimachine systems. If multiple FACTS controllers are installed in more than one line, we can still apply the control strategy in a decentralized fashion by considering only W_k (energy in a line) in place of W_{PE}. Since W_{PE} is the sum of energies in individual lines, the decentralized control strategy works.

11.6 Case Studies of Discrete Control for Stability Improvement

11.6.1 A SMIB System with a TCSC

This example is taken from [25]. A synchronous machine is connected to an infinite bus through a line of reactance 0.7 p.u. A TCSC with a nominal capacitive reactance of 0.1 p.u. and maximum capacitive reactance of 0.4 p.u. is connected in the line. The generator is represented by the classical model of a constant voltage source E_g behind a transient reactance of 0.32 p.u. The initial and final operating point is $V_g = E_b = 1.0$ p.u., $P_g = 1.0$ p.u. The initial and the post-fault stable equilibrium angle (with $X_{TCSC} = 0.1$) is $\delta_0 = 53°$. The control strategy is simpler than what is presented in section 11.5.2 and is given below:

1. The TCSC (capacitive) reactance is switched to the maximum value as soon the disturbance is detected (at the time of clearing of a fault).
2. The TCSC is switched to the nominal value when W_{PE} (computed for the nominal value of TCSC reactance) is maximum and $\frac{d\delta}{dt} \leq 0$.
3. The TCSC reactance is switched to the maximum when $\frac{d\delta}{dt}$ is at a maximum provided that it exceeds a tolerance (ε).

Note that the TCSC was not switched to a minimum value (corresponding to inductive reactance) to avoid inductive vernier operation.

For a three phase fault at the generator terminals, the critical clearing time is increased from 0.1 s to 0.178 s when the switching strategy was used. The u.e.p. (unstable equilibrium point) for the system with nominal value of TCSC reactance is 127°. With the switching strategy, $\delta_{\max}$ can be increased up to 143° (u.e.p. with maximum value of TCSC reactance). The rotor angle oscillations were damped in less than 3.5 s (after three swings).

The strategy was also tried with detailed one-axis model of the generator with the following data:

$$x_d = 1.6, x'_d = 0.32, T'_{do} = 6s, x_q = 1.55, H = 5, f_0 = 60 \text{ Hz}.$$

The critical clearing time is increased from 0.075 to 0.134 s (without AVR) and from 0.092 to 0.166 s (with AVR).

11.6.2 A UPFC in a 10 Machine System

Fig. 11.13 shows the single line diagram of the 10 machine, 39 bus New England System. The data are given in [1]. The generators are represented

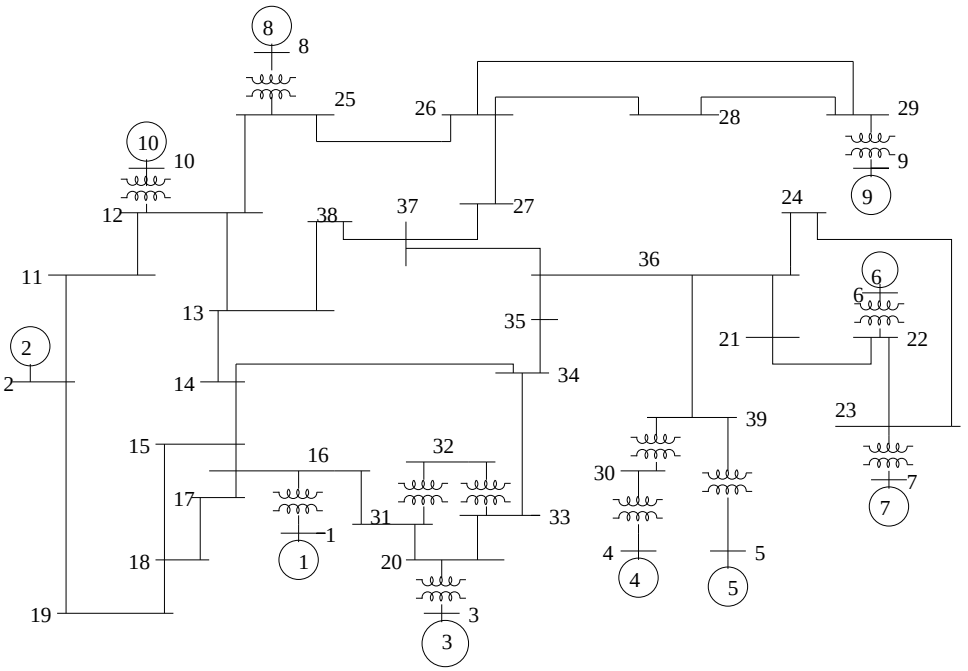

Figure 11.13: Single line diagram of 10 machine system

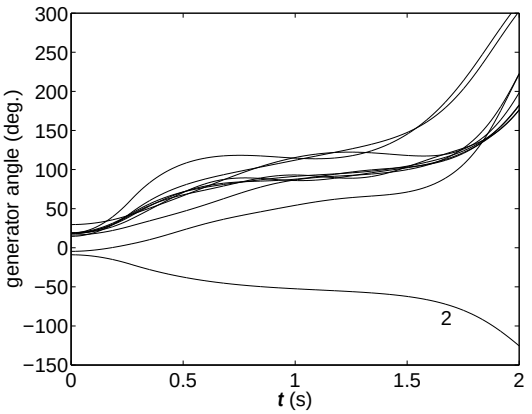

Figure 11.14: Swing curves without control

by classical models and loads are assumed to be of constant impedance type. The network losses are ignored.

Fig. 11.14 shows the swing curves without any control for a fault at bus 34 cleared by tripping the line 34-35 at 0.267 s. The system is unstable; generator 2 separates from the rest of the system. The lines 11-12 and 18-19 form the critical cutset. The same disturbance is simulated with a UPFC

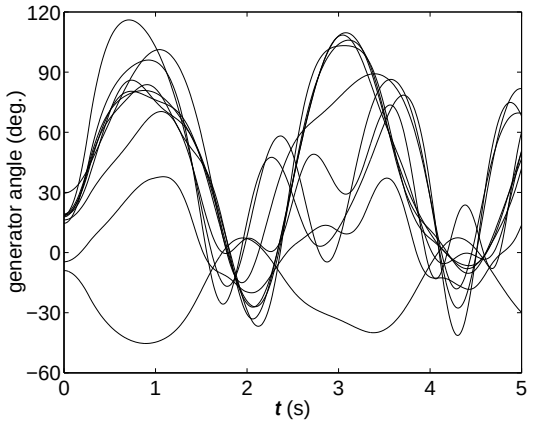

Figure 11.15: Swing curves with control action initiated at the instant of fault clearing

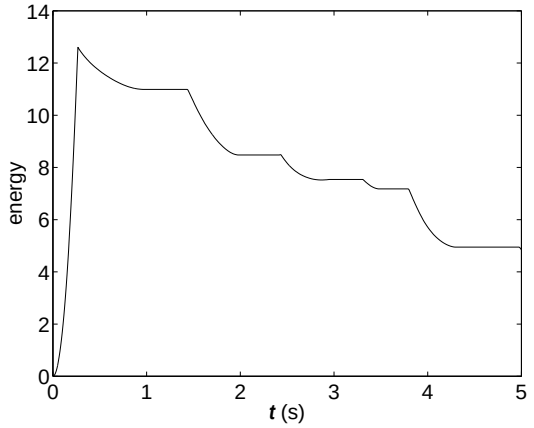

Figure 11.16: System energy variation with time

connected in line 11-12 with shunt converter connected to bus 11. A rating of 0.2 p.u. is used for both series voltage and shunt current of UPFC. It is assumed that UPFC does not inject any voltage or current in steady state. With the discrete control initiated at the instant of fault clearing, the system remains stable as shown in Fig. 11.15. Fig. 11.16 shows the variation of the total system energy (computed for the nominal power flow conditions). With every switching of the UPFC control variables to maximize or minimize the power flow in the line, the energy decreases, thus contributing to system damping. In the absence of the control, the energy would have remained constant.

The control strategy for a multimachine power system was derived by assuming strict coherency in each of the two areas separated by the critical

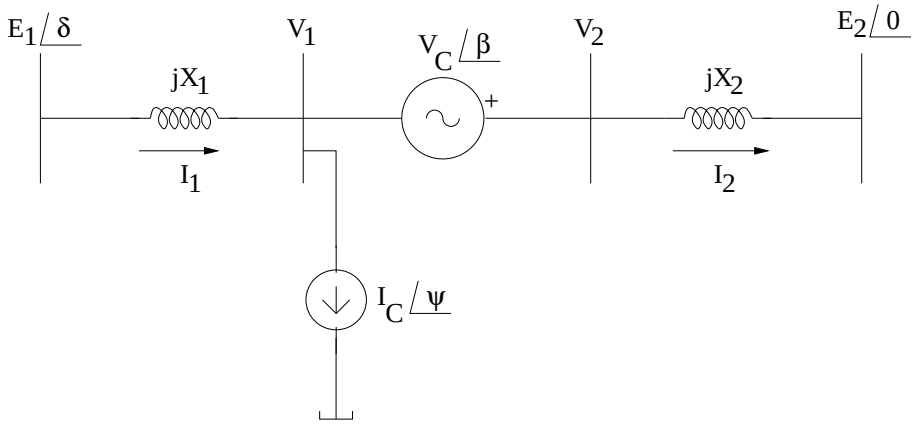

Figure 11.17: A UPFC connected in a line

cutset. While this assumption is not strictly valid, the energy in the lines forming the cutsets is primarily the energy that is responsible for system separation. The provision of FACTS controllers in the lines forming the critical cutset definitely helps in improving transient stability and damping of oscillations, using the control strategy.

The investigation of the critical cutsets in a large practical system (of 355 buses, 587 lines and 55 generators) indicated that there is a small subset of critical lines that have a high probability (occurrence) of membership in a critical cutset even when a large set of credible contingencies (disturbances) are considered [42]. This result simplifies the problem of locating a FACTS controller for stability improvement.

Power Flow Control with UPFC

Consider a line with Thevenin equivalents at the two ends (See Fig. 11.17). The total series reactance between the two voltage sources is $X_1 + X_2$. The current $\hat{I}_2$ can be obtained by superposition as

$$\hat{I}_2 = \frac{E_1\angle\delta - E_2\angle 0}{jX} + \frac{V_C\angle\beta}{jX} - \frac{X_1}{X_1 + X_2} I_C\angle\psi \tag{11.72}$$

The power flow P in the line and the voltage V_1 are given by

$$P = Re[E_2 I_2^*], \quad V_1 = E_1\angle\delta - jI_1X_1$$

where $\hat{I}_1 = \hat{I}_2 + I_C\angle\psi$, $X = X_1 + X_2$.

The problem of maximizing or minimizing the power flow P is a constrained optimization problem with 4 control variables (V_C, I_C, β and ψ) with one equality and two inequality constraints given by

$$Re[V_1 I_C^*] = Re[V_C I_2^*] \tag{11.73}$$

$$0 \leq V_C \leq V_{C\max} \tag{11.74}$$

$$0 \leq I_C \leq I_{C\max} \tag{11.75}$$

where $V_{C\max}$ and $I_{C\max}$ represent the ratings of the series and the shunt converter respectively.

For a general case, the problem has to be solved by numerical methods. However, for the special case when $E_1 = E_2 = E$, $X_1 = X_2 = \frac{X}{2}$, we get the analytical result (see chapter 8) as follows.

For maximum power flow in the line,

$$\beta = \frac{\delta}{2} + \frac{\pi}{2}, \quad \psi = \frac{\delta}{2} + \frac{\pi}{2}, \quad 0 < \delta < \pi \tag{11.76}$$

For minimum power flow in the line,

$$\beta = \frac{\delta}{2} - \frac{\pi}{2}, \quad \psi = \frac{\delta}{2} - \frac{\pi}{2}, \quad 0 < \delta < \pi \tag{11.77}$$

The expression for the maximum and minimum power are

$$P_{\max} = \frac{EV_{C\max}}{X}\cos\frac{\delta}{2} + \frac{EI_{C\max}}{2}\sin\frac{\delta}{2} + \frac{E^2\sin\delta}{X} \tag{11.78}$$

$$P_{\min} = \frac{-EV_{C\max}}{X}\cos\frac{\delta}{2} - \frac{EI_{C\max}}{2}\sin\frac{\delta}{2} + \frac{E^2}{X}\sin\delta \tag{11.79}$$

Note that for both $P_{\max}$ and $P_{\min}$, $V_C = V_{C\max}$ and $I_C = I_{C\max}$: It can also be shown (for both cases), the power in the DC link (exchanged between the series and shunt converters) is given by

$$P_{DC} = \frac{V_{C\max}I_{C\max}}{2} \tag{11.80}$$

The power is transferred from the series converter to the shunt converter.

References and Bibliography

1. K.R. Padiyar, **Power System Dynamics - Stability and Control**, Second Edition, Hyderabad: B.S. Publications, 2002.
2. J.W. Chapman, M.D. Ilic, C.A. King, L. Eng and H. Kaufman, "Stabilizing a multimachine power system via decentralized feedback linearizing excitation control", IEEE Trans. on Power System, v.8, n. 3, 1993, pp. 830-839.
3. D.J. Hill and J.M.Y. Mareels, "Stability theory for differential/algebraic systems with application to power system", IEEE Trans. on Circuits and Systems, v. 37, n. 11, 1990, pp. 1416-1423.

4. V. Rajkumar and R.R. Mohler, "Nonlinear control methods for power systems: A comparison", IEEE Trans. on Control Systems Technology, v. 3, n. 2, 1995, pp. 231-237.
5. G. Guo, Y. Wang and D.J. Hill, "Nonlinear output stabilization control of multimachine power systems" IEEE Trans. on Circuits and Systems, Part I, v. 47, n.1, 2000, pp. 46-53.
6. Y. Guo, D.J. Hill and Y. Wang, "Global transient stability and voltage regulation for power systems", IEEE Trans. on Power Systems, v. 16, n. 4, 2001, pp. 678-688.
7. Y.J. Cao et al, "Nonlinear control of power system multi-mode oscillations", Elect. Power & Energy Syst., v. 20, n. 1, 1998, pp. 61-68.
8. N. Kakimoto, A. Nakanishi and K. Tomiyama, "Instability of interarea oscillation mode by autoparametric resonance", IEEE Trans. on Power Systems, v. 19, n. 4, 2004, pp. 1961-1970.
9. V. Venkatasubramanian, K.W. Schneider and C.W. Taylor, "Improving Pacific intertie stability using existing static VAR compensators and Thyristor Controlled Series Compensation", Bulk Power System Dynamics and Control IV – Restructuring, Santorini, Greece, August
10. D.N. Kosterev, C.W. Taylor and W.A. Mittelstadt, "Model validation for the August 10, 1996 WSCC system outage", IEEE Trans. on Power Systems, v. 14, n. 3, 1999, pp. 967-979.
11. R.J. Davy and I.A. Hiskens, "Lyapunov functions for multimachine power systems with dynamic loads", IEEE Trans. on Circuits and Systems-I: Fund. Theory and Applications, v. 44, n.9, 1997, pp. 796-812.
12. M. Ghandhari, G. Andersson and I.A. Hiskens, "Control Lyapunov functions for controllable series devices", IEEE Trans. on Power Systems, v. 16, n. 4, 2001, pp. 689-694.
13. M. Ghandhari, G. Andersson, M. Pavella and D. Ernst, "A control strategy for controllable series capacitor in electric power systems", Automatica, v. 37, 2001, pp. 1575-1583.
14. M.A. Pai, **Energy Function Analysis for Power System Stability**, Boston: Kluwer Academic Publishers, 1989.
15. M. Pavella, D. Ernst and D. Ruiz-Vega, **Power System Transient Stability Analysis and Control**, Boston: Kluwer Academic Publishers, 2000
16. Y. Zou, M. Hin and H.D. Chiang, "Theoretical foundation of the controlling UEP method for direct transient stability analysis of netowrk-preserving power system models", IEEE Tran. on Circuits and Systems-I: Fund. Theory and Appl., v. 50, n. 10, 2003, pp. 1324-1336.

17. K.R. Padiyar and K.K. Ghosh, "Direct stability evaluation of power systems with detailed generator models using structure preserving energy functions", Elect. Power & Energy Syst., v. 11, n. 1, 1989, pp. 47-56.

18. K.R. Padiyar and H.S.Y. Sastry, "A structure preserving energy function for stability analysis of AC/DC systems", Sadhana (Proc. in Engg. Sciences, Indian Academy of Sciences), v. 18, Part 5, 1993, pp. 787-799.

19. K.R. Padiyar and Vijayan Immanuel, "Modelling of SVC for stability evaluation using structure preserving energy function", Elect. Power & Energy Syst., v. 16, n. 5, 1994, pp. 339-348.

20. E.W. Kimbark, "Improvement of system stability by switched series capacitors", IEEE Trans., v. PAS-85, 1966, pp. 180-188.

21. O.J.M. Smith, "Power system transient control by capacitor switching", IEEE Trans., v. PAS-88, 1969, pp. 28-35.

22. N. Rama Rao and D.K. Reitan, "Improvement of power system transient stability using optimal control: Bang-bang control of reactance", IEEE Trans., v. PAS-89, 1970, pp. 975-983.

23. D.N. Kosterev and W.J. Kolodziej, "Bang-bang series capacitor transient stability control", IEEE Trans. on Power Systems, v. 10, n. 2, 1995, pp. 915-923.

24. J.F. Gronquist et al, "Power oscillation damping control strategies for FACTS devices using locally measurable quantities", IEEE Trans. on Power Systems, v. 10, n.3, 1995, pp. 1598-1605.

25. K.R. Padiyar and K. Uma Rao, "Discrete control of series compensation for stability improvement in power systems", Elec. Power & Energy Syst., v. 19, n. 5, 1997, pp. 311-319.

26. J. Chang and J.H. Chow, "Time-optimal control of power systems requiring multiple switchings of series capacitors", IEEE Trans. on Power Systems, v. 13, n. 2, 1998, pp. 367-373.

27. S. Krishna and K.R. Padiyar, "Discrete control of unified power flow controller for stability improvement", Electric Power Systems Research, 2005, pp. 178-189.

28. K.R. Padiyar and P. Varaiya, "A network analogy for power system stability analysis", Preprint, Dec. 1983.

29. R. Mihalic, P. Zunko and D. Povh, "Improvement of transient stability using unified power flow controller", IEEE Trans. on Power Delivery, v. 11, n. 1, 1996, pp. 485-492.

30. K.R. Padiyar and K. Uma Rao, "Modeling and control of unified power flow controller for transient stability", Elect. Power & Energy Syst., v. 21, 1991, pp. 1-11.

31. K.R. Padiyar and S. Krishna, "On-line detection of loss of synchronism using energy function criterion", IEEE Trans. on Power Delivery, v. 21, n. 1, 2006, pp. 46-55.

32. R. Mihalic and U. Gabrijel, "A structure-preserving energy function for a static series synchronous compensator", IEEE Trans. on Power Systems, v. 19, n.3, 2004, pp. 1501-1507.

33. V. Azbe, U. Gabrijel, D. Povh and R. Mihalic, "The energy function of a general multimachine system with a unified power flow controller", IEEE Trans. on Power Systems, v. 23, n. 3, 2005, pp. 1478-1485.

34. IEEE/CIGRE Joint Task Force, "Definition and classification of power system stability", IEEE Trans. on Power Systems, v. 19, n.2, 2004, pp. 1387-1401.

35. C.A. Desoer and E.S. Kuh, **Basic Circuit Theory**, New York, McGraw Hill, 1969.

36. S. Krishna, **Dynamic Security Assessment and Control using Unified Power Flow Controller**, Ph.D. Thesis submitted to IISc, Bangalore, March 2003.

37. H.D. Chiang, F.F. Wu and P. Varaiya, "Foundations of direct methods for power system transient stability analysis", IEEE Trans. Circuits Syst., v. CAS-34, Feb. 1987, pp. 160-173.

38. Y. Zhang, L. Wehenkel, P. Rousseaux and M. Pavella, "SIME: A hybrid approach to fast transient stability assessement and contingency selection", Elect. Power & Energy and Syst., v. 19, n.3, 1997, pp. 195-208.

39. H.D. Chiang, F.F. Wu and P. Varaiya, "Foundations of Potential Energy Boundary Surface method for power system transient stability analysis", IEEE Trans. Circuits and Syst., v. CAS-35, June 1988, pp. 712-728.

40. A.A. Found and V. Vittal, **Power System Transient Stability Analysis Using the Transient Energy Function Method**, Englewood Cliffs, NJ: Prentice-Hall, 1991.

41. M. Athans and P.L. Falb, **Optimal Control: An Introduction to the Theory and its Applications**, New York: McGraw-Hill, 1966.

42. K.R. Padiyar, S. Krishna and Nagesh Prabhu, "On-line detection of loss of synchronism is large power systems", Int. Conf. on Power Systems, Katmandu, Nepal, November 2004.

This page intentionally left blank

Chapter 12

Power Quality and Introduction to Custom Power Devices

12.1 General

The concept of custom power was introduced by N.G. Hingorani [1] in 1995 as an extension of the FACTS concept to distribution systems. The major objective is to improve power quality (PQ) and enhance reliability of power supply. The concept of FACTS was also proposed by Hingorani in 1988.

The term 'custom power' describes the value-added power that electric utilities will offer their customers. The value addition involves the application of high power electronic controllers (similar to FACTS) to distribution systems, at the supply end of industrial, commercial customers and industrial parks [1]. The provision of custom power devices (CPD) is complementary to the individual end-use equipment at low voltages (such as UPS (Uninterruptible Power Supply) or standby generators).

The traditional electric power reliability focuses on availability of power supply (no sustained interruptions). The reliability in distribution systems is usually measured in terms of frequency and duration of the outages. One of the reliability indices, the Average Service Availability Index (ASAI) is the ratio of hours of available service in a year to the hours in a year. In developed countries such as in U.S.A., the average utility customer is subjected to only one hour of interruption in a year. This works out to the ASAI of typically 0.99989 (99.99%). Although this looks impressive, the problems of power quality affect many customers with sensitive loads. Momentary interruptions lasting less than 3 seconds can affect process industries such as plastic injection moulding plants, computers networks etc.

The power quality has serious economic implications for customers, utilities and electrical equipment manufacturers. Modernization and automation of industry involves increasing use of computers, microprocessors and power electronic systems such as adjustable speed drives. Integration of non-conventional generation technologies such as fuel cells, wind turbines and photo-voltaics with utility grids often requires power electronic interfaces. The power electronic systems also contribute to power quality prob-

lems (generating harmonics).

Under the deregulated environment, in which electric utilities are expected to compete with each other, the customer satisfaction becomes very important. The impact of power quality problems is increasingly felt by customers - industrial, commercial and even residential. The equipment suppliers have to take hard decisions about including features that will tolerate (or withstand) power quality problems. This adds to the cost of the equipment.

12.2 Electromagnetic Phenomena and Power Quality

The power quality problems are primarily due to electromagnetic disturbances which are broadly classified by IEC as follows.

1. Conducted low frequency phenomena
2. Radiated low frequency phenomena
3. Conducted high frequency phenomena
4. Radiated high frequency phenomena
5. Electrostatic discharge phenomena (ESD)
6. Nuclear electromagnetic pulse (NEMP)

For power quality applications, the following categories are defined along with their characteristics.

12.2.1 Temporary Phenomena

1. Transients

These are undesirable but decay with time and hence not a steady state problem. A broad definition is that a transient is "that part of the change in a variable that disappears during transition from one steady state operating condition to the other" [34]. Another synonymous term is 'surge'.

Transients are classified into two categories:

(a) Impulsive

(b) Oscillatory

An impulsive transient has unidirectional (positive or negative) polarity and is characterized by the rise and decay times. For example, a 1.2/50 μs, 1000 V impulsive transient rises from zero to the peak value in 1.2 μs and then decays to half its peak value in 50 μs. An impulsive transient is mathematically defined by

$$I(t) = A(e^{-\alpha t} - e^{-\beta t}) \tag{12.1}$$

The peak value, rise time and decay time can be found from the parameters, A, α and β.

Impulsive transients can be due to (i) lightning discharge or (ii) switching due to opening and closing of circuit breakers.

An oscillatory transient is a sudden non-power frequency change that is bi-directional (both positive and negative polarities). Depending on the frequency range, the oscillatory transients are classified as (i) high frequency (>500 kHz), (ii) medium frequency (5-500 kHz) and (iii) low frequency (<5 kHz). The high frequency transients are often due to the response of the network to an impulsive transient. The medium frequency transient can result from back-to-back capacitor energization or cable switching. Low frequency transients can be due to capacitor bank energization. Ferroresonance and transformer energization can cause oscillatory transients with principal frequencies below 300 Hz. A mathematical description of oscillatory transient is given by

$$O(t) = \sum_n A_n e^{-\alpha_n t} \sin(\omega_n t + \phi_n) \tag{12.2}$$

Note that there could be more than one frequency involved in the transient.

It is possible to categorize transients according to their mode. A transient in a 3 phase system with a neutral conductor can be either common mode or normal mode depending on whether ground is involved or not.

2. Long Duration Voltage Variations

When rms (root mean square) deviations at power frequency last longer than one minute, we say they are long duration voltage variations.

They can be either overvoltages (greater than 1.1 p.u.) or undervoltages (less than 0.9 p.u.).

Overvoltages are usually the result of switching off a load or energizing a capacitor bank. Incorrect tap settings on transformers can also result in overvoltages. Undervoltages are the result of events which are the reverse of events that cause overvoltages - switching in a load or switching off a capacitor bank.

3. Sustained Interruptions

When the supply voltage has been zero for a period of time greater than one minute, then we say it is a sustained interruption. Generally, voltage interruptions lasting over one minute are often permanent and requires human intervention to restore the supply. The term 'outage' used by utilities is synonymous, however it does not bring out the true impact of the power interruption. For a customer with a sensitive load, even an interruption of half a cycle can be disastrous.

4. Short Duration Voltage Variations

These are further classified as

(a) Instantaneous (0.5-30 cycles)

(b) Momentary (30 cycles - 3 s)

(c) Temporary (3 s - 1 min)

Short duration voltage variations are generally caused by (i) fault conditions (ii) energization of large loads such as induction motors. The voltage variations can be temporary voltage dips (sags) or voltage rises (swells) or a complete loss of voltage (interruptions).

Interruption

An interruption occurs when the supply voltage or load current decreases to less than 0.1 p.u. for a period of time not exceeding one minute. Interruptions can be due to either system faults, equipment failures or control malfunctions. The interruptions are measured by their duration alone. The duration due to a fault is determined by the operating time of the protective devices. Instantaneous reclosure will limit the interruption caused by a non-permanent fault to less than 30 cycles. Duration of an interruption due to equipment malfunction can be irregular.

Some interruptions may be preceded by a voltage sag when there are faults on the source side. The voltage sag occurs between the initiation of the fault and the operation of the protective device to clear the fault.

Voltage Sags

A sag is a decrease of rms voltage to a value between 0.1 and 0.9 p.u. and lasting for duration between 0.5 cycle to 1 minute. IEC defines voltage sag as a voltage dip. Voltage sags are mainly due to system faults and last for durations ranging from 3 cycles to 30 cycles depending on the fault clearing time. It is to be noted that undervoltages (lasting over a minute) can be

handled by voltage regulation equipment. The magnitudes of the voltages sags caused by faults depend upon the distance of the fault location from the bus where the sag is measured.

Starting of large induction motors can result in voltage sags as the motor draws a current up to 10 times the full load current during the starting. Also, the power factor of the starting current is generally poor.

Voltage Swells

A voltage swell is defined as an increase to between 1.1 and 1.8 p.u. in rms voltage at the power frequency for duration between 0.5 cycle to 1 minute. A voltage swell (like a sag) is characterized by its magnitude (rms) and duration. As with sags, swells are associated with system faults. A SLG fault can result in a voltage swell in the unfaulted phases. Swells can also result form energizing a large capacitor bank.

The magnitude of a voltage swell depends on the system impedance, fault location and grounding. On an ungrounded system, the line to ground voltages on the ungrounded phases are 1.73 p.u. during a SLG fault. However in a grounded system, there will be negligible voltage rise on the unfaulted phases close to a substation where the delta connected windings of the transformer (usually connected delta-wye) provide a low impendence paths for the zero sequence current during the SLG fault.

12.2.2 Steady State Phenomena

1. Voltage Imbalance (Unbalance)

Voltage imbalance can be defined using symmetrical components. The ratio of the negative sequence (or zero sequence) component to the positive sequence component is a measure of unbalance.

The main source of voltage unbalance are single phase loads on a three phase circuit resulting in load imbalance. Severe imbalance can be caused by single-phasing conditions.

2. Waveform Distortion

This is defined as a steady-state deviation from an ideal sine wave of power frequency. There are five types of waveform distortion:

(a) DC offset

(b) Harmonics

(c) Interharmonics

(d) Notching

(e) Noise

The presence of DC voltage or current in AC power systems is termed as DC offset. This can occur as the result of a geomagnetic disturbance or ground return operating mode in monopolar HVDC links. The DC current flow in transformers cause magnetic saturation, increased heating and loss of transformer life.

Nonlinear loads and power electronic controllers are the primary source of harmonics. Fourier analysis can be used to characterize harmonic distortion. Total Harmonic Distortion (THD) is one of the most commonly used measures for harmonics and is defined as

$$THD = \frac{\left[\sum_{h=2}^{h_{\max}} M_h^2\right]^{1/2}}{M_1} \tag{12.3}$$

where M_h is the rms value of the harmonic (h) component of M (current or voltage).

Major problems that arise from harmonic distortion are

1. Extra losses and heating in rotating machines and capacitors
2. Overvoltages due to resonance
3. Interference with ripple control systems used in Demand Side Management (DSM)
4. Telephone interference caused by noise on telephone lines.

Voltages or currents having frequency components that are not integer multiples of the supply frequency (50 or 60 Hz) are called interharmonics. The main sources of interharmonics are static frequency converters, cycloconverters and back to back HVDC links. Interharmonics can affect power line carrier signalling and cause visual flicker in display devices such as cathode ray tubes (CRT).

Notching is a periodic disturbance in the voltage waveform introduced by power converters when current is commutated from one phase to another (under normal operation). Since notching is a steady state phenomenon, it can be analyzed using Fourier series that gives the harmonic spectrum of the affected voltage. However, notching is treated as a special case as the frequency components associated with notching can be high and outside the range of measuring equipment normally used for harmonic analysis.

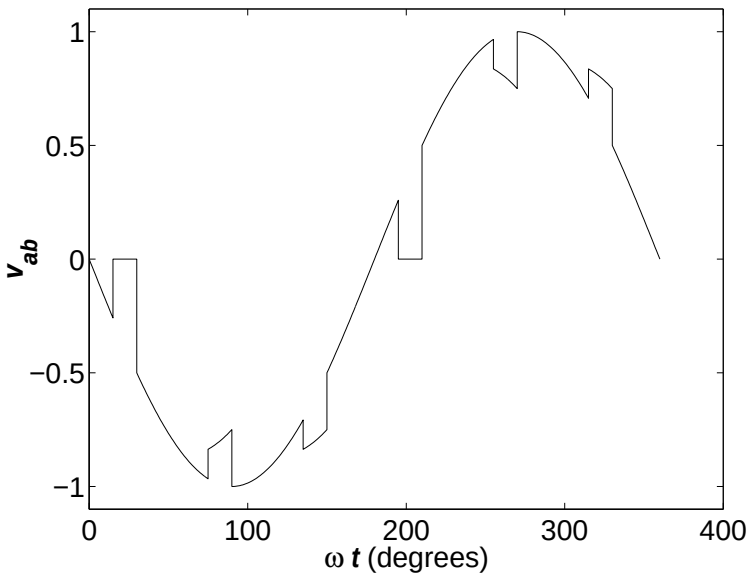

Figure 12.1: An example of voltage notching

An example of the notching produced by a three phase Graetz bridge supplying continuous DC current is shown in Fig. 12.1. The notches result from momentary short circuit across two phases during the commutation period.

Notching can result in multiple zero voltage crossing which can cause digital clocks to run fast as their design is based on two crossing per cycle.

Noise can be defined as unwanted electrical signals with broadband spectral content less than 200 kHz which is superimposed on the voltage or current in distribution lines. Noise can be caused by power converters, arcing equipment or switched mode power supplies. Noise affects electronic devices such as microcomputer and programmable controllers. The noise problem can be mitigated by using filters, isolation transformers and line conditioners.

12.2.3 Voltage Fluctuations and Flicker

Voltage fluctuations are systematic variations of the voltage envelope or a series of random changes in the voltage magnitude (which lies in the range of 0.9 to 1.1 p.u.)

High power loads that draw fluctuating current, such as large motor drives and arc furnaces, cause low frequency cyclic voltage variations that result in flickering of light sources (incandescent and fluorescent lamps) which

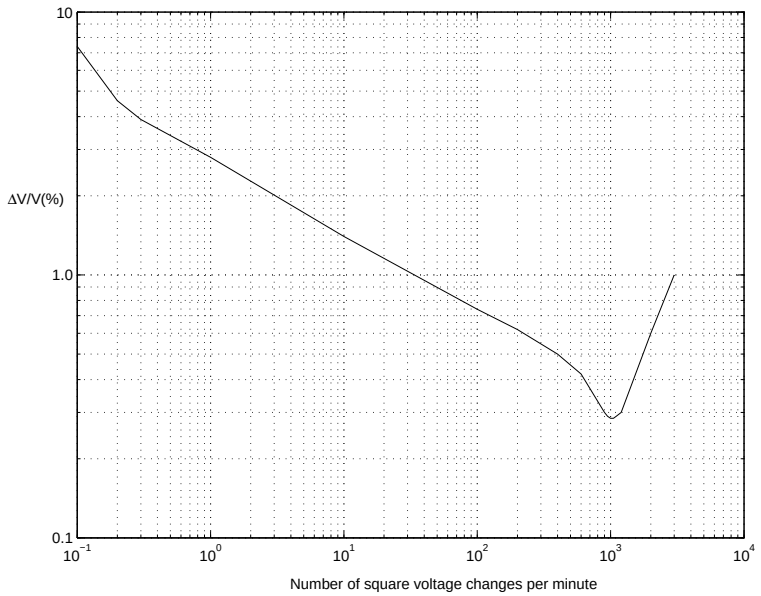

Figure 12.2: Flicker perception characteristic for square shape voltage changes applied to 60 W bulbs

can cause significant physiological discomfort or irritation in human beings. The voltage flicker can also affect stable operation of electrical and electronic devices such as motors and CRT devices. The typical frequency spectrum of voltage flicker lies in the range from 1 Hz to 30 Hz.

The luminous flux of the lamps fluctuate with voltage flicker. The perception of human eye varies with the frequency of variations and is most sensitive in the range of 6 to 12 Hz. For example, the variations in the voltage amplitude of 0.3% at 10 Hz can be detected. Figure 12.2 shows the threshold of perception of flicker (measured as percentage of $\Delta V/V$) as a function of frequency of voltage changes. It is assumed that the voltage waveform is sinusoidal (at power frequency) and the magnitude is varying as a periodic square wave of a specified frequency. The measurements of the flicker perception are shown for a 60 W, 230 V tungsten bulb.

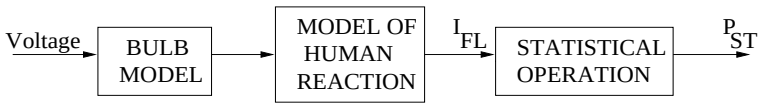

Figure 12.3: Block diagram of flickermeter

International Electrotechnical Commission (IEC) has brought out a standard IEC 1000-4-15 for flicker measurement based on the protocol developed by Union of Electroheat (UIE) [35]. The block diagram of the flick-

(a) Block diagram of the bulb model

(b) Block diagram of model of human reaction

Figure 12.4: Details of flickermeter

ermeter is shown in Fig. 12.3. The input is the voltage signal in the analog or digital form. The fluctuating components of the voltage are obtained by demodulating the signal $v(t)$. This is realized by using a squaring circuit followed by a high pass and a low pass filter (see Fig. 12.4(a)). The high pass filter with a cut off frequency of 0.05 Hz serves to remove the constant component. The low pass filter with a cut off frequency of 35 Hz represents the dynamic properties of a 60 W, 230 V tungsten lamp.

The model of the human reaction (eye and the brain) to the fluctuations in the lamp luminosity is the weighing curve in the frequency domain. The weighing curve is represented as the Bode plot (magnitude versus frequency) of a band pass filter with the following transfer function

$$H(s) = \frac{k\omega_1 s}{s^2 + 2\lambda s + \omega_1^2} \cdot \frac{1 + \frac{s}{\omega_2}}{\left(1 + \frac{s}{\omega_3}\right)\left(1 + \frac{s}{\omega_4}\right)} \tag{12.4}$$

where, for a 60 W, 230 V incandescent lamp,

$$k = 1.74802, \quad \lambda = 2\pi \cdot 4.05981, \quad \omega_1 = 2\pi \cdot 9.15494$$
$$\omega_2 = 2\pi \cdot 2.27979, \quad \omega_3 = 2\pi \cdot 1.22535, \quad \omega_4 = 2\pi \cdot 21.9$$

This filter is designed based on the psycho-physiological research on the influence of luminous flux changes on the human being. The weighing filter is followed by a squaring multiplier and 0.53 Hz low pass (smoothing) filter that models the fatigue effect of luminous flux changes. The block diagram of the model of human reaction is shown in Fig. 12.4(b). The output of this model is the instantaneous flicker (I_{FL}). The Bode plot of the weighing filter is shown in Fig. 12.5.

The instantaneous flicker, $I_{FL}(t)$ is given as input to statistical processing or evaluation block. This computes Cumulative Probability Function (CPF) based on samples of I_{FL} collected over an observation time of 10 minutes. For convenience, I_{FL} is divided into a number of groups (or classes)

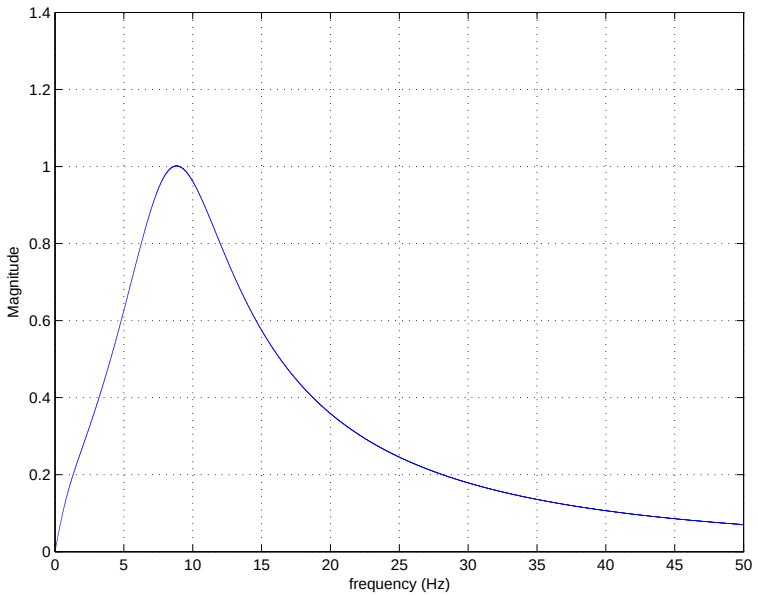

Figure 12.5: Bode plot of weighing filter

see Fig. 12.6(a) which shows I_{FL} plotted as a function of time (over a period of 10 minutes). Signal duration in a particular class say 7 is indicated as $T_7 = \sum t_i = t_1+t_2+t_3+t_4+t_5$. This can be converted into percentage of the observation time. From the knowledge of the percentage of time for which I_{FL} belongs to a class, we can compute CPF. A typical variation of CPF as a function of the I_{FL} (discretized into classes) is shown in Fig. 12.6(b). The y axis indicates percentiles corresponding to a level k such that the instantaneous flicker exceeds the level for the percentage of the time indicated on the y axis.

The short term flicker severity (P_{ST}) is defined by

$$P_{ST} = [0.0314P_{0.1} + 0.0525P_{1s} + 0.0657P_{3s} + 0.28P_{10s} + 0.08P_{50s}]^{1/2} \quad (12.5)$$

where $P_{0.1}$ is the flicker level corresponding to 0.1%. Similar definitions apply to P_1, P_3, P_{10} and P_{50}. The subscript s indicates that averaging (or smoothing) is applied according to the following formulae:

$$\begin{aligned} P_{1s} &= (P_{0.7} + P_1 + P_{1.3})/3 \\ P_{3s} &= (P_{2.2} + P_3 + P_4)/3 \\ P_{10s} &= (P_6 + P_8 + P_{10} + P_{13} + P_{17})/5 \\ P_{50s} &= (P_{30} + P_{50} + P_{80})/3 \end{aligned}$$

The short term flicker values are used to evaluate long term flicker severity

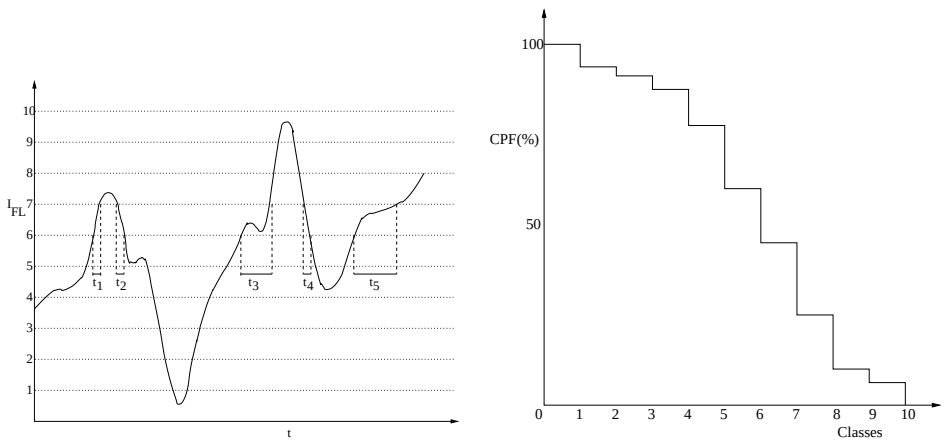

(a) Variation of I_{FL} with time

(b) Cumulative probability function

Figure 12.6: Statistical operation

from,

$$P_{LT} = \left[\frac{\sum_{i=1}^{N} P_{ST_i}^3}{N} \right]^{1/3} \tag{12.6}$$

where N is the number of 10 minute intervals within the observation time of P_{LT}. For example, there are 12 P_{ST} measurements in a two hour period over which P_{LT} is calculated.

P_{ST} is used as a measure of voltage flicker instead of maximum value of instantaneous flicker as a higher level of flicker can be tolerated for a very short time. The value of $P_{ST} > 1$ corresponds to the threshold of irritability for 50% of the persons subjected to the measured flicker.

12.2.4 Power Frequency Variations

These are defined as the deviations of the system (fundamental) frequency from its specified value of 50 or 60 Hz. The variations in the frequency arise from the changes in the load and the response of the generators to meet the load. Thus the load characteristics (dependence on the frequency) and the control characteristics of the generators (turbine-governors and automatic generation control (AGC) system if they are operational) affect the shift in the frequency.

In modern interconnected power systems, frequency variations are insignificant most of the time unless governor and load frequency controls are disabled under a regime of power shortages and a lack of grid discipline.

Economic incentives or disincentives that ensure balance between available generation and load may help control over frequency variations under normal operating conditions. For example, Availability Based Tariff (ABT) that charges inadvertent tie line flows according to the system frequency is claimed to be a solution to the problem of large frequency excursions. In this scheme, a state utility overdrawing from the central generating stations when the frequency is low, is penalized. On the other hand, economic incentives are provided to increase load (and disincentives to decrease generation) when the frequency is high.

12.3 Custom Power Devices

The problem of voltage sags can affect sensitive loads. However, there are no specific standards for different categories of equipment except in the case of data processing equipment. Computer Business Equipment Manufacturers Association (CBEMA) has developed the CBEMA curve to describe the tolerance of main frame computers to the magnitude and duration of voltage variations on the power systems. Although many modern computers have different tolerances, the CBEMA curve (see Fig. 12.7) has become a standard design target for sensitive equipment and also a common format for reporting power quality variations.

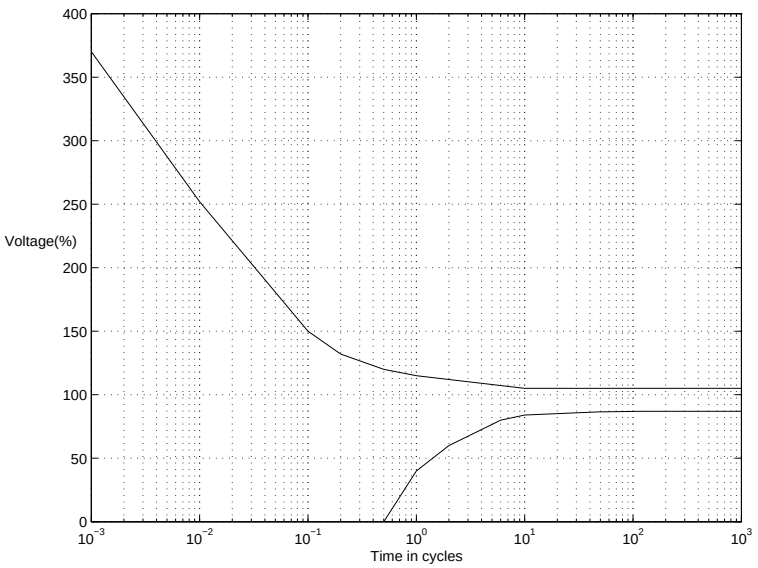

Figure 12.7: CBEMA operating voltage envelope

The vertical axis in Fig. 12.7 represents the voltage magnitude and the horizontal axis represents the duration (in cycles of 60 Hz operating

frequency) of the event. The points below the envelope are presumed to cause the load to drop out due to lack of energy. The points above the envelope are presumed to cause malfunctions such as insulation failure, overvoltage trip etc. The CBEMA curve is primarily used in the range of the duration exceeding 0.1 cycle.

Actual plant equipment has a variety of operational characteristics during voltage sags. For example, motor contactors and electromechanical relays will drop out at 50% to 70% voltage if the dip lasts for over one cycle. Mercury lamps are extinguished around 80% normal voltage and require time to restrike. Although some adjustable speed drives are designed to ride through voltage sags, the ride through time can be anywhere from 0.05 s to 0.5 s, depending on the manufacturer and the model [4].

Some of the process industries are very sensitive to voltage sags. For example, an event of uncompensated voltage sag can result in losses exceeding a million dollars in a semiconductor plant.

There are standards for the current and voltage harmonics based on THD. Typically, the voltage THD should be below 5%. The standards on voltage flicker (mentioned in the previous section) are for $P_{ST} \leq 1$. One can also specify standards for voltage unbalance.

The previous discussion indicates the requirement for compensating equipment to improve power quality and meet the specified standards. The major problems relate to voltage magnitude and waveform distortion. Also, it is essential to provide reactive power compensation to improve power factor or regulate voltage under dynamic conditions. The operation of load at unity power factor is beneficial in (a) reduction of losses and improved voltage profile and (b) better utilization of distribution feeders.

The custom power devices that can be used in distribution systems are:

1. Solid State (Thyristor Controlled) Transfer Switch (SSTS)
2. Solid State Circuit Breaker (SSCB)
3. Solid State Current Limiter (SSCL)
4. Static Synchronous Compensator (STATCOM)
5. Dynamic Voltage Restorer (DVR)
6. Active Filter (AF)
7. Static Var Compensator (SVC)
8. Thyristor Controlled Voltage Regulator (TCVR)

The items 2 and 3 (SSCB and SSCL) have been discussed in chapter 9. The Solid State Transfer Switch (SSTS) is used to transfer the feed to a sensitive load from one feeder to another on the detection of voltage sag or power interruption. SSTS improves reliability by using duplicate supplies without degradation of power quality.

The distribution STATCOM is similar to a transmission STATCOM in that it uses a VSC of the required rating. However, the VSC used in a DSTATCOM is a Type 1 converter with PWM control over the magnitude of the injected AC voltage while maintaining a constant DC voltage across the capacitor. Faster power semiconductor devices such as IGBT or IGCT are used instead of GTO. The rapid switching capability provided by IGBT (or IGCT) switches enable the use of more sophisticated control schemes to provide functions of balancing (by injecting negative sequence current), active filtering (by injecting harmonic currents) and flicker mitigation.

A DSTATCOM can be viewed as a variable current source determined by the control functions. To increase the dynamic rating in the capacitive range, a fixed capacitor/filter can be used in parallel with DSTATCOM. By connecting an energy storage device such as a Superconducting Magnetic Energy Storage (SMES) on the DC side through a DC/DC power conditioner, it is possible to exchange real power with the network for a limited time (during momentary interruptions or large voltage sags).

The Dynamic Voltage Restorer (DVR) is a series connected device analogous to a SSSC. The main function of a DVR is to eliminate or reduce voltage sags seen by sensitive loads such as semiconductor manufacturing plant or a paper mill. DVR that have been installed so far are modular with ratings of 2 MVA per module. They have been designed to compensate three phase voltage sags up to 35% for a duration of time less than half a second (depending on the requirement). If the voltage sag occurs only in one phase (caused by SLG faults) then the DVR may be designed to provide compensation for sags exceeding 50%. The energy storage required in capacitors is typically in the range of 0.2 to 0.4 MJ per MW of load served. A DVR is connected in series with the feeder using a transformer. The low voltage winding is connected to the converter. If the objective of a DVR is mainly to regulate the voltage at the load bus, it remains for most of the time in stand-by mode during which the converter is bypassed (no voltage is injected). Only when a sag is detected, the DVR injects a series voltage of the required magnitude. It is necessary to protect a DVR against the fault currents (as in the case of a SSSC).

A DVR with IGBT/IGCT devices can be controlled to act as a series active filter to isolate the load from voltage harmonics on the source side. It is also possible to balance the voltage on the load side by injecting negative and/or zero sequence voltages in addition to harmonic voltages.

Active Filters

There is a proliferation of power electronic loads in the distribution system, primarily due to the need for energy efficiency and improved productivity. However, this leads to generation of harmonic currents which can flow in the feeder lines and contribute to increased losses and voltage distortion at the point of common coupling (PCC). Passive filters made up of tuned L–C filters (at characteristic harmonics) and high pass filters have traditionally been used to absorb the harmonics generated by large industrial load or high power electronic equipment (HVDC converter and SVC). These have the advantage of low cost and high efficiency. However, they have the following drawbacks:

1. Supply impedance strongly influences the effectiveness of the passive filters. As the supply impedance reduces, the effectiveness also reduces.
2. They are prone to resonances.
3. Tuned passive filters are sensitive to L–C component tolerances. They are detuned also by system frequency variations. The detuning reduces the effectiveness of these filters.
4. Tuned filters are prone to overloading as the ambient harmonics (generated elsewhere) tend to flow in them. Often, these filters are deliberately detuned to prevent their overloading. This is an undesirable solution as it defeats the very purpose of their installation.
5. The design of passive filters requires extensive studies involving considerable engineering effort. This restricts their application mainly to high power (nonlinear) loads.

The active filters based on VSC have been developed to solve the problems associated with passive filters. Although the principles of the active filters have been proposed over 30 years ago, the developments in power semiconductor devices and control technology have made their implementation practical. For example, active DC filters have been proposed to compensate for the harmonic currents injected by the HVDC converters in the DC line [36]. However, most of the applications are in the AC systems.

The active filters are classified according to their configuration as follows.

1. Shunt Active Filters
2. Series Active Filters
3. Hybrid Active Filters
4. Unified Power Quality Conditioners (UPQC)

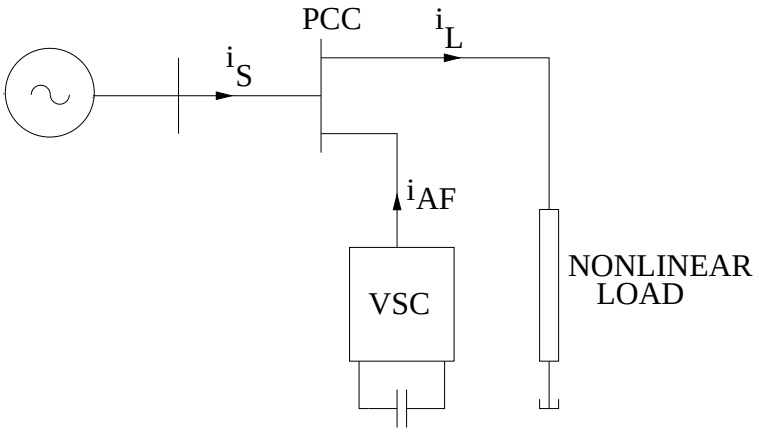

Figure 12.8: A shunt active filter

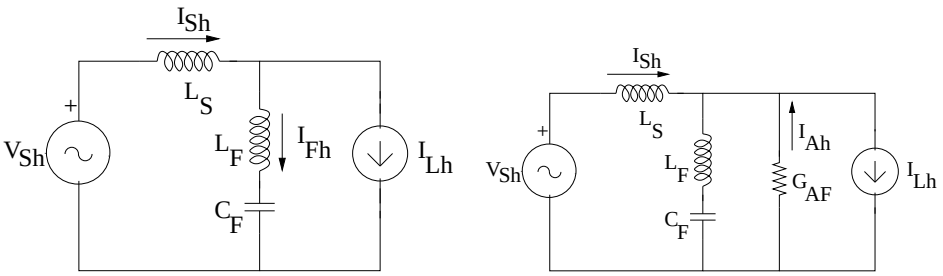

(a) Without active filter (b) With active filter

Figure 12.9: Harmonic equivalent circuit

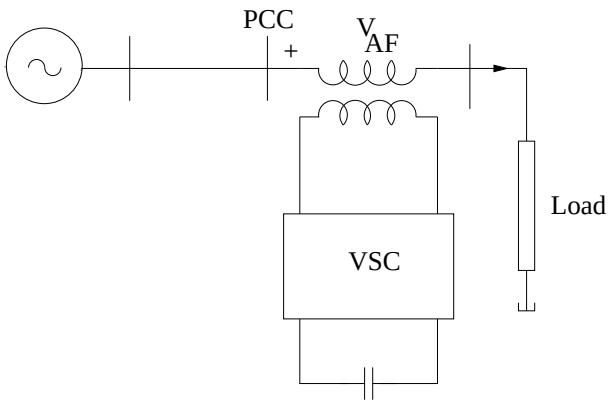

Figure 12.10: A series active filter

A shunt active filter is shown in Fig. 12.8. This may be used in isolation or in parallel with a passive filter. In such cases, the shunt active filter has the capability to damp the harmonic resonance between the existing passive filter and the supply impedance. This can be explained with reference to the harmonic equivalent circuit shown in Fig. 12.9.

Considering a single harmonic (of order h), the filter is tuned for the frequency (hf_1). As seen from the load side (represented by a current source), the passive filter forms with source inductance, a parallel resonance at the frequency (f_{res}) given by

$$f_{res} = \frac{1}{2\pi} \cdot \frac{1}{\sqrt{(L_F + L_S)C_F}} \tag{12.7}$$

If there is a harmonic current source of frequency f_{res}, in parallel with the load, it will result in very high harmonic voltages and high harmonic currents flowing in the line and the filter. Also, if the source voltage has a harmonic at the resonant frequency, this will also result in high harmonic voltage at the PCC and high harmonic currents in the system.

If an active filter is connected in parallel with the passive filter, it can be used to damp the harmonic resonance by injecting a current i_{Ah} such that

$$i_{Ah} = -G_{AF} v_h = G_{AF} L_S \frac{di_{Sh}}{dt} \tag{12.8}$$

The above control law has the effect of inserting an equivalent conductance (only for harmonics - not at fundamental frequency) G_{AF} which will damp the harmonic resonance.

The combination of shunt active and passive filters have been applied for harmonic compensation of high power cycloconverters used in steel mill drives.

A series active filter is shown in Fig. 12.10. It is connected in series with the line through an isolation transformer. It injects a voltage v_{AF} whereas a shunt active filter injects a current i_{AF}. If the nonlinear load injects voltage harmonics, a series active filter blocks their transfer to the PCC. On the other hand, harmonic voltages present on the source side are also prevented from reaching the load bus. Thus, a series active filter acts as a harmonic isolator in addition to damping resonances. A typical control law for a series active filter is,

$$v_{AF} = k i_{Sh} \tag{12.9}$$

where i_{Sh} is the harmonic current in the line. This control law ensures that for all harmonic frequencies, the series active filter appears as a large resistance (except for the fundamental).

A hybrid active filter consists of both an active and a passive filter. There are two configurations (i) a series active filter with a passive (shunt connected) filter (ii) a series active filter connected in series with the passive filter. Both the configurations are shown in Fig. 12.11.

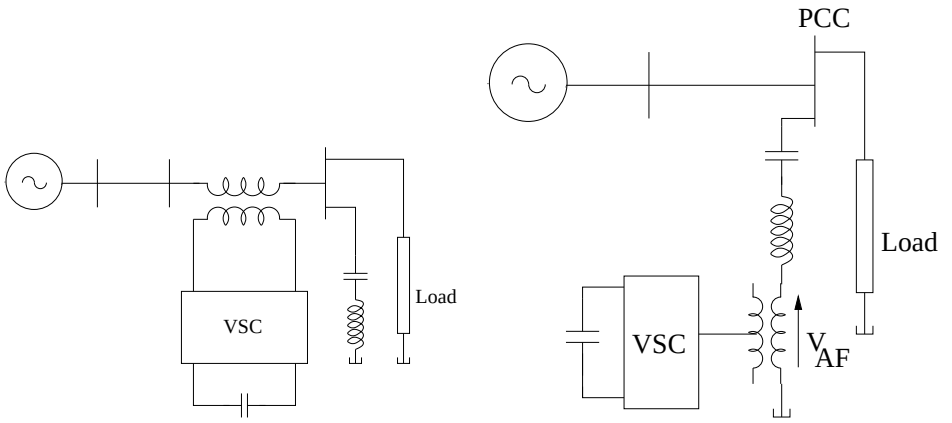

(a) A series active filter with shunt passive filter

(b) An active filter in series with shunt passive filter

Figure 12.11: Hybrid filters

The second configuration of an active filter connected in series with a shunt passive filter is an interesting combination that has already been used for active DC filters in a HVDC converter stations.

The control law suggested [37] is based on source current detection and is given by

$$v_{AF} = ki_{Sh} \tag{12.10}$$

(Note that this control law is same as what is suggested for a pure series active filter).

For the single phase equivalent circuit of the hybrid filter shown in Fig. 12.12, we can derive

$$I_{Sh} = \frac{Z_{Fh}}{k + Z_{Sh} + Z_{Fh}} I_{Lh} + \frac{1}{k + Z_{Sh} + Z_{Fh}} V_{Sh} \tag{12.11}$$

$$V_h = \frac{-Z_{Sh}Z_{Fh}}{k + Z_{Sh} + Z_{Fh}} I_{Lh} + \frac{k + Z_{Fh}}{k + Z_{Sh} + Z_{Fh}} V_{Sh} \tag{12.12}$$

If k is selected such that $|k| \gg |Z_{Sh}+Z_{Fh}|$, I_{Sh} is significantly reduced. However, the harmonics in the source voltage (V_{Sh}) appear at the PCC. Thus, the application of this hybrid filter would depend on the level of harmonics

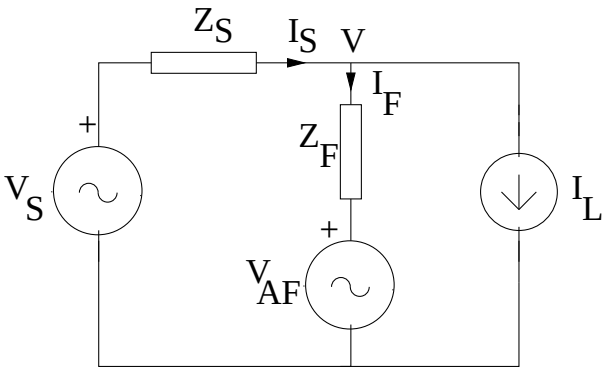

Figure 12.12: Single phase equivalent circuit of the hybrid filter

present on the source side. A study of the characteristics of the hybrid filter shows that the filtering characteristics of the passive filter are significantly improved by the active filter and the parallel and series resonance is effectively damped. The cost of the hybrid filter is significantly less compared to the case when a shunt active filter is used alone. This is due to the fact that the rating of the active filter required is much smaller, typically 2–3% of harmonic producing load (with high quality factor of the passive filter, $Q > 35$). With ideal filtering characteristics of the hybrid filter (with high k), we have.

$$V_{AF} = Z_{Fh} I_{Lh} + V_{Sh} \tag{12.13}$$

$$I_{AF} = I_{Lh} - I_{F1} \tag{12.14}$$

where I_{F1} is the fundamental frequency current flowing in the passive filter due to the source voltage. The rating of the active filter is the product of V_{AF} and I_{AF}.

Unified Power Quality Conditioner

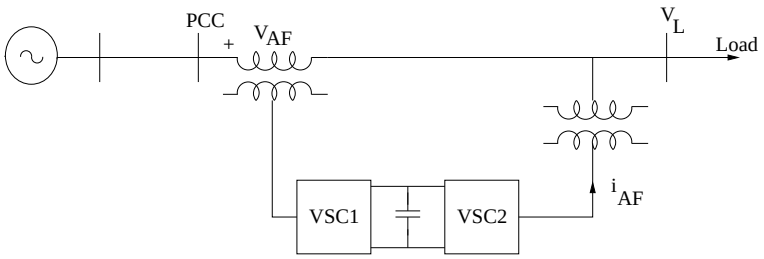

Figure 12.13: Unified Power Quality Conditioner (UPQC)

This is a combination of shunt and series active filters which are connected on the DC side (see Fig. 12.13). This configuration is inspired by the

UPFC discussed in chapter 8. The reference [8] suggest the possibility of a centralized UPQC at the distribution substation that will provide harmonic isolation between the subtransmission system and distribution system. The series branch of UPQC provides this harmonic isolation in addition to voltage regulation and imbalance compensation. The shunt branch provides for harmonic and negative sequence current compensation in addition to DC link voltage regulation.

Shunt Active Filters for Power Distribution Systems

Reference [8] also proposes application of shunt active filters in distribution systems located at appropriate locations. It is mentioned that for a radial system, the location of a shunt active filter at the end terminal of a primary feeder is desirable rather than at the beginning terminal. Also, the control law suggested is (based on voltage detection scheme) given by

$$I_{AF} = \frac{-K_v}{1+Ts} V_h \tag{12.15}$$

The proposed control law implies that an active filter is represented by an inductive impedance (R in series with L).

Remarks

1. We should note the fact that the terminology on custom power devices is not yet standardized. Although specific term such as DSTATCOM had the connotation of a device meant for reactive power compensation and load balancing, the present trend is to include the task of harmonic compensation also. Similarly, while active filters generally address the problem of harmonic compensation, they can also be used for functions originally assigned to DSTATCOM. Thus, there is a convergence of the functions expected of a multi-purpose power quality compensator. Incidentally, different manufactures have also used different terminology. For example, ABB call DSTATCOM as SVC Light.

2. The need for combining different functions in a device arises from the constraint to minimize the overall costs.

3. It is possible to use a single control law that ensures achieving the various objectives for a particular device. This integration of the control functions comes about from the concept of a generalized definition of the reactive current or power. Hence we need to examine the concept of reactive power with non-sinusoidal voltages and currents. This is done in the next section.

12.4 Definitions of Reactive Power

As discussed in the previous section, the reactive power control is important for system operation and improving quality of power supply. The reactive power is well defined in circuits with sinusoidal voltage and currents. However the concept of reactive power is not so well defined in circuits with non-sinusoidal voltages and currents.

In this section, the definitions of reactive power will be reviewed in the context of reactive power compensation and improvement of power factor.

12.4.1 Sinusoidal Excitation and Current - Review of Basic Definitions

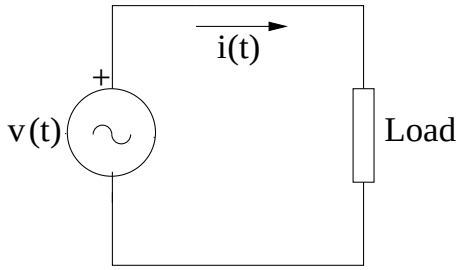

Figure 12.14: A single phase circuit

For simplicity, consider a single phase circuit shown in Fig. 12.14 where a sinusoidal voltage is applied across a linear passive load (An equivalent impedance is shown to represent any general linear, passive 1-port network). If the voltage $v(t)$ and current $i(t)$ are expressed as

$$v(t) = \sqrt{2}V\cos(\omega t) \tag{12.16}$$

$$i(t) = \sqrt{2}I\cos(\omega t - \phi) \tag{12.17}$$

(Note: The current is sinusoidal in steady state).

The voltage and current phasors are related by

$$\hat{V} = \hat{Z}\hat{I} \tag{12.18}$$

where $\hat{Z}$ is the impedance with magnitude Z and phase angle ϕ.

The instantaneous power p, is given by

$$\begin{aligned} p &= vi = 2VI\cos\omega t\cos(\omega t - \phi) \\ &= VI[\cos\phi + \cos(2\omega t - \phi)] \end{aligned} \tag{12.19}$$

The average power P is defined as

$$P = \frac{1}{T}\int_0^T vidt = VI\cos\phi \tag{12.20}$$

The reactive power Q is defined as

$$Q = \sqrt{S^2 - P^2} \tag{12.21}$$

where $S = VI$ is defined as apparent power. Substituting (12.20) in (12.21) we have

$$Q = \pm VI\sin\phi \tag{12.22}$$

The sign is taken to be positive if $\hat{I}$ lags $\hat{V}$ by angle ϕ. The power factor (PF) is defined as

$$PF = \frac{P}{S} = \frac{P}{\sqrt{P^2 + Q^2}} \tag{12.23}$$

From (12.23) it is obvious that if PF is to be improved to unity, the reactive power consumed by the load is to be compensated, (by using shunt capacitors of appropriate size).

The apparent power S is the magnitude of the complex power $\hat{S}$ which is defined as

$$\hat{S} = P + jQ = \hat{V}\cdot\hat{I}^* \tag{12.24}$$

Hence, reactive power Q is also defined as the imaginary part of the complex power [38].

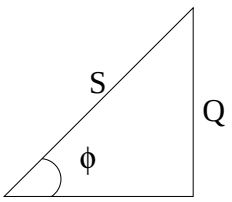

P = S Cos ϕ
Q = S Sin ϕ

Figure 12.15: Power triangle

The power triangle is shown in Fig 12.15 which shows the relationship between P, Q and S.

Remarks:

1. Although P, Q and S have same dimension, they have different units that is Watt, Var and VA.

2. The importance of apparent power (S) is that the rating of an equipment - say a generator or transformer is expressed in terms of Volt Amperes.

Physical Interpretation of Reactive power

The physical meaning of reactive power is not evident from the definition of (12.21) or (12.24). The reactive power is not required to be supplied to a resistive load. It is consumed or generated by reactive load made up of pure inductors and capacitors. When a sinusoidal voltage source $v(t)$ is connected across an inductor, the current $i_L(t)$ is given by

$$i_L(t) = \sqrt{2} I_L \cos(\omega t - \pi/2) = \sqrt{2} I_L \sin(\omega t) \tag{12.25}$$

where $I_L = \frac{V}{\omega L}$.

The instantaneous power $p_L(t)$ is given by

$$p_L(t) = V I_L \sin(2\omega t) = Q_L \sin(2\omega t) \tag{12.26}$$

Equation (12.26) shows that Q_L is the peak value of the alternating power supplied to an inductor. Note that the instantaneous power is a sinusoidal quantity of twice the frequency of the supply voltage.

If the voltage v is applied to a capacitor C, the instantaneous power p_C is given by

$$p_C = -V I_C \sin(2\omega t) = Q_C \sin(2\omega t) \tag{12.27}$$

where $I_C = \omega C V$ is the rms value of the capacitor current given by

$$i_C(t) = -\sqrt{2} I_C \sin(\omega t) \tag{12.28}$$

It is to be noted that Q_C is negative in general. It can be shown that if the voltage $v(t)$ defined in Eq. (12.16) is applied to a single port linear reactive network, the instantaneous power supplied to the network can be expressed as

$$p_B(t) = Q \sin(2\omega t) \tag{12.29}$$

where Q is the net reactive power consumed by the network.

The above equation indicates that the reactive power can be defined as the amplitude (peak value) of the instantaneous power supplied to the reactive component of the load. However, it is to be noted that the peak value of the instantaneous power drawn by a load is *not equal* to the reactive

power. This follows from the fact that a pure resistor of conductance G, has both a dc and a sinusoidal component in the instantaneous power given by

$$\begin{aligned} p_G(t) &= Gv^2(t) = GV^2[1 + \cos(2\omega t)] \\ &= P[1 + \cos(2\omega t)] \end{aligned} \tag{12.30}$$

Hence the reactive power is not equal to the peak value of the sinusoidal component of the total instantaneous power.

It is to be noted that although a pure resistor draws oscillatory power, it does not consume reactive power. This follows from the fact that a resistor always consumes (dissipates) energy (at all instants). On the other hand, a pure reactive component such as an inductor or a capacitor does not dissipate energy but only stores it. The energy is stored in the magnetic field in the case of an inductor and in the electric field in the case of a capacitor. In one half cycle of the alternating supply, the energy is stored and returned in the other half cycle. It is this continual exchange of energy between the energy storage element and the source that contributes to the flow of reactive power. In an inductor, the maximum energy stored is given by

$$W_L = \frac{1}{2}Li_{\max}^2 = LI^2 = \frac{Q_L}{\omega} \tag{12.31}$$

In general, it can be shown that the reactive power supplied to a load is equal to ω times the peak energy stored in the load.

It is obvious that in an alternating current network, the exchange of energy between the energy storage components of the load and the source is inevitable and this does not contribute to the flow of real power which is consumed by the load. The flow of reactive power not only puts a burden on the generating capacity (because of limitations of the apparent power) but also loads the transmission and distribution network and increases losses. The control of reactive power in the load and the network is essential for optimum utilization of the facilities.

There can be types of energy storage elements other than inductor and capacitor. For example, a separately excited DC motor (see Fig. 12.16) excited by an AC voltage source behaves like a capacitor in which the energy is stored in the rotor in the form of kinetic energy. This can be shown as follows.

DC Machine

The voltage equation is given by

$$v = Kn \tag{12.32}$$

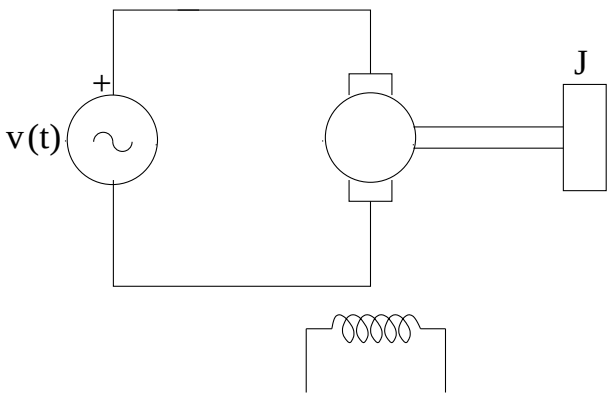

Figure 12.16: A separately excited motor

where n is the angular speed of the machine rotor. (K is a constant). Assuming that

$$v(t) = \sqrt{2}V\cos(\omega t)$$

We have

$$n = \frac{\sqrt{2}V}{K}\cos(\omega t) \tag{12.33}$$

The torque equation is given by

$$J\frac{dn}{dt} = T_e = Ki \tag{12.34}$$

where T_e is the electric torque and is proportional to the alternating current i. Substituting Eq. (12.33) in (12.34) we have,

$$\begin{aligned} i(t) &= -\frac{\omega J}{K^2}\sqrt{2}V\sin(\omega t) \\ &= -\omega C_{eq}\sqrt{2}V\sin(\omega t) \end{aligned} \tag{12.35}$$

This shows that the DC machine appears as a capacitor (C_{eq}) defined by

$$C_{eq} = \frac{J}{K^2} \tag{12.36}$$

It can be shown that peak kinetic energy stored in the rotor is given by

$$W_{KE} = \frac{1}{2}Jn_{\max}^2 = \frac{1}{2}J\left(\frac{\sqrt{2}V}{K}\right)^2 = \frac{J}{K^2}V^2 = C_{eq}V^2 \tag{12.37}$$

The following is an example (although not realistic) of the energy stored in the form of heat.

Time-Varying Resistor

Let a voltage $v(t) = \sqrt{2}V\cos(\omega t)$ be applied across a time-varying resistor whose conductances is given by

$$g(t) = -G\tan(\omega t) \tag{12.38}$$

The current through the resistor is given by

$$i(t) = g(t)v(t) = -\sqrt{2}VG\sin(\omega t) \tag{12.39}$$

This shows, the resistor is actually generating reactive power with the instantaneous power given by

$$p(t) = vi = -V^2G\sin(2\omega t) = Q\sin(2\omega t) \tag{12.40}$$

The active power consumed by the resistor is zero. This may appear surprising, but it is worth noting that the conductance changes sign during a half cycle, as

$$\begin{aligned} g(t) < 0, \qquad & 0 < \omega t < \frac{\pi}{2} \\ g(t) > 0, \qquad & \frac{\pi}{2} < \omega t < \pi \end{aligned}$$

12.4.2 Reactive Power in Non-Sinusoidal Conditions

The definition of reactive power is not simple when non-sinusoidal voltages and currents are considered. Nonlinear loads such as power electronic converters produce non-sinusoidal currents even when the voltage applied is sinusoidal. In this condition, the harmonic currents do not contribute to active (real) power.

The flow of non-sinusoidal currents through system impedances result in non-sinusoidal voltages. In general, both the voltage and current can be considered as non-sinusoidal. To simplify analysis, it will be assumed that the load is linear and thus the current harmonics result from voltage harmonics.

Definitions of Power in Time and Frequency Domain

It is worth nothing that definition of active power in time domain (see Eq. (12.20)) applies even if $v(t)$ and $i(t)$ are non-sinusoidal.

We will assume that both $v(t)$ and $i(t)$ are periodic in steady state and have only AC components (no DC components). The active power P, is defined by

$$P = \frac{1}{T}\int_0^T vidt \tag{12.41}$$

From Fourier analysis, both $v(t)$ and $i(t)$ can be expressed as

$$v(t) = \sum_{n=1}^{\infty} v_n = \sum_{n=1}^{\infty} \sqrt{2}V_n \cos(n\omega t + \alpha_n) \tag{12.42}$$

$$i(t) = \sum_{n=1}^{\infty} i_n = \sum_{n=1}^{\infty} \sqrt{2}I_n \cos(n\omega t + \beta_n) \tag{12.43}$$

Substituting Eqs (12.42) and (12.43) in (12.41), it is possible to express P as

$$P = \sum_{n=1}^{\infty} P_n \tag{12.44}$$

where

$$P_n = V_n I_n \cos\phi_n \tag{12.45}$$

$$\phi_n = \alpha_n - \beta_n \tag{12.46}$$

It is to be noted that P_n is the harmonic power due to the harmonic component v_n and i_n.

It is also possible to define Q_n as the reactive power at the nth harmonic, namely

$$Q_n = V_n I_n \sin\phi_n \tag{12.47}$$

The definition of the apparent power (S) and the power factor (PF) given earlier with sinusoidal excitation and current, can be extended to the general case of any periodic functions. Thus,

$$S = VI \tag{12.48}$$

where

$$V^2 = \frac{1}{T}\int_0^T v^2 dt \tag{12.49}$$

$$I^2 = \frac{1}{T}\int_0^T i^2 dt \tag{12.50}$$

V and I are rms values of voltage and current respectively. Using Eqs. (12.42) and (12.43),

$$V^2 = \sum_{n=1}^{\infty} V_n^2, \quad I^2 = \sum_{n=1}^{\infty} I_n^2 \tag{12.51}$$

The power factor can be expressed as

$$PF = \frac{P}{S} \tag{12.52}$$

Budeanu Concept of Reactive Power

C. Budeanu, a Romanian engineer defined the reactive power (Q_B) in a manner similar to the definition of P given in (12.44), namely

$$Q_B = \sum_{n=1}^{\infty} Q_n = \sum_{n=1}^{\infty} V_n I_n \sin\phi_n \tag{12.53}$$

However, it can be shown that, in general

$$S^2 \neq P^2 + Q_B^2 \tag{12.54}$$

Budeanu defined distortion power (D_B) to express the apparent power as

$$S^2 = P^2 + Q_B^2 + D_B^2 \tag{12.55}$$

Using Fourier components, it can be shown that

$$\begin{aligned} D_B^2 &= \frac{1}{2}\sum_{m=1}^{\infty}\sum_{n=1}^{\infty}[V_m^2 I_n^2 + V_n^2 I_m^2 - 2V_m V_n I_m I_n \cos(\phi_m - \phi_n)] \qquad (12.56)\\ &= \frac{1}{2}\sum_{m=1}^{\infty}\sum_{n=1}^{\infty}[(V_m I_n - V_n I_m)^2 + 2V_m V_n I_m I_n[1 - \cos(\phi_m - \phi_n)]] \end{aligned}$$

The distortion power is zero only if

$$\frac{V_m}{I_m} = \frac{V_n}{I_n} \tag{12.57}$$

and

$$\phi_m = \phi_n \tag{12.58}$$

Thus, a pure resistor does not have any distortion power. Budeanu's definition of reactive power has been adopted by ANSI/IEEE Standard 100-1977.

L.S. Czarnecki [25] has shown the drawbacks of the Budeanu concept. The first and the foremost drawback is that while Q_B is zero, individual components of (Q_n) are non-zero signifying energy exchange (between the source and the load) taking place at different harmonic frequencies. Thus, even when a compensatory element (such as a shunt capacitor) may be chosen to reduce Q_B to zero on the source side, the power factor may not be improved. (The reduction of Q_B is accompanied by increase in D_B).

The second objection is regarding the definition of the distortion power. This power does not provide any information about waveform distortion. It is possible that in a circuit, there is no waveform distortion (both current and voltage waveforms are similar) and yet D_B is not zero. On the other hand, $D_B = 0$ does not guarantee that the waveform is not distorted.

Thirdly, both Q_B and D_B are difficult to instrument. But the major problem is the uselessness of Q_B as an index of power factor improvement.

Fryze Definition of Reactive Power

S. Fryze, proposed in 1931, the concept of reactive power as follow:

$$Q_F = \pm\sqrt{S^2 - P^2} \tag{12.59}$$

However, this cannot be interpreted as the rate of energy transfer to energy storage elements. For example, a sinusoidal voltage source supplying energy to a resistor through a diode results in non-zero Q_F. Actually it can be shown that both P and Q_F in this circuit are equal and given by

$$P = Q_F = \frac{V^2}{2R}$$

and the apparent power S is given by

$$S = VI = \frac{V^2}{\sqrt{2}R}$$

Yet, Fryze definition of reactive power has been recommended by International Electrotechnical Commission. This is because Q_F has two merits over Q_B as follows:

1. It represents a measure of uselessly transmitted power and the extent to which a power system is not utilized. In addition, it is directly related to the ratings of the compensating equipment which can improve the source side power factor to unity.
2. Q_F is defined without reference to the Fourier series representation of the voltage and current and can be easily measured.

Actually, Q_F can be defined strictly from time domain quantities. The load current can be divided in to two orthogonal components as follows:

$$i = i_p + i_q \tag{12.60}$$

where

$$i_p = G_e v \tag{12.61}$$

G_e is the effective conductance of the load defined by

$$G_e = \frac{P}{V^2} \tag{12.62}$$

where V is the rms value of the applied voltage.

P and Q_F are defined from

$$P = VI_p,\ Q_F = VI_q \tag{12.63}$$

where I_p and I_q are rms values of i_p and i_q.

Remarks

1. If a sinusoidal voltage is applied across a nonlinear load, the current in the circuit consists of harmonics in addition to the reactive component (at the supply frequency) due to the energy storage elements in the load. It is obvious that i_q consists of both these wattless components. This observation can be extended even if the source voltage is not sinusoidal.

2. In general, with nonsinusoidal voltage and currents, the current i_q (which is defined as the difference between i and i_p) can have components that may not be fully compensated by passive L-C networks (passive filters). Essentially, i_q contains components that are not required for instantaneous power transfer and can be compensated by an (active) compensator with no energy storage.

12.5 Reactive Power Compensation in Single Phase Circuits

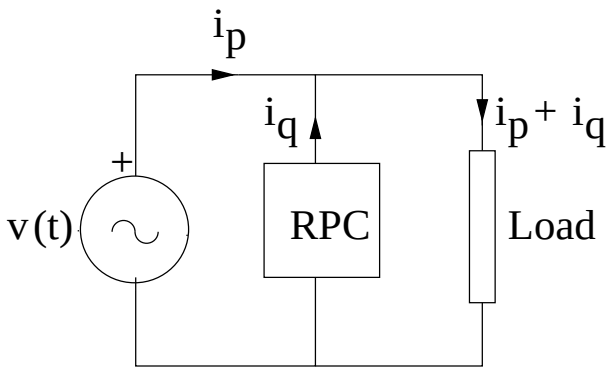

Figure 12.17: A RPC in a single phase circuit

In the previous section, the instantaneous active current (i_p) and reactive current (i_q) are defined. Since, $Q_F = VI_q$ where I_q is the rms value of $i_q(t)$, defined as

$$I_q^2 = \frac{1}{T}\int_0^T i_q^2 dt \tag{12.64}$$

the full compensation of Q_F in the load, will result in only active current (i_p) being supplied by the source, (see Fig. 12.17) which results in minimum losses in the line and unity power factor on the source side. The reactive power compensator (RPC) can be a shunt active filter or a combination of passive filter and active filter. While it is possible for a shunt active filter to fully compensate for i_q, the question we would like to pose is whether a passive filter can do the job on its own. Also, what is the optimal solution

for the passive filter that will minimize the reactive power supplied by the source?

The answer to the first question is no; that is a pure passive network (filter) is inadequate in general to fully compensate for the reactive power (Q_F) in the load. We will answer the second question next. We will consider two cases: (a) when the passive filter is a capacitor or an inductor (as one would apply in sinusoidal conditions for reactive power compensation) and (b) when the passive filter is made up of a one port L-C network connected across the load. Needless to say that the second case is more general than the first one.

Case 1: A Capacitor or Inductor Across the Load

Kusters and Moore [43] showed that the instantaneous reactive current i_q in a single phase network can be divided into two orthogonal components in two ways. That is,

$$(a) \qquad i_q = i_{qc} + i_{qcr} \tag{12.65}$$

$$(b) \qquad i_q = i_{ql} + i_{qlr} \tag{12.66}$$

where i_{qc} and i_{ql} are defined as instantaneous capacitive and inductive reactive currents, defined by

$$i_{qc} = \frac{\dot{v}(\frac{1}{T}\int_0^T \dot{v}idt)}{(\dot{V})^2} \tag{12.67}$$

$$i_{ql} = \frac{\bar{v}(\frac{1}{T}\int_0^T \bar{v}idt)}{(\bar{V})^2} \tag{12.68}$$

Here, $\dot{v} = \frac{dv}{dt}$, $\bar{v} = \int vdt$ and

$$\dot{V}^2 = \frac{1}{T}\int_0^T \left(\frac{dv}{dt}\right)^2 dt, \quad \bar{V}^2 = \frac{1}{T}\int_0^T (\bar{v})^2 dt$$

i_{qcr} and i_{qlr} are defined as instantaneous residual reactive currents, capacitive and inductive respectively. The rms inductive and capacitive reactive currents are defined as,

$$I_{ql}^2 = \frac{1}{T}\int_0^T i_{ql}^2 dt, \quad I_{qc}^2 = \frac{1}{T}\int_0^T i_{qc}^2 dt \tag{12.69}$$

Similar definitions also apply for rms residual currents I_{qlr} and I_{qcr}. We can show that,

$$I_q^2 = I_{ql}^2 + I_{qlr}^2 = I_{qc}^2 + I_{qcr}^2 \tag{12.70}$$

The above equation shows that i_{ql} and i_{qlr} are orthogonal. We say, that two periodic functions f_1 and f_2 are orthogonal if

$$\int_0^T f_1(t) f_2(t) dt = 0 \tag{12.71}$$

Note that i_{qc} and i_{qcr} are also orthogonal.

With sinusoidal voltage and linear load (which results in sinusoidal current), the residual reactive components of the current are zero and the inductive and capacitive reactive currents are equal in magnitude but opposite in sign. Complete compensation of an inductive load can be realized by a shunt capacitor and that of a capacitive load by a shunt inductor. With a non-sinusoidal voltage and linear loads, the residual reactive current components need not be zero. The inductive and capacitive reactive currents may be unequal, and both positive or opposite in sign. If the capacitive reactive current in the load is negative, that is $\int_0^T \dot{v} i dt < 0$, then a shunt capacitor can compensate for i_{qc}. Similarly if $\int_0^T \bar{v} i dt < 0$, then a shunt inductor can be used to compensate for i_{ql} in the load. The following result gives the optimum value of the shunt capacitor or inductor required for the (partial) compensation of the reactive current in the load.

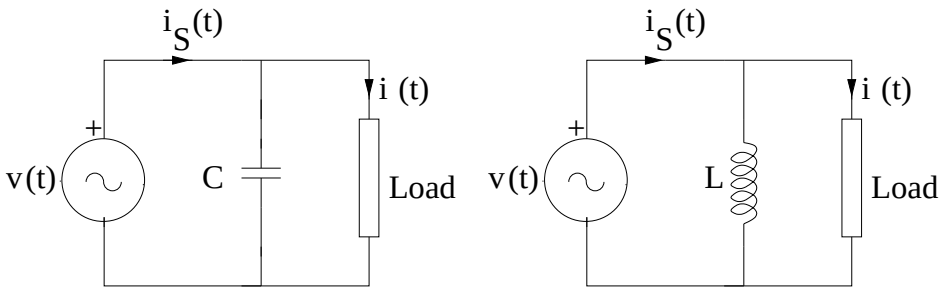

(a) Shunt capacitor compensation

(b) Shunt inductor compensation

Figure 12.18: Shunt reactive compensation

Theorem: The optimum value of the shunt capacitor (C_{opt}) required is given by $-C_{eq}$ where C_{eq} is defined by

$$C_{eq} = \left(\frac{1}{T} \int_0^T \dot{v} i dt \right) / \dot{V}^2 \tag{12.72}$$

Similarly, the optimum shunt inductor (L_{opt}) required is given by $L_{opt} = -L_{eq}$ where L_{eq} is given by

$$L_{eq} = (\bar{V})^2 / \left(\frac{1}{T} \int_0^T \bar{v} i dt \right) \tag{12.73}$$

Proof:
Let us consider the first part. If $\int_0^T \dot{v} i dt < 0$, a shunt capacitor can be used for compensation as shown in Fig. 12.18. The source current (i_S) is given by

$$i_S(t) = i(t) + C\frac{dv}{dt} \tag{12.74}$$

where $i(t)$ is the load current. The rms value of the source current is given by

$$I_S^2 = \frac{1}{T}\int_0^T i_S^2(t)dt = \frac{1}{T}\int_0^T (i + C\dot{v})^2 dt \tag{12.75}$$

The value of the shunt capacitor (C) is optimum when it minimizes the rms value of $i_S(t)$. The necessary condition for this is given by

$$\frac{dI_S^2}{dC} = 0 = \int_0^T (i + C\dot{v})\dot{v}dt \tag{12.76}$$

From the above we get $C_{opt} = -C_{eq}$. It is obvious that C_{opt} results in cancellation of i_{qc} in the source current and $i_S(t)$ will contain only $i_p(t) + i_{qcr}(t)$. Hence, $C_{opt} = -C_{eq}$ is both a necessary and sufficient condition for the minimization of the rms value of the source current.

If instead of a shunt capacitor, a shunt inductor is connected in parallel with the load, the source current is given by

$$i_S(t) = i(t) + \frac{1}{L}\int vdt = i(t) + \frac{\bar{v}}{L} \tag{12.77}$$

We can derive the result $L_{opt} = -L_{eq}$ in a similar fashion as above.

Example 12.1

Consider a switched resistor load shown in Fig. 12.19. The switch is made up of two thyristors connected back to back. The applied voltage is sinusoidal with rms value of 10 V and frequency = 50 Hz. R = 10 ohms. The switch is on when

$$\frac{\pi}{2}(2n-1) \leq \omega t \leq \pi n, \quad n = 1, 2$$

The voltage and current waveforms are also shown in Fig. 12.19

(a) Find the power and power factor of the load

(b) What is the maximum power factor achievable by connecting a capacitor in parallel with the load. What is the value of the capacitor for this condition?

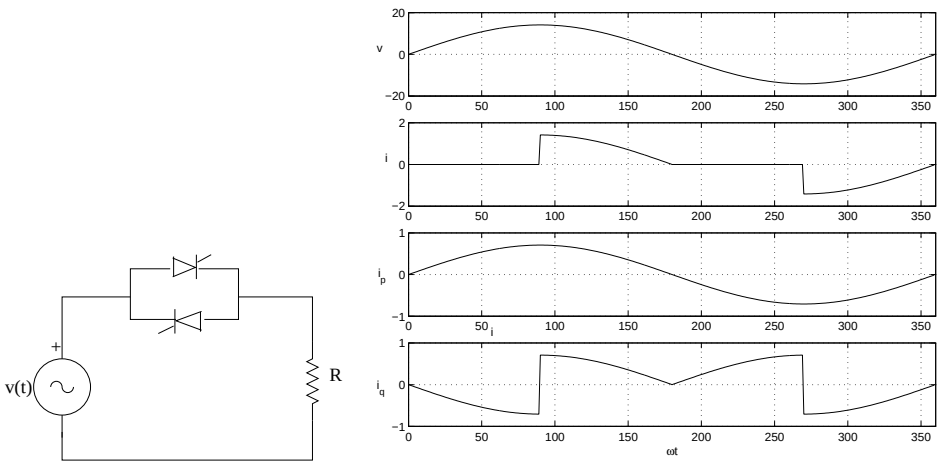

(a) A switched resistive load (b) Voltage and current waveforms

Figure 12.19: Example 12.1

Solution

(a) The voltage $v(t)$ is given by

$$v(t) = \sqrt{2}.10 \sin \omega t, \quad \omega = 2\pi.50$$

The load current $i(t)$ defined over one cycle, is

$$\begin{aligned} i(t) &= \sqrt{2} \sin \omega t, \quad \frac{\pi}{2} \leq \omega t \leq \pi \quad \text{and} \quad \frac{3\pi}{2} \leq \omega t \leq 2\pi \\ &= 0 \text{ elsewhere.} \end{aligned}$$

The average power

$$\begin{aligned} P &= \frac{1}{T} \int_0^T vidt \\ &= \frac{1}{\pi} \int_{\pi/2}^{\pi} 20 \sin^2 \theta \; d\theta, \quad \theta = \omega t \\ &= 5 \text{ Watts} \end{aligned}$$

The rms value of the load current is given by

$$I^2 = \frac{1}{\pi} \int_{\pi/2}^{\pi} 2 \sin^2 \theta d\theta = \frac{1}{2}$$

$$\text{Power Factor} = \frac{P}{VI} = \frac{5.\sqrt{2}}{10} = 0.707$$

Note that

$$G_e = \frac{P}{V^2} = \frac{5}{100} = 0.05 \text{ mho}$$

$$\begin{aligned} i_p(t) &= G_e v(t) = 0.707 \sin \omega t \\ i_q(t) &= i(t) - i_p(t) \end{aligned}$$

The waveforms of v, i, i_p and i_q are shown in Fig. 12.19(b).

(b) The optimum value of the shunt capacitor connected across the load is given by

$$\begin{aligned} C_{opt} &= -C_{eq} = -\frac{1}{\dot{V}^2}\left(\frac{1}{T}\int_0^T \dot{v} i dt\right) \\ \dot{V} &= \omega V = 10\omega, \quad \frac{1}{T}\int_0^T \dot{v} i dt = \frac{1}{\pi}\int_{\pi/2}^{\pi} 10\omega \sin(2\omega t) d\omega t = \frac{-10\omega}{\pi} \\ C_{opt} &= \frac{1}{10\omega\pi} F = 101.32 \mu F \end{aligned}$$

The instantaneous capacitive reactive current (i_{qc}) is given by

$$i_{qc}(t) = C_e \dot{v}(t) = -\frac{\sqrt{2}}{\pi} \cos \omega t$$

The rms value $(I_{qc}) = \frac{1}{\pi} = 0.3183A$. The rms source current after shunt capacitor compensation

$$I_s = \sqrt{I^2 - I_{qc}^2} = 0.6314A$$

The maximum PF achievable is:

$$PF = \frac{P}{VI_s} = \frac{5}{10 \times 0.6314} = 0.792$$

It is interesting to observe that if the thyristor switch shown in Fig. 12.19(a) is replaced by a (single) diode, the power consumed in the load is same $(\frac{V^2}{2R})$. However, $\int_0^T \dot{v} i dt = 0$ and it is not possible to improve the power factor by using a shunt capacitor.

Case 2: A One-Port L-C filter across the Load

Czarnecki [26] showed that i_q in a linear load can be expressed as

$$i_q = i_s + i_r \tag{12.78}$$

where i_r is the reactive current caused by the susceptances in the load and i_s is termed as the scattered component caused by the variations in the

conductances of the load with frequency. If the applied voltage $v(t)$ can be expressed as

$$v(t) = \sum_{h=1}^{n_s} \sqrt{2} V_h \sin(h\omega_1 t + \alpha_h) \tag{12.79}$$

then i_p, i_s and i_r are expressed as

$$i_p(t) = G_e v(t) = G_e \sum_{h=1}^{n_s} \sqrt{2} V_h \sin(h\omega_1 t + \alpha_h) \tag{12.80}$$

$$i_s(t) = \sqrt{2} \sum_{h=1}^{n_s} (G_h - G_e) V_h \sin(h\omega_1 t + \alpha_h) \tag{12.81}$$

$$i_r(t) = \sqrt{2} \sum_{h=1}^{n_s} B_h V_h \cos(h\omega_1 t + \alpha_h) \tag{12.82}$$

The total load current $i(t)$ is the sum of i_p, i_s and i_r and is given by

$$i(t) = \sqrt{2} \sum_{h=1}^{n_s} [G_h V_h \sin(h\omega_1 t + \alpha_h) + B_h V_h \cos(h\omega_1 t + \alpha_h)] \tag{12.83}$$

It can be shown that i_p, i_s and i_r are mutually orthogonal. Also, i_r can be compensated by connecting a one-port L-C filter across the load with the susceptances (B_{ch}) such that

$$B_{ch} = -B_h, \quad h = 1, 2, \ldots n_s \tag{12.84}$$

Note that n_s is the highest order of the harmonics in the applied voltage.

Example 12.2

A non-sinusoidal voltage $v(t) = 10\sqrt{2}\left(\sin t + \frac{\sin 3t}{3}\right)$ is connected across a load represented by a series connection of 1 ohm resistor and 1 H inductor. Compute i_p, i_r and i_s.

Solution

The average power (P) can be expressed on

$$P = V_1 I_1 \cos\phi_1 + V_3 I_3 \cos\phi_3$$

where $\hat{I}_1 = \frac{\hat{V}_1}{|Z_1|\angle\phi_1}, \hat{I}_3 = \frac{\hat{V}_3}{|Z_3|\angle\phi_3}$

$$\begin{aligned} Z_1 &= 1 + j1 = \sqrt{2}\angle 45^\circ, \quad Z_3 = 1 + j3 = 3.1623\angle 71.57^\circ \\ I_1 &= \frac{V_1}{|Z_1|} = \frac{10}{\sqrt{2}} = 7.07, \quad I_3 = \frac{V_3}{|Z_3|} = \frac{10}{3 \times 3.1623} = 1.054 \end{aligned}$$

$$\begin{aligned}
\cos\phi_1 &= \cos 45 = 0.707, \cos\phi_3 = \cos 71.57^\circ = 0.3161 \\
P &= 10 \times 7.07 \times 0.707 + \frac{10}{3} \times 1.054 \times 0.3161 \\
&= 50 + 1.11 = 51.11 \text{ Watts} \\
G_e &= \frac{P}{V^2}, \quad V^2 = V_1^2 + V_3^2 = 10^2 + \frac{10^2}{9} = 111.11 \\
G_e &= 0.460 \text{ mho} \\
i_p(t) &= G_e v(t) = \sqrt{2} \times 4.6 \left(\sin t + \frac{\sin 3t}{3} \right)
\end{aligned}$$

The instantaneous load current $i(t)$ is given by

$$i(t) = \sqrt{2}[I_1 \sin(t - \phi_1) + I_3 \sin(3t - \phi_3)]$$

Substituting the values, we get

$$\begin{aligned}
i(t) &= 7.07(\sin t - \cos t) + \frac{\sqrt{2}}{3}(\sin 3t - 3\cos 3t) \\
i_r(t) &= -\sqrt{2}(5\cos t + \cos 3t) \\
i_s(t) &= (G_1 - G_e)v_1(t) + (G_3 - G_e)v_3(t) \\
G_1 &= \frac{1}{2} = 0.5, \quad G_3 = \frac{1}{10} = 0.01 \\
i_s(t) &= 0.04 \times 10\sqrt{2}\sin t - 0.36 \times \frac{10\sqrt{2}}{3}\sin 3t \\
&= \sqrt{2} \times 0.4 \sin t - \sqrt{2} \times 1.2 \sin 3t
\end{aligned}$$

Czarnecki claimed in [26] that the scattered current cannot be compensated by any passive one port network and the source current will contain i_s in addition to i_p. The maximum power factor for such a case is given by

$$PF_{\max} = \frac{I_p}{(I_p^2 + I_s^2)^{1/2}} \tag{12.85}$$

However, in a recent paper [45] Czarnecki has proved that the power factor can be made unity (by fully compensating for i_q) by using two one-port L-C networks (one connected in parallel with the load and the other connected in series with the load). The susceptance B_{ph}, of the shunt connected compensating reactive network is chosen such that the parallel combination has constant resistance $(1/G_e)$ for all values of h. The value of B_{ph} is given by

$$B_{ph} = -B_h \pm G_h \sqrt{\left(\frac{G_e}{G_h}\right) - 1} \tag{12.86}$$

Here, we assume that $G_e > G_h$ for all h.

The series one-port L-C network is designed such that its reactance value (X_{sh}) at harmonic 'h', compensates for the reactive voltage across the parallel combination of the load and shunt compensating reactive network. We obtain X_{sh} as

$$X_{sh} = -\frac{1}{B_{ph} + B_h} \tag{12.87}$$

The structure of the reactive compensator that fully compensates for the reactive and scattered power in the load is shown in Fig. 12.20.

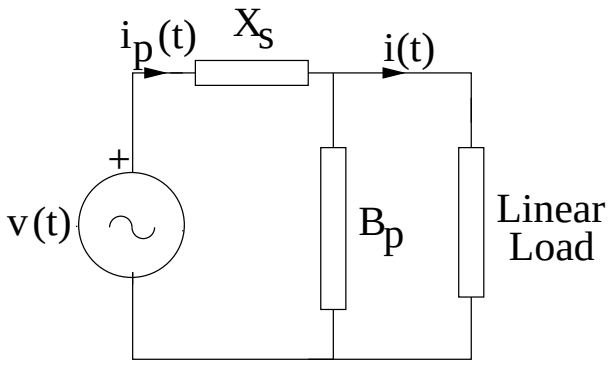

Figure 12.20: Structure of RPC for full compensation of linear load

12.6 Reactive Power Compensation in Three Phase Circuits

12.6.1 Instantaneous Reactive Power (IRP) Theory

This was proposed by Akagi et al [27] in 1984. They used Clarke's transformation and the $\alpha - \beta$ components defined from

$$\begin{bmatrix} v_\alpha \\ v_\beta \end{bmatrix} = \sqrt{\frac{2}{3}} \begin{bmatrix} 1 & -\frac{1}{2} & -\frac{1}{2} \\ 0 & -\frac{\sqrt{3}}{2} & \frac{\sqrt{3}}{2} \end{bmatrix} \begin{bmatrix} v_a \\ v_b \\ v_c \end{bmatrix} \tag{12.88}$$

$$\begin{bmatrix} i_\alpha \\ i_\beta \end{bmatrix} = \sqrt{\frac{2}{3}} \begin{bmatrix} 1 & -\frac{1}{2} & -\frac{1}{2} \\ 0 & -\frac{\sqrt{3}}{2} & \frac{\sqrt{3}}{2} \end{bmatrix} \begin{bmatrix} i_a \\ i_b \\ i_c \end{bmatrix} \tag{12.89}$$

The instantaneous power in the three phase circuit is given by

$$p(t) = v_a(t)i_a(t) + v_b(t)i_b(t) + v_c(t)i_c(t) \tag{12.90}$$

This is also equal to

$$p(t) = v_\alpha(t)i_\alpha(t) + v_\beta(t)i_\beta(t) + v_0(t)i_0(t) \tag{12.91}$$

where v_0 and i_0 are the zero-sequence voltage and current in the circuit respectively. These are defined as,

$$\begin{aligned} v_0(t) &= \frac{1}{\sqrt{3}}[v_a(t) + v_b(t) + v_c(t)] \\ i_0(t) &= \frac{1}{\sqrt{3}}[i_a(t) + i_b(t) + i_c(t)] \end{aligned}$$

For a three wire system, (without a neutral wire) $i_0 = 0$. Hence the instantaneous power, $p(t)$ is given by

$$p(t) = v_\alpha(t)i_\alpha(t) + v_\beta(t)i_\beta(t) \tag{12.92}$$

Akagi et al [27] defined the 'instantaneous imaginary (reactive) power' as

$$q(t) = v_\alpha i_\beta - v_\beta i_\alpha \tag{12.93}$$

Combining Eqs (12.92) and 12.93), we can write,

$$\begin{bmatrix} i_\alpha \\ i_\beta \end{bmatrix} = \begin{bmatrix} v_\alpha & v_\beta \\ -v_\beta & v_\alpha \end{bmatrix}^{-1} \begin{bmatrix} p \\ q \end{bmatrix} \tag{12.94}$$

It was claimed in [27] that the instantaneous reactive power in the load can be fully compensated by connecting a compensator (with switching devices) without energy storage in parallel with the load. The ideal compensator does not absorb any power and hence the compensator currents are given by

$$\begin{bmatrix} i_{C\alpha} \\ i_{C\beta} \end{bmatrix} = \begin{bmatrix} v_\alpha & v_\beta \\ -v_\beta & v_\alpha \end{bmatrix} \begin{bmatrix} 0 \\ -q(t) \end{bmatrix} \tag{12.95}$$

Note that $i_{C\alpha}$ and $i_{C\beta}$ are assumed to be currents drawn by the compensator.

Remarks

1. It can be proved that (when $i_0 = 0$),

$$i_a^2 + i_b^2 + i_c^2 = i_\alpha^2 + i_\beta^2 = \frac{p^2(t) + q^2(t)}{v_\alpha^2 + v_\beta^2} \tag{12.96}$$

This shows that the source current magnitudes (and hence the power losses in the line) can be reduced by compensating for $q(t)$.

Note that for sinusoidal, balanced voltages, $v_\alpha^2+v_\beta^2 =$ constant. Also, for a balanced load connected to a balanced, sinusoidal voltage supply, $p(t)$ and $q(t)$ are constants. In general, with unbalanced, nonlinear load supplied by nonsinusoidal voltages, $p(t)$ and $q(t)$ can both have DC and AC components. It was claimed that the AC components in $p(t)$ and $q(t)$ represent the contribution from harmonic and unbalanced currents. However, this is true only if $v_\alpha^2 + v_\beta^2 =$ constant and $i_0 = 0$.

2. The definition of instantaneous reactive power is contradictory to the concept of reactive power associated with energy storage elements (inductor and capacitor). Actually, it is more appropriate to use the concept of instantaneous reactive (and non-active) current.

3. As mentioned in [29], there are the following drawbacks of the IRP theory.

(i) The theory cannot be easily extended to the four wire systems when i_0 and v_0 are non-zero.

(ii) The single phase situation cannot be treated as a special case of the theory.

(iii) There is no generalization to systems with more than three phases.

An extension of IRP theory to three phase, four wire systems has been proposed in [31] by introducing p-q-r theory. They define p-q-r components of the currents and voltages given by

$$\begin{bmatrix} f_p \\ f_q \\ f_r \end{bmatrix} = \frac{1}{v_{0\alpha\beta}} \begin{bmatrix} v_0 & v_\alpha & v_\beta \\ 0 & -\frac{v_{0\alpha\beta}v_\beta}{v_{\alpha\beta}} & \frac{v_{0\alpha\beta}v_\alpha}{v_{\alpha\beta}} \\ v_{\alpha\beta} & -\frac{v_0 v_\alpha}{v_{\alpha\beta}} & -\frac{v_0 v_\beta}{v_{\alpha\beta}} \end{bmatrix} \begin{bmatrix} f_0 \\ f_\alpha \\ f_\beta \end{bmatrix} \tag{12.97}$$

where f represents current (i) or voltage (v) and

$$v_{0\alpha\beta} = \sqrt{v_0^2 + v_\alpha^2 + v_\beta^2}, \quad v_{\alpha\beta} = \sqrt{v_\alpha^2 + v_\beta^2}$$

The instantaneous (real) power is given by

$$p = v_p i_p = v_{0\alpha\beta} i_p \tag{12.98}$$

Both v_q and v_r are zero. The instantaneous reactive power has two components (q_q and q_r) given by

$$q_q = -v_p i_r, \quad q_r = v_p i_q \tag{12.99}$$

4. The α, β components defined by Eqs. (12.88) and (12.89) are consistent with the definitions of $d-q$ components used in this book given

by

$$\begin{bmatrix} f_d \\ f_q \end{bmatrix} = \sqrt{\frac{2}{3}} \begin{bmatrix} \cos\theta & \cos\left(\theta - \frac{2\pi}{3}\right) & \cos\left(\theta + \frac{2\pi}{3}\right) \\ \sin\theta & \sin\left(\theta - \frac{2\pi}{3}\right) & \sin\left(\theta + \frac{2\pi}{3}\right) \end{bmatrix} \begin{bmatrix} f_a \\ f_b \\ f_c \end{bmatrix} \tag{12.100}$$

where f can be current (i) or voltage (v). The $\alpha - \beta$ components are defined by letting $\theta = 0$ in Eq. (12.100). In defining $d - q$ components above, we have assumed that d-axis leads q-axis.

It can be shown that the definition of $q(t)$ given in [27] (Eq. (12.93)) is consistent with the definitions of v_β and i_β given in Eqs. (12.88) and (12.89). However, in [27] both v_β and i_β are defined as the negative of what is defined here.

12.6.2 A General Theory for Reactive Compensation

Here, we remove the restrictions that apply to IRP theory proposed in [27]. We will be using untransformed quantities that are applicable in all situations – single phase or multi-phase. Also, some of the confusion prevailing in the literature will be clarified. The presentation is based on the ideas given in the papers [29] and [41].

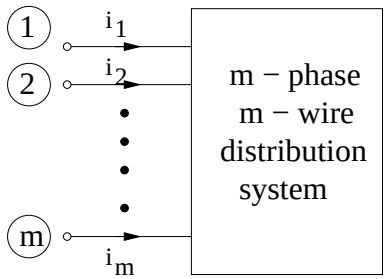

Figure 12.21: A m-phase, m-wire system

Consider a load supplied by a m-phase, m-wire system (see Fig. 12.21). The three phase, 4 wire system becomes a special case. We assume that all the voltages are measured with respect to a reference bus (typically ground). The total instantaneous power transmitted to the load is a scalar $p_\Sigma(t)$, given by

$$p_\Sigma(t) = v(t)^T i(t) \tag{12.101}$$

where both $v(t)$ and $i(t)$ are m-dimensional vectors and the superscript T denotes transposition. We define a vector $i_p(t)$, proportional to $v(t)$ as

$$i_p(t) = G(t)v(t) \tag{12.102}$$

where

$$G(t) = \frac{p_\Sigma(t)}{(v^T v)} \tag{12.103}$$

It is easy to show that $p_\Sigma(t) = v(t)^T i_p(t)$. The current vector $i_p(t)$ is defined as the instantaneous active current. The difference in the two currents ($i(t)$ and $i_p(t)$) is defined as the instantaneous non-active (or reactive) current given by

$$i_q(t) = i(t) - i_p(t) \tag{12.104}$$

The current $i_q(t)$ does not contribute to the transfer of power and essentially relates to the oscillation of the energy between phases. Hence, it should be possible to compensate for this current by a compensator without energy storage. After this compensation, the instantaneous power is unaffected. The collective source current magnitude is reduced from I_Σ to $I_{\Sigma p}$ where I_Σ and $I_{\Sigma p}$ are defined as

$$I_\Sigma^2 = \frac{1}{T}\int_0^T |i(t)|^2 dt, \quad I_{\Sigma p}^2 = \frac{1}{T}\int_0^T |i_p(t)|^2 dt$$

where

$$|i(t)|^2 = (i^T \cdot i), \quad |i_p(t)|^2 = (i_p^T \cdot i_p)$$

The collective source current magnitude can be reduced further if there are variations in the instantaneous power. However, this requires compensation with energy storage. The minimum collective source current magnitude required is one that supplies the average total power (P_Σ) for a specified voltage vector, at minimum losses in the line (and maximum collective PF). The source currents resulting after (a) compensation without energy storage and (b) the compensation with energy storage are termed as instantaneous active current defined by

$$i_{act}(t) = Gv(t) \tag{12.105}$$

where

$$\begin{aligned} G &= \frac{P_\Sigma}{V_\Sigma^2}, \quad P_\Sigma = \frac{1}{T}\int_0^T p_\Sigma(t) dt, \\ V_\Sigma^2 &= \frac{1}{T}\int_0^T |v(t)|^2 dt, \quad |v(t)|^2 = v^T v \end{aligned}$$

The currents supplied by the compensator with energy storage are given by

$$\begin{aligned} i_{CE}(t) &= i_p(t) - i_{act}(t) \\ &= [G(t) - G]v(t) \end{aligned} \tag{12.106}$$

It is claimed in the previous literature that the compensator has to provide for the AC component in the total instantaneous power and $i_{CE}(t)$ is wrongly computed as

$$i_{CE}(t) = \frac{[p_\Sigma(t) - P_\Sigma]}{|v(t)|} v(t)$$

Note that the correct computation of $i_{CE}(t)$ from Eq. (12.106) gives

$$i_{CE}(t) = \left[\frac{p_\Sigma(t)}{|v(t)|^2} - \frac{P_\Sigma}{V_\Sigma^2} \right] v(t)$$

Note that the two expressions are different unless $|v(t)|$ is a constant (in which case it is same as V_Σ).

Remarks

1. For the general case of m wires presented above, it is possible to define the instantaneous imaginary (reactive) power as

$$q(t) = |v(t)| \cdot |i_q(t)|$$

For three phase systems without zero sequence components, the currents and voltages can be represented in a plane (of $\alpha - \beta$ quantities). Here, $q(t)$ can be associated with a cross product of the current and voltage vectors ($q = v \times i$) [28]. The sign of $q(t)$ can be associated with the direction of the vector perpendicular to the plane of the voltage and current vectors. However, for the general case, this sign interpretation is not possible.

In any case, as mentioned earlier, the concept of instantaneous reactive power is not consistent with reactive power defined for energy storage elements. In general, we can say that a load may draw non-active currents which include reactive currents (associated with linear L-C networks) and currents that do not contribute to the flow of instantaneous power to the load.

2. For a single phase system, i_p defined in Eq. (12.61) is same as the active current defined in (12.105) for the general case. Hence, $i_q(t)$ for the single phase systems requires a compensator with energy storage.

3. The presence of the zero sequence current does not affect the analysis presented here. If zero sequence voltage is not zero, then there is zero sequence power that contributes to $p_\Sigma(t)$. Only if the zero sequence power is zero, then i_0 contributes only to non-active currents.

4. It is mentioned in [31] that negative sequence components of the load voltages result in AC component in $|v(t)|$. This is not always true. In [42] a counter example is given which shows that even with unbalanced voltages, $|v(t)|$ can be a constant.

12.6.3 Application to a 3 Phase, 4 Wire System

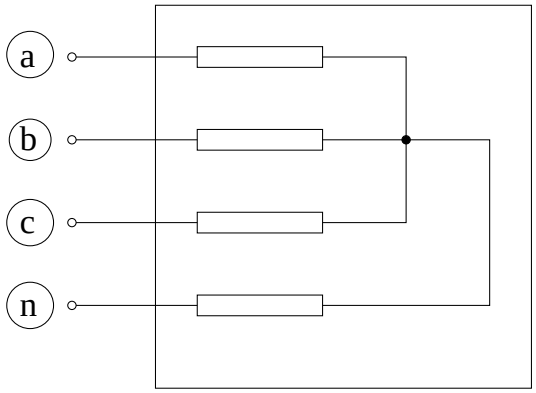

Figure 12.22: A 3-phase, 4-wire system

Here we consider the practical case of three phase, four wire system (with $m = 4$). Figure 12.22 shows the load supplied by a three phase, four wire supply. The compensator (based on VSC) is connected in parallel (not shown in the Fig.). The configuration of the VSC can be a two level four leg type or other types that enable it to inject zero sequence current components.

The total instantaneous power ($p_\Sigma(t)$) is given by

$$\begin{aligned} p_\Sigma(t) &= v_a i_a + v_b i_b + v_c i_c + v_n i_n \\ &= v_{an} i_a + v_{bn} i_b + v_{cn} i_c \end{aligned} \tag{12.107}$$

where $v_{an} = v_a - v_n$. Similar definition applies to v_{bn} and v_{cn}. Eq. (12.107) is derived by noting that $i_a + i_b + i_c + i_n = 0$.

The desired source current, $i_S(t)$, can be assumed to be $i_p(t)$ which is defined by

$$i_S(t) = i_p(t) = \frac{p_\Sigma(t)}{(v_{an}^2 + v_{bn}^2 + v_{cn}^2)} [v_{an} \quad v_{bn} \quad v_{cn}]^T \tag{12.108}$$

The currents injected by the compensator without energy source are given by

$$i_C(t) = i_L(t) - i_S(t) = i(t) - i_S(t) \tag{12.109}$$

With an ideal compensator with negligible losses, the instantaneous power supplied on the AC and DC side of the compensator are equal. Thus, we have the constraint

$$v_{an} i_{Ca} + v_{bn} i_{Cb} + v_{cn} i_{Cc} = v_{dc} i_{dc} \tag{12.110}$$

Since, the LHS of the above equation is zero (as the compensator is supplying i_q with zero instantaneous power), we derive $i_{dc} = 0$ as v_{dc} is non-zero.

Remarks

1. According to the modified IRP theory [44], we can express the desired compensator currents in terms of $\alpha\beta 0$ components of the voltage (v_{an}, v_{bn} and v_{cn}) and currents. The desired source currents are,

$$i_{S(0\alpha\beta)} = \frac{p_\Sigma(t)}{v_{0\alpha\beta}^2}[v_0 \quad v_\alpha \quad v_\beta]^T$$

where

$$i_{S(0\alpha\beta)} = [i_{S0} \quad i_{S\alpha} \quad i_{S\beta}]^T, \quad v_{0\alpha\beta}^2 = v_0^2 + v_\alpha^2 + v_\beta^2$$

The desired compensator currents in $\alpha\beta 0$ components are obtained as

$$i_{C(0\alpha\beta)} = i_{0\alpha\beta} - i_{S(0\alpha\beta)}$$

2. If it is desired to compensate for the variations in the instantaneous power, we have to design a compensator with energy storage. We can use a common compensator to inject both i_q and i_{pv} where the latter is defined by

$$i_{pv} = [G(t) - G]v$$

Note that the computation of G involves averaging and filtering and cannot be performed on an instantaneous basis. Further, as the compensator now modifies the instantaneous power in the line, $i_{dc} \neq 0$ (although the average value of i_{dc} is zero in steady state). Since finite capacitor is used, the variation in i_{dc} introduces ripples in the capacitor voltage (v_{dc}) depending on the magnitude of the injected currents i_{pv}.

The injected AC voltages by the compensator are related to the DC (capacitor voltage) and the switching functions. These are given by

$$[e_{Ca} \quad e_{Cb} \quad e_{Cc}]^T = [S_a(t) \quad S_b(t) \quad S_c(t)]^T v_{dc} \tag{12.111}$$

where e_C is the injected voltage vector. S_a, S_b and S_c are the switching functions that are determined by the control (modulation) strategy. If the compensator is assumed to be ideal (lossless), then

$$i_{dc} = S_a(t)i_{Ca} + S_b(t)i_{Cb} + S_c(t)i_{Cc} \tag{12.112}$$

Generally, the capacitor voltage is regulated. The shunt connected compensator functions like a controlled current source by controlling the injected currents by PWM techniques.

12.6.4 Reactive Power Compensation by Series Connected Compensators

The reactive power compensation considered in the previous subsections assumed that the load can be represented as a (variable) current source that draws power from a specified voltage source. The reactive compensator is assumed to be connected in parallel with the load. There are loads (including arc furnaces) that cannot be modelled as controllable current sources. For example, in an arc furnace, the arc resistance is not only nonlinear, but also varies over a wide range. In general, the load may be modelled as variable impedances or voltage sources in series with impedances that are comparable to the source impedances. In such cases, it is convenient to assume the load current as specified and analyze the quality of the voltage across the load. The general theory presented in section 12.6.2 can be extended to these cases.

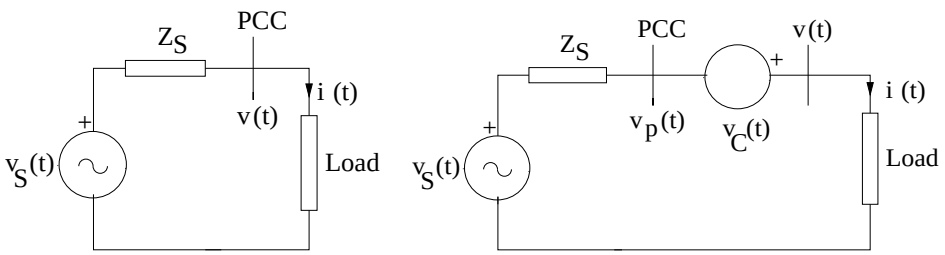

(a) Without compensator (b) With series compensator (no energy storage)

Figure 12.23: A circuit with series compensator

Consider the circuit shown in Fig. 12.23 (only single phase representation is shown). We can express the voltage vector (corresponding to the PCC) as a sum of two components.

$$v(t) = v_p(t) + v_q(t) \tag{12.113}$$

where,

$$v_p(t) = R(t)i(t), \quad R(t) = \frac{p_\Sigma(t)}{(i^T i)} \tag{12.114}$$

It is possible to compensate for $v_q(t)$ at PCC by connecting a compensator in series with the load. This compensator does not require any energy storage since $v_q(t)$ does not affect the total instantaneous active power ($p_\Sigma(t)$). We can prove that

$$p_\Sigma(t) = i^T(t) \cdot v_p(t), \quad i^T(t)v_q(t) = 0 \tag{12.115}$$

If $R(t)$ is not a constant and has periodically varying components, it is possible to further compensate for the variations of the instantaneous power, $p_\Sigma(t)$. The total average power (P_Σ) can be met by the voltage vector $v_a(t)$ defined by

$$v_a(t) = Ri(t), R = \frac{P_\Sigma}{I_\Sigma^2} \tag{12.116}$$

$$I_\Sigma^2 = \frac{1}{T}\int_0^T |i(t)|^2 dt, \quad |i(t)|^2 = i^T \cdot i$$

To compensate for the variations in $p_\Sigma(t)$, we require a compensator with energy storage that can inject a voltage, $(v_p - v_a)$ in addition to $v_q(t)$.

The advantages of a series compensator are to (a) improve the power quality for loads connected to PCC and (b) to improve the utilization of power for the load that is compensated. A compensated load can draw more power for a given supply.

The series reactive compensator can also be used to compensate for the voltage variations in the supply caused by voltage sags or harmonics. If the compensator requires active power in steady state for satisfactory performance, this has to be arranged by connecting an energy source. For example, a shunt connected rectifier can supply power on the DC side of the VSC based compensator.

References and Bibliography

1. N.G. Hingorani, "Introducing Custom Power", IEEE Spectrum, v. 32, n. 6, 1995, pp. 41-48.
2. R.C. Dugan, M.F. McGranaghan and H.W. Beaty, **Electrical Power Systems Quality**, New York: McGraw-Hill, 1996
3. D.D. Sabin and A. Sundaram, "Quality enhances reliability", IEEE Spectrum, v. 33, n. 2, 1996, pp. 34-41
4. M.F. McGranagan, D.R. Mueller and M.J. Samotyj, "Voltage sags in industrial systems", IEEE Trans. on Industry Applications, v. 29, n. 2, 1993, pp. 397-403
5. D.O. Koval, "Power system disturbance patterns", IEEE Trans. on Industry Appl., v. 26, n. 3, 1990, pp. 556-562
6. IEEE 519-1992, "IEEE Recommended practices and requirements for harmonic control in electric power systems".
7. W.M. Grady, M.J. Samotyj and A.H. Noyola, "Survey of active power line conditioning methodologies", IEEE Trans. on Power Delivery, v. 5, n. 3, 1990, pp. 1536- 1542

8. H. Akagi, "New trends in active filters for power conditioning", IEEE Trans. Industry Appl., v. 32, n. 6, 1996, pp. 1312-1322

9. H. Akagi, "Control strategy and site selection of a shunt active filter for damping harmonic propagation in power distribution systems", IEEE Trans. on Power Delivery, v. 12, n. 1, 1997, pp. 354-363

10. J. Hafner, M. Aredes and K. Heumann, "A shunt active filter applied to high voltage distribution lines", IEEE Trans. on Power Delivery, v. 12, n. 1, 1997, pp. 266- 272

11. A. van Zyl, J.H.R. Enslin and R. Spee, "Converter based solution to power quality problems on radial distribution lines", IEEE Trans. Industry Appl., v. 32, n. 6, 1996, pp. 1323-1330

12. F.Z. Peng, H. Akagi and A. Nabae, "A new approach to harmonic compensation in power systems - a combined system of shunt passive and active filters", IEEE Trans. on Industry Appl., v. 26, n. 6, 1990, pp. 983-990

13. S.M. Williams, G.T. Brownfield and J.W. Duffus, "Harmonic propagation on an electric distribution system: field measurements compared to computer simulation", IEEE Trans. on Power Delivery, v. 8, n. 2, 1993, pp. 547-552

14. A.E. Emanuel and M. Yang, "On the harmonic compensation in non-sinusoidal systems", IEEE Trans., Power Delivery, v. 8, n. 1, 1993, pp. 393-399

15. R.S. Thallam and S. Eckroad, "Multimode battery energy storage system for custom power applications", IEEE Power Engineering Society 1999 Winter Meeting, v. 2, 1999, pp. 1147-1150

16. J.J. Paserba et al., "Coordination of a distribution level continuously controlled compensation device with existing substation equipment for long term var management", IEEE Trans. on Power Delivery, v. 9, n. 2, 1994, pp. 1034-1040

17. S. Santoso et al., "Power quality assessment via wavelet transform analysis", IEEE Trans. on Power Delivery, v. 11, n. 2, 1996, pp. 924-930

18. S. Santoso et al, "Power quality disturbance waveform recognition using wavelet-based neural classifier- Part I: Theoretical foundation", IEEE Trans. on Power Delivery, v. 15, n. 1, 2000, pp. 222-228

19. S. Santoso et al., " Power quality disturbance waveform recognition using wavelet-based neural classifier- Part II: Application", IEEE Trans. on Power Delivery, v. 15, n. 1, 2000, pp. 229-235

20. T.N. Le et al., "Active damping of resonances in power systems", IEEE Trans. on Power Delivery, v. 9, n. 2, 1994, pp. 1001-1008

21. K. Srinivasan, "Digital measurement of voltage flicker", IEEE Trans. on Power Delivery, v. 6, n. 4, 1991, pp. 1593-1598

22. G. Manchur and C.C. Erven, "Development of a model for predicting flicker from electric arc furnaces", IEEE Trans. on Power Delivery, v. 7, n. 1, 1992, pp. 416-426

23. G.C. Montanari et al, "Arc-furnace model for the study of flicker compensation in electrical networks", IEEE Trans. on Power Delivery, v. 9, n. 4, 1994, pp. 2026- 2034

24. A. Nabae and M. Yamaguchi, "Suppression of flicker in an arc-furnace supply system by an active capacitance - A novel voltage stabilizer in power systems", IEEE Trans., Industry Appl., v. 31, n. 1, 1995, pp. 107-111

25. L.S. Czarnecki, "What is wrong with Budeanu concept of reactive and distortion power and why it should be abandoned", IEEE Trans. on Instrumentation and Measurement, v. IM-36, n. 3, 1987, pp. 834-837

26. L.S. Czarnecki, "Considerations on the reactive power in non-sinusoidal situations", IEEE Trans. on Instrum. Meas., v. IM-34, n. 3, 1985, pp. 399-404

27. H. Akagi, Y. Kanazawa and A. Nabae, "Instantaneous reactive power compensators comprising switching devices without energy storage components", IEEE Trans., Industry Appl., v. IA-20, 1984, pp. 625-631

28. F.Z. Peng and J.S. Lai, "Generalized instantaneous reactive power theory for three-phase power systems", IEEE Trans., Instrum. Meas., v. 45, n. 1, 1996, pp. 293-297

29. J.L. Willems, "A new interpretation of the Akagi-Nabae power components for nonsinusoidal three-phase situations", IEEE Trans., Instrum. Meas., v. 41, n. 4, 1992, pp. 523-527.

30. M. Aredes, J. Hafner and K. Heumann, "Three-phase four-wire shunt active filter control strategies", IEEE Trans., Power Electronics, v. 12, n. 2, 1997, pp. 311- 318

31. H. Kim et al, "Instantaneous power compensation in three-phase systems by using p-q-r theory", IEEE Trans., on Power Electronics, v. 17, n. 5, 2002, pp. 701- 710

32. H. Kim, F. Blaabjerg and B. Bak-Jensen, "Spectral analysis of instantaneous powers in single-phase and three-phase systems with use of p-q-r theory", IEEE Trans. on Power Electronics, v. 17, n. 5, 2002, pp. 711-720

33. J.C. Montano and P. Salmeron, "Instantaneous and full compensation in three-phase systems", IEEE Trans., Power Delivery, v. 13, n. 4, 1998, pp. 1342-1347

34. IEEE Standard 100-1988, IEEE Standard Dictionary of Electrical and Electronic Terms

35. IEC 61000-4-15: 1997, Electromagnetic Compatibility (EMC)-Part 4: Testing and measurement techniques - Section 15: Flicker meter - Functional and design specifications

36. W. Zhang et al., "Active dc filter for HVDC system - A test installation in the Konti-Skan at Lindome converter station", IEEE Trans., Power Delivery, v. 8, 1993, pp. 1599-1605

37. H. Fujita and H. Akagi, "A practical approach to harmonic compensation in power systems – series connection of passive and active filters", IEEE Trans., Industry Appl., v. 27, 1991, pp. 1020-1025

38. W.H. Hayt and J.E. Kemmerly, **Engineering Circuit Analysis, Second Edition**, New York: McGraw-Hill, 1971

39. L.S. Czarnecki, "Orthogonal decomposition of the currents in a 3-phase nonlinear asymmetrical circuit with a nonsinusoidal voltage source", IEEE Trans., Instr. and Meas., v. 37, n. 1, 1988, pp. 30-34

40. A. E. Emmanuel, "Powers in nonsinusoidal situations: A review of definition and physical meaning", IEEE Trans., Power Delivery, v. 5, n. 3, 1990, pp. 1377-1389

41. M. Depenbrock, "The FBD-method, a generally applicable tool for analyzing power relations", IEEE Trans., Power Systems, v. 8, n. 2, 1993, pp. 381-387

42. M. Depenbrock, V. Staudt and H. Wrede, "Concerning Instantaneous power compensation in three-phase systems by using p-q-r theory", IEEE Trans. on Power Electronics, v. 19, n. 4, 2004, pp. 1151-1152

43. N.L. Kusters and W.J.M. Moore, "On definition of reactive power under non-sinusoidal conditions", IEEE Trans., Power Apparatus and Systems, v. PAS-99, n. 5, 1980, pp. 1845-1854

44. M. Depenbrock, V. Staudt and H. Wrede, "A theoretical investigation of original and modified instantaneous power theory applied to four-wire systems", IEEE Trans., Industry Appl., v. 39, n. 4, 2003, pp. 1160-1167

45. L.S. Czarnecki, "Scattered and reactive current, voltage and power in circuits with nonsinusoidal waveforms and their compensation", IEEE Trans., Instr. and Meas., v. 40, n. 3, 1991, pp. 563-567

Chapter 13

Load Compensation and Distribution STATCOM

13.1 Introduction

Large fluctuating loads such as arc furnaces, steel rolling mills, electric traction cause current unbalance and large variations in the reactive power demand. The load compensation by shunt connected compensators that are fast acting, helps to maintain unity power factor while balancing the load. The improvement of power factor reduces the line current for a given load demand and enables better utilization of the distribution system. It also helps to reduce the line losses.

The unbalanced load currents with large reactive components results in voltage fluctuations and unbalance due to the source (system) impedances. A shunt compensator also helps to reduce voltage fluctuations at the point of common coupling (PCC). If the source voltages are unbalanced and varying, it is also possible for a shunt compensator to achieve this [14]. However, the effectiveness of the voltage regulation, in this case, is a function of the system impedance. As discussed in the previous chapter, fast voltage regulation also helps to improve voltage flicker.

The first power electronics based static shunt compensator applied for load compensation was SVC using thyristor-controlled reactor in parallel with fixed or thristor-switched capacitors. The emerging technology of high power voltage source converters using pulse width modulation (PWM) is replacing thyristor-based controllers. The application of VSC also permits multi-function (or composite) compensation that includes active filtering to prevent the flow of harmonic currents on the source side.

In this chapter, we will consider load compensation using both SVC and Distribution STATCOM. We consider both three phase, three wire and four wire systems and discuss various control algorithms that are applicable. Finally, we present a case study of composite compensation using DSTATCOM.

13.2 Three Phase Three Wire Systems

In a three wire system, the sum of the phase currents is zero, implying that there is no zero-sequence current flowing in the system. The load may be connected in delta or star (with floating neutral). To simplify the analysis, we will assume the source voltage to be balanced and sinusoidal. We will also assume that the source impedances are symmetric. There is no loss of generality in assuming the mutual impedances between the phases are zero.

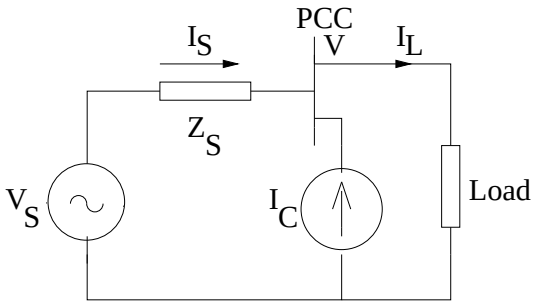

Figure 13.1: Single phase equivalent circuit

Linear Loads

If we assume that the loads are linear (although time-varying), the load currents are sinusoidal in steady state as the supply voltages are sinusoidal. However, the load currents may be unbalanced with the presence of negative sequence components. Fig. 13.1 shows the equivalent system with the unbalanced load and the shunt compensator.

In Fig. 13.1, the source current I_S is given by

$$I_S = I_L - I_C \tag{13.1}$$

With an ideal compensator, the current I_C supplied by the compensator is equal to the sum of the negative sequence component and the (positive sequence) reactive current drawn by the load. This ensures that the source current contains only the active component of the positive sequence current drawn by the load. This also results in the load voltage (V) becoming balanced.

Incidentally, it was shown by Steinmetz that a delta-connected reactive network (see Fig. 13.2) can work as an ideal compensator. This concept can be used to design a SVC whose susceptances depend on the sequence components of the load current.

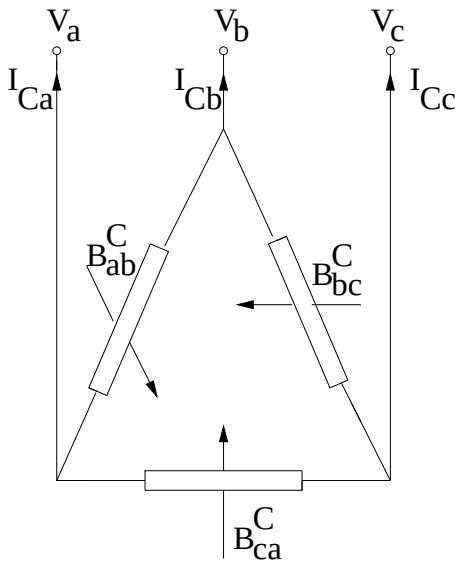

Figure 13.2: A delta connected reactive compensator

Neglecting the source impedance Z_S we get $V = V_S$. Thus, V is a positive sequence voltage independent of the load. If we assume V_a as reference, we can write

$$V_a = V, \quad V_b = h^2 V, \quad V_c = hV \tag{13.2}$$

where, h is the operator defined by

$$h = e^{j\frac{2\pi}{3}} = -\frac{1}{2} + j\frac{\sqrt{3}}{2} \tag{13.3}$$

The compensator currents injected are given by

$$I_{Ca} = -(I^C_{ab} - I^C_{ca}) = -j[B^C_{ab}(1-h^2) - B^C_{ca}(h-1)]V \tag{13.4}$$
$$I_{Cb} = -(I^C_{bc} - I^C_{ab}) = -j[B^C_{bc}(h^2-h) - B^C_{ab}(1-h^2)]V \tag{13.5}$$
$$I_{Cc} = -(I^C_{ca} - I^C_{bc}) = -j[B^C_{ca}(h-1) - B^C_{bc}(h^2-h)]V \tag{13.6}$$

The symmetrical components of the phase currents are defined (using power invariant transformation) by

$$I_0 = \frac{1}{\sqrt{3}}(I_a + I_b + I_c) \tag{13.7}$$
$$I_1 = \frac{1}{\sqrt{3}}(I_a + hI_b + h^2 I_c) \tag{13.8}$$
$$I_2 = \frac{1}{\sqrt{3}}(I_a + h^2 I_b + hI_c) \tag{13.9}$$

Note that the power-invariant transformation implies that

$$V_a I_a^* + V_b I_b^* + V_c I_c^* = V_1 I_1^* + V_2 I_2^* + V_0 I_0^* \tag{13.10}$$

The symmetrical components of the delta connected reactive compensator are given by

$$\begin{aligned} I_{C0} &= 0 \\ I_{C1} &= -j\sqrt{3}(B_{ab}^C + B_{bc}^C + B_{ca}^C)V \\ I_{C2} &= j\sqrt{3}(h^2 B_{ab}^C + B_{bc}^C + hB_{ca}^C)V \end{aligned}$$

Since load compensation requires

$$I_{C2} = I_{L2}, \quad \text{Im}[I_{C1}] = \text{Im}[I_{L1}] \tag{13.11}$$

we can derive the desired compensator susceptances as follows

$$B_{ab}^C = \frac{-1}{3\sqrt{3}V}[\text{Im}(I_1^L) + \text{Im}(I_2^L) - \sqrt{3}\text{Re}(I_2^L)] \tag{13.12}$$

$$B_{bc}^C = \frac{-1}{3\sqrt{3}V}[\text{Im}(I_1^L) - 2\text{Im}(I_2^L)] \tag{13.13}$$

$$B_{ca}^C = \frac{-1}{3\sqrt{3}V}[\text{Im}(I_1^L) + \text{Im}(I_2^L) + \sqrt{3}\text{Re}(I_2^L)] \tag{13.14}$$

(Note that the superscript C refers to compensator). It is possible to express the quantities on the R.H.S of the Eqs. (13.12) to (13.14) in terms of the phase variables. The final result is

$$B_{ab}^C = -\frac{1}{3V}[\text{Im}(I_a^L) + \text{Im}(hI_b^L) - \text{Im}(h^2 I_c^L)] \tag{13.15}$$

$$B_{bc}^C = -\frac{1}{3V}[\text{Im}(hI_b^L) + \text{Im}(h^2 I_c^L) - \text{Im}(I_a^L)] \tag{13.16}$$

$$B_{ca}^C = -\frac{1}{3V}[\text{Im}(h^2 I_c^L) + \text{Im}(I_a^L) - \text{Im}(hI_b^L)] \tag{13.17}$$

Thus, we have two sets of expressions for the susceptances of the reactive compensator – one in terms of the symmetrical components, the other in terms of phase variables of the load currents. The latter can also be expressed in terms of load reactive powers. Eqs. (13.15) to (13.17) can be recast as

$$B_{ab}^C = \frac{1}{3V^2}[Q_{La} + Q_{Lb} - Q_{Lc}] \tag{13.18}$$

$$B_{bc}^C = \frac{1}{3V^2}[Q_{Lb} + Q_{Lc} - Q_{La}] \tag{13.19}$$

$$B_{ca}^C = \frac{1}{3V^2}[Q_{Lc} + Q_{La} - Q_{Lb}] \tag{13.20}$$

where $Q_{Lm} = \text{Im}[V_m(I_{Lm})^*], \quad m = a, b \text{ or } c.$

Q_a, Q_b and Q_c can be computed as the average values (over a period) of the products of currents and phase shifted voltages. For example, Q_a is obtained as

$$Q_a = \frac{1}{T}\int_T v_a \left(\omega t - \frac{\pi}{2}\right) i_a(\omega t)dt$$

Since, $v_{bc} = \sqrt{3}v_a(\omega t - \frac{\pi}{2})$, we get

$$Q_a = \frac{1}{\sqrt{3}T}\int_T v_{bc} i_a dt$$

Similarly,

$$Q_b = \frac{1}{\sqrt{3}T}\int_T v_{ca} i_b dt, \quad Q_c = \frac{1}{\sqrt{3}T}\int_T v_{ab} i_c dt$$

(Note that the subscript L is dropped for convenience) Although the integration is over one period of the fundamental frequency, it is not strictly essential to reset the electronic integrator (used as part of the SVC control system) every cycle and it is possible to get continuous signals representing the desired susceptances. The integrator time constant can even be reduced to speed up the compensator response.

Compensation Using DSTATCOM

The equations (13.18) to (13.20) essentially define the delta connected susceptances in a SVC, that are required to compensate for the unbalance and the reactive power drawn by a three phase, 3 wire connected linear load. If a distribution STATCOM is used for compensation instead of a SVC, it is more appropriate to define the currents injected by the DSTATCOM. It is mentioned in [15] that a compensator with switching devices (such as a DSTATCOM) without energy storage can compensate for the instantaneous reactive power (q) defined as

$$q = v_\alpha i_\beta - v_\beta i_\alpha \tag{13.21}$$

It is worthwhile examining the conditions under which the above statement holds good. In the previous chapter (section 12.6.2) we presented a general theory for reactive compensation applicable for a m-phase (m-wire) system of which 3 phase - 3 wire system is a special case. However, let us first consider a balanced linear load connected across a constant (sinusoidal) voltage balanced supply with the instantaneous voltages defined by

$$\begin{aligned} v_a &= \sqrt{\frac{2}{3}}V\cos\omega_0 t, \quad v_b = \sqrt{\frac{2}{3}}V\cos\left(\omega_0 t - \frac{2\pi}{3}\right), \\ v_c &= \sqrt{\frac{2}{3}}V\cos\left(\omega_0 t + \frac{2\pi}{3}\right) \end{aligned}$$

As the load is balanced and linear, the currents are also balanced and sinusoidal defined by

$$\begin{aligned} i_a &= \sqrt{\frac{2}{3}} I \cos(\omega_0 t - \phi), \quad i_b = \sqrt{\frac{2}{3}} I \cos\left(\omega_0 t - \frac{2\pi}{3} - \phi\right), \\ i_c &= \sqrt{\frac{2}{3}} I \cos\left(\omega_0 t + \frac{2\pi}{3} - \phi\right) \end{aligned}$$

For this special case, it can be shown that,

$$\begin{aligned} p_\Sigma &= v_a i_a + v_b i_b + v_c i_c = V I \cos\phi = P_\Sigma \\ |v(t)| &= [v_a^2 + v_b^2 + v_c^2]^{1/2} = V = V_\Sigma \end{aligned}$$

Hence, the instantaneous active current $i_{act}(t)$ and $i_p(t)$ (defined as $p_\Sigma(t)/v(t)|$) are identical given by

$$i_p(t) = i_{act}(t) = Gv(t) = \left(\frac{P_\Sigma}{V_\Sigma}\right) v(t) \tag{13.22}$$

This clearly shows that $i_q(t)$ defined by

$$i_q(t) = i(t) - i_p(t) \tag{13.23}$$

can be compensated by a switching converter without energy storage as

$$v^T i_q = 0 \tag{13.24}$$

Remarks

1. From Eq. (13.23), it can be shown that i_q is obtained as

$$\begin{aligned} i_{qa} &= \sqrt{\frac{2}{3}} \left(\frac{q}{V}\right) \sin\omega_0 t, \quad i_{qb} = \sqrt{\frac{2}{3}} \left(\frac{q}{V}\right) \sin\left(\omega_0 t - \frac{2\pi}{3}\right) \\ i_{qc} &= \sqrt{\frac{2}{3}} \left(\frac{q}{V}\right) \sin\left(\omega_0 t + \frac{2\pi}{3}\right) \end{aligned}$$

where $q = VI\sin\phi$ is the reactive power. It is to be noted that q is also the 'instantaneous reactive power' (IRP) defined by Eq. (13.21).

The important conclusion from this result is that reactive power compensation can be achieved *without* energy storage elements (such as capacitors or inductors). A VSC based compensator can do the job.

2. The concept of IRP is valid only for three phase, three wire systems. For these systems, the zero sequence components in the currents are zero. To define instantaneous powers, we will use $d - q$ components

(defined with respect to a synchronously rotating reference frame), defined as follows.

$$f_d = \sqrt{\frac{2}{3}}\left[f_a\cos\theta + f_b\cos\left(\theta-\frac{2\pi}{3}\right) + f_c\cos\left(\theta+\frac{2\pi}{3}\right)\right] \quad (13.25)$$

$$f_q = \sqrt{\frac{2}{3}}\left[f_a\sin\theta + f_b\sin\left(\theta-\frac{2\pi}{3}\right) + f_c\sin\left(\theta+\frac{2\pi}{3}\right)\right] \quad (13.26)$$

where f can be voltage or current vector. $\theta = \omega_0 t$ if the network frequency is ω_0. (Note that the definition of d-q components is according to the convention used in reference [16] that d-axis leads q-axis).

From Eqs (13.25) and (13.26), we obtain

$$\begin{aligned}(f_d - jf_q) &= \sqrt{\frac{2}{3}}\left[f_a e^{-j\theta} + f_b e^{-j(\theta-\frac{2\pi}{3})} + f_c e^{-j(\theta+\frac{2\pi}{3})}\right] \\ &= \sqrt{\frac{2}{3}}\left[f_a + f_b e^{j\frac{2\pi}{3}} + f_c e^{-j\frac{2\pi}{3}}\right] e^{-j\theta} \\ &= F_s e^{-j\theta} \end{aligned} \quad (13.27)$$

where F_s is sometimes described as 'space vector'.

We can also define $\alpha-\beta$ components with respect to a stationary reference frame. These are defined from Eqs. (13.25) and (13.26), letting $\theta = 0$. Thus, we get

$$f_\alpha = \sqrt{\frac{2}{3}}\left[f_a - \frac{1}{2}f_b - \frac{1}{2}f_c\right] \quad (13.28)$$

$$f_\beta = \sqrt{\frac{2}{3}}\left[-\frac{\sqrt{3}}{2}f_b + \frac{\sqrt{3}}{2}f_c\right] \quad (13.29)$$

Substituting from the above equations, we can express F_s as

$$F_s = (f_\alpha - jf_\beta) \quad (13.30)$$

(Note that if we assume q-axis leading d-axis, the definition of f_β would involve a reversal of sign and $F_s = f_\alpha + jf_\beta$).

Since d-q components are defined as instantaneous quantities, we can define instantaneous complex power as

$$p + jq = (v_d - jv_q)(i_d - jiq)^* \quad (13.31)$$

Substituting from Eqs. (13.27) and (13.30), we get

$$\begin{aligned} p + jq &= (v_\alpha - jv_\beta)(i_\alpha + ji_\beta)e^{-j\theta}\cdot e^{j\theta} \\ &= (v_\alpha - jv_\beta)(i_\alpha + ji_\beta) \\ &= (v_\alpha i_\alpha + v_\beta i_\beta) + j(v_\alpha i_\beta - v_\beta i_\alpha) \end{aligned} \quad (13.32)$$

Equating real and imaginary parts, we get the expression for IRP(q) defined in Eq. (13.21).

Many references (including [15]) define i_β (or v_β) according to the following equation

$$f_\beta = \sqrt{\frac{2}{3}}\left[\frac{\sqrt{3}}{2}f_b - \frac{\sqrt{3}}{2}f_c\right] \tag{13.33}$$

However q is still defined according to Eq. (13.21). The two equations are inconsistent. If f_β is defined according to Eq. (13.33) instead of Eq. (13.29), the expression for q will be negative of what is defined in Eq. (13.21). For the balanced, linear load supplied by positive sequence voltage supply, we get

$$\begin{aligned} v_\alpha &= V\cos\omega_0 t, \quad v_\beta = -V\sin\omega_0 t \\ i_\alpha &= I\cos(\omega_0 t - \phi), \quad i_\beta = -I\sin(\omega_0 t - \phi) \end{aligned}$$

(Note that both v_β and i_β are defined according to Eq. (13.29)). The expression for q (according to Eq. (13.21)) results in

$$q = VI\sin\phi$$

3. Since the zero sequence component (i_0) of the load current is always zero in a 3 wire system, we can express the total instantaneous power (p_Σ)

$$p_\Sigma = v_\alpha i_\alpha + v_\beta i_\beta \tag{13.34}$$

Note that i_0 is defined as

$$i_0 = \frac{1}{\sqrt{3}}[i_a + i_b + i_c] \tag{13.35}$$

Since we are using power-invariant transformation, p_Σ is given by the general expression

$$p_\Sigma = v_\alpha i_\alpha + v_\beta i_\beta + v_0 i_0$$

Using $\alpha - \beta$ coordinates instead of phase (a,b and c) coordinates, we can define

$$i_p = \frac{p_\Sigma}{v_\alpha^2 + v_\beta^2}\begin{bmatrix} v_\alpha \\ v_\beta \end{bmatrix}, \quad i_q = \frac{q}{v_\alpha^2 + v_\beta^2}\begin{bmatrix} -v_\beta \\ v_\alpha \end{bmatrix} \tag{13.36}$$

Note that using α-β-0 transformation, we can define i_p and i_q as two-dimensional vectors. This is valid even if $v_0 \neq 0$. The compensator injects a current vector i_q (as defined above) and the source current now contains only i_p. If p_Σ and $(v_\alpha^2 + v_\beta^2)$ are constants, the compensation is complete and the source currents have minimum rms values.

If $(v_\alpha^2 + v_\beta^2)$ remains constant even in the presence of unbalanced (negative sequence) and harmonic currents in the (nonlinear) load, the instantaneous powers p and q contain time-varying (periodic) components in addition to constant components. The expression for i_q is unaltered in this case also. However, the minimum source current is now expressed as

$$i_{act}(t) = \frac{P_\Sigma}{V_\Sigma^2} \begin{bmatrix} v_\alpha \\ v_\beta \end{bmatrix} \tag{13.37}$$

where

$$P_\Sigma = \frac{1}{T}\int_0^T p_\Sigma(t)dt, \quad V_\Sigma^2 = \frac{1}{T}\int_0^T (v_\alpha^2 + v_\beta^2)dt = v_\alpha^2 + v_\beta^2$$

The compensation of the current $[i_p(t) - i_{act}(t)]$ requires energy storage elements. If a STATCOM is used for compensation, the DC capacitor must absorb and provide the required energy as $p_\Sigma(t)$ varies over a period (of supply frequency).

The compensator currents can be expressed in terms of phase coordinates using the relationships given below.

$$\begin{aligned} i_{Ca} &= \sqrt{\frac{2}{3}} i_{C\alpha}, \quad i_{Cb} = \sqrt{\frac{2}{3}}\left[-\frac{1}{2} i_{C\alpha} - \frac{\sqrt{3}}{2} i_{C\beta}\right] \\ i_{Cc} &= \sqrt{\frac{2}{3}}\left[-\frac{1}{2} i_{C\alpha} + \frac{\sqrt{3}}{2} i_{C\beta}\right] \end{aligned}$$

$i_{C\beta}$ and $i_{C\beta}$ are defined from

$$\begin{bmatrix} i_{C\alpha} \\ i_{C\beta} \end{bmatrix} = i_p(t) - i_{act}(t) + i_q(t) \tag{13.38}$$

Expressions for Current and Power Components Using Phase Coordinates

In reference [8], the expressions for the instantaneous current (and power) components are given using phase coordinates (a,b and c) without transformation. This is based on the application of linear vector spaces.

In a three dimensional vector space, there are three independent orthogonal vectors that span the space. We call these as basis vectors if their lengths are unity. Note that a vector V has length unity if

$$(V, V) = V^T V = 1$$

The inner product of two vectors U and V is defined as

$$(U, V) = \sum_i U_i V_i$$

Two vectors are said to be orthogonal if their inner product is zero.

For a specified set of three phase voltages, we can define three orthogonal vectors as follows

$$\begin{aligned} V_0^T &= \frac{v_0}{\sqrt{3}}[1 \;\; 1 \;\; 1], \quad v_0 = \frac{1}{\sqrt{3}}(v_a + v_b + v_c) \\ V_p^T &= V^T - V_0^T, \quad V^T = [v_a \;\; v_b \;\; v_c] \\ V_q^T &= \frac{1}{\sqrt{3}}[v_b - v_c \;\; v_c - v_a \;\; v_a - v_b] \end{aligned}$$

A current vector I defined by

$$I^T = [i_a \;\; i_b \;\; i_c]$$

can be expressed as a linear combination of the three vectors as follows.

$$I = \alpha_0 V_0 + \alpha_p V_p + \alpha_q V_q \tag{13.39}$$

where,

$$\begin{aligned} \alpha_0 &= \frac{p_0}{|V_0|^2}, \quad \alpha_p = \frac{p}{|V_p|^2}, \quad \alpha_q = \frac{q}{|V_q|^2} \\ p_0 &= I^T V_0, \quad p = I^T V_p, \quad q = I^T V_q \end{aligned}$$

For a three wire system, p_0 is always zero. Hence I can be expressed as

$$I = I_p + I_q \tag{13.40}$$

where

$$I_p^T = [i_{pa} \;\; i_{pb} \;\; i_{pc}], \quad I_q^T = [i_{qa} \;\; i_{qb} \;\; i_{qc}]$$

and

$$I_p = \frac{p}{|V_p|^2} V_p, \quad I_q = \frac{q}{|V_q|^2} V_q$$

It can be shown that $|V_p|^2$ defined by

$$\begin{aligned} |V_p|^2 &= \frac{2}{3}(v_a^2 + v_b^2 + v_c^2) - \frac{1}{3}(v_a v_b + v_b v_c + v_c v_a) \\ &= v_\alpha^2 + v_\beta^2 \end{aligned}$$

Similarly, $|V_q|^2 = v_\alpha^2 + v_\beta^2$.

The concept of orthogonal decomposition of vectors can be extended to electrical networks with m phases (and m wires). This is presented in the next section.

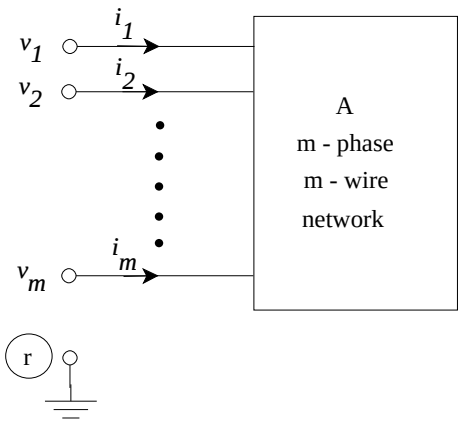

Figure 13.3: A m-phase, m-wire network

13.3 Three Phase Four Wire Systems

The analysis of a three phase, four wire systems can be considered as a special case of m-phase, m-wire system (see Fig. 13.3). We can define the current and voltage vectors for this system as

$$\begin{aligned} I^T &= [i_1 \;\; i_2 \;\; i_3 \;\; \ldots \;\; i_m] \\ V^T &= [v_1 \;\; v_2 \;\; v_3 \;\; \ldots \;\; v_m] \end{aligned}$$

with the constraint

$$\sum_{k=1}^{m} i_k = 0 \tag{13.41}$$

Note that all the voltages are expressed with reference to a bus 'r' (not necessarily ground bus).

There is a general result which is useful in defining instantaneous power in a m-phase, m-wire system. This is given below.

Lemma: Given two m-dimensional vectors, V and I, we can express

$$V = V_p + V_0, \quad I = I_p + I_0 \tag{13.42}$$

where

$$\begin{aligned} V_0 &= \frac{v_0}{\sqrt{m}}E, \quad I_0 = \frac{i_0}{\sqrt{m}}E, \\ v_0 &= \frac{1}{\sqrt{m}}(v_1 + v_2 + \ldots v_m), \quad i_0 = \frac{1}{\sqrt{m}}(i_1 + i_2 + \ldots i_m) \\ E^T &= [1 \;\; 1 \;\; \ldots \;\; 1] \end{aligned}$$

The scalar product (V, I) can be expressed as

$$(V, I) = (V_p, I_p) + (V_0, I_0)$$

The proof is straightforward as we can show

$$\begin{aligned} V^T I &= (V_p^T + V_0^T)(I_p + I_0) \\ &= V_p^T I_p + V_0^T I_0 \quad \text{as} \quad V_0^T I_p = V_p^T I_0 = 0 \end{aligned}$$

In a m-wire system, $I_0 = 0$ due to the constraint expressed by Eq. (13.41). Hence the total instantaneous power p_Σ can be expressed as

$$p_\Sigma(t) = V_p^T(t) I_p(t) = V_p^T I \tag{13.43}$$

In reference [17], V_0 is termed as a vector of common mode (or homopolar) voltages. It is obvious that these voltages do not contribute to the total instantaneous power as the power is affected only by the differences in the voltages. (The choice of the reference bus has no effect). Reference [17] also refers to $\frac{v_0}{\sqrt{m}}$ as the voltage of a virtual star point (of a symmetrical load of m unit resistances connected in star). Note that this is only a physical explanation of the voltage $\frac{v_0}{\sqrt{m}}$. The actual load can have any configuration. The voltages V_p can be viewed as the terminal voltages with reference to the virtual star point (see Fig. 13.4).

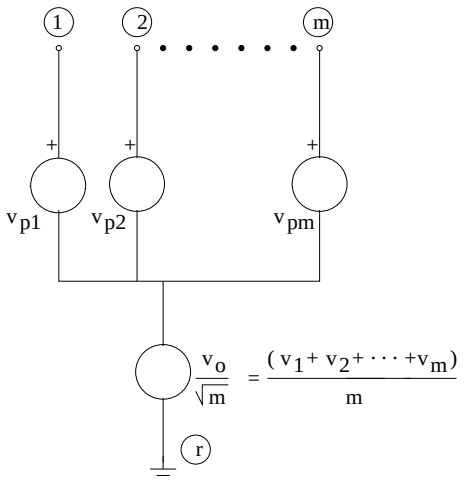

Figure 13.4: Representation of applied voltages

It is obvious that the vector V_p can be expressed as a linear combination of $(m-1)$ independent m dimensional vectors as $V_p^T V_0 = 0$.

Remarks

1. It is to be noted that v_0 is not to be confused with zero sequence voltage defined for a 3 phase, 3 wire system (Although for $m = 3$, the two are identical).

2. In 3 phase, 3-wire systems, it is obvious that V_p can be expressed as a linear combination of two independent vectors. In reference [15] these are chosen using $\alpha - \beta$ components.

3. The concept of IRP cannot be extended to systems with $m > 3$.

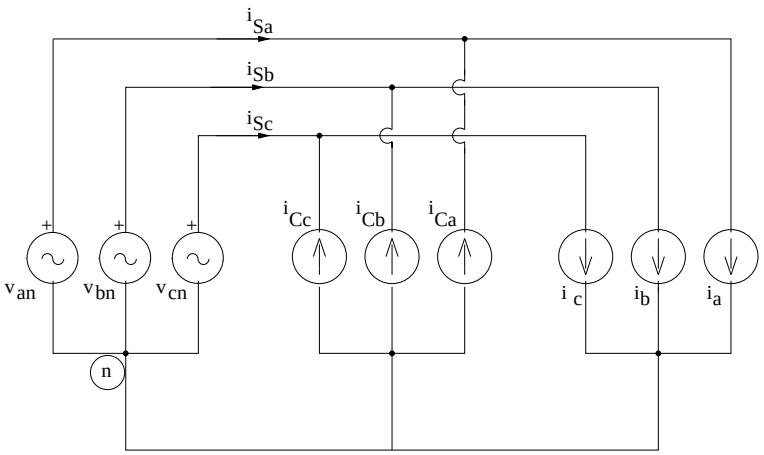

Figure 13.5: A three-phase, four wire system with shunt compensator

The application of this general theory to three phase, 4-wire systems (see Fig. 13.5) gives the following results.

$$V_0^T = \frac{(v_{ar} + v_{br} + v_{cr} + v_{nr})}{4}[1\ 1\ 1\ 1] \tag{13.44}$$

where V_{jr} ($j = a, b, c$ or n) indicates the voltage of terminal j with respect to a reference bus r. The vector V_p can be expressed in terms of three independent orthogonal vectors (V_x, V_y and V_z) as follows.

$$V_p = v_x V_x + v_y V_y + v_z V_z \tag{13.45}$$

where

$$v_x = (V, V_x), v_y = (V, V_y), v_z = (V, V_z)$$

V_x, V_y and V_z vectors are each of unit length. They are defined as [17]

$$V_x^T = \left[\sqrt{\frac{2}{3}} \quad -\frac{1}{\sqrt{6}} \quad -\frac{1}{\sqrt{6}} \quad 0\right] \tag{13.46}$$

$$V_y^T = \left[0 \quad \frac{1}{\sqrt{2}} \quad -\frac{1}{\sqrt{2}} \quad 0\right] \tag{13.47}$$

$$V_z^T = \left[\frac{1}{\sqrt{12}} \quad \frac{1}{\sqrt{12}} \quad \frac{1}{\sqrt{12}} \quad -\sqrt{\frac{3}{4}}\right] \tag{13.48}$$

If the neutral terminal is selected as reference, then $v_{nr} = 0$. In this case, v_x, v_y and v_z are expressed in terms of v_{an}, v_{bn} and v_{cn} by the following vector equation

$$\begin{bmatrix} v_x \\ v_y \\ v_z \end{bmatrix} = \sqrt{\frac{2}{3}} \begin{bmatrix} 1 & -\frac{1}{2} & -\frac{1}{2} \\ 0 & \frac{\sqrt{3}}{2} & -\frac{\sqrt{3}}{2} \\ \frac{1}{2\sqrt{2}} & \frac{1}{2\sqrt{2}} & \frac{1}{2\sqrt{2}} \end{bmatrix} \begin{bmatrix} v_{an} \\ v_{bn} \\ v_{cn} \end{bmatrix} \tag{13.49}$$

By comparing this equation to the definition of α, β and zero components, we get,

$$v_x = v_\alpha, \quad v_y = -v_\beta, \quad v_z = \frac{1}{2} v_h \tag{13.50}$$

Note that we have used the symbol v_h (instead of v_0) to denote the usual zero-sequence voltage component defined for three phase systems. This is done to avoid the clash with the symbol v_0 we have used to denote common mode voltage. Also note that v_β is defined in some of the literature as negative of the expression used here.

It is also possible to express the current vector $I^T = [i_a \;\; i_b \;\; i_c \;\; i_n]$ in terms of three orthogonal independent vectors V_x, V_y and V_z as follows

$$I = i_x V_x + i_y V_y + i_z V_z \tag{13.51}$$

where $i_x = (I, V_x), i_y = (I, V_y)$ and $i_z = (I, V_z)$.

Equation (13.51) follows from the fact that

$$i_a + i_b + i_c + i_n = 0 \tag{13.52}$$

When Eq. (13.52) is substituted in (13.51) we can express i_x, i_y and i_z in terms of i_a, i_b and i_c as

$$\begin{bmatrix} i_x \\ i_y \\ i_z \end{bmatrix} = \sqrt{\frac{2}{3}} \begin{bmatrix} 1 & -\frac{1}{2} & -\frac{1}{2} \\ 0 & \frac{\sqrt{3}}{2} & -\frac{\sqrt{3}}{2} \\ \sqrt{2} & \sqrt{2} & \sqrt{2} \end{bmatrix} \begin{bmatrix} i_a \\ i_b \\ i_c \end{bmatrix} \tag{13.53}$$

In comparison with i_α, i_β and i_h (zero sequence component), we get,

$$i_x = i_\alpha, i_y = -i_\beta, i_z = 2i_h \tag{13.54}$$

The desired compensator currents that are to be injected are obtained as

$$\begin{aligned} i_{Cx} &= i_x - i_{Sx} \\ i_{Cy} &= i_y - i_{Sy} \\ i_{Cz} &= i_z - i_{Sz} \end{aligned} \tag{13.55}$$

The desired source currents are obtained as

$$\begin{bmatrix} i_{Sx} \\ i_{Sy} \\ i_{Sz} \end{bmatrix} = \frac{p_\Sigma(t)}{(v_x^2 + v_y^2 + v_z^2)} \begin{bmatrix} v_x \\ v_y \\ v_z \end{bmatrix} \tag{13.56}$$

where $p_\Sigma(t) = I^T V_p = i_x v_x + i_y v_y + i_z v_z$.

The compensator currents (i_{Ca}, i_{Cb} and i_{Cc}) are obtained after transformation from x, y and z components and are given by

$$\begin{bmatrix} i_{Ca} \\ i_{Cb} \\ i_{Cc} \end{bmatrix} = \sqrt{\frac{2}{3}} \begin{bmatrix} 1 & 0 & -\frac{1}{2\sqrt{2}} \\ -\frac{1}{2} & \frac{\sqrt{3}}{2} & -\frac{1}{2\sqrt{2}} \\ -\frac{1}{2} & -\frac{\sqrt{3}}{2} & \frac{1}{2\sqrt{2}} \end{bmatrix} \begin{bmatrix} i_{Cx} \\ i_{Cy} \\ i_{Cz} \end{bmatrix} \tag{13.57}$$

Remarks

1. The major difference with the modified IRP theory is that

$$v_x^2 + v_y^2 + v_z^2 = v_\alpha^2 + v_\beta^2 + \frac{v_h^2}{4} \tag{13.58}$$

Note that L.H.S $\neq v_h^2 + v_\alpha^2 + v_\beta^2$ unless $v_h = 0$.

2. In reference [18], the original IRP theory is modified to define a new reactive current component (i_r) and modify i_p. The current i_p is modified to

$$i_p = \frac{p_\Sigma(t)}{|v_{0\alpha\beta}|^2} v_{0\alpha\beta} \tag{13.59}$$

where

$$\begin{aligned} p_\Sigma &= v_{0\alpha\beta}^T i_{0\alpha\beta} = v_{0\alpha\beta}^T i_p, \\ v_{0\alpha\beta}^T &= [v_0 \;\; v_\alpha \;\; v_\beta], \quad i_{0\alpha\beta}^T = [i_0 \;\; i_\alpha \;\; i_\beta] \end{aligned}$$

The current component i_r is defined as

$$i_r = (i_0 - i_{p0}) \frac{|v_{0\alpha\beta}|}{|v_{\alpha\beta}|} \tag{13.60}$$

where i_0 is the zero sequence current, $|v_{\alpha\beta}|$ is defined as $\sqrt{v_\alpha^2 + v_\beta^2}$. Similarly $|v_{0\alpha\beta}| = (v_0^2 + v_\alpha^2 + v_\beta^2)^{1/2}$. Note that i_r represents the reactive current component in the zero sequence current.

There is no need to define multiple components of the instantaneous reactive current. The basic definition of $i_q = i - i_p$ is valid for all cases. The major problem arises from the desire to extend the concept of IRP (q) to four wire systems and this is not feasible.

13.4 A Case Study

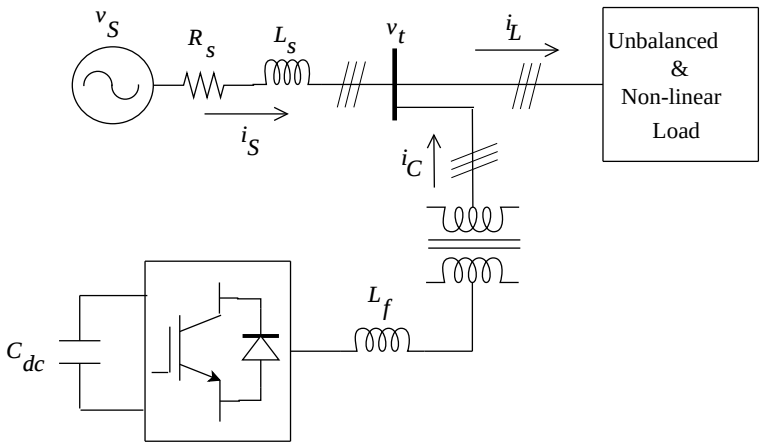

Figure 13.6: System diagram

A distribution system supplying an unbalanced and nonlinear load is taken up for study. The system diagram is shown in Fig. 13.6 which shows the source impedance (R_s and L_s). A STATCOM of suitable rating is connected in parallel with the load. In general, the STATCOM is connected through a step-up transformer. The load consists of a linear unbalanced load and a nonlinear rectifier load. It is assumed that the supply voltage is sinusoidal positive sequence voltage. However, the flow of load currents through the system impedance causes the voltage at PCC (V_t) to be unbalanced and contain harmonics. The source and the load data are given below.

Source: $V_s = 415$ V, $f = 50$ Hz, $L_s = 40$ mH, $\frac{X_s}{R_s} = 8$

Load: Unbalanced R-L load: $R_a = 50\ \Omega$, $L_a = 200$ mH $R_b = 75\ \Omega$,

$L_b = 225$ mH, $R_c = 25\ \Omega$, $L_c = 175$ mH

Nonlinear load: Three phase diode rectifier with $R_d = 125\ \Omega$, $L_d = 30$ mH (on DC side).

The objectives of the compensator are:

1) The source currents should be sinusoidal and contain only positive sequence components

2) The power factor or the voltage magnitude at PCC should be controlled.

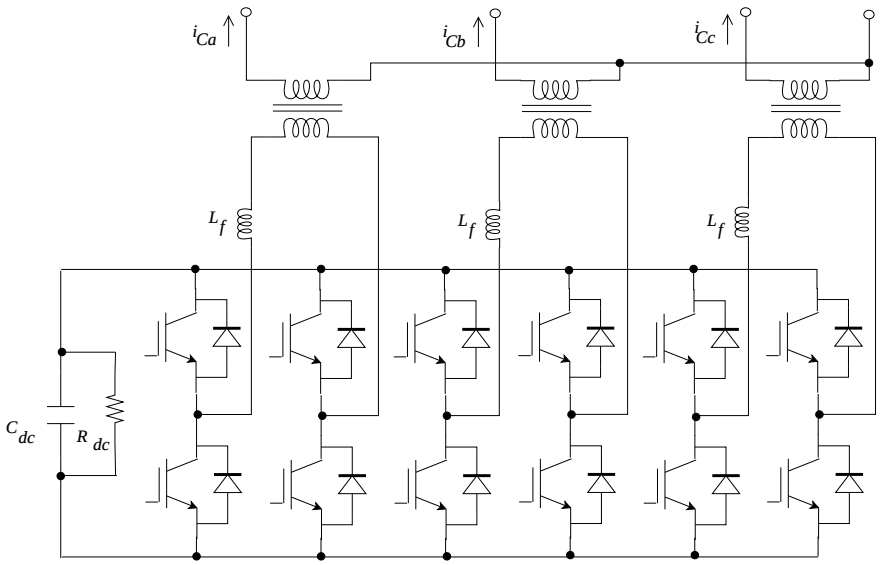

Figure 13.7: Configuration of DSTATCOM

Since V_S is assumed to be positive sequence and sinusoidal, the PCC voltage would also be sinusoidal and contain only positive sequence components, if the first objective is met. To achieve this objective, the compensator should be able to inject negative, zero sequence fundamental frequency components in addition to harmonic currents of all sequences. The configuration of DSTATCOM chosen is shown in Fig. 13.7. It contains three single phase full bridge converters connected to a common DC bus. The DC bus voltage is held by the capacitor C_{dc}. Since there is no energy source connected to the DC bus, the average power exchanged by the DSTATCOM is zero if the switches are ideal and losses in the reactors and capacitor are zero. However, in practice, the losses are to be supplied by the active power drawn from the AC system. To stabilize the capacitor voltage in steady state, a DC bus voltage control is necessary. It is to be noted that as the power supplied to

the load varies over the time period (of fundamental (supply) frequency), the capacitor will charge and discharge resulting in a voltage ripple. This is required to minimize the rms current supplied from the source to achieve unity factor at PCC.

As discussed in the previous section, the reference for the source current vector is first computed and the desired compensator currents are obtained as the difference between the load and the source (reference) currents. To inject the desired currents, DSTATCOM must have a high bandwidth closed loop current control loop. We will discuss the current control scheme later. The determination of reference source current vector is based on two approaches

1) Based on Synchronous Reference Frame (SRF)

2) Based on computation of $I_{act}(t)$

The data for the STATCOM selected are: $V_{dc} = 400$ V, $C_{dc} = 5000$ μF, $R_{dc} = 6000$ Ω, $L_f = 25$ mH.

13.5 Synchronous Reference Frame Based Extraction of Reference Currents

The block diagram of the control scheme to generate the reference values of the compensator currents is shown in Fig. 13.8. The desired source currents (in d-q components) are obtained as

$$i_{Sd}^{*} = \bar{i}_{Ld} + i_{Cd} \tag{13.61}$$

$$i_{Sq}^{*} = K_q \bar{i}_{Lq} + u i_{Cq} \tag{13.62}$$

where $\bar{i}_{Ld}$ and $\bar{i}_{Lq}$ are the average values of the d- and q- axis components of the load current, i_{Cd} is the output of the DC voltage controller and i_{Cq} is the output of the AC voltage controller (if the bus voltage (V_t) is to be regulated). u is a logical variable equal to (a) zero if PF is to be regulated and (b) one if bus voltage is to regulated. $K_q = 1$ in the latter case. When PF is to be controlled, K_q is determined by the required power factor as follows.

$$K_q = \frac{Q_S^{*}}{\bar{Q}_L} \tag{13.63}$$

where Q_S^{*} is the reference reactive power supplied by the source (at PCC) and $\bar{Q}_L$ is the average reactive power (at fundamental frequency) defined by

$$\bar{Q}_L = |V_t| \bar{i}_{Lq} \tag{13.64}$$

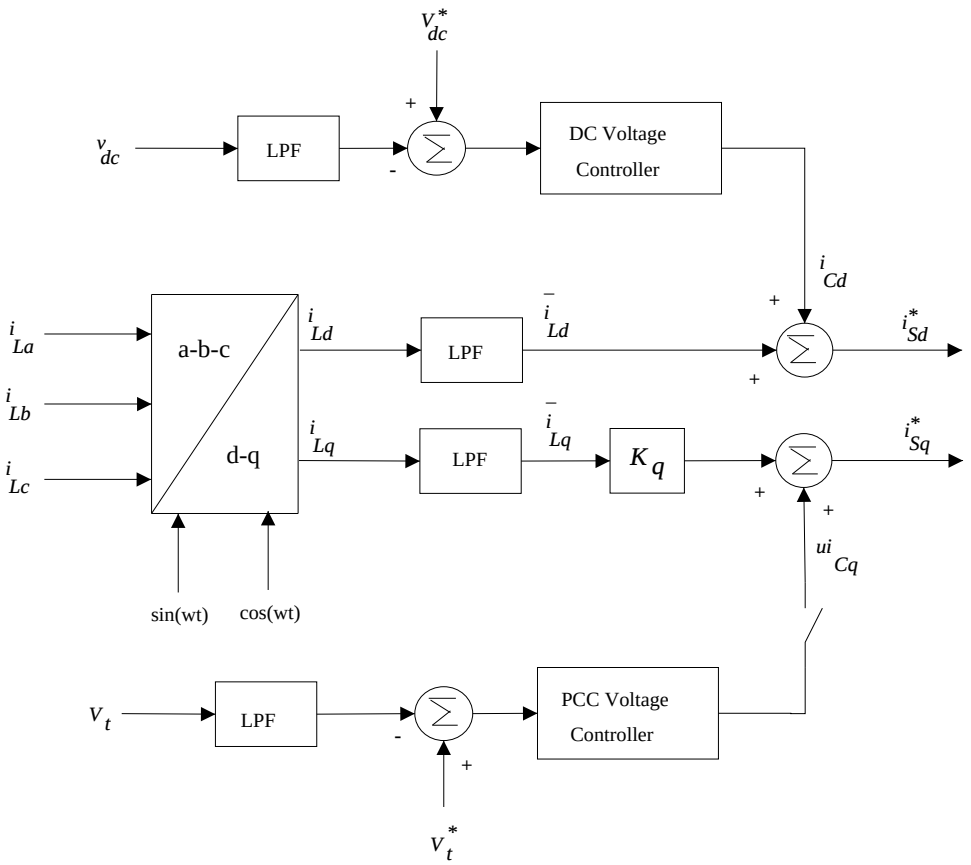

(a) Computation of reference source currents (d and q components)

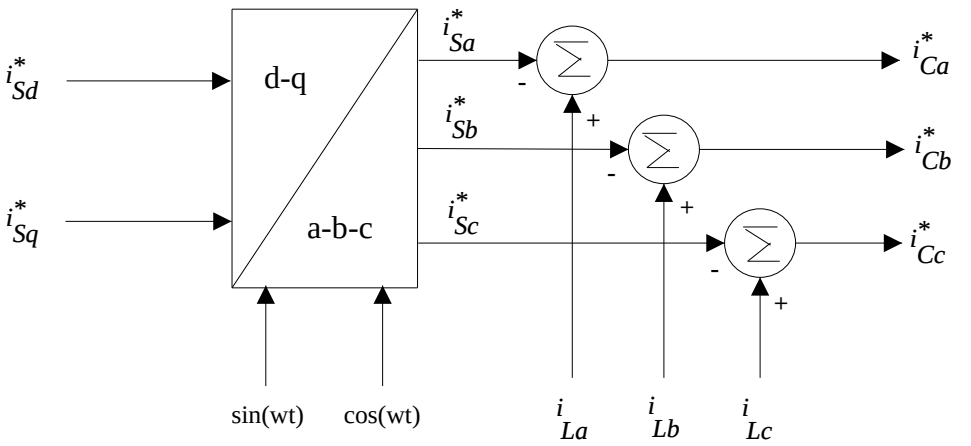

(b) Generation of reference compensator currents

Figure 13.8: Block diagram of the control scheme using SRF

For unity power factor, $Q_S^* = 0$ and $K_q = 0$. The average values of i_{Ld} and i_{Lq} are obtained as the outputs of two identical low pass filters and are defined as

$$\begin{bmatrix} \bar{i}_{Ld} \\ \bar{i}_{Lq} \end{bmatrix} = G(s) \begin{bmatrix} i_{Ld} \\ i_{Lq} \end{bmatrix} \tag{13.65}$$

where $G(s)$ is chosen as the transfer function of a 2nd order Butterworth low pass filter (with a corner frequency of 30 Hz). The d-q components are computed from the following relations

$$\begin{bmatrix} i_{Ld} \\ i_{Lq} \end{bmatrix} = \begin{bmatrix} \cos\omega t & -\sin\omega t \\ \sin\omega t & \cos\omega t \end{bmatrix} \begin{bmatrix} i_{L\alpha} \\ i_{L\beta} \end{bmatrix} \tag{13.66}$$

where the $\alpha - \beta$ components are obtained as

$$\begin{bmatrix} i_{L\alpha} \\ i_{L\beta} \end{bmatrix} = \sqrt{\frac{2}{3}} \begin{bmatrix} 1 & -\frac{1}{2} & -\frac{1}{2} \\ 0 & -\frac{\sqrt{3}}{2} & \frac{\sqrt{3}}{2} \end{bmatrix} \begin{bmatrix} i_{La} \\ i_{Lb} \\ i_{Lc} \end{bmatrix} \tag{13.67}$$

The reference vector of source currents is given by

$$\begin{bmatrix} i_{Sa}^* \\ i_{Sb}^* \\ i_{Sc}^* \end{bmatrix} = \sqrt{\frac{2}{3}} \begin{bmatrix} 1 & 0 \\ -\frac{1}{2} & -\frac{\sqrt{3}}{2} \\ -\frac{1}{2} & \frac{\sqrt{3}}{2} \end{bmatrix} \begin{bmatrix} i_{S\alpha}^* \\ i_{S\beta}^* \end{bmatrix} \tag{13.68}$$

where the $\alpha - \beta$ currents are given by

$$\begin{bmatrix} i_{S\alpha}^* \\ i_{S\beta}^* \end{bmatrix} = \begin{bmatrix} \cos\omega t & \sin\omega t \\ -\sin\omega t & \cos\omega t \end{bmatrix} \begin{bmatrix} i_{Sd}^* \\ i_{Sq}^* \end{bmatrix} \tag{13.69}$$

Note that ω is the supply frequency expressed in radians/sec. The unit vectors $\sin\omega t$ and $\cos\omega t$ are obtained from Phase-Locked Loop (PLL) which is locked to the PCC voltage.

Results of the Case Study

The DC voltage regulator is designed as a proportional controller with a gain of 0.6. The AC voltage controller is designed as a PI controller with $K_p = -0.2$ and $K_I = -40$ (Note that a positive error requires i_{Sq}^* to be reduced. This implies that i_{Cq} should be reduced when the error, $(V_t^* - V_t)$ is positive).

For the case of (a) power factor correction with $K_q = 0.0$, the steady state wave forms of the (i) load currents (ii) compensator currents (iii) source currents and (iv) PCC voltages are shown in Fig. 13.9. The PCC voltage

(v_{ta}) and source current (i_{Sa}) are shown in Fig. 13.10 with and without compensation. Note that the source current not only becomes sinusoidal, but also remains in phase with the PCC voltage after compensation. Fig. 13.11 shows the zero sequence component in the source current before and after compensation.

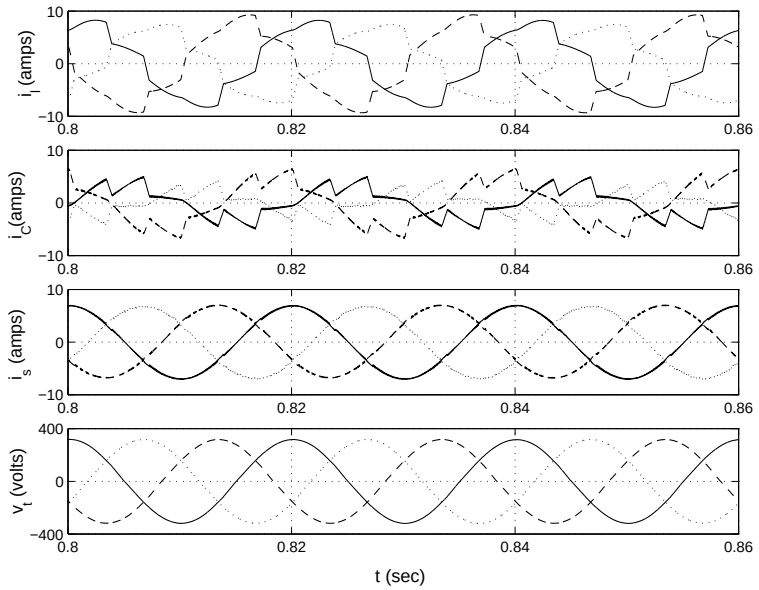

Figure 13.9: Current and PCC voltage waveforms

The Total Harmonic Distortion (THD) in the load current is in the range of 15 to 17% for the three phases. (Note that the load is unbalanced). After compensation, the THD in source currents is reduced to about 2.3%. The THD in voltages reduces from 1.6% to 0.6%.

If AC voltage regulator is included, and $V_t^* = 415$ V, the variation of $|V_t|$ is shown in Fig. 13.12 as the compensator is switched on at $t = 0.2$ s. The settling time is less than 0.1 s. The ripple in the voltage magnitude is negligible.

13.6 Instantaneous Active and Reactive Current Based Extraction of Reference Currents

In this method, the vector of reference source currents is expressed as

$$i_S^* = Gv_t + Bv_t^q \tag{13.70}$$

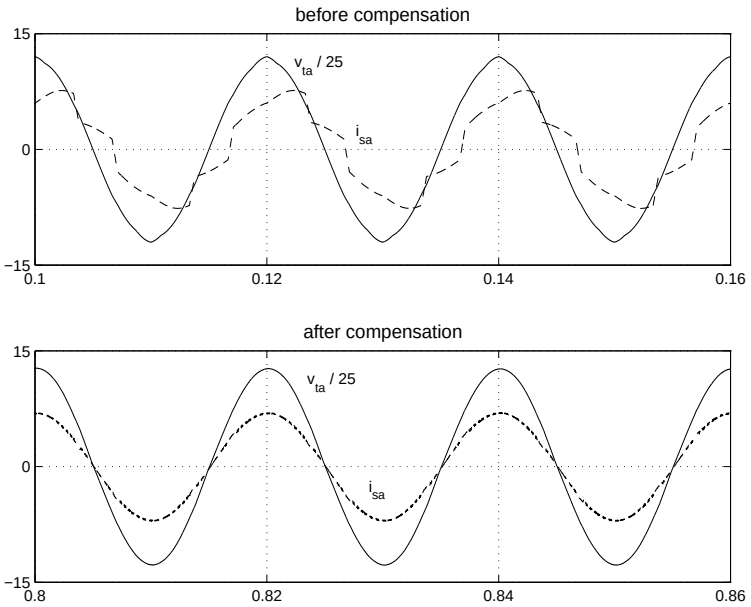

Figure 13.10: PCC voltage and source current

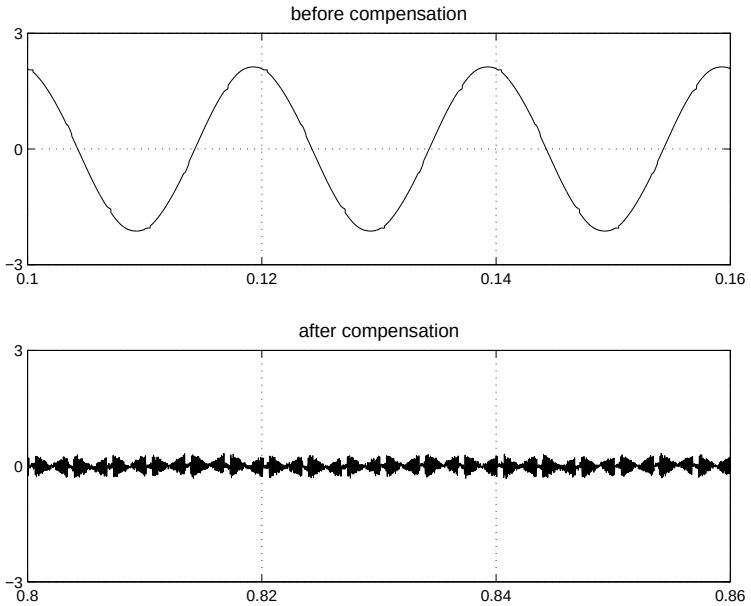

Figure 13.11: Zero sequence component of the source current

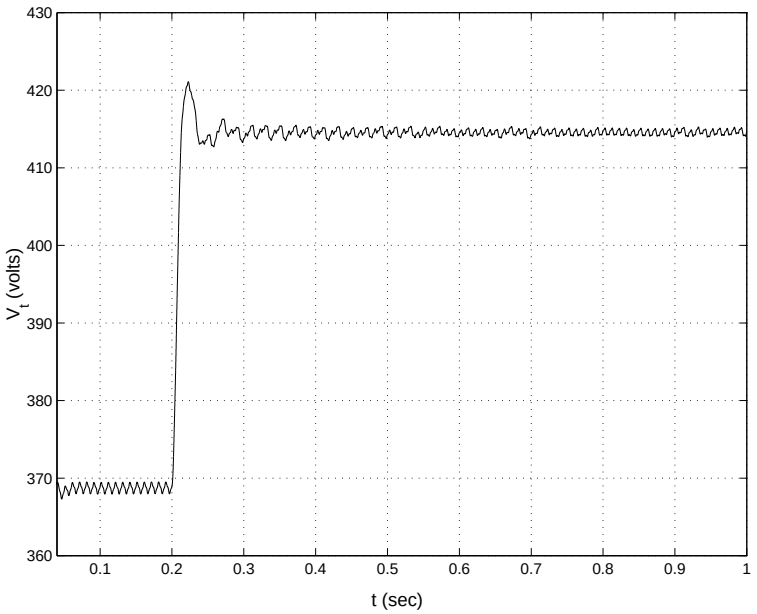

Figure 13.12: PCC voltage (line to line) magnitude

where G and B are defined as

$$G = \frac{P_S^*}{V_\Sigma^2}, \quad B = \frac{Q_S^*}{V_\Sigma^2} \tag{13.71}$$

where P_S^* and Q_S^* are the average power and reactive power (reference values) supplied by the source and are expressed as

$$P_S^* = P_L + \Delta P_S, \quad Q_S^* = r^* P_S^* \tag{13.72}$$

The value of r determines the reactive power to be supplied by the source. ΔP_S is the output of the DC voltage controller. P_L and V_Σ^2 are defined from the following equations.

$$P_L = \frac{1}{T}\int_0^T p_\Sigma(t)dt = \frac{1}{T}\int_0^T (v_t^T i_L)dt \tag{13.73}$$

$$V_\Sigma^2 = \frac{1}{T}\int_0^T (v_{ta}^2 + v_{tb}^2 + v_{tc}^2)dt \tag{13.74}$$

The voltage vector v_t^q is a unit vector that is orthogonal to v_t and thus satisfies

$$v_t^T v_t^q = 0 \tag{13.75}$$

in addition to the constraint

$$\sum_m v_{tm}^q = 0, \quad m = a, b \text{ and } c \tag{13.76}$$

The above equation implies that the zero sequence component of v_t^q is zero. v_t^q that satisfies both Eq. (13.75) and (13.76) is obtained as

$$v_t^q = \frac{1}{\sqrt{3}} \begin{bmatrix} 0 & 1 & -1 \\ -1 & 0 & 1 \\ 1 & -1 & 0 \end{bmatrix} \begin{bmatrix} v_{ta} \\ v_{tb} \\ v_{tc} \end{bmatrix} \tag{13.77}$$

Note that the length of the vector v_t^q is unity.

We can have two options for the choice of the reactive power or the ratio r.

1) Reactive power or power factor control. Here the reference value of r is specified as

$$r^* = \tan \phi_S^* \tag{13.78}$$

For unity power factor control, $r^* = 0$.

2) PCC Voltage control. Here, r^* is obtained as the output of the integral controller used for regulating the PCC voltage. Thus,

$$r^* = \frac{K_I}{s}[(V_t^*)^2 - V_t^2] \tag{13.79}$$

Fig. 13.13 shows the block diagram of the controller for determining the reference current vector (for the source and the compensator). Both cases (a) reactive power control and (b) PCC voltage control are considered.

Results of the Case Study

The results were found to be comparable or even slightly better than that presented in the previous control scheme using SRF. For case (a), the PCC voltage (v_{ta}) and the source current (i_{Sa}) with and without compensation are shown in Fig. 13.14. The compensator is started at $t = 0.2$ s and the variation of the DC voltage (V_{dc}) is shown in Fig. 13.15. It is observed that V_{dc} settles down in about 100 ms (5 cycles). The average steady state value of $V_{dc} = 400.5$ V.

For case (b) with PCC voltage control, the variation of PCC voltage magnitude (with $V_t^* = 415$ V) is shown in Fig. 13.16. (Note that the compensator is started at 0.2 s). The overshoot for this case is less than what was observed for the case with SRF control scheme. The DC voltage also settles down within 0.1 s (see Fig. 13.17).

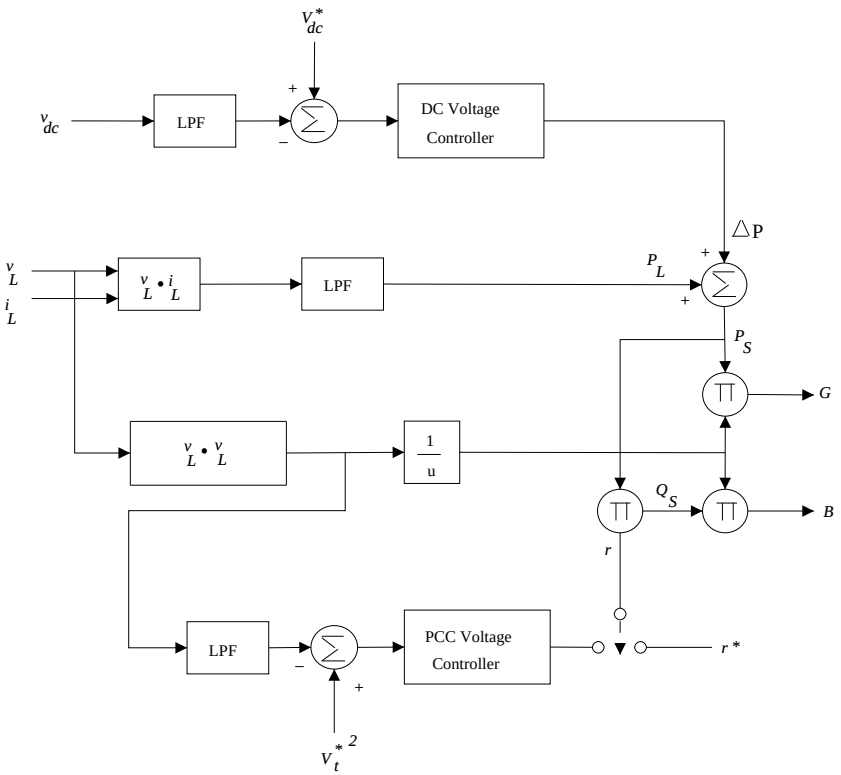

(a) Computation of G and B

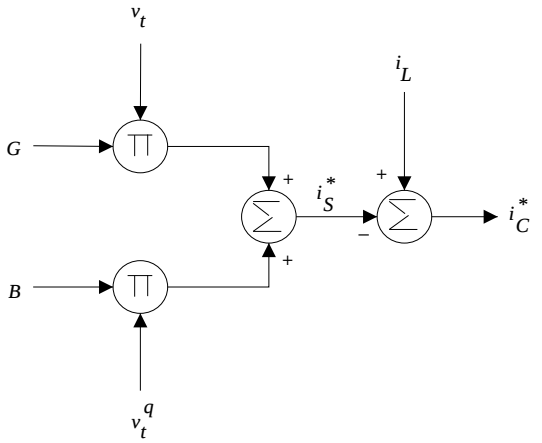

(b) Generation of reference compensator currents

Figure 13.13: Block diagram of the control scheme based on the extraction of i_p and i_q

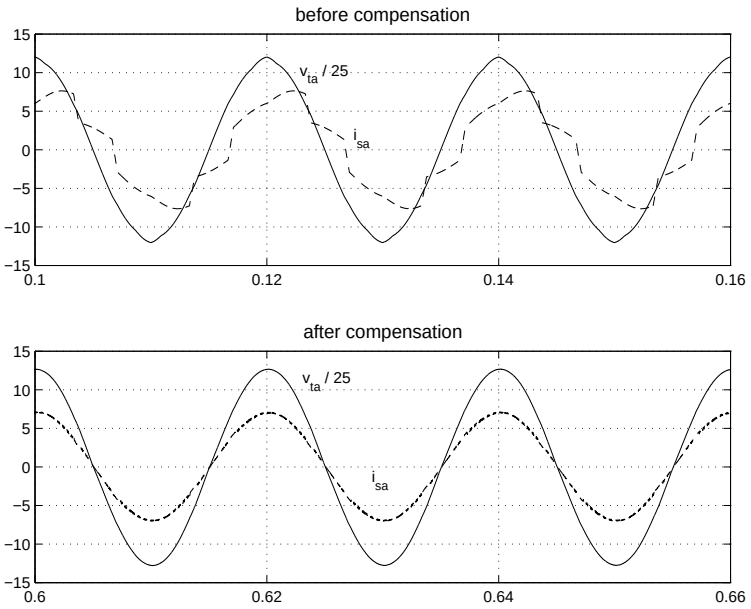

Figure 13.14: PCC voltage and source current

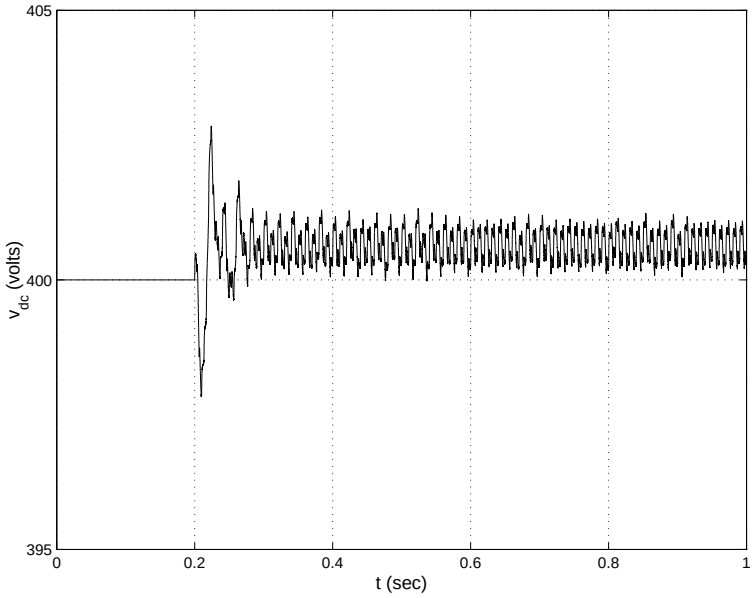

Figure 13.15: DC bus voltage (power factor control)

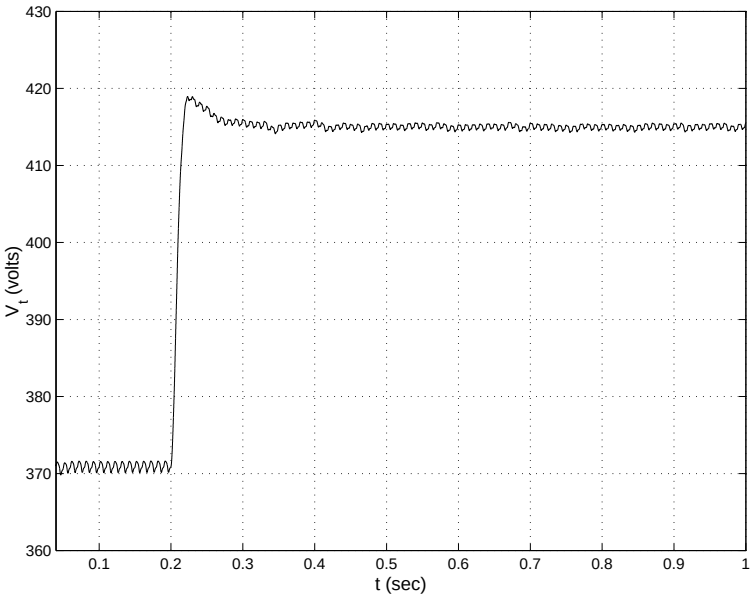

Figure 13.16: PCC voltage (line to line) magnitude

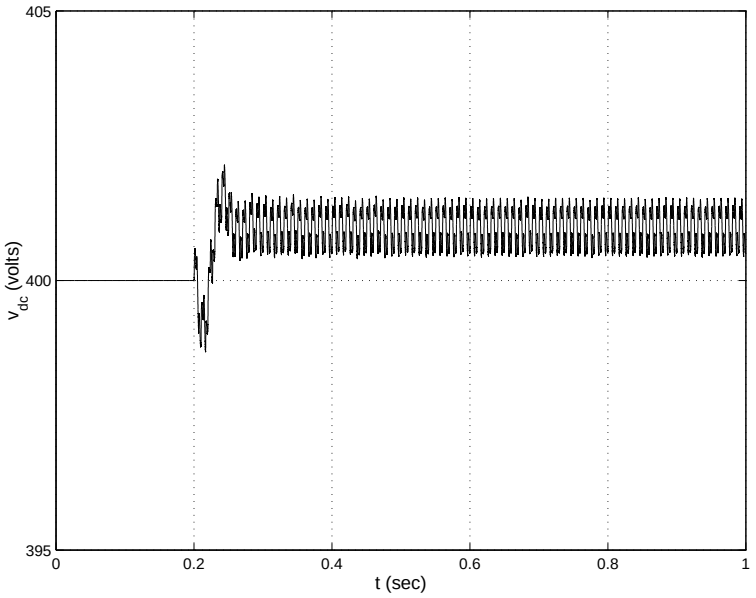

Figure 13.17: DC bus voltage (PCC voltage control)

Discussion

In this control scheme, there is no need for PLL and thus simpler to implement. The average values of power (P_L) and V_Σ^2 are obtained as the outputs of the low pass filters as shown in Fig. 13.13. It is also possible to use moving average filter that computes the average over a period (corresponding to the supply frequency).

The results obtained from both control schemes are excellent. The modulation used is sine PWM using a triangular carrier wave of frequency 5 kHz.

13.7 Application of DSTATCOM for Reactive Power Compensation and Voltage Regulation

Initial application of DSTATCOM (using GTO devices) was primarily for the control of (fundamental frequency) reactive power control and voltage regulation. SVCs have been applied for this purpose earlier. A DSTATCOM has obvious advantages over a SVC as discussed in chapter 6. A major advantage relates to the improved speed of response, capacity for transient overload (up to one second) in addition to the improved performance at reduced voltages.

Reference [2] describes a case study on a ± 12 MVAR STATCOM connected at a 12.5 kV, 150 MW substation of Commonwealth Edison of Chicago, U.S.A. The benefits achieved are

1. Limiting voltage swells caused by capacitor switching
2. Reduction of voltage sags due to common feeder faults
3. Controlling the voltage fluctuations caused by customer load variations. It was found that voltage fluctuations were reduced from 2.5% to 0.2% with DSTATCOM. This reduces voltage flicker substantially.
4. Based on the control algorithm, the frequency of mechanical switching operations (involving load tap changing (LTC) transformers and mechanically switched capacitors) is reduced that is beneficial for maintenance.
5. Increase in the maximum loadability of the system (in particular, increase in the induction motor load that can remain stable through a major disturbance, such as a loss of primary infeed).

The controller of DSTATCOM suggested in [2] has three levels given below

1. Fast voltage regulator
2. Fast current limiter and overload management control
3. Slow reset control

The voltage regulator has a response time of few cycles. The second level of control allows the inherent short-term overload capability of DSTATCOM to be utilized for better performance while protecting the equipment. The third level of control involving slow reset ensures that the DSTATCOM does not remain near limits over an extended period of time. The objective is to ensure that the DSTATCOM remains ready to respond quickly to subsequent disturbances. The reset control acts on the voltage reference (within limits) and works with a delay (of typically 2 minutes). The output of DSTATCOM is ramped back to lie within a specified deadband of $\pm$ 1.2 MVAR, at a rate of 0.5 MVAR per minute. The control is coordinated with existing mechanically switched devices.

The voltage flicker can be reduced by 50% from applying a DSTATCOM in comparison with a SVC [19]. The controller design of a DSTATCOM based on analytical model is presented in [13] and the predictions on the performance are validated by experimental results. In reference [20] a unified control to mitigate voltage sag and flicker is presented, based on Kalman filter.

13.8 Current Control Techniques for PWM Converters

Compensators based on voltage source pulse-width modulated (VS-PWM) converters use a control structure comprising an internal current feedback loop [10]. The basic block diagram of current controlled PWM (CC-PWM) converter is shown in Fig. 13.18. The design of current controller has to consider the following aspects or constraints.

1. Modulation that involves hard switching or soft switching (using RDCL (Resonant DC Link) converter). There are constraints on the switching instants for the latter case. Further, modulation generates high order voltage harmonics located around switching frequency which should be high enough.

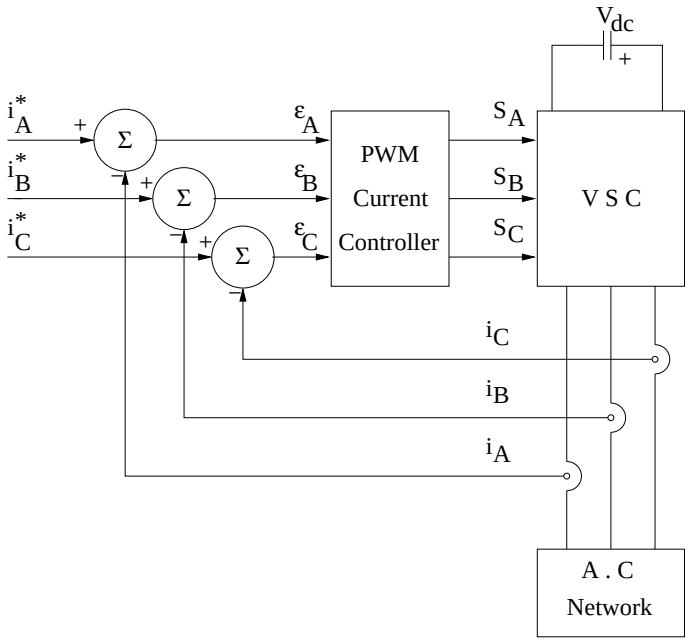

Figure 13.18: Basic block diagram of CC-PWM converter

2. Current ripple and switching frequency. Modulation produces current ripple that depends on the average AC voltage, DC voltage and switching frequency. If switching frequency remains constant, the ripple varies with the AC voltage. On the other hand, for constant ripple magnitude, the modulation frequency has to vary. The power losses put a limitation on the average switching frequency. Filtering requirements may also enforce a constant switching frequency.

3. Phase interference effect: While phase voltage can be controlled independently, phase currents are determined often by all the phase voltages. Thus a phase interference occurs that must be taken into account.

4. DC link voltage limit: A voltage reserve is required to force an AC side current according to its reference value.

The basic requirements of current control are listed below:

1. No phase and amplitude errors over a wide output frequency range.

2. High dynamic response

3. Limited or constant switching frequency to guarantee safe operation of the power semiconductor devices

4. Low harmonic content
5. Good DC link voltage utilization.

A criterion for the evaluation of the performance of the current control is based on the RMS value of the error vector, defined by

$$RMS = \left[\frac{1}{T}\int_0^T (\varepsilon_A^2 + \varepsilon_B^2 + \varepsilon_C^2)dt\right]^{1/2}$$

The current control (CC) techniques can be classified into two main groups, linear and nonlinear controllers [10]. There are four types of linear controllers, namely

(a) Stationary (PI) controller also called the ramp comparison current controller, uses 3 PI controllers to produce voltage commands for a three phase sinusoidal PWM. In this scheme, comparison with the triangular carrier signal generates the control signals (switching functions) S_a, S_b and S_c.

(b) Synchronous vector controller (PI). Here two PI controllers are used to drive the errors in the d-q components (of currents) to zero.

(c) State feedback controller working in stationary ($\alpha\beta$) or synchronously rotating (reference frame) coordinates. The feedback gain matrix is usually based on the pole assignment technique to guarantee sufficient damping.

(d) Predictive and deadbeat controllers: This technique predicts at the beginning of each sampling period, the current error vector on the basis of the present error and the AC side parameters. The voltage vector to be generated by PWM during the next sampling period is determined to minimize the forecast error. The prediction controller that aims at reducing the error to zero is often called a deadbeat controller.

Nonlinear control methods include hysteresis, delta modulation and on-line optimized controllers [10]. For hard switched converters, hysteresis current controllers are simple to implement. The switching signals, S_a, S_b and S_c are produced directly when the error exceeds an assigned tolerance band. The advantages of hysteresis CC are simplicity, robustness, no tracking errors and good dynamics limited only by the switching speed. However, the converter switching frequency is not constant and the operation can be affected by the limit cycle which may complicate the protection of the converter.

13.9 Application of Composite Compensation

As installation of DSTATCOMs is expensive a composite compensation scheme involving not only reactive power compensation/voltage regulation (at fundamental frequency) but also active filtering becomes important [12]. High power IGBT devices that can operate up to 2 kHz switching frequency are already used in VSC based HVDC converters (rated below 300 MW). It is anticipated that faster devices will be available at reasonable costs to apply composite shunt compensation in distribution systems.

References and Bibliography

1. L. Gyugyi, R.A. Otto and T.H. Putman, "Principles and application of static thyristor-controlled shunt compensators", IEEE Trans., PAS. v. 97, Sept./Oct. 1978, pp. 1935-1945.

2. J.J. Paserba et al, "Coordination of a distribution level continuously controlled compensation device with existing substation equipment for long term VAR management", IEEE Trans., Power Delivery, v. 9, n.2, 1994, 1034-1040.

3. M. Aredes, J. Hafner and K. Heumann, "Three-phase four-wire shunt active filter control strategies", IEEE Trans., Power Electronics, v. 12, n.2, 1997, pp. 311-318.

4. S. Bhattacharya, D.M. Divan and B. Banerjee, "Synchronous frame harmonic isolator using active series filter", Proc. 4th Euro Conf. on Power Electronics and Appl., Florence, Italy, 1991, v. 3, pp. 30-35.

5. S. Bhattacharya and D.M. Divan, "Active filter solutions for utility interface of industrial loads", Proc. IEEE Int. Conf. Power Electronics, Drives and Energy Systems, New Delhi, 1996, pp. 1078-1084

6. P.T. Cheng, S. Bhattacharya and D.M. Divan, "Application of dominant harmonic active filter systems with 12-pulse nonlinear loads", IEEE Trans., Power Delivery, v. 14, n. 2, 1999, pp. 642-647.

7. J. Hafner, M. Aredes and K. Heumann, "A shunt active power filter applied to high voltage distribution lines", IEEE Trans., Power Delivery, v. 12, n. 1, 1997, pp. 266-272.

8. J.C. Montano and P. Salmeron, "Instantaneous and full compensation in three-phase systems", IEEE Trans., Power Delivery, v. 13, n.4, 1998, pp. 1342-1347.

9. M.K. Mishra, A. Joshi and A. Ghosh, "A new compensation algorithm for balanced and unbalanced distribution systems using generalized instantaneous reactive power theory", Electric Power Systems Research, 60, 2001, pp. 29-37.

10. M.P. Kazmierkowski and L. Malesani, "Current control techniques for three-phase voltage-source PWM converters: A survey", IEEE Trans., Industrial Electronics, v. 45, n. 5, 1998, pp. 691-703.

11. P.S. Sen Sarma, K.R. Padiyar and V. Ramanarayanan, "A STATCOM for composite power line conditioning", IEEE Int. Conf. on Industrial Technology, v. 1, 2000, pp. 542-547.

12. A.K.S.N. Polisetty and K.R. Padiyar, "A composite compensation scheme for distribution STATCOM", National Power Electronics Conference, December 2005, I.I.T. Kharaghpur.

13. P.S. Sen Sarma, K.R. Padiyar and V. Ramanarayanan, "Analysis and performance evaluation of a distribution STATCOM for compensating voltage fluctuations", IEEE Trans., Power Delivery, v. 16, n. 2, 2001, pp. 259-264.

14. C. Gueth, P. Enstedt, A. Rey and R.W. Menzies, "Individual phase control of a static compensator for load compensation and voltage balancing and regulation", IEEE Trans., Power Systems, v. 2, n. 4, 1987, pp. 898-905.

15. H. Akagi et al, "Instantaneous reactive power compensators comprising switching devices without energy storage components", IEEE Trans., Industry Appl., v. IA-20, 1984, pp. 625-631.

16. K.R. Padiyar, **Power System Dynamics - Stability and Control**, Second Edition, B.S. Publications, Hyderabad, 2002.

17. M. Depenbrock, V. Staudt and H. Wrede, "A theoretical investigation of original and modified instantaneous power theory applied to four-wire systems", IEEE Trans., Industry Appl., v. 39, n.4, 2003, pp. 1160-1167.

18. H. Kim et al, "Instantaneous power compensation in three-phase systems by using p-q-r theory", IEEE Trans., Power Electronics, v. 17, n. 5, 2002, pp. 701-710.

19. C. Poumarede et al, "Present and future flicker mitigation techniques", CIGRE Regional Meeting on Power Quality-Assessment of Impact, September, 1997, New Delhi, India.

20. A Elnady and M.M.A. Salama, "Unified approach for mitigating voltage sag and voltage flicker using DSTATCOM", IEEE Trans., Power Delivery, v. 20, n.2, 2005, pp. 992-1000.

This page intentionally left blank

Chapter 14

Dynamic Voltage Restorer and Unified Power Quality Conditioner

14.1 Introduction

In the previous chapter, the load compensation techniques using shunt compensators were considered. The major objectives are to increase the capacity utilization of distribution feeders (by minimizing the rms values of the line currents for a specified power demand), reduce the losses and improve power quality at the load bus. The major assumption was to neglect the variations in the source voltages. This essentially implies that the dynamics of the source voltage is much slower than the load dynamics.

When the fast variations in the source voltage cannot be ignored, these can affect the performance of critical loads such as (a) semiconductor fabrication plants (b) paper mills (c) food processing plants and (d) automotive assembly plants. The most common disturbances in the source voltages are the voltage sags or swells that can be due to (i) disturbances arising in the transmission system, (ii) adjacent feeder faults and (iii) fuse or breaker operation. Voltage sags of even 10% lasting for 5-10 cycles can result in costly damage in critical loads. The voltage sags can arise due to symmetrical or unsymmetrical faults. In the latter case, negative and zero sequence components are also present.

Uncompensated nonlinear loads in the distribution system can cause harmonic components in the supply voltages. To mitigate the problems caused by poor quality of power supply, series connected compensators are used. These are called as Dynamic Voltage Restorer (DVR) in the literature as their primary application is to compensate for voltage sags and swells. Their configuration is similar to that of SSSC, discussed in chapter 7. However, the control techniques are different. Also, a DVR is expected to respond fast (less than 1/4 cycle) and thus employs PWM converters using IGBT or IGCT devices.

The first DVR entered commercial service on the Duke Power System in U.S.A. in August 1996. It has a rating of 2 MVA with 660 kJ of energy

storage and is capable of compensating 50% voltage sag for a period of 0.5 second (30 cycles). It was installed to protect a highly automated yarn manufacturing and rug weaving facility. Since then, several DVRs have been installed to protect microprocessor fabrication plants, paper mills etc. Typically, DVRs are made of modular design with a module rating of 2 MVA or 5 MVA. They have been installed in substations of voltage rating from 11 kV to 69 kV.

A DVR has to supply energy to the load during the voltage sags. If a DVR has to supply active power over longer periods, it is convenient to provide a shunt converter that is connected to the DVR on the DC side. As a matter of fact one could envisage a combination of DSTATCOM and DVR connected on the DC side to compensate for both load and supply voltage variations. The combined compensator is termed as Unified Power Quality Conditioner (UPQC) which has a configuration similar to UPFC discussed in chapter 8. However, the control objectives are different.

In this chapter, both series connected DVR and UPQC are described. Their operation and control methods are explained. The performance of a DVR and a UPQC are illustrated with the help of case studies.

14.2 Dynamic Voltage Restoration

In this section, we discuss the application of DVR for fundamental frequency voltage (magnitude) restoration. The configuration of a DVR is shown in Fig. 14.1. The voltage source converter is typically one or more converters connected in series to provide the required voltage rating. The DVR can inject a (fundamental frequency) voltage in each phase of required magnitude and phase. The DVR has two operating modes

1. Standby (also termed as short circuit operation (SCO) mode) where the voltage injected has zero magnitude.
2. Boost (when the DVR injects a required voltage of appropriate magnitude and phase to restore the prefault load bus voltage).

The power circuit of DVR shown in Fig. 14.1 has four components listed below.

1. Voltage Source Converter (VSC)

This could be a 3 phase - 3 wire VSC or 3 phase - 4 wire VSC. The latter permits the injection of zero-sequence voltages. Either a conventional two level converter (Graetz bridge) or a three level converter is used.

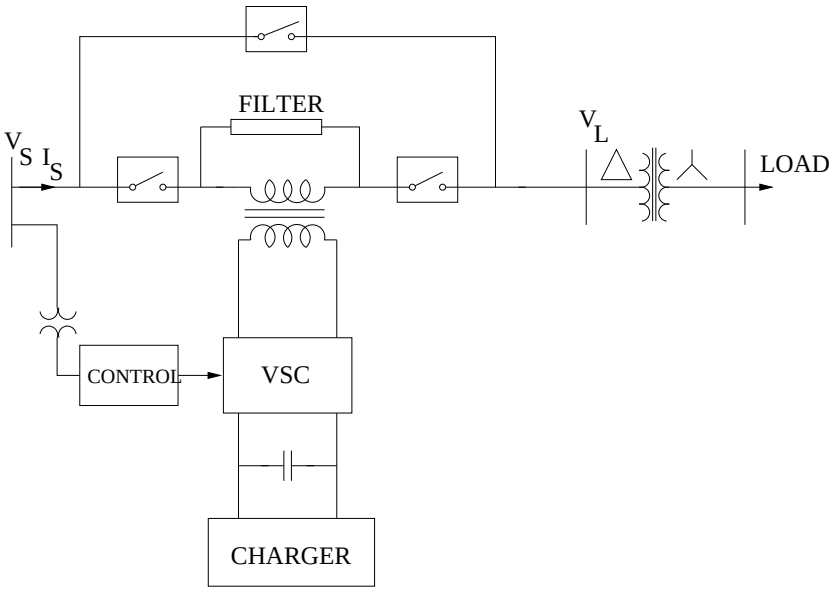

Figure 14.1: Dynamic Voltage Restorer

2. Boost or Injection Transformers

Three single phase transformers are connected in series with the distribution feeder to couple the VSC (at the lower voltage level) to the higher distribution voltage level. The three single transformers can be connected with star/open star winding or delta/open star winding. The latter does not permit the injection of the zero sequence voltage. The choice of the injection transformer winding depends on the connections of the step down transformer that feeds the load. If a $\Delta - Y$ connected transformer (as shown in Fig. 14.1) is used, there is no need to compensate the zero sequence voltages. However if $Y - Y$ connection with neutral grounding is used, the zero sequence voltage may have to be compensated.

It is essential to avoid the saturation in the injection transformers.

3. Passive Filters

The passive filters can be placed either on the high voltage side or the converter side of the boost transformers. The advantages of the converter side filters are (a) the components are rated at lower voltage and (b) higher order harmonic currents (due to the VSC) do not flow through the transformer windings. The disadvantages are that the filter inductor causes voltage drop and phase (angle) shift in the (fundamental component of) voltage injected. This can affect the control scheme of DVR. The location of the filter on

the high voltage side overcomes the drawbacks (the leakage reactance of the transformer can be used as a filter inductor), but results in higher ratings of the transformers as high frequency currents can flow through the windings.

4. Energy Storage

This is required to provide active power to the load during deep voltage sags. Lead-acid batteries, flywheel or SMES can be used for energy storage.

It is also possible to provide the required power on the DC side of the VSC by an auxiliary bridge converter that is fed from an auxiliary AC supply [5].

Control Strategy [5]

There are three basic control strategies as follows.

1. Pre-Sag Compensation

The supply voltage is continuously tracked and the load voltage is compensated to the pre-sag condition. This method results in (nearly) undisturbed load voltage, but generally requires higher rating of the DVR.

Before a sag occur, $V_S = V_L = V_o$. The voltage sag results in drop in the magnitude of the supply voltage to V_{S1}. The phase angle of the supply also may shift (see Fig. 14.2). The DVR injects a voltage V_{C1} such that the load voltage ($V_L = V_{S1} + V_{C1}$) remains at V_o (both in magnitude and phase). It is claimed that some loads are sensitive to phase jumps and it is necessary to compensate for both the phase jumps and the voltage sags.

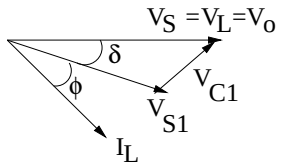

Figure 14.2: Phasor diagram showing injected voltage by DVR

2. In-phase Compensation

The voltage injected by the DVR is always in phase with the supply voltage regardless of the load current and the pre-sag voltage (V_o). This control strategy results in the minimum value of the injected voltage (magnitude). However, the phase of the load voltage is disturbed. For loads which are

not sensitive to the phase jumps, this control strategy results in optimum utilization of the voltage rating of the DVR.

The power requirements for the DVR are not zero for this strategy.

3. Minimum Energy Compensation

Neglecting losses, the power requirements of the DVR are zero if the injected voltage (V_C) is in quadrature with the load current. To raise the voltage at the load bus, the voltage injected by the DVR is capacitive and V_L leads V_{S1} (see Fig. 14.3). Fig. 14.3 also shows the in-phase compensation for comparison. It is to be noted that the current phasor is determined by the load bus voltage phasor and the power factor of the load.

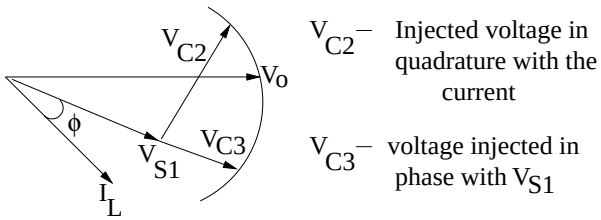

Figure 14.3: Alternate DVR control strategy

Implementation of the minimum energy compensation requires the measurement of the load current phasor in addition to the supply voltage.

When V_C is in quadrature with the load current, DVR supplies only reactive power. However, full load voltage compensation is not possible unless the supply voltage is above a minimum value that depends on the load power factor.

When the magnitude of V_C is not constrained, the minimum value of V_S that still allows full compensation is

$$V_S^{\min} = V_o \cos\phi \tag{14.1}$$

where ϕ is the power factor angle and V_o is the required magnitude of the load bus voltage.

If the magnitude of the injected voltage is limited ($V_C^{\max}$), the minimum supply voltage that allows full compensation is given by

$$V_S^{\min} = [V_o^2 - 2V_oV_C^{\max}\sin\phi + (V_C^{\max})^2]^{1/2} \tag{14.2}$$

The expressions (14.1) and (14.2) follow from the phasor diagrams shown in Fig. 14.4. Note that at the minimum source voltage, the current is in phase with V_S for the case (a).

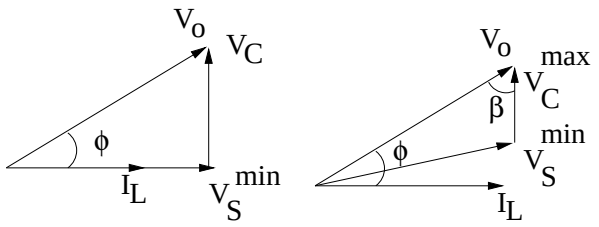

(a) (b)

V_C unlimited V_C is limited

Figure 14.4: Phasor diagrams determining V_S^{min} with quadrature injection

If the source voltage magnitude is less than $V_S^{\min}$, the DVR has to supply non-zero energy to provide full compensation. But it is possible to devise a strategy that results in minimum energy requirement for full compensation [4].

Control and Protection

The control and protection of a DVR designed to compensate voltage sags must consider the following functional requirements.

1. When the supply voltage is normal, the DVR operates in a standby mode with zero voltage injection. However if the energy storage device (say batteries) is to be charged, then the DVR can operate in a self-charging control mode.
2. When a voltage sag/swell occurs, the DVR needs to inject three single phase voltages in synchronism with the supply in a very short time. Each phase of the injected voltage can be controlled independently in magnitude and phase. However, zero sequence voltage can be eliminated in situations where it has no effect.

   The DVR draws active power from the energy source and supplies this along with the reactive power (required) to the load.
3. If there is a fault on the downstream of the DVR, the converter is bypassed temporarily using thyristor switches to protect the DVR against overcurrents. The threshold is determined by the current ratings of the DVR.

The controller is generally an open loop type as shown in Fig. 14.5. The three phase supply voltages are measured and transformed into d-q components through $\alpha - \beta$ components. The transformation to d-q components

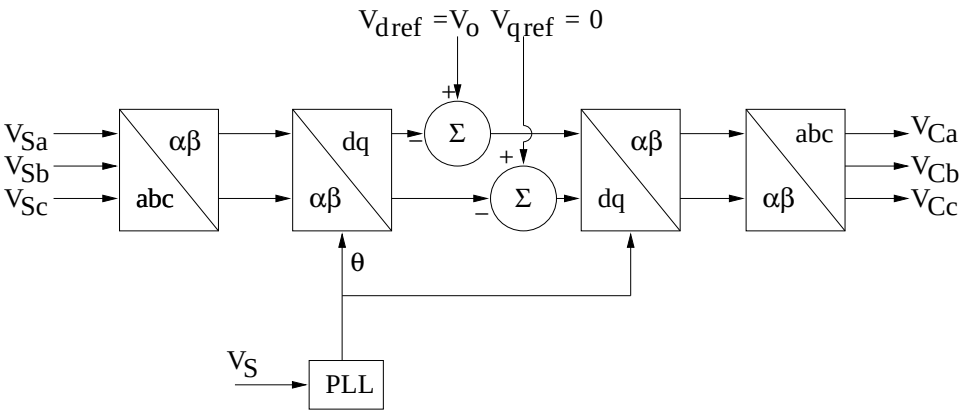

Figure 14.5: Open loop controller for DVR

requires a PLL with inputs from the supply voltage. The d-q components of the supply voltage are subtracted from the reference values of the (desired) load bus voltage d-q components to give the required values of the injected voltage (d-q components). These are transformed to the required three phase injected voltages.

The overall design of DVR must consider the following parameters:

1. Ratings of the load and power factor
2. Voltage rating of the distribution line
3. Maximum single phase sag (in percentage)
4. Maximum three phase sag (in percentage)
5. Duration of the voltage sag (in milliseconds)
6. The voltage time area (this is an indication of the energy requirements)
7. Recovery time for the DC link voltage to 100%
8. Overcurrent capability without going into bypass mode.

Typically, a DVR may be designed to protect a sensitive load against 35% of three phase voltage sag or 50% of the single phase sag. The duration of the sag could be 200 ms. The DVR can compensate higher voltage sags lasting for shorter durations or allow longer durations (up to 500 ms) for smaller voltage sags. The response time could be as small as 1 ms.

14.3 Series Active Filtering

The series connected power (quality) conditioner can be designed as an active filter to provide harmonic isolation between the source and the load. The

harmonics in the source voltage can be compensated by series connected VSC and the load bus voltage will contain only fundamental frequency balanced voltages. If the load has linear characteristics, then the line currents will be balanced (contain only positive sequence components) and sinusoidal. The series converter can also compensate for the unbalance in the supply without having to supply active power in steady state. Note that, here, we are referring to steady state compensation against source harmonics and unbalance. In the previous section, we dealt with transient compensation of the voltage sags.

Control Strategies for Active Filtering

Fig. 14.6 shows a single phase equivalent circuit for harmonics, representing a distribution feeder supplying a load. The load is assumed to be nonlinear with I_{Lh} as the harmonic current. Z_{Fh} represents the harmonic impedance of the shunt passive filter. V_{Th} and Z_{Th} represent Thevenin (harmonic) voltage and impedance on the supply side. V_{Ch} is the harmonic voltage injected in series.

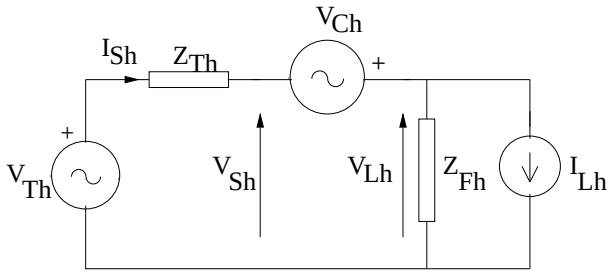

Figure 14.6: Harmonic equivalent circuit for series active filtering

Reference [7] suggests three control methods for the series active filter. These are,

1. Current detection method. Here V_{Ch} is controlled according to the equation
$$V_{Ch} = -KI_{Sh} \tag{14.3}$$

2. Voltage detection method. Here V_{Ch} is controlled as
$$V_{Ch} = -V_{Sh} \tag{14.4}$$

3. Combined method when V_{Ch} is obtained as
$$V_{Ch} = -KI_{Sh} - V_{Sh} \tag{14.5}$$

K is a real number that represents a proportional gain of the controller.

The equivalent circuits of the system taking into account the three control strategies listed above, are shown in Fig. 14.7. From these circuits we can easily obtain the expressions for the load voltage harmonic (V_{Lh}) and the source current harmonic (I_{Sh}). These are given below.

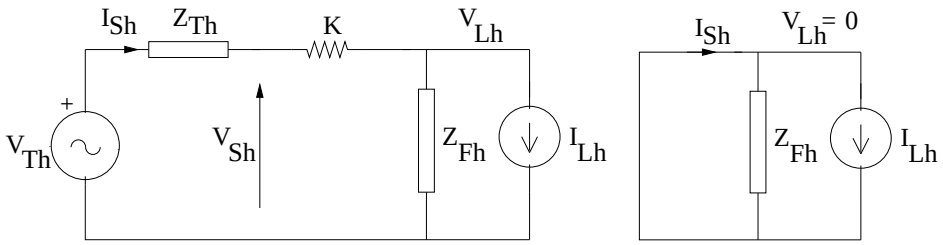

(a) Current detecting method

(b) Voltage detecting method

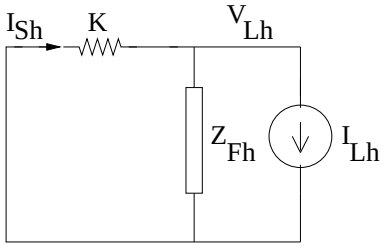

(c) Combined method

Figure 14.7: Equivalent circuits for three control methods

1. Current detection method

$$V_{Lh} = \frac{Z_{Fh}}{Z_{Th} + Z_{Fh} + K} V_{Th} - \frac{(Z_{Th} + K) Z_{Fh}}{Z_{Th} + Z_{Fh} + K} I_{Lh} \tag{14.6}$$

$$I_{Sh} = \frac{1}{Z_{Th} + Z_{Fh} + K} V_{Th} + \frac{Z_{Fh}}{Z_{Th} + Z_{Fh} + K} I_{Lh} \tag{14.7}$$

2. Voltage detection method

$$V_{Lh} = 0 \tag{14.8}$$

$$I_{Sh} = I_{Lh} \tag{14.9}$$

3. Combined method

$$V_{Lh} = \frac{-KZ_{Fh}}{Z_{Fh}+K} I_{Lh} \tag{14.10}$$

$$I_{Sh} = \frac{Z_{Fh}}{Z_{Fh}+K} I_{Lh} \tag{14.11}$$

It is to be noted that the subscript 'h' represents not only a harmonic (of order h) but also any frequency component including low frequency components corresponding to voltage flicker.

In method 1, both V_{Lh} and I_{Sh} are minimized if $K \gg |Z_{Th} + Z_{Fh}|$. However, for low frequencies, it is difficult to satisfy this condition as the filter exhibits a high capacitive impedance at fundamental or lower frequency. Thus, while the source current is unaffected by the harmonic currents in the load, the load bus voltage is affected by the low frequency components in the source voltage (such as voltage flicker).

In method 2, the load voltage remains sinusoidal, but the source current harmonics are not attenuated. Actually, the passive filter in this case, fails to filter the load current harmonics as the source appears as a short circuit.

The combined method eliminates the disadvantages of the first two methods. Not only the source voltage disturbances have no effect on the load bus voltage, the source current harmonics are eliminated if $K \gg |Z_{Fh}|$. This is easy to arrange for harmonic frequencies of $5f_0$ and above, where f_0 is the fundamental (supply) frequency.

Remarks

1. If the source currents are balanced and sinusoidal, the series active filter that compensates for harmonic voltages (from the source side) does not have to supply or draw active power in steady state if losses in the converter are neglected.

   Similar comments also apply if the series active filter has to compensate for the negative sequence voltages (at fundamental frequency). However, the converter draws an oscillating power of frequency $2f_0$. If the DC capacitor is finite, this results in a voltage ripple across the DC capacitor.

2. If the series active filter has to compensate for the zero sequence voltages, the instantaneous power exchanged by the converter remains zero (as the zero sequence current in the line is zero).

3. Only voltage variations at the fundamental frequency caused by flicker requires a variable power exchange by the converter which can cause large excursions in the capacitor voltage as the frequency of the disturbances is variable and low. Hence, the compensation of low frequency flicker in the source voltage requires an energy source for satisfactory operation of the series active filter.

4. Note that, in the absence of standardized terminology, we can label the series active filter also as a DVR or series power quality conditioner (SPQC) that compensates not only for the harmonic voltages but also for the unbalance and flicker in the source voltages.

14.4 A Case Study on DVR

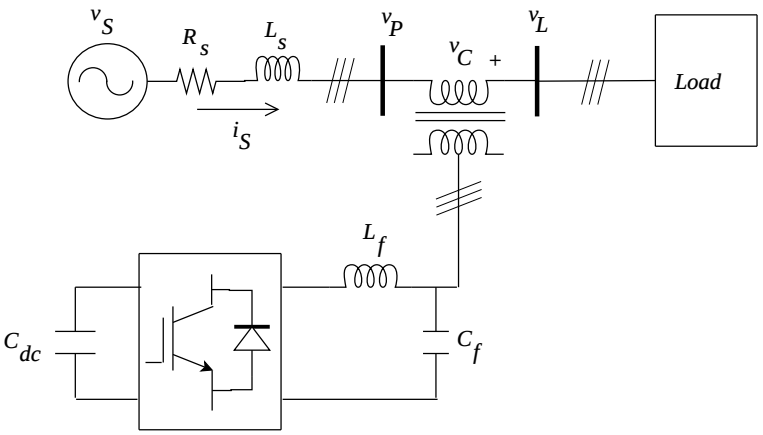

Figure 14.8: System diagram

A DVR is connected in series with the linear load to compensate for the harmonics and unbalance in the source voltages and improve the power factor on the source side (at PCC). The system diagram is shown in Fig. 14.8 which represents a 3 phase 50 Hz, 415 V distribution system. The source inductance is 40 mH and $R_s = 1.57$ ohms. A Y connected balanced R-L load is considered with $R = 50$ ohms, $L = 200$ mH. The harmonic distortion in the source voltage is simulated by adding 20% of the 5th harmonic and 14% of the 7th harmonic. The unbalance in the source voltage is simulated by adding 10% negative sequence and 10% of the zero sequence voltage to the positive sequence (fundamental frequency voltage).

Control Scheme

The major objective of the control strategy is to ensure that the load bus voltages remain balanced and sinusoidal (positive sequence). Since the load is assumed to be balanced and linear, the load currents will also remain balanced (positive sequence) and sinusoidal. An additional objective is to ensure that the source current remains in phase with the fundamental frequency component of the PCC voltage. This requires that the reactive power of the load is met by the DVR. It is also possible to arrange that DVR supplies a specified fraction of the reactive power required by the load.

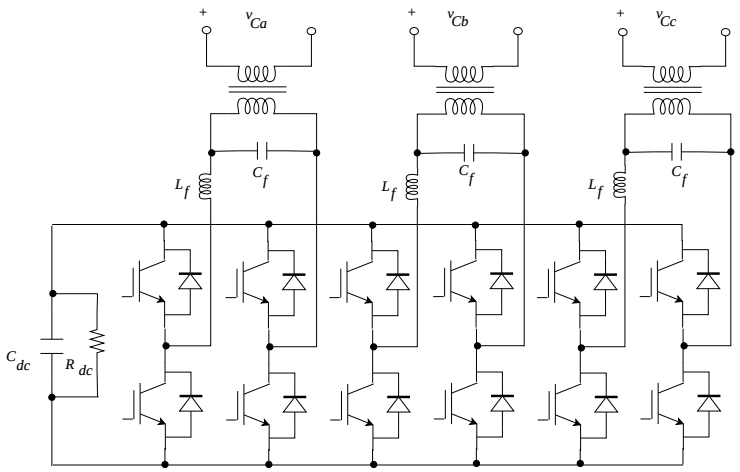

Figure 14.9: Configuration of DVR

The DVR configuration chosen is shown in Fig. 14.9. Here, three single phase full bridge converters are connected to a common DC bus. The sine PWM technique is used to control the DVR. The DC bus voltage is held by the capacitor C_{dc}. Since no energy source is connected, the net real power exchanged by the DVR is zero in steady state, if the losses are neglected. However, to stabilize the operating point, a DC bus voltage control loop is necessary.

The phasor diagram (see Fig. 14.10) shows the current phasor I_s in phase with the voltage phasor V_P (PCC voltage). The source and the load bus voltage phasors are also shown here. ϕ is the power factor angle of the load. The voltage injected by the DVR (V_C) ensures that the current I_S is in phase with V_P.

From the phasor diagram, the d-q components of the load bus voltage are given by

$$V_{Ld} = V_P + V_{Cd} \tag{14.12}$$

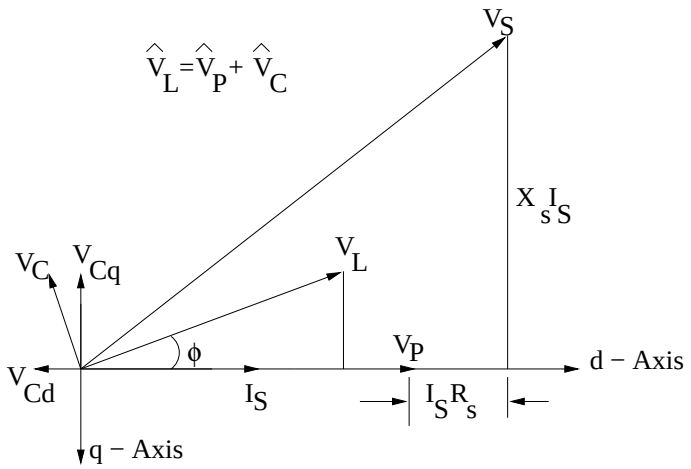

Figure 14.10: Phasor diagram for the system

$$V_{Lq} \quad = \quad -V_{Ld} \tan \phi \tag{14.13}$$

The Synchronous Reference Frame (SRF) approach is used to generate the reference voltages for the DVR.

Fig. 14.11 shows the control scheme using SRF. The PCC voltage V_{Pa}, V_{Pb} and V_{Pc} are transformed into d-q components using the following equations.

$$\begin{bmatrix} V_{P\alpha} \\ V_{P\beta} \end{bmatrix} = \sqrt{\frac{2}{3}} \begin{bmatrix} 1 & -\frac{1}{2} & -\frac{1}{2} \\ 0 & -\frac{\sqrt{3}}{2} & \frac{\sqrt{3}}{2} \end{bmatrix} \begin{bmatrix} V_{Pa} \\ V_{Pb} \\ V_{Pc} \end{bmatrix} \tag{14.14}$$

$$\begin{bmatrix} V_{Pd} \\ V_{Pq} \end{bmatrix} = \begin{bmatrix} \cos \omega_0 t & -\sin \omega_0 t \\ \sin \omega_0 t & \cos \omega_0 t \end{bmatrix} \begin{bmatrix} V_{P\alpha} \\ V_{P\beta} \end{bmatrix} \tag{14.15}$$

where ω_0 is the operating system frequency. In the synchronously rotating reference frame, the positive sequence, fundamental frequency components are transformed into DC quantities. The negative sequence components and harmonic components (irrespective of the sequence) are transformed into oscillating quantities of frequency (f_{dq}) given by

$$f_{dq} = f_{abc} \mp 1 \tag{14.16}$$

where f_{abc} is the frequency of the positive or negative sequence components in the phase coordinates. The sign associated with the second term in the R.H.S. of Eq. (14.16) is negative for positive sequence components and positive for negative sequence components. Note that zero sequence components in the phase coordinates do not contribute to d-q components.

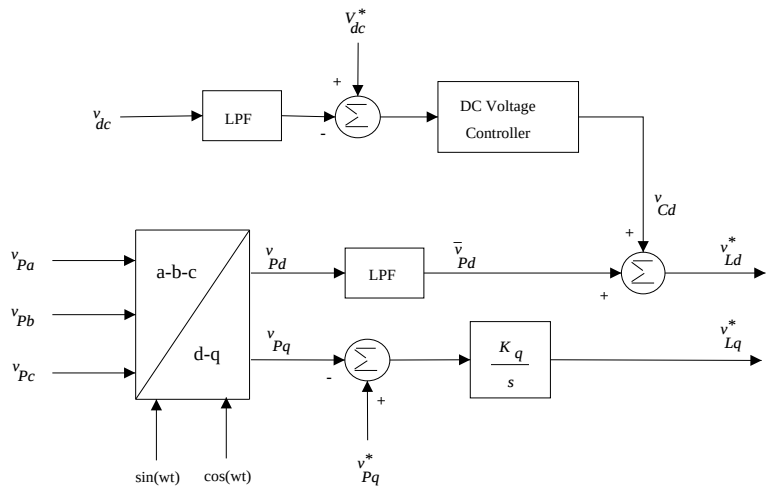

(a) Computation of reference load voltages (d and q components)

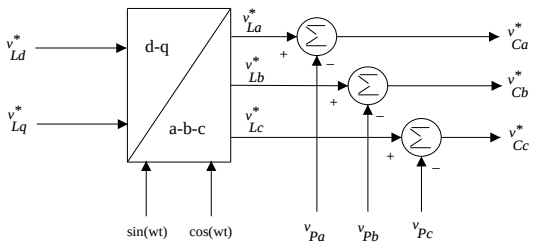

(b) Generation of reference compensator voltages

Figure 14.11: Block diagram of the DVR controller

The synchronously rotating reference frame is synchronized with the source current (I_S) using a PLL. Therefore, the components V_{Pd} and V_{Pq} are the active and reactive components of the PCC voltage.

The DC components in V_{Pd} and V_{Pq} are extracted by using a low pass filter. Thus,

$$\begin{bmatrix} \bar{V}_{Pd} \\ \bar{V}_{Pq} \end{bmatrix} = G(s) \begin{bmatrix} V_{Pd} \\ V_{Pq} \end{bmatrix} \tag{14.17}$$

where $\bar{V}_{Pd}$ and $\bar{V}_{Pq}$ are the DC components. From Eq. (14.12) we derive the reference for the active component of the load voltage (V^*_{Ld}) as

$$V^*_{Ld} = \bar{V}_{Pd} + V_{Cd} \tag{14.18}$$

where V_{Cd} is obtained as the output of the DC voltage controller (with a proportional gain K_p). A second order Butterworth low pass filter is used in

the feedback path of the DC voltage controller to filter out high frequency ripple in the DC voltage signal.

In steady state, $V_{Pq} = 0$ and $V_{Lq} = -V_{Ld} \tan\phi$. These two conditions can be met by arranging

$$V_{Lq}^* = \frac{K_q}{s} \cdot V_{Pq} \tag{14.19}$$

K_q is chosen to optimize the controller response.

From the reference values of V_{Ld}^* and V_{Lq}^* we can obtain the desired load voltages in phase coordinates from the following equations.

$$\begin{bmatrix} V_{L\alpha}^* \\ V_{L\beta}^* \end{bmatrix} = \begin{bmatrix} \cos\omega_0 t & \sin\omega_0 t \\ -\sin\omega_0 t & \cos\omega_0 t \end{bmatrix} \begin{bmatrix} V_{Ld}^* \\ V_{Lq}^* \end{bmatrix} \tag{14.20}$$

$$\begin{bmatrix} V_{La}^* \\ V_{Lb}^* \\ V_{Lc}^* \end{bmatrix} = \sqrt{\frac{2}{3}} \begin{bmatrix} 1 & 0 \\ -\frac{1}{2} & -\frac{\sqrt{3}}{2} \\ -\frac{1}{2} & \frac{\sqrt{3}}{2} \end{bmatrix} \begin{bmatrix} V_{L\alpha}^* \\ V_{L\beta}^* \end{bmatrix} \tag{14.21}$$

Finally, the reference voltages for the DVR are given by

$$\begin{aligned} V_{Ca}^* &= V_{La}^* - V_{Pa} \\ V_{Cb}^* &= V_{Lb}^* - V_{Pb} \\ V_{Cc}^* &= V_{Lc}^* - V_{Pc} \end{aligned} \tag{14.22}$$

Digital Simulation and Results

The DVR parameters are chosen as,

$C_{dc} = 5000\ \mu$F, $R_{dc} = 6000\ \Omega$, $V_{dc} = 400$ V

$L_f = 9.6$ mH, $C_f = 4.2\ \mu$F, $K_p = -40$, $K_q = 7$

The carrier frequency is assumed to be 5 kHz. The cut-off frequency for both low pass filters is chosen as 30 Hz. The simulation is performed using MATLAB/SIMULINK for the system shown in Fig. 14.8.

Fig. 14.12 shows the waveforms of v_L, v_C and i_S before and after the DVR is switched on at $t = 0.2$ s. It is observed that the load voltages and consequently the source currents become balanced and sinusoidal after DVR is switched on. Fig. 14.12 also shows the DC bus voltage (V_{dc}). The DC voltage control loop stabilizes within 5 cycles and the average steady state value of V_{dc} is 400.2 V.

The computation of the harmonic voltages in load bus voltages showed that both 5th and 7th harmonics are reduced below 0.5% after the DVR is switched on.

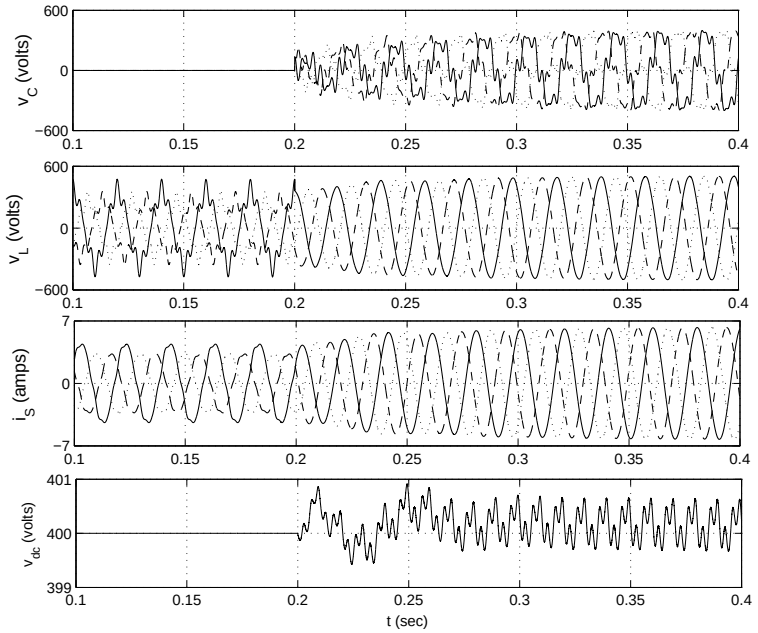

Figure 14.12: Voltage and current waveforms

The fundamental frequency component of the PCC voltage V_{Pa1} and the source current i_{sa} are shown in Fig. 14.13. It is observed that V_{Pa1} and i_{Sa} remain in phase after the DVR is switched on. Fig. 14.14 shows the zero sequence component of the load bus voltage in phase a before and after the DVR is connected.

The results from the system simulation demonstrate the effectiveness of the DVR in providing balanced, sinusoidal voltages at the load bus, even though the supply voltages are unbalanced and contain appreciable harmonics. The improvement of power factor at the PCC is also achieved by a simple control scheme that drives the source current in phase with the fundamental frequency component of the PCC voltage.

It is to be noted that the DVR will not be able to compensate for the harmonics in the load current produced by nonlinear loads. This would require shunt connected DSTATCOM. When both load compensation and harmonic isolation (from the source) are required, then Unified Power Quality Conditioner (UPQC), to be described in the next section, is the appropriate device for improvement of power quality. UPQC also helps in regulating the load bus voltage in the presence of large variations (sag or swell) in the supply voltages. The DVR with capacitor on the DC side has the limitations of having to inject only reactive voltage in steady state. This may not be able to compensate fully large variations in the PCC voltage.

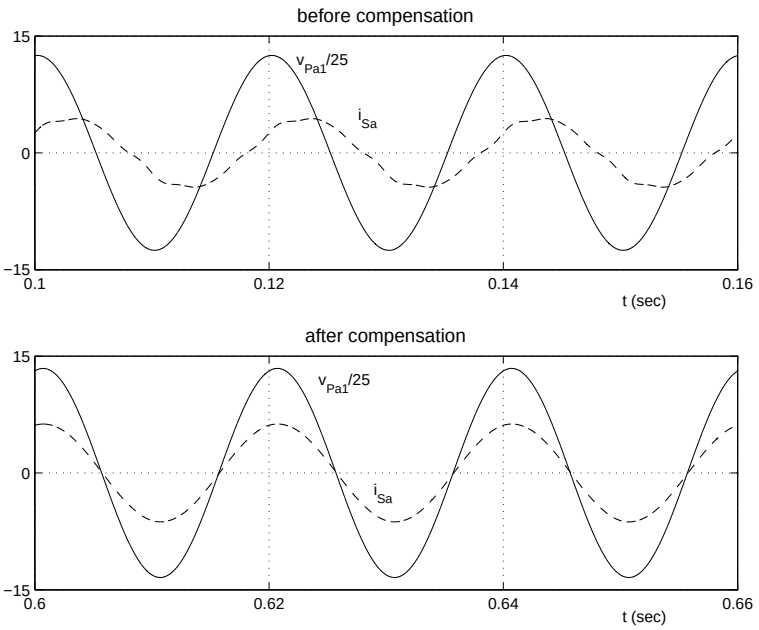

Figure 14.13: Fundamental PCC voltage and source current

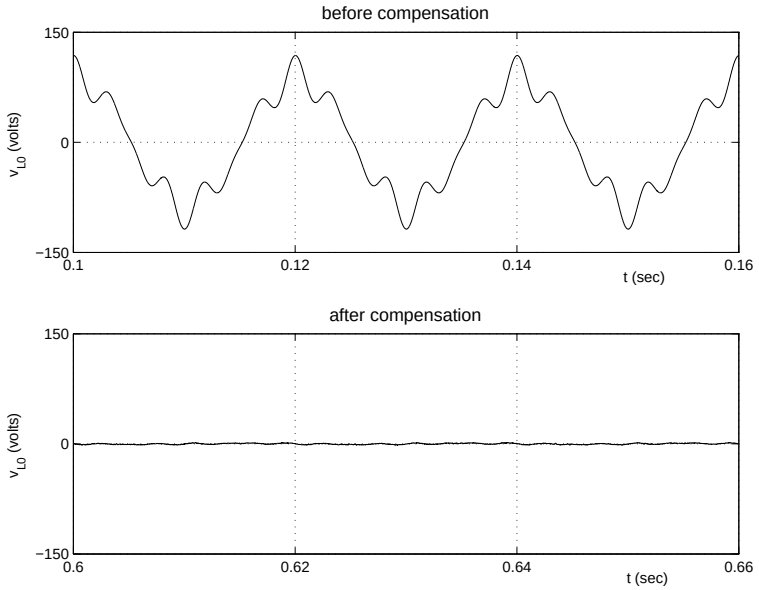

Figure 14.14: Zero sequence load bus voltage

14.5 Unified Power Quality Conditioner

It was shown in the previous chapter that a shunt connected DSTATCOM can balance the source currents and eliminate the harmonics in them in the presence of unbalanced nonlinear loads. By injecting reactive current of desired magnitude, the power factor (or displacement factor) on the source side can be controlled. Instead of controlling the power factor, it is possible to control the load bus voltage magnitude (within limits determined by the source impedance). It was shown in the previous sections that a series connected DVR can balance the voltages at the load bus in addition to isolation of the harmonics from the source side.

The provision of both DSTATCOM and DVR can control the power quality of the source current and the load bus voltage. In addition, if the DVR and STATCOM are connected on the DC side, the DC bus voltage can be regulated by the shunt connected DSTATCOM while the DVR supplies the required energy to the load in case of the transient disturbances in source voltage. The configuration of such a device (termed as Unified Power Quality Conditioner (UPQC)) is shown in Fig. 14.15. This is a versatile device similar to a UPFC. However, the control objectives of a UPQC are quite different from that of a UPFC.

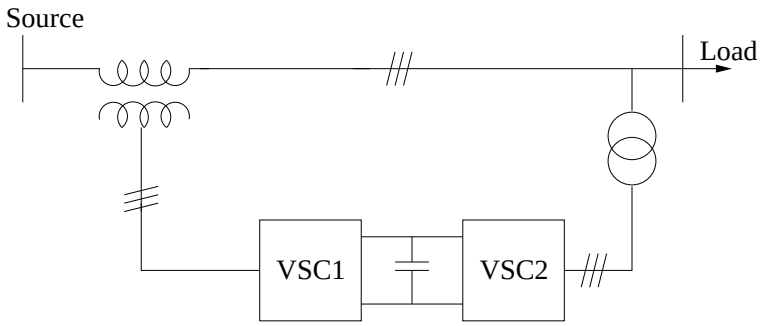

Figure 14.15: A Unified Power Quality Conditioner

Control Objectives of UPQC

The shunt connected converter has the following control objectives

1. To balance the source currents by injecting negative and zero sequence components required by the load
2. The compensate for the harmonics in the load current by injecting the required harmonic currents.

3. To control the power factor by injecting the required reactive current (at fundamental frequency)
4. To regulate the DC bus voltage.

The series connected converter has the following control objectives

1. To balance the voltages at the load bus by injecting negative and zero sequence voltages to compensate for those present in the source.
2. To isolate the load bus from harmonics present in the source voltages, by injecting the harmonic voltages
3. To regulate the magnitude of the load bus voltage by injecting the required active and reactive components (at fundamental frequency) depending on the power factor on the source side
4. To control the power factor at the input port of the UPQC (where the source is connected. Note that the power factor at the output port of the UPQC (connected to the load) is controlled by the shunt converter.

Operation of UPQC

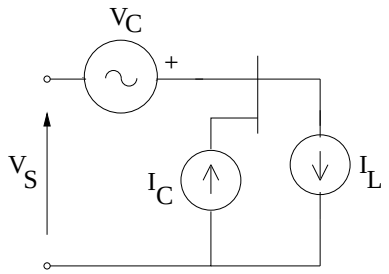

Figure 14.16: Equivalent circuit of ideal UPFC

The operation of a UPQC can be explained from the analysis of the idealized equivalent circuit shown in Fig. 14.16. Here, the series converter is represented by a voltage source V_C and the shunt converter is represented by a current source I_C. Note that all the currents and voltages are 3 dimensional vectors with phase coordinates. Unlike in the case of a UPFC (discussed in chapter 8), the voltages and currents may contain negative and zero sequence components in addition to harmonics. Neglecting losses in the converters, we get the relation

$$\langle V_L, I_C \rangle + \langle V_C, I_S \rangle = 0 \tag{14.23}$$

where $\langle X, Y \rangle$ denote the inner product of two vectors, defined by

$$\langle X, Y \rangle = \frac{1}{T} \int_0^T X^t(\tau) Y(\tau) d\tau. \tag{14.24}$$

Let the load current I_L and the source voltage V_S be decomposed into two components given by

$$I_L = I_L^{1p} + I_L^r \tag{14.25}$$

$$V_S = V_S^{1p} + V_S^r \tag{14.26}$$

where I_L^{1p} contains only positive sequence, fundamental frequency components. Similar comments apply to V_S^{1p}. I_L^r and V_S^r contain rest of the load current and the source voltage including harmonics. I_L^{1p} is not unique and depends on the power factor at the load bus. However, the following relation applies for I_L^{1p}.

$$P_L = \langle V_L, I_L \rangle = \langle V_L, I_L^{1p} \rangle \tag{14.27}$$

This implies that $\langle I_L^r, V_L \rangle = 0$. Thus, the fundamental frequency, positive sequence component in I_L^r does not contribute to the active power in the load.

To meet the control objectives, the desired load voltages and source currents must contain only positive sequence, fundamental frequency components and

$$P_L = |V_L^* \ I_S^*| \cos\phi_l = |V_S^{1p} I_S^*| \cos\phi_s \tag{14.28}$$

where V_L^* and I_S^* are the reference quantities for the load bus voltage and the source current respectively. ϕ_l is the power factor angle at the load bus while ϕ_s is the power factor angle at the source bus (input port of UPQC). Note that $V_L^*(t)$ and $I_S^*(t)$ are sinusoidal and balanced.

If the reference current (I_C^*) of the shunt converter and the reference voltage (V_C^*) of the series converter are chosen as

$$I_C^* = I_L^*, \quad V_C^* = -V_S^r + V_C^{1p} \tag{14.29}$$

with the constraint

$$\langle V_C^{1p}, I_S^* \rangle = 0 \tag{14.30}$$

we have,

$$I_S^* = I_L^{1p}, \quad V_L^* = V_S^{1p} + V_C^{1p} \tag{14.31}$$

Note that the constraint (14.30) implies that V_C^{1p} is the reactive voltage in quadrature with the desired source current, I_S^*. It is easy to derive that

$$\langle V_C^*, I_S^* \rangle = 0 = \langle I_C^*, V_L^* \rangle \tag{14.32}$$

The above equation shows that for the operating conditions assumed, a UPQC can be viewed as a combination of a DVR and a STATCOM with no active power flow through the DC link. However, if the magnitude of V_L^* is to be controlled, it may not be feasible to achieve this by injecting only

reactive voltage. The situation gets complicated if V_S^{1p} is not constant, but changes due to system disturbances or faults. To ensure the regulation of the load bus voltage it may be necessary to inject variable active voltage (in phase with the source current). If we express

$$V_C = V_C^* + \Delta V_C, I_C = I_C^* + \Delta I_C \tag{14.33}$$

we get,

$$I_S = I_S^* - \Delta I_C, V_L = V_S^{1p} + V_C^{1p} + \Delta V_C \tag{14.34}$$

Substituting Eq. (14.34) in (14.23), we get

$$\langle I_S, \Delta V_C \rangle + \langle V_L, \Delta I_C \rangle = 0 \tag{14.35}$$

In deriving the above, we assume that

$$\langle I_S, V_C^* \rangle = 0 = \langle V_L, I_C^* \rangle \tag{14.36}$$

This implies that both ΔV_C and ΔI_C are perturbations involving positive sequence, fundamental frequency quantities (say, resulting from symmetric voltage sags).

Equation (14.35) expresses the power balance on the DC side of the shunt and series converter. The perturbation in V_C is initiated to ensure that

$$|V_C^* + \Delta V_C + V_S| = |V_L| = \text{constant}. \tag{14.37}$$

Thus, the objective of the voltage regulation at the load bus may require exchange of power between the shunt and series converters.

Remarks

1. The unbalance and harmonics in the source voltage can arise due to uncompensated nonlinear and unbalanced loads in the upstream of the UPQC.
2. The injection of capacitive reactive voltage by the series converter has the advantage of raising the source voltage magnitude.

14.6 A Case Study on UPQC

The system considered is the same as in section 14.4 on DVR. However, instead of a balanced $R-L$ load, the load is assumed to consist of a 3 phase half bridge diode rectifier in parallel with a Y connected unbalanced $R-L$ impedances. The configuration of the shunt converter is the same as that used for the case study on the DSTATCOM in chapter 13.

The control scheme for the shunt compensator is shown in Fig. 14.17. The controller ensures that a fraction (K_q) of the reactive current (at the fundamental frequency) required by the load is met by the source. If the desired power factor is unity, then $K_q = 0.0$. The shunt compensator regulates the DC bus voltage in addition to compensating for the harmonics and unbalance in the load.

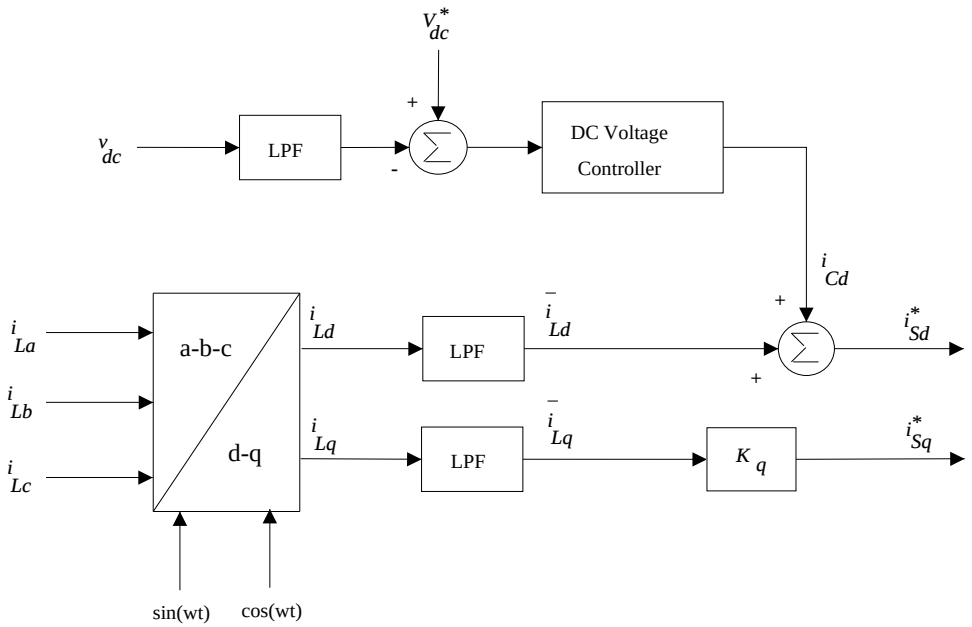

(a) Computation of reference source currents (d and q components)

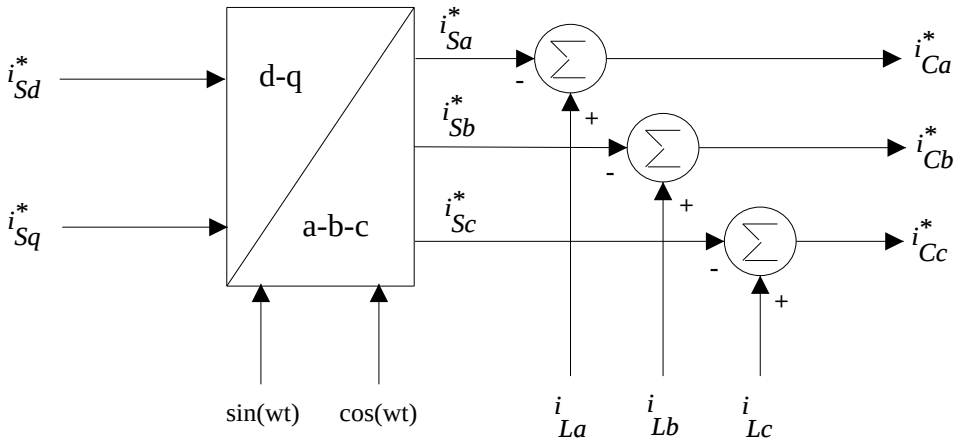

(b) Generation of reference compensator currents

Figure 14.17: Shunt compensator control scheme

The control scheme for the series compensator is shown in Fig. 14.18. The controller ensures the displacement factor at the source bus by modifying $\bar{v}_{Pq}$ (not shown here). In addition, the voltage magnitude at the load bus is regulated and the unbalance, harmonics in the source voltages are compensated.

Fig. 14.19 shows the waveforms of the currents and voltages in the network. It is observed that the UPQC results in sinusoidal, balanced source currents and the load voltages.

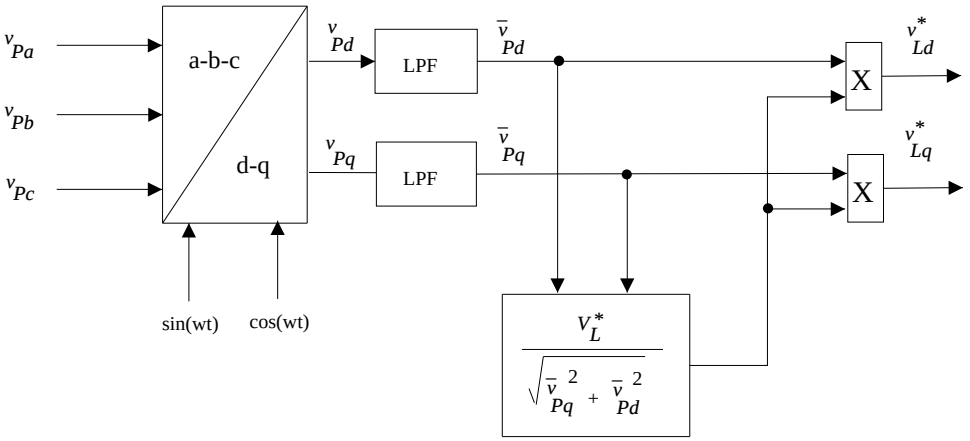

(a) Computation of reference source voltages (d and q components)

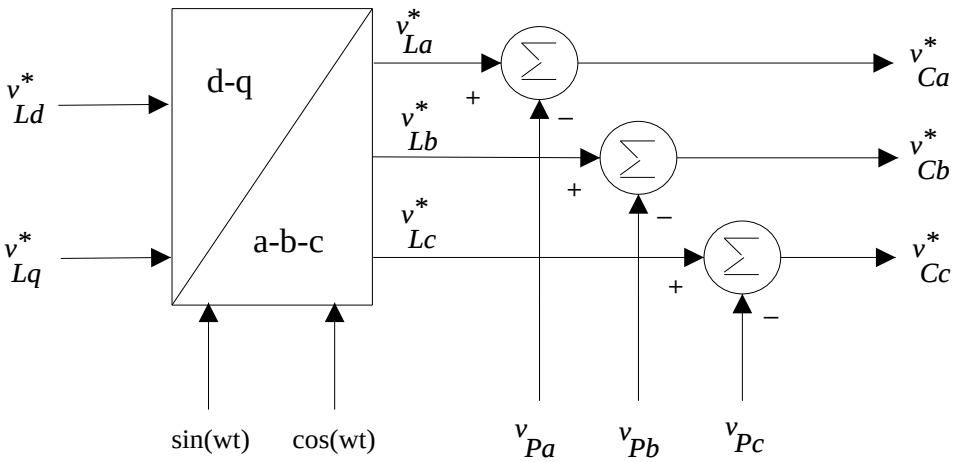

(b) Generation of reference compensator voltages

Figure 14.18: Series compensator control scheme

At 0.6 sec, a voltage sag of 20% for a duration of 0.4 sec is simulated by reducing the (fundamental frequency) positive sequence component of the

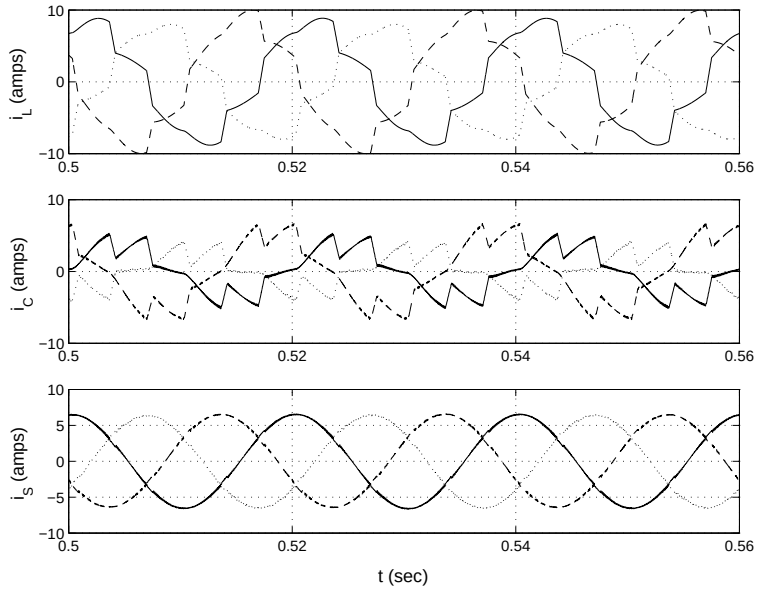

(a) Currents

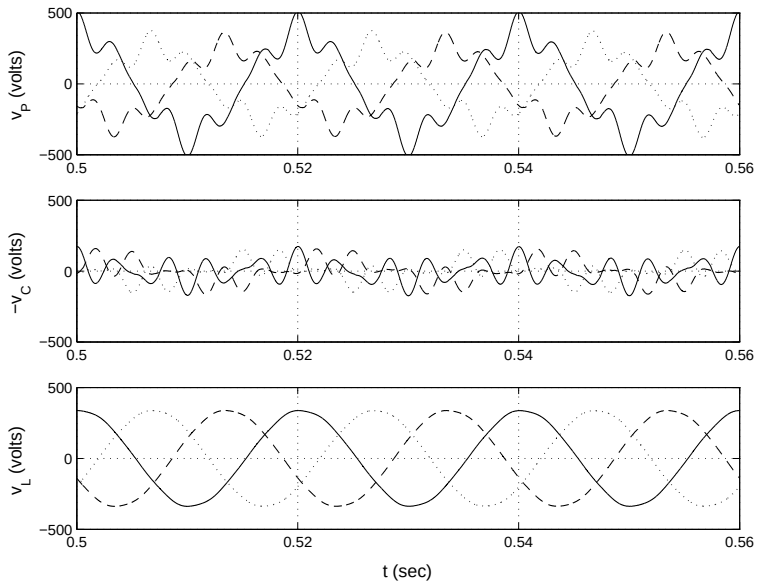

(b) Voltages

Figure 14.19: Current and voltage waveforms

source voltage from 1.0 pu to 0.8 pu. The line to line voltage magnitudes at the input and output ports of the UPQC are shown in Fig. 14.20. The UPQC is started at 0.2 sec. The reduction in the source voltage at 0.6 sec has no effect on the load bus voltage magnitude. The active and reactive powers

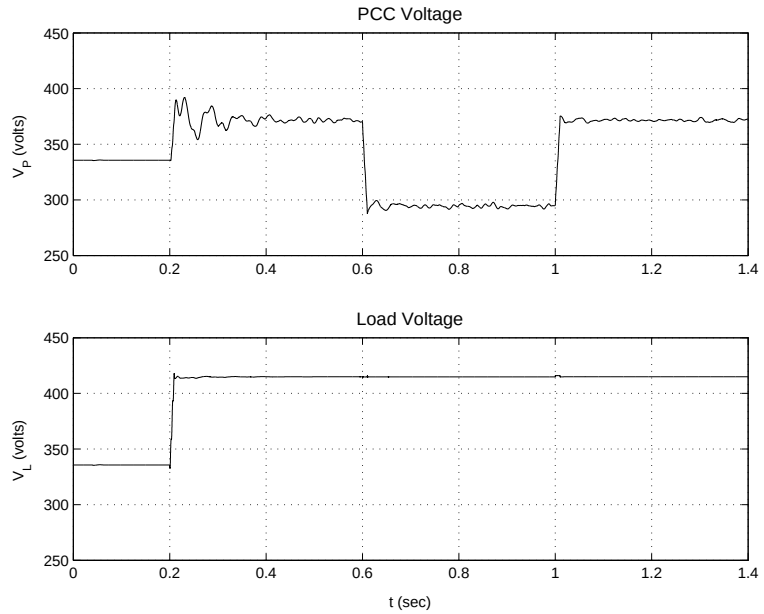

Figure 14.20: Magnitude of PCC and load bus voltages

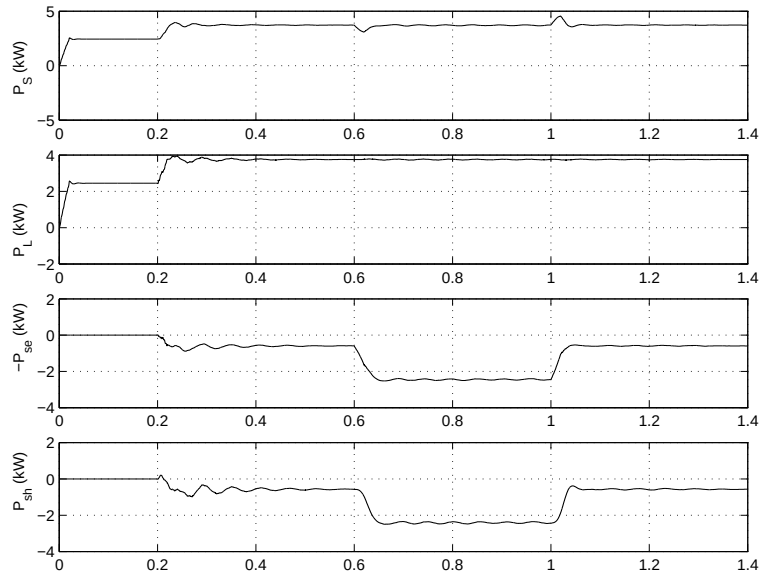

Figure 14.21: Variation of active powers

supplied by the source (P_S, Q_S), drawn by the load (P_L, Q_L), supplied by the series compensator (P_{se}, Q_{se}) and the shunt compensator (P_{sh}, Q_{sh}) are

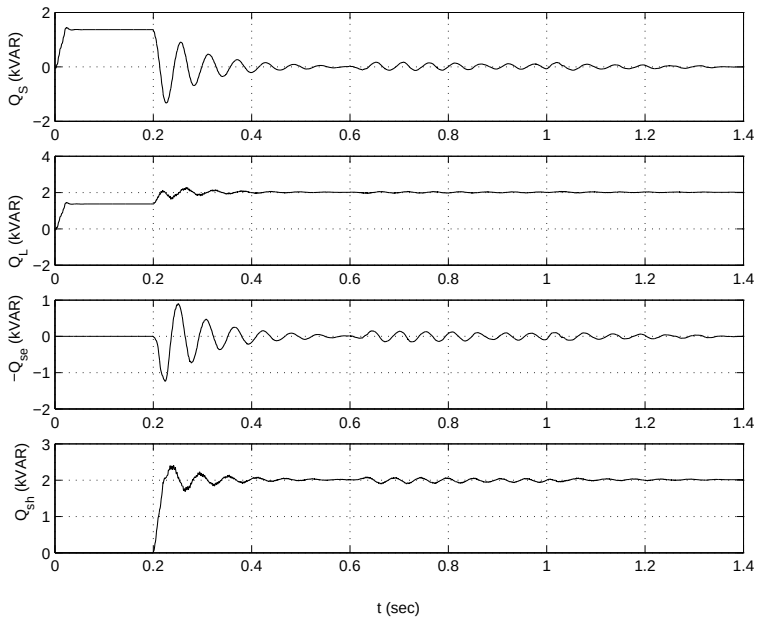

Figure 14.22: Variation of reactive powers

shown in Fig. 14.21 and 14.22. Since V_{Pq}^* is assumed to be zero, the series compensator and the source do not supply any reactive power (except during a transient). It is interesting to observe that the variations in the reactive powers during the voltage sag are small. The maintenance of the desired voltage magnitude at the load bus requires positive power output from the series compensator which is supplied by the shunt compensator through the DC link. The voltage sag results in increase in the power exchange between the series and shunt compensators. However, the load power and reactive powers drawn are unaltered by the voltage sag.

References and Bibliography

1. N. Hingorani, "Introducing Custom Power", IEEE Spectrum, v. 32, n. 6, June 1995, pp. 41-48.

2. N.H. Woodley, L. Morgan and A. Sundaram, "Experience with an inverter-based Dynamics Voltage Restorer", IEEE Trans., Power Delivery, v. 14, n. 3, 1999, pp. 1181-1186.

3. P.T. Cheng and R.H. Lasseter, "Dynamic voltage restoration for unbalanced systems", EPRI Conf. on the Future of Power Delivery, Washington, DC, April 9-11, 1996.

4. S.S. Choi, B.H. Li and D.M. Vilathgamuwa, "Dynamic voltage restoration with minimum energy injection", IEEE Trans., Power Systems, v. 15, n. 1, 2000, pp. 51-57.

5. J.G. Nielsen, F. Blaabjerg and N. Mohan, "Control strategies for dynamic voltage restorer compensating voltage sags with phase jump", Appl. Power Electron. Conf. Expos, 2001; 2; pp. 1267-1273.

6. D.M. Vilathgamuwa, A.A.D.R. Perera and S.S. Choi, "Voltage sag compensation with energy optimized dynamic voltage restorer", IEEE Trans., Power Delivery, v. 18, n. 3, 2003, pp. 928-936.

7. H. Fujita and H. Akagi, "The unified power quality conditioner: The integration of series and shunt- active filters", IEEE Trans., Power Electronics, v. 13, n. 2, 1998, pp. 315-322.

8. K.R. Padiyar and S.N.P. Anand Kumar, "Control and simulation of DVR for improving power quality", National Power Systems Conf. (NPSC-06), I.I.T. Roorkee, December 2006.

9. A.K.S.N. Polisetty, "Application of custom power devices for improving power quality", M.E. Project Report, Indian Institute of Science, July 2005.

10. H.M. Wijekoon, D.M. Vilathgamuwa and S.S. Choi, "Interline dynamic voltage restorer: an economical way to improve interline power quality", IEE Proc., Gener. Trans. Distrib., v. 150, n. 5, 2003, pp. 513-520.

11. C. Zhan et al, "Dynamics voltage restorer based on voltage space vector PWM control", Appl. Power Electron. Conf. Expos., 2001; 2; pp.1301-1307.

12. R.S. Weissbach, G.G. Karady and R.G. Farmer, "Dynamic voltage compensation on distribution feeders using flywheel energy storage", IEEE Trans., Power Delivery, v. 14, n. 2, 1999, pp. 465-471.

13. J.H.R. Enslin, J. Zhao and R. Spee, "Operation of the unified power flow controller as harmonic isolator", IEEE Trans., Power Electronics, v. 11, n. 6, 1996, pp. 776- 784.

This page intentionally left blank

Appendix A

Modelling of Synchronous Generator

In this Appendix, we consider the modelling of a synchronous machine (stator and rotor circuits) and the mechanical mass-spring system made up of the generator rotor, turbines and the rotating excitor masses and the connecting elastic shafts.

A.1 Synchronous Machine Model

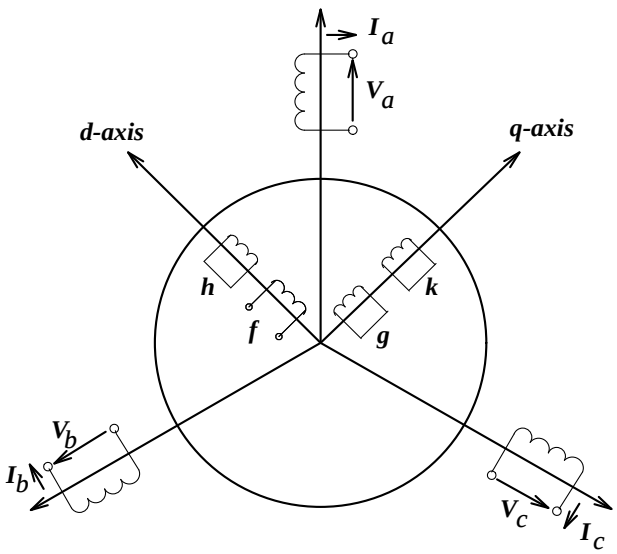

Figure A.1: Synchronous machine

The synchronous machine considered is shown in Fig. A.1. This shows three phase armature windings (a,b and c) on the stator and four windings on the rotor including the field winding 'f'. The amortisseur (or damper) circuits in the salient pole machine or the eddy current effects in the solid rotor are represented by a set of coils. Three damper coils, 'h' in the d-axis and g,k in the q-axis are shown in Fig. A.1. Generally, three

damper windings are the most detailed model of the rotor electrical circuits that represent both transient and subtransient effects in the machine. If subtransient effects are not important, one damper winding in the q-axis may be adequate.

Modelling of the Stator

Three representations of the stator circuits are considered here depending on the requirement

1. Transient simulation using three phase model
2. Transient simulation using d-q coordinates
3. Stability simulation neglecting stator transients

1. Three Phase Equivalent Circuit of the Stator

The synchronous machine equations are, in general, nonlinear and time varying. The solution of synchronous machine equations along with the stationary network equations requires a suitable interface technique.

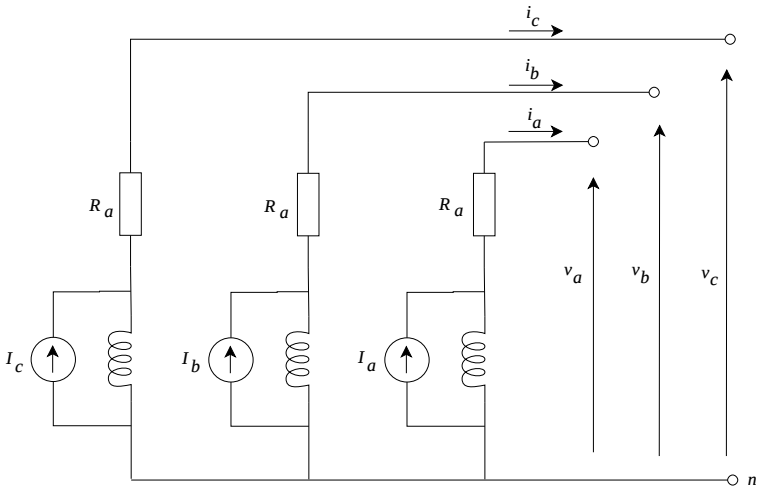

Figure A.2: Equivalent circuit of stator

If the stator of a synchronous machine can be represented by an equivalent circuit, this will simplify considerably, the problem of interfacing the machine and the network. Ramshaw and Padiyar [3] presented such a model where the stator of a synchronous generator is represented by constant (substransient) inductances $[L_s'']$ in parallel with current sources I_s which are

dependent on the rotor flux linkages (see Fig. A.2). The inductances matrix $[L_s'']$ is naturally a constant matrix if $L_d'' = L_q''$ (there is no subtransient saliency). However, if $L_d'' \neq L_q''$, the matrix can still be made constant by introducing a dummy coil on the rotor along the q-axis. The mutually coupled stator inductances can be included as part of the external network in the same manner as any other mutually coupled three phase branch.

The current source I_s is given by

$$I_s = [I_a \ I_b \ I_c]^t = I_d C + I_q S \tag{A.1}$$

where

$$C^t = \sqrt{\frac{2}{3}}\left[\cos\theta \ \cos\left(\theta - \frac{2\pi}{3}\right) \ \cos\left(\theta + \frac{2\pi}{3}\right)\right] \tag{A.2}$$

$$S^t = \sqrt{\frac{2}{3}}\left[\sin\theta \ \sin\left(\theta - \frac{2\pi}{3}\right) \ \sin\left(\theta + \frac{2\pi}{3}\right)\right] \tag{A.3}$$

$$I_d = -(C_1\psi_f + C_2\psi_h) \tag{A.4}$$

$$I_q = -(C_3\psi_g + C_4\psi_k + C_5\psi_c) \tag{A.5}$$

$$\theta = \omega_0 t + \delta \tag{A.6}$$

$$C_1 = \frac{x_{df}x_h - x_{dh}x_{fh}}{x_d''(x_f x_h - x_{fh}^2)}, \quad C_2 = \frac{x_{dh}x_f - x_{fh}x_{df}}{x_d''(x_f x_h - x_{fh}^2)},$$

$$C_3 = \frac{x_{qg}x_k - x_{qk}x_{gk}}{x_d''(x_g x_k - x_{gk}^2)}, \quad C_4 = \frac{x_{qk}x_g - x_{gk}x_{qg}}{x_d''(x_g x_k - x_{gk}^2)},$$

$$C_5 = \frac{1}{x_d''}\sqrt{\frac{(x_q'' - x_d'')}{x_c}}$$

x_c is the self reactance of the dummy coil which can be chosen as $x_q \cdot \psi_c$ is the flux linkage of the dummy coil. $[L_s'']$ is defined by

$$[L_s''] = \frac{L_0}{3}\begin{bmatrix} 1 & 1 & 1 \\ 1 & 1 & 1 \\ 1 & 1 & 1 \end{bmatrix} + \frac{2L_d''}{3}\begin{bmatrix} 1 & -\frac{1}{2} & -\frac{1}{2} \\ -\frac{1}{2} & 1 & -\frac{1}{2} \\ -\frac{1}{2} & -\frac{1}{2} & 1 \end{bmatrix} \tag{A.7}$$

where L_0 is the zero sequence inductance and L_d'' is the d-axis subtransient inductance.

ω_0 is the operating speed of the rotor (corresponding to a two pole machine). δ is the rotor angle measured with respect to a synchronously rotating reference frame.

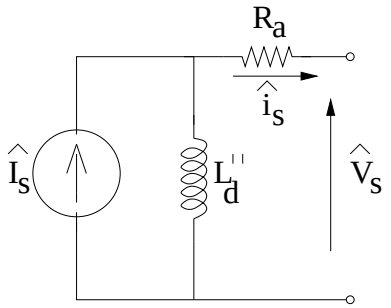

Figure A.3: Equivalent circuit using $d-q$ coordinates

2. Equivalent Circuit Using $d-q$ Coordinates

If the network (connected to the stator) is represented using $d-q$ coordinates it is adequate to model the stator also using $d-q$ coordinates (with respect to a rotating reference frame fixed to the rotor). The single phase equivalent circuit of the stator is shown in Fig. A.3.

In this single phase circuit, $\hat{I}_s$, $\hat{i}_s$ are all complex variables defined by

$$\left.\begin{array}{ll} \hat{I}_s = (I_d - jI_q)e^{j\theta}, & \hat{i}_s = (i_d - ji_q)e^{j\theta}, \\ \hat{v}_s = (v_d - jv_q)e^{j\theta} & \end{array}\right\} \tag{A.8}$$

The complex equation for the equivalent circuit in Fig. A.3 is given by

$$L''_d \frac{d}{dt}(\hat{I}_s - \hat{i}_s) - R_a \hat{i}_s = \hat{v}_s \tag{A.9}$$

Substituting Eq. (A.8) in (A.9) and separating the real and imaginary parts, we get

$$-\frac{d\psi_d}{dt} - \dot{\theta}\psi_q - R_a i_d = v_d \tag{A.10}$$

$$-\frac{d\psi_q}{dt} + \dot{\theta}\psi_d - R_a i_q = v_q \tag{A.11}$$

where,

$$\begin{aligned} \psi_d &= -L''_d(I_d - i_d), \quad \psi_q = -L''_d(I_q - i_q) \\ \dot{\theta} &= \frac{d\theta}{dt} = \omega_0 + \frac{d\delta}{dt} \end{aligned}$$

3. Equivalent Circuit in $d-q$ Coordinates, Neglecting Stator Transients

For transient stability simulation, it is usual to neglect stator transients and the variations in $\dot{\theta}$. What this implies is that the derivative terms in

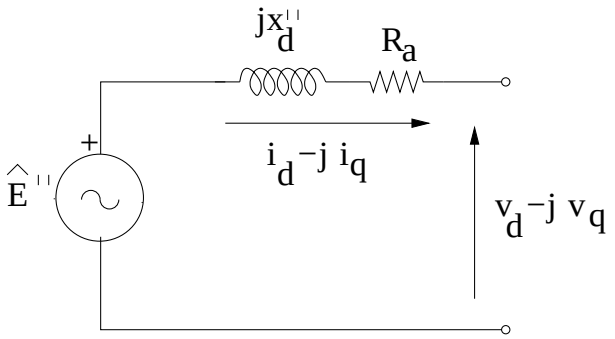

Figure A.4: Equivalent circuit neglecting transients

Eqs. (A.10) and (A.11) are neglected and $\dot{\theta}$ is assumed to be equal to ω_B (the rated speed). With these approximations, it is possible to derive an equivalent circuit shown in Fig. A.4 where the complex voltage source $\hat{E}''$ is defined as

$$\hat{E}'' = E''_d - jE''_q \tag{A.12}$$

where

$$E''_d = x''_d I_q \tag{A.13}$$

$$E''_q = -x''_d I_d \tag{A.14}$$

If subtransient phenomenon is not considered, then only one damper winding in the q-axis is adequate. In this case, the equivalent circuit is shown in Fig. A.5. Here, E'_d and E'_q are defined by

$$E'_d = -\frac{x_{qg}}{x_g}\psi_g - x'_d C'_5 \psi_c, \quad E'_q = \frac{x_{df}}{x_f}\psi_f \tag{A.15}$$

$$C'_5 = \frac{1}{x'_d}\sqrt{\frac{(x'_q - x'_d)}{x_c}} \tag{A.16}$$

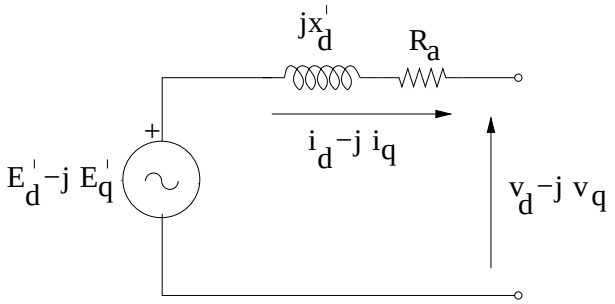

Figure A.5: A simplified equivalent circuit (with one damper winding)

Rotor Electrical Equations

The equations for the rotor flux linkages can be written in the state space form as

$$\dot{\psi}_R = [A_R]\psi_R + [B_R]U_R \tag{A.17}$$

where

$$\psi_R = [\psi_f \ \psi_h \ \psi_g \ \psi_k \ \psi_c]^t, \quad U_R = [i_d \ i_q \ E_{fd}]^t \tag{A.18}$$

The nonzero elements of the $[A_R]$ and $[B_R]$ matrices are given below,

$$\begin{aligned}
A_R(1,1) &= -\frac{\omega_B R_f x_h}{x_f x_h - x_{fh}^2}, \quad A_R(1,2) = \frac{\omega_B R_f x_{fh}}{x_f x_h - x_{fh}^2} \\
A_R(2,1) &= -\frac{\omega_B R_h x_{fh}}{x_f x_h - x_{fh}^2}, \quad A_R(2,2) = -\frac{\omega_B R_h x_f}{x_f x_h - x_{fh}^2} \\
A_R(3,3) &= -\frac{\omega_B R_g x_k}{x_g x_k - x_{gk}^2}, \quad A_R(3,4) = \frac{\omega_B R_g x_{gk}}{x_g x_k - x_{gk}^2} \\
A_R(4,3) &= \frac{\omega_B R_k x_{gk}}{x_g x_k - x_{gk}^2}, \quad A_R(4,4) = -\frac{\omega_B R_k x_g}{x_g x_k - x_{gk}^2} \\
A_R(5,5) &= -\frac{1}{T_c} \\
B_R(1,1) &= \frac{\omega_B R_f (x_h x_{df} - x_{dh} x_{fh})}{x_f x_h - x_{fh}^2}, \quad B_R(1,3) = \frac{\omega_B R_f}{x_{df}} \\
B_R(2,1) &= \frac{\omega_B R_h (x_f x_{dh} - x_{fh} x_{df})}{x_f x_h - x_{fh}^2} \\
B_R(3,2) &= \frac{\omega_B R_g (x_k x_{qg} - x_{qk} x_{gk})}{x_g x_k - x_{gk}^2} \\
B_R(4,2) &= \frac{\omega_B R_k (x_g x_{qk} - x_{gk} x_{qg})}{x_g x_k - x_{gk}^2} \\
B_R(5,2) &= \sqrt{x_c (x_q'' - x_d'')}/T_c
\end{aligned}$$

In these expressions, x_f, x_h, x_g and x_k represent the self reactances of the windings 'f', 'h', 'g' and 'k' respectively. The reactance x_{ij} represents the mutual reactance between the windings i and j. Without loss of generality, we can assume $x_{df} = x_{dh}$ and $x_{qg} = x_{qk} = x_{gk}$. However, $x_{fh} \neq x_{df}$ in general.

T_c is the time constant of the dummy coil in the q-axis given by $T_c = \frac{x_c}{\omega_B R_c}$. T_c can be arbitrarily chosen for the required accuracy. For stability studies T_c can be chosen not smaller than 10 ms for adequate accuracy. For transient simulation, $T_c = 0.1$ ms gives accurate results. (Note that $T_c = 0.0$ for exact results).

A.2 Modelling of Turbine Generator Mechanical Systems

A.2.1 General

The rotor of a Turbine Generator (T-G) unit is a complex mechanical system made up of several rotors of different sizes, each with mechanical shaft sections and couplings. Turbine sections contain a number of discs which may be integral or attached to the rotor. The length of the rotor system may extend over 50 m and weigh several hundred tons. The system also has a number of smaller components including turbine blades, rotor coils, retaining rings, blowers and pumps.

While an exact analysis of the rotor system may require an advanced continuum model, for the study of torsional interactions, lumped multimass model is adequate [4]. Here, each major rotor element (generator, various turbine stages and rotating exciter) is considered to be a rigid mass connected to adjacent elements by shafts that are modelled as massless springs. This lumped multimass model has natural resonant frequencies below the system (electrical) frequency. The torsional mode oscillations, induced by a transient (such as a sudden change in the air gap torque caused by network switching) are lightly damped even when torsional interaction with the transmission network is neglected. The total damping forces are due to (A) Steam pressure on turbine blades (B) bearing friction and windage on shaft elements (C) hysteritic damping in the rotor steel and (D) electrical damping due to generator, exciter and the transmission network. The first component is dependent on the generator loading while the last component can be negative. The hysteritic damping arises due to the energy dissipated in the material subjected to alternating stress.

A.2.2 State Equations

The state equations for the mechanical system can be expressed either based on (a) coupled multimass model or (b) decoupled modal model. Both approaches will be illustrated by taking an example of a four mass system made up of High Pressure (HP), Intermediate Pressure (IP), Low Pressure (LP) turbines and the generator rotor. (see Fig. A.6). There are four masses and three shafts sections. The number of state variable is eight and defined by,

$$X_m = [\delta \ S_m \ T_{LG} \ S_{LP} \ T_{IL} \ S_{IP} \ T_{HI} \ S_{HP}]^t$$

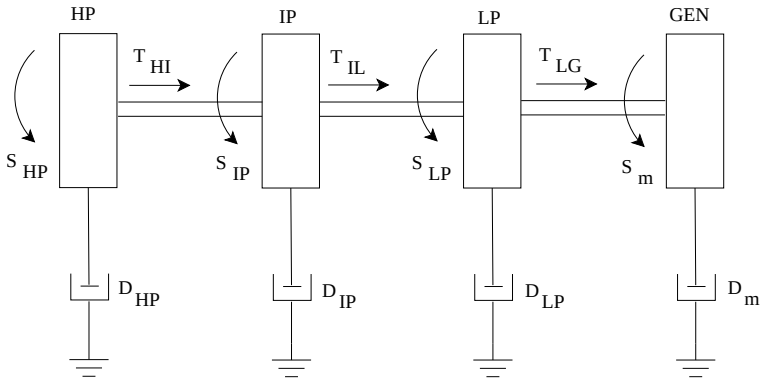

Figure A.6: A four mass system

T_{ij} is the torque in the shaft connecting rotor masses i and j. S_i is the per unit slip of the rotor mass defined by

$$S_i = \frac{\omega_i - \omega_B}{\omega_B}$$

The state equations are given below.

$$\frac{d\delta}{dt} = \omega_B S_m \tag{A.19}$$

$$2H_m \frac{dS_m}{dt} = -(D_m + D_{LG})S_m + T_{LG} + D_{LG}S_{LP} - T_e \tag{A.20}$$

$$\frac{dT_{LG}}{dt} = \omega_B K_{LG}(S_{LP} - S_m) \tag{A.21}$$

$$\begin{aligned} 2H_{LP}\frac{dS_{LP}}{dt} &= -(D_{LG} + D_{LP} + D_{IL})S_{LP} + D_{LG}S_m \\ &\quad + D_{IL}S_{IP} + T_{IL} - T_{LG} + F_{LP}T_m \end{aligned} \tag{A.22}$$

$$\frac{dT_{IL}}{dt} = \omega_B K_{IL}(S_{IP} - S_{LP}) \tag{A.23}$$

$$\begin{aligned} 2H_{IP}\frac{dS_{IP}}{dt} &= -(D_{HI} + D_{IP} + D_{IL})S_{IP} + D_{HI}S_{HP} \\ &\quad + D_{IL}S_{LP} + T_{HI} - T_{IL} + F_{IP}T_m \end{aligned} \tag{A.24}$$

$$\frac{dT_{HI}}{dt} = \omega_B K_{HI}(S_{HP} - S_{IP}) \tag{A.25}$$

$$\begin{aligned} 2H_{HP}\frac{dS_{HP}}{dt} &= -(D_{HP} + D_{HI})S_{HP} + D_{HI}S_{IP} - T_{HI} \\ &\quad + F_{HP}T_m \end{aligned} \tag{A.26}$$

where D_{HI}, D_{IL} and D_{LG} are mutual damping terms associated with shaft sections connecting HP-IP, IP-LP and LP-GEN respectively. T_m is the net mechanical torque produced by the prime mover. F_{HP}, F_{IP} and F_{LP} are the fractions of the mechanical torque (or power) produced by HP, IP and LP turbines respectively. H_i is the inertia constant of rotor mass i. It is assumed that initial slip (S_{mo}) is zero.

Eqs. (A.19) to (A.26) can be expressed in the compact form as

$$\dot{X}_m = [A_m]X_m + [B_{m1}]T_m + [B_{m2}]T_e \tag{A.27}$$

where A_m is a matrix of order 2m $\times$ 2m where m is the number of masses, B_{m1} and B_{m2} are column vectors of order 2m.

State Equations Using Modal Quantities

As mentioned earlier, it is possible to transform the system equations into decoupled form using modal inertias, spring constants and damping parameters. These equations for the four mass system shown in Fig. A.6 are given below. To simplify the notation, the modal quantities are denoted by subscripts.

$$\frac{d\delta_0}{dt} = \omega_B S_0 \tag{A.28}$$

$$2H_0\frac{dS_0}{dt} = -D_0S_0 + (T_m - T_e) \tag{A.29}$$

$$\frac{d\delta_1}{dt} = \omega_B S_1 \tag{A.30}$$

$$2H_1\frac{dS_1}{dt} = -D_1S_1 - K_1\delta_1 + (T_m^1 - T_e) \tag{A.31}$$

$$\frac{d\delta_2}{dt} = \omega_B S_2 \tag{A.32}$$

$$2H_2\frac{dS_2}{dt} = -D_2S_2 - K_2\delta_2 + (T_m^2 - T_e) \tag{A.33}$$

$$\frac{d\delta_3}{dt} = \omega_B S_3 \tag{A.34}$$

$$2H_3\frac{dS_3}{dt} = -D_3S_3 - K_3\delta_3 + (T_m^3 - T_e) \tag{A.35}$$

$$S_m = S_0 + S_1 + S_2 + S_3 \tag{A.36}$$

$$\delta = \delta_0 + \delta_1 + \delta_2 + \delta_3 \tag{A.37}$$

where H_0, H_1, H_2 and H_3 are modal inertias corresponding to modes zero, one, two and three respectively. The frequency of mode zero is zero and

the mode three has the highest frequency. D_0, D_1, D_2 and D_3 are modal dampings. T_m^1, T_m^2 and T_m^3 are defined by

$$T_m^1 = q_1^t F T_m, T_m^2 = q_2^t F T_m, T_m^3 = q_3^t F T_m \tag{A.38}$$

$$F^t = [F_{HP}\ F_{IP}\ F_{LP}\ 0]$$

q_1, q_2 and q_3 are columns of [Q] matrix (eigenvectors of the matrix $[M^{-1}][K]$ corresponding to the torsional modes 1,2 and 3). $[M]$ and $[K]$ are defined below

$$[M] = \frac{1}{\omega_B}\begin{bmatrix} 2H_{HP} & 0 & 0 & 0 \\ 0 & 2H_{IP} & 0 & 0 \\ 0 & 0 & 2H_{LP} & 0 \\ 0 & 0 & 0 & 2H_m \end{bmatrix}$$

$$[K] = \begin{bmatrix} K_{HI} & -K_{HI} & 0 & 0 \\ -K_{HI} & (K_{HI}+K_{IL}) & -K_{IL} & 0 \\ 0 & -K_{IL} & (K_{IL}+K_{LG}) & -K_{LG} \\ 0 & 0 & -K_{LG} & K_{LG} \end{bmatrix}$$

The eigenvectors of $[M]^{-1}[K]$ are chosen such that their last elements (corresponding to generator rotor angle) are all equal to unity.

It is to be noted that

$$D_0 = D_T = D_{HP} + D_{IP} + D_{LP} + D_m$$
$$H_0 = H_T = H_{HP} + H_{IP} + H_{LP} + H_m$$

The modal dampings are normally obtained directly from test results or assumed.

A.3 Relationship between Park and Kron Transformation

It is to be noted that the three phase, transient model of the synchronous machine described in section A.1, is derived from first principles without utilizing Park's transformation. However, the application of Park's transformation that involves a rotating reference frame fixed to the machine rotor, results in the equivalent circuit of the stator shown in Fig. A.3 or A.4 depending on whether stator transients are considered or neglected. The zero sequence component in the armature windings has no effect on the electromagnetic torque produced.

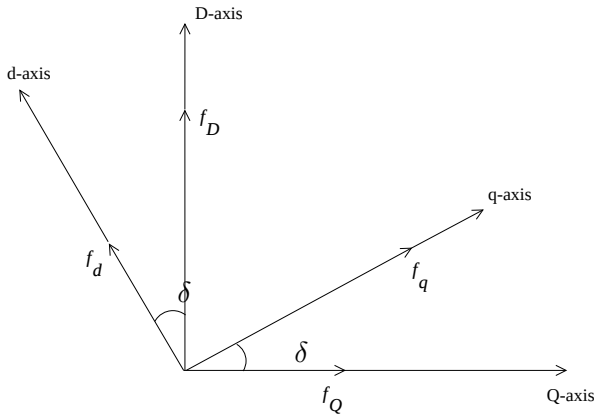

Figure A.7: Phasor diagram showing relationship between $D-Q$ and $d-q$ components

For the stationary network, it is convenient to utilize a synchronously rotating reference frame with a constant speed. In power system literature, the associated transformation is termed as Kron's transformation. (In some papers by power electronics specialists, this is also (mistakenly) labelled as Park's transformation). The relationship between the d-q (Park's components) and D-Q (Kron's components) is given by

$$(f_Q + jf_D) = (f_q + jf_d)e^{j\delta} \tag{A.39}$$

where f can be a voltage or current (dynamic) phasor. (Note that lower case letters refer to Park's components while the upper case letters refer to Kron's components). Typically, the reference phasor is considered to be along Q-axis. The machine q-axis leads Q-axis by δ (rotor angle). See Fig. A.7. Typically, the infinite bus voltage E_b is assumed to be along the Q-axis.

If there are no synchronous generators to be represented (as in a distribution system) there is no need for Park's components. Often, Kron's components are labelled using lower case d-q letters, when there is no confusion.

References

1. K.R. Padiyar, **Analysis of Subsynchronous Resonance in Power Systems**, Kluwer Academic Publishers, Boston, 1999.
2. K.R. Padiyar, **Power System Dynamics - Stability and control**, (Second Edition), B S Publications, Hyderabad, 2002.
3. R.S. Ramshaw and K.R. Padiyar, "Generalized system model for slipring machines", Proc. IEE, (London) v. 120, n. 6, 1973, pp. 647-658.

4. D.G. Ramey, A.C. Sismour and G.C. Kung, "Important parameters in considering transient torques on turbine-generator shaft systems", IEEE Trans., PAS-99, n.1, 1980, pp. 311-317.

Appendix B

Pulse Width Modulation for Voltage Source Converters

There is a large body of literature on Pulse Width Modulation (PWM) techniques for different applications [1,2]. Here, we consider only three widely used techniques for high power applications – Selected Harmonic Elimination (SHE), Sinusoidal PWM (SPWM) and Space Vector Modulation (SVM). Actually, PWM methods are often categorized as open loop (feedforward) and closed loop schemes. The first category is further subdivided into carrier-based PWM, carrierless PWM, overmodulation and optimized feedforward schemes. The closed loop or feedback PWM control schemes are classified into nonoptimal methods involving hysteresis or space vector current control, optimization in real-time involving predictive current control or trajectory tracking control etc. [1].

B.1 Introduction

We consider PWM techniques applied to a three phase, two level VSC shown in Fig. B.1. In the absence of modulation, the waveform of phase voltage e_a referred to (i) midpoint (N) of the DC capacitor and (ii) supply neutral are shown in Fig. B.2. The line-to-line voltage (e_{ab}) waveform is shown in Fig. B.3. The VSC without modulation is termed as a square wave or six-step converter. The peak value of the fundamental frequency component of the phase voltage (E_1) is given by

$$E_1 = \frac{4}{\pi}\left(\frac{V_{dc}}{2}\right) = \sqrt{2}(0.90)\left(\frac{V_{dc}}{2}\right) \tag{B.1}$$

where $\left(\frac{V_{dc}}{2}\right)$ is the level of the square wave shown in Fig. B.2. 0.90 is the rms value of the fundamental frequency component of a square wave whose level is 1.0.

Generally, we wish to regulate the DC capacitor voltage (V_{dc}) and yet control the output AC voltage magnitude (in addition to its phase). Since the maximum value of the phase voltage injected is limited by V_{dc} we can

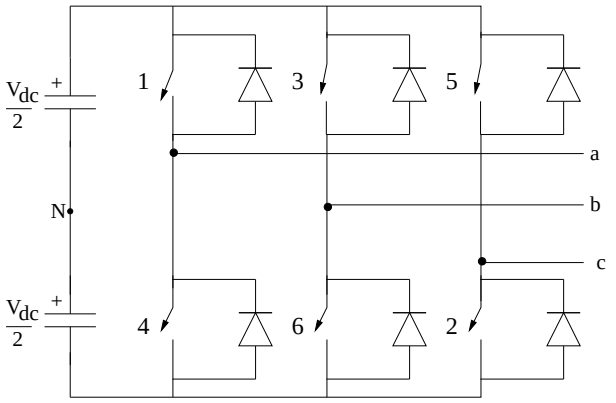

Figure B.1: A three phase, two level (Graetz bridge) VSC

only control the width of the voltage pulses generated by switching between complementary devices (1 and 4 for phase a). Note that we can reverse the voltage polarity by switching off device 1 and switching on 4 (or vice versa). For simplicity, we ignore the dead time (blanking time) between the switching of devices 1 and 4 (and similarly in other two legs).

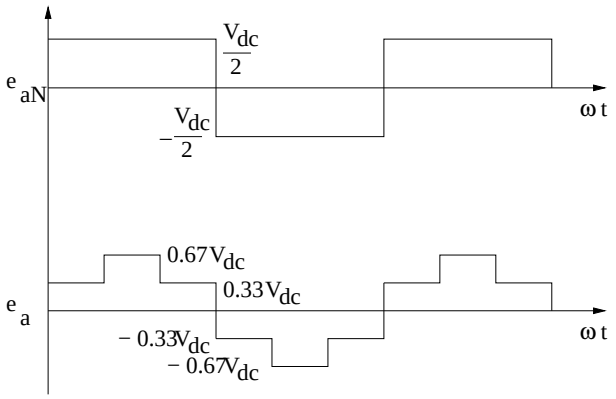

Figure B.2: Waveform of e_{aN} and e_a

The objectives of PWM can be stated as follows.

1. To control the output AC voltage for a constant DC voltage.
2. To minimize the harmonics in the load subject to the constraints on the switching losses, generation of noise etc.

The characteristics of the load may vary. However, typically the load behaves as a low pass filter. Hence, if we reduce the lower order harmonics in the output AC voltage, it is advantageous in minimizing load current

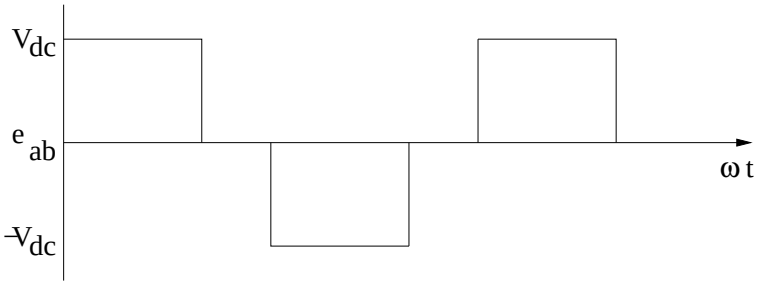

Figure B.3: Waveform of e_{ab}

harmonics. Thus shifting the frequency spectrum of the injected voltage to the higher level is beneficial in improving the performance of the PWM-VSC.

The frequency ratio

$$p = \frac{F}{f} \tag{B.2}$$

where F is the modulation frequency and f is the fundamental output frequency is an important parameter. p is also called as the pulse number. Higher the value of p, broader the spectrum of harmonics that can be eliminated. The switching frequency (F) is dependent on the devices used. The maximum switching frequency for GTO thyristors is only around 100 Hz. This is why PWM is not used in GTO based VSC employed in high power FACTS controllers. Multi-pulse or multilevel converters which require only one switching (on and off) in a cycle are used with GTO devices. On the other hand, IGBT devices can be operated up to 10 kHz. However, switching losses increase with frequency and are a limiting factor in the choice of F.

For $p > 20$, the modulating (carrier) wave and the reference (output) voltage need not be synchronized. It is not necessary that p be an integer. For comparing various modulation schemes, the modulation index (m) is normalized by taking the ratio of actual fundamental component of the modulated output voltage to that of the unmodulated output voltage, that is,

$$\bar{m} = \frac{E_{mod1}}{0.45V_{dc}} \tag{B.3}$$

where E_{mod1} is the rms value of the fundamental component of the modulated output voltage.

B.2 Selective Harmonic Elimination (SHE)

By reversing the phase voltages a few times during each half cycle, it is possible to eliminate low order harmonics selectively. However, the high

order harmonics may increase in magnitudes, but the current harmonics are not significantly affected due to the low pass filter characteristics of the load.

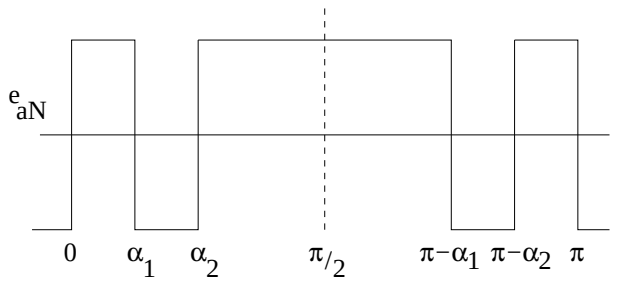

(a) 4 voltage reversals in a half cycle

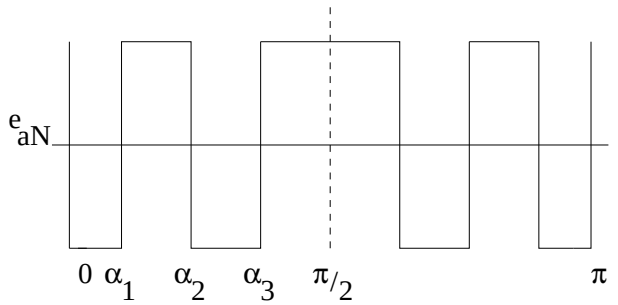

(b) 6 voltage reversals in a half cycle

Figure B.4: Waveforms of e_{aN} with voltage reversals

Fig. B.4 shows the waveforms of the phase voltage (e_{aN}) with four and six reversals within one half cycle. The voltage reversals are effected at chosen instants such that the notches (caused by the voltage reversals) are placed symmetrically about the centre line of each half cycle. If there are 'p' switching (voltage reversals) in a quarter cycle, the rms value of the nth harmonic voltage is given by

$$\begin{aligned} E_n &= \pm\frac{1}{\sqrt{2}}\cdot\frac{4}{\pi}\cdot\frac{V_{dc}}{2}\left[-\int_0^{\alpha_1}\sin n\theta\ d\theta+\int_{\alpha_1}^{\alpha_2}\sin n\theta\ d\theta...\pm\int_{\alpha_p}^{\pi/2}\sin n\theta\ d\theta\right] \\ &= \pm\frac{0.45}{n}V_{dc}[2(\cos n\alpha_1-\cos n\alpha_2+\cos n\alpha_3-\cdots)-1] \end{aligned} \tag{B.4}$$

where $\alpha_1, \alpha_2, \cdots, \alpha_p$ are switching angles within each quarter cycle. There are p degrees of freedom and are used to cancel $(p-1)$ harmonic components in the voltage and control the fundamental voltage. For example, if there

are 3 switchings at α_1, α_2 and α_3, we can eliminate the fifth and seventh harmonics in addition to controlling the fundamental voltage. We get 3 transcendental equations given by

$$\begin{aligned} \bar{m} &= 2[\cos\alpha_1 - \cos\alpha_2 + \cos\alpha_3] - 1 && \text{(B.5)} \\ 0 &= 2[\cos 5\alpha_1 - \cos 5\alpha_2 + \cos 5\alpha_3] - 1 && \text{(B.6)} \\ 0 &= 2[\cos 7\alpha_1 - \cos 7\alpha_2 + \cos 7\alpha_3] - 1 && \text{(B.7)} \end{aligned}$$

Note that although the phase voltage contain triplen harmonics, the line to line voltages are free from them. Hence a three phase six-step (square wave) converter has only harmonics of the order

$$h = 6k \pm 1, \quad k = 1, 2, 3, \cdots \tag{B.8}$$

Example

If there are two voltage reversals in a quarter cycle, the values of α, and α_2 are 16.2° and 22.0° such that the 5th and 7th voltage harmonics are zero. The modulation index ($\bar{m}$) is given by

$$\bar{m} = 1 - 2(\cos\alpha_1 - \cos\alpha_2) = 0.934 \tag{B.9}$$

B.3 Sinusoidal PWM

The sinusoidal PWM technique is widely used for industrial converters. The method is also known as suboscillation method and uses a triangular carrier wave of frequency F to generate a sinusoidal reference voltage of frequency f. Actually, the modulated output voltage of the converter approximates a staircase shape in which each step is the average value over each cycle of the carrier wave.

The sine PWM technique can be compared to the SHE PWM discussed in the previous section. Here, the instants of voltage reversals are determined by the intersections between a reference sinusoidal voltage of peak value m and a triangular voltage of amplitude 1. Fig. B.5 shows the operation of sine PWM for $p = \frac{F}{f} = 9$ with $m = 0.5$. The modulation is said to be in the linear range, if $0 < m \leq 1$. The same carrier wave can be used for all three phases with reference voltages in each phase-phase shifted from each other by 120° (for generating balanced output voltages). The fundamental frequency voltage $e_1(t)$ is given by

$$e_1(t) = m\sin(2\pi f t) \tag{B.10}$$

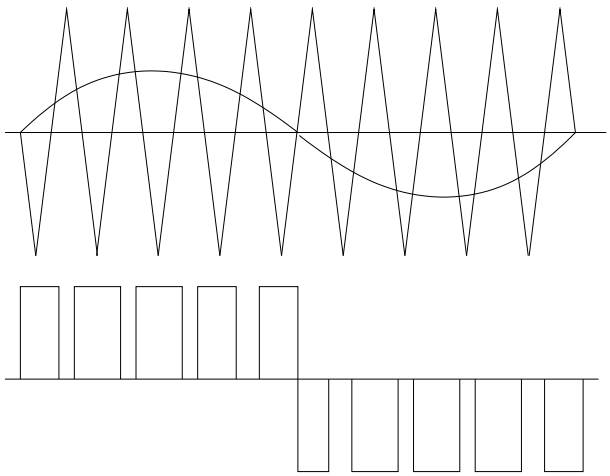

Figure B.5: Sinusoidal PWM

The harmonics are present in the output and have frequencies given by

$$f_h = MF \pm Nf \tag{B.11}$$

where M and N are integers. The harmonics are significant only around the frequency $= MF$. In general, the harmonics are determined by the frequency spectrum of the reference wave and that due to the modulation. With a sinusoidal reference wave, all harmonics are generated by the PWM process.

The reference wave can be divided into p intervals with each interval representing one cycle of the carrier wave. In each interval, the reference wave can be sampled by representing it as a constant value which is the mean of the reference wave within the interval. Thus, the reference wave is represented by a staircase waveform shown in Fig. B.6.

Two sampled waveforms with identical mean values have approximately the same fundamental component and low order harmonics. Thus, the waveforms shown in Fig. B.7(a) and (b) (which represent one stair and a notched waveform generated by the triangular wave shown in (c)) have the same mean value (L). This shows that sine PWM results in the output voltage equivalent to a voltage having a staircase waveform. As the pulse number p is increased, the staircase waveform approximates closely the reference sine wave.

Note that the reference wave is not necessarily sinusoidal in general. For active filtering applications, the reference wave includes low order harmonics. However, the method of obtaining instants of voltage reversal by comparing the reference wave with triangular wave is unaltered. In this case,

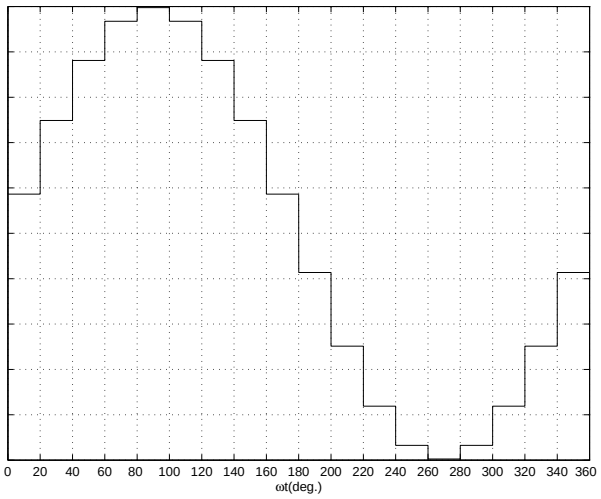

Figure B.6: Staircase waveform (after sampling)

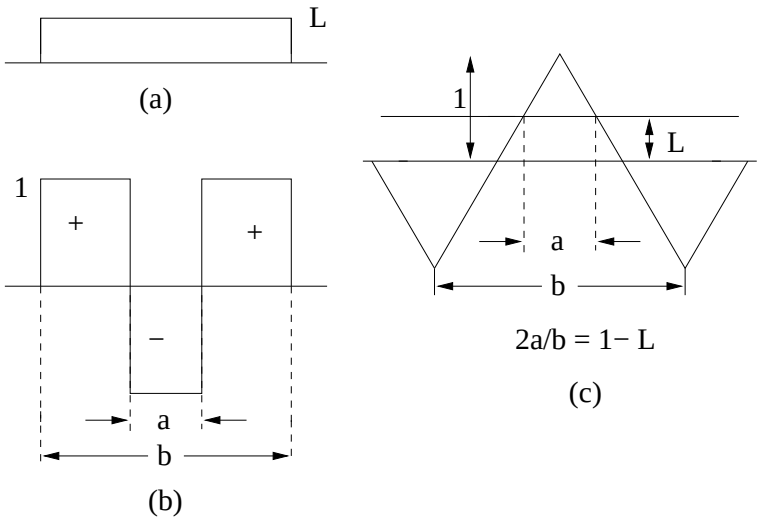

Figure B.7: Equivalence of a stair and a notched waveform (a) A stair(step) (b) Notched waveform (c) Triangular waveform

f represents the fundamental frequency of the reference wave.

Quasine Modulation [3]

The maximum value of the fundamental voltage (E_1) with sine PWM is 0.5 V_{dc} (for $m = 1$). The maximum value of the fundamental voltage for square wave (six-step) converter is $\frac{2}{\pi}V_{dc}$. Thus, the maximum value of the normalized modulation index ($\bar{m}$) for sine PWM is given by

$$\bar{m}_{\max} = \frac{\pi}{4} = 0.785 \tag{B.12}$$

The value of $\bar{m}$ can be increased by adding triplen harmonics to the reference wave without affecting the output line to line voltages. This technique follows from the fact that in three phase converters, line to line voltages have no zero sequence components. In symmetrical three phase converters, the triplen harmonics present in the phase voltages are of zero sequence.

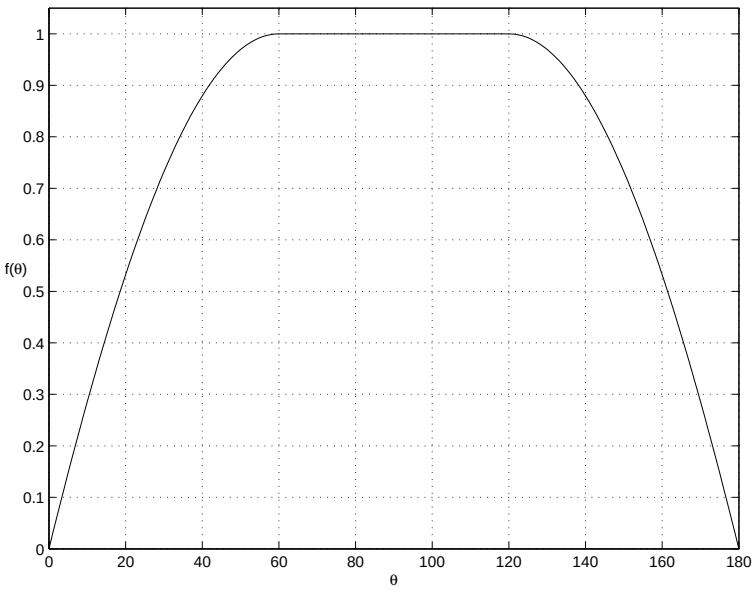

Figure B.8: Quasine waveform

The basic concept in the addition of triplen harmonics is to make the reference wave flat topped and come closer to a rectangular (or square) wave which has maximum value of the fundamental component. The maximum fundamental voltage is obtained if the reference wave has the quasine waveform shown in Fig. B.8. (over half cycle). It is defined by,

$$f(\theta) \quad = \quad 2\sin(\theta + 30^\circ) - 1, \quad 0 \leq \theta \leq 60^\circ$$

$$\begin{aligned} &= 1, \quad 60 \leq \theta \leq 120^\circ \\ &= 2\sin(\theta - 30^\circ) - 1, \quad 120^\circ \leq \theta \leq 180^\circ \end{aligned}$$

The quasine waveform can be expressed in Fourier series as,

$$f(\theta) = b_1 \sin\theta + b_3 \sin 3\theta + b_9 \sin\theta + \ldots$$

where

$$b_1 = \frac{2}{\sqrt{3}}, \quad b_3 = \frac{1}{2\pi}, \quad b_9 = \frac{1}{60\pi}$$

In general,

$$b_n = \frac{4}{\pi} \cdot \frac{3}{n(n-1)(n+1)}, \quad n = 3(2k+1)$$

where k is an integer.

It can be shown that

$$f(\theta) - f(\theta - 120^\circ) = 2\sin(\theta + 30^\circ) \tag{B.13}$$

This indicates that the line to line reference voltages are sinusoidal and unaltered by the injection of triplen harmonics to the phase reference wave.

The maximum (normalized) modulation index is given by

$$\bar{m}_{\max} = \frac{\pi}{2\sqrt{3}} = 0.907 \tag{B.14}$$

Remark

It is not necessary to use a quasine waveform to maximize the fundamental component of the output voltage. Another waveform with injected third harmonic which is one sixth of the fundamental also gives same results. This waveform is defined by

$$f'(\theta) = b_1 \sin\theta + \frac{b_1}{6} \sin 3\theta \tag{B.15}$$

where b_1 is same as before, equal to $\frac{2}{\sqrt{3}} = 1.155$.

B.4 Space Vector Modulation (SVM)

Consider one leg of the converter shown in Fig. B.9(a). Although there are two switches connected in series across the terminals 'p' and 'n', their operation is complementary. Neglecting dead time, when one of the switches is on, the other is off. Hence it is possible to get an equivalent circuit (see Fig.

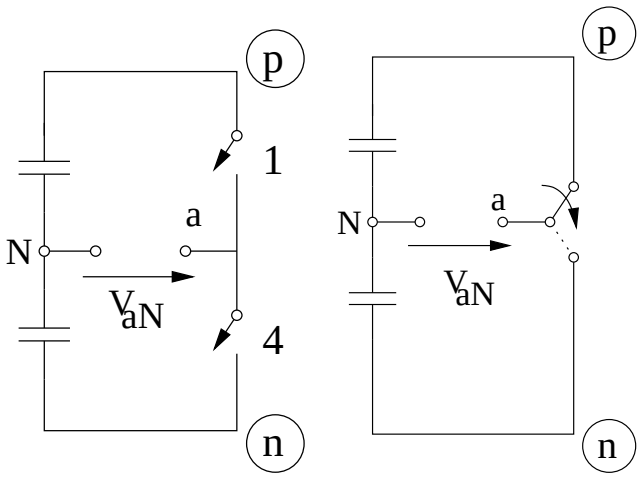

(a) A converter leg (b) Equivalent circuit

Figure B.9: Converter leg and its equivalent circuit

B.9(b)) in which there is only one switch connecting phase 'a' to terminal 'p' or 'n'. Thus, there are a total of 3 switches for a Graetz bridge (voltage source) converter with 2^3 possible switching states. Table B.1 shows the phase voltages referred to the terminal 'n' for each switching state. For each leg, we denote the switching state as 1 if the phase is connected to the terminal 'p' and 0 if the phase is connected to the terminal 'n'.

Note that $V_{an} = V_{aN} + \frac{V_{dc}}{2}$. Similarly, $V_{bn} = V_{bN} + \frac{V_{dc}}{2}$ and $V_{cn} = V_{cN} + \frac{V_{dc}}{2}$.

Neglecting zero sequence component, three phase voltages can be represented by the complex space vector defined by

$$\hat{V} = \sqrt{\frac{2}{3}}\left[V_a(t) + V_b(t)e^{j\frac{2\pi}{3}} + V_c(t)e^{j\frac{4\pi}{3}}\right] \tag{B.16}$$

Since

$$\begin{aligned} V_\alpha &= \sqrt{\frac{2}{3}}\left[V_a(t) - \frac{1}{2}V_b(t) - \frac{1}{2}V_c(t)\right] \\ V_\beta &= \sqrt{\frac{2}{3}}\left[-\frac{\sqrt{3}}{2}V_b(t) + \frac{\sqrt{3}}{2}V_c(t)\right] \end{aligned}$$

we get

$$\hat{V} = V_\alpha - jV_\beta \tag{B.17}$$

Table B.1:

S. No.	S_a	S_b	S_c	V_{an}	V_{bn}	V_{cn}
1	1	0	0	V_{dc}	0	0
2	1	1	0	V_{dc}	V_{dc}	0
3	0	1	0	0	V_{dc}	0
4	0	1	1	0	V_{dc}	V_{dc}
5	0	0	1	0	0	V_{dc}
6	1	0	1	V_{dc}	0	V_{dc}
7	1	1	1	V_{dc}	V_{dc}	V_{dc}
8	0	0	0	0	0	0

We can also express $\hat{V}$ as

$$\hat{V} = (V_d - jV_q)e^{j\omega t} = |V|e^{j(\omega t - \phi)} \tag{B.18}$$

where V_d and V_q are components with reference to a synchronously rotating reference frame. For positive sequence, sinusoidal phase voltages, V_d and V_q are constants. In this case, the space vector has a constant magnitude (V) and a phase angle which is linearly increasing with time. Note that $V = \sqrt{V_d^2 + V_q^2}$ and $\phi = \tan^{-1}\frac{V_q}{V_d}$.

Note that a voltage space vector is defined for any set of voltages not necessarily sinusoidal. For the phase voltages given in Table B.1, the space vector has only eight discrete values, each corresponding to a particular switching state. These are defined below.

$$\begin{aligned}
\hat{V}_1 &= R\angle 0, \quad \hat{V}_2 = R\angle 60^\circ, \quad \hat{V}_3 = R\angle 120^\circ, \\
\hat{V}_4 &= R\angle 180^\circ, \quad \hat{V}_5 = R\angle 240^\circ, \quad \hat{V}_6 = R\angle 300^\circ, \\
\hat{V}_7 &= \hat{V}_8 = 0
\end{aligned}$$

where $R = \sqrt{\frac{2}{3}}V_{dc}$. The first six vectors form a hexagon as shown in Fig. B.10(a). The vectors V_7 and V_8 correspond to the origin in the complex plane. It is interesting to note that $\hat{V}_7$ is zero although the phase voltages are not zero. However, the phase voltages contain only zero sequence components and these do not contribute to the space vector. There are six sectors in the hexagon, each bounded by the two adjacent space vectors.

The objective in space vector modulation is to generate the desired space vector (that may lie within any of the six sectors) by switching between the two adjacent vectors (that define a sector) and the zero vector represented by V_7 or V_8 or both. For a specified switching cycle, there is an

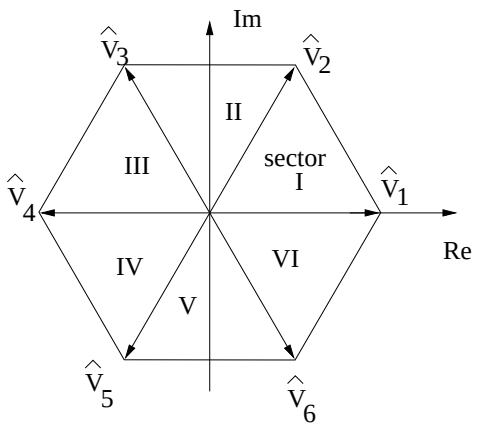

(a) Converter output voltage space vectors

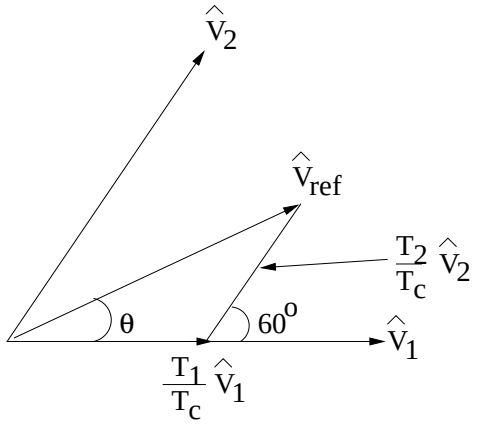

(b) Determination of switching times in sector I

Figure B.10: Voltage space vectors

average value of $\bar{V}_{ref}$ that is approximated by switching the three vectors for the predetermined times within the cycle.

For the reference space vector $\hat{V}_{ref}$ lying in sector I, we can determine the switching times from the following equation

$$\bar{V}_{ref} = \frac{1}{T_c}\int_0^{T_c} \hat{V}_{ref}dt = \frac{1}{T_c}\left[\int_0^{T_1} \hat{V}_1 dt + \int_{T_1}^{T_1+T_2} \hat{V}_2 dt + \int_{T_1+T_2}^{T_c} \hat{V}_7 dt\right] \tag{B.19}$$

where T_c is the period of the switching cycle, T_1 and T_2 are the switching

times of the vectors $\hat{V}_1$ and $\hat{V}_2$ respectively.

Since $\hat{V}_1$ and $\hat{V}_2$ are constants and $\hat{V}_7 = 0$, we get,

$$\hat{V}_1 T_1 + \hat{V}_2 T_2 = \hat{V}_{ref} T_c \tag{B.20}$$

Using rectangular coordinates, we can express the above equation as

$$\begin{aligned} T_1 \cdot \sqrt{\frac{2}{3}} V_{dc} \begin{bmatrix} 1 \\ 0 \end{bmatrix} \quad + \quad & T_2 \cdot \sqrt{\frac{2}{3}} V_{dc} \begin{bmatrix} \cos 60^\circ \\ \sin 60^\circ \end{bmatrix} \\ = \quad & T_c \cdot \sqrt{\frac{2}{3}} V_{dc} \cdot r \begin{bmatrix} \cos\theta \\ \sin\theta \end{bmatrix} \end{aligned} \tag{B.21}$$

where θ is defined in Fig. B.10(b) which also shows how T_1 and T_2 are related to $\hat{V}_{ref}$. r is defined from

$$r = \frac{|\hat{V}_{ref}|}{\sqrt{\frac{2}{3}} V_{dc}} \tag{B.22}$$

T_1 and T_2 are computed from Eq. (B.21). These are obtained as

$$T_1 = r \cdot T_c \cdot \frac{\sin(60^\circ - \theta)}{\sin 60^\circ} \tag{B.23}$$

$$T_2 = r \cdot T_c \cdot \frac{\sin\theta}{\sin 60^\circ} \tag{B.24}$$

The time (T_7) in a switching cycle corresponding to the vector $\hat{V}_7$ is given by

$$T_7 = T_c - T_1 - T_2 \tag{B.25}$$

Similar calculations apply to sectors II to VI also. Note that vector $\hat{V}_8$ can be used in place of $\hat{V}_7$. The choice is based on the requirement to minimize the average number of switchings per cycle. Fig. B.11 shows the voltages V_{aN}, V_{bN} and V_{cN} normalized by dividing by $V_{dc}/2$. This also shows the optimum pulse pattern of space vector modulation over two switching cycles. T_0 is the switching time of vector $\hat{V}_7$ or $\hat{V}_8$. Although the figure refers to the sector I, it can also apply to other sectors if T_1 and T_2 are replaced by appropriate variables (say T_2 and T_3 in sector II).

For sector I, we get the average values of V_{aN}, V_{bN} and V_{cN} (in a switching cycle) as

$$\bar{V}_{aN} = \frac{2}{\sqrt{3}} \cdot r \cdot \frac{V_{dc}}{2} \cdot \sin(\theta + 60^\circ) \tag{B.26}$$

$$\bar{V}_{bN} = 2r \cdot \frac{V_{dc}}{2} \cdot \sin(\theta - 30^\circ)$$

$$\bar{V}_{cN} = -\bar{V}_{aN} \tag{B.27}$$

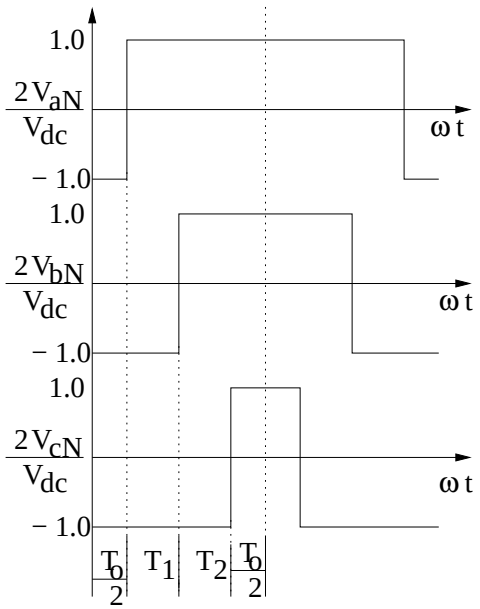

Figure B.11: Optimum pulse pattern of SVM

The maximum value of r is obtained when $\theta = 30°$ and when $|V_{ref}|$ is given by

$$\max |V_{ref}| = \cos 30° \cdot \sqrt{\frac{2}{3}} V_{dc} = \frac{V_{dc}}{\sqrt{2}} \tag{B.28}$$

This is the maximum (rms) value of the line to line (sinusoidal) voltage injected by the converter. Note that the maximum magnitude of $\hat{V}_{ref}$ is also the radius of the circle inscribed in the hexagon shown in Fig. B.10. Since the square wave converter generates a space vector of magnitude $\frac{\sqrt{6}}{\pi} V_{dc}$, we obtain the maximum value of the normalized modulation index as

$$\bar{m}_{\max} = \frac{\pi}{\sqrt{6} \cdot \sqrt{2}} = \frac{\pi}{2 \cdot \sqrt{3}} = 0.907 \tag{B.29}$$

This is also the same as that produced by quasine modulation or the injection of triplens in the reference wave.

Constraints on Ideal Switching

The analysis has neglected the dead time (T_d) that is introduced between the switching off one device and switching on the complementary device in the same leg. This is required to prevent both devices in a leg conducting simultaneously and thereby short circuiting the DC bus (This condition is called as shoot-through). The dead time provides a safety zone which allows for device dependent effects such as charge storage.

The minimum pulse width has to be greater than T_d to prevent shoot through. This constraint (termed as lock-out) puts a limit on the maximum voltage that can be achieved. The dead time requirements increase as the device switching speeds decrease (as power levels of switches increase). The increase in the output voltage can be achieved only by elimination of the pulses having widths below the permissible level. This process is termed as dropout. The pulse dropout effect needs to be considered especially for multilevel converters using PWM.

The effect of the dead time is also to add an effective resistance in series with the reference voltage. It is possible to compensate for the dead time effect by the current or voltage feedback methods. In the latter method, the detected output phase voltage is compared with the voltage reference signal and the error signal alters the reference modulating wave to compensate the error.

References

1. Joachim Holtz, "Pulsewidth Mudulation - A survey", IEEE Trans., Industrial Electronics, v. 39, n.5, 1992, pp. 410-420.
2. D.G. Holmes and T.A. Lipo, **Pulse Width Modulation for Power Converters**, IEEE Press, 2003.
3. K. Thorborg, **Power Electronics - in Theory and Practice**, Overseas Press, New Delhi, 2005.
4. B.K. Bose, **Modern Power Electronics and AC Drives**, Pearson Education, Singapore, 2002.
5. H.W. Van Der Broeck, H.C. Skudelny and G.V. Stanke, "Analysis and realization of a pulsewidth modulation based on voltage space vectors", IEEE Trans., Industry Appl., v. 24, n.1, 1988, pp. 142-150.

This page intentionally left blank

Appendix C

Per Unit System for STATCOM

It is convenient to express the parameters of a STATCOM in per unit (expressed on a base of STATCOM ratings) as they tend to lie in a narrow range even if the ratings vary widely. The MVA or MVAR rating of a STATCOM is expressed as $\pm S_B$ and the voltage rating (line to line) of the high voltage winding of the step-down or coupling transformer is expressed as V_B in kV. We select S_B as the base MVA and V_B as base voltage. The base current (I_B) and base impedance (Z_B) are defined by

$$I_B = \frac{S_B}{V_B}, \quad Z_B = \frac{V_B}{I_B} \tag{C.1}$$

Note that $I_B = \sqrt{3} I_n$, where I_n is the nominal rating of the line current. However, the expression for Z_B gives the same result if we use line to neutral voltage and line current. The advantages of the choice given in (C.1) are explained in [1].

The base values of inductance (L_B) and capacitance (C_B) are selected as

$$L_B = \frac{Z_B}{\omega_B}, \quad C_B = \frac{1}{(Z_B \omega_B)} \tag{C.2}$$

where ω_B is the base frequency (nominal frequency) in radians/sec.

To select the base values on the DC side, we redraw the equivalent circuit of a STATCOM shown in Fig. 6.10(a). This is shown in Fig. C.1. which shows two ideal transformers. The first transformer represents the coupling transformer while the second is a fictitious transformer with fixed or variable turns ratio depending on whether k is fixed or variable. Alternately, we can consider a fixed turns ratio (k_{fix}) and the secondary voltage as variable (mV_{dc}) where m is the modulation index (normalized) where $0 < m < 1$. The phase angle of the secondary voltage is also a variable.

If we select V_{dcB} as

$$V_{dcB} = \frac{N_2}{N_1} \frac{V_B}{k} = \left(\frac{N_2}{N_1} \frac{6}{p} \right) \frac{\pi}{\sqrt{6}} V_B \tag{C.3}$$

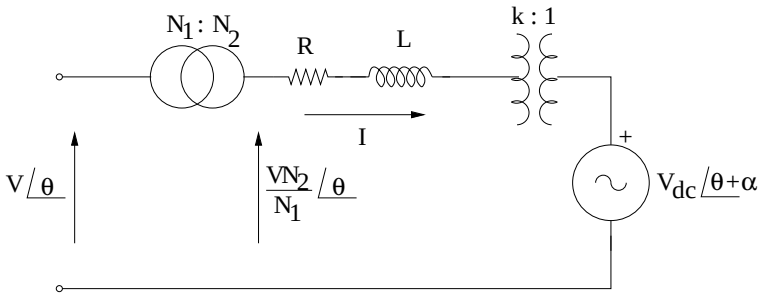

Figure C.1: Equivalent circuit of a STATCOM showing AC quantities

we can simplify the equivalent circuit to that shown in Fig. C.2. with parameters expressed in per unit. Note that we can express Eq. (C.3) also as

$$V_{dcB} = (nV_B)\frac{\pi}{\sqrt{6}} \tag{C.4}$$

where (nV_B) is the nominal AC voltage across a 3 phase Graetz bridge. $\left(n = \frac{N_2}{N_1} \cdot \frac{6}{p}\right)$. Thus, Eq. (C.4) is independent of the pulse number.

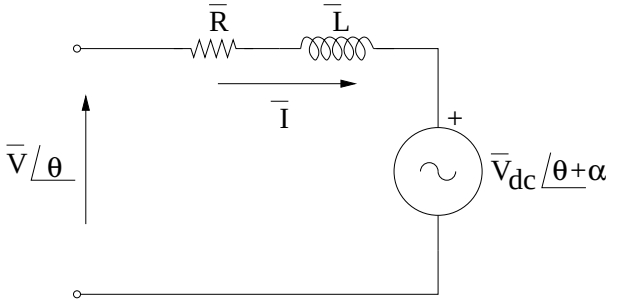

Figure C.2: Equivalent circuit in per unit quantities

The DC capacitor (C) can be referred to the AC side from the transformation,

$$C_e = \frac{C}{k^2} \tag{C.5}$$

where C_e is the equivalent capacitor on the AC side.

An Example

The first prototype STATCOM installation in USA is at 161 kV Sullivan substation of the Tennessee Valley Authority (TVA). It has the following data.

Nominal DC voltage : 6.6 kV.

Energy stored in the DC capacitor: 65 kJ.

The nominal converter output voltage is

$$V_n = \frac{\sqrt{6}}{\pi} V_{dc} = 0.78 \times 6.6 = 5.15\ kV \tag{C.6}$$

The value of the DC capacitor (C) is

$$C = \frac{65 \times 2 \times 10^3}{(6.6)^2 \times 10^6} \simeq 3000 \mu F \tag{C.7}$$

The equivalent capacitance (C_e) is given by

$$C_e = \frac{C}{(0.78)^2} = 4931 \mu F \tag{C.8}$$

This value corresponds to a voltage of 5.15 kV.

At 161 kV, the equivalent capacitor is

$$C'_e = \frac{C}{(161)^2}(5.15)^2 \simeq 5.0 \mu F \tag{C.9}$$

The rating of the STATCOM is ±100 MVA. The base impedance (Z_B) = $\frac{V_B^2}{S_B} = \frac{(161)^2}{100} = 259.2$ ohms. The capacitor susceptance (in per unit) is given by

$$b_c = \omega_B C'_e Z_B = 377 \times 5 \times 10^{-6} \times 259.2 \simeq 0.49 p.u.$$

This shows the DC capacitor rating is about 50% of the STATCOM rating. However, it is to be noted that the current in the ideal DC capacitor is zero in steady state (except for a small ripple).

Reference

1. K.R. Padiyar, **Power System Dynamics - Stability and Control**,(Second Edition), BS Publications, Hyderabad, 2002.

This page intentionally left blank

Appendix D

Abbreviations

AC	:	Alternating Current
AVR	:	Automatic Voltage Regulator
AF	:	Active Filter
CA	:	Constant Angle (control)
CC	:	Constant Current (control)
CSC	:	Convertible Static Compensator
CPD	:	Custom Power Device
CSI	:	Current Source Inverter
DSTATCOM	:	Distribution STATCOM
DC	:	Direct Current
DVR	:	Dynamic Voltage Restorer
FACTS	:	Flexible AC Transmission System
FCL	:	Fault Current Limiter
GPU	:	Gate Pulse Unit
GTO	:	Gate Turn-Off (Thyristor)
GUPFC	:	Generalized UPFC
HP	:	High Pressure (Turbine)
HVDC	:	High Voltage Direct Current
Hz	:	Hertz
IGBT	:	Insulated Gate Bipolar Transistor
IGE	:	Induction Generator Effect
IGCT	:	Integrated Gate Commutated Thyristor
IPFC	:	Interline Power Flow Controller
IP	:	Intermediate Pressure (turbine)
IPC	:	Interphase Power Controller
KCL	:	Kirchhoff's Current Law
KVL	:	Kirchhoff's Voltage Law

LPF	:	Low Pass Filter
LP	:	Low Pressure (turbine)
LCC	:	Line Commutated Converter
MCT	:	Metal-oxide semiconductor Controlled Thyristor
MOV	:	Metal Oxide Varistor
PLL	:	Phase-Locked Loop
POD	:	Power Oscillation Damping
PSDC	:	Power Swing Damping Controller
PSS	:	Power System Stabilizer
PST	:	Phase Shifting Transformer
PWM	:	Pulse Width Modulation
PQ	:	Power Quality
rad	:	radian
rms	:	root mean square
s	:	second
SC	:	Synchronous Condenser
SCR	:	Short Circuit Ratio
SMC	:	Supplementary Modulation Controller
SPST	:	Static PST
SR	:	Susceptance Regulator
SSDC	:	Subsynchronous Damping Controller
SSO	:	Subsynchronous Oscillation
SSR	:	Subsynchronous Resonance
SSSC	:	Static Synchronous Series Compensator
STATCOM	:	Static (Synchronous) Compensator
STATCON	:	Static Condenser
SVC	:	Static Var Compensator
SVR	:	Synchronous Voltage Reversal
TCBR	:	Thyristor Controlled Braking Resistor
TCPAR	:	Thyristor Controlled Phase Angle Regulator
TCR	:	Thyristor Controlled Reactor
TCPST	:	Thyristor Controlled PST
TCSC	:	Thyristor Controlled Series Capacitor
TCVL	:	Thyristor Controlled Voltage Limiter
TSC	:	Thyristor Switched Capacitor
TSR	:	Thyristor Switched Reactor
TSSC	:	Thyristor Switched Series Capacitor
T-G	:	Turbine Generator
TI	:	Torsional Interaction
UPFC	:	Unified Power Flow Controller
UPQC	:	Unified Power Quality Conditioner
VSC	:	Voltage Source Converter
VSI	:	Voltage Source Inverter

Index